

GREAT AUSTRALIAN BIGHT RESEARCH PROGRAM

RESEARCH REPORT SERIES

Petroleum migration in the Bight Basin: a fluid inclusion approach to constraining source, composition and timing

Final Report GABRP Project 5.3

Richard Kempton, Julien Bourdet and Se Gong

GABRP Research Report Series Number 14

June 2017



DISCLAIMER

The partners of the Great Australian Bight Research Program advises that the information contained in this publication comprises general statements based on scientific research. The reader is advised that no reliance or actions should be made on the information provided in this report without seeking prior expert professional, scientific and technical advice. To the extent permitted by law, the partners of the Great Australian Bight Research Program (including its employees and consultants) excludes all liability to any person for any consequences, including but not limited to all losses, damages, costs, expenses and any other compensation, arising directly or indirectly from using this publication (in part or in whole) and any information or material contained in it.

The GABRP Research Report Series is an Administrative Report Series which has not been reviewed outside the Great Australian Bight Research Program and is not considered peer-reviewed literature. Material presented may later be published in formal peer-reviewed scientific literature.

COPYRIGHT

©2017

THIS PUBLICATION MAY BE CITED AS:

Kempton, R., Bourdet, J. and Gong, S. (2017). Petroleum migration in the Bight Basin: a fluid inclusion approach to constraining source, composition and timing. Final Report GABRP Project 5.3. Great Australian Bight Research Program, GABRP Research Report Series Number 14, 342pp.

CONTACT

Dr Richard Kempton
CSIRO
e: richard.kempton@csiro.au

FOR FURTHER INFORMATION

www.misa.net.au/GAB

GREAT AUSTRALIAN BIGHT RESEARCH PROGRAM

The Great Australian Bight Research Program is a collaboration between BP, CSIRO, the South Australian Research and Development Institute (SARDI), the University of Adelaide, and Flinders University. The Program aims to provide a whole-of-system understanding of the environmental, economic and social values of the region; providing an information source for all to use.

Contents

LIST OF FIGURES.....	i
LIST OF TABLES.....	viii
ACKNOWLEDGEMENTS.....	x
EXECUTIVE SUMMARY	xi
Part I Introduction	1
INTRODUCTION.....	2
Overview	2
Background and Need.....	2
Objectives	3
REGIONAL GEOLOGY OF THE BIGHT BASIN	4
Basin Outline	4
Basin Evolution and Tectonostratigraphic Framework.....	5
Mid-Jurassic–Lower Cretaceous Extension (BP1)	5
Post-Rift Subsidence (BP2).....	5
Mid-Cretaceous Accelerated Subsidence (BP3).....	5
Australian–Antarctic sea-floor spreading and post-breakup subsidence (BP4)	6
Exploration History	6
Petroleum Geology	8
Hydrocarbon Indications and Shows	9
Part II GOI & hydrocarbon migration	11
Lead author	11
Richard Kempton	11
INTRODUCTION.....	12
Overview	12
Previous Fluid Inclusion Studies.....	12
Samples for GOI	14
Selection Criteria.....	14
Sample Preparation	15
Methods.....	19
RESULTS	20
GOI Results.....	20
Mineral Host	20

Oil Inclusion Description	24
Gnarlyknots-1A	28
Greenly-1.....	29
Duntroon-1.....	30
Potoroo-1	31
Fluorescence Colour.....	32
Gnarlyknots-1A	35
Greenly-1.....	36
Duntroon-1.....	37
Potoroo-1	38
Location.....	39
Gnarlyknots-1A	42
Greenly-1.....	44
Duntroon-1.....	46
Potoroo-1	47
Bubble Size and Variance.....	48
Gnarlyknots-1A	51
Greenly-1.....	52
Duntroon-1.....	53
Potoroo-1	54
DISCUSSION.....	55
Interpreting Palaeo-Oil Saturation from GOI Data	55
Factors Affecting GOI Interpretation	56
Implications for trapping sites in the Bight Basin	56
Gnarlyknots-1A	57
Greenly-1.....	59
Duntroon-1.....	61
Potoroo-1	63
Jerboa-1 (Revised GOI).....	65
Hydrocarbon Migration in the Bight Basin	67
Central Ceduna Sub-basin	67
Eastern Ceduna/Duntroon Sub-basins.....	70
Eyre Sub-basin.....	72
Hydrocarbon Types	73

API Gravity.....	73
Relative Timing of Hydrocarbon Migration.....	74
Part IV MCI & geochemical composition	76
Lead author	76
Se Gong	76
INTRODUCTION.....	77
Overview	77
Previous MCI studies.....	77
Samples	77
Methods.....	77
MCI sample cleaning	78
System blanks	78
Off-line MCI.....	78
On-line MCI	79
Carbon isotopes of fluid inclusion gases.....	80
RESULTS	82
Gnarlyknots-1A	82
Off-line MCI.....	82
On-line MCI	88
Carbon isotopes of fluid inclusion gases.....	89
Greenly-1.....	90
Off-line MCI.....	90
DISCUSSION.....	95
Potential Source Rocks in the Bight Basin.....	95
Tiger Supersequence.....	95
White Pointer Supersequence	95
Blue Whale Supersequence	96
Upper Bronze Whaler Supersequence.....	96
Fluid Inclusion Source Characteristics and Palaeo-depositional Conditions	96
Gnarlyknots-1A FI Oil	101
Greenly-1 FI Oil	102
Molecular Thermal Maturity.....	103
Gnarlyknots-1A FI oil.....	103
Greenly-1 FI oil	103

Fluid Inclusion Gases in Gnarlyknots-1A.....	103
Part II PVTx modelling & timing of hydrocarbon migration.....	107
Lead author	107
Julien Bourdet	107
INTRODUCTION.....	108
Overview	108
Previous temperature studies.....	108
Samples	109
Methods.....	109
Microthermometry	109
Raman Spectroscopy.....	112
Fluid Modelling	113
RESULTS	115
Gnarlyknots-1A (4410-15 mMD).....	115
Fluid Inclusion Assemblages	116
Microthermometry	117
PVT Analysis	124
Summary of <i>PT</i> Trapping Conditions.....	126
Greenly-1 (4809-12 mMD).....	128
Fluid Inclusion Assemblage Descriptions	129
Microthermometry	130
PVT Analysis	135
Summary of <i>PT</i> Trapping Conditions.....	136
Duntroon-1 (2505-10 mMD).....	138
Fluid Inclusion Assemblage Descriptions	139
Microthermometry	140
PVT analysis.....	149
Summary of <i>PT</i> Trapping Conditions.....	151
Potoroo-1 (2505-10 mMD)	153
Fluid Inclusion Assemblage Descriptions	154
Microthermometry	155
Water Inclusion Assemblages	157
PVT Analysis	162
Summary of <i>PT</i> Trapping Conditions.....	163

DISCUSSION.....	165
Timing of Hydrocarbon Entrapment in the Central Ceduna Sub-basin	165
Gnarlyknots-1A	165
Potoroo-1	167
Generation-Expulsion Modelling (Literature)	169
Timing of Hydrocarbon Entrapment in the Eastern Ceduna/Duntroon Sub-basins	171
Greenly-1.....	171
Duntroon-1.....	173
Consequences of Entrapment in Quartz for Understanding Migration	175
CONCLUSIONS.....	176
Contributions to Petroleum Systems Knowledge in the Bight Basin	176
Grains containing Oil Inclusions (GOI)	176
Molecular Composition of Oil Inclusions (MCI)	176
Timing of Hydrocarbon Entrapment (PVT)	177
Implications for natural Bitumen Strandings in South Australia (Link to Project 5.2)	179
REFERENCES.....	182
APPENDIX 1: DATA MANAGEMENT	192
Raw Datasets Created.....	192
Data Processing and Derived Datasets	193
Data Curation and Archive	194
Data Access, Use Agreements and Licensing	194
Publication of Datasets	194
APPENDIX 2: PROJECT PUBLICATIONS	195
Papers	195
Presentations	195
Patents	195
Media Releases	195
APPENDIX 3: INTELLECTUAL PROPERTY	196
Unique discoveries.....	196
Action plan	196
APPENDIX 4: Molecular Composition of oil Inclusions (MCI) – Tables & Figures	197
APPENDIX 5: MCI – Peak Assignments & Abbreviations.....	214
APPENDIX 6: OFF-LINE MCI – Gnarlyknots-1A	230
APPENDIX 7: ON-LINE MCI – Gnarlyknots-1A	272

APPENDIX 8: OFF-LINE MCI – Greenly-1	279
APPENDIX 9: PT diagrams Gnarlyknots-1A	321
APPENDIX 10: PT diagrams Greenly-1.....	325
APPENDIX 11: PT diagrams Duntroon-1.....	330
APPENDIX 12: PT diagrams Potoroo-1	339
APPENDIX 13: Phase envelopes of hydrocarbon fluid showing reversible precipitation at low temperatures	342

LIST OF FIGURES

Figure 1: Location of the Bight Basin with component sub-basins.....	4
Figure 2: Bight Basin stratigraphic correlation chart showing basin phases and predicted source rock intervals.....	7
Figure 3: Bight Basin and location of petroleum wells (with exploration permits current as of 2016).	8
Figure 4: Summary chart of the petroleum systems in the Bight Basin.	9
Figure 5: GOI microscope and partitioning of a thin section.....	19
Figure 6: Photomicrographs of oil inclusions from Gnarlyknots-1A. TL (left), UV (right).	20
Figure 7: Oil inclusions within detrital quartz grains. UV light.....	20
Figure 8: GOI results ranked by GOI number.....	22
Figure 9: GOI results ranked by number of grains with oil inclusions.	23
Figure 10: Oil inclusion descriptions for all GOI.....	24
Figure 11: Bar chart of oil inclusion descriptions for GOI—all samples.	26
Figure 12: Photomicrographs of oil and gas-rich inclusions.	27
Figure 13: Pie charts of oil inclusion descriptions for GOI—Gnarlyknots-1A.	28
Figure 14: Pie charts of oil inclusion descriptions for GOI—Greenly-1.	29
Figure 15: Pie charts of oil inclusion descriptions for GOI—Duntroon-1.	30
Figure 16: Pie charts of oil inclusion descriptions for GOI—Potoroo-1.....	31
Figure 17: Pie chart of OIA fluorescence colour—all samples.	32
Figure 18: Bar chart of OIA fluorescence colour—all samples.	34
Figure 19: Pie charts of OIA fluorescence colour—Gnarlyknots-1A.....	35
Figure 20: Pie charts of OIA fluorescence colour—Greenly-1.....	36
Figure 21: Pie charts of OIA fluorescence colour—Duntroon-1.	37
Figure 22: Pie charts of OIA fluorescence colour—Potoroo-1.	38
Figure 23: Pie chart of OIA locations—all samples.....	39
Figure 24: Bar chart of OIA locations—all samples. For oil-bearing inclusions counted in GOI only.....	41
Figure 25: Pie charts of OIA location—Gnarlyknots-1A.	42
Figure 26: Oil-bearing inclusions in Gnarlyknots-1A.....	43
Figure 27: Pie charts of OIA location—Greenly-1.....	44
Figure 28: Oil-bearing inclusions in Greenly-1.....	45
Figure 29: Pie charts of OIA location—Duntroon-1.....	46
Figure 30: Pie charts of OIA location—Potoroo-1.	47
Figure 31: Pie chart of OIA bubble size and variability—all samples.	48
Figure 32: Bar chart of OIA bubble size and variability-all samples. For oil-bearing inclusions counted in GOI only.....	50
Figure 33: Pie charts of OIA bubble size and variability—Gnarlyknots-1A.....	51
Figure 34: Pie charts of OIA bubble size and variability—Greenly-1.....	52
Figure 35: Pie charts of OIA bubble size and variability—Duntroon-1.....	53
Figure 36: Pie charts of OIA bubble size and variability—Potoroo-1.	54
Figure 37 GOI values recorded in oil and water legs from selected oilfields in Australasia	55
Figure 38: GOI log – Gnarlyknots-1A.....	58
Figure 39: GOI log – Greenly-1.....	60
Figure 40: GOI log – Duntroon-1.....	62

Figure 41: GOI log – Potoroo-1	64
Figure 42: GOI log – Jerboa-1.....	66
Figure 43: GOI summary by supersequence age. Includes data of Lisk et al (2001).	68
Figure 44: Structural elements of the central Ceduna Sub-basin.....	69
Figure 45: 2D transects across the Ceduna Sub-basin showing potential source rock intervals.....	70
Figure 46: Structural elements of the eastern Ceduna and Duntroon sub-basins.....	71
Figure 47: Hydrocarbon types observed in fluids inclusions from the Bight Basin.	73
Figure 48: Schematic representation of crude oil fluorescence colour and gravity °API, showing the range of near-white fluorescent oil inclusions from this study.	74
Figure 49: Relative timing of oil inclusions.	75
Figure 50: the effect of fractionation in the cryo-trapping system using three gas standards.	81
Figure 51: Gnarlyknots-1A — samples for MCI (off-line and on-line) and gas isotopes.....	83
Figure 52: Artefacts of alkene based synthetic drilling fluid from GC-MS chromatogram of saturated hydrocarbons extracted from Gnarlyknots-1A 4412.0 m SWC sample.....	84
Figure 53: GC-MS chromatogram of saturated hydrocarbons from the final outside rinse of the Gnarlyknots-1A sample.....	85
Figure 54: Carbon isotopic composition of FI gases from Gnarlyknots-1A (4410-15 mMD) showing reproducibility of the duplicates.....	89
Figure 55: Greenly-1 — samples for MCI (off-line only).	91
Figure 56: Comparison of normalized n-alkane distributions in the Gnarlyknots-1A and Greenly-1 FI oils.....	98
Figure 57: Comparison of pristane/n-C ₁₇ versus phytane/n-C ₁₈ ratios in the Gnarlyknots-1A and Greenly-1 FI oils.	99
Figure 58: Comparison of C ₂₄ tetracyclic/C ₂₃ tricyclic terpanes versus (C ₁₉ +C ₂₀)/C ₂₃ tricyclic terpanes in the Gnarlyknots-1A and Greenly-1 FI oils.	99
Figure 59: Comparison of C ₂₇ , C ₂₈ , C ₂₉ steranes in the Gnarlyknots-1A and Greenly-1 FI oils.	100
Figure 60: Comparison of dibenzothiophene/phenanthrene (DBT/P) versus pristane/phytane ratios in the Gnarlyknots-1A and Greenly-1 FI oils.	100
Figure 61: Modelled present-day transformation ratios of three potential source rock units within the Blue Whale, upper White Pointer and Tiger supersequences in the Ceduna Sub-basin.	101
Figure 62: Schematic cross section (NE-SW) showing potential type III terrigenous source rocks (Bronze Whaler and White Pointer) for the Greenly-1 FI oil.	102
Figure 63: End member values for stable carbon isotopes of methane and the potential for mixing between these two sources. Base image from Stalker (2013).	104
Figure 64: Natural gas interpretative diagram showing carbon isotopic composition of methane in Gnarlyknots-1A FI gases.....	104
Figure 65: Natural gas interpretative diagram showing carbon isotopic compositions of methane and ethane in the Gnarlyknots-1A FI gases.	105
Figure 66: Thermometric observations and measurements acquired in the laboratory from oil inclusions, water inclusions or gas inclusions.....	110
Figure 67: Phase diagrams illustrating the thermometric observations and measurements acquired in the laboratory from oil inclusions, water inclusions or gas inclusions.	111
Figure 68: Phase envelopes of aqueous and petroleum fluids at different scenarios of gas saturation in liquid at entrapment.	114
Figure 69: GOI log for Gnarlyknots-1A showing location of sample for PVT analysis.	115

Figure 70: Fluid inclusions types observed in Gnarlyknots-1A sample (at room temperature).....	116
Figure 71 Petroleum fluid inclusion assemblages observed from 4410-15 mMD in Gnarlyknots-1A	117
Figure 72: Homogenisation temperatures of oil and associated water inclusion from 4410-15 mMD in Gnarlyknots-1A.	118
Figure 73: Homogenisation temperatures of water inclusion assemblages at the quartz overgrowth boundary from 4410-15 mMD in Gnarlyknots-1A.	119
Figure 74: Transmitted light photomicrographs of Gnarlyknots-1A oil inclusion assemblages 2, 3, 5, 8, 15.	123
Figure 75: Trapping conditions at 4410-15 mMD in Gnarlyknots-1A derived from PVTx modelling of gas, oil and water fluid inclusion assemblages.	127
Figure 76: GOI log for Greenly-1 showing location of sample for PVT analysis.....	128
Figure 77 Petroleum fluid inclusion assemblages observed from 4809-12 mMD in Greenly 1,.	129
Figure 78: Homogenisation temperatures of oil and associated water inclusions from 4809-12 mMD in Greenly-1.....	130
Figure 79: Paired transmitted light and UV photomicrographs of Greenly-1 oil inclusion assemblages 1, 4, 6.....	133
Figure 80: Paired transmitted light and UV photomicrographs of Greenly-1 oil inclusion assemblages 2, 4, 8.....	134
Figure 81: Trapping conditions at 4809-12 mMD in Greenly-1 derived from PVTx modelling of oil and water fluid inclusion assemblages.	137
Figure 82: GOI log for Duntroon-1 showing location of sample for PVT analysis.....	138
Figure 83. Fluid inclusions types observed at room temperature in the sample from Duntroon-1. .	139
Figure 84: Petroleum fluid inclusion assemblages observed from 2505-10 mMD in Duntroon 1.	140
Figure 85: Homogenisation temperatures of petroleum and associated water inclusion assemblages from 2505-10 mMD in Duntroon-1.....	142
Figure 86: Homogenisation temperatures of water inclusions from 2505-10 mMD in Duntroon-1..	142
Figure 87: Paired transmitted light and UV photomicrographs of Duntroon-1 oil inclusion assemblages 1, 2, 6.	147
Figure 88: Paired transmitted light and UV photomicrographs of Duntroon-1 oil inclusion assemblages 2, 4, 8.	148
Figure 89: Trapping conditions at 2505-10 mMD in Duntroon-1 derived from PVTx modelling of gas, oil and water fluid inclusion assemblages.	152
Figure 90: GOI log for Potoroo-1 showing location of sample for PVT analysis.	153
Figure 91: Petroleum fluid inclusion assemblages observed from 1778-86 mMD in Potoroo-1.	155
Figure 92 Homogenisation temperatures of petroleum and associated water inclusion assemblages from 1778-86mMD in Potoroo-1.	156
Figure 93: Homogenisation temperatures of water inclusions from 1778-86mMD in Potoroo-1.....	157
Figure 94: Paired transmitted light and UV photomicrographs of Potoroo-1 oil inclusion assemblages 2, 5, 6, 9 and 14.....	161
Figure 95: Trapping conditions at 1178-86 mMD in Potoroo-1 derived from PVTx modelling of oil and water fluid inclusion assemblages.	164
Figure 96: Pressure-time and Temperature-time plots for entrapment of oil and gas bearing inclusion assemblages at 4410-15 mMD in Gnarlyknots-1A.....	166
Figure 97: Maturation of organic matter.....	167

Figure 98: Pressure-time and Temperature-time plots for entrapment of oil and gas bearing inclusion assemblages at 1778-86 mMD in Potoroo-1 (hotter PT modelled conditions).....	168
Figure 99: Predicted accumulations and the percentage of liquids contribution from three potential source units in the central Ceduna transect.....	170
Figure 100: Pressure-time and Temperature-time plots for entrapment of oil bearing inclusion assemblages at 4809-12 mMD in Greenly-1.....	172
Figure 101: Pressure-time and Temperature-time plots for entrapment of oil bearing inclusion assemblages at 2505-10 mMD in Duntroon-1.....	174
Figure 102: Dendrogram of the hierarchical cluster analysis (HCA) of 26 source variables showing similarity and dissimilarity between Gnarlyknots-1A and Greenly-1 FI oils and asphatites and waxy bitumens from the GAB.	181
Figure A4-103: Diagram of the 55 mL stainless steel crushing cylinder used for off-line analyses of FI oils.	206
Figure A4-104: Schematic diagram of the Quantum MSSV1B Thermal Analysis System used for the on-line crushing of quartz grains containing oil-bearing fluid inclusions directly onto a GC-MS capillary column.....	207
Figure A4-105: Aliphatic hydrocarbon distributions in the Gnarlyknots-1A (4390-4425 m) MCI sample.....	208
Figure A4-106: Aliphatic hydrocarbon distributions in the Greenly-1 (4806-4818 m) MCI sample...	209
Figure A4-107: Plot of Ph/n-C ₁₈ versus Pr/n-C ₁₇ ratios of Gnarlyknots-1A (4390-4425 m) FI oil.....	210
Figure A4-108: Plot of Ph/n-C ₁₈ versus Pr/n-C ₁₇ ratios of Greenly-1 (4806-4818 m) FI oil.	210
Figure A4-109: Distribution of alkylbenzenes, naphthalene, phenanthrene, biphenyl, dibenzothiophene and alkylated homologues of Gnarlyknots-1A (4390-4425 m) FI oil.....	211
Figure A4-110: Distribution of alkylbenzenes, naphthalene, phenanthrene, biphenyl, dibenzothiophene and alkylated homologues of Greenly-1 (4806-4818 m) FI oil.	212
Figure A4-111: Normalised distribution of low molecular weight compounds in the Gnarlyknots-1A FI oil.	213
Figure A6-112: Partial m/z 85 mass chromatograms for the Gnarlyknots-1A (4390-4425m) FI oil. .	231
Figure A6-113: Partial m/z 85 mass chromatograms for the Gnarlyknots-1A (4390-4425m) FI system blank.....	232
Figure A6-114: Partial m/z 113 and 125 mass chromatograms for the Gnarlyknots-1A (4390-4425m) FI oil.....	233
Figure A6-115: Partial m/z 113 and 125 mass chromatograms for the Gnarlyknots-1A (4390-4425m) FI system blank.....	234
Figure A6-116: Partial m/z 123 and 191 mass chromatograms for the Gnarlyknots-1A (4390-4425m) FI oil.....	235
Figure A6-117: Partial m/z 123 and 191 mass chromatograms for the Gnarlyknots-1A (4390-4425m) FI system blank.....	236
Figure A6-118: Partial m/z 191, 177 and 205 mass chromatograms for the Gnarlyknots-1A (4390-4425m) FI oil.	237
Figure A6-119: Partial m/z 191, 177 and 205 mass chromatograms for the Gnarlyknots-1A (4390-4425m) FI system blank.	238
Figure A6-120: Partial MRM chromatograms (m/z 370.4, 398.4 and 398.4 → 191.2) of the aliphatic hydrocarbons from the Gnarlyknots-1A (4390-4425m) FI oil.....	239

Figure A6-121: Partial MRM chromatograms (m/z 412.4, 426.4 and 440.4 → 191.2) of the aliphatic hydrocarbons from the Gnarlyknots-1A (4390-4425m) FI oil.....	240
Figure A6-122: Partial MRM chromatograms (m/z 454.5, 468.5 and 482.5 → 191.2) of the aliphatic hydrocarbons from the Gnarlyknots-1A (4390-4425m) FI oil.....	241
Figure A6-123: Partial m/z (a) 217 and (b) 218 mass chromatograms for the Gnarlyknots-1A (4390-4425m) FI oil.	242
Figure A6-124: Partial m/z (a) 217 and (b) 218 mass chromatograms for the Gnarlyknots-1A (4390-4425m) FI system blank.	243
Figure A6-125: Partial m/z (a) 259 and (b) 231 mass chromatograms for the Gnarlyknots-1A (4390-4425m) FI oil.	244
Figure A6-126: Partial m/z (a) 259 and (b) 231 mass chromatograms for the Gnarlyknots-1A (4390-4425m) FI system blank.	245
Figure A6-127: Partial MRM chromatograms (m/z 372.4, 386.4 and 400.4 → 217.2) of the aliphatic hydrocarbons from the Gnarlyknots-1A (4390-4425m) FI oil.....	246
Figure A6-128: Partial MRM chromatograms (m/z 358.4 and 414.4 → 217.2; 414.4 → 231.2) of the aliphatic hydrocarbons from the Gnarlyknots-1A (4390-4425m) FI oil.....	247
Figure A6-129: Partial m/z (a) 253.2 and (b) 231.12 mass chromatograms for the Gnarlyknots-1A (4390-4425m) FI oil.	248
Figure A6-130: Partial m/z (a) 253.2 and (b) 231.12 mass chromatograms for the Gnarlyknots-1A (4390-4425m) FI oil.	249
Figure A6-131: Partial m/z 106, 120 and 134 mass chromatograms for the Gnarlyknots-1A (4390-4425m) FI oil.	250
Figure A6-132: Partial m/z 106, 120 and 134 mass chromatograms for the Gnarlyknots-1A (4390-4425m) FI system blank.	251
Figure A6-133: Partial m/z 128, 142 and 156 mass chromatograms for the Gnarlyknots-1A (4390-4425m) FI oil.	252
Figure A6-134: Partial m/z 128, 142 and 156 mass chromatograms for the Gnarlyknots-1A (4390-4425m) FI system blank.	253
Figure A6-135: Partial m/z 170, 184 and 198 mass chromatograms for the Gnarlyknots-1A (4390-4425m) FI oil.	254
Figure A6-136: Partial m/z 170, 184 and 198 mass chromatograms for the Gnarlyknots-1A (4390-4425m) FI system blank.	255
Figure A6-137: Partial m/z 197, 183 and 198 mass chromatograms for the Gnarlyknots-1A (4390-4425m) FI oil.	256
Figure A6-138: Partial m/z 197, 183 and 198 mass chromatograms for the Gnarlyknots-1A (4390-4425m) FI system blank.	257
Figure A6-139: Partial m/z 178, 192 and 206 mass chromatograms for the Gnarlyknots-1A (4390-4425m) FI oil.	258
Figure A6-140: Partial m/z 178, 192 and 206 mass chromatograms for the Gnarlyknots-1A (4390-4425m) FI system blank.	259
Figure A6-141: Partial m/z 220 and 234 mass chromatograms for the Gnarlyknots-1A (4390-4425m) FI oil.....	260
Figure A6-142: Partial m/z 220 and 234 mass chromatograms for the Gnarlyknots-1A (4390-4425m) FI system blank.....	261

Figure A6-143: Partial m/z 154, 168 and 182 mass chromatograms for the Gnarlyknots-1A (4390-4425m) FI oil.	262
Figure A6-144: Partial m/z 154, 168 and 182 mass chromatograms for the Gnarlyknots-1A (4390-4425m) FI system blank.	263
Figure A6-145: Partial m/z 166, 180, 202 and 216 mass chromatograms for the Gnarlyknots-1A (4390-4425m) FI oil.	264
Figure A6-146: Partial m/z 166, 180, 202 and 216 mass chromatograms for the Gnarlyknots-1A (4390-4425m) FI system blank.	265
Figure A6-147: Partial m/z 184, 198 and 212 mass chromatograms for the Gnarlyknots-1A (4390-4425m) FI oil.	266
Figure A6-148: Partial m/z 184, 198 and 212 mass chromatograms for the Gnarlyknots-1A (4390-4425m) FI system blank.	267
Figure A6-149: Partial m/z 136.1, 135.1,149.1, 163.1 and 177.1 mass chromatograms for the Gnarlyknots-1A (4390-4425m) FI oil.	268
Figure A6-150: Partial m/z 136.1, 135.1,149.1, 163.1 and 177.1 mass chromatograms for the Gnarlyknots-1A (4390-4425m) FI system blank.	269
Figure A6-151: Partial m/z 188.2, 187.1, 201.2 and 215.2 mass chromatograms for the Gnarlyknots-1A (4390-4425m) FI oil.	270
Figure A6-152: Partial m/z 188.2, 187.1, 201.2 and 215.2 mass chromatograms for the Gnarlyknots-1A (4390-4425m) FI system blank.	271
Figure A7-153: Partial m/z 57, 70, 71, 85 mass chromatograms for the Gnarlyknots-1A (4410-4415 m) FI oil (on-line crushing method).	273
Figure A7-154: Partial m/z 56, 78,68 and 82 mass chromatograms for Gnarlyknots-1A (4410-4415 m) FI oil (on-line crushing method).	274
Figure A7-155: Partial m/z 57, 70,71 and 85 mass chromatograms for the Gnarlyknots-1A (4410-4415 m) FI oil (on-line crushing method).	275
Figure A7-156: Partial m/z 55, 91,97 and 99 mass chromatograms for the Gnarlyknots-1A (4410-4415 m) FI oil (on-line crushing method).	276
Figure A7-157: Partial m/z 57, 55,97 and 106 mass chromatograms for the Gnarlyknots-1A (4410-4415 m) FI oil (on-line crushing method).	277
Figure A7-158: TIC, partial m/z 57 and 55 mass chromatograms for the Gnarlyknots-1A (4410-4415 m) FI oil (on-line crushing method).	278
Figure A8-159: Partial m/z 85 mass chromatograms for the Greenly-1 (4806-4818 m) FI oil.	280
Figure A8-160: Partial m/z 85 mass chromatograms for the Greenly-1 (4806-4818 m) FI system blank.	281
Figure A8-161: Partial m/z 113 and 125 mass chromatograms for the Greenly-1 (4806-4818 m) FI oil.	282
Figure A8-162: Partial m/z 113 and 125 mass chromatograms for the Greenly-1 (4806-4818 m) FI system blank.	283
Figure A8-163: Partial m/z 123 and 191 mass chromatograms for the Greenly-1 (4806-4818 m) FI oil.	284
Figure A8-164: Partial m/z 123 and 191 mass chromatograms for the Greenly-1 (4806-4818 m) FI system blank.	285
Figure A8-165: Partial m/z 191, 177 and 205 mass chromatograms for the Greenly-1 (4806-4818 m) FI oil.	286

Figure A8-166: Partial m/z 191, 177 and 205 mass chromatograms for the Greenly-1 (4806-4818 m) FI system blank.....	287
Figure A8-167: Partial MRM chromatograms (m/z 370.4, 398.4 and 398.4 → 191.2) of the aliphatic hydrocarbons from the Greenly-1 (4806-4818 m) FI oil.....	288
Figure A8-168: Partial MRM chromatograms (m/z 412.4, 426.4 and 440.4 → 191.2) of the aliphatic hydrocarbons from the Greenly-1 (4806-4818 m) FI oil.....	289
Figure A8-169: Partial MRM chromatograms (m/z 454.5, 468.5 and 482.5 → 191.2) of the aliphatic hydrocarbons from the Greenly-1 (4806-4818 m) FI oil.....	290
Figure A8-170: Partial m/z (a) 217 and (b) 218 mass chromatograms for the Greenly-1 (4806-4818 m) FI oil.....	291
Figure A8-171: Partial m/z (a) 217 and (b) 218 mass chromatograms for the Greenly-1 (4806-4818 m) FI system blank.....	292
Figure A8-172: Partial m/z (a) 259 and (b) 231 mass chromatograms for the Greenly-1 (4806-4818 m) FI oil.....	293
Figure A8-173: Partial m/z (a) 259 and (b) 231 mass chromatograms for the Greenly-1 (4806-4818 m) FI system blank.....	294
Figure A8-174: Partial MRM chromatograms (m/z 372.4, 386.4 and 400.4 → 217.2) of the aliphatic hydrocarbons from the Greenly-1 (4806-4818 m) FI oil.....	295
Figure A8-175: Partial MRM chromatograms (m/z 358.4 and 414.4 → 217.2; 414.4 → 231.2) of the aliphatic hydrocarbons from the Greenly-1 (4806-4818 m) FI oil.....	296
Figure A8-176: Partial m/z (a) 253.2 and (b) 231.12 mass chromatograms for the Greenly-1 (4806-4818 m) FI oil.....	297
Figure A8-177: Partial m/z (a) 253.2 and (b) 231.12 mass chromatograms for the Greenly-1 (4806-4818 m) FI oil.....	298
Figure A8-178: Partial m/z 106, 120 and 134 mass chromatograms for the Greenly-1 (4806-4818 m) FI oil.....	299
Figure A8-179: Partial m/z 106, 120 and 134 mass chromatograms for the Greenly-1 (4806-4818 m) FI system blank.....	300
Figure A8-180: Partial m/z 128, 142 and 156 mass chromatograms for the Greenly-1 (4806-4818 m) FI oil.....	301
Figure A8-181: Partial m/z 128, 142 and 156 mass chromatograms for the Greenly-1 (4806-4818 m) FI system blank.....	302
Figure A8-182: Partial m/z 170, 184 and 198 mass chromatograms for the Greenly-1 (4806-4818 m) FI oil.....	303
Figure A8-183: Partial m/z 170, 184 and 198 mass chromatograms for the Greenly-1 (4806-4818 m) FI system blank.....	304
Figure A8-184: Partial m/z 197, 183 and 198 mass chromatograms for the Greenly-1 (4806-4818 m) FI oil.....	305
Figure A8-185: Partial m/z 197, 183 and 198 mass chromatograms for the Greenly-1 (4806-4818 m) FI system blank.....	306
Figure A8-186: Partial m/z 178, 192 and 206 mass chromatograms for the Greenly-1 (4806-4818 m) FI oil.....	307
Figure A8-187: Partial m/z 178, 192 and 206 mass chromatograms for the Greenly-1 (4806-4818 m) FI system blank.....	308

Figure A8-188: Partial m/z 220 and 234 mass chromatograms for the Greenly-1 (4806-4818 m) FI oil.	309
Figure A8-189: Partial m/z 220 and 234 mass chromatograms for the Greenly-1 (4806-4818 m) FI system blank.	310
Figure A8-190: Partial m/z 154, 168 and 182 mass chromatograms for the Greenly-1 (4806-4818 m) FI oil.	311
Figure A8-191: Partial m/z 154, 168 and 182 mass chromatograms for the Greenly-1 (4806-4818 m) FI system blank.	312
Figure A8-192: Partial m/z 166, 180, 202 and 216 mass chromatograms for the Greenly-1 (4806-4818 m) FI oil.	313
Figure A8-193: Partial m/z 166, 180, 202 and 216 mass chromatograms for the Greenly-1 (4806-4818 m) FI system blank.	314
Figure A8-194: Partial m/z 184, 198 and 212 mass chromatograms for the Greenly-1 (4806-4818 m) FI oil.	315
Figure A8-195: Partial m/z 184, 198 and 212 mass chromatograms for the Greenly-1 (4806-4818 m) FI system blank.	316
Figure A8-196: Partial m/z 136.1, 135.1, 149.1, 163.1 and 177.1 mass chromatograms for the Greenly-1 (4806-4818 m) FI oil.	317
Figure A8-197: Partial m/z 136.1, 135.1, 149.1, 163.1 and 177.1 mass chromatograms for the Greenly-1 (4806-4818 m) FI system blank.	318
Figure A8-198: Partial m/z 188.2, 187.1, 201.2 and 215.2 mass chromatograms for the Greenly-1 (4806-4818 m) FI oil.	319
Figure A8-199: Partial m/z 188.2, 187.1, 201.2 and 215.2 mass chromatograms for the Greenly-1 (4806-4818 m) FI system blank.	320

LIST OF TABLES

Table 1: Hydrocarbon indications and shows.	10
Table 2: Previous GOI data reported by Lisk et al (2001).	13
Table 3: GAB — Sample selection for GOI, PVTx and MCI and rationale.	16
Table 4: GOI results from this study.	21
Table 5: Oil inclusion descriptions for GOI and non-GOI fluorescing features (not counted).	25
Table 6: OIA fluorescence colour.	33
Table 7: OIA locations.	40
Table 8: OIA bubble size and variability-all samples.	49
Table 9: Revised GOI for Jerboa-1.	65
Table 10: MCI and gas isotope sample information – Gnarlyknots-1A.	82
Table 11: MCI sample information – Greenly-1.	90
Table 12: Summary of biomarker related source indicators in the Gnarlyknots-1A and Greenly-1 fluid inclusion oil.	97
Table 13: Sources of CO ₂ in petroleum basins and carbon isotopic values.	105
Table 14: Sample information.	109
Table 15: Gnarlyknots-1A thermometric results.	120
Table 16: Gnarlyknots-1A Raman results for gas detection.	122

Table 17: Oil inclusions compositions calculated for Gnarlyknots-1A using PIT.	125
Table 18: Summary of PT entrapment conditions in Gnarlyknots-1A.	126
Table 19: Greenly-1 thermometric results.....	131
Table 20: Greenly-1 Raman results for gas detection.....	132
Table 21: Oil inclusion compositions calculated in Greenly-1 using PIT.....	136
Table 22: Summary of PT entrapment conditions in Greenly-1.	137
Table 23: Duntroon-1 thermometric results.....	143
Table 24: Duntroon-1 Raman-derived pressure and fluid compositions.	146
Table 25: Duntroon-1 oil inclusion compositions calculated using PIT.	150
Table 26: Summary of PT entrapment conditions in Duntroon-1.	152
Table 27: Potoroo-1 thermometric results.	158
Table 28: Potoroo-1 Raman-derived pressure and fluid compositions.....	160
Table 29: Potoroo-1 oil inclusion compositions calculated using PIT.....	162
Table 30: Summary of PT entrapment conditions in Potoroo-1.....	163
Table A4-31: Aliphatic hydrocarbon concentrations of the FI oil, associated system blank and final outside rinse.....	198
Table A4-32: Aliphatic hydrocarbon parameters.....	199
Table A4-33: Terpane parameters.	200
Table A4-34: Sterane and diasterane parameters.....	201
Table A4-35: Aromatic hydrocarbon parameters.....	202
Table A4-36: Diamondoid hydrocarbon parameters.....	204
Table A4-37: Low molecular weight hydrocarbon parameters (on-line).....	205
Table A4-38: Carbon isotopic composition of fluid inclusion gases.	205
Table A5-39: Peak assignments for terpanes in the m/z 191, 177 and 205 mass chromatograms and MRM chromatograms.....	215
Table A5-40: Peak assignments for steranes, diasteranes and methylsteranes in the m/z 217, 218, 259 and 231 mass chromatograms and MRM chromatograms.	216
Table A5-41: Peak assignments for monoaromatic (MA) and rearranged dia-monoaromatic (DMA) steroids in the m/z 253 mass chromatogram.....	218
Table A5-42: Peak assignments for triaromatic steroids in the m/z 231 mass chromatogram.	218
Table A5-43: Peak abbreviations for the aromatic hydrocarbons, with diagnostic m/z ions.....	219
Table A5-44: Peak assignments for diamondoid hydrocarbons (adamantanes and diamantanes), with the diagnostic m/z ions.....	223
Table A5-45: Peak assignments for low molecular weight hydrocarbons, with structures.	224

ACKNOWLEDGEMENTS

The Great Australian Bight Research Program is a collaboration between BP, CSIRO, the South Australian Research and Development Institute (SARDI), the University of Adelaide, and Flinders University. The Program aims to provide a whole-of-system understanding of the environmental, economic and social values of the region; providing an information source for all to use.

A portion of this work was subcontracted to, and undertaken in collaboration with, the Centre de Recherches sur la Geologie des Matieres Premieres Minerales et Energetiques (CREGU) in Nancy, France and Nathalie Foucal (Director). Acknowledgement is given to Jacques Pironon, Director of the GeoResources Laboratory, University of Lorraine, Nancy, France, for allowing the use of Petroleum Inclusion Thermodynamic (PIT) software, and Vanessa Dyja for performing laser scanning confocal microscopy.

Selected images in this report © Commonwealth of Australia (Geoscience Australia) 2016. These products are released under the Creative Commons Attribution 4.0 International Licence.

<http://creativecommons.org/licenses/by/4.0/legalcode>

EXECUTIVE SUMMARY

Project 5.3 (fluid inclusions) forms a component in Theme 5 (petroleum systems) of the Great Australian Bight Research Program. The perceived risk of hydrocarbon charge in the Bight Basin, and the Ceduna Sub-basin, was a significant driver for the application of unique fluid inclusion-based methods to address objectives of; (1) constraining key elements of the petroleum system(s), namely migration, source and timing, and (2) providing geochemical analogues for potentially addressing the origin of coastal bitumen strandings in the GAB (link to Project 5.2).

To screen the Bight Basin for hidden hydrocarbon indications, 36 samples were analysed from 7 historic exploration wells—central Ceduna Sub-basin; Potoroo-1, and the previously untested Gnarlyknots-1A well and eastern Ceduna/Duntroon sub-basins; Borda-1, Duntroon-1, Greenly-1, Jerboa-1 and Platypus-1—using CSIRO's *Grains with Oil Inclusions (GOI™)* technique. The identification of not only oil-bearing, but in some samples gas-rich inclusions at low abundance (GOI <0.7%, up to a maximum of 1.1% in Greenly-1) is positive evidence for widespread oil and gas migration in the Bight Basin. These hidden oil indications are more frequent in intervals from the Late Cretaceous White Pointer, Tiger and Hammerhead supersequences and are a significant improvement over conventional oil indications that are limited to Greenly-1. The presence of these hydrocarbon inclusions implies generation and expulsion from active petroleum systems, and therefore the presence of effective source rocks. The result improves exploration potential, particularly in the poorly understood deepwater part of the Ceduna Sub-basin. In attempting to integrate previous GOI results into this investigation, palaeo-oil zones in Jerboa-1 from the Eyre Sub-basin are no longer supported by repeat GOI measurements.

To geochemically fingerprint hydrocarbons, CSIRO's *Molecular Composition of oil Inclusions (MCI)* and gas-isotope techniques were performed on minute quantities of oil and gas extracted from the fluid inclusions. Fluid inclusion (FI) oil from Gnarlyknots-1A (4,390 to 4,425 mMD; Tiger Supersequence) comprises a mixture of types including oil and gas-condensate. The *n*-alkane and biomarker characteristics show a mixed organic matter input from both algae and terrestrial plants and was generated from source rock(s) deposited in suboxic-oxic marine environment(s). The wide range of maturities, 0.65% to 1.3% equivalent vitrinite reflectance (VRE), in the Gnarlyknots-1A FI oil suggests either a mixture of oils generated from different source rocks—Blue Whale and Tiger having potential marine algal input, while the White Pointer has potential terrestrial plant input—or from the same source rock at different maturity stages—perhaps an unrecognised paralic facies of the White Pointer, containing both algal and terrestrial organic matter. Either way, the recognition of some algal input is the first direct evidence for generation from rocks containing type II kerogen and this significantly improves the prospectivity in the deepwater Ceduna Sub-basin. The light gasoline range hydrocarbons are dominated by toluene and originated, in part, from coeval aqueous inclusions. The bulk $\delta^{13}\text{C}$ isotopic composition of methane (-28.4 ‰ and -28.6 ‰ replicates) and ethane (-17.6 ‰ and -18.1 ‰ replicates) indicates a thermogenic origin for these hydrocarbon gases, probably derived from type III (humic/coaly) organic matter. The bulk $\delta^{13}\text{C}$ isotopic composition of carbon dioxide (-3.9 ‰ and -4.4 ‰ replicates) indicates a wholly inorganic origin from inherited inclusions of probable magmatic or metamorphic sources.

By comparison, FI oil from Greenly-1 (4,806-4,818 mMD; White Pointer Supersequence) comprises only oil, with no gas-condensate visually detected. The *n*-alkane and biomarker characteristics indicate significant organic matter input from terrestrial plants, and a minor contribution from

bacteria, and generation from a source rock deposited in an oxic, clay-rich fluvio/deltaic depositional environment. This FI oil represents a pristine oil sample that was generated over a narrow maturity band at the early to peak oil window (0.8% to 1.1% VRE), and lacks the mixed algal input of the current oil indications in the same well. Previous suggestions that these oil indications correlate to a Bronze Whaler source sequence is not supported by the MCI data, which lacks algal input and potentially indicates a White Pointer source sequence instead.

To understand the timing of oil migration, the *pressure-temperature (PT)* trapping conditions of hydrocarbon inclusions were determined in Gnarlyknots-1A, Greenly-1, Duntroon-1 and Potoroo-1. The intra-Coniacian primary well target in Gnarlyknots-1A (4,410-4,415 mMD; Tiger Supersequence) was a migration pathway, over an extended period of time, for a variety of hydrocarbon fluid compositions modelled by Petroleum Inclusion Thermodynamic (PIT) as black oil, light oil, gas-condensate and gas+CO₂. There is good concordance in the measured *PT* data with independent *PT* curves from basin models. The earliest oil entrapment took place at a minimum of 58°C, with constrained *PT* conditions of light oil (240-270 bar; 69.2°C) in the Late Cretaceous at ~70-75 Ma (Campanian). Phase separation of light oil, and entrapment of both gas-rich phases and gas-depleted black oil, occurred at *PT* conditions (285-308 bar; 80-85°C) consistent with the Late Cretaceous at ~70 Ma (Maastrichtian). Subsequent entrapment of gas-condensate took place at pressure conditions (350-410 bar; 80°C) reached later at ~35-15 Ma (Oligocene to Early Miocene), followed by gas+CO₂ at *PT* conditions (370-408 bar; 78-88°C) reached at ~27-15 Ma (Late Oligocene to Early Miocene). This apparent sequence of hydrocarbon entrapment from oil to gas over time might simply be explained by generation from a single mixed organic source unit over a range of thermal maturity stages—perhaps an unrecognised paralic facies of the White Pointer? The earlier oil-rich assemblages are easily explained by sediment loading of the Upper Cretaceous succession by the Hammerhead Supersequence, but a mechanism for generation of later stage gas-rich inclusions, plus late stage oil, in the Miocene is less clear.

The Cenomanian interval in Greenly-1 (4,808-4,812 mMD; Tiger Supersquence) trapped remarkably consistent hydrocarbon assemblages modelled by PIT as black oil. While this consistency is also reflected in the measured *PT* entrapment conditions (270-340 bar; 127-135°C), they are not concordant with the independently modelled *PT* curve. If the temperatures reflect the entrapment conditions, then this constrains oil charge from the Early Miocene (~23 Ma onwards) and at a depth equivalent to about 2 km less than modelled. Tertiary carbonate progrades over the Late Cretaceous deltas, and rapid burial peaking around 15 Ma, might explain this, with a terrestrial White Pointer source favoured from the MCI result. If, however, the pressures reflect the entrapment conditions, then this possibly constrains oil charge in Greenly-1 to the Campanian–early Eocene (~75-52 Ma) and at temperatures about 30°C higher than modelled. One explanation might be a transient period of hotter fluids that were in thermal disequilibrium with the rock. This earlier timing of entrapment, however, would require generation from a Bronze Whaler source, which is not favoured by the MCI.

The Turonian-Santonian interval in Duntroon-1 (2,505-10 mMD; Tiger Supersequence) and the Cenomanian-Santonian interval in Potoroo-1 (1,778-86 mMD; Tiger Supersquence) were migration pathways for a variety of hydrocarbon fluid compositions modelled by PIT as black oil, light oil and, in the case of Duntroon-1, gas (+N₂ and CO₂). In both these wells from the margins of the basin, hydrocarbon charge appears to be late. Because pressure evolution over much of the Cenozoic in Duntroon-1 was static, temperature constraints (81-95°C) suggest entrapment of oil from the mid

Miocene (~17 Ma) and, if Tertiary loading is considered, would constrain generation to the White Pointer, or even the Tiger, source sequences. CO₂ and N₂ rich hydrocarbon gases entrapped in the Holocene potentially have volcanic origins similar to those in the Otway Basin. In Potoroo-1, hydrocarbon entrapment occurred either from the Oligocene (~32 Ma), or from the Early Miocene (~25 Ma), to recent. Only the Blue Whale/lower White Pointer source sequence reached thermal maturities capable of generating this oil locally, but because of its location on the basin margin a variety of potential source/charge scenarios could be envisaged including earlier re-migrated oil.

Multivariate statistical analysis of Gnarlyknots-1A and Greenly-1 FI oils with naturally stranded asphaltites and waxy bitumens along the South Australian coast, postulated as having a local southern margin origin, reveals that neither are closely related to the asphaltites. The Greenly-1 FI oil is also not closely related to any waxy bitumen type, whereas the Gnarlyknots-1A FI oil can be correlated to some waxy bitumen types. While the majority of waxy bitumen types have distinctive biomarkers indicative of an Indonesian Archipelago origin and therefore transport into southern Australian waters by a complex system of surface ocean currents, there are other waxy bitumen types which lack these diagnostic biomarkers emerging from more detailed geochemical investigations as part of Project 5.2.

This study has, for the first time, proven the existence of hydrocarbons in the central deepwater Ceduna Sub-basin, the primary focus of the renewed exploration activities in the Bight Basin. In addition, through geochemical analysis of the composition of both liquids and gases there is now a clearer understanding of possible source rocks that generated these hydrocarbons, including the eastern Ceduna/Duntroon sub-basins. Detailed information of the timing of entrapment and oil type has permitted constraints on when hydrocarbon charge took place which, in turn, helps to validate petroleum systems models. The outcomes of this project have significantly enhanced prospectivity and reduced exploration risks within the Bight Basin.

Part I Introduction

INTRODUCTION

Overview

BP Developments Australia, CSIRO, the South Australian Research and Development Institute (SARDI), the University of Adelaide and Flinders University are working on a 4 year, \$20 million research program to improve the understanding of the environmental, economic and social value of the Great Australian Bight (GAB). The GAB Research Program is administered by a Management Committee with representation from BP, CSIRO, SARDI Adelaide University and Flinders University and is advised by an independent Science Panel (ISP) comprising internationally recognised experts in key discipline areas.

The GAB Research Program comprises 7 themes and 16 research projects. This report presents the findings of research conducted for Theme 5 (Petroleum Geology & Geochemistry) and Project 5.3 (Fluid Inclusions).

Background and Need

The previous 44 years of petroleum activity in the Bight Basin have seen only 13 exploration wells drilled, with no significant liquid hydrocarbons recovered. A petroleum system capable of producing commercial quantities of hydrocarbons has yet to be proven. Despite this, palaeo-hydrocarbon migration routes from fluid inclusions have been identified within some vintage exploration wells (Lisk et al., 2001), together with reports of coastal bitumen strandings along the southern coastline of Australia that date back to the mid-1800s (Padley, 1995; Edwards et al., 1998; Hall et al., 2014).

Early exploration efforts of the Bight Basin were focused on the shallower northern and eastern parts of the continental shelf. Subsequent technology changes allowed for drilling in deeper water toward the continental shelf and this resulted in the Gnarlyknots-1/1A well in 2003 that tested the petroleum potential of the Ceduna Sub-basin. Although the well failed to recover hydrocarbons, a fluid inclusion-based methane-depleted, wet-gas to gas-condensate response was detected over the intra-Santonian (Late Cretaceous) primary objective, consistent with a highly mature palaeo-charge (Tapley et al., 2005). This was supported by the frequent visual occurrence of yellow to blue-white fluorescent inclusions in quartz grains. Despite uncertainty expressed in regard to the liquids-generation capability of potential source intervals within the Ceduna Sub-basin, no further fluid inclusion work was undertaken.

Given the current level of renewed interest in the Bight Basin, there is an opportunity to understand, in greater detail the nature of hydrocarbon-bearing fluid inclusions in the Gnarlyknots-1A well and other wells previously studied (Borda-1, Duntroon-1, Echidna-1, Greenly-1, Jerboa-1, Platypus-1, Potoroo-1 and Vivonne-1). This will inform Project 5.2, which aims to address the origin of coastal bitumen strandings in the GAB.

Modern fluid inclusion techniques enable retrospective re-assessment of exploration wells to investigate palaeo-oil (and gas) charge and hydrocarbon sources. The detection and characterisation of hidden oil enables the risk in the source–generation–migration chain to be assessed independently of forward models and to identify which elements of the petroleum system were active. An important advantage of fluid inclusion data is that the inclusions represent sealed artifacts

of hydrocarbons that are impervious to subsequent changes. The inclusions are not altered by contamination introduced during drilling and are unaffected by time or conditions of storage.

Numerous fluid-inclusion techniques, some developed by CSIRO, are applicable to this study.

- Grains with Oil Inclusions (GOI™): to detect hidden hydrocarbons and characterise properties such as fluid type, gas content and relative timing of entrapment.
- Molecular Composition of oil Inclusions (MCI™): to geochemically fingerprint bulk liquid hydrocarbons extracted from fluid inclusions for potential source-rock characteristics.
- Carbon isotopic composition of bulk fluid inclusion gases for source characteristics.
- Pressure-temperature (PT) modelling: to constrain the timing of hydrocarbon charge and evolution in fluid composition.

Objectives

The perceived risk of hydrocarbon charge in the Bight Basin was a significant driver for Project 5.3 and in undertaking detailed fluid inclusion-based studies of oil/gas migration. The outputs of this project were ultimately intended to provide source-analogues of liquid hydrocarbons in addressing the origin of coastal bitumen strandings in the GAB (Project 5.2).

The petroleum system is a core concept of petroleum geology that consists of a mature source rock, migration pathway, reservoir rock, trap and seal. Appropriate relative timing of formation of these elements and the processes of generation, migration and accumulation are necessary for hydrocarbons to accumulate and be preserved.

In this context, the main objectives of Project 5.3 were to constrain several key elements of the petroleum system(s) in the GAB. Unlike conventional basin modelling approaches, an important factor for this project was to acquire baseline data directly from the rocks.

1. MIGRATION: detect hidden hydrocarbon migration pathways in the GAB.
2. SOURCE: obtain source-specific molecular geochemical data from fluid inclusions (oil and gas) to identify probable source rock types.
3. TIMING: constrain the timing of hydrocarbon migration events from pressure-temperature reconstructions.

Each of these key petroleum system elements are discussed forthwith as separate sections after the Introduction.

REGIONAL GEOLOGY OF THE BIGHT BASIN

The Bight Basin formed during the break-up of eastern Gondwana in the Late Jurassic–Early Cretaceous. It extends for ~2,000 km along the Australian southern margin and comprises a series of extensional depocentres in modern day water depths between 200 m and >4,000 m. No significant hydrocarbons have been found in the basin, which remains an exploration frontier.

Basin Outline

The Bight Basin is a large, mainly offshore basin situated along the western and central parts of the continental margin of southern Australia (Figure 1). The basin extends from the Leeuwin Fracture Zone in the west, to just south of Kangaroo Island in the east, where it adjoins the Otway Basin (The basin contains a number of sub-basins that formed by the rifting and thinning of the Australian Plate and includes; the Ceduna, Duntroon, Eyre, Bremer and Recherche sub-basins (Figure 1). The current sub-divisions of the Bight Basin are based on those defined by Bradshaw et al. (2003) and Totterdell and Bradshaw (2004) and have evolved from many previous basin definitions published by various researchers. Within the revised definition of the Bight Basin, the former Duntroon Basin has been remapped as a smaller, genetically related rift system along the margin of the main rift basin, and has been reclassified as a sub-basin. The Bight Basin is overlain unconformably by dominantly cool-water carbonates of the Cenozoic Eucla Basin (Feary and James, 1998; Messent, 1996).

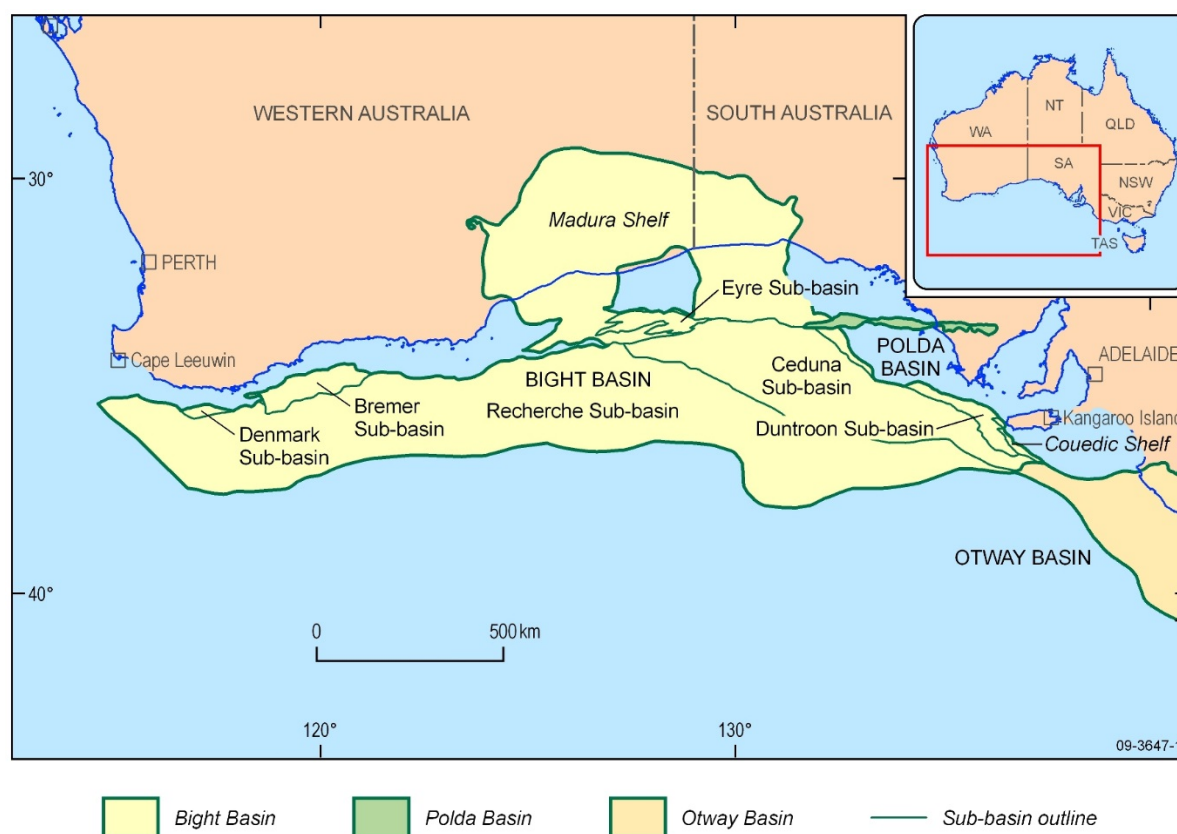


Figure 1: Location of the Bight Basin with component sub-basins.
© Commonwealth of Australia (Geoscience Australia) 2016

Basin Evolution and Tectonostratigraphic Framework

The Bight Basin is a large Mesozoic to Cenozoic depocentre, which formed during the breakup of Gondwana (Fraser and Tilbury, 1979; Bein and Taylor, 1981; Willcox and Stagg, 1990; Hill, 1995; Totterdell et al., 2000; Norvick and Smith, 2011; Teasdale et al., 2003). The basin evolved through repeated episodes of extension and thermal subsidence leading up to, and following, the commencement of seafloor spreading between Australia and Antarctica (Totterdell and Bradshaw, 2004). The sequence stratigraphic framework of the Bight Basin is based on work conducted by Geoscience Australia (Totterdell et al., 2000) and supersequences are named after marine fauna, many of which are characteristic of the Southern Ocean (Figure 2). This largely replaces previous formation-based nomenclature which emphasised lithostratigraphic correlations (e.g. Smith and Donaldson, 1994; Messent et al., 1996) rather than chronostratigraphic relationships. The tectonostratigraphic development of the basin can be described in terms of four basin phases (following synopsis taken from various work by Geoscience Australia).

Mid-Jurassic–Lower Cretaceous Extension (BP1)

The Bight Basin was initiated during a period of Middle–Late Jurassic to Early Cretaceous upper crustal Extension. Extensive *en-echelon* half grabens formed the Bremer, Eyre, inner Recherche, Ceduna and Duntroon sub-basins and were filled with largely fluvial and lacustrine clastic sediments of the Sea Lion and Minke supersequences.

Post-Rift Subsidence (BP2)

The Early Cretaceous was characterised by post-rift thermal subsidence in the Bight Basin. By the mid-Cretaceous, an open ocean lay to the west and a seaway extended along the margin to the eastern Bight Basin. Deposition during the initial extensional phase and the subsequent period of thermal subsidence was largely dominated by non-marine sediments and the previous syn-rift successions are overlain by widespread fluvio-lacustrine to marine sediments of the Southern Right and Bronze Whaler supersequences.

Mid-Cretaceous Accelerated Subsidence (BP3)

An abrupt increase in subsidence rate in the mid-Albian (Totterdell et al., 2000; Totterdell and Bradshaw, 2004) signaled the onset of the third phase of basin development. This period of accelerated subsidence, which continued until the commencement of sea-floor spreading between Australia and Antarctica in the late Santonian, coincided with a period of rising global sea level. As a result, accommodation space rapidly increased and the first major marine flooding event in the basin occurred and marine silts and shales of the Albian–Cenomanian Blue Whale Supersequence were deposited widely. Progradation of deltaic sediments into a narrow seaway commenced in the Cenomanian, depositing the White Pointer Supersequence. High depositional rates resulted in a short-lived period of shale mobilization and growth faulting throughout the northern half of the Ceduna Sub-basin (Figure 1, Figure 3). The Cenomanian deltaic facies include a broad band of coaly sediments in the inner part of the Ceduna Sub-basin. The White Pointer Supersequence is overlain by the marginal marine, deltaic and open marine sediments of the Turonian–Santonian Tiger Supersequence. The Tiger Supersequence thickens markedly to the south reflecting a shift in the locus of deltaic deposition during this time (MacDonald et al., 2013).

Australian–Antarctic sea-floor spreading and post-breakup subsidence (BP4)

The commencement of ultra-slow to very slow sea-floor spreading in the latest Santonian was followed by a period of thermal subsidence and the establishment of the southern Australian passive margin. This phase of basin development is represented by the latest Santonian–Maastrichtian Hammerhead Supersequence, a sand-rich deltaic system characterised by strongly prograding stratal geometries. Because of the slow rate of sea-floor spreading, the seaway into which the deltas prograded would have been relatively narrow. A dramatic reduction in sediment supply at the end of the Cretaceous saw the cessation of deltaic deposition. Regional uplift resulted in the erosion of the Hammerhead Supersequence, much of the underlying Tiger Supersequence from the Eyre Sub-basin and the progressive erosion of the Cretaceous section across the Madura Shelf.

From the late Paleocene to the present, the largely cool-water carbonates of the Eucla Basin accumulated on a sediment-starved passive margin. In the middle Eocene (around 45 Ma) there was a dramatic increase in the rate of seafloor spreading (Tikku and Cande, 1999), which resulted in widespread subsidence of the margin. A short phase of magmatism coincided with the onset of rapid spreading. This magmatic phase was characterised by both extrusive volcanism (volcanoes, flows, volcanic build-ups) and the intrusion of sills, dykes and deeper igneous bodies in the central Ceduna Sub-basin (Schofield and Totterdell, 2008).

Exploration History

Petroleum exploration in the eastern Bight Basin (Eyre, Ceduna and Duntroon sub-basins) has occurred in three major cycles – the late 1960s to early 1970s, the early 1990s, and 2000–present (see O’Neil, 2003). After nearly fifty years of exploration in the offshore Bight Basin, only fourteen petroleum exploration wells have been drilled; Apollo-1 (1975), Borda-1 (1993), Columbia-1 (1982), Duntroon-1 (1986), Echidna-1 (1972), Gemini-1/1A (1975), Gnarlyknots-1/1A (2003), Greenly-1 (1993), Jerboa-1 (1980), Mercury-1 (1981), Platypus-1 (1972), Potoroo-1 (1975) and Vivinne-1 (1993). With the exception of Gnarlyknots-1/1A, all wells have been drilled in relatively shallow water near the basin margin. No significant hydrocarbons have been discovered and the deep-water parts of the basin remain largely untested and a frontier area. In 2009, six areas in the central Ceduna Sub-basin were made available for bidding and, in January 2011, BP Developments Australia Pty Ltd was awarded four permits (EPP 37–40).

During the last phase of exploration in the 2000s, exploration permits were awarded to a joint venture operated by Woodside Energy in the Ceduna Sub-basin. The joint venture acquired approximately 15,400 line km of 2D seismic data and in 2003, drilled Gnarlyknots-1/1A (Tapley et al., 2005). The well was the first and only attempt to test the deep-water Ceduna Sub-basin and failed to reach its objective due to adverse weather conditions.

In 2007, Geoscience Australia embarked on a regional geological and sampling survey of the Bight Basin as part of the Australian Government’s Offshore Energy Security program. The survey targeted and sampled potential source rocks of late Cenomanian to early Turonian age on the northwest margin of the Ceduna Sub-basin. Analytical results indicated that the organic rich rocks recovered by the survey are capable of generating liquid hydrocarbons (Totterdell et al., 2008; Totterdell and Mitchell, 2009).

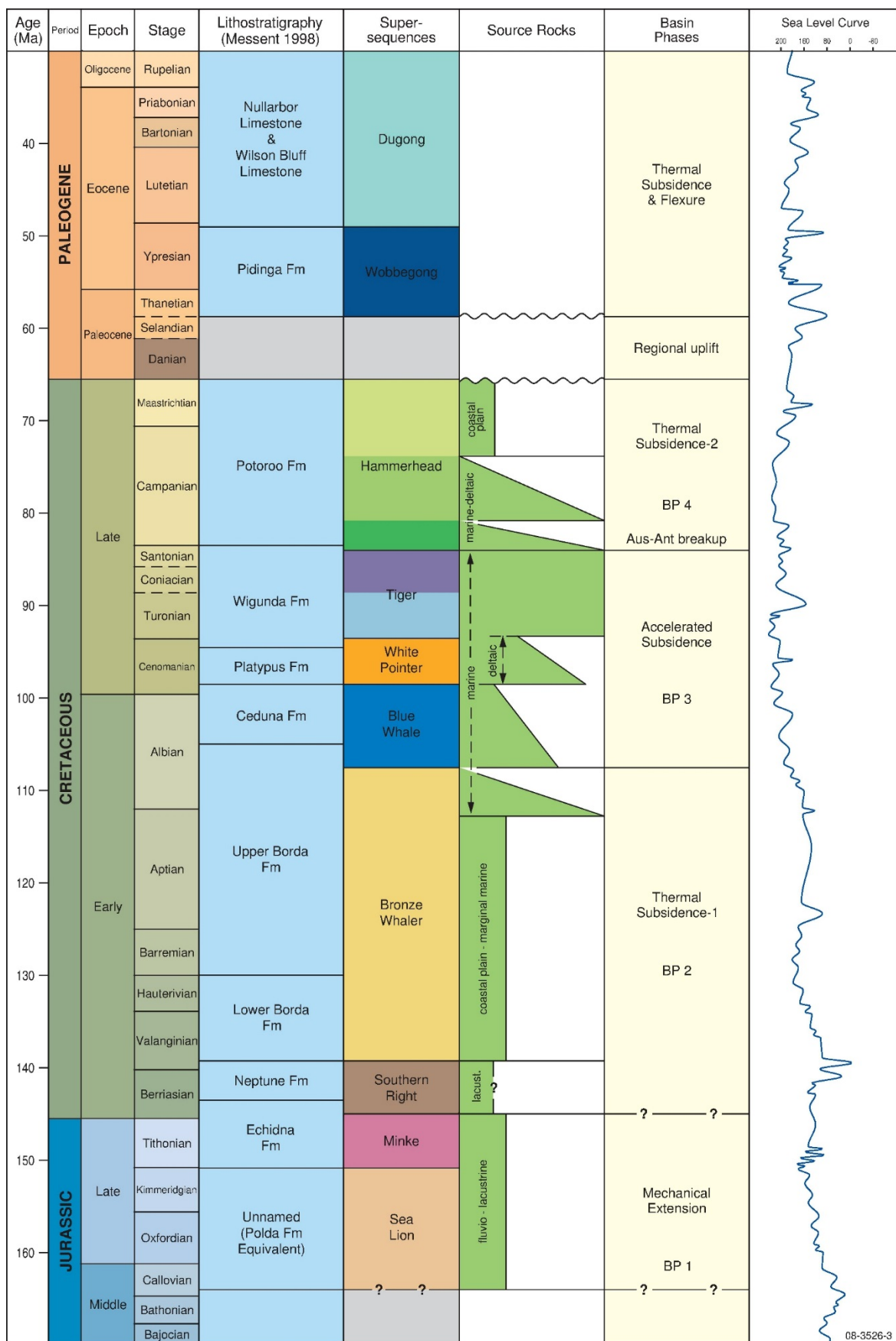


Figure 2: Bight Basin stratigraphic correlation chart showing basin phases and predicted source rock intervals.
© Commonwealth of Australia (Geoscience Australia) 2016.

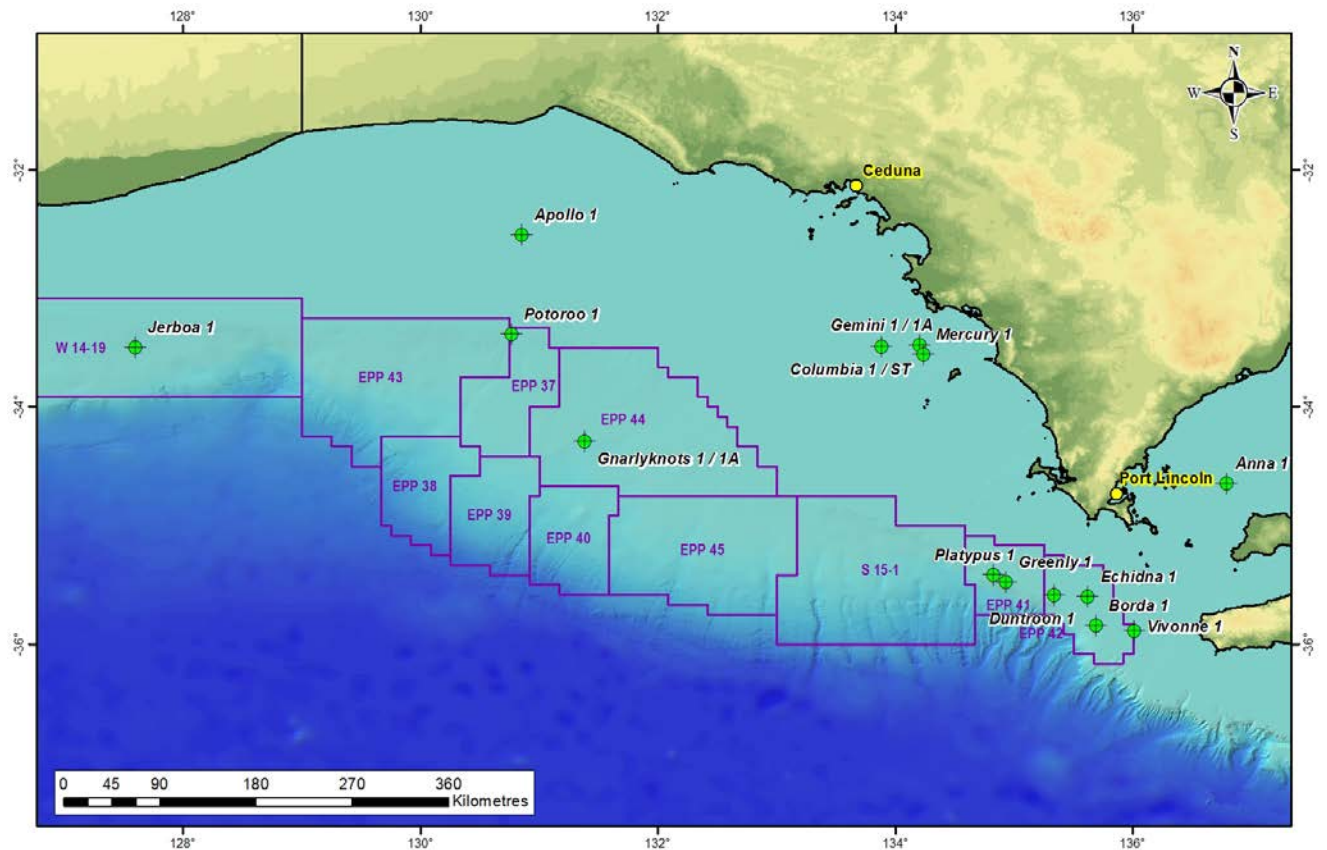


Figure 3: Bight Basin and location of petroleum wells (with exploration permits current as of 2016).

Petroleum Geology

The eastern part of the Bight Basin (Ceduna, Eyre and Duntroon sub-basins) is potentially one of the most prospective deepwater frontier basins in offshore Australia. The thick sedimentary succession, in excess of 15 km thick in places, and its evolution from local half grabens depocentres during the Jurassic, to an extensive sag basin in the Early Cretaceous and passive margin during the Late Cretaceous to Holocene, implies that there is significant potential for the presence of multiple petroleum systems.

The most prospective petroleum systems are believed to be associated with thick mid to Late Cretaceous deltaic and marine sediments (Blue Whale, White Pointer, Tiger and Hammerhead supersequences), which provide reservoirs, seals and potential oil-prone source rocks at several stratigraphic levels, together with a wide range of structural and stratigraphic plays (Blevin et al., 2000; Totterdell et al., 2000; Struckmeyer et al., 2001; Totterdell et al., 2008) – Figure 4.

Despite mounting evidence for oil-prone marine source rocks in the Ceduna Sub-basin (Totterdell et al., 2008), and speculation they might be present in distal facies of deep water areas in the Ceduna Sub-basin, hydrocarbon generation is a key uncertainty for explorers.

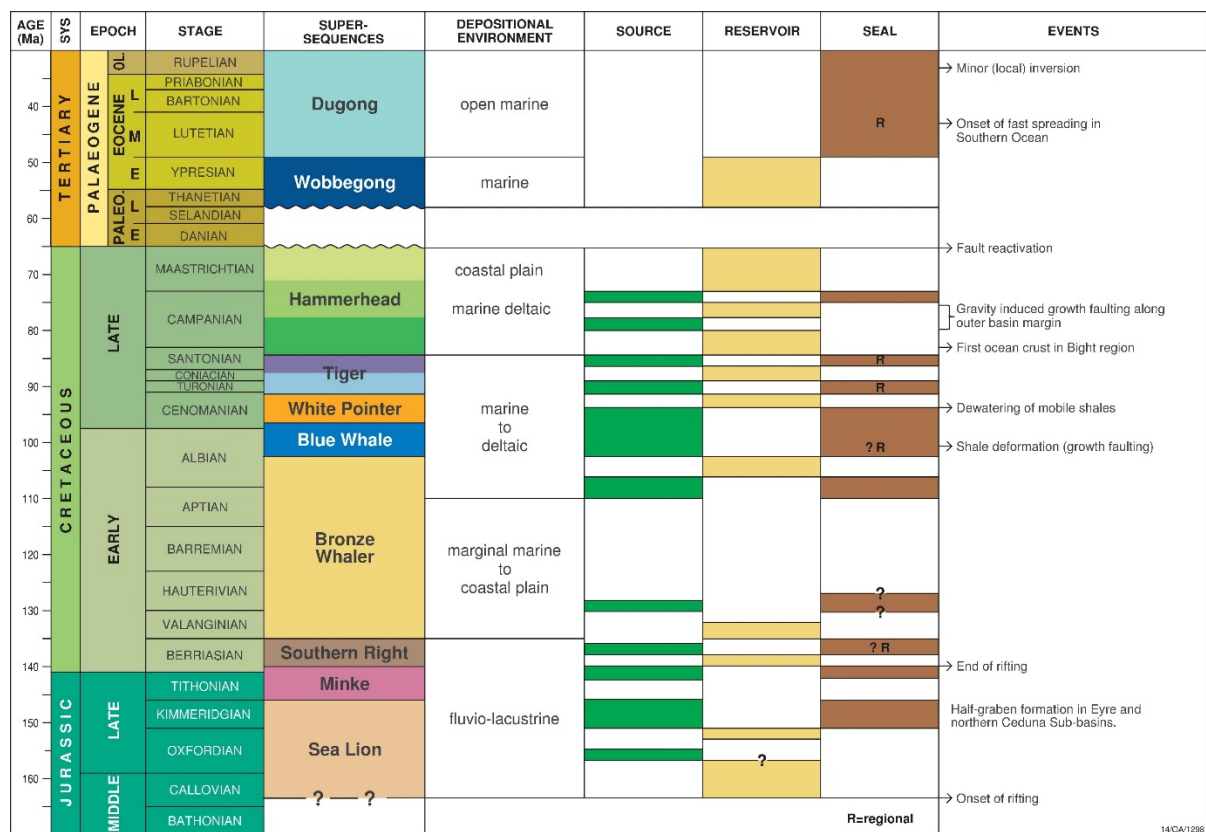


Figure 4: Summary chart of the petroleum systems in the Bight Basin.
© Commonwealth of Australia (Geoscience Australia) 2016.

Hydrocarbon Indications and Shows

None of the wells drilled in the Bight Basin have encountered either potential or proven hydrocarbon zones (oil or gas). In fact, hydrocarbon indications and shows are infrequent (Table 1). The only significant oil shows reported are from Greenly-1, which recovered oil, as a surface scum from a water/oil mixture, and gas (repeat formation test – 4,209.2 m). At the time, these represented the first major indications of hydrocarbons in the basin, indicating the presence of a valid source rock, and significantly upgraded the prospectivity of the Ceduna Sub-basin.

Apart from Greenly-1, none of the other wells in the Ceduna and Duntroon sub-basins have convincing evidence for hydrocarbon shows. This is particularly relevant for the current phase of exploration in the Bight Basin that centers on exploration permits in the deeper parts of the basin. Only one well, Gnarlyknots-1A, tests this area. While oil, potentially from synthetic based mud fluorescence, and gas indications were minor, this provides a unique opportunity to test the hydrocarbon generation and migration potential of the area by using fluid inclusions as a tool to access potential hidden oil shows.

Table 1: Hydrocarbon indications and shows.

Well	Year	TD (mRT)	HC shows	Comment	Formation	Interval (mRT)
Borda-1	1993	2,800	None reported	–	–	–
Duntroon-1	1986	3,515.6	L1 - oil indication	Fluorescence	Upper Borda	3,061; 3,200
Echidna-1	1972	3,832	L1 - oil indication	Black soft bituminous material, fluorescence	Lower Borda	2,648; 2,652
Gnarlyknots-1/1A	2003	4,736	L1 - oil indication* G1 – gas indication L1 - oil indication*	Fluorescence Trace C ₄ Fluorescence	Wigunda Wigunda Wigunda	4,379-4,712.5 (SWC) 4,505-TD; max 4,710 4,685-4,725
Greenly-1	1993	,4860	L1, L2 – strong oil indications	Fluorescence	Wigunda	3,430-4,542 (SWC, Cuttings)
			L1 - oil indication	Fluorescence	Platypus	4,770-4818
			L3, G3 – oil/gas show	Recovered oil as surface scum and water/oil mixture; gas recovered	Wigunda	4,209.2 (RFT)
Jerboa-1	1980	2,538	None reported	–	–	–
Platypus-1	1972	3,893	None reported	–	–	–
Potoroo-1	1975	2,924	G1 – gas indication	18,000ppm C ₁	Platypus	2,128-2,132
Vivonne-1	1993	3,000	None reported	–	–	–

Data summarised from Messent (1998). RFT = Repeat Formation test. SWC = side-wall core. * considered likely to be synthetic based mud fluorescence. L1 = oil indication (fluorescence or cut); L2 = strong oil indication (fluorescence or cut & other oil indication e.g. log anomaly); L3 = oil show (oil recovered from core, test, mud); L4 – potential oil zone (oil show with convincing log anomaly); L5 = proven oil zone (oil flow on test or RFT & log anomaly proving accumulation). G1 = gas indication (anomalously high gas readings); G2 = strong gas indication (anomalously high gas readings and other indications e.g. core, logs or shakers); L3 = gas low on tests; L4 = potential gas zone (gas show with convincing log anomaly or other indication); L5 = proven gas zone (sustained gas flow on test or RFT and log anomaly or pressure data proving an accumulation).

Part II **GOI & hydrocarbon migration**

Lead author

Richard Kempton

INTRODUCTION

Overview

To reveal hidden hydrocarbon shows trapped as fluid inclusions within the rocks of the Bight Basin, CSIRO's *Grains with Oil Inclusion (GOI)* method was attempted from 8 historic exploration wells, including the previously untested Gnarlyknots-1A well. The aim was to identify palaeo-migration routes through these rocks and, if possible, any evidence for accumulation. The results of this analysis determined the intervals suitable for PVTx modelling and the Molecular Composition of oil Inclusions (MCI) geochemical technique.

Previous Fluid Inclusion Studies

Grains with Oil Inclusion (GOI)

An investigation of the oil migration risks in the GAB was undertaken by Lisk et al. (2001), who detected fluid inclusion 'oil shows' by the *Grains with Oil Inclusion (GOI)* method (Table 2). Oil inclusions were identified in 6 wells from the Ceduna and, what was then classified as, the Duntroon Sub-basin; Borda-1, Duntroon-1, Greenly-1, Platypus-1, Potoroo-1 and Vivonne-1.

In the Duntroon Sub-basin, oil expulsion and migration was indicated from possible Middle to Lower Cretaceous source rocks by the presence of oil inclusions within intercalated sandstones. Evidence for oil migration into shallower Upper Cretaceous and Tertiary sandstones was also recorded. Oil inclusions from the Lower Cretaceous in Potoroo-1 were interpreted as first evidence of an operating migration system in the Ceduna Sub-basin, whilst those observed in Jerboa-1 corroborated minor oil indications in the Upper Jurassic (Bein and Taylor, 1981). At the time, the Jerboa-1 result was significant as they reflected the presence of a palaeo-oil column (here revised in this report) within Upper Jurassic sandstones.

Fluid Inclusion Stratigraphy (FIS)

Fluid Inclusion Stratigraphy (FIS) has previously been performed on cuttings samples from Duntroon-1 and Platypus-1 and, more recently, Gnarlyknots-1A. The technique involves automated crushing and on-line GC-MS analysis of volatile species trapped within fluid inclusions (Hadley et al., 1997).

In Gnarlyknots-1A, a methane-depleted wet gas to gas-condensate response was observed in the primary well objective, consistent with a highly mature palaeo-charge (Tapley et al., 2005). This was supported by the frequent occurrence of yellow to blue-white fluorescent inclusions in quartz grains, in a broad stratigraphic interval. Strong proximal pay indications were indicated within local shale seals below 4,600 mMD and interpreted as proximity to a potential oil column below the TD of the well.

In Duntroon-1 and Platypus-1, FIS data were acquired to provide continuous screening of strongly intercalated sand-shale sequences within the White Pointer (Platypus Fm.) and Tiger (Wigunda Fm.) supersequences, where potential fluid migration pathways were too numerous to allow comprehensive analysis by petrographic methods (Lisk et al., 2001). The results revealed a background of wet-gas range species through the tested sections, with a distinct increase in higher molecular weight species (paraffins and alkylated naphthenes) in the lower parts of the sections, particularly Duntroon-1. No proximal pay indications were identified.

Table 2: Previous GOI data reported by Lisk et al (2001).

Well	CSIRO No	Depth (MMD)	GOI (%)	Total grains counted	GWOI	blue	white	yellow	orange	fcdm	ob	fco
Borda-1	125315	2,150-53	0.0	3149	0	0	0	0	0	0	0	0
Borda-1	125316	2,162-65	0.1	2161	2	0	0	0	2	1	1	0
Borda-1	125317	2,324-27	<0.1	3386	1	0	0	0	1	1	0	0
Borda-1	125318	2,369-72	0.1	5046	7	5	2	0	0	7	0	0
Borda-1	125319	2,411-14	0.2	6101	11	10	0	1	0	11	0	0
Borda-1	125320	2,438-41	0.2	1663	3	2	0	0	1	3	0	0
Borda-1	125321	2,480-83	0.0	428	0	0	0	0	0	0	0	0
Borda-1	125322	2,546-49	0.2	3732	8	7	0	1	0	8	0	0
Duntroon-1	125323	1,630-35	<0.1	5018	5	3	0	3	0	5	0	0
Duntroon-1	125324	1,845-50	0.4	3864	17	9	1	8	1	17	0	0
Duntroon-1	125325	1,890-95	0.2	4899	11	5	2	6	3	11	0	0
Duntroon-1	125326	2,510-15	0.4	5220	20	14	4	7	0	20	0	0
Duntroon-1	125327	2,605-10	0.1	6933	9	7	0	4	0	9	0	0
Duntroon-1	125328	2,950-55	<0.1	13315	2	0	2	1	0	2	0	0
Duntroon-1	125391	3,165-70	0.0	7344	0	0	0	0	0	0	0	0
Duntroon-1	125392	3,200-05	<0.1	13156	5	2	1	2	0	5	0	0
Duntroon-1	125393	3,245-50	0.3	2450	8	6	1	1	0	8	0	0
Duntroon-1	125394	3,275-80	<0.1	18845	2	1	0	1	0	2	0	0
Duntroon-1	125395	3,460-65	0.1	2392	3	2	1	0	0	3	0	0
Greenly-1	125329	1,885-90	<0.1	9906	1	0	0	0	1	1	0	0
Greenly-1	125330	2,060-65	<0.1	4112	1	1	0	0	0	1	0	0
Greenly-1	125331	2,215-20	<0.1	8528	5	5	0	0	0	5	0	0
Greenly-1	125332	2,460-65	0.0	794	0	0	0	0	0	0	0	0
Greenly-1	125333	2,555-60	0.0	690	0	0	0	0	0	0	0	0
Greenly-1	125334	2,965-70	<0.1	1283	1	1	0	0	0	1	0	0
Greenly-1	125335	2,975-80	0.1	2818	3	1	1	0	1	3	0	0
Greenly-1	125336	2,995-00	0.2	2624	6	5	0	1	0	6	0	0
Greenly-1	125337	3,015-20	0.2	1480	3	0	3	0	0	3	0	0
Greenly-1	125338	3,205-10	0.5	813	4	4	0	0	0	4	0	0
Greenly-1	125339	3,445-50	0.2	1053	2	2	0	0	0	2	0	0
Greenly-1	125340	4,107-10	0.6	4039	24	16	8	0	0	23	1	0
Greenly-1	125341	4,161-64*	0.3	3772	13	11	1	1	0	13	0	0
Greenly-1	125342	4,185-88	0.1	4950	5	5	0	0	0	5	0	0
Greenly-1	125343	4,455-58	0.1	5227	8	4	4	0	0	8	0	0
Greenly-1	125344	4,533-36	0.6	3464	19	14	4	1	0	19	0	0
Greenly-1	125345	4,812-15*	0.7	2520	18	8	10	0	0	18	0	0
Jerboa-1	125360	2,495-00	<0.1	2250	1	0	0	1	0	1	0	0
Jerboa-1	125361	2,500-05	<0.1	2726	0	0	0	0	0	0	0	0
Jerboa-1	125362	2,505-10	0.2	1635	4	1	3	0	0	4	0	0
Jerboa-1 [†]	124056	2,140-50	<0.1	13469	9	8	1	0	0	9	0	0
Jerboa-1 [†]	124057	2,240-50	<0.1	4191	2	0	0	0	2	2	0	0

Well	CSIRO No	Depth (MMD)	GOI (%)	Total grains counted	GWOI	blue	white	yellow	orange	fcdm	ob	fco
Jerboa-1 †	124054	2,292-23	0.0	8260	0	0	0	0	0	0	0	0
Jerboa-1 †	124055	2,295-77	<0.1	49875	5	0	0	0	5	5	0	0
Jerboa-1 †	124058	2,385-90	<0.1	4501	1	0	0	0	1	1	0	0
Jerboa-1 †	124059	2,470-80	6.6	348	23	0	22	0	1	23	0	0
Jerboa-1 †	125194	2,490-95	10.4	106	11	6	4	1	0	11	0	0
Platypus-1	125346	1,759-62	0.0	5300	0	0	0	0	0	0	0	0
Platypus-1	125347	1,896-99	0.3	2960	9	3	1	7	0	9	0	0
Platypus-1	125348	1,957-60	0.2	2006	4	2	0	2	0	4	0	0
Platypus-1	125369	3,212-15	0.1	9631	8	6	1	3	0	8	0	0
Platypus-1	125370	3,502-05	0.1	4324	4	2	1	1	0	3	1	0
Platypus-1	125371	3,730-33*	<0.1	11405	10	9	0	1	0	10	0	0
Platypus-1	125372	3,859-62*	0.2	16091	28	28	8	7	2	28	0	0
Potoroo-1	125383	900-10	0.0	70	0	0	0	0	0	0	0	0
Potoroo-1	125385	2,562-66	0.0	325	0	0	0	0	0	0	0	0
Potoroo-1	125386	2,566-70	0.0	1442	0	0	0	0	0	0	0	0
Potoroo-1	125387	2,702-06	0.0	4267	0	0	0	0	0	0	0	0
Potoroo-1	125388	2,706-10	0.0	3990	0	0	0	0	0	0	0	0
Potoroo-1	125389	2,734-38	0.5	1257	6	2	2	0	2	6	0	0
Potoroo-1	125390	2,738-42	0.1	885	1	1	0	0	0	1	0	0
Vivonne-1	125373	1,059-62	0.0	1277	0	0	0	0	0	0	0	0
Vivonne-1	125374	1,065-68	0.0	8216	0	0	0	0	0	0	0	0
Vivonne-1	125375	1,077-80	<0.1	6698	1	0	1	0	1	1	0	0
Vivonne-1	125376	1,101-04	<0.1	4211	3	1	1		2	3	0	0
Vivonne-1	125377	1,362-65	0.0	1777	0	0	0	0	0	0	0	0
Vivonne-1	125378	1,341-44	0.1	2989	4	2	2	0	0	4	0	0
Vivonne-1	125379	2,010-13	0.0	1998	0	0	0	0	0	0	0	0
Vivonne-1	125380	2,013-16	0.0	430	0	0	0	0	0	0	0	0
Vivonne-1	125381	2,361-64	<0.1	1663	1	0	0	1	0	0	0	1
Vivonne-1	125382	2,634-37	0.0	3671	0	0	0	0	0	0	0	0

gwoi = grains with oil inclusions; fcdm = fracture cutting detrital mineral; ob = overgrowth boundary; fco = fracture cutting overgrowth *samples contain oil inclusions in carbonate. † Data re-reported from Liu and Eadington (1998).

Samples for GOI

Selection Criteria

Fluid inclusion GOI sample selection was limited to wells in the Bight Basin and focused principally on the Tiger and Hammerhead supersequences in Gnarlyknots-1A. Samples were also selected from Borda-1, Duntroon-1, Greenly-1, Jerboa-1, Platypus-1, Potoroo-1 and Vivonne-1 to test: (1) the continuity in height of anomalous GOI sample zones identified in a previous study by Lisk et al. (2001), (2) untested sandstone intervals in these wells, and to (3) re-visit the Jerboa-1 palaeo-oil zone result of Lisk et al. (2001).

Echidna-1, from the Duntroon Sub-basin, was not sampled due to the low net-to-gross of the interval and previous sampling by Lisk et al (2001). No wells from the Polda Basin were sampled (i.e. Apollo-1, Columbia-1, Gemini-1/1A or Mercury-1). The Polda Basin is primarily a much older Neoproterozoic basin that was reactivated during southern margin rifting, and is thus considered a separate sedimentary basin that underlies the continental platform succession (Totterdell and Bradshaw, 2004).

Approval to view and sample petroleum wells for GOI from the Great Australian Bight was granted by the National Offshore Petroleum Data & Core Repository (NOPDCR) – Approval No's: N00074, extension to N00074 and N00335.

A total of fifty six cuttings samples from seven wells were collected from the Western Australian Department of Mines and Petroleum's Carlisle core library in Perth. Of these:

- 40 samples for GOI analysis, with 4 of these doubling as PVTx samples.
- 2 additional PVTx samples as backup.
- 11 samples for online MCI.
- 3 samples for online MCI and gas isotopes (2 unused).

The details and rationale for each selected sample is listed in Table 3.

Sample Preparation

To reduce the potential for unwanted fluorescence from the surface of the grains, all cuttings samples were cleaned by; (i) digestion in dilute hydrogen peroxide for 48 hours, (ii) ultrasonicated to remove fine clay particles from mineral surfaces, (iii) sieved to isolate the sand-sized particle fraction (<63 micron fraction typically not used), and (iv) mineral separated to remove magnetic fractions such as shale.

Only one sample, from 2,853-56 m in Vivonne-1, did not yield enough detrital grains for preparation of a thin section. The 1,778-82 m/1,782-86 m, 2,398-2,402 m/402-06 m samples in Potoroo-1 and 2,470-75 m/2,475-80 m samples in Jerboa-1 were aggregated into single samples to achieve a minimum recovery of grains to prepare a thin section.

A total of 36 polished fluid inclusion thin sections were prepared to a nominal thickness of 80 microns. Irgalite blue pigment was added to suppress fluorescence from the epoxy. The thin section making process itself has little effect on the preservation of fluid inclusions, particularly in quartz. There have been reported instances of fluorescing materials being introduced into softer minerals like barite during thin sectioning (Dutkiewicz and Ridley, 2003) but, because the GOI process is a visual technique, there are tell-tale features that allow these to be distinguished.

Table 3: GAB — Sample selection for GOI, PVTx and MCI and rationale.

Well	CSIRO No	Depth (MD)	Supersequence (Totterdell et al 2000)	Period (WCR)	Stage (WCR)	Rationale for sampling	Analysis
Borda-1	134500	2,678-81 m	Hammerhead	L. Cretaceous	Maastrichtian	Untested sand below shale (Potoroo Fm – WCR)	GOI
Borda-1	134501	2,774-77 m	Hammerhead	L. Cretaceous	Maastrichtian	Untested sand at base of well (Potoroo Fm – WCR)	GOI
Duntroon-1	134502	1,855-60 m	Hammerhead	L. Cretaceous	Maastrichtian	Previous GOI 0.4% @ 1845-50 m – migration zone	GOI
Duntroon-1	134503	2,150-55 m	Hammerhead	L. Cretaceous	Santonian	Untested sand below shale	GOI
Duntroon-1	134504	2,505-10 m	Tiger	L. Cretaceous	Turonian	Previous GOI 0.4% @ 2510-15 m – migration zone	GOI, PVTx
Duntroon-1	134505	3,025-30 m	Blue Whale	E. Cretaceous	Aptian –Albian	Untested sand below shale	GOI
Duntroon-1	134506	3,235-40 m	Bronze Whaler	E. Cretaceous	Aptian –Albian	Previous GOI 0.3% @ 3245-50 m – migration zone	GOI
Duntroon-1	134507	3,345-50 m	Bronze Whaler	E. Cretaceous	Aptian –Albian	Untested sand below shale	GOI
Greenly-1	134508	3,275-80 m	Hammerhead	L. Cretaceous	Santonian	Untested sand below shale	GOI
Greenly-1	134509	3,753-56 m	Tiger	L. Cretaceous	Cenom-Sant.	Untested sand below shale	GOI
Greenly-1	134510	4,110-13 m	White Pointer	L. Cretaceous	Cenom-Sant.	Previous GOI 0.6% @ 4107-10 m – migration zone	GOI
Greenly-1	134511	4,377-80 m	White Pointer	L. Cretaceous	Cenom-Sant.	Untested sand below shale	GOI
Greenly-1	134512	4,530-33 m	White Pointer	L. Cretaceous	Cenom-Sant.	Previous GOI 0.6% @ 4533-36 m – migration zone	GOI
Greenly-1	134607	4,806-09 m	White Pointer	L. Cretaceous	Cenomanian	Additional sample for MCI	Offline MCI
Greenly-1	134513	4,809-12 m	White Pointer	L. Cretaceous	Cenomanian	Previous GOI 0.7% @ 4812-15 m – migration zone	GOI, PVTx
“	“	4,809-12 m	White Pointer	L. Cretaceous	Cenomanian	Additional sample for MCI	Offline MCI
Greenly-1	134608	4,812-15 m	White Pointer	L. Cretaceous	Cenomanian	Additional sample for MCI	Offline MCI
Greenly-1	134609	4,815-18 m	White Pointer	L. Cretaceous	Cenomanian	Additional sample for MCI	Offline MCI
Gnarlyknots-1A	134514	2,170-80 m	Hammerhead	L. Cretaceous	Maastrichtian	Untested sand below shale	GOI

Well	CSIRO No	Depth (MD)	Supersequence (Totterdell et al 2000)	Period (WCR)	Stage (WCR)	Rationale for sampling	Analysis
Gnarlyknots-1A	134515	2,535-40 m	Hammerhead	L. Cretaceous	Maastrichtian	Untested sand below shale	GOI
Gnarlyknots-1A	134516	2,865-70 m	Hammerhead	L. Cretaceous	Maast–Camp.	Untested sand below shale	GOI
Gnarlyknots-1A	134517	3,175-80 m	Hammerhead	L. Cretaceous	Campanian	Untested sand below shale	GOI
Gnarlyknots-1A	134713	3,750-55 m	Tiger	L. Cretaceous	Coniac-Sant.	Backup sample for PVTx	Unused
Gnarlyknots-1A	134518	3,760-65 m	Tiger	L. Cretaceous	Coniac-Sant.	Secondary well objective: FIS CH ₄ depleted WG-GC	GOI
Gnarlyknots-1A	134714	3,760-65 m	Tiger	L. Cretaceous	Coniac-Sant.	Backup sample for PVTx	Unused
Gnarlyknots-1A	134519	3,770-75 m	Tiger	L. Cretaceous	Coniac-Sant.	Secondary well objective: FIS CH ₄ depleted WG-GC	GOI
Gnarlyknots-1A	134520	3,930-40 m	Tiger	L. Cretaceous	Coniac-Sant.	Untested sand below shale. FIS CH ₄ depleted WG-GC	GOI
Gnarlyknots-1A	134521	4,135-40 m	Tiger	L. Cretaceous	Coniac-Sant.	Untested sand below shale	GOI
Gnarlyknots-1A	134522	4,390-95 m	Tiger	L. Cretaceous	Coniacian	Primary well objective: FIS WG-GC PTPL	GOI
“	“	4,390-95 m	Tiger	L. Cretaceous	Coniacian	Additional sample for MCI	Offline MCI
Gnarlyknots-1A	134715	4,390-95 m	Tiger	L. Cretaceous	Coniacian	Backup sample for gas isotopes	Unused
Gnarlyknots-1A	134603	4,395-00 m	Tiger	L. Cretaceous	Coniacian	Additional sample for MCI	Offline MCI
Gnarlyknots-1A	134523	4,400-05 m	Tiger	L. Cretaceous	Coniacian	Primary well objective: FIS WG-GC PTPL	GOI
“	“	4,400-05 m	Tiger	L. Cretaceous	Coniacian	Additional sample for MCI	Offline MCI
Gnarlyknots-1A	134716	4,400-05 m	Tiger	L. Cretaceous	Coniacian	Backup sample for gas isotopes	Unused
Gnarlyknots-1A	134604	4,405-10 m	Tiger	L. Cretaceous	Coniacian	Additional sample for MCI	Offline MCI
Gnarlyknots-1A	134524	4,410-15 m	Tiger	L. Cretaceous	Coniacian	Primary well objective: FIS WG-GC PTPL	GOI, PVTx
“	“	4,410-15 m	Tiger	L. Cretaceous	Coniacian	Additional sample for MCI	Offline MCI
Gnarlyknots-1A	134717	4,410-15 m	Tiger	L. Cretaceous	Coniacian	Sample for gas isotopes	GI, online MCI

Well	CSIRO No	Depth (MD)	Supersequence (Totterdell et al 2000)	Period (WCR)	Stage (WCR)	Rationale for sampling	Analysis
Gnarlyknots-1A	134605	4,415-20 m	Tiger	L. Cretaceous	Coniacian	Additional sample for MCI	Offline MCI
Gnarlyknots-1A	134606	4,420-25 m	Tiger	L. Cretaceous	Coniacian	Additional sample for MCI	Offline MCI
Gnarlyknots-1A	134525	4,520-25 m	Tiger	L. Cretaceous	Coniacian	Untested sand below shale. FIS dry to wet gas	GOI
Gnarlyknots-1A	134526	4,605-10 m	Tiger	L. Cretaceous	Coniacian	Untested sand below shale. FIS dry to wet gas, PTPL	GOI
Gnarlyknots-1A	134527	4,705-10 m	Tiger	L. Cretaceous	Turon-Coniac.	Untested sand below shale. FIS dry to wet gas, PTPL	GOI
Jerboa-1	134718	2,470-75 m	Sea Lion	L. Jurassic	Callov-Kimmerid.	Re-visit palaeo-oil zone of Lisk et al. (2001)	GOI (combined)
Jerboa-1	134719	2,475-80 m	Sea Lion	L. Jurassic	Callov-Kimmerid.	Re-visit palaeo-oil zone of Lisk et al. (2001)	
Jerboa-1	134720	2,490-95 m	Sea Lion	L. Jurassic	Callov-Kimmerid.	Re-visit palaeo-oil zone of Lisk et al. (2001))	GOI
Platypus-1	134528	9,560-9570 ft	Tiger	E-L. Cretaceous	Albian-Cenoman.	Untested sand below shale	GOI
Platypus-1	134529	9,640-9,650 ft	Tiger	E-L. Cretaceous	Albian-Cenoman.	Untested sand below shale	GOI
Platypus-1	134530	11,090-11,100 ft	Blue Whale	E. Cretaceous	Albian	Untested sand below coals	GOI
Potoroo-1	134721	1,778-82 m	Tiger	L. Cretaceous	Turon-Coniac.	Untested silt below thick shale	GOI , PVTx (combined)
Potoroo-1	134722	1,782-86 m	Tiger	L. Cretaceous	Turon-Coniac.	Untested silt below thick shale	
Potoroo-1	134531	2,398-2402 m	White Pointer	L. Cretaceous	Cenomanian	Untested sand below shale	GOI (combined)
Potoroo-1	134532	2,402-06 m	White Pointer	L. Cretaceous	Cenomanian	Untested sand below shale	
Potoroo-1	134533	2,730-34 m	Blue Whale	E. Cretaceous	Albian	Previous GOI 0.5% @ 2734-38 m – migration zone	GOI
Vivonne-1	134534	2,853-56 m	Bronze Whaler	E. Cretaceous	Barremian	Untested sand below claystone Lower Borda Fm – WCR	No sample

GOI = Grains with Oil Inclusions, MCI = Molecular Composition of oil Inclusions, PVTx = Pressure-Volume-Temperature-composition, GI = gas isotopes. FIS = Fluid Inclusion Stratigraphy, WG = wet gas, GC = gas condensate, PTPL = proximity to pay liquids. Period/Stage derived from well completion reports. Note that Stages differ (somewhat) to those reported by Messent (1998). Supersequence names derived by comparison of depth to Figure 4 and Figure 6 of Totterdell et al. (2000). Supersequence names for Borda-1, Gnarlyknots-1A and Vivonne-1 derived by cross-referencing WCR age with supersequence names in the stratigraphic chart from Totterdell et al. (2008). All cuttings samples referred to in this report are quoted in meters (m) or feet (ft) measured depth (MD) relative to the drilling datum (RT or KB).

Methods

The Grains with Oil Inclusion (GOI™) technique is a petrographic point counting method that records the number of quartz and feldspar grains containing oil inclusions, expressed as a percentage of the total number of grains in each sample (Eadington et al., 1996; Lisk et al., 2002). A computer controlled microscope stepping stage is used to determine the number of quartz grains containing oil inclusions by partitioning the fluid inclusion thin section into approximately 2,000 Fields of View (FOV), each 0.5 x 0.5 mm (Figure 5).

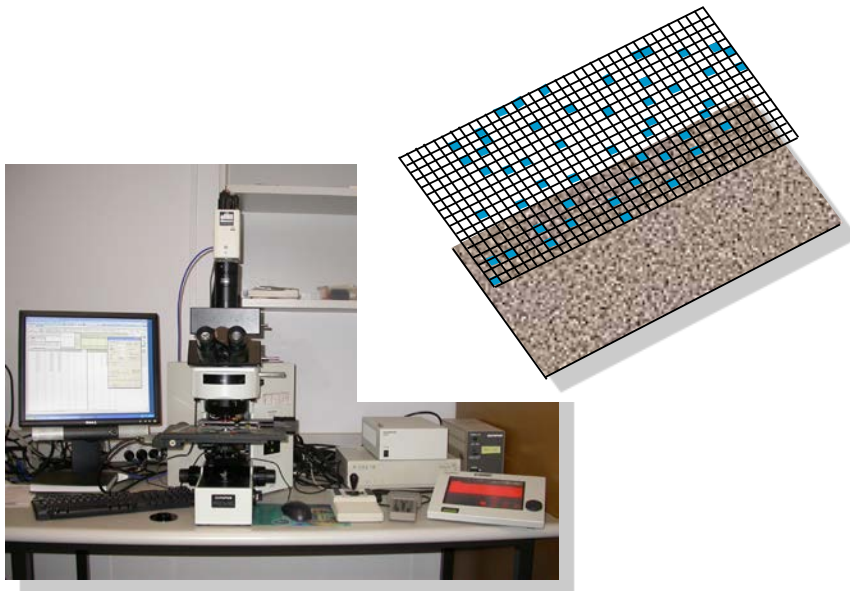


Figure 5: GOI microscope and partitioning of a thin section

There are three methods for counting GOI. The number of FOV and tracks scanned is determined on a sample-by-sample basis by reference to statistics associated with the random selection of grains.

1. The Square Grid (GOI_SG) scan protocol applies to samples where preliminary examination suggests an elevated GOI (>5%) is likely. Square fields of view (0.5 mm x 0.5 mm) are selected at random and a count made of the total grains and grains containing oil inclusions (GWOI). Typically hundreds of grains are counted.
2. The Rectangular Grid (GOI_RG) scan protocol applies to samples where preliminary examination suggests a low GOI (<5%) is likely. Grains containing oil inclusions are counted in randomly selected rectangular fields and grains counted in a sub-set of the fields used to compute the total number of grains scanned. Typically thousands of grains are counted.
3. The Point Grid (GOI_PG) count protocol applies to samples where preliminary examination shows that 200X magnification is not adequate to detect and identify oil inclusions due to their small size or high background fluorescence. This technique uses 500X magnification for positive identification of oil inclusions. Grains and associated oil inclusions are counted on a grain-by-grain basis. Typically one to two hundred grains are counted.

RESULTS

GOI Results

Oil inclusions were observed in 32 of 36 samples and in all wells, with the exception of Jerboa-1 (Figure 6). Their visual abundance, as measured by GOI, are <1.1% (Table 4; Figure 8). The numbers of grains with oil inclusions (GWOI) counted are shown graphically for reference (Figure 9) and were used in the assessment of sample for PVTx and MCI geochemistry.

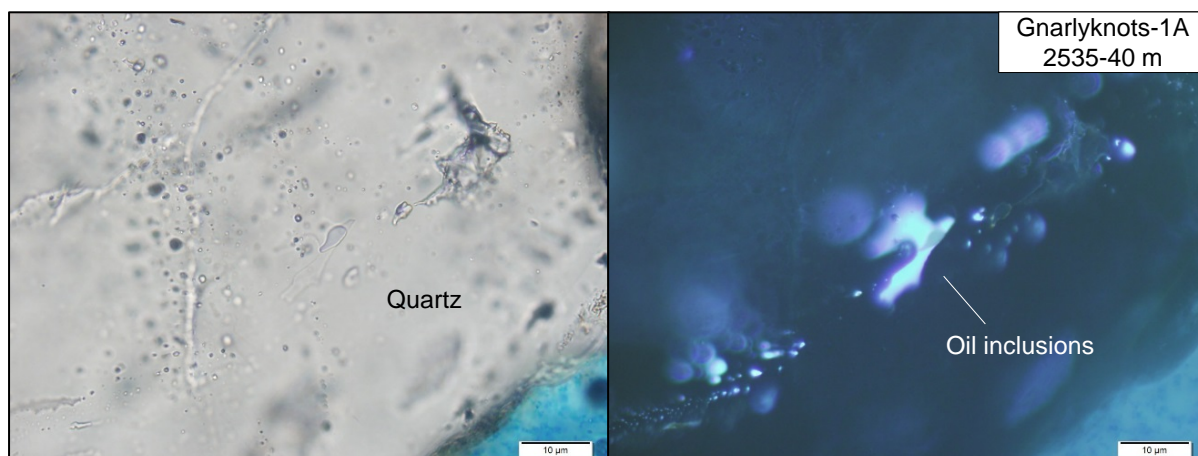


Figure 6: Photomicrographs of oil inclusions from Gnarlyknots-1A. TL (left), UV (right).

Oil inclusions were not observed in samples from 2,774-77 m in Borda-1, 11,090-11,100 ft in Platypus-1, and 2,470-80 m and 2,490-95 m from Jerboa-1. Their GOI are reported as 0.0%. This does not exclude the possibility that oil inclusions may be present at low abundance, but were not detected in the Area of Interest.

Mineral Host

Oil-bearing inclusions are hosted primarily within detrital grains of quartz (Figure 7) and, to a lesser extent, feldspar. Oil-bearing inclusions were noted in carbonate cement in Greenly-1 (as discussed later), but were not included in the GOI count.

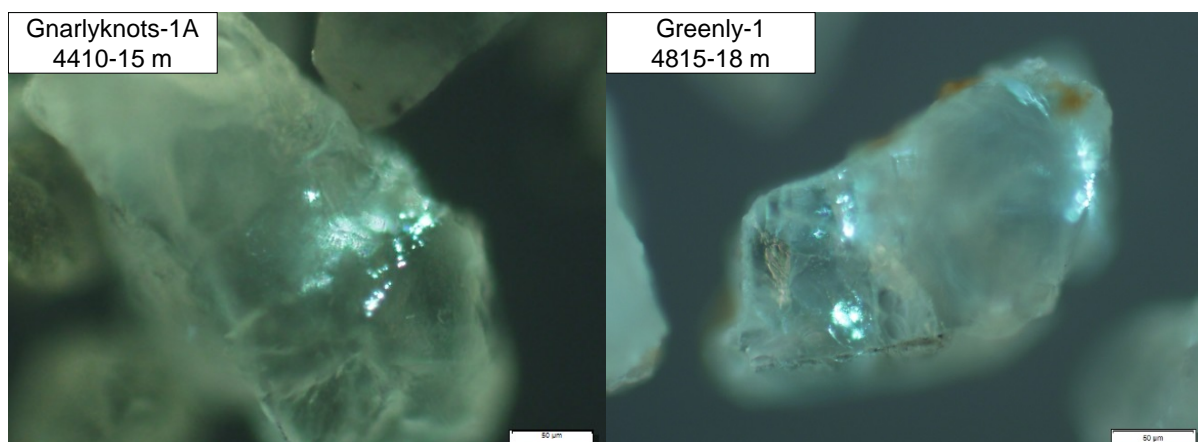


Figure 7: Oil inclusions within detrital quartz grains. UV light.

Table 4: GOI results from this study.

Well	CSIRO No	Depth (MMD)	Count Protocol	Grains with oil inclusions	Total grains counted	GOI (%)
Borda-1	134500	2678-81 m	RG	4	6819	<0.1%
Borda-1	134501	2774-77 m	RG	0	2272	0.0%
Duntroon-1	134502	1855-60 m	RG	2	2160	<0.1%
Duntroon-1	134503	2150-55 m	RG	7	2253	0.3%
Duntroon-1	134504	2505-10 m	RG	12	3316	0.4%
Duntroon-1	134505	3025-30 m	RG	1	2718	<0.1%
Duntroon-1	134506	3235-40 m	RG	2	3840	<0.1%
Duntroon-1	134507	3345-50 m	RG	1	4015	<0.1%
Greenly-1	134508	3275-80 m	RG	6	3326	0.2%
Greenly-1	134509	3753-56 m	RG	2	2298	<0.1%
Greenly-1	134510	4110-13 m	RG	14	6661	0.2%
Greenly-1	134511	4377-80 m	RG	15	8520	0.2%
Greenly-1	134512	4530-33 m	RG	20	6192	0.3%
Greenly-1	134513	4809-12 m	RG	16*	1425	1.1%
Gnarlyknots-1A	134514	2170-80 m	RG	10	3360	0.3%
Gnarlyknots-1A	134515	2535-40 m	RG	8	2540	0.3%
Gnarlyknots-1A	134516	2865-70 m	RG	7	3648	0.2%
Gnarlyknots-1A	134517	3175-80 m	RG	5	3878	0.1%
Gnarlyknots-1A	134518	3760-65 m	RG	11	4994	0.2%
Gnarlyknots-1A	134519	3770-75 m	RG	6	3775	0.2%
Gnarlyknots-1A	134520	3930-40 m	RG	20	4778	0.4%
Gnarlyknots-1A	134521	4135-40 m	RG	19	4352	0.4%
Gnarlyknots-1A	134522	4390-95 m	RG	9	4143	0.2%
Gnarlyknots-1A	134523	4400-05 m	RG	12	7594	0.2%
Gnarlyknots-1A	134524	4410-15 m	RG	29	7027	0.4%
Gnarlyknots-1A	134525	4520-25 m	RG	6	6353	<0.1%
Gnarlyknots-1A	134526	4605-10 m	RG	19	5954	0.3%
Gnarlyknots-1A	134527	4705-10 m	RG	13	8046	0.2%
Jerboa-1	134718 + 134719	2470-75 m + 2475-80 m	RG	0	517	0.0%
Jerboa-1	134720	2490-95 m	RG	0	345	0.0%
Platypus-1	134528	9560-70 ft	RG	3	3720	<0.1%
Platypus-1	134529	9640-50 ft	RG	3	2700	0.1%
Platypus-1	134530	11090-100 ft	RG	0	201	0.0%
Potoroo-1	134721 + 134722	1778-82 m + 1782-86 m	RG	34	21384	0.2%
Potoroo-1	134531 + 134532	2398-2402 m + 2402-06 m	RG	3	2352	0.1%
Potoroo-1	134533	2730-34 m	RG	2	500	0.4%

GOI rounded to nearest 0.1% except for values between 0.01 and 0.09% which are reported as <0.1%. Rectangle Grid (RG), Point Grid (PG), Square Grid (SG or Random). * Excludes of oil inclusions in carbonate cement.

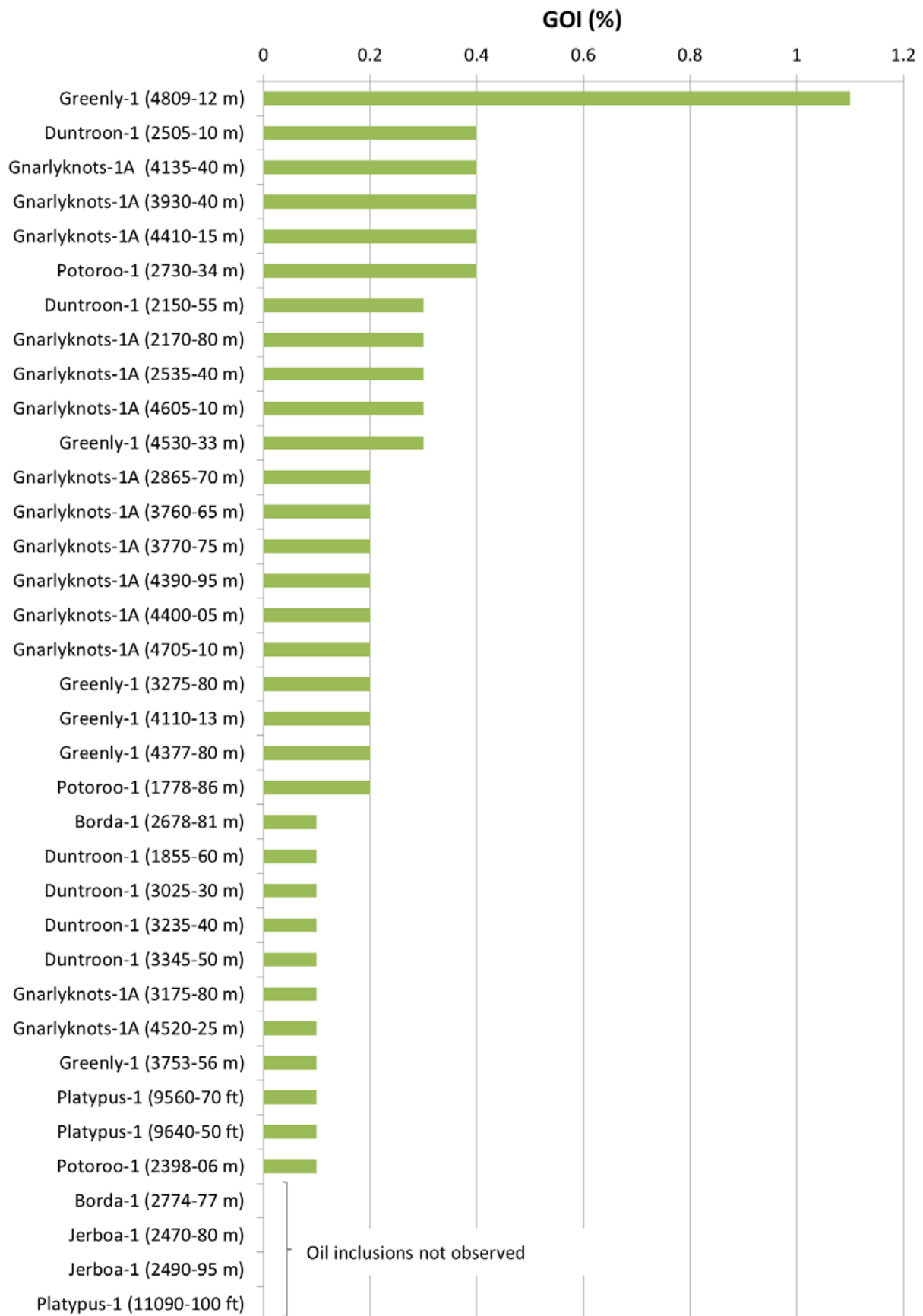


Figure 8: GOI results ranked by GOI number.

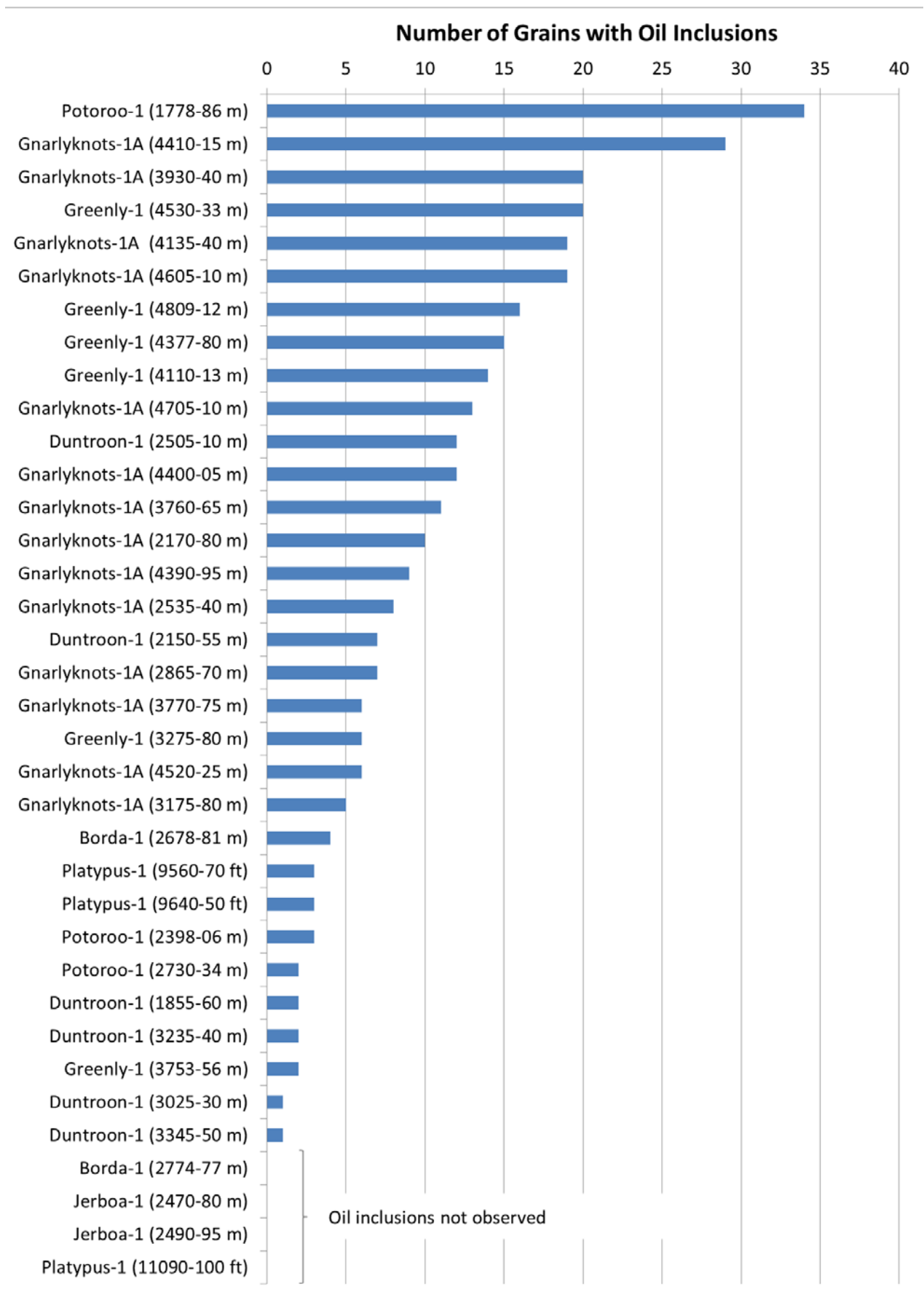


Figure 9: GOI results ranked by number of grains with oil inclusions.

Oil Inclusion Description

Only one oil-bearing inclusion is needed in the description for a grain to be counted in GOI. Oil-bearing inclusions used as the criterion to count GOI contain a fluorescing phase in the inclusion chamber that lacks internal structure and conforms (CONFRM CLR FLR), either wholly or partly, to a spherical or lobate (LOBAT) vapour bubble. The vapour, or contraction, bubble may be moving (MVNG) or non-moving (NO MV). Where the vapour bubble occupies >50% of the inclusion volume they are termed large vapour bubble (LARGE VB). Where a water phase is present they are classified as oil-water inclusions (OWI).

Fluorescence-types NOT INCLUDED in the GOI count are; fluorescing particles in aqueous inclusions (FL PART AQ INCL), thin shell oil-water inclusions, fluorescing features (FL FEAT) and monophase fluorescent inclusions (MONOPHSE INCL). Thin shell oil-water inclusions (THIN SHELL OWI) show conformance of a thin fluorescing oil-film around a vapour bubble. Fluorescing features cannot be assigned to an inclusion chamber that contains a vapour bubble and common types include fluorescing clays and solid inclusions. Where the fluorescence does not conform to a vapour bubble and forms discrete particles within an aqueous inclusion, either attached or dislocated from the vapour bubble, they are classified as “fluorescing particles in aqueous inclusions”.

1. MVNG BUBL CONFRM CL FL; 2. NO MV LOBAT CONFRM CL FL; 3. LARGE VB; 4. OWI MVG BUBL CONFRM CL FL; 5. OWI NO MV LOBAT CONFRM CL FL; 6. THIN SHELL OWI; 7. MONO-PHASE INCL; 8. FL PART AQ INCL; 9. FL FEAT

The dominant type of oil-bearing inclusion recorded in the GOI counts are those with a small vapour bubble in relation to the size of the inclusion (<50% of the inclusion volume; Table 5; Figure 11; Figure 12A-B). While generally small, the vapour bubbles vary in size (Figure 12C). Inclusions of this type are likely to homogenise into the liquid phase at reservoir conditions and were likely trapped as oil.

Other inclusion types included in the GOI count, but at lower relative proportions, include; (i) inclusions with a large vapour phase and a small amount of fluorescing liquid oil (Figure 12D) and, (ii) oil-water inclusions where the dominant phase is water with a minor amount of oil. The inclusions with large vapour bubbles are likely to homogenise into the vapour phase at reservoir conditions and were probably trapped as gas.

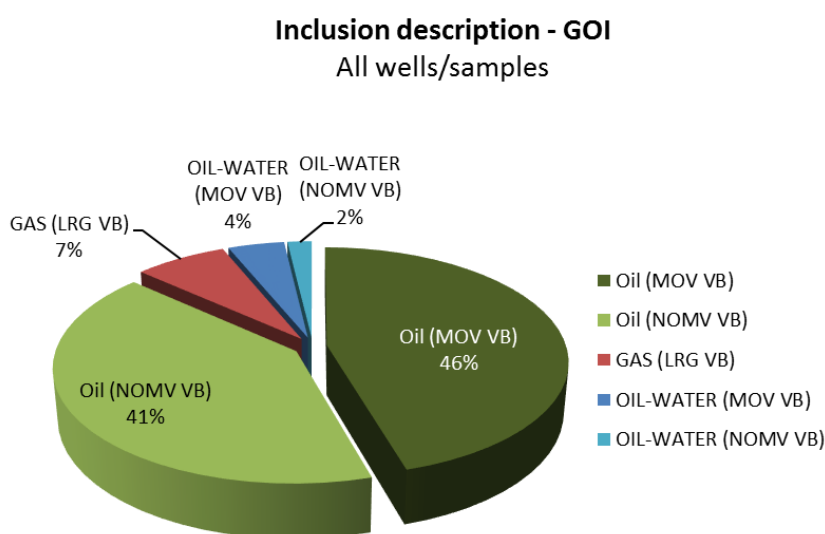











Figure 10: Oil inclusion descriptions for all GOI.

Table 5: Oil inclusion descriptions for GOI and non-GOI fluorescing features (not counted).

CSIRO NO	DEPTH METRES (MD)	OIL		GAS	OWI		NON GOI FLUORESCING FEATURES			
										
Borda-1	2678-81 m	2	1	1	-	-	-	-	-	-
Borda-1	2774-77 m	-	-	-	-	-	-	-	-	-
Duntroon-1	1855-60 m	-	2	-	-	-	-	-	-	-
Duntroon-1	2150-55 m	2	-	2	3	-	-	-	-	-
Duntroon-1	2505-10 m	1	8	3	-	-	-	-	-	-
Duntroon-1	3025-30 m	-	1	-	-	-	-	-	-	-
Duntroon-1	3235-40 m	2	-	-	-	-	-	-	-	-
Duntroon-1	3345-50 m	1	-	-	-	-	-	-	-	-
Greenly-1	3275-80 m	1	3	-	2	-	-	-	-	1
Greenly-1	3753-56 m	1	1	-	-	-	-	-	-	-
Greenly-1	4110-13 m	7	5	1	1	-	-	-	-	1
Greenly-1	4377-80 m	6	9	-	-	-	-	1	-	1
Greenly-1	4530-33 m	11	9	-	-	-	1	-	1	-
Greenly-1	4809-12 m	6	9	-	1	-	-	-	-	-
Gnarlyknots-1A	2170-80 m	4	3	1	1	1	-	-	-	1
Gnarlyknots-1A	2535-40 m	3	4	1	-	-	-	-	-	1
Gnarlyknots-1A	2865-70 m	2	4	1	-	-	-	-	-	-
Gnarlyknots-1A	3175-80 m	5	-	-	-	-	-	1	-	2
Gnarlyknots-1A	3760-65 m	4	3	2	1	1	1	-	1	-
Gnarlyknots-1A	3770-75 m	5	-	-	-	1	-	2	-	3
Gnarlyknots-1A	3930-40 m	9	9	-	1	1	-	-	-	1
Gnarlyknots-1A	4135-40 m	13	4	1	1	-	1	1	-	-
Gnarlyknots-1A	4390-95 m	-	8	-	1	-	-	-	-	-
Gnarlyknots-1A	4400-05 m	6	4	2	-	-	1	1	-	-
Gnarlyknots-1A	4410-15 m	17	7	4	-	1	1	-	1	2
Gnarlyknots-1A	4520-25 m	4	2	-	-	-	-	1	-	0
Gnarlyknots-1A	4605-10 m	9	8	1	1	-	-	2	-	1
Gnarlyknots-1A	4705-10 m	10	2	-	1	-	-	-	-	-
Jerboa-1	2470-80 m	-	-	-	-	-	-	-	2	-
Jerboa-1	2490-95 m	-	-	-	-	-	1	-	-	-
Platypus-1	9560-70 ft	2	1	-	-	-	-	1	-	2
Platypus-1	9640-50 ft	2	1	-	-	-	-	-	-	1
Platypus-1	11090-100 ft	-	-	-	-	-	1	-	-	-
Potoroo-1	1778-86 m	10	21	3	-	-	-	-	-	-
Potoroo-1	2398-06 m	1	1	-	-	1	-	-	-	1
Potoroo-1	2730-34 m	-	2	-	-	-	-	-	-	3

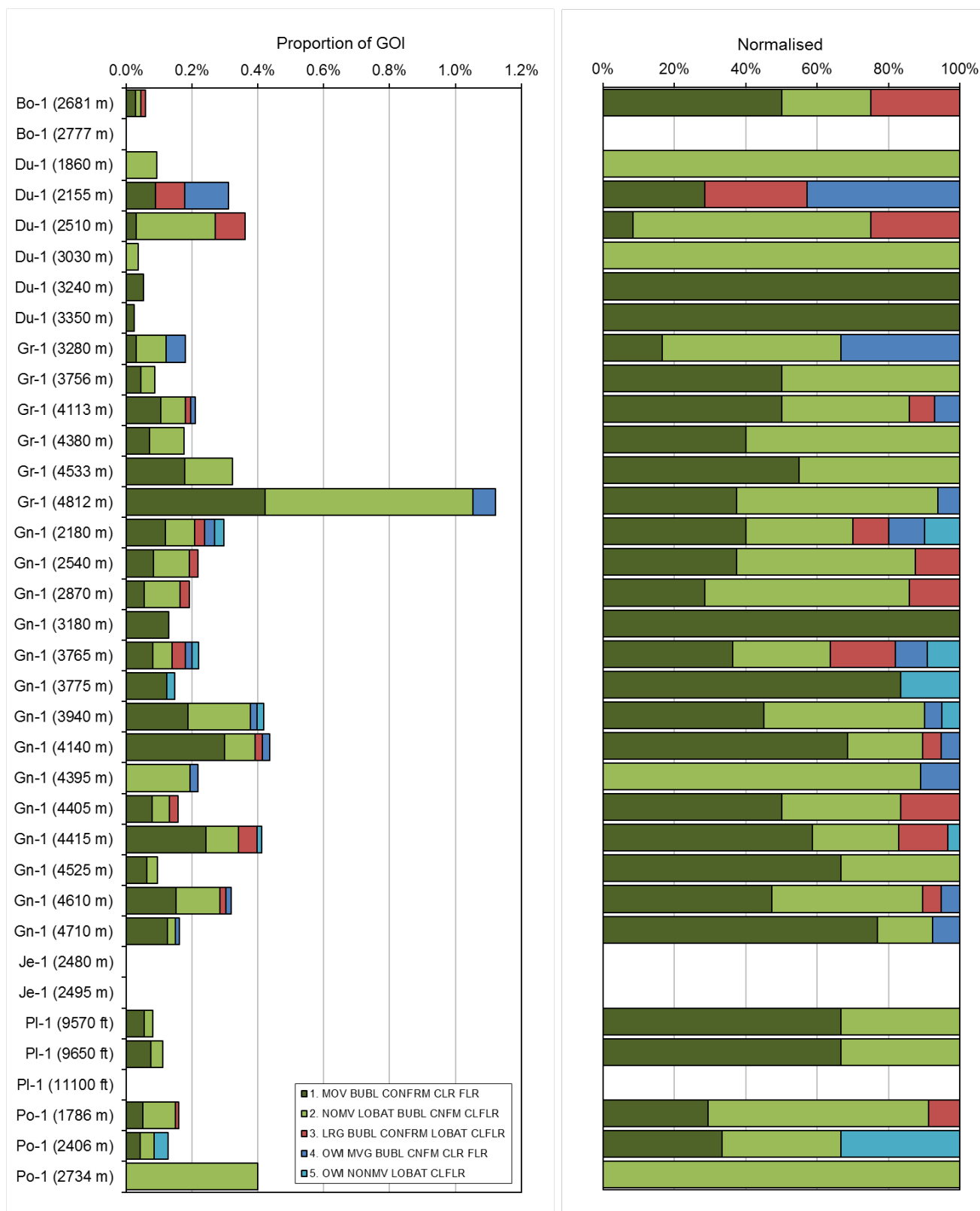


Figure 11: Bar chart of oil inclusion descriptions for GOI—all samples.
For oil-bearing inclusions counted in GOI only. Well annotations shortened to first two letters of name. Depth = base of cuttings interval.

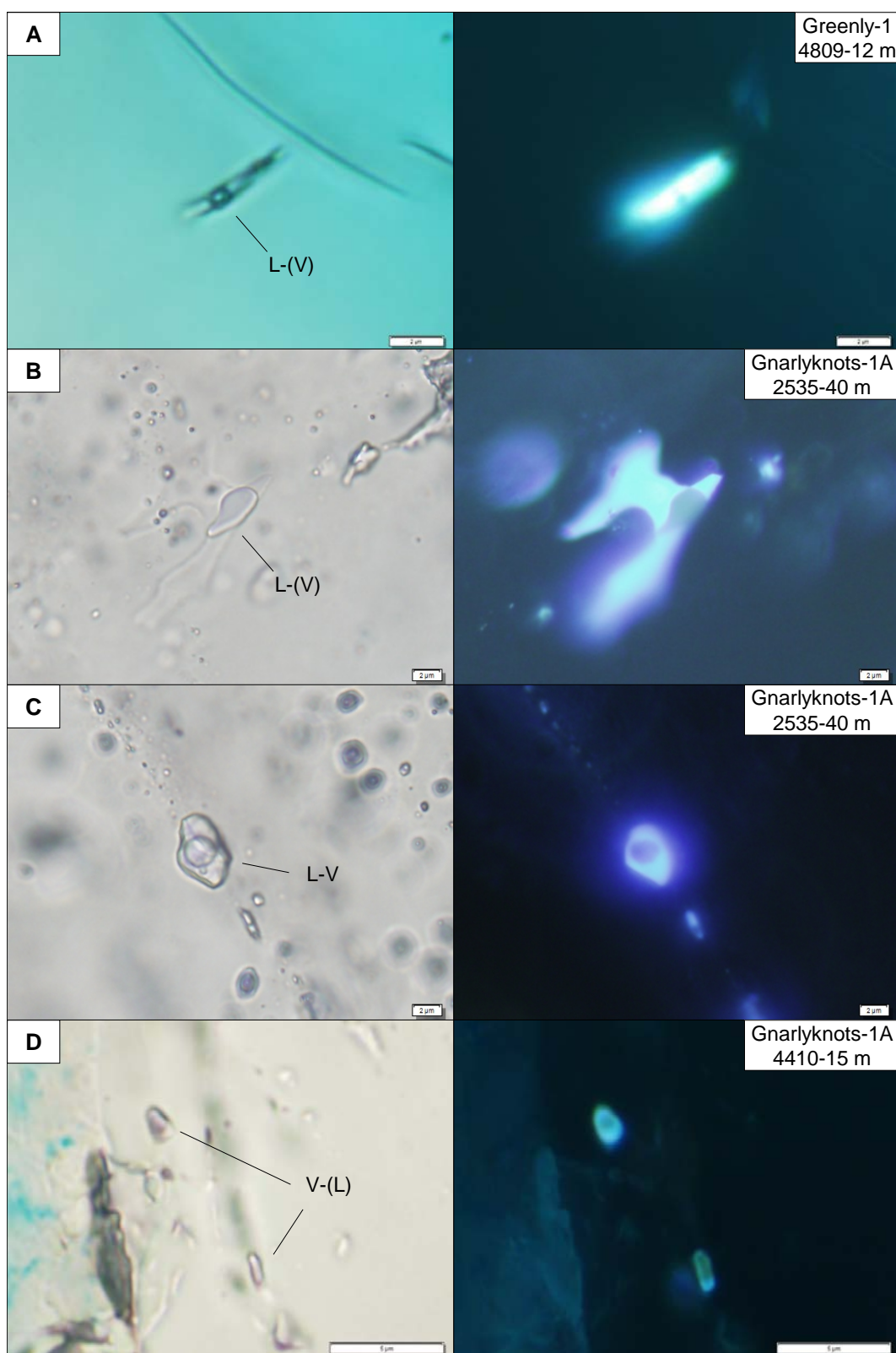


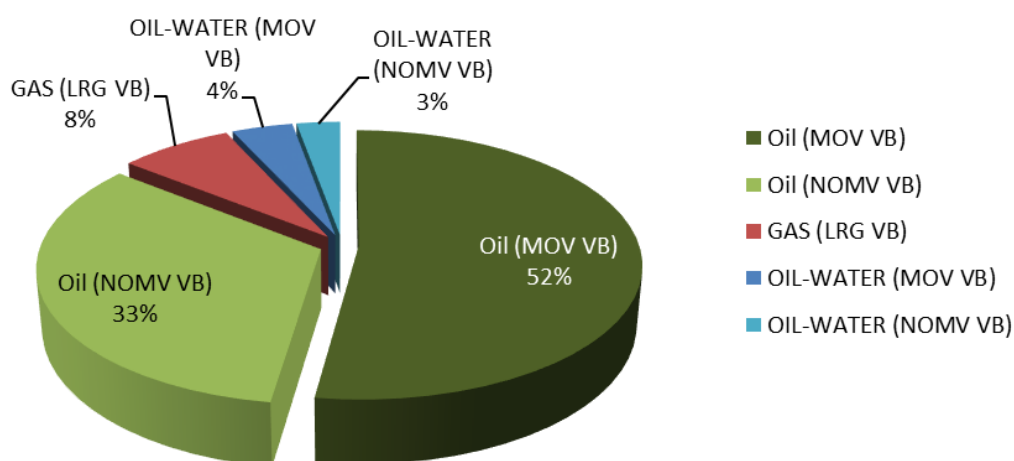
Figure 12: Photomicrographs of oil and gas-rich inclusions.

(A-B) liquid oil (L) inclusions with small vapour phase (V). (C) Liquid oil inclusion with larger vapour phase compared to size of the inclusions. (D) vapour (gas) dominated inclusions with a small component of fluorescent liquid oil. Paired transmitted light (left) and UV illumination (right) photomicrographs.

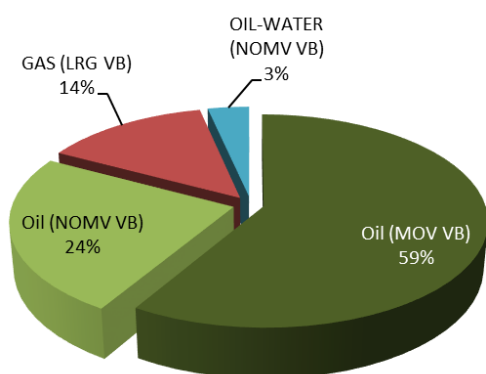
Gnarlyknots-1A

Hydrocarbon inclusions in all samples from Gnarlyknots-1A are dominantly oil-bearing (92% of the GOI count if oil-water inclusions are included), but also includes a minor proportion of gas-bearing inclusions (8%; Figure 13A). The 4410-15 m sample for PVTx and gas isotope analysis, and the larger interval for MCI, contains between 86-88% oil-bearing (if oil-water inclusions are included) and 12-14% gas-bearing inclusions in the GOI count (Figure 13B, C).

A. Inclusion description in GOI Gnarlyknots-1A (all samples)



B. Inclusion description in GOI Gnarlyknots-1A (4410-15 m) PVTx Gas isotopes



C. Inclusion description in GOI Gnarlyknots-1A (4390-4415 m) MCI

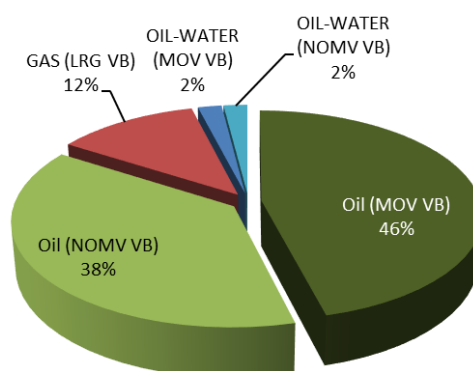


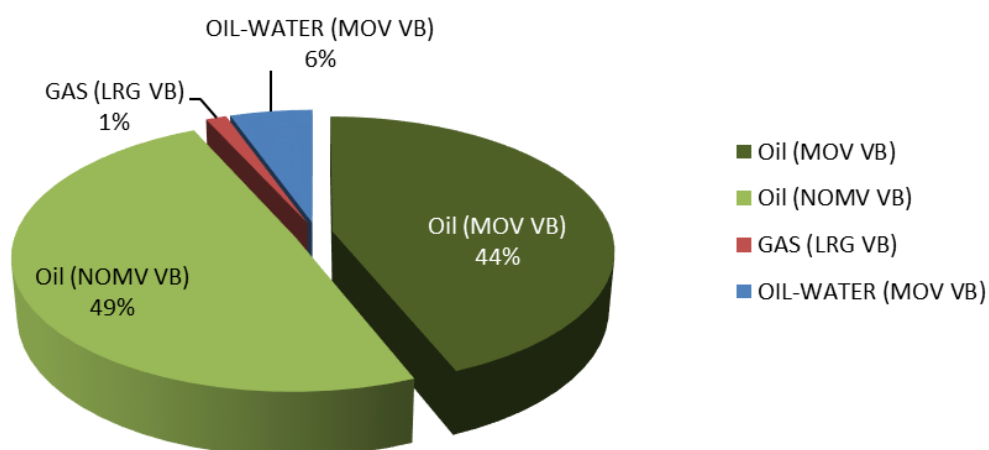
Figure 13: Pie charts of oil inclusion descriptions for GOI–Gnarlyknots-1A.

Greenly-1

Hydrocarbon inclusions in all samples from Greenly-1 are dominantly oil-bearing (99% of the GOI count if oil-water inclusions are included), with very few gas-bearing inclusions (Figure 14A). The 4,809-12 m sample for PVTx and MCI analysis contains only oil-bearing inclusions (100% of the GOI count if oil-water inclusions are included; Figure 14B). No gas-bearing inclusions were recorded.

A. Inclusion description in GOI

Greenly-1 (all samples)



B. Inclusion description in GOI

Greenly-1 (4809-12 m) PVTx MCI

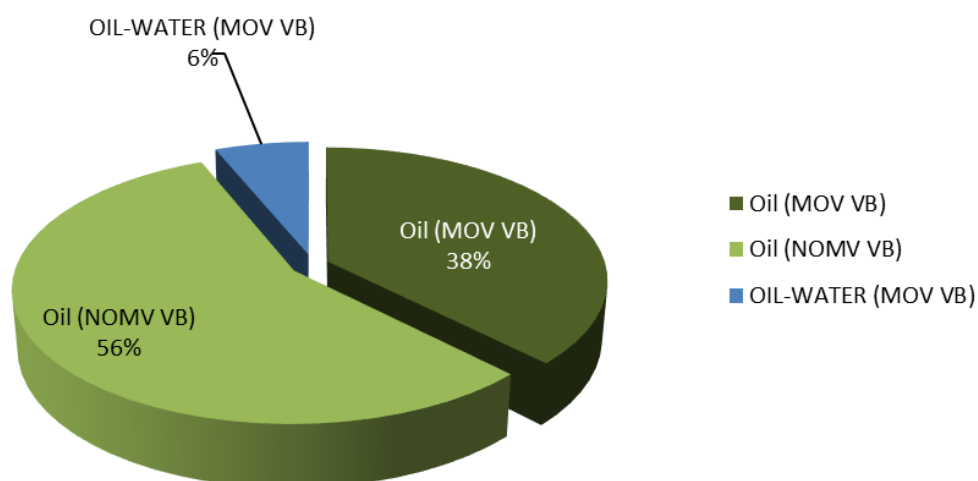


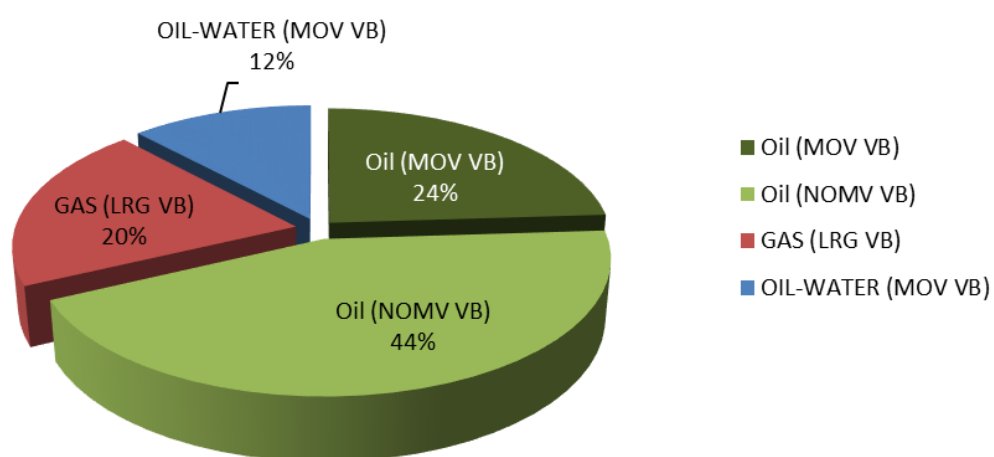
Figure 14: Pie charts of oil inclusion descriptions for GOI–Greenly-1.

Duntroon-1

Hydrocarbon inclusions in all samples from Duntroon-1 are dominantly oil-bearing (80% of the GOI count if oil-water inclusions are included), but also includes a significant proportion of gas-bearing inclusions with large vapour bubbles (20%; Figure 15A). The 2,505-10 m sample for PVTx analysis is similar and contains 75% oil-bearing and 25% gas-bearing inclusions in the GOI count (Figure 15B).

A. Inclusion description in GOI

Duntroon-1 (all samples)



B. Inclusion description in GOI

Duntroon-1 (2505-10 m) PVTx

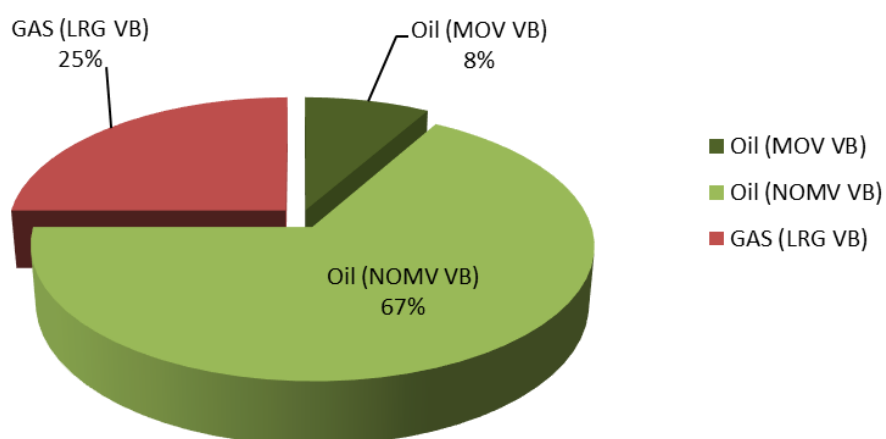


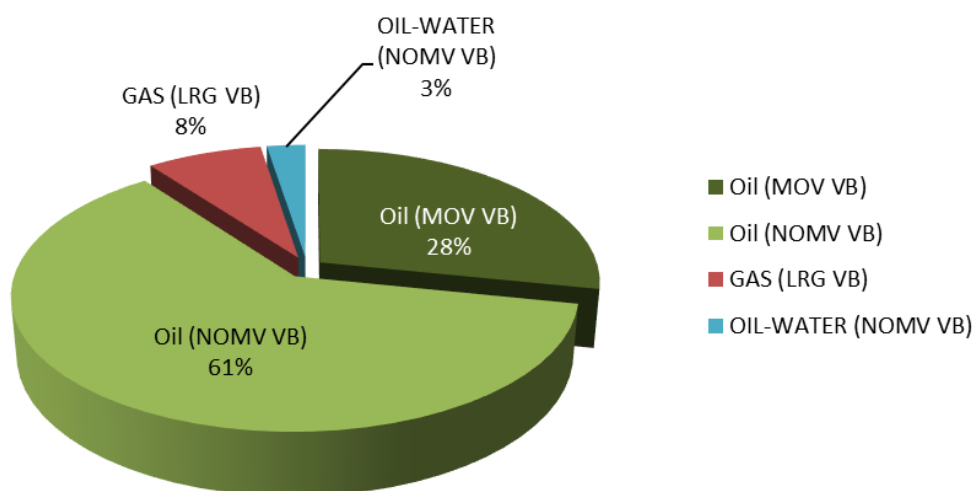
Figure 15: Pie charts of oil inclusion descriptions for GOI–Duntroon-1.

Potoroo-1

Hydrocarbon inclusions in all samples from Potoroo-1 are dominantly oil-bearing (92% of the GOI count if oil-water inclusions are included), but also includes a minor proportion of gas-bearing inclusions (8%; Figure 16A). The 1,778-86 m sample for PVTx analysis is similar and contains 91% oil-bearing and 9% gas-bearing inclusions in the GOI count (Figure 16B).

A. Inclusion description in GOI

Potoroo-1 (all samples)



B. Inclusion description in GOI

Potoroo-1 (1778-86 m) PVTx

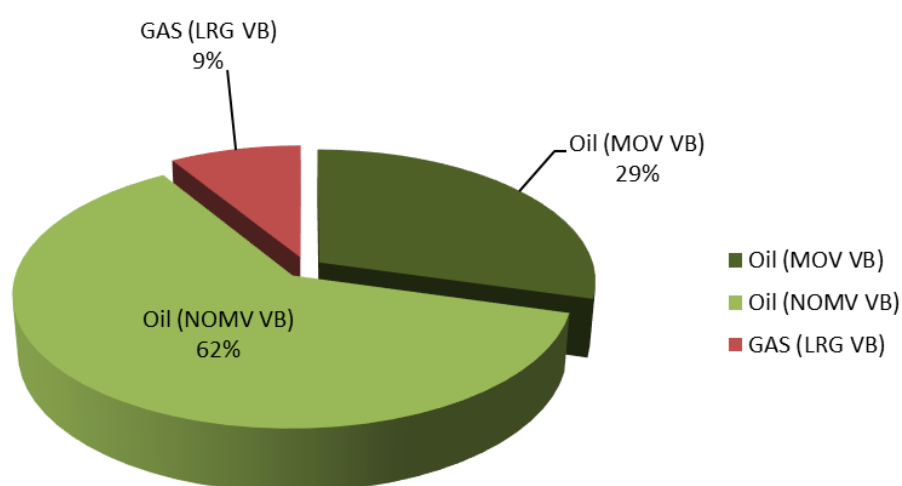


Figure 16: Pie charts of oil inclusion descriptions for GOI–Potoroo-1.

Fluorescence Colour

Groups of oil inclusions called assemblages are classified by visual assignment of fluorescence colour on a three colour classification being near-blue, near-white, or near-yellow, also recognizing where oil inclusion assemblages have more than one fluorescence colour. The latter are described as having gradational blue to white, white to yellow or blue to yellow fluorescence. Fluorescence was excited by UV illumination at 365 nm excitation wavelength and observed after passing through a 420 nm barrier filter.

1. Near-blue; 2 Gradational blue- white; 3. Near-white; 4 Gradational white-yellow.; 5 Near-yellow; 6. Gradational blue- yellow.

The dominant type of oil-bearing inclusion recorded in the GOI counts are those with near-white visual fluorescence colour (Table 6; Figure 17; Figure 18). These white fluorescence assemblages are mostly uniform, but do encompass small colour variations to include those with slightly bluish or yellowish tints.

While there are local variances between wells and individual samples, assemblages with uniform near-blue and near- yellow fluorescence colours generally occur at lower proportions, together with those that exhibit gradational variants of near-white, near-blue and near- yellow.

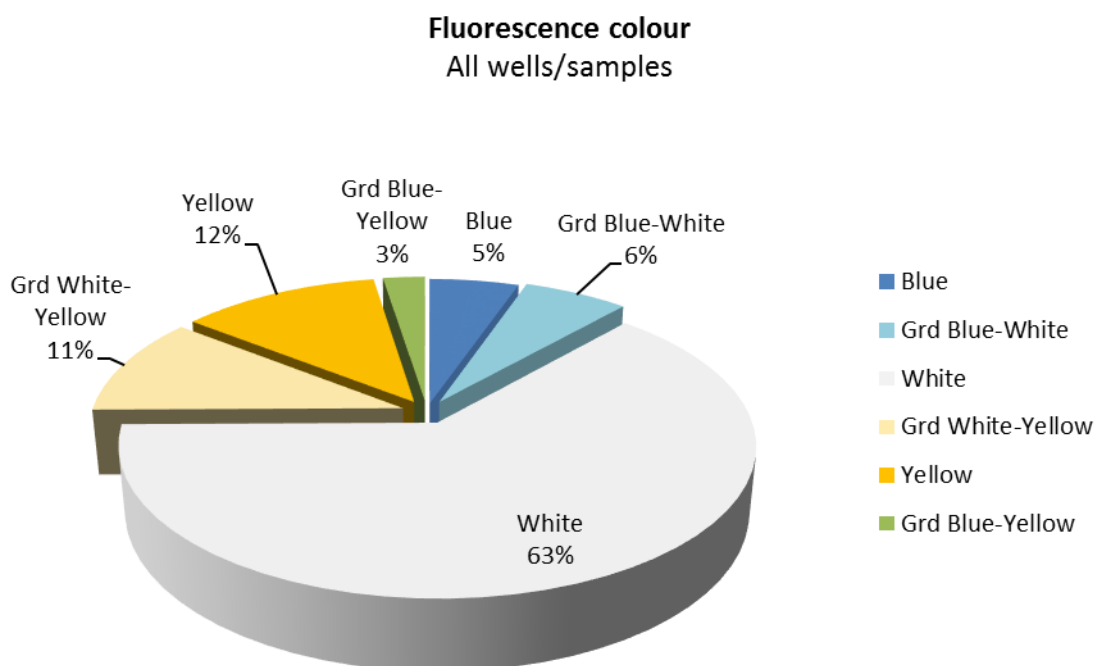

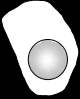






Figure 17: Pie chart of OIA fluorescence colour—all samples.

Table 6: OIA fluorescence colour.

WELL	DEPTH METRES (MDRT)	1. BLUE 	2. WHITE 	3. YELLOW 	4. GRAD BLUE- WHITE 	5. GRAD. WHITE- YELLOW 	6. GRAD. BLUE- YELLOW 
Borda-1	2678-81 m	-	3	-	1	-	-
Borda-1	2774-77 m	-	-	-	-	-	-
Duntroon-1	1855-60 m	-	-	2	-	-	-
Duntroon-1	2150-55 m	3	3	-	-	1	-
Duntroon-1	2505-10 m	-	7	1	1	2	1
Duntroon-1	3025-30 m	-	1	-	-	-	-
Duntroon-1	3235-40 m	-	2	-	-	-	-
Duntroon-1	3345-50 m	-	1	-	-	-	-
Greenly-1	3275-80 m	-	3	1	-	2	-
Greenly-1	3753-56 m	-	-	-	-	2	-
Greenly-1	4110-13 m	1	9	2	-	1	1
Greenly-1	4377-80 m	-	12	-	1	2	-
Greenly-1	4530-33 m	2	15	2	-	1	-
Greenly-1	4809-12 m	-	10	-	3	-	-
Gnarlyknots-1A	2170-80 m	2	5	1	1	-	1
Gnarlyknots-1A	2535-40 m	1	4	2	1	-	-
Gnarlyknots-1A	2865-70 m	1	5	-	-	1	-
Gnarlyknots-1A	3175-80 m	-	1	2	-	2	-
Gnarlyknots-1A	3760-65 m	1	7	-	-	2	1
Gnarlyknots-1A	3770-75 m	-	5	1	-	-	-
Gnarlyknots-1A	3930-40 m	-	16	2	2	-	-
Gnarlyknots-1A	4135-40 m	-	11	3	3	1	1
Gnarlyknots-1A	4390-95 m	-	6	2	1	-	-
Gnarlyknots-1A	4400-05 m	2	6	1	1	2	-
Gnarlyknots-1A	4410-15 m	-	21	2	1	5	-
Gnarlyknots-1A	4520-25 m	-	5	1	-	-	-
Gnarlyknots-1A	4605-10 m	1	10	4	1	2	1
Gnarlyknots-1A	4705-10 m	-	8	-	1	3	1
Jerboa-1	2470-80 m	-	-	-	-	-	-
Jerboa-1	2490-95 m	-	-	-	-	-	-
Platypus-1	9560-70 ft	-	3	-	-	-	-
Platypus-1	9640-50 ft	-	2	-	-	1	-
Platypus-1	11090-100 ft	-	-	-	-	-	-
Potoroo-1	1778-86 m	3	15	9	2	4	1
Potoroo-1	2398-06 m	-	3	-	-	-	-
Potoroo-1	2730-34 m	-	2	-	-	-	-

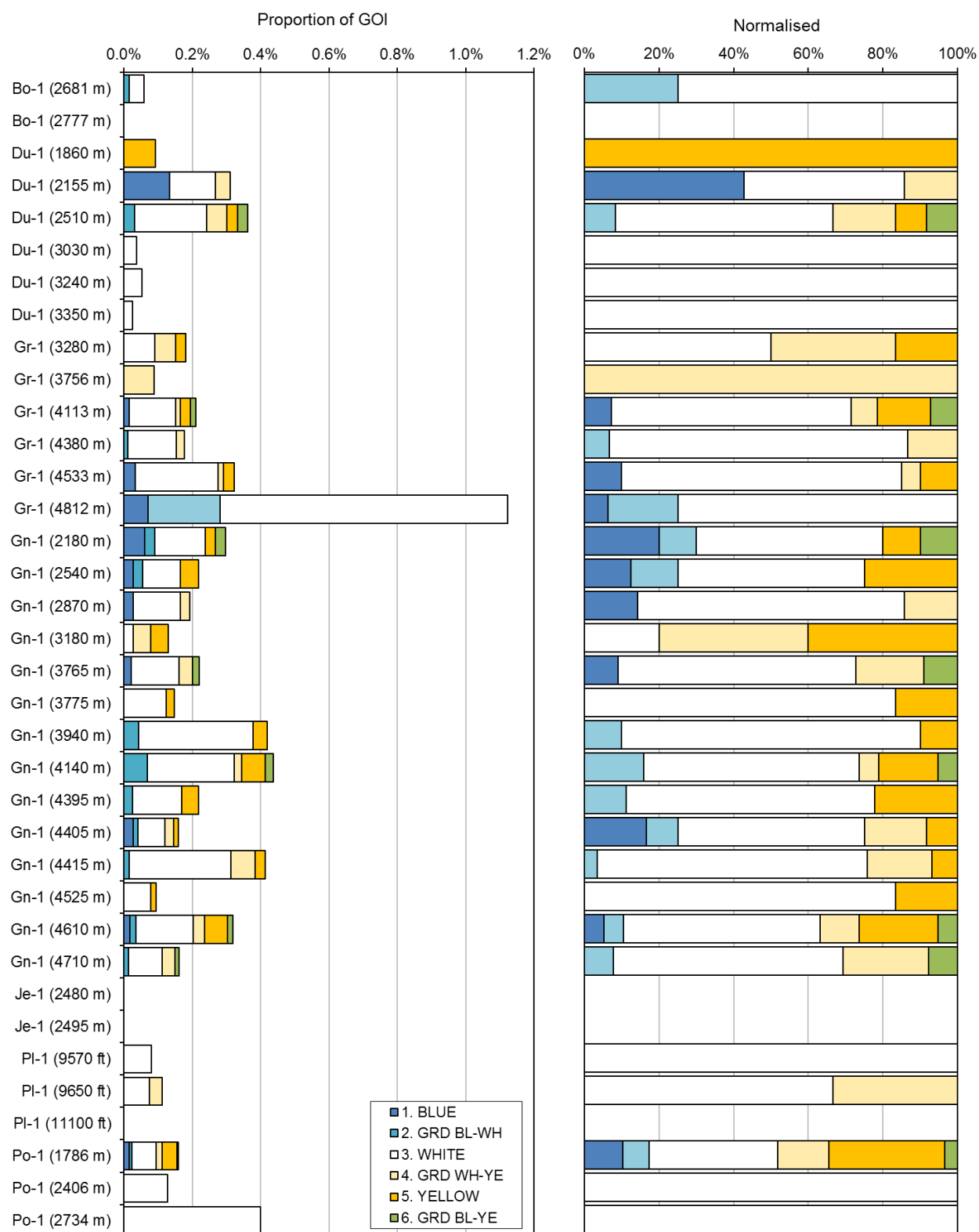


Figure 18: Bar chart of OIA fluorescence colour—all samples.

For oil-bearing inclusions counted in GOI only. Well annotations shortened to first two letters of name. Depth = base of cuttings interval.

Gnarlyknots-1A

Hydrocarbon assemblages from Gnarlyknots-1A fluoresce mostly white and are uniform (63% of the GOI count; Figure 19A). The remainder being uniform near-blue and near-yellow with gradational variants. Between two thirds and three quarters (66-72%) of the oil inclusions in the 4,410-15 m sample for PVTx and gas isotope analysis, and the larger interval for MCI, are uniform white, with the remainder being near-blue, near yellow and associated variants (Figure 19B, C).

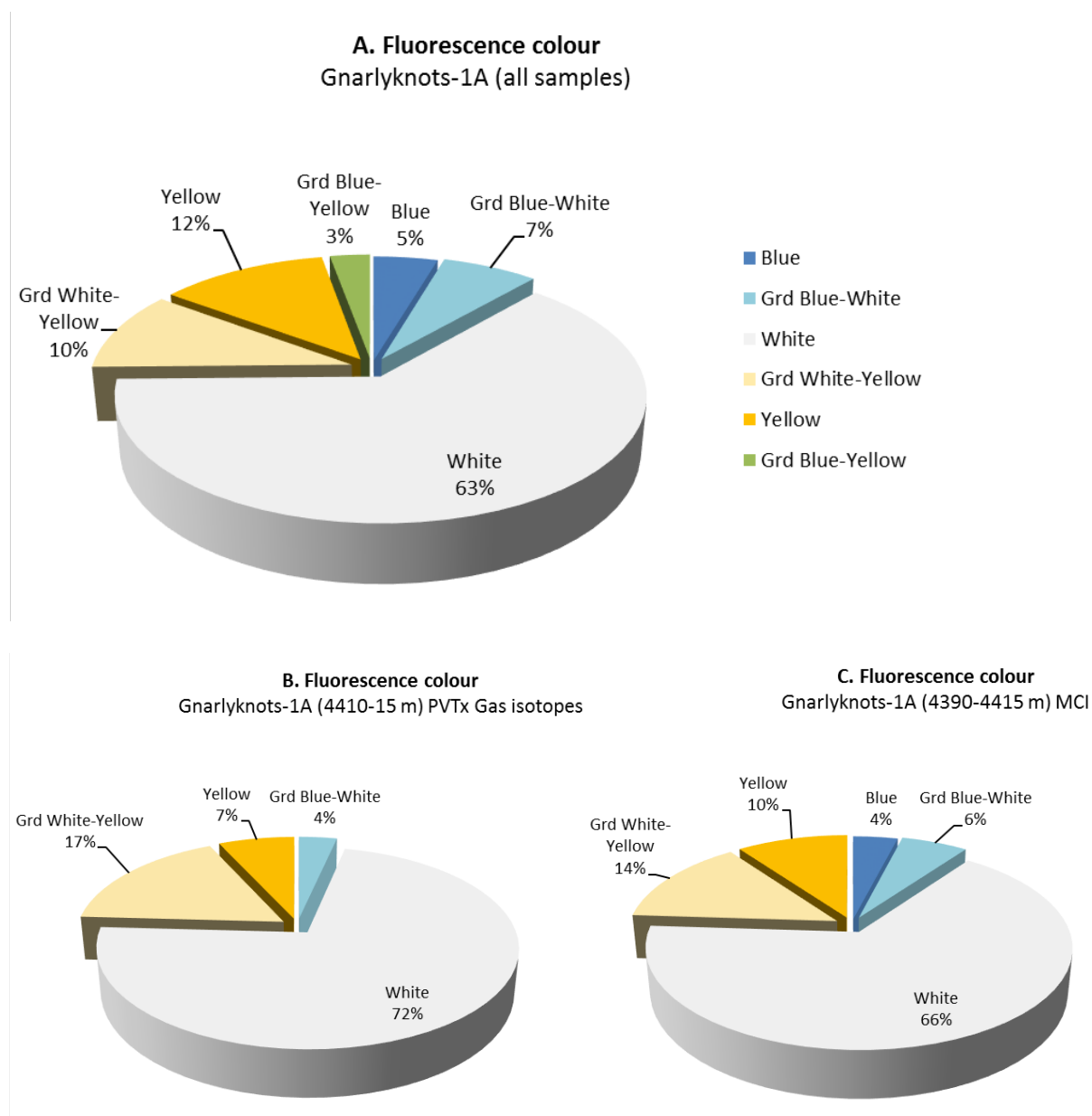


Figure 19: Pie charts of OIA fluorescence colour–Gnarlyknots-1A.

Greenly-1

Hydrocarbon assemblages from Greenly-1 fluoresce mostly white and are uniform (70% of the GOI count; Figure 20A). The remainder being uniform near-blue and near-yellow, with gradational variants. About three quarters (77%) of the oil inclusions in the 4,809-12 m sample for PVTx and MCI analysis are uniform white, with the remainder assigned as gradational blue-white variants (Figure 20B). This confers some degree of consistency in the trapped oil and, perhaps, composition.

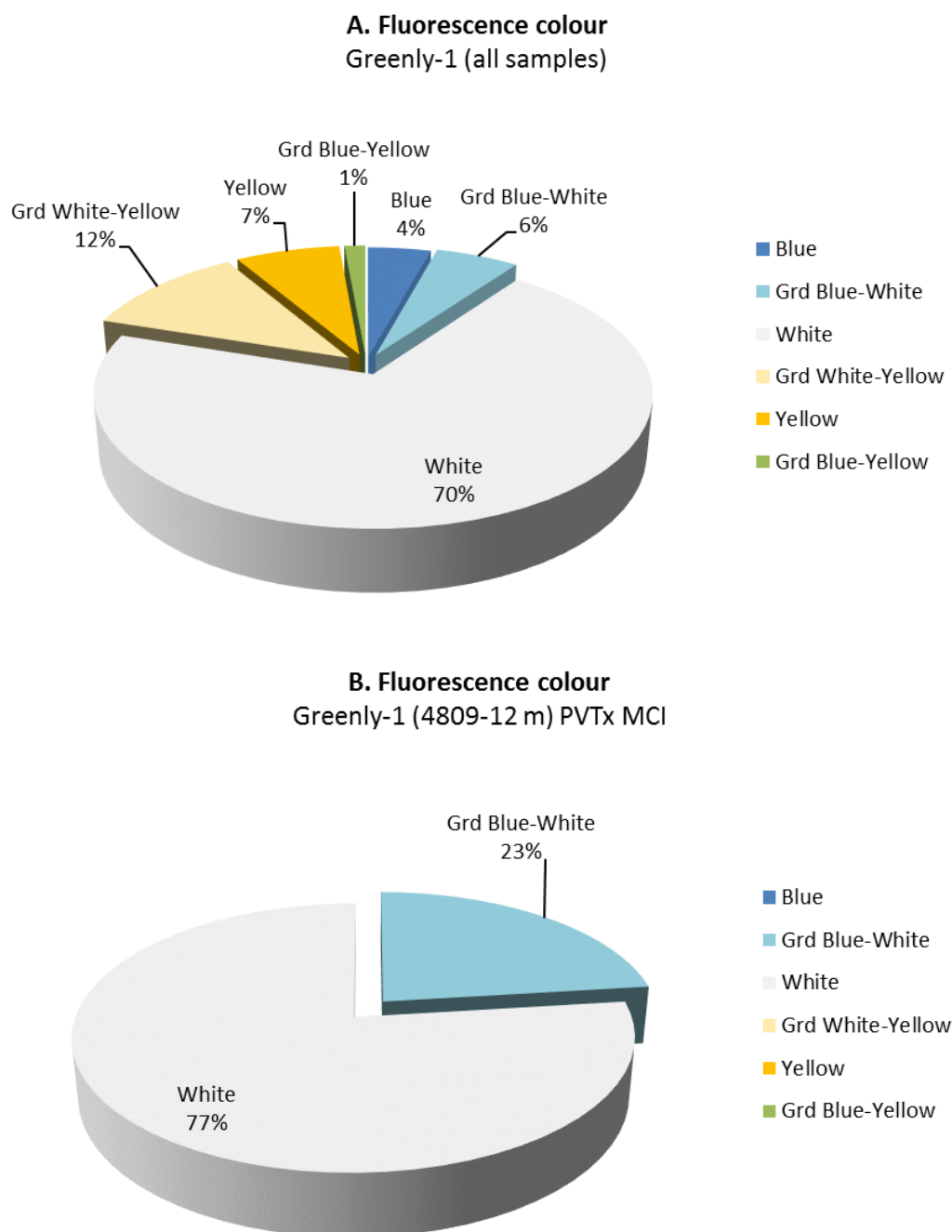


Figure 20: Pie charts of OIA fluorescence colour–Greenly-1.

Duntroon-1

Hydrocarbon assemblages from Duntroon-1 frequently fluoresce white and are uniform (56% of the GOI count (Figure 21A). The remainder being uniform near-blue and near-yellow, with gradational variants. About half (59%) of the oil inclusions in the 2,505-10 m sample for PVTx analysis are uniform white, with the remainder assigned as near-yellow with gradational variants (Figure 21B).

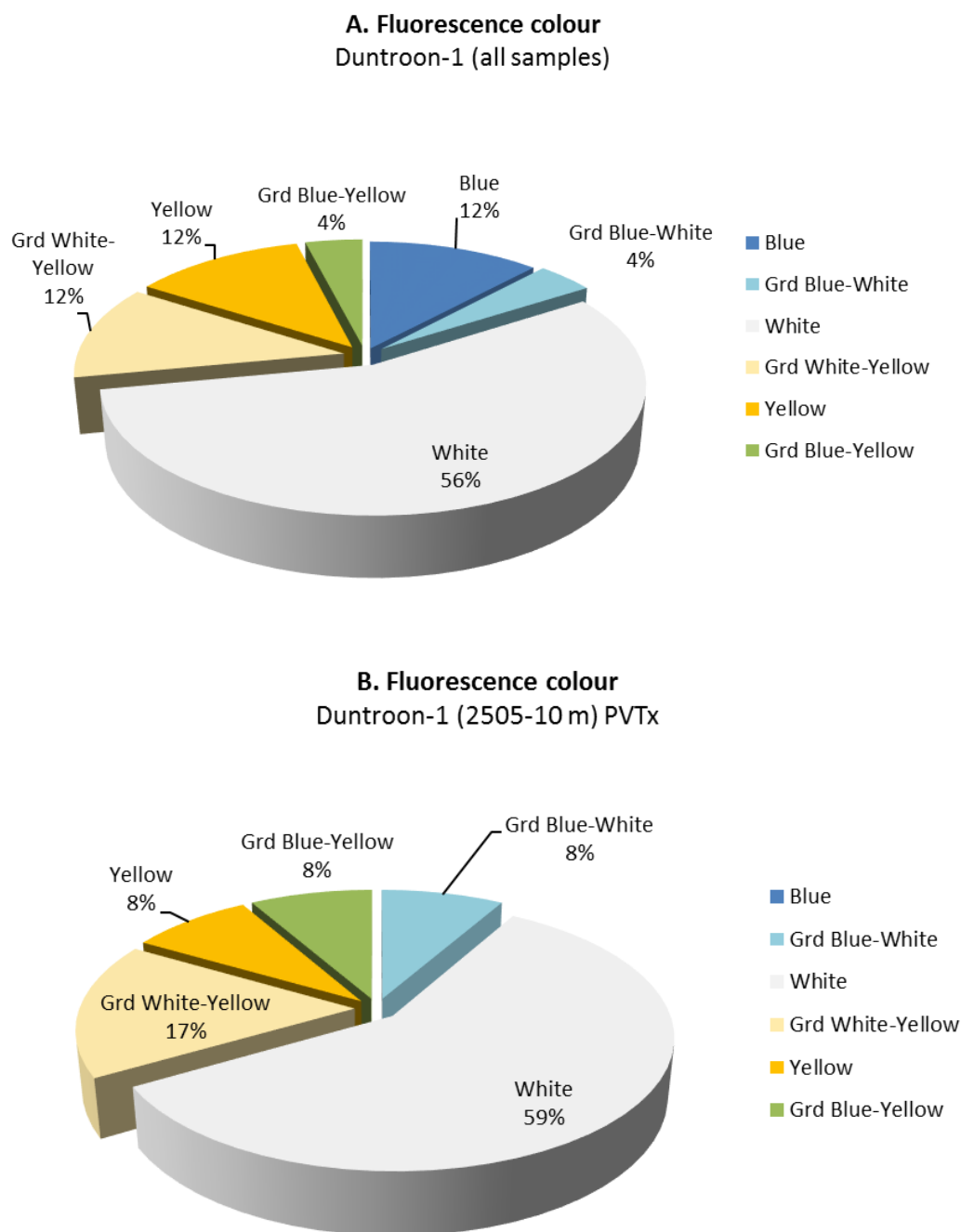


Figure 21: Pie charts of OIA fluorescence colour–Duntroon-1.

Potoroo-1

Hydrocarbon assemblages from Potoroo-1 frequently fluoresce white and are uniform (51% of the GOI count). The remainder being uniform near-blue and near-yellow, with gradational variants (Figure 22A). While about half (44%) of the oil inclusions in the 1,778-86 m sample for PVTx analysis are uniform white, there is a significant proportion of uniform near-yellow inclusions, with the remainder assigned as near-blue and associated gradational variants (Figure 22B). At 56.5°C current day temperature (and having not reached sterilization temperatures), this sample is still within the biodegradation window and may account for the “heavier–lower API” yellow fluorescing oil.

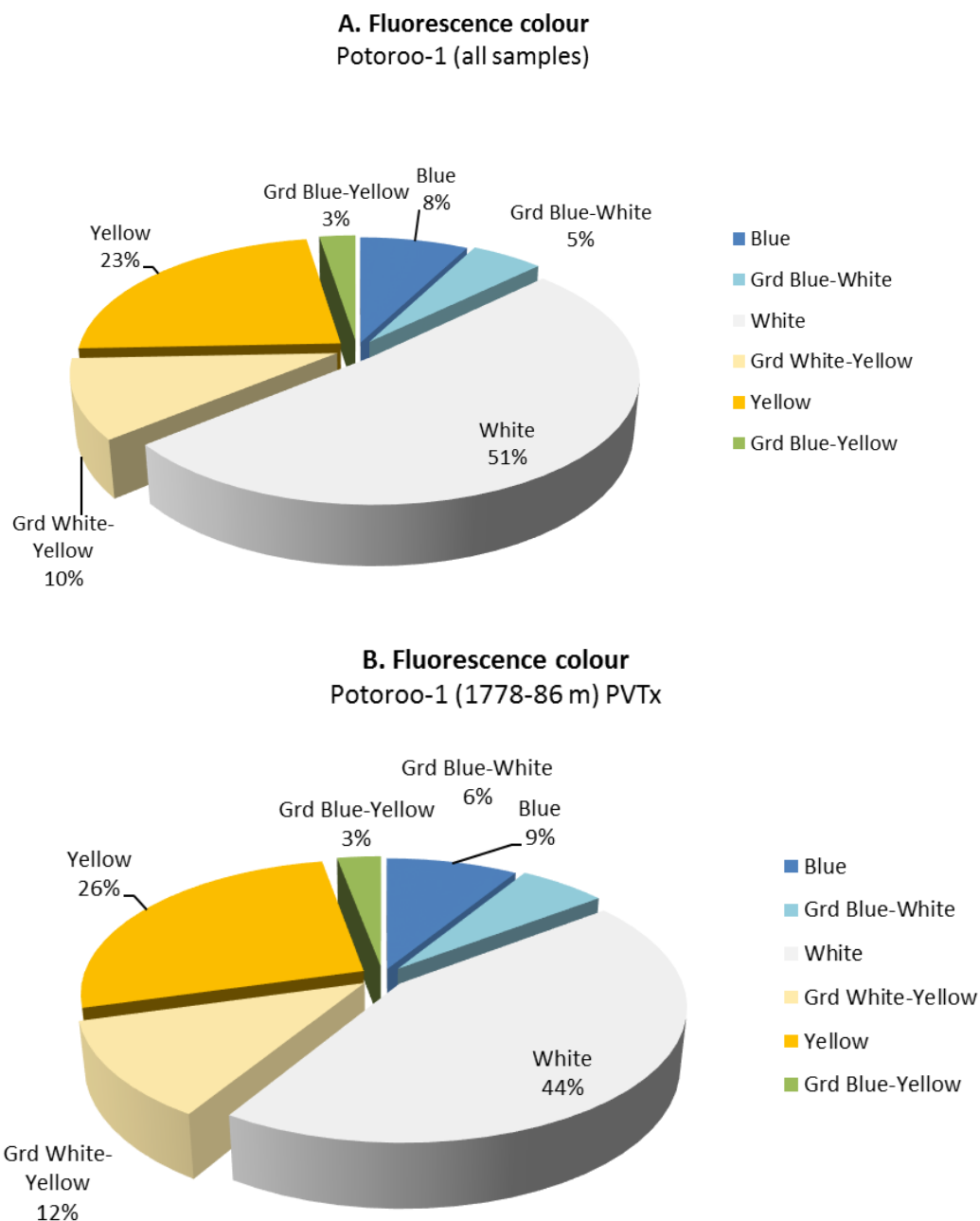


Figure 22: Pie charts of OIA fluorescence colour–Potoroo-1.

Location

Location attributes in quartz and feldspar are recorded for each grain with oil inclusion using the following descriptions: (i) unresolved location in the grain, (ii) trail(s) of inclusions along fractures within detrital grains, (iii) in fracture trails terminating at the quartz overgrowth boundary (QOB), (iv) at the QOB, (v) within quartz overgrowth (QO), (vi) fractures that transect QO, and (vii) fractures that are penetrative through the fabric of the rock.

1. UNR LOCN; 2. FRAC INTRA; 3. FRAC TERM QO; 4. QOB; 5. WQO; 6. FRAC TRANS QO; 7. PEN FRAC

Oil-bearing inclusions recorded in the GOI counts are those located, almost exclusively, along unconstrained healed micro-fractures in detrital quartz (Table 7; Figure 23; Figure 24). Diagenetic fractures are common trapping sites for fluid inclusions and typically form by brittle grain-grain compaction as the sediment is buried. Due to temperature constraints, this process typically occurs earlier in the burial cycle than cementation processes, like quartz cement, that tend to retard the compaction process. No relationship with quartz cement could be established and they are termed fracture intragrain.

Some oil-bearing diagenetic fractures appear to terminate at the quartz overgrowth boundary, being noted in four samples from Gnarlyknots-1A and one sample from Duntroon-1.

Trace numbers of oil inclusions were observed at the quartz overgrowth boundary in Potoroo-1 and Duntroon-1, but at abundances too low to be statistically significant.

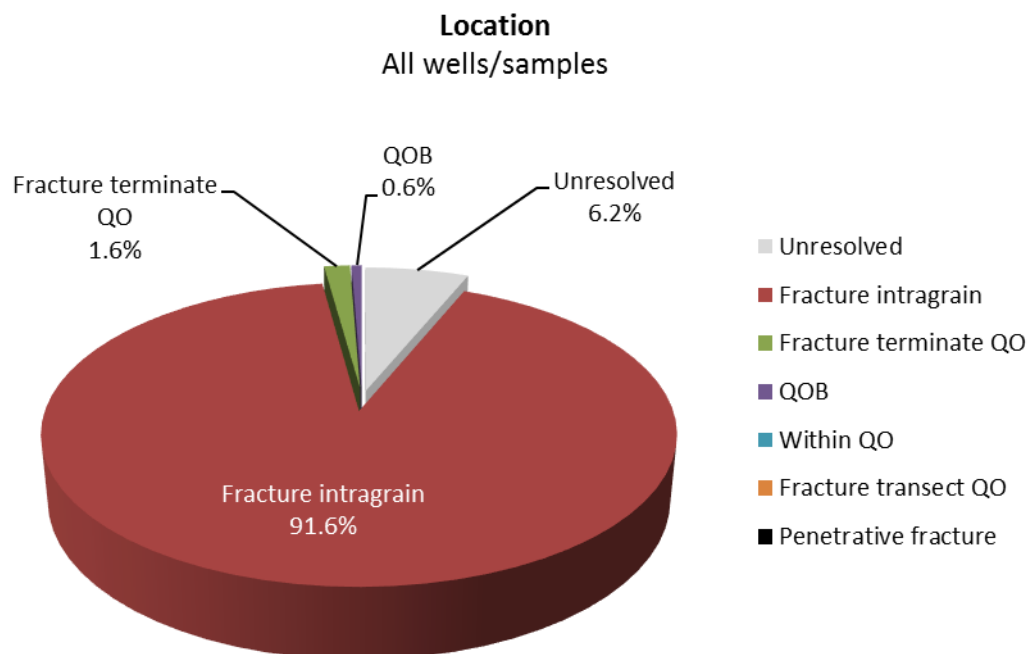









Figure 23: Pie chart of OIA locations—all samples.

Table 7: OIA locations.

WELL	DEPTH METRES (MDRT)	1. UNR LOCN 	2. FRAC INTRA 	3. FRAC TERM QO 	4. QOB 	5. WQO 	6. FRAC TRANS QO 	7. PEN FRAC 
Borda-1	2678-81 m	-	4	-	-	-	-	-
Borda-1	2774-77 m	-	-	-	-	-	-	-
Duntroon-1	1855-60 m	1	1	-	-	-	-	-
Duntroon-1	2150-55 m	-	7	-	-	-	-	-
Duntroon-1	2505-10 m	1	9	1	1	-	-	-
Duntroon-1	3025-30 m	-	1	-	-	-	-	-
Duntroon-1	3235-40 m	-	2	-	-	-	-	-
Duntroon-1	3345-50 m	-	1	-	-	-	-	-
Greenly-1	3275-80 m	-	6	-	-	-	-	-
Greenly-1	3753-56 m	-	2	-	-	-	-	-
Greenly-1	4110-13 m	-	14	-	-	-	-	-
Greenly-1	4377-80 m	2	13	-	-	-	-	-
Greenly-1	4530-33 m	2	18	-	-	-	-	-
Greenly-1	4809-12 m	5	11	-	-	-	-	-
Gnarlyknots-1A	2170-80 m	-	10	-	-	-	-	-
Gnarlyknots-1A	2535-40 m	-	8	-	-	-	-	-
Gnarlyknots-1A	2865-70 m	-	7	-	-	-	-	-
Gnarlyknots-1A	3175-80 m	-	5	-	-	-	-	-
Gnarlyknots-1A	3760-65 m	-	11	-	-	-	-	-
Gnarlyknots-1A	3770-75 m	1	5	-	-	-	-	-
Gnarlyknots-1A	3930-40 m	-	19	1	-	-	-	-
Gnarlyknots-1A	4135-40 m	-	18	1	-	-	-	-
Gnarlyknots-1A	4390-95 m	-	9	-	-	-	-	-
Gnarlyknots-1A	4400-05 m	-	12	-	-	-	-	-
Gnarlyknots-1A	4410-15 m	3	26	-	-	-	-	-
Gnarlyknots-1A	4520-25 m	-	5	1	-	-	-	-
Gnarlyknots-1A	4605-10 m	-	19	-	-	-	-	-
Gnarlyknots-1A	4705-10 m	-	12	1	-	-	-	-
Jerboa-1	2470-80 m	-	-	-	-	-	-	-
Jerboa-1	2490-95 m	-	-	-	-	-	-	-
Platypus-1	9560-70 ft	-	3	-	-	-	-	-
Platypus-1	9640-50 ft	-	3	-	-	-	-	-
Platypus-1	11090-100 ft	-	-	-	-	-	-	-
Potoroo-1	1778-86 m	4	30	-	-	-	-	-
Potoroo-1	2398-06 m	-	3	-	-	-	-	-
Potoroo-1	2730-34 m	1	-	-	1	-	-	-

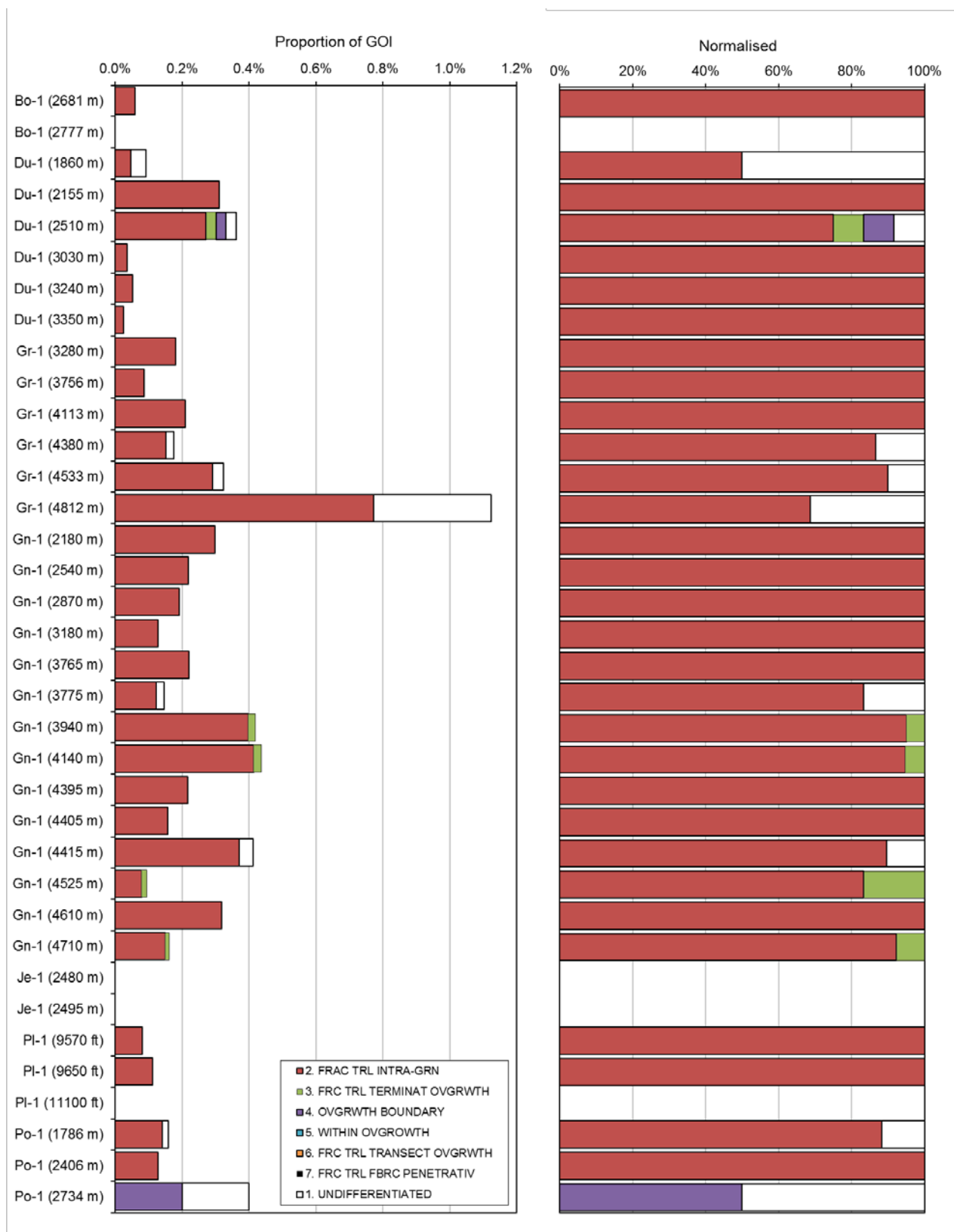


Figure 24: Bar chart of OIA locations—all samples. For oil-bearing inclusions counted in GOI only. Well annotations shortened to first two letters of name. Depth = base of cuttings interval.

Gnarlyknots-1A

Hydrocarbon assemblages from Gnarlyknots-1A are located, almost exclusively, along unconstrained healed micro-fractures in detrital quartz (Figure 25A; Figure 26A, B). Some fractures in each of the samples from 3,930-40 m, 4,135-40 m, 4,520-25 m and 4,705-10 m do, however, show evidence for termination at the quartz overgrowth boundary (Figure 26C). This suggests that some oil was trapped in fractures before significant quartz cementation. In the 4,410-15 m sample for PVTx and gas isotope analysis, and the larger interval for MCI, oil inclusion assemblages were recorded only in unconstrained diagenetic fractures within quartz (Figure 25B, C).

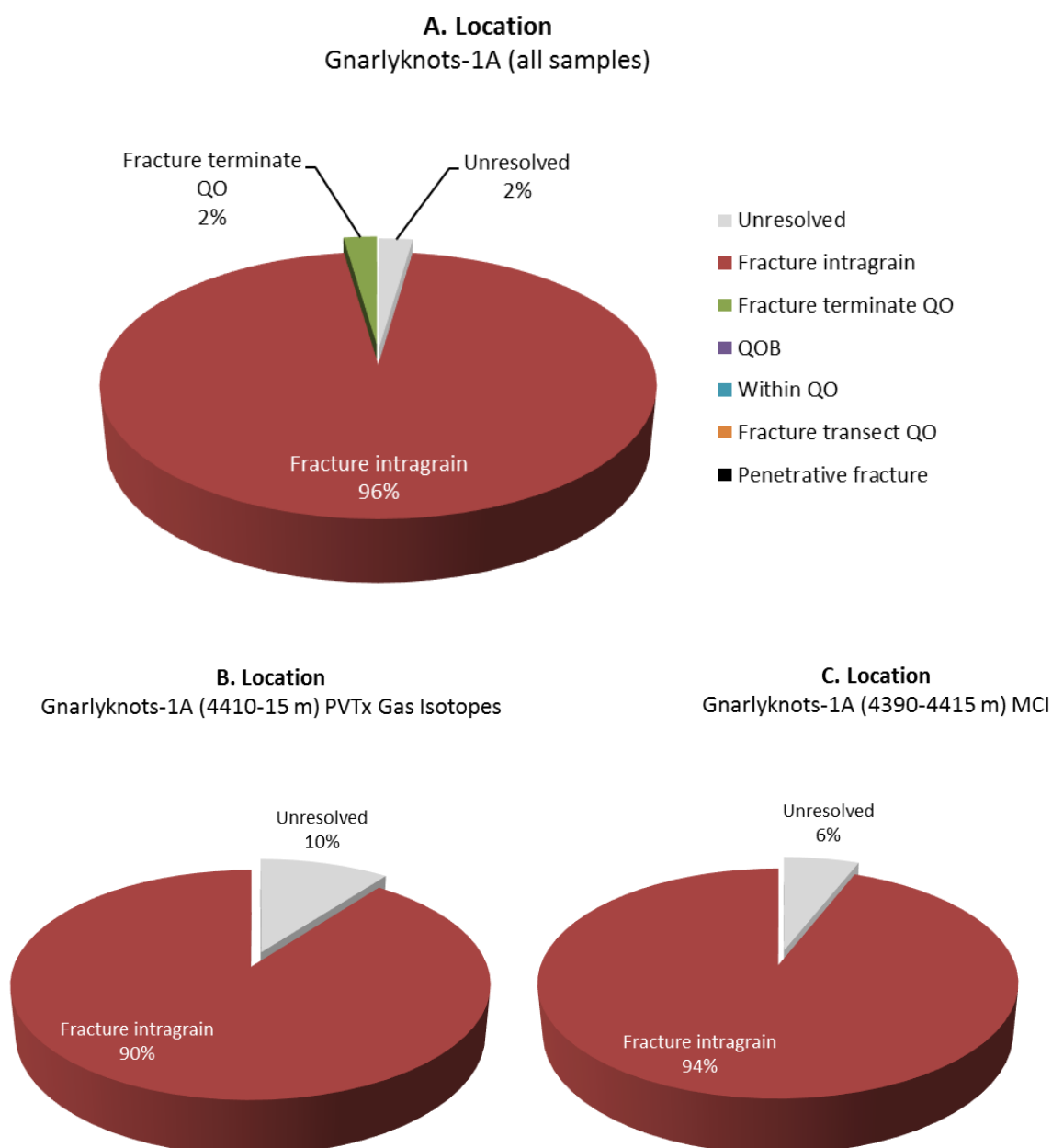


Figure 25: Pie charts of OIA location—Gnarlyknots-1A.

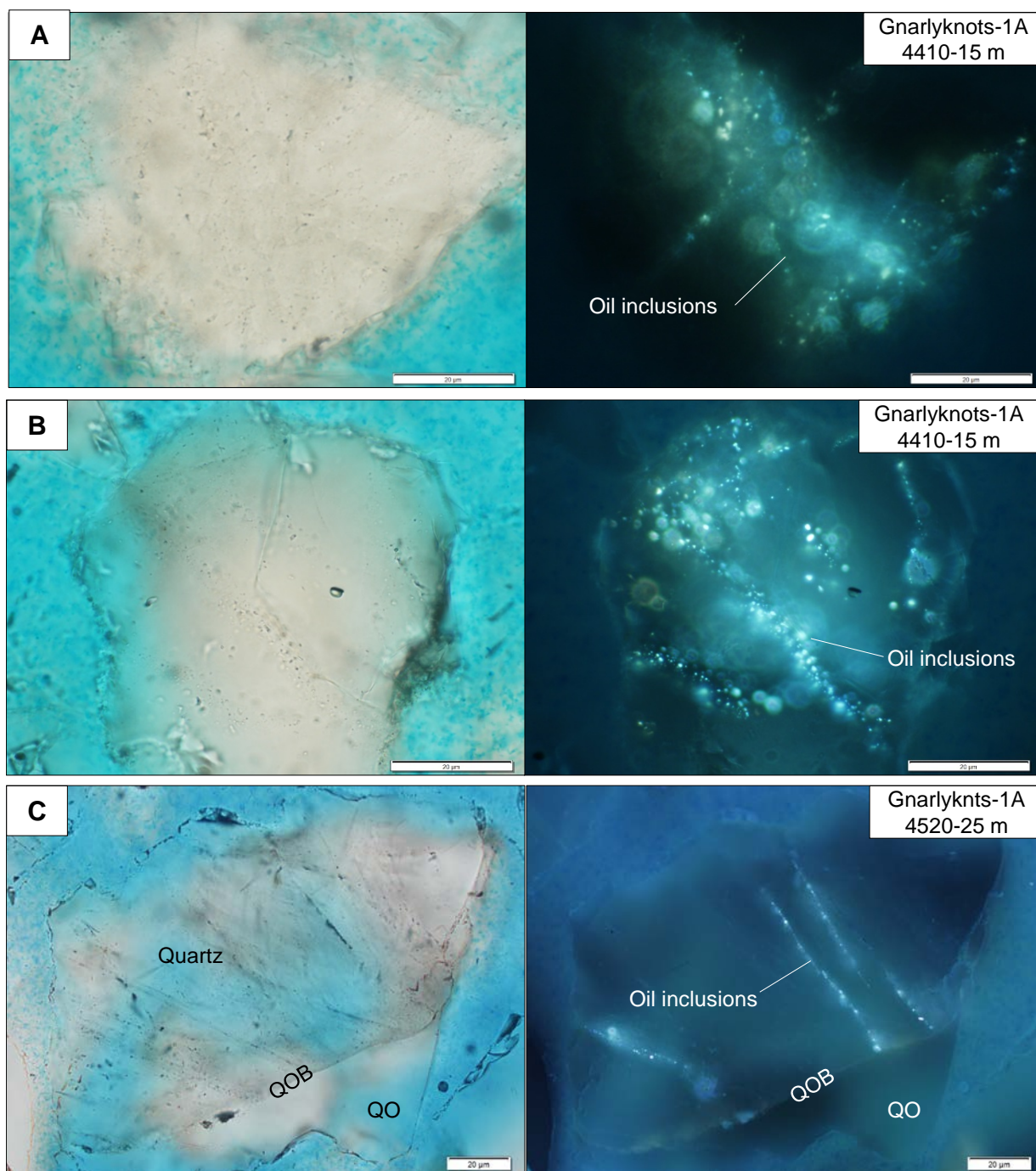


Figure 26: Oil-bearing inclusions in Gnarlyknots-1A. (A-B) diagenetic fractures within quartz and, (C) diagenetic fractures showing termination at the quartz overgrowth boundary (QOB). Paired transmitted light (top) and UV illumination (bottom) photomicrographs.

Greenly-1

Hydrocarbon assemblages from Greenly-1, that are counted in GOI, are all located along unconstrained healed micro-fractures in detrital quartz (Figure 27A; Figure 28A). In the 4,809-12 m sample for PVTx and MCI analysis the same is true, but a higher proportion are in unresolved locations. This was because there was some difficulty in resolving these from oil-bearing inclusions contained in carbonate cement that were not included in the GOI count.

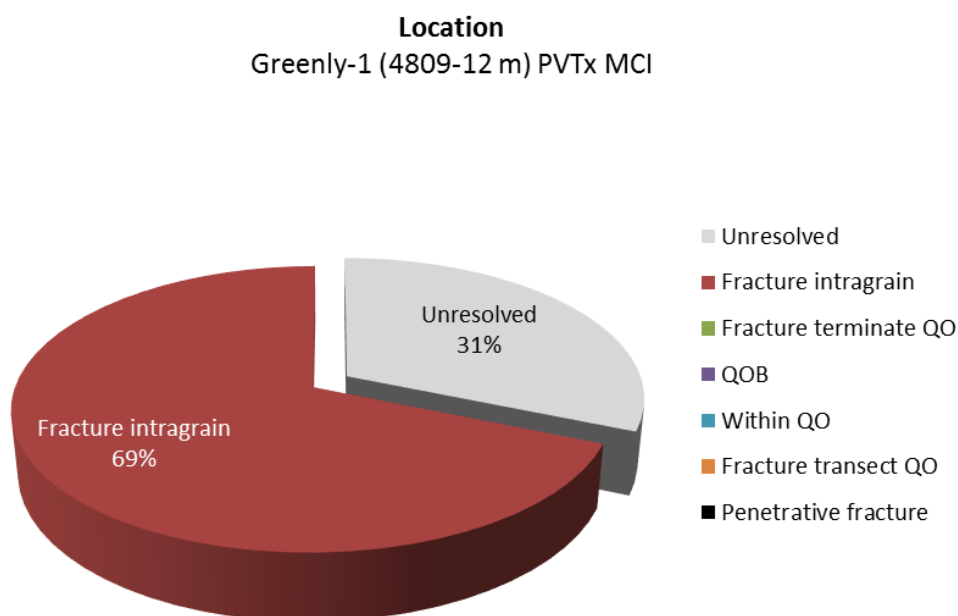
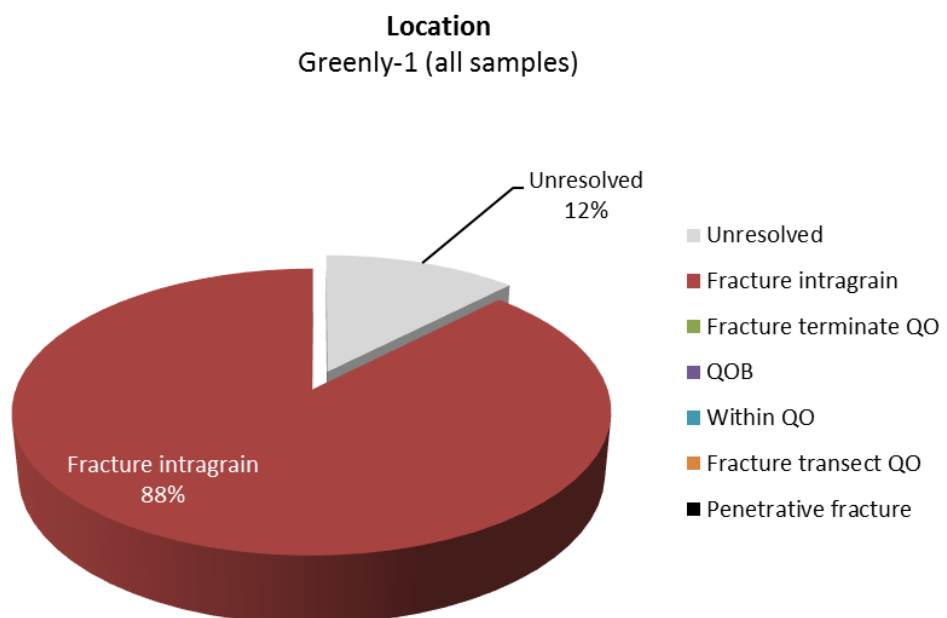


Figure 27: Pie charts of OIA location—Greenly-1.

Oil-bearing inclusions in carbonate cement

A significant number of oil inclusion assemblages are hosted by carbonate cement, in addition to quartz, in the 4,809-12 m sample from Greenly-1. Similar occurrences were also noted by Lisk et al (2001) in the 4,161-64 m and 4,812-15 m samples from Greenly-1 and the 3,730-33 m and 3,859-62 m samples from Platypus-1 (Table 2). The fluorescence colour and inclusion descriptions are the same as those trapped in quartz, and this implies a similar timing and composition. The oil inclusions appear to be trapped in pore-filling carbonate cements between detrital grains (Figure 28B) and filling voids after the dissolution of grains (Figure 28C). They are not so common in brownish isopachous (early) cement (siderite?).

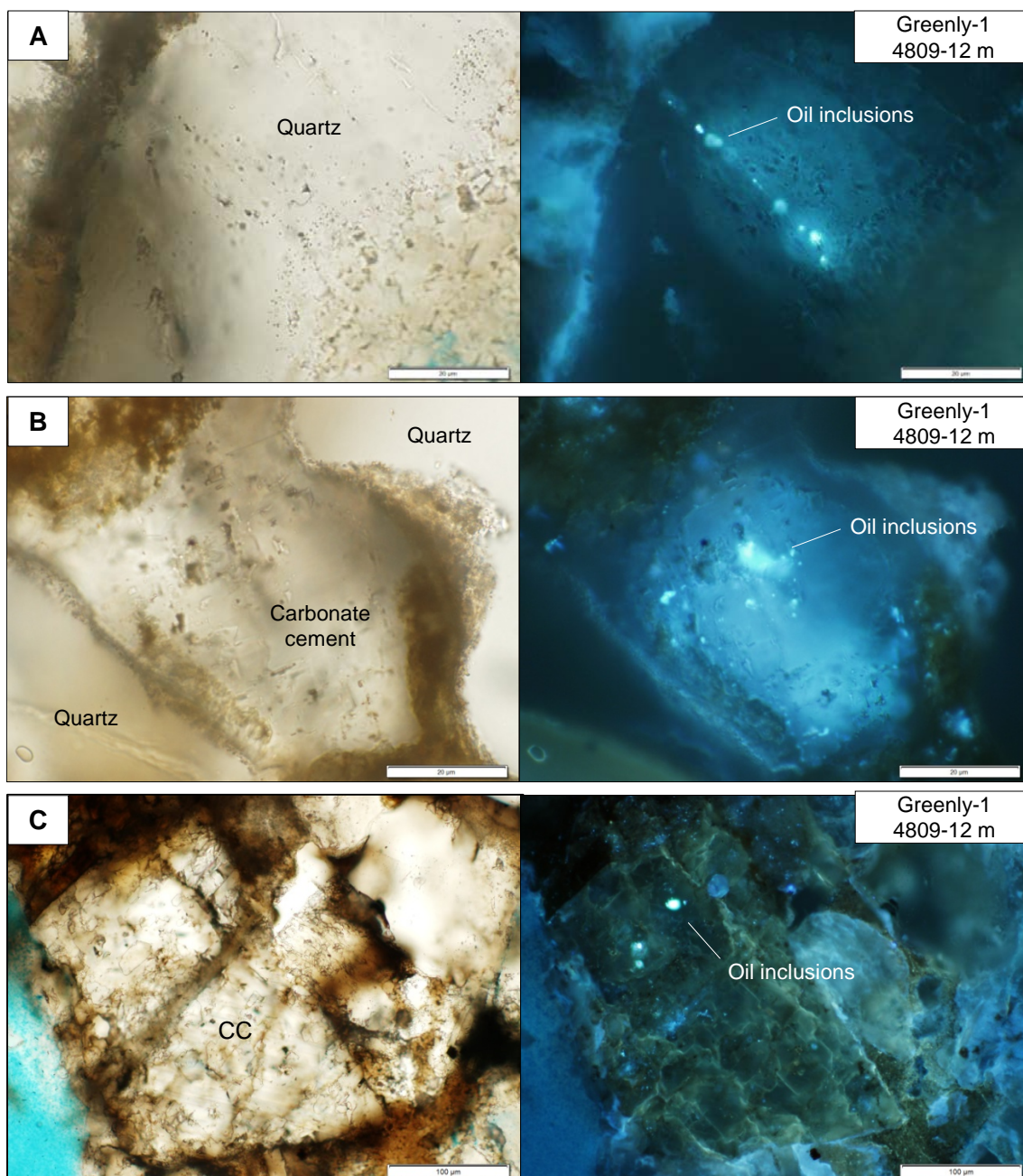


Figure 28: Oil-bearing inclusions in Greenly-1. (A) diagenetic fractures with unconstrained location in quartz, (B) pore-filling cement between grains and (C) pore-filling cement filling voids after dissolution of grains?

Duntroon-1

Hydrocarbon assemblages from Duntroon-1 are located, almost exclusively, along unconstrained healed micro-fractures in detrital quartz (Figure 29; Figure 25A). Some fractures of these fractures in the 2,505-10 m PVTx sample show evidence for termination at the quartz overgrowth boundary (Figure 29B). Oil inclusions were also noted at trace abundance at the quartz overgrowth boundary. Together this suggests that some oil was trapped before significant quartz cementation.

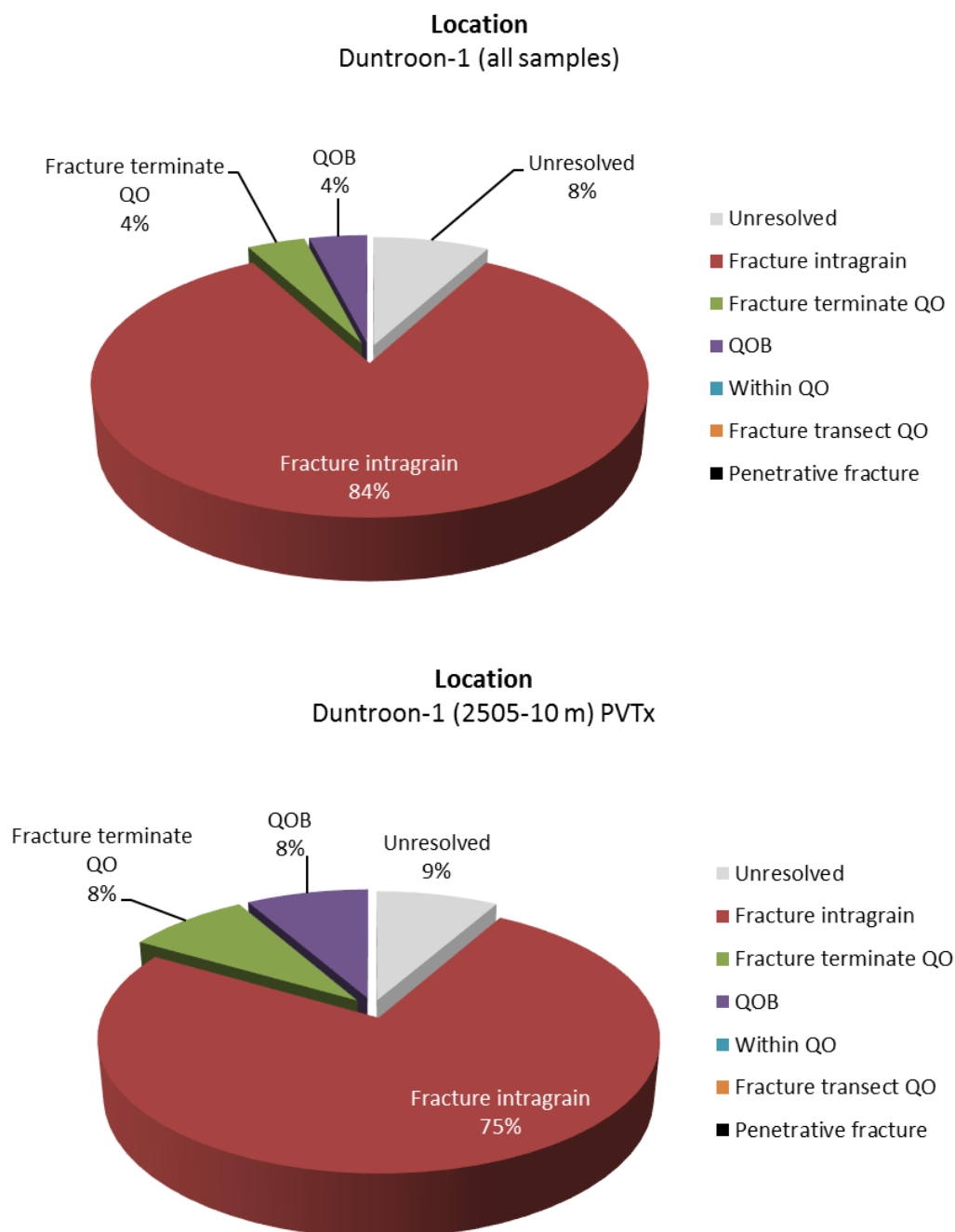


Figure 29: Pie charts of OIA location–Duntroon-1.

Potoroo-1

Hydrocarbon assemblages from Potoroo-1, including the PVTx sample at 1,778-86 m, are located along unconstrained healed micro-fractures in detrital quartz, (Figure 30 and Figure 25A, B). Oil inclusion assemblages were also noted at trace abundance at the quartz overgrowth boundary in the deeper 2,730-34 m sample however, given the low grains with oil inclusions count, this is statistically insignificant.

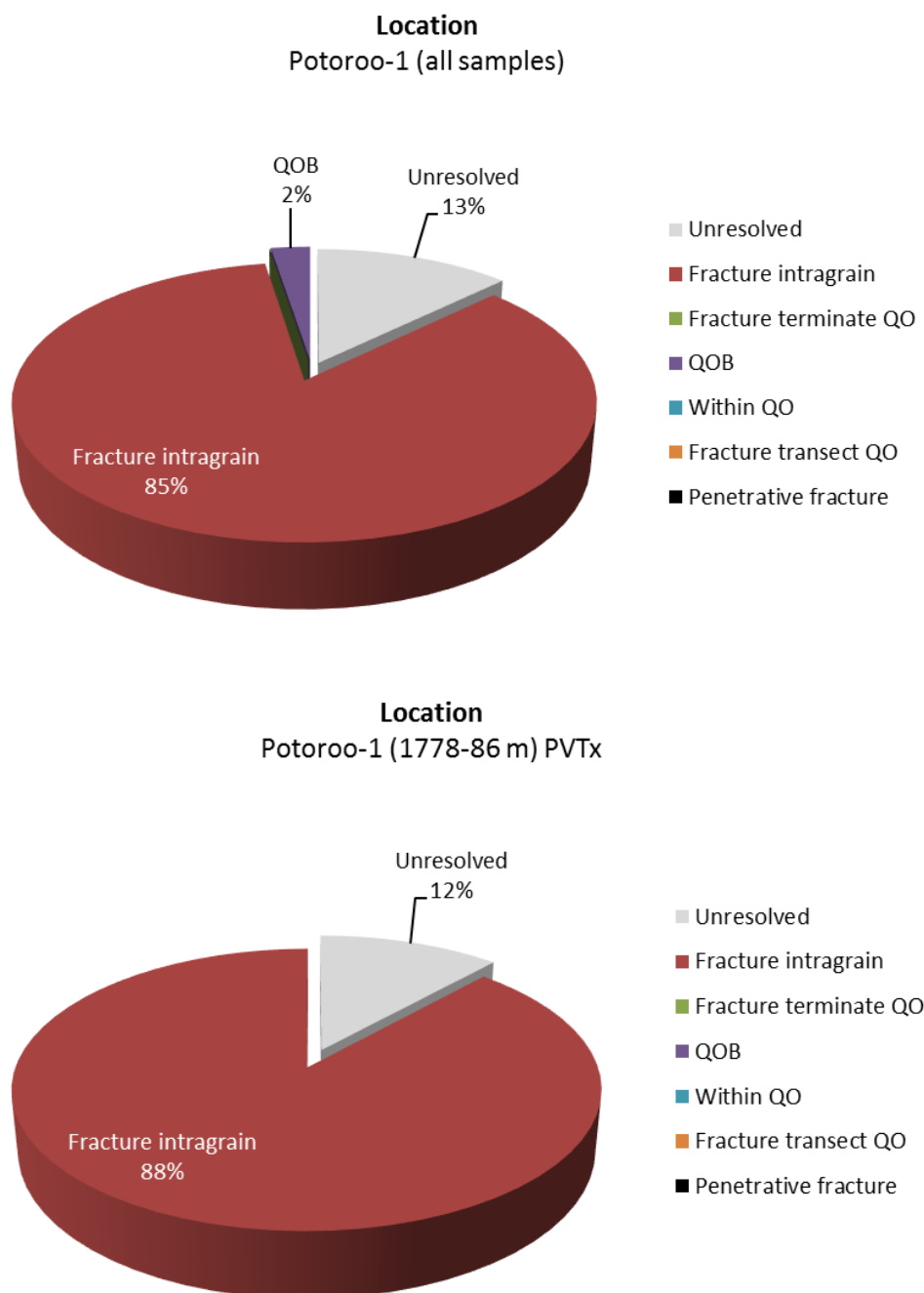


Figure 30: Pie charts of OIA location–Potoroo-1.

Bubble Size and Variance

Oil inclusion assemblages are described according to the size of the vapour bubble and the variability. Oil inclusion assemblages with a vapour bubble that occupies less than 50% of the volume at room temperature (Small; SM) are differentiated from oil- inclusions where the vapour bubble is greater than 50% of the volume of the inclusion (large; LR or LRG). Assemblages with the same fluorescence colour and uniform or small variance (SV) are differentiated from those with variable vapour bubble size (VAR) or where the vapour bubble shows co-variance with (fluorescence) colour (COVAR). Inclusion assemblages where variance could not be observed are termed indeterminate (INDET). This is usually the case where two or less inclusions are observed in any given assemblage.

1. SMBUBL SMLVAR; 2. LRBUBL SMLVAR; 3. LRG VAR; 4. COVAR COL; 5. INDETERMINATE

The dominant type of oil-bearing assemblage recorded in the GOI counts are those with a small vapour bubbles at room temperature and little variance in their bubble size (Table 8; Figure 31; Figure 32). While mostly small, the vapour bubbles (<50% the size of the inclusion) are likely to homogenise into the liquid phase at reservoir conditions and were likely trapped as oil.

Although less common, inclusion assemblages with large vapour bubbles and small variance are likely to homogenise into the vapour phase at reservoir conditions and were probably trapped as gas-condensate. The condensate being the thin rim of fluorescing oil that surrounds the vapour bubbles at room temperature.

Assemblages with large variance in vapour fraction are more common in Duntroon-1 than other wells and, together with those that co-vary with colour, suggest that both oil (residual?) and gas were in the pore space at the time of trapping.

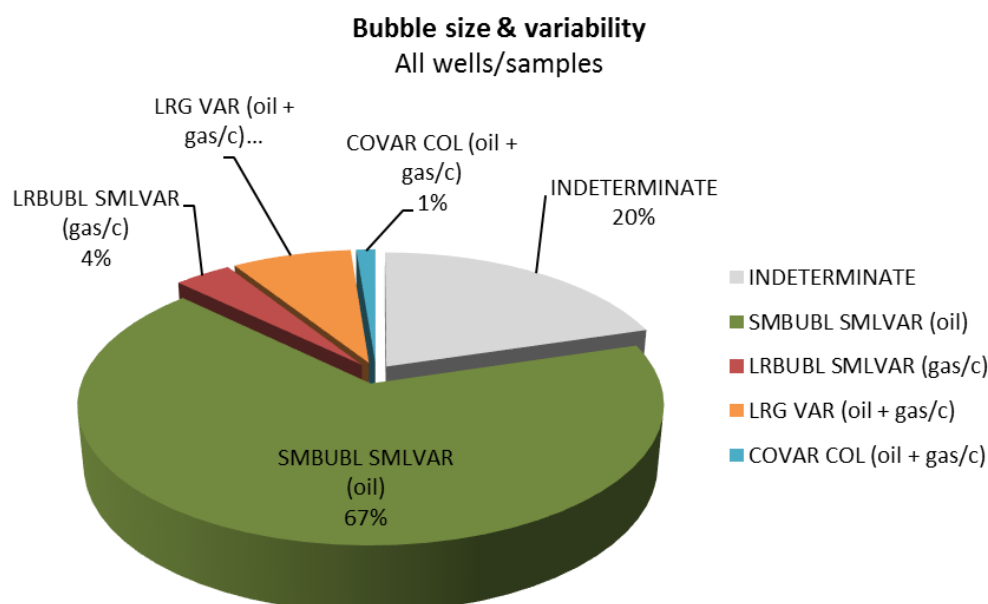






Figure 31: Pie chart of OIA bubble size and variability—all samples.

Table 8: OIA bubble size and variability-all samples.

CSIRO NO.	DEPTH METRES (MDRT)	1. SMBUBLSV 	2. LRBUBLSV 	3. LRG VAR 	4. COVAR COL 	5. INDET
Borda-1	2678-81 m	3	1	-	-	-
Borda-1	2774-77 m	-	-	-	-	-
Duntroon-1	1855-60 m	1	-	-	-	1
Duntroon-1	2150-55 m	3	1	3	-	-
Duntroon-1	2505-10 m	8	2	2	-	-
Duntroon-1	3025-30 m	-	-	1	-	-
Duntroon-1	3235-40 m	2	-	-	-	-
Duntroon-1	3345-50 m	1	-	-	-	-
Greenly-1	3275-80 m	3	-	2	-	1
Greenly-1	3753-56 m	2	-	-	-	-
Greenly-1	4110-13 m	10	-	-	1	3
Greenly-1	4377-80 m	11	-	-	-	4
Greenly-1	4530-33 m	13	-	2	-	5
Greenly-1	4809-12 m	14	-	-	-	2
Gnarlyknots-1A	2170-80 m	8	1	-	-	1
Gnarlyknots-1A	2535-40 m	4	1	1	-	2
Gnarlyknots-1A	2865-70 m	4	-	1	-	2
Gnarlyknots-1A	3175-80 m	5	-	-	-	-
Gnarlyknots-1A	3760-65 m	6	-	2	2	1
Gnarlyknots-1A	3770-75 m	5	-	1	-	-
Gnarlyknots-1A	3930-40 m	13	-	-	-	7
Gnarlyknots-1A	4135-40 m	13	1	1	-	4
Gnarlyknots-1A	4390-95 m	6	-	2	-	1
Gnarlyknots-1A	4400-05 m	7	1	2	-	2
Gnarlyknots-1A	4410-15 m	13	1	4	-	11
Gnarlyknots-1A	4520-25 m	4	-	-	-	2
Gnarlyknots-1A	4605-10 m	15	1	-	-	3
Gnarlyknots-1A	4705-10 m	8	-	1	-	4
Jerboa-1	2470-80 m	-	-	-	-	-
Jerboa-1	2490-95 m	-	-	-	-	-
Platypus-1	9560-70 ft	2	-	-	-	1
Platypus-1	9640-50 ft	3	-	-	-	-
Platypus-1	11090-100 ft	-	-	-	-	-
Potoroo-1	1778-86 m	25	2	1	1	5
Potoroo-1	2398-06 m	2	-	-	-	1
Potoroo-1	2730-34 m	-	-	-	-	2

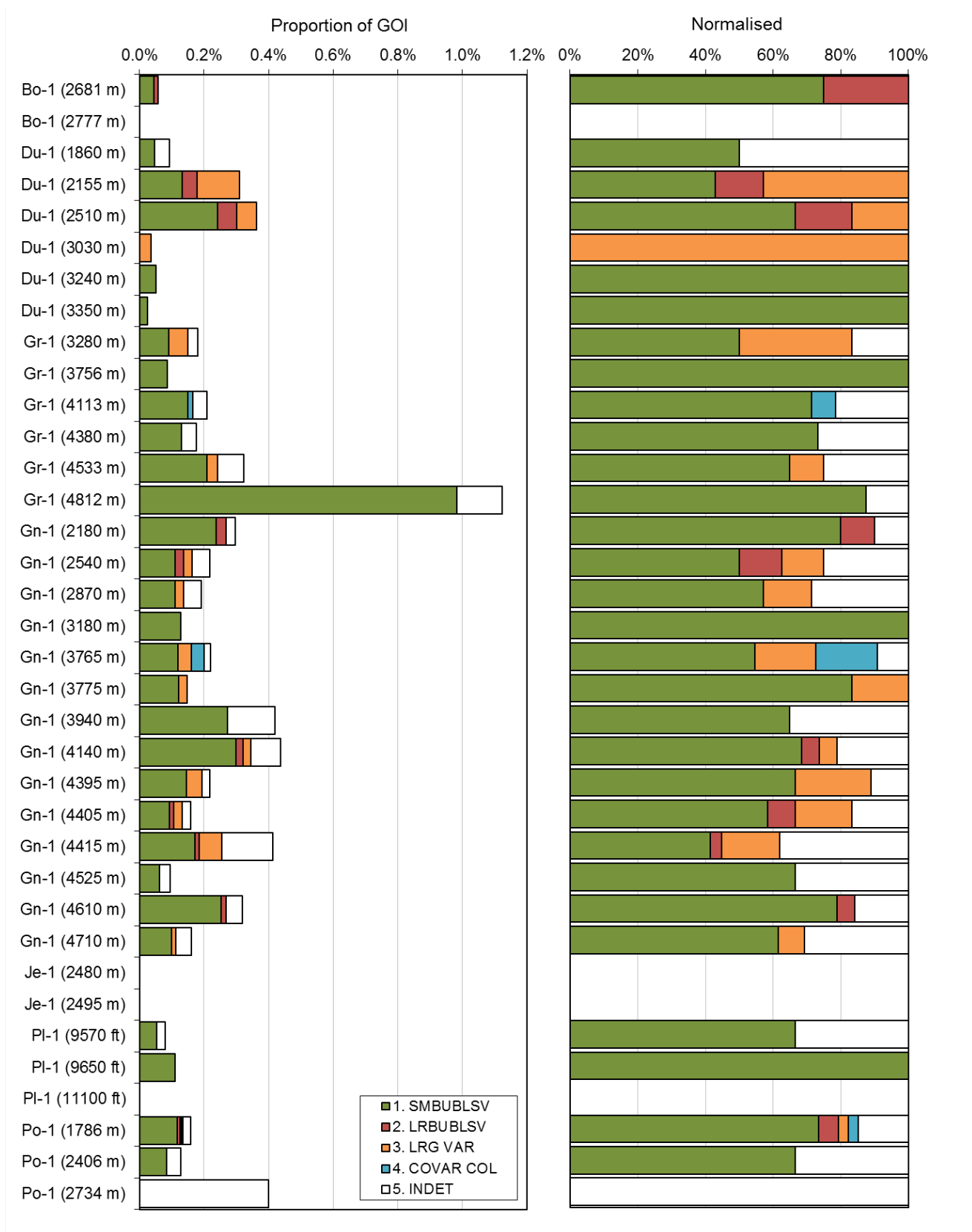


Figure 32: Bar chart of OIA bubble size and variability-all samples. For oil-bearing inclusions counted in GOI only. Well annotations shortened to first two letters of name. Depth = base of cuttings interval.

Gnarlyknots-1A

Hydrocarbon assemblages from Gnarlyknots-1A comprise mostly those with small vapour bubbles at room temperature and little variance in their bubble size and were trapped as oil (64%; Figure 33A). This is likely to be higher as most indeterminate assemblages (23%) are recorded as having small vapour bubbles in the oil inclusion description (Figure 13A). In addition, there are small numbers of assemblages with large, uniform vapour bubbles that were trapped as gas-condensate (3%) and those with large variance that trapped both oil and gas (10%, including those that co-vary with colour). In the 4,410-15 m sample for PVTx and gas isotope analysis, and the larger interval for MCI, the bubble size and variability of the oil inclusion assemblages are essentially the same (Figure 33B, C).

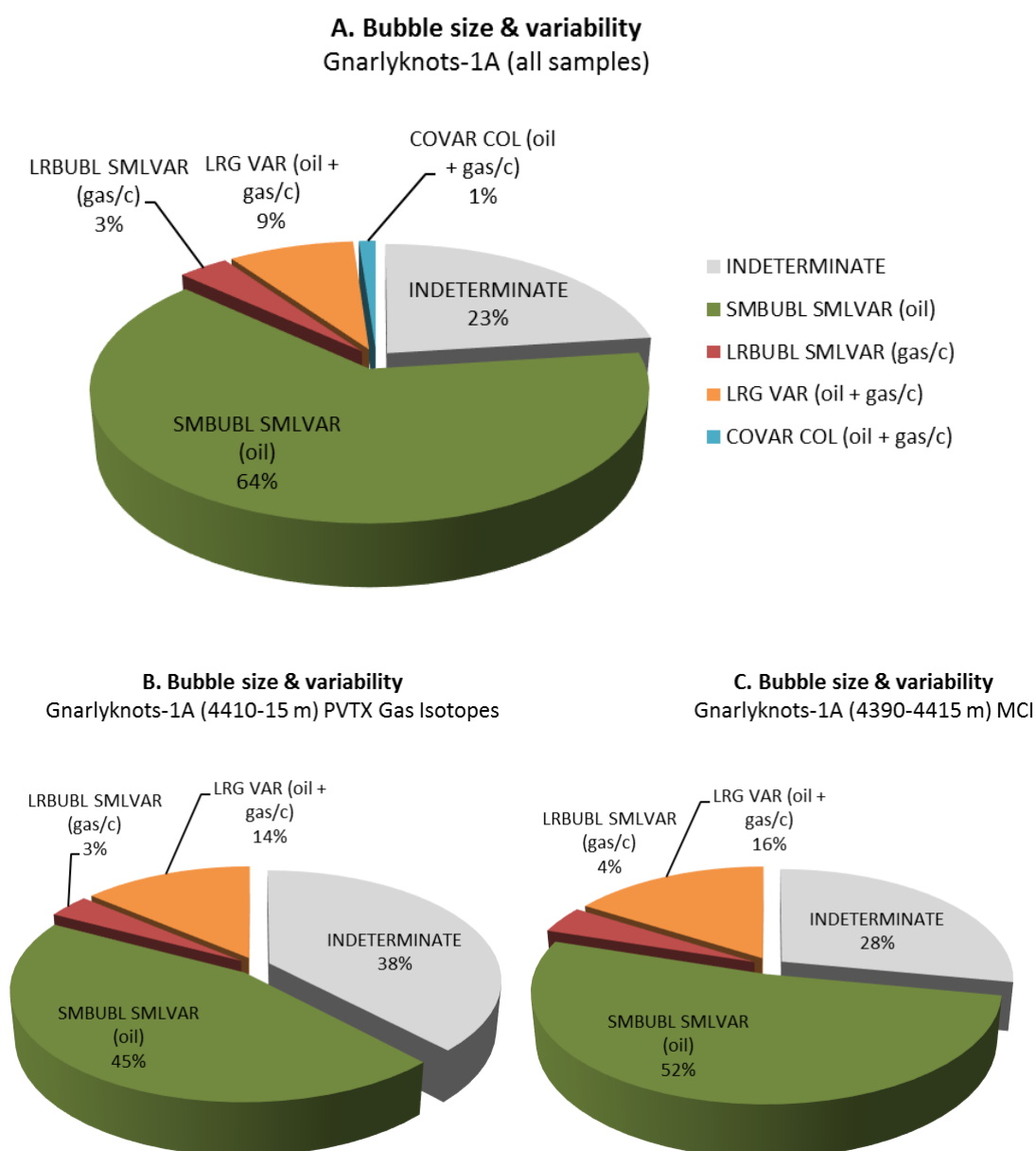


Figure 33: Pie charts of OIA bubble size and variability—Gnarlyknots-1A.

Greenly-1

Hydrocarbon assemblages from Greenly-1 comprise mostly those with small vapour bubbles at room temperature and little variance in their bubble size and were trapped as oil (73%; Figure 34A). This is likely to be higher as most indeterminate assemblages (21%) are recorded as having small vapour bubbles in the oil inclusion description (Figure 14A). Assemblages with large, uniform vapour bubbles (gas-condensate) are absent and only a few occurrences of those with large variance, that trapped both oil and gas, are recorded (6%, including those that co-vary with colour). In the 4,809-12 m sample for PVTx and MCI, the assemblages only comprise with those that trapped oil with small bubble size and variability (Figure 34B).

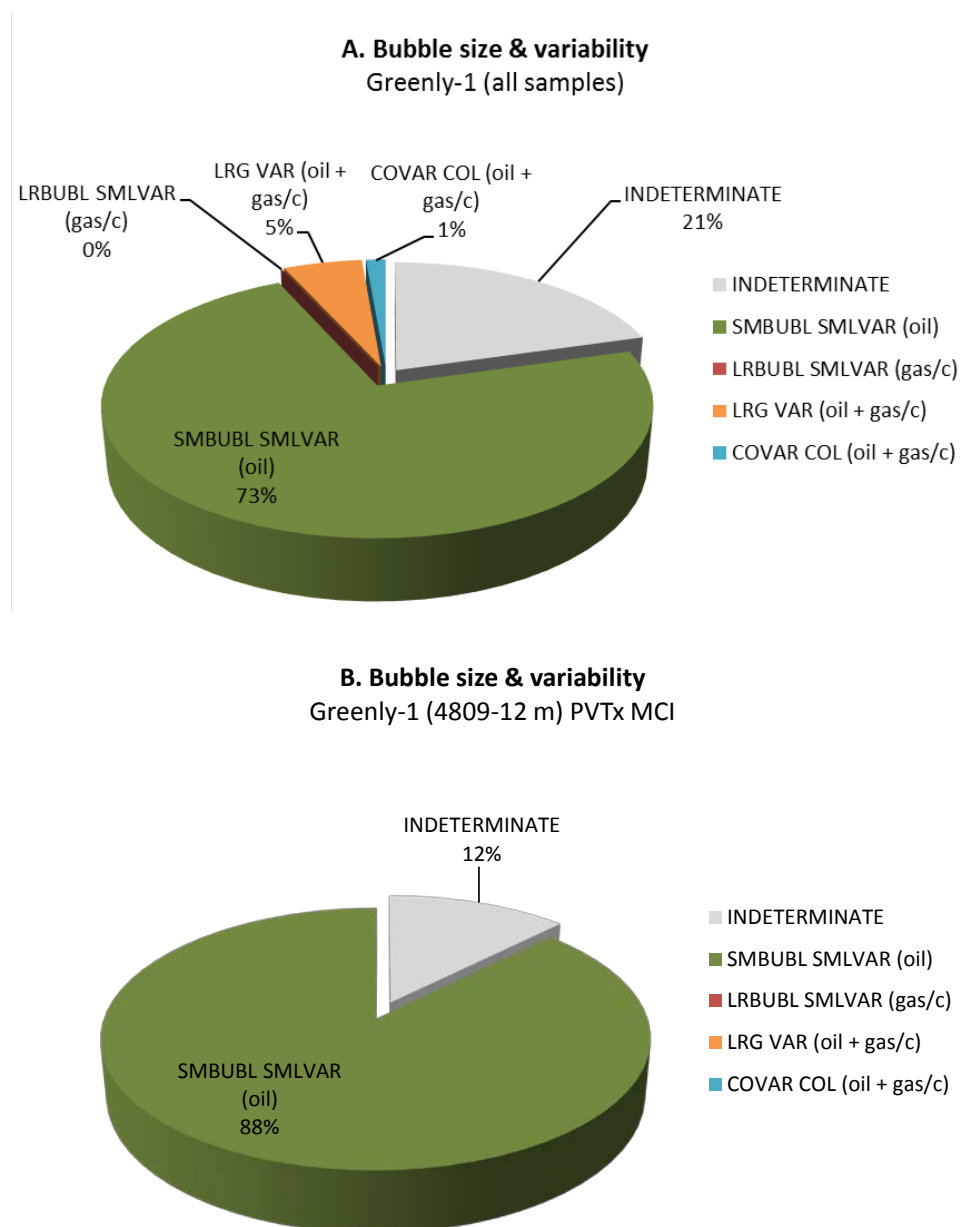


Figure 34: Pie charts of OIA bubble size and variability—Greenly-1.

Duntroon-1

Hydrocarbon assemblages from Duntroon-1 are the most variable of the study. They comprise those that were trapped as oil, with small vapour bubbles at room temperature and little variance in their bubble size (62%; Figure 35A), together with a significant proportion that trapped gas. Assemblages with large, uniform vapour bubbles (13%; gas-condensate) are significant, together with those that trapped both oil and gas with large variance in vapour bubble size (21%). In the 2,505-10 m sample for PVTx analysis, the assemblages proportions are essentially the same with about a quarter trapping gas (27% Figure 35B).

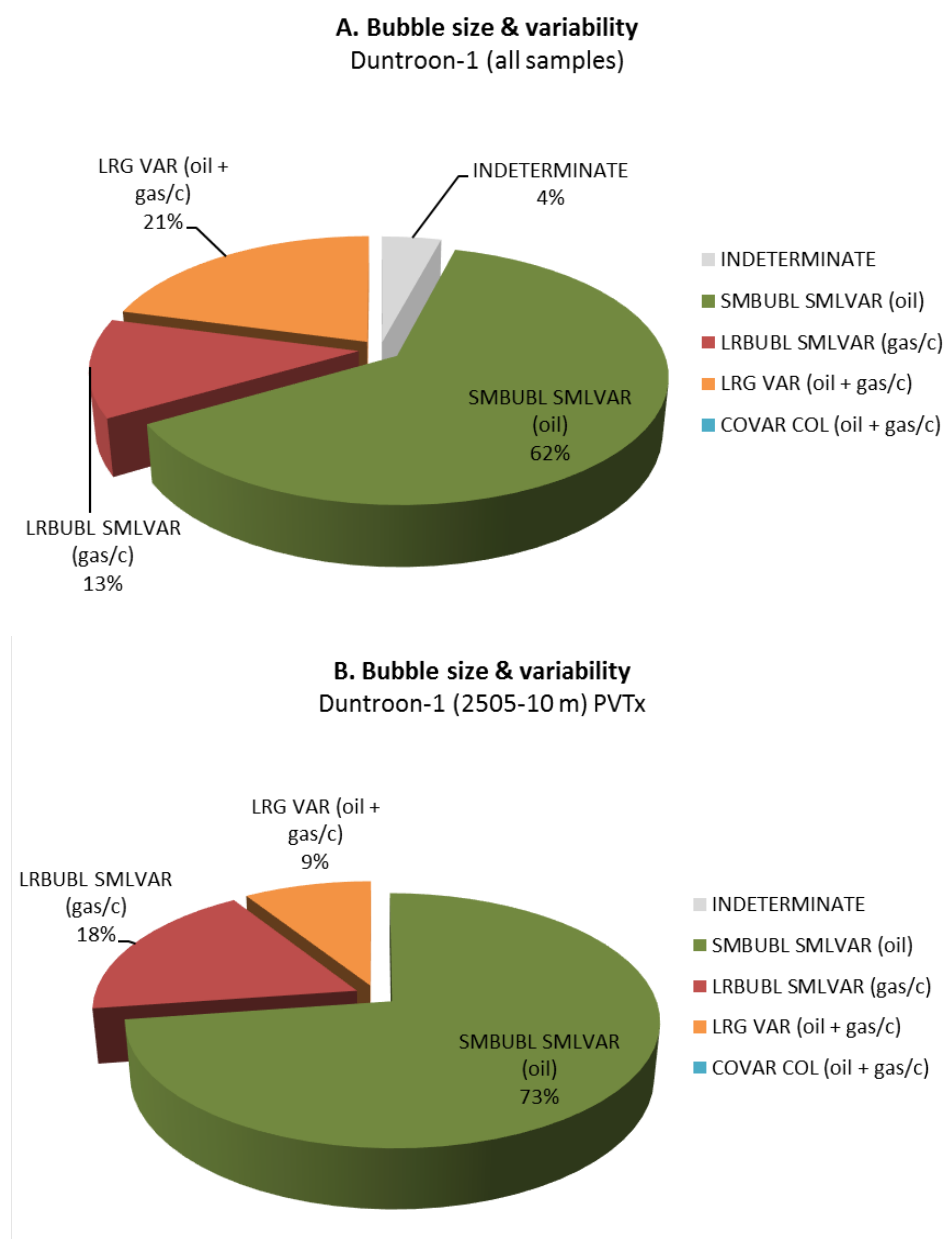


Figure 35: Pie charts of OIA bubble size and variability–Duntroon-1.

Potoroo-1

Hydrocarbon assemblages from Potoroo-1 comprise mostly those with small vapour bubbles at room temperature and little variance in their bubble size and were trapped as oil (69%; Figure 36A). This is likely to be higher as most indeterminate assemblages (20%) are recorded as having small vapour bubbles in the oil inclusion description (Figure 16A). Assemblages that trapped gas and gas-condensate (with both large and variable vapour bubbles) account for only 11% off the assemblage types. In the 1,778-86 m sample for PVTx analysis, the assemblages proportions are essentially the same with oil being the dominant phase trapped (Figure 36B).

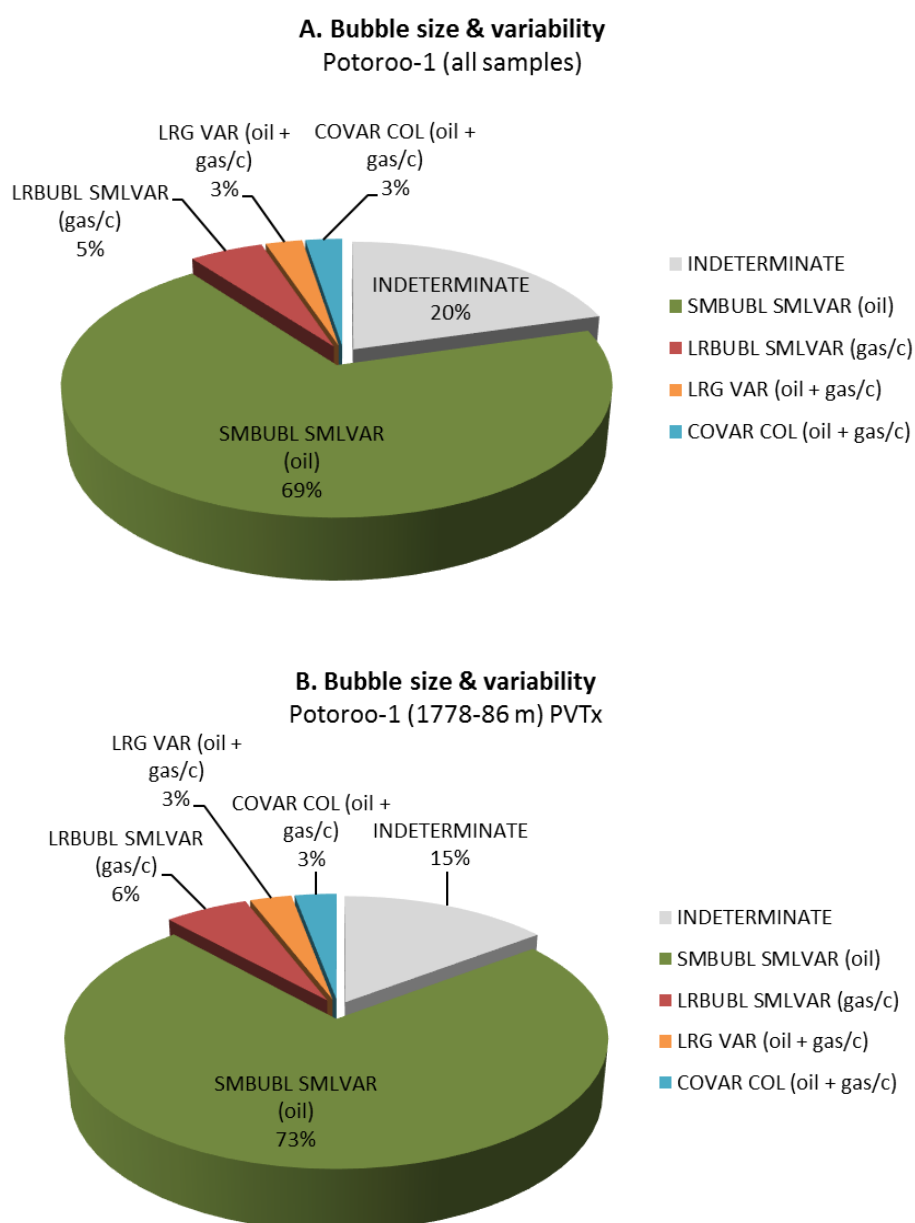


Figure 36: Pie charts of OIA bubble size and variability–Potoroo-1.

DISCUSSION

Interpreting Palaeo-Oil Saturation from GOI Data

Palaeo-oil zones can be mapped using the GOI™ (Grains containing Oil Inclusions) technique (Eadington et al., 1996). GOI values in producing oil zones vary widely from <0.1% to about 95% (Figure 37). Samples with GOI values >5% are only from producing oil zones, from palaeo-oil zones recognised by solid fluorescence, or from locations that can reasonably be expected to have been in closure. Such GOI data usually show stratification that reflects buoyant confinement of oil. GOI values >5% have not been measured in samples where closure and high oil saturation are unlikely to have occurred. Consequently GOI values >5% can be readily identified as palaeo-oil zone by empirical comparison.

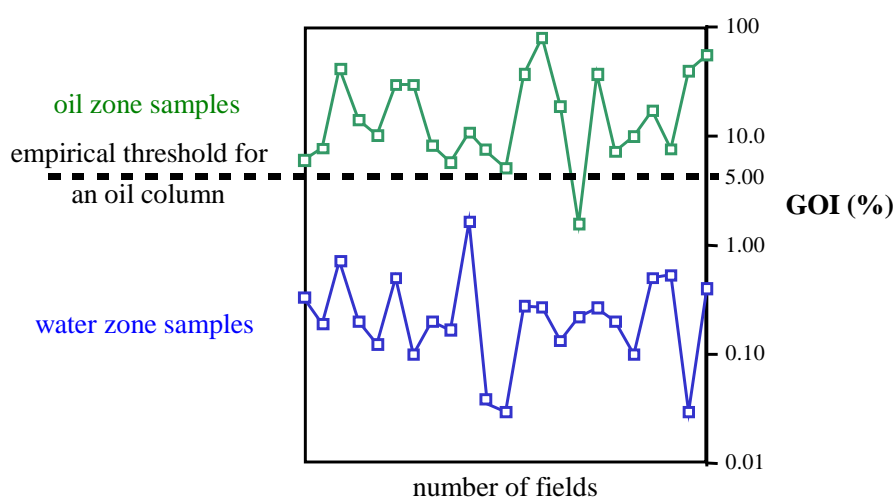


Figure 37 GOI values recorded in oil and water legs from selected oilfields in Australasia

Each point represents an oil field with the highest value in oil zone and water zone reported

GOI values <5% also occur in current oil zones and the reverse logic that they indicate there was no palaeo-oil zone is not valid. GOI values <5% may result from:

1. fluid inclusions having formed before or after the residence time of oil,
2. fluid inclusion trapping sites having formed at low frequency in the presence of oil,
3. the presence of fine grained minerals increasing the displacement pressure (i.e. poor reservoir quality),
4. low buoyancy pressure at the base of the oil zone or migration pathway, or
5. dilution where a cuttings interval brackets a palaeo oil-water contact (palaeo-OWC) or inferred palaeo gas-oil contact (palaeo-GOC).

The GOI method does not readily detect gas–condensate or other hydrocarbon inclusions if they are non-fluorescent at optical wavelengths.

Factors Affecting GOI Interpretation

Interpretation of GOI data should be informed both by the quality of porosity and permeability in the reservoir and by the abundance of trapping sites for diagenetic fluid inclusions in the grains. Rock-type has a significant effect on GOI because capillary pressures in shale, claystone and siltstone may be too high for oil to migrate through the pore network. Rocks of these types are not regarded as good tests of palaeo-oil saturation and typically yield low GOI.

In sandstones, sites for the formation of fluid inclusions, including those that trap oil, commonly include diagenetic fractures in detrital grains and in cements, such as quartz and carbonate. GOI refers to the time at which fluid inclusions formed in these locations. Typically, diagenetic fractures form within detrital grains due to mechanical compaction as a result of burial. During the early stages of burial the principal process of compaction is probably the rearrangement and packing of grains (i.e. grain boundary slip), while at later stages the physical strain at grain contacts is accommodated by brittle deformation and the formation of diagenetic fractures. The common observation in cemented sandstones of intra-grain fractures terminating at grain boundaries suggests that crystallisation of cement (particularly quartz) slows the formation of diagenetic fractures. In sandstones from different localities, ages and burial histories, the temperatures for the onset of quartz cementation, deduced from grain-boundary fluid inclusions, is highly variable but usually within the 60-150°C range (Walderhaug, 1994).

Where trapping sites for fluid inclusions formed at low frequency or were absent, then palaeo-oil saturation may remain equivocal because there is uncertainty about what constrained the abundance of inclusions (the lack of trapping sites or oil saturation). Thus palaeo-oil may remain undetected by fluid-inclusion-based methods if the trapping sites formed before or after the residence time of oil or at low frequency in the presence of oil. The GOI method may not detect gas or other hydrocarbon inclusions if they are non-fluorescent at optical wavelengths.

Implications for trapping sites in the Bight Basin

Quartz cement is not well developed in the samples studied for GOI. This is because, even at depths approaching 4 km (e.g. Gnarlyknots-1A), the temperatures are not sufficiently elevated to promote significant amounts of quartz cementation. As a consequence, the trapping sites for fluid inclusions in diagenetic fractures probably formed over a more extended period of time in the Bight Basin compared to many other basins. In the Vulcan Sub-basin, for instance, quartz cement is a common site for trapping of oil inclusions and the frequency of diagenetic fracture formation was subsequently impacted by this cementation phase.

As a consequence, most of the oil and gas-bearing inclusion assemblages identified in this study are located in diagenetic fractures in quartz. The exception being those that also occur in carbonate cement in Greenly-1.

Gnarlyknots-1A

Operator	Woodside	Date spud	20 April 2003
Type	Exploration	Rig release	29 May 2003
Status	P & A - dry	KB/RT datum (m)	25.1
Sub-basin	Ceduna	Water depth (m)	1316
		TD (m)	4736
Structural style	Fault block with low relief 4-way dip closure at primary objective		
Target horizon(s)	Primary: "intra-Santonian" (post-drill Coniacian) – Tiger Supersequence Secondary: near-top Santonian – Tiger Supersequence Secondary (not penetrated and undated): top Coniacian, top Turonian, top Cenomanian)		
Cause of failure	Failure to encounter hydrocarbons is attributed to the well being drilled outside any fault independent closure and the absence of valid fault seal on the northern bounding fault. The sand content was higher than predicted and too high to form adequate cross-fault seal – either by fault gauge and juxtaposition of sealing units – at both the primary and secondary objective levels.		

Palaeo-oil saturation, as measured by GOI, is low in Gnarlyknots-1A. There is no positive evidence for saturations consistent with a palaeo-oil zone. Oil-bearing inclusion assemblages were, however, recorded in all samples from the Tiger and Hammerhead supersequences and with all GOI <0.4% (Figure 38). At these abundances the GOI indicate low level oil and gas-condensate saturation in water-bearing rock by reference to Figure 37. While in-situ generation of hydrocarbons from sample depths below the top oil window at 4,100 mMD (Gnarlyknots-1A Well Completion Report) is a possibility, the rocks are only marginally mature at total depth and the maturation gradient is clearly low. This indicates that the rate of maturation would have been low and the presence of oil inclusion assemblages throughout Gnarlyknots-1A is good evidence for hydrocarbon migration over multiple depth intervals of the well.

The intra-Santonian primary objective (post-drill dated as top Coniacian), tested by three samples, contains a statistically significant number of grains with oil inclusions (Figure 9), comprising both oil and gas-condensate (Figure 13; Figure 33). This correlates with a methane-depleted wet gas to gas-condensate FIS response over this same interval (Tapley, 2005) and was the focus for further PVTx and MCI geochemistry presented in this report. Other intervals in the Tiger Supersequence contain similarly moderate to significant numbers of grains with oil inclusions, while those in the overlying Hammerhead Supersequence (post-break-up sequence) generally contain lower numbers. The migration signature in Gnarlyknots-1A, therefore, appears to increase in intensity with depth.

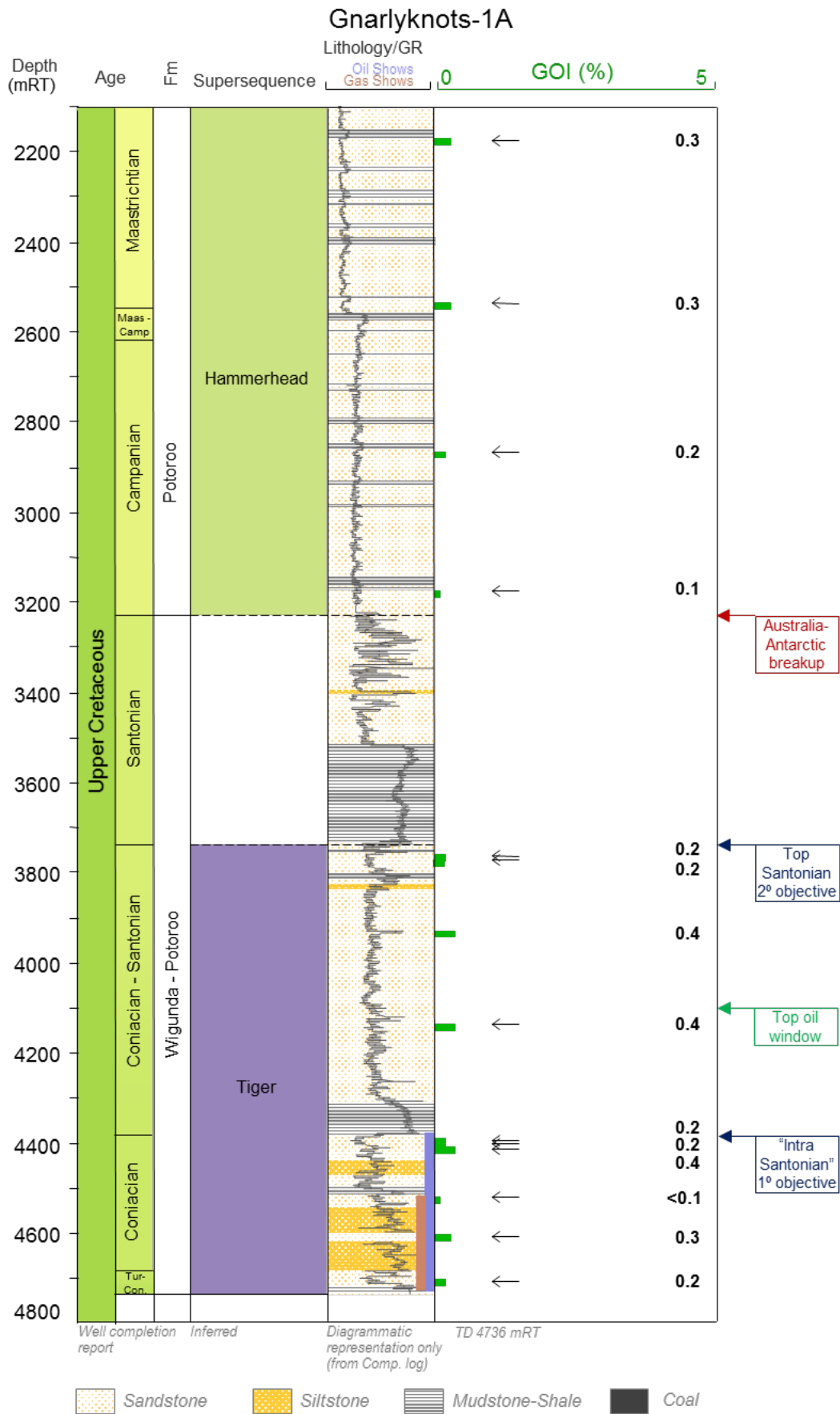


Figure 38: GOI log – Gnarlyknots-1A.

Greenly-1

Operator	BHP Petroleum	Date spud	04 June 1993
Type	Exploration	Rig release	14 August 1993
Status	P & A - dry	KB (m)	25
Sub-basin	Ceduna	Water depth (m)	156.1
		TD (m)	4860
Structural style	Fault block (low side)		
Target horizon(s)	Primary: basal sandstone of the Wigunda Formation (Wombat Sandstone) – White Pointer Supersequence.		
Cause of failure	Invalid test: The most likely cause of failure was a combination of poor reservoir quality and the lack of closure at the target horizon. The structural interpretation was in error and the well was drilled on the down-thrown block of a major fault. The target horizon was in excess of 2000 m deep to prognosis.		

Palaeo-oil saturation, as measured by GOI, is generally low in Greenly-1. There is no positive evidence for saturations consistent with a palaeo-oil zone. Together with previous GOI data of Lisk et al (2001), oil-bearing inclusion assemblages are recorded in all samples from the White Pointer and Tiger supersequences and in some samples from the Hammerhead Supersequences, with all GOI <1.1% (Figure 39). At these abundances the GOI indicate low level oil saturation in water-bearing rock by reference to Figure 37. The Tiger and White Pointer supersequences, at the base of the well, are mature below 3,405 mMD (VR 0.66%; Geoscience Australia, Petroleum Wells Database, 2017), so the presence of oil inclusions above this is good evidence for hydrocarbon migration. The possibility that some oil inclusions from below this depth might have arisen from in-situ generation cannot be discounted.

The Cenomanian Platypus Formation (White Pointer Supersequence), near the total depth of the well, was tested by two samples with anomalous GOI of 0.7% and 1.1%, comprising only oil (Figure 14; Figure 34). In addition, oil inclusions with similar physical properties were also noted in pore-filing carbonate cement (Figure 28B, C) which would only increase the inclusion abundances. Given the structural misinterpretation and lack of closure at the shallower target horizon, the GOI is, at a minimum, strong evidence for migration. The 4,809-12 m was selected for PVTx with PIT modelling indicating black oil was entrapped at very similar *PT* conditions (i.e. one event). There is then the possibility that the anomalous GOI might reflect lower oil saturations near the base of a small palaeo-oil column, however this remains speculative.

Other intervals in the White Pointer and basal Tiger supersequences have similarly strong evidence for migration, with GOI of 0.1% up to 0.6%. These are consistent with oil indications over this same general interval, from which oil was also recovered as a surface scum on water at 4,209 mMD (Table 1). Those intervals with the strongest oil indications tend to also have the higher oil inclusion abundances. The abundance of grains with oil inclusions generally decreases in samples above the oil window from the mid Tiger and Hammerhead supersequences. Like Gnarlyknots-1A, migration intensity therefore appears to increase with depth and presumed proximity to mature sources.

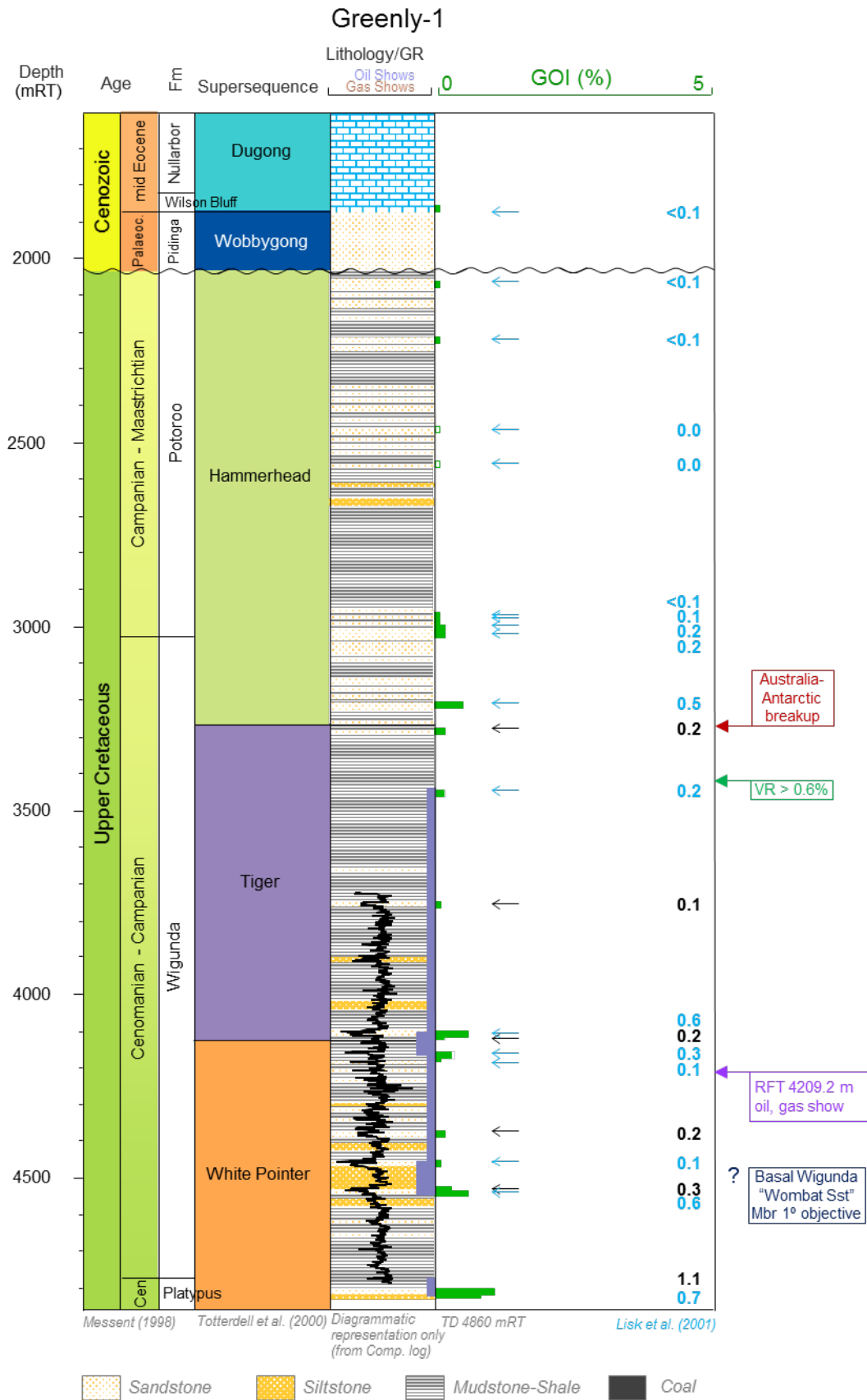


Figure 39: GOI log – Greenly-1.

Duntroon-1

Operator	BP Petroleum Dev Aust	Date spud	11 January 1986
Type	Exploration	Rig release	5 March 1986
Status	P & A - dry	KB/RT datum (m)	26.8
Sub-basin	Duntroon	Water depth (m)	144.0
		TD (m)	3515.6
Structural style	Tilted fault block		
Target horizon(s)	Primary: top Platypus Formation – White Pointer Supersequence.		
Cause of failure	Possible valid test (small Cenomanian closure) but the cause of failure is not clear. There is considerable doubt as to the validity of the structure mapped, and the source potential near the well is limited. The absence of a suitable migration pathway (possible migration shadow) also contributed to the failure of the well.		

Palaeo-oil saturation, as measured by GOI, is generally low in Duntroon-1. There is no positive evidence for saturations consistent with a palaeo-oil zone. Together with previous GOI data of Lisk et al. (2001), oil inclusion assemblages are variably recorded in samples from the Bronze Whaler, Blue Whale, Tiger and Hammerhead supersequences, with all GOI <0.4% (Figure 40). At these abundances the GOI indicate low level oil and gas-condensate (Figure 35) saturation in water-bearing rock by reference to Figure 37. The Bronze Whaler Supersequence is marginally mature below 3,100 mMD (VR 0.58%; Geoscience Australia, Petroleum Wells Database, 2017), so the presence of oil inclusions above this is good evidence for hydrocarbon migration. The possibility that some oil inclusions from below this depth might have arisen from in-situ generation, however, cannot be discounted.

In general, GOI abundances from the Lower Cretaceous Bronze Whaler and Blue Whale supersequences are slightly lower than for the Upper Cretaceous Tiger and Hammerhead supersequences. This is the opposite of what was observed in Gnarlyknots-1A and Greenly-1 where abundances generally increase with depth. Whether circumstantial or not, the White Pointer Supersequence is faulted out in Duntroon-1 by a major down-to-basin growth fault. Faults like this can act as major fluid conduits and potentially plumb deeper, more mature sections down dip. The 0.4% GOI samples from the base of the Tiger Supersequence in Duntroon-1 were selected for PVTx analysis presented in this report.

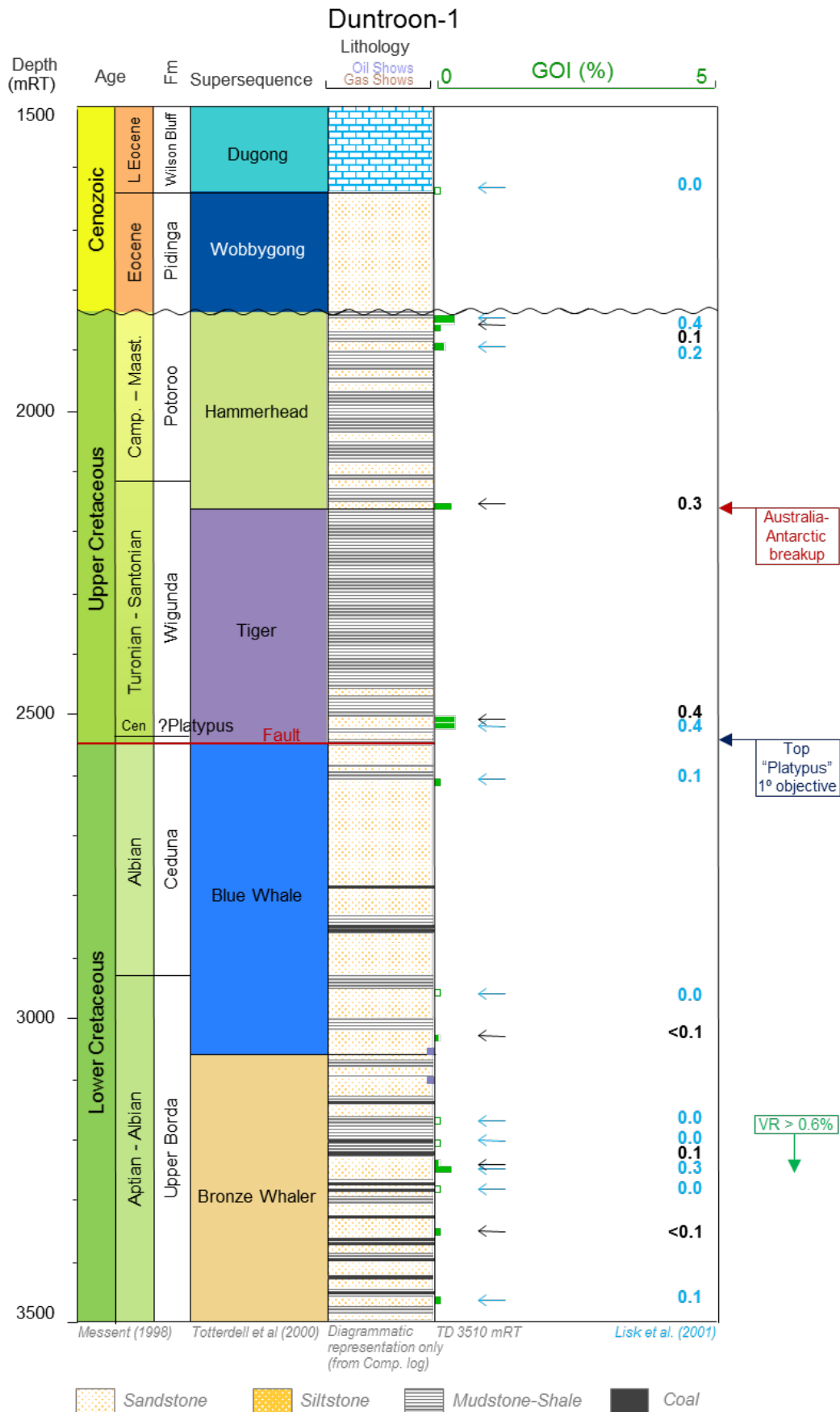


Figure 40: GOI log – Duntroon-1.

Potoroo-1

Operator	Shell Development Aust	Date spud	7 March 1975
Type	Exploration	Rig release	29 April 1975
Status	P & A - dry	KB/RT datum (m)	9
Sub-basin	Ceduna	Water depth (m)	261
		TD (m)	2924
Structural style	Fault block		
Target horizon(s)	Primary: interval of strong seismic reflection character similar to the 'Platypus sands' in Platypus-1 – White Pointer Supersequence. Secondary: Tertiary sands below Eocene "A" horizon.		
Cause of failure	Invalid test: the primary cause of failure is the lack of reservoir at the primary target horizon, the Platypus Formation, and no closure.		

Palaeo-oil saturation, as measured by GOI, is rather low in Potoroo-1. There is no positive evidence for saturations consistent with a palaeo-oil zone. Together with previous GOI data of Lisk et al (2001), oil-bearing inclusion assemblages are variably recorded in samples from the Blue Whale, White Pointer and Tiger supersequences, with all GOI <0.5% (Figure 41). At these abundances the GOI indicate low level oil and minor gas-condensate (Figure 36) saturation in water-bearing rock by reference to Figure 37. The Bronze Whaler Supersequence, at the very base of the well, is marginally mature below 2,788 mMD (VR 0.64%; Geoscience Australia, Petroleum Wells Database, 2017), so the presence of oil inclusions over much of the well intersection is good evidence for low level hydrocarbon migration rather than in-situ generation.

The counting statistics of the highest GOI in this study of 0.4% from the basal Blue Whale Supersequence is poor and due, in part, to the very coarse-grained nature of the sand at this depth (<500 grains; Table 4). The 0.4% GOI was based on only 2 grains with oil inclusions and the confidence level for assigning them as oil inclusions was low (i.e. very small and difficult to observe vapour bubbles). This potentially lowers the confidence in a 0.5% GOI in the interval below this where 6 grains with oil inclusion were recorded Lisk et al. (2001).

The 0.2% GOI from the base of the Tiger Supersequence, however, has numerous grains with oil inclusions (34 in total; Figure 9) and was from a lithology logged as siltstone (Figure 41). On the basis of oil inclusion abundance, this sample was selected for further PVTx analysis presented in this report.

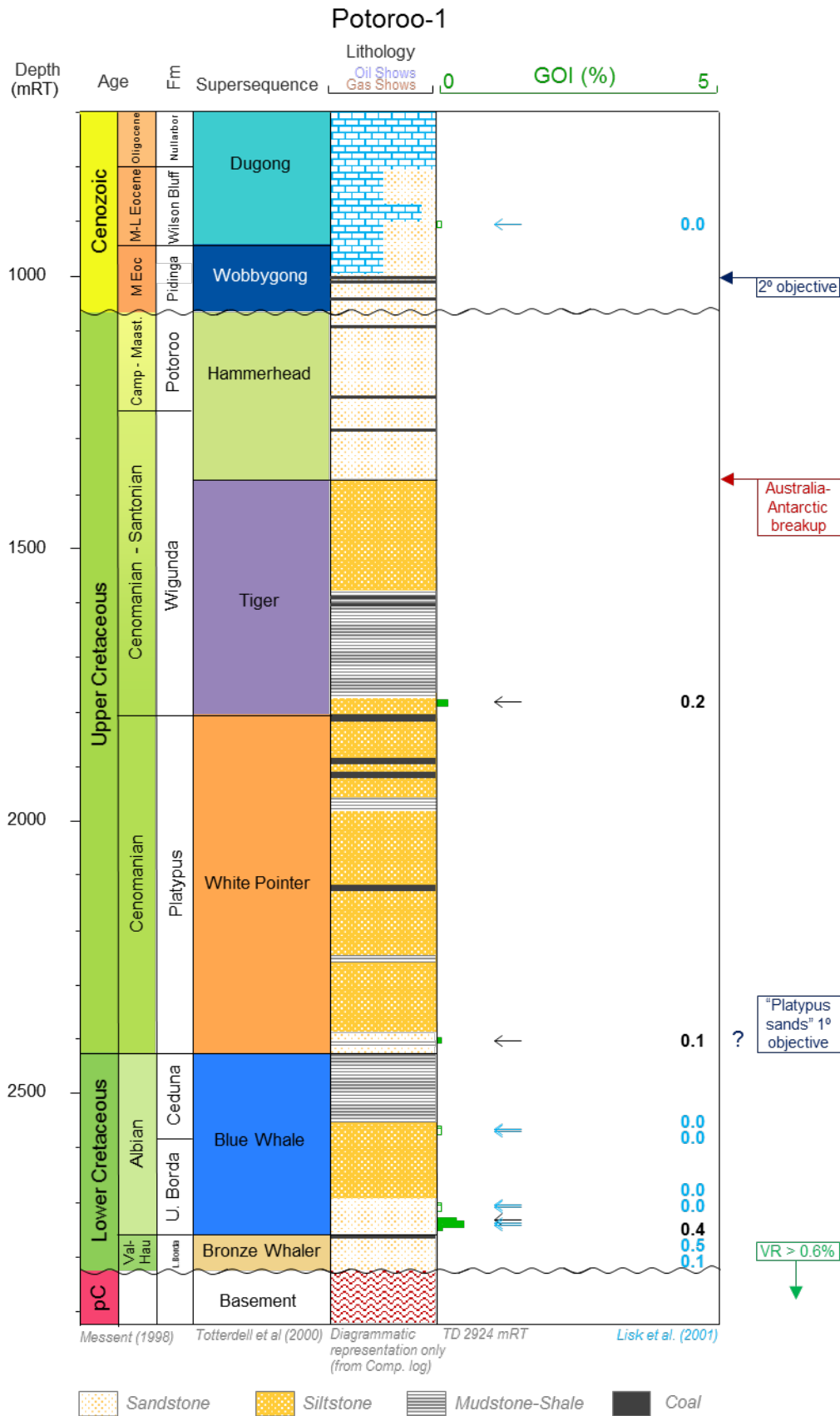


Figure 41: GOI log – Potoroo-1.

Jerboa-1 (Revised GOI)

Operator	Esso Explor. & Prod.	Date spud	3 April 1980
Type	Exploration	Rig release	29 April 1980
Status	P & A - dry	KB/RT datum (m)	10.4
Sub-basin	Eyre	Water depth (m)	760.5
		TD (m)	2537.5
Structural style	Basement drape		
Target horizon(s)	Primary: sandstone of early Cretaceous age – Bronze Whaler Supersequence		
Cause of failure	Valid structural test: failure due to lack of maturity of potential source rocks and/or lack of effective migration pathways from deeper levels.		

Previous Jerboa-1 GOI results were significant and, at the time, were interpreted to reflect the presence of a palaeo-oil column within unnamed Upper Jurassic sandstones (Lisk et al., 2001 and Ruble et al., 2001). As part of this study, these samples, with a 6.6% GOI from 2,470-80 m and a 10.4% from 2,490-95 m, were revisited as potential candidates for PVTx analysis.

Repeat GOI on new samples from 2,470-80 m and 2,490-95 m sample have now revised these down to 0.0% (Table 9) and oil inclusions were not observed in either sample. Inspection of the original thin sections for GOI reveals high background fluorescence in the epoxy used to prepare the thin sections and significant fluorescence contamination of grains, probably caused by inadequate sample preparation. It can only be surmised that non-oil bearing fluorescing features were included in the GOI by error. Such features were not observed in the new thin section preparations and the current methods include robust criteria for counting oil-bearing inclusions and ensuring potential contamination is excluded from the count.

The revised GOI of 0.0% for the 2,470-80 m or 2,490-95 m samples do not provide evidence for saturations consistent with a palaeo-oil zone. Moreover, there is no positive evidence for hydrocarbon migration either. Oil shows were not encountered during drilling, and gas readings within the drilling mud were low.

Table 9: Revised GOI for Jerboa-1.

Well	Depth (MD)	Previous GOI (%) (Lisk et al., 2001)	Revised GOI (%) – this study
Jerboa-1	2470-75 m + 2475-80 m	6.6%	0.0%
Jerboa-1	2490-95 m	10.4%	0.0%

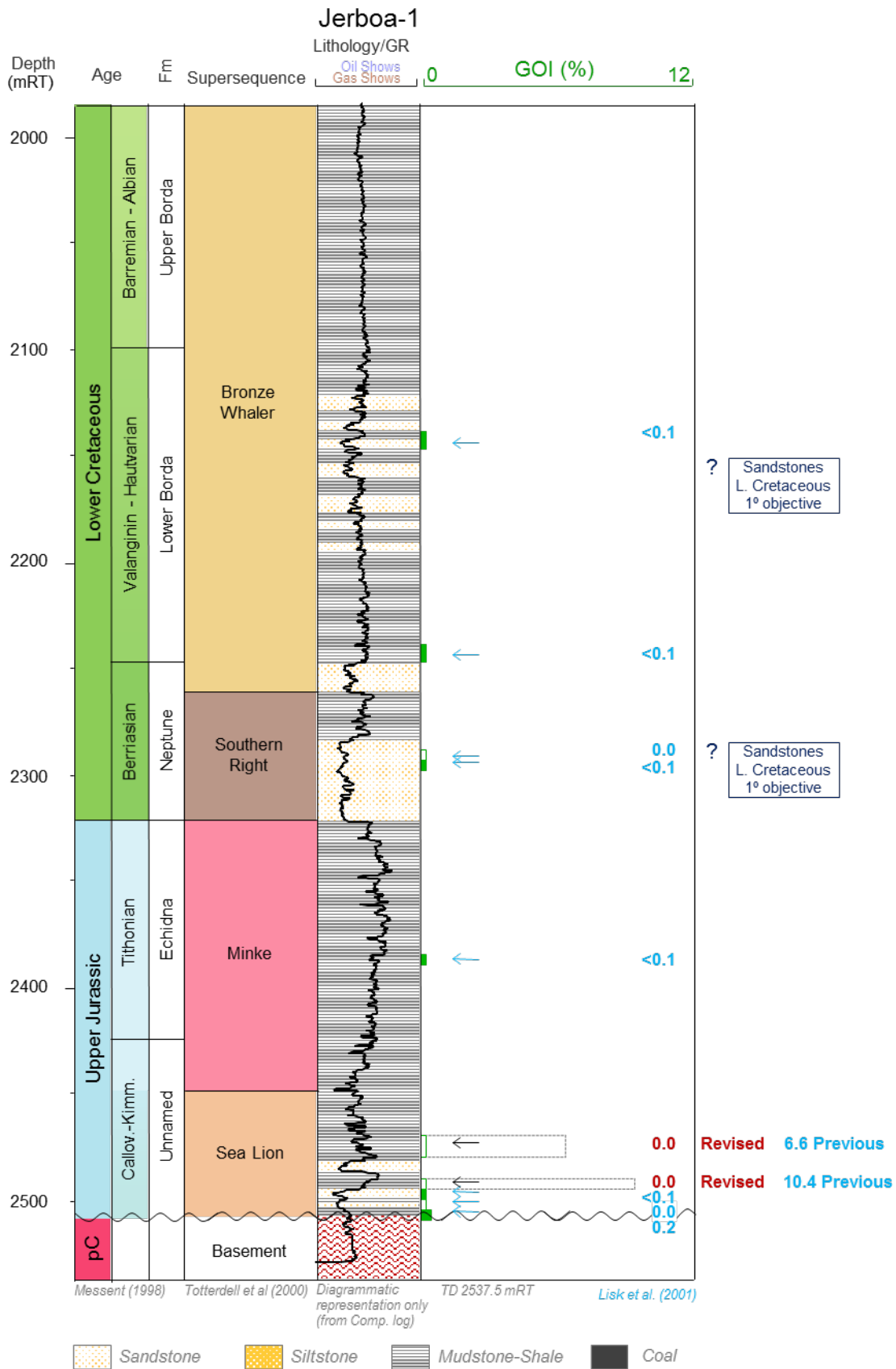


Figure 42: GOI log – Jerboa-1.

Hydrocarbon Migration in the Bight Basin

Historically, evidence for hydrocarbon migration in the Bight Basin was supported only by strong oil indications and shows in Greenly-1 from the eastern Ceduna/Duntroon sub-basins. Subsequent fluid inclusion analysis by Lisk et al. (2001) revealed evidence of widespread oil migration over much of the Bight Basin, coupled with abundant reservoirs at multiple levels, numerous potential seals and a range of trap styles that pointed to productive petroleum systems that were inadequately tested by previous drilling. The wells themselves failed for a variety of reasons, primarily the lack of a valid structural test that contributed to the failure of more than 50% of the wells (Messent, 1998).

Many of wells drilled prior to Gnarlyknots-1/1A in 2003 were located on the margins of the Bight Basin in a series of extensional half grabens comprising Late Jurassic to Early Cretaceous syn-rift continental sediments. These were predominantly in the vicinity of the Duntroon and Eyre sub-basins. The drilling of Gnarlyknots-1/1A, in 1,316 m water depth (Tapley et al., 2005), represented the first test of the under-explored deepwater area of the central Ceduna Sub-basin. While this well failed to encounter hydrocarbons, the fluid inclusion results of this study have revealed hidden evidence for hydrocarbon migration, both oil and gas, over multiple intervals in Gnarlyknots-1A. This, in turn, implies the potential for active petroleum systems in the deepwater Ceduna Sub-basin.

Integrated with the previous fluid inclusions data from the basin, the oil and some gas-bearing inclusions are more frequent in intervals from the Late Cretaceous White Pointer, Tiger and Hammerhead supersequences, on a measure of GOI (Figure 43). While these intervals, themselves, were the more common target for exploration, oil inclusions are less frequent in samples from the Early Cretaceous Bronze Whaler and Blue Whale supersequences and in the Palaeogene Wobbegong and Dugong supersequences of the overlying Eucla Basin. While not prescriptive, this perhaps implies that the more active source-rocks belong to the Late Cretaceous intervals.

Central Ceduna Sub-basin

Potoroo-1 and Gnarlyknots-1A are located in the central Ceduna Sub-basin (Figure 44). Potoroo-1 lies on the inboard margin of the sub-basin, close to the structural hinge that separates it from the Madura Shelf, and Gnarlyknots-1/1A in a more basinward position.

The strongest evidence for hydrocarbon migration is in the Gnarlyknots-1A well and particularly intervals in the Tiger Supersequence that include the primary objective of Coniacian age (Figure 38). These intervals, at the base of the well, are only marginally mature for oil generation at a depth of 4,100 mMD, so the oil inclusions, and almost certainly the gas-condensate inclusions, arise from migrated hydrocarbons. The source of these hydrocarbons is presumably beneath or down dip of the well intersection where they are more thermally mature for hydrocarbon generation. Based solely on the presence of oil and gas-condensate inclusions, the Tiger, upper White Pointer and Blue Whale supersequences are all potential sources of the hydrocarbons in Gnarlyknots-1A (Figure 45).

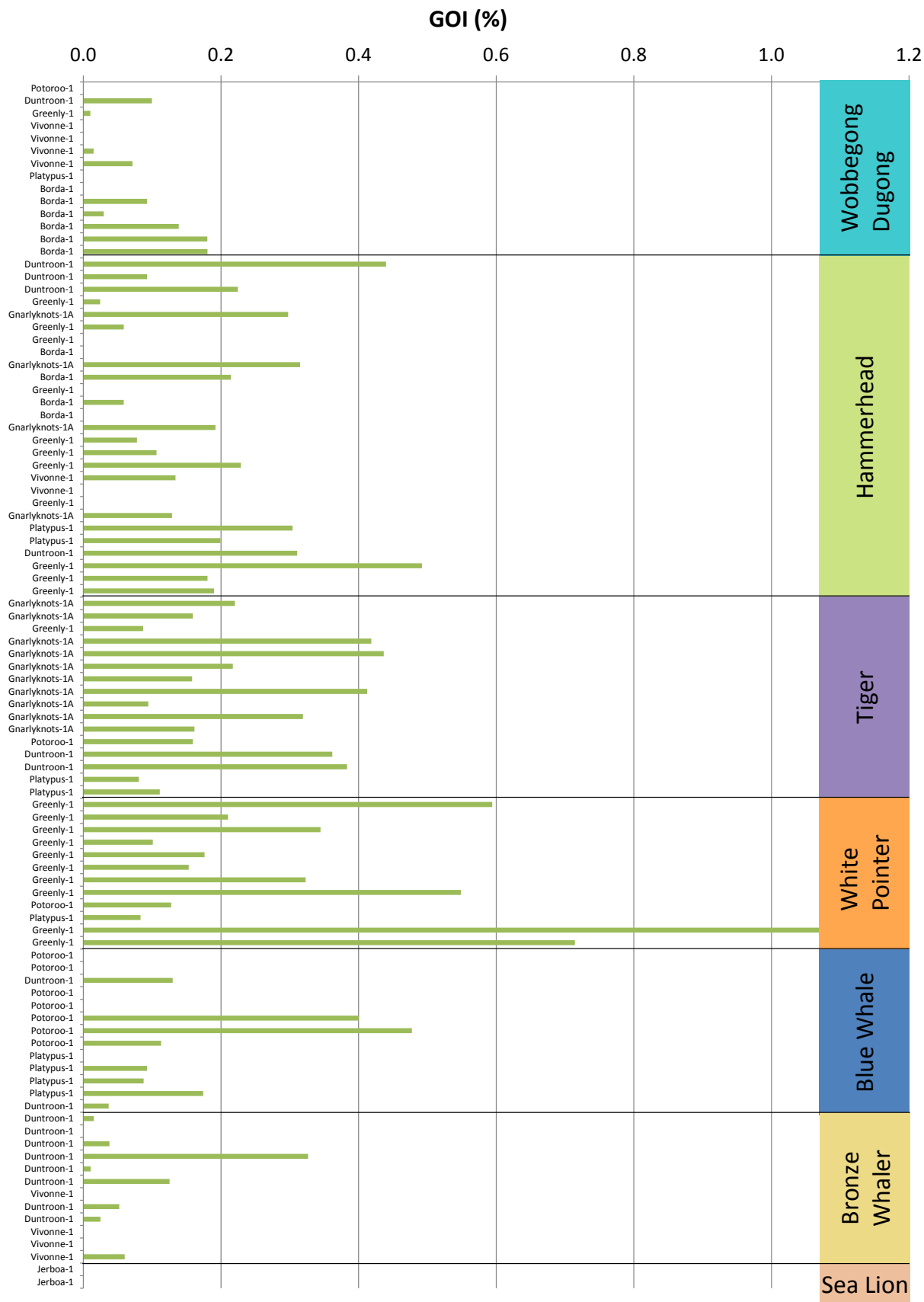


Figure 43: GOI summary by supersequence age. Includes data of Lisk et al (2001).
GOI % are shown to 0.01% precision (i.e. not rounded to nearest 0.1%).

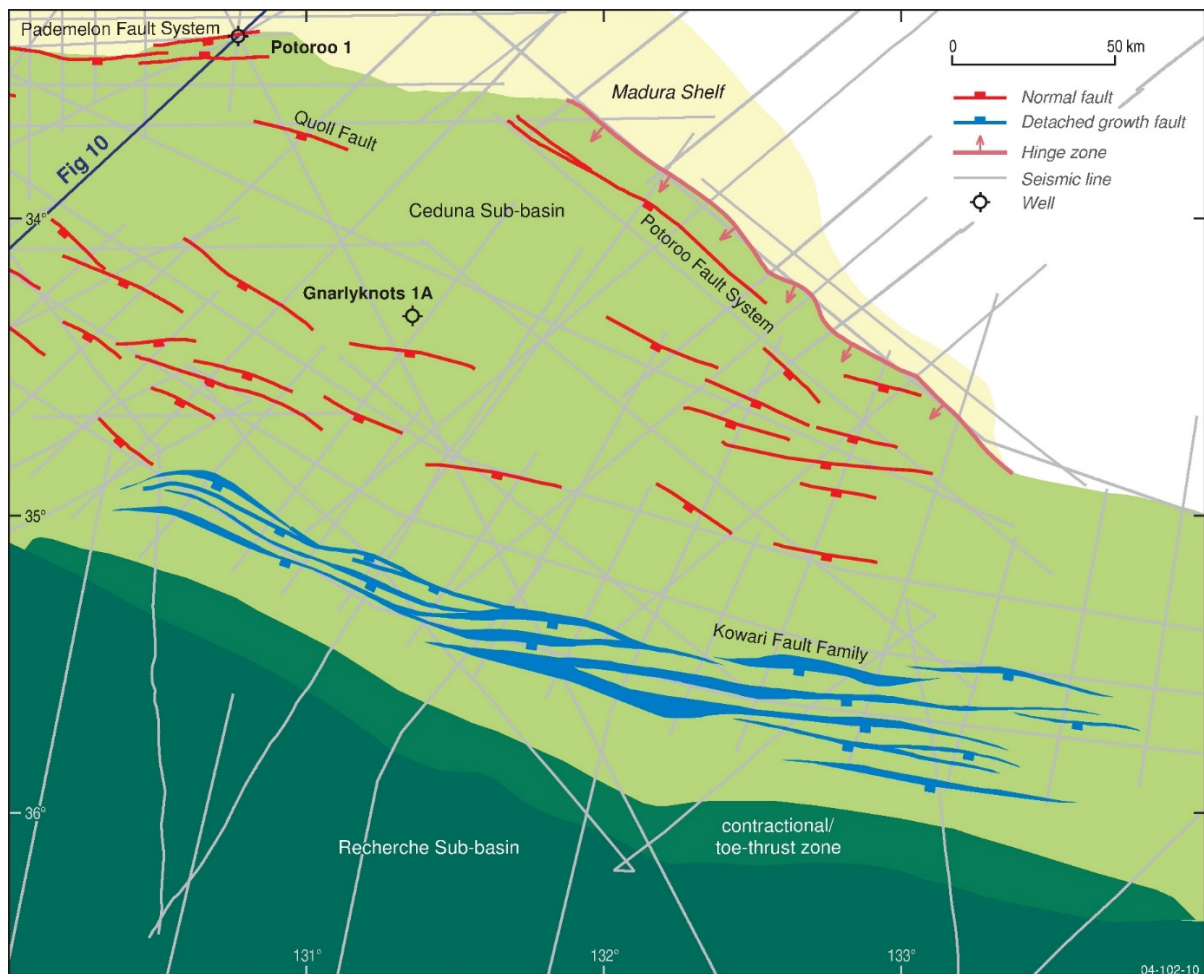


Figure 44: Structural elements of the central Ceduna Sub-basin.
© Commonwealth of Australia (Geoscience Australia) 2016.

In Potoroo-1 the evidence for hydrocarbon migration is somewhat less intense. Reservoir quality is generally poor in the Blue Whale, White Pointer and Tiger supersequences and capillarity effects may be limiting the ingress of hydrocarbons into what are largely siltstones. As the base of the well is only marginally mature, the presence of some oil inclusions is evidence that oil migrated rather than being locally generated. This weak GOI migration signal in Potoroo-1 is consistent with its location further up-dip from thermally mature hydrocarbon sources, compared to Gnarlyknots-1A. Any migration signal would be expected to have diminished in response to the longer lateral distances required to reach Potoroo-1. Similar effects have been reported by Liu et al. (2005) in the Vulcan Sub-basin from North West Shelf of Australia.

The 1,778-86 m sample from the base of the Tiger Supersequence in Potoroo-1 has 34 grains with oil inclusions recorded in GOI of 0.2%, all from a siltstone interval below shale. This is anomalous compared to other samples below this and the question arises as to the potential source of this fluid inclusion oil. Clearly they do not arise from local in-situ generation. The Tiger and upper White Pointer are potentially mature at distances greater than 50 km basinward of Potoroo-1 toward the Ceduna depocentre. Only the Blue Whale source is thermally mature in the immediate vicinity down-dip of Potoroo-1.

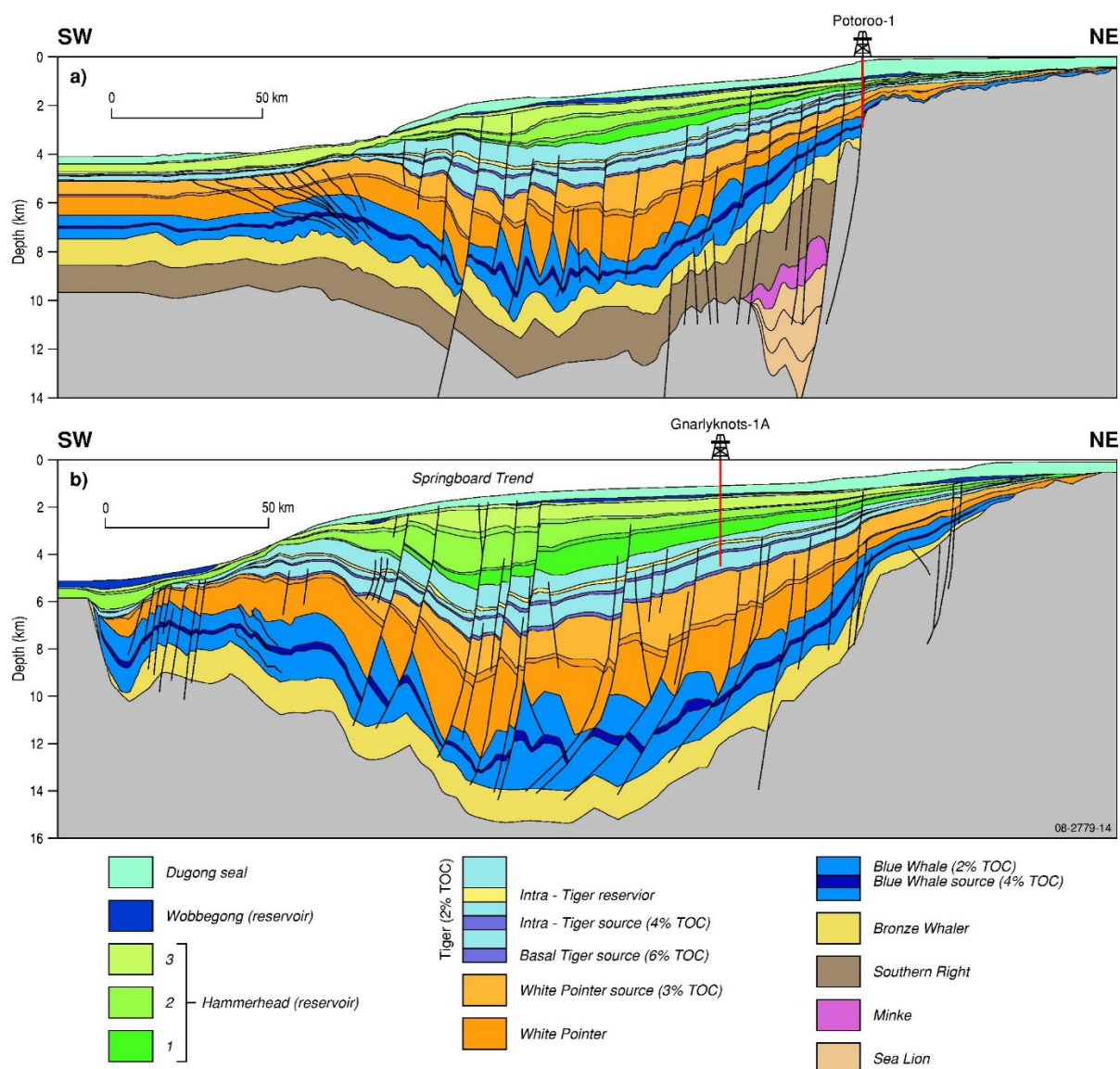


Figure 45: 2D transects across the Ceduna Sub-basin showing potential source rock intervals.
© Commonwealth of Australia (Geoscience Australia) 2016.

Eastern Ceduna/Duntroon Sub-basins

Borda-1, Duntroon-1, Echidna-1, Greenly-1, Platypus-1 and Vivonne-1 were originally defined in the former Duntroon Basin (Messent, 1998). A revised definition for sedimentary basins along the southern continental margin was subsequently developed by Geoscience Australia and is documented in Bradshaw et al. (2003) and Totterdell and Bradshaw (2004). In this scheme, the Duntroon Basin was remapped as smaller, genetically related rift system along the margin of the main rift basin, and reclassified as a sub-basin (Figure 46). As a result Borda-1, Duntroon-1, Greenly-1 and Platypus-1 are now re-classified as being in the eastern Ceduna Sub-basin.

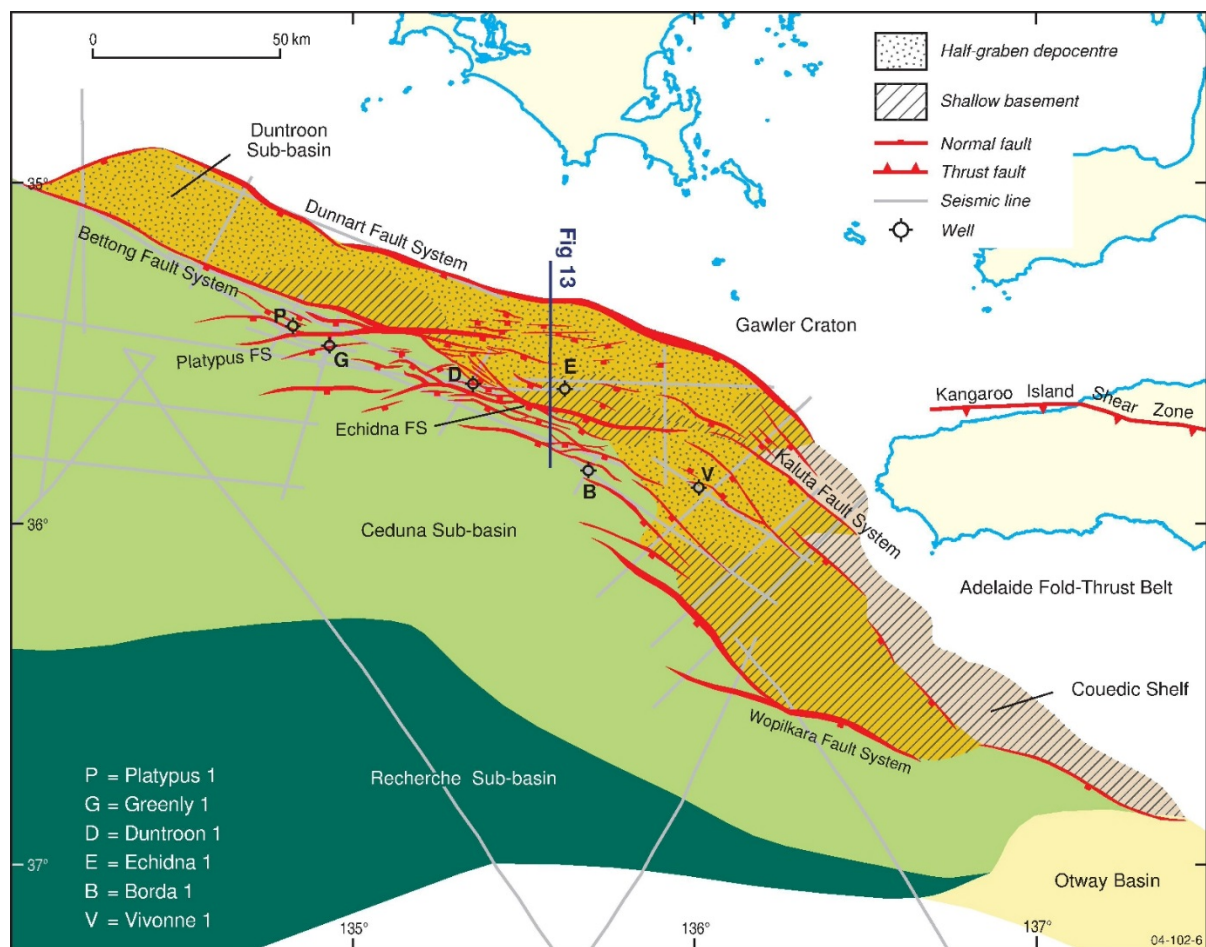


Figure 46: Structural elements of the eastern Ceduna and Duntroon sub-basins. Duntroon Sub-basin (yellow) lies to the northeast of the 'Late Cretaceous Hinge' that separates it from the seaward Ceduna Sub-basin. © Commonwealth of Australia (Geoscience Australia) 2016.

From fluid inclusions, Greenly-1 has the strongest evidence for oil migration in the eastern Ceduna Sub-basin. This occurs over multiple intervals, primarily within the White Pointer and, to a lesser extent, the Tiger supersequences. This is consistent with abundant oil shows reported from the same intervals, along with minor amounts of oil recovered from an RFT. Migration was thought to have occurred vertically and from the south (Messent, 1998).

Duntroon-1 has moderate evidence for oil and gas migration in both the Hammerhead and Tiger supersequences. Migration was thought to have been from the south and west of the structure. The quality of the source rocks in the immediate vicinity of the well was, however, limited, and the major migration pathway was likely from the south (Messent, 1998). While some complexity for migration is involved due to the number of fault zones, these fault zones may themselves have acted as conduits for migration. The sample from the Tiger Supersequence at 2,505-10 m has the highest number of grains with oil inclusions, and a GOI of 0.4%, and is located just above a significant fault zone that juxtaposes Tiger and Blue Whale supersequences.

While oil inclusions are recorded in some samples from Platypus-1 and Borda-1, the generally lower GOI values are weaker evidence for oil migration in these wells. Migration in Borda-1 was predicted to have been vertical, via faults from the Upper Borda Formation (Bronze Whaler) to the Lower

Pidinga Formation (Wobbeygong) reservoirs. As the Wigunda (Tiger) Formation is interpreted to be relatively thick in this area and predominantly consists of claystones, it was considered likely that the faults were sealing within the catchment area of Borda-1 rather than providing a migration pathway (Messent, 1998). Some oil inclusions were recorded in the Lower Pidinga and Potoroo (Hammerhead) formations (including Lisk et al., 2001; Table 2), and some oil clearly reached these shallower reservoirs. Given that the reservoir sands at these depths are immature to marginally mature for hydrocarbon generation (VR <0.6%; Geoscience Australia, Petroleum Wells database), the oil inclusions probably represent migrated hydrocarbons.

While in Platypus-1 there is no evidence for hydrocarbon shows (Messent, 1998), oil-bearing inclusions in the Upper Borda (Bronze Whaler) and Ceduna (Blue Whale) formations (Table 2; Table 4) suggests that some oil was present in these deeper sections. Given that the reservoir sands at these depths are immature to marginally mature for hydrocarbon generation (VR <0.6%; Geoscience Australia, Petroleum Wells database), the oil inclusions probably represent migrated hydrocarbons.

Vivonne-1 is the only well from the Duntroon Sub-basin, *sensu stricto*, and was not a focus for this investigation. Several samples were attempted for GOI, however not enough sand could be recovered to perform an analysis. In the sand intervals studied by Lisk et al. (2001) – Lower Pidinga (Wobbegong), Potoroo (Hammerhead) and Upper/Lower Borda (Bronze Whaler) formations – there were very few oil inclusions and generally most GOI were <0.1%. There are potentially two sources to feed the Vivonne structure, the Echidna (Minke) and Upper Borda formations (Bronze Whaler). The Early Cretaceous Upper Borda Formation is immature to marginally mature in Vivonne-1 (down to 2,140 mMD; Geoscience Australia, Petroleum Wells database) and throughout most of the Duntroon Sub-basin. Consequently, any migration would have to be from the south and in more mature areas of the Ceduna Sub-basin. For the Late Jurassic Echidna Formation in the Duntroon Sub-basin, any hydrocarbons are likely to have migrated prior to development of the structure (Messent, 1998).

Eyre Sub-basin

Hydrocarbon migration and accumulation in the Eyre Sub-basin has been re-interpreted in this report as a result of reviewing and re-measuring GOI data from Jerboa-1. Previous evidence for palaeo-oil zones at 2,470-80 mMD and 2,490-95 mMD from in the Upper Jurassic Sea Lion Supersequence is no longer supported. Higher molecular weight hydrocarbons (oil) were not extracted from the 2,470-80 mMD sample during Molecular Composition of oil Inclusion analysis and, as originally presented by Ruble et al. (2001), there was a low biomarker yield, relative to high background levels of components in the associated system blanks, in the 2,490-95 mMD sample. This result was itself suspect, given that MCI from high GOI samples >5% typically yield robust biomarker data, and suggests that there were insufficient numbers of oil inclusions in both samples to begin with.

Traces of residual oil (stains) were reported by Bein and Taylor (1981) in thin sections from 2,145 mMD and within the upper MCI interval from 2,472.5 mMD in Jerboa-1. If these oil stains represent the migration of oil, then this is not trapped in the fluid inclusion record of this well. At the well location, any source rocks are immature to marginally mature (67°C at 2,507 mMD; vitrinite reflectance 0.51% at 2,490 mMD), but possible Jurassic source rocks are likely to be mature in the deeper parts of the half graben (Messent, 1998).

Hydrocarbon Types

The types of trapped hydrocarbons in the fluid inclusion record from the Ceduna and Duntroon sub-basins are oil and gas-condensate (Figure 31; Figure 47). Where these are mapped by GOI, the number of grains containing only oil inclusions is greater than those containing gas-condensate or mixtures. Fluorescence-based techniques are biased for detecting liquid oil and because dry-gas is non-fluorescent at optical wavelengths.

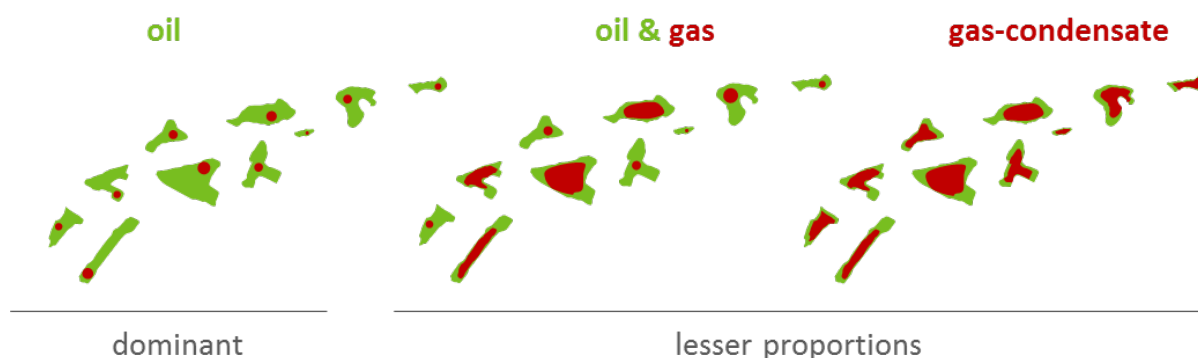


Figure 47: Hydrocarbon types observed in fluids inclusions from the Bight Basin.

Where oil un-mixes from gas at surface conditions, this is observed in fluid inclusions as large uniform vapour bubbles surrounded by a thin rim of fluorescing oil. These likely were trapped as gas-condensate, which is a low-density mixture of hydrocarbon liquids that are present as gaseous components in raw natural gas at reservoir conditions. They are a small component of assemblage types in Gnarlyknots-1A and Potoroo-1 in the Ceduna Sub-basin, and a relatively higher component in Duntroon-1 in the eastern Ceduna/Duntroon sub-basins. Gas-condensate was not observed in Greenly-1 and Platypus-1, which are co-located (Figure 46), perhaps suggesting these wells did not plumb a gassier source rock(s) in this part of the eastern Ceduna/Duntroon sub-basins.

Perhaps the more common occurrence of gas within inclusions from the Bight Basin are those assemblages that contain both oil and gas-condensate. This suggests two phase trapping of both oil and gas-condensate at the same time, perhaps from residual oil interacting with later gas or oil un-mixing from gas-condensate at reservoir conditions (phase separation). They are a small component of assemblage types in Gnarlyknots-1A, Greenly-1 and Potoroo-1, but a relatively high component in Duntroon-1 (Figure 35). Perhaps the area around Duntroon-1 plumbed a gassier source rock(s) in this part of the eastern Ceduna/Duntroon sub-basins.

API Gravity

API gravity is a measure of how heavy or light a petroleum liquid is compared to water; if its API gravity is greater than 10, it is lighter and floats on water; if less than 10, it is heavier and sinks. Generally speaking, oil with an API gravity between 40 and 45° is more valuable to refineries. Above 45°, the molecular chains become shorter and below 40°, longer. Crude oil is classified as; 'light crude oil' with an API gravity higher than 31.1°, 'medium oil' with an API gravity between 22.3 and 31.1°, 'heavy crude oil' with an API gravity below 22.3° and 'extra heavy oil' with an API gravity below 10°.

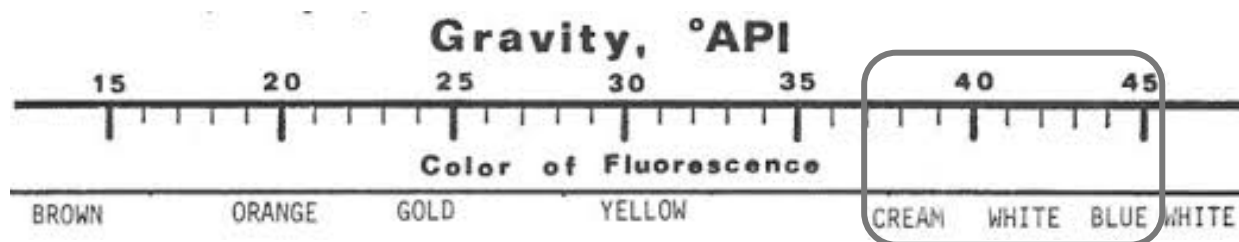


Figure 48: Schematic representation of crude oil fluorescence colour and gravity °API, showing the range of near-white fluorescent oil inclusions from this study.

Image from Crain's petrophysical handbook; <https://www.spec2000.net/08-samples.htm>.

API gravity can be inferred on the basis of fluorescence colour; that is, the colour emitted in the visible spectrum by oil illuminated by ultraviolet light. Empirically, oil that fluoresces toward the red wavelengths (those that appear orange/yellow) tend to have lower API gravities while oil that fluoresces toward the blue wavelengths have higher API gravities (Figure 48). A similar correlation between API gravity of fluid inclusion oil and fluorescence colour has been reported by Stasiuk and Snowdon (1997) and more recently by Bourdet et al. (2014).

While the oil inclusion assemblages in individual samples from the Bight Basin exhibit a range of fluorescence colours from yellow to white and blue, the dominant colour in most samples were those with near-white fluorescence (Figure 17). Fluorescence in the near-white region of the visible spectrum indicates light crude oil, with inferred API gravities between 37° to about 45°. The near-white classification allows for small variations (tints) to the yellow (cream) and blue parts of the visible spectrum (Figure 48). Those inclusions assigned with near-blue fluorescence tend to be associated with larger vapour bubbles and gas, and the API would be >45° in this case.

The Gnarlyknots -1A well completion report (interpretive data; 2004) reports API gravities from fluid inclusions in two cuttings (2,745 m and 3,950 m) and two sidewall core (4,467 m and 4,593 m) samples. API gravities in the 40-48° range were recorded in the deeper section at 4,467 m and 4,593 m and lower API's of between 36-42° at 2,745 m and 3,950 m. These API gravities are in general agreement with those inferred from visual assessment in this investigation, both of which suggest light crude oils.

Relative Timing of Hydrocarbon Migration

The timing of hydrocarbon migration can be deduced from the location of fluid inclusions relative to diagenetic cements that form in the sands during burial and compaction. The oil inclusions in the Bight Basin occur, almost exclusively, along healed fracture trails in detrital quartz (Figure 23). While the relative timing of fracture trail formation is difficult to constrain, because cements are generally poorly developed, there is evidence to suggest that some may have formed prior to the onset of quartz cementation (Figure 49A). Fracture trails with oil inclusions that appear to terminate at the quartz overgrowth boundary were identified in Gnarlyknots-1A (4,705-10 m, 4,520-25 m (Figure 26C), 4,135-40 m, 3,930-40 m) and Duntroon-1 (2,510 m). This, however, does not necessarily confer an early timing for oil migration in the burial history. On a global basis, the temperatures often reported for the onset of quartz cementation from fluid inclusions are highly variable but usually within the 75-150°C range (Walderhaug, 1994). The temperature at the Coniacian depth level in Gnarlyknots-1A is currently about 86°C at 4,000 m, which places it just within the window for the

formation of quartz cement. Thus the diagenetic fractures that host the oil-bearing inclusions may have formed at any time in the burial history.

In Greenly-1 at 4,809-12 m, there are numerous occurrences of oil inclusions in pore-filling carbonate cement in addition to those in fractures in quartz (Figure 49B). The carbonate cement phases are complex and a relationship relative to quartz cement and the diagenetic fractures could not be established. The oil inclusions in both locations, however, have similar fluorescence colour and bubble size attributes and, on this basis, are considered to have formed at the same time.

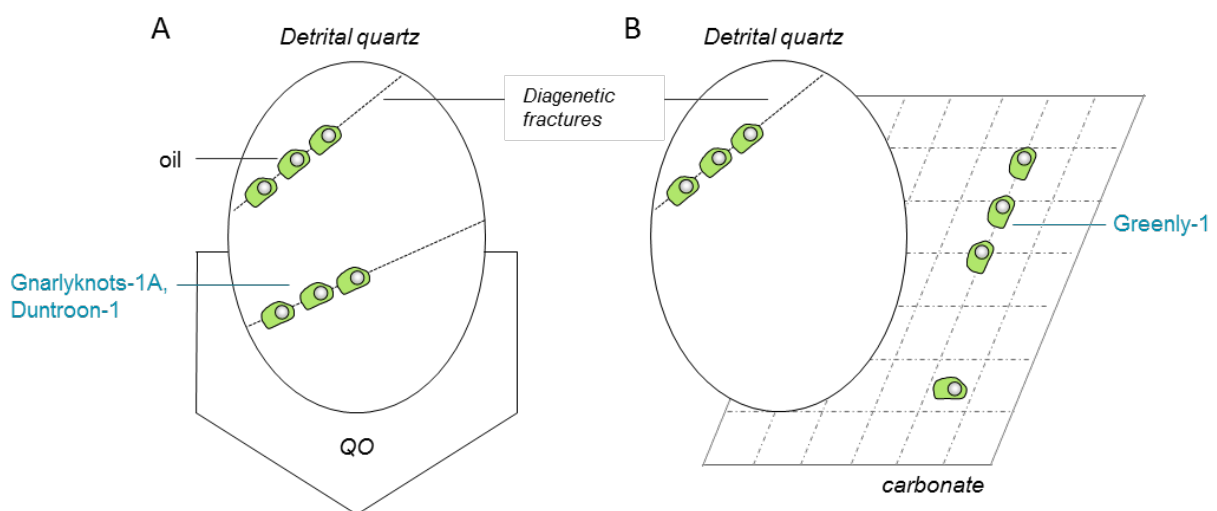


Figure 49: Relative timing of oil inclusions.

(A) Diagenetic fractures that terminate at the quartz overgrowth (QO) boundary. (B) Carbonate cement containing oil.

Part IV MCI & geochemical composition

Lead author

Se Gong

INTRODUCTION

Overview

To characterise the fluid inclusion oils and gases within the rocks of the Bight Basin, the CSIRO's *Molecular Composition of Inclusions (MCI)* method was applied to two wells; Gnarlyknots-1A and Greenly-1. The purpose was to geochemically fingerprint the hydrocarbons for source-related information and thermal maturity. Potential source rocks in the Bight Basin are largely inferred and the MCI technique has direct application for compositional information not otherwise obtainable by conventional techniques.

Previous MCI studies

Geochemical characterisation of palaeo-oil inclusions by MCI from 2,490-95 mMD in Jerboa-1 was discussed by Ruble et al. (2001). Aliphatic biomarkers suggested that the inclusion oil was derived from a carbonate-rich source rock containing algal and bacterial organic material, which was likely deposited in a lacustrine environment. Low levels of organosulfur compounds were believed consistent with non-marine deposition and an absence of plant-derived waxes suggested an environment with minimal terrestrial input.

Repeat analysis of the 2,490-95 mMD sample by GOI in this study (Figure 42), however, did not detect any visible fluorescent oil inclusions and the geochemical data, as presented, is not likely to have a fluid inclusion origin. The geochemical evidence presented by Ruble et al. (2001) should therefore be viewed with caution, as indeed the authors alluded to remarking “low biomarker concentrations and high background levels of components in the associated system blanks”.

Samples

Prior to MCI geochemical analysis, samples were screened for sufficient oil and gas inclusions using the Grains with Oil Inclusion (GOI) method, as outlined in the previous section. Samples for MCI can include those with high abundances of oil inclusions, such as in current or palaeo-oil reservoirs, but also, in the case of the Bight Basin, samples with low amounts of oil inclusions, such as those from oil migration pathways. Two sample intervals from Gnarlyknots-1A and Greenly-1 were selected for MCI and, in the case of Gnarlyknots-1A, carbon isotopes of gases. Each sample interval is discussed further in the results section.

Approval to view and sample petroleum wells for MCI and carbon isotopes of gases was granted by the National Offshore Petroleum Data & Core Repository (NOPDCR) – Approval No's: N00074, extension to N00074 and N00335.

Methods

Reliable geochemical information of similar quality to conventional analyses of crude oils and source rocks can be obtained from oil-bearing fluid inclusions (FI). Carefully controlled analytical procedures including sample clean-up, procedural blanks and attention to detail are essential for successful analysis and a description of the methodology is provided by George et al. (2007). A full range of hydrocarbons can be measured from inclusions by MCI, including:

- Offline MCI: *n*-alkanes, aliphatic biomarkers such as isoprenoids, hopanes and steranes, and aromatic hydrocarbons (C₁₂–C₃₆).

- Online MCI: low molecular weight 'gasoline-range' hydrocarbons (C₅–C₉).
- Carbon isotopes of gases: gaseous compounds (C₁–C₄) and CO₂.

Due to the relatively low oil inclusion abundances (Gnarlyknots-1A) and low detrital grain recovery (Greenly-1) off-line MCI was prioritised over on-line MCI and gas isotopes.

MCI sample cleaning

The uncleaned cuttings samples from Gnarlyknots-1A and Greenly-1 were treated successively with hydrogen peroxide, chromic acid and aqua regia to remove carbonate cements and organic matter from the surfaces of quartz and other detrital grains. To ensure thorough cleanliness, the samples were subjected to further solvent cleaning using triplicate 10 min sonications in 20 mL of methanol (MeOH), followed by triplicate 10 min sonications in a 20 mL azeotropic mixture of dichloromethane (DCM) and MeOH (93:7 vol%) and triplicate 10 min sonications of 20 mL DCM (all discarded). This was followed by the collection of an additional triplicate rinse of 20 mL DCM as an outside rinse blank. The outside rinse blank was spiked with an internal standard (squalane), passed through a Pasteur pipette packed with 5 cm of silica gel using DCM, the eluant was concentrated, and then checked for cleanliness by gas chromatography–mass spectrometry (GC-MS) analyses. Only when the outside rinse blank was deemed low enough to be considered background, was the inclusion oil from the cleaned samples extracted for analysis.

System blanks

Before fluid inclusion extraction, system blank experiments using the same experimental procedures detailed below were carried out in order to determine the extent of any hydrocarbon contribution from the off-line crushing cylinder, glassware and any residual oil from previously analysed samples. A system blank that was deemed to be sufficiently clean was acquired one day prior to crushing of the samples, and the samples crushed subsequently using the same crushing cylinder and glassware. The results from the system blank prior to the extraction are provided throughout the report in order to demonstrate the level of background hydrocarbons. Similar to the FI extracts, the system blank extracts were quantified by adding known amounts of internal standard. Chromatograms of the blank are scaled to the same amounts as for the corresponding FI oil chromatograms (using the internal standard and proportionality factors), to enable direct visual comparison.

Off-line MCI

Off-line extraction of oil was carried out after crushing the quartz concentrates containing the inclusions in a sealed metal crusher under solvent. The oil recovered was then analysed in the same manner as conventional oils or source rock extracts.

Aliquots of the cleaned quartz grains were crushed to a fine paste under DCM using a stainless steel crushing cylinder with a 55 mL capacity. Two stainless steel balls were placed in the cylinder above the sample and 25 mL of DCM was added before closure of the cylinder in air at atmospheric pressure. The cylinder was vigorously shaken for 3 x 10 mins in a vertical motion with a throw of about 40 mm, using a modified piston pump. This procedure enables crushing of the rock chips, thereby releasing the trapped oil into the solvent. In between the crushing phases, the crusher was allowed to cool in order to minimise evaporative loss of the liberated FI oil. This procedure crushes the mineral grains and releases the trapped oil, which partitions into the solvent. The resultant suspension of finely crushed mineral in solvent is poured into a beaker, and the crushing bomb is

rinsed with an additional 25 mL of solvent. The solution in the beaker is then ultrasonicated for 10 min, allowed to settle for a few minutes and then the supernatant solvent layer, containing the FI extract and suspended mineral fines, is transferred to a round bottom flask. The residual mineral powder is ultrasonicated twice with fresh DCM (25 mL), and the supernatant is transferred into the same round bottom flask. The solvent containing the oil extracted from the FIs (total=100 mL) is reduced in a rotary evaporator and by blowing down with purified nitrogen. Suspended rock powder is removed by passing the extract reduced to ~2 mL through a short Pasteur pipette plugged with glass wool and packed with silica gel (C60: 60 - 210 μ m). Particular care is taken to avoid blowing the sample dry, so as to preserve the low-molecular-weight hydrocarbons (see Ahmed and George, 2004). Generally, hydrocarbons as low as \sim C₈ are recovered using this technique, and those from C₁₂ to C₃₆ quantitatively. The amount of oil obtained from each FI oil is determined by adding small amounts (~0.6 μ g) of an internal standard (squalane), since the yields are too low for gravimetric determination.

GC-MS analysis of the FI oil was performed on a Thermo Trace Ultra GC interfaced with a high resolution Thermo DFS GC-MS system. Gas chromatography was carried out on a DB-5MS (J&W) fused silica column (60 x 0.25 mm i.d., 0.25 μ m film thickness). Samples were injected (1 μ L) using a splitless technique with an injector temperature of 260 °C and constant flow of 1.5 mL/min. The mass spectrometer was tuned to 1,000 resolution (electron energy 70 eV; source temperature 280 °C). The oven was programmed in two ways for different GC-MS runs: (a) for an initial temperature of 40°C for 2 min., followed by heating at 4°C min⁻¹ to 310°C, and (b) for an initial temperature of 40°C for 2 min., followed by heating at 20°C min⁻¹ to 200°C and then a second heating ramp at 2°C min⁻¹ to 310°C. The FI oil, final outside rinse and laboratory system blank samples were analysed using five different multiple ion detection (MID) programmes:

- MID_A, GC programme a: m/z 83, 85, 97, 106, 113, 120, 123, 125, 128.
- MID_B, GC programme a: m/z 128, 134, 142, 154, 156, 166, 168, 170, 178, 183.2
- MID_C, GC programme a: m/z 178, 180, 182, 183.1, 183.2, 184.03, 184.13, 192.1, 198.05, 198.14, 202, 206, 212, 216, 220, 234.
- MID_D, GC programme b: m/z 177, 183, 191, 205, 217, 218, 231.11, 231.21, 253, 259.
- MID_F, GC programme c: m/z 135, 136, 149, 163, 177, 187, 188, 201, 215.
- The FI oils were also analysed using two metastable reaction monitoring (MRM) programmes, using GC programme (b):
- MRM_HOPS: m/z 370, 384, 398, 412, 426, 440, 454, 468, 482 \rightarrow 191.
- MRM_STER: m/z 358, 372, 386, 400, 414 \rightarrow 217; 414 \rightarrow 231.

On-line MCI

Gasoline-range hydrocarbons were analysed using a direct on-line crushing GC-MS method. This utilises a device mounted on an Agilent 6890-5973 GC-MS which allows crushing of mineral grains and release of volatile products from the FIs directly onto the chromatography column via a carrier gas. A small amount of cleaned quartz (~ 50 mg) was hand crushed in the glass-lined metal insert of a customised MSSV-1B Thermal Analysis System using a metal plunger. The thermal analysis port was mounted in a cryogenic trap prior to GC separation. Chromatography was performed using a BPX5 column (5% phenyl 95% methyl silicone, 0.5 μ m film thickness, SGE), with the oven programmed from an initial temperature of -20°C at the start of the crushing (7 min hold), followed

by heating at 4°C min⁻¹ to 30°C, with a 8 min. hold, followed by heating at 4°C min⁻¹ to 300°C, with a 15 min, hold. The cryogenic trap was removed after 3 min. Hydrocarbons liberated from the inclusions were analysed by the GC-MS using a SIM programme:

- FI-MSSV1B: *m/z* 55, 56, 57, 68, 70, 71, 78, 82, 85, 91, 97, 99, 106.

Areas of peaks in mass chromatograms were converted to TIC-equivalent areas and then to FID-equivalent data using response factors, before data manipulation. Day to day variations in tuning and calibration were accounted for by measuring a standard sample from the well Buffalo-2.

Carbon isotopes of fluid inclusion gases

Carbon isotopes of fluid inclusion gases were analysed by an online crushing–trapping–analysis system comprising a gas-tight crusher and a concentrator with micro-trap connected to a GC-C-IRMS. This technique was recently developed in CSIRO and has made carbon isotope analysis of inclusion gases possible, especially for samples with low observed abundances of hydrocarbon inclusions. The novel design of this technique imparts no isotopic fractionation during the cryo-trapping stage or subsequent thermal release from the trap, as shown by running three gas standards (pure CH₄, CH₄/CO₂ mixture (50:50) and pure CO₂) with and without cryo-trapping (Figure 50).

Cleaned quartz grains were loaded into a crusher. With vertical vibration of the crusher, the fluid inclusion gases were released and carried into a micro-trap by high-flow helium. The gases were cryo-trapped for 5 minutes by liquid nitrogen. The gases were then released into a GC-C-IRMS, via the GC injector, by heating the trap to 250°C. The carbon isotopic composition of the released fluid inclusions gases was measured by GC-C-IRMS (gas chromatography/combustion/isotope-ratio mass spectrometry). The GC-C-IRMS system comprises a GC unit (6890N, Agilent Technologies, USA) connected to a GC-C/TC III combustion device coupled via open split to a Delta V Plus mass spectrometer (ThermoFisher Scientific, Germany). The analytes of the GC effluent stream were oxidised to CO₂ in a combustion furnace held at 1,000°C on a CuO/Ni/Pt catalyst. CO₂ was transferred on-line to the mass spectrometer to determine carbon isotope ratios. 20 -100 µL of sample gas was injected into the GC unit working in split mode (20:1 ratio). The injector was held at a temperature of 200°C. The gas components were separated on a fused silica capillary column (PoraPlot Q, 25 m x 0.32 mm ID, Varian). The GC was held isothermally at 40°C. Helium was used as a carrier gas, set to a constant pressure of 14.3 psi. A system blank was run before each crush to ensure that there was no potential contamination from the system. Carbon isotope values are reported in the δ¹³C notation:

$$\delta = \frac{R_{\text{sample}} - R_{\text{standard}}}{R_{\text{standard}}} \times 1000 (\text{‰})$$

Where the isotope ratio measurement is the delta value (δ) given in per mille (‰) relative to Vienna Pee Dee Belemnite (VPDB) standard. *R*_{sample} is the isotope ratio measured in the laboratory. *R*_{standard} = ¹³C/¹²C of VPDB = 0.010743.

Three gas standards (100% CH₄, 50:50 CH₄:CO₂ and 100% CO₂), of known isotopic composition, were measured in duplicate as a calibration of the system prior to analysis, with a standard deviation of ≤0.5‰. These same gas standards are checked on a yearly basis by inter-comparison on dual bellows inlet mode on a Finnigan MAT 252, against international primary carbonate standards (IAEA-CO-1, IAEA-CO-8, IAEA-CO-9, LSVEC and NBS19) prepared by the phosphoric acid method.

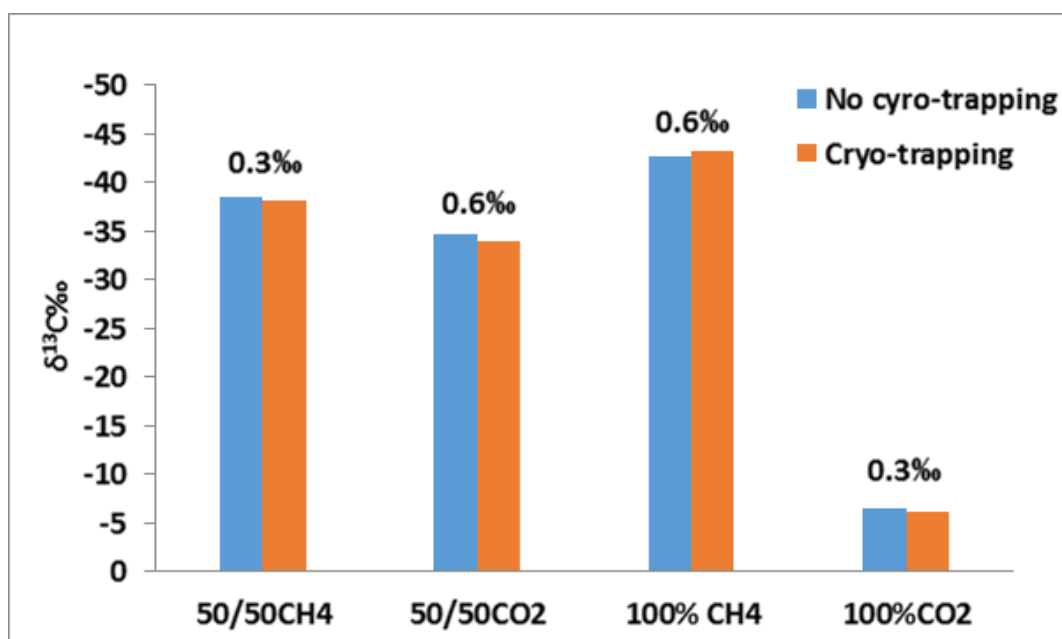


Figure 50: the effect of fractionation in the cryo-trapping system using thee gas standards.

RESULTS

Gnarlyknots-1A

A sand-rich cuttings interval from the Upper Cretaceous (Coniacian) Tiger Supersequence in Gnarlyknots-1A, central Ceduna Sub-basin, was selected for the full suite of inclusion analysis (Table 10; Figure 51):

- Off-line MCI sample: 4,390 m to 4,425 mMD (7 consecutive cuttings samples combined).
- On-line MCI sample: 4,410-15 mMD cuttings sample only.
- Fluid inclusion gas isotopes: 4,410-15 mMD cuttings sample only.

The Gnarlyknots-1A sample combined seven intervals of cuttings, three of which had confirmed low GOI abundance (0.2% - 0.4%). Due to the low expected recovery of fluid inclusion (FI) oil, instead of crushing one aliquot of sample (normally 5 g -15 g), six aliquots of cleaned detrital grains (total 78.68 g) were crushed to obtain enough FI oil for biomarker analysis.

Table 10: MCI and gas isotope sample information – Gnarlyknots-1A.

Well	Depth (mMD)	GOI (%)	Off-line MCI	On-line MCI	Gas isotopes
Gnarlyknots-1A	4390-95 m	GOI–0.2%	134522	-	-
Gnarlyknots-1A	4395-00 m	Not analysed	134603	-	-
Gnarlyknots-1A	4400-05 m	GOI–0.2%	134523	-	-
Gnarlyknots-1A	4405-10 m	Not analysed	134604	-	-
Gnarlyknots-1A	4410-15 m	GOI–0.4%	134524	134717	134717
Gnarlyknots-1A	4415-20 m	Not analysed	134605	-	-
Gnarlyknots-1A	4420-25 m	Not analysed	134606	-	-

Sample denoted by CSIRO sample no.

Off-line MCI

Geochemical parameters obtained from the FI oils are shown in Appendix 4. Mass chromatograms for the FI oils and the associated blanks are shown in Appendix 6, with peak assignment nomenclature shown in Appendix 5.

n-Alkane and Branched Alkanes

The m/z 85 mass chromatogram (Figure A6-112) was used to calculate the abundances of *n*-alkanes and isoprenoids in the Gnarlyknots-1A FI oil. The quantitative data were derived from comparison of the area of the internal standard Squalane with the *n*-alkanes, taking into account the response factor for the instrument used. Yields of *n*-alkanes of the Gnarlyknots-1A FI oil and system blank are provided in Table A4-31. Various *n*-alkane and isoprenoid ratios are provided in Table A4-32.

Normalised distributions of *n*-alkanes in the Gnarlyknots-1A FI oil and system blank are shown in Figure A4-105. *n*-Alkane recovery in the range of *n*-C₁₂ to *n*-C₃₂ from the Gnarlyknots-1A FI oil is 887.4 ng, which is 77 times more than that of the system blank and 46 times more than that of the final outside rinse (Table A4-31). Therefore, the results presented in this study can be interpreted with a high degree of confidence.

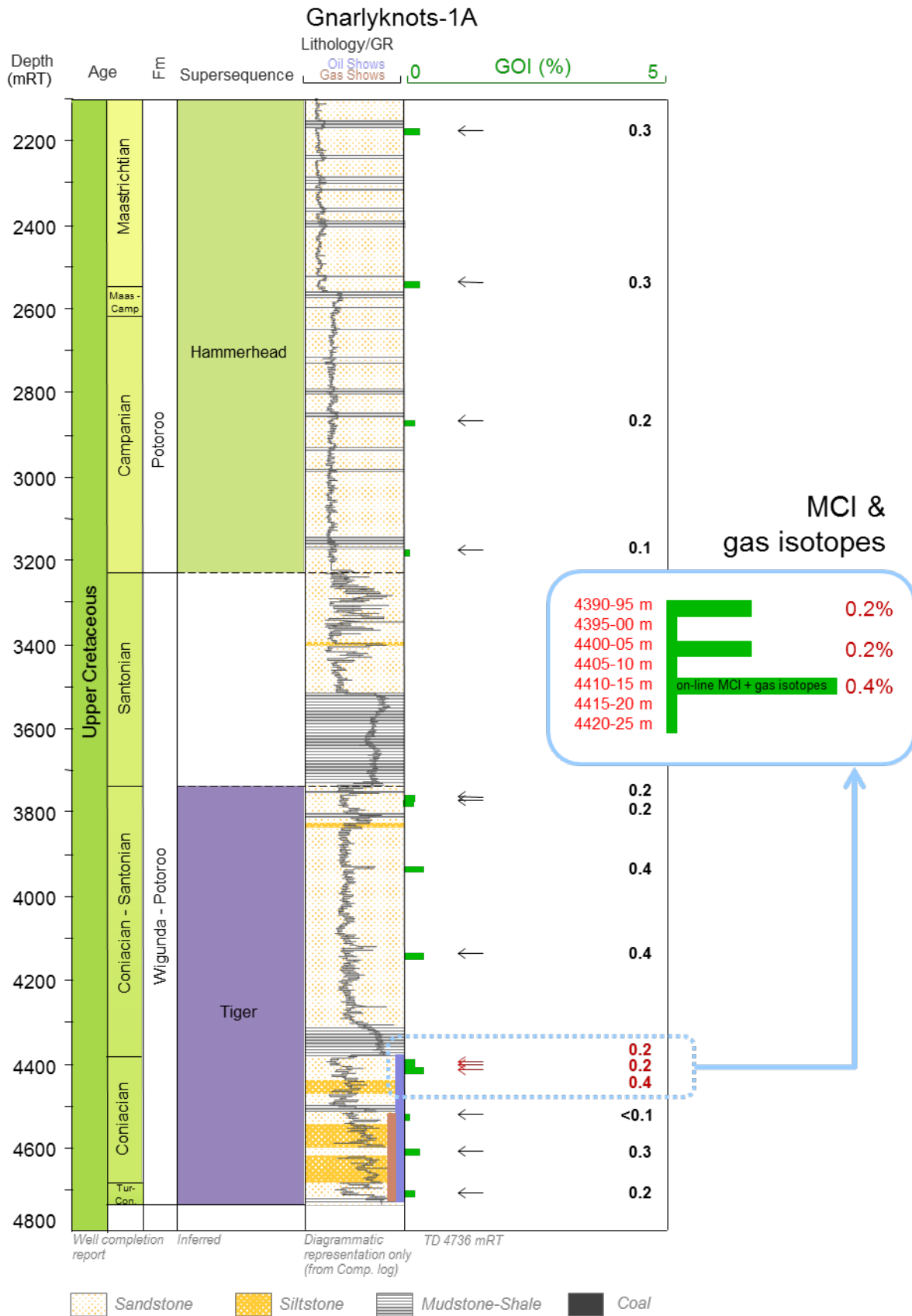


Figure 51: Gnarlyknots-1A — samples for MCI (off-line and on-line) and gas isotopes.

The m/z 85 mass chromatogram of the Gnarlyknots-1A FI oil shows a distinct bimodal distribution of n -alkanes with maxima at n -C₁₆ and n -C₂₇ (Figure A4-105), suggesting the Gnarlyknots-1A FI oil was generated from a source rock(s) with both algal and terrestrial organic matter inputs.

The predominance of even C-number n -alkanes (particularly n -C₁₆ and n -C₁₈) is observed in the Gnarlyknots-1A FI oil but it is not present in the final outside rinse. This is uncommon and possibly arises from the alkene-based synthetic drilling mud used in the well (Figure 52). While the abundance of n -alkanes in the Gnarlyknots-1A FI oil is about 200 times more than that in the outside rinse (Figure 53), the compounding effect of six aliquots (78.68 g) of crushed grains, rather than the standard one aliquot, may have amplified small amounts of this alkene-based drilling fluid. The n -C₁₆ and n -C₁₈ peaks are not prominent in the final outside rinse, which suggests that the alkene-based drilling fluid was potentially extracted during crushing of the grains (note that system blanks for the glassware and crushing apparatus were similarly baseline). There are several possibilities for the preservation of drilling fluid in the sample after the cleaning process: (1) in disconnected pores within grain aggregates and, (2) along drilling induced micro-fractures within the quartz grains. Despite some potential contamination effects from the drilling fluid, it appears that only the even C-number peaks n -C₁₄, n -C₁₆, n -C₁₈ and n -C₂₀ are affected and the remainder of the n -alkanes can be interpreted with more confidence. The predominance of the odd C-number (n -C₂₅ and n -C₂₇) in the higher molecular weight n -alkanes is typical of immature hydrocarbons from terrestrial plant wax (Eglinton and Hamilton, 1967; Elias et al., 1997).

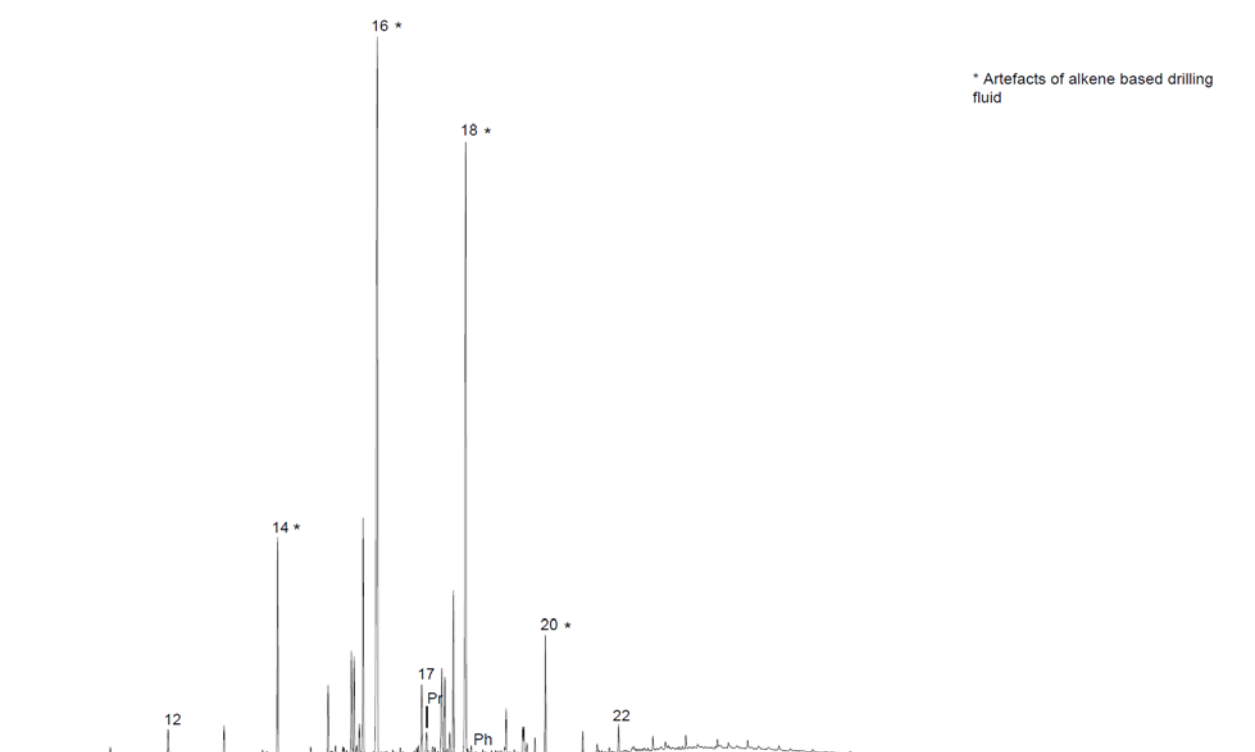


Figure 52: Artefacts of alkene based synthetic drilling fluid from GC-MS chromatogram of saturated hydrocarbons extracted from Gnarlyknots-1A 4412.0 m SWC sample.

Image by Geotechnical Services Pty Ltd reported in the Gnarlyknots-1 & 1A (2003) well completion report (basic data).

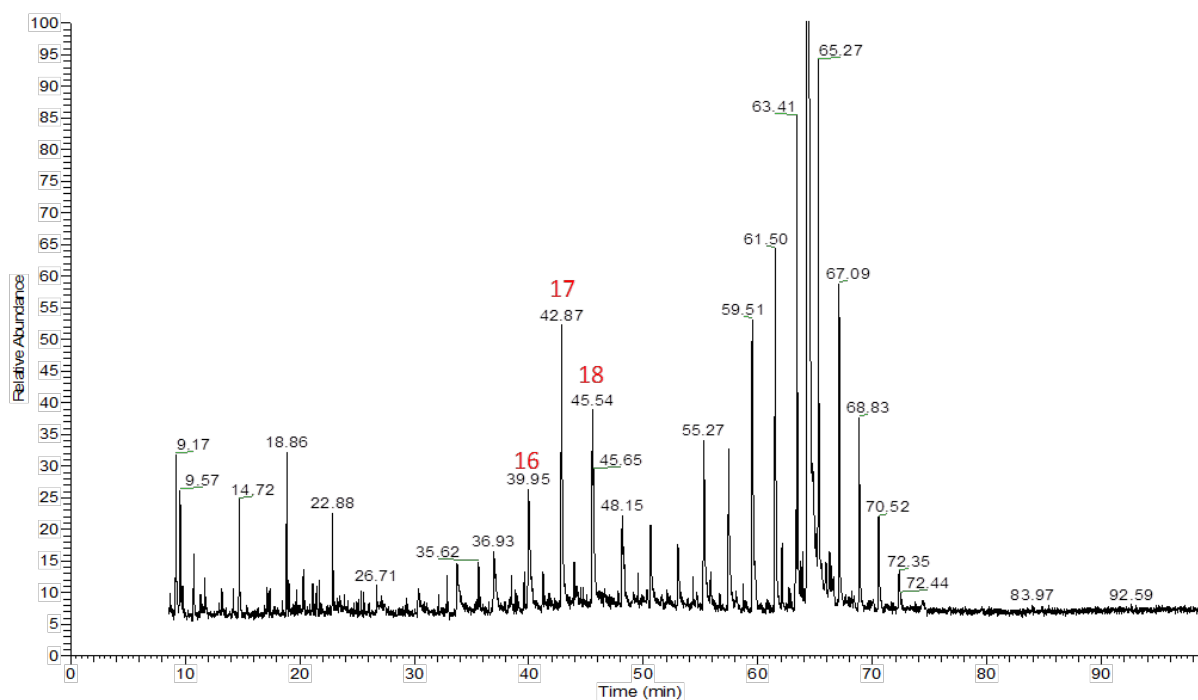


Figure 53: GC-MS chromatogram of saturated hydrocarbons from the final outside rinse of the Gnarlyknots-1A sample.

A Pr/Ph ratio of 1.5 suggests a sub-oxic depositional environment (Peters et al., 2005). Carbon preference index (CPI) for C_{22-32} shows a slight odd-over-even predominance (Table A4-32). Based on a plot of Ph/ n - C_{18} versus Pr/ n - C_{17} (Figure A4-107), the source rock of the Gnarlyknots-1A FI oil contains type III/II kerogen deposited in relatively reducing sub-oxic condition. Since the n - C_{18} peak was partly contaminated by drilling mud, the ratio of Ph/ n - C_{18} would likely be higher and more type II kerogen.

Terpanes

Terpanes were monitored using four SIM mass chromatograms and also by MRM chromatograms. The m/z 123 mass chromatogram (Figure A6-116a) shows that C_{14} to C_{16} bicyclic sesquiterpanes are present in the Gnarlyknots-1A FI oil. Diterpanes are either absent or below the limits of detection (Figure A6-116b) and this indicates that the source rock(s) contained no, or only minor amounts of, coniferous organic matter (Noble et al., 1985a, 1985b, 1986).

Hopanes, moretanes (Figure A6-118a) and the tricyclic and tetracyclic terpanes (Figure A6-116c) were monitored using the m/z 191 mass chromatograms. The presence of dimethylhopanes was evaluated using the m/z 177 mass chromatogram (Figure A6-118b), whereas methylhopanes were analysed using the m/z 205 mass chromatogram (Figure A6-118c). Peak annotations are defined in Table A5-39. Mass chromatograms of the system blank scaled to the same extent by using the internal standard (Squalane) demonstrate that the FI oil data can be interpreted with confidence. Ratios based on terpanes are shown in Table A4-33.

Tricyclic terpanes in the Gnarlyknots-1A FI oil are dominated by the C_{21} and C_{23} homologues. The abundant C_{23} tricyclic terpane commonly occurs in oil samples from marine source rocks (Aquino Neto et al., 1983). The C_{23} tricyclic terpane is relatively high compared to C_{30} $\alpha\beta$ hopane with C_{23} tricyclic terpane/ C_{30} $\alpha\beta$ hopane = 0.87, suggesting moderate to high thermal maturity. The C_{24} tetracyclic terpane is much higher than C_{26} tricyclic terpane (C_{24} tetracyclic/ C_{26} tricyclic terpanes =

2.2), indicating terrestrial organic matter input (Philp and Gilbert, 1986; Preston and Edwards, 2000; Grice et al., 2001; Peters et al., 2005). The C₂₅ tricyclic terpane is more abundant than C₂₆ tricyclic terpane (C₂₆/C₂₅ tricyclic terpanes = 0.73), indicating that the source rock(s) was probably not deposited in a lacustrine environment.

Hopanes in the Gnarlyknots-1A FI oil are dominated by C₃₀ αβ hopane. The relative abundances of C₂₉Ts and diahopanes are low (e.g. C₂₉Ts/C₂₉ αβ hopane = 0.28, C₃₀*/C₃₀ αβ hopane = 0.07). A relatively high abundance of 28, 30-bisnorhopane (28, 30-BNH/C₃₀ αβ hopane = 0.36) indicates that the source rock(s) was deposited under an anoxic depositional environment with bacterial inputs (Mello et al., 1990). Relatively low C₂₉ αβ hopane/C₃₀ αβ hopane (0.79) and low C₃₀ 30-norhopane (C₃₀ 30-norhopane/C₃₀ αβ hopane = 0.04) indicate the source rock(s) was not calcareous (Subroto et al., 1991). Oleanane, the biomarker for angiosperm higher plants that evolved during the Early Cretaceous- Late Jurassic (Moldowan et al., 1994; Zheng and Wang, 2010), could not be detected. Methylhopanes, an indicator of oxygen-producing cyanobacteria (Summons and Jahnke, 1990), are present in low abundance which is consistent with the low abundance of C₂₉ αβ hopane. Gammacerane, a biomarker suggesting water column stratification under a saline depositional environment or hypersalinity for the source rock (Sinninghe Damsté et al., 1995), is present at low abundance.

The higher abundance of rearranged hopane, Ts relative to Tm (Ts/Tm = 1.06), may be due to relatively high thermal maturity or due to generation from a source rock rich in clay. Maturity rather than source is the likely control on the abundance of rearranged diahopanes in this case. The C₃₁ 22S/(22S+22R) hopane ratio (0.52) is close to the equilibrium value (0.55), and typical for most oils in the early oil generation window.

Steranes and Diasteranes

Sterane and diasterane were monitored by SIM analyses using the *m/z* 217 and *m/z* 218 mass chromatograms (Figure A6-123), while the diasteranes were monitored using the *m/z* 217 and *m/z* 259 mass chromatograms (Figure A6-123a and Figure A6-125a). Peak annotations are defined in Table A5-40. A MRM experiment was also acquired to examine the distribution of C₂₇-C₃₀ steranes, diasteranes and methylsteranes in greater detail (Figure A6-127 and Figure A6-128).

The commonly occurring series of C₂₇ to C₂₉ αββ steranes and βα diasteranes were detected in the Gnarlyknots-1A FI oil. The sterane distribution is characterised by higher abundances of C₂₇ steranes compared to C₂₉ steranes with C₂₇:C₂₈:C₂₉ sterane distribution of 57:14:29, indicating predominant inputs from algal organic matter (Huang and Meinschein, 1979). The diasterane distribution is characterised by equal abundances between C₂₇ and C₂₉ βα diasteranes (C₂₇:C₂₈:C₂₉ βα diasterane = 32:34:33). The diasterane/sterane ratio is moderate (0.6), indicating the source rock(s) was not calcareous (Mello et al., 1988), which is consistent with the low C₂₉ αβ hopane/C₃₀ αβ hopane ratio. Steranes with carbon number C₂₆ or C₃₀ could not be detected in the MRM chromatograms and these compounds are either absent or below detection limits. Therefore, it was not possible to; (i) assess the geological age of the source rock(s) from the distribution of C₂₆ steranes (Holba et al., 1998a; 1998b), (ii) verify the input of marine organic matter from the presence of *n-propyl* cholestanes (Moldowan et al., 1990) and (iii) assess the distribution of C₃₀ methylsteranes (Summons et al., 1987).

Thermal maturity parameters determined from the distribution of steranes suggest an early oil window thermal maturity of the source rock(s) that generated the Gnarlyknots-1A FI oil. The C₂₉ sterane $\alpha\alpha\alpha$ 20S/(20S+20R) ratio is 0.38 which is significantly lower than their empirical end values (0.52-0.55) reached at a VRE of ca. 0.8%. A correlation of C₂₉ sterane $\alpha\alpha\alpha$ 20S/20R with vitrinite reflectance according to Sofer (1993) provides a VRE value of ca. 0.65%. This low maturity is supported by the C₂₉ $\alpha\beta\beta$ /($\alpha\beta\beta$ + $\alpha\alpha\alpha$) sterane ratio of 0.5 which is lower than the theoretical endpoint of 0.7 reached at peak oil window maturity (Seifert and Moldowan, 1986).

Aromatic Hydrocarbons

Eight major classes of aromatic hydrocarbons were monitored to assess variations in thermal maturity and source characteristics of the Gnarlyknots-1A FI oil. These compound classes include alkylbenzenes, alkylnaphthalenes, alkylphenanthrenes, alkylbiphenyls, alkylfluorenes, alkylpyrenes, alkylfluoranthrenes and alkyldibenzothiophenes. All chromatograms, including system blanks, are shown Figure A6-131 to Figure A6-148. A wide variety of source and maturity related parameters were determined from the integrated SIM mass chromatograms, and selected ratios are reported in Table A4-35. Abbreviations for aromatic hydrocarbons are defined in Table A5-43.

The distribution of aromatic compound classes for the Gnarlyknots-1A FI oil is characterised by very high abundances of C₂ alkylbenzenes which are about 10 times more abundant than phenanthrene (Figure A4-109). A predominance of aromatics with lesser degrees of alkylation are also apparent for naphthalenes, phenanthrenes, biphenyls and dibenzothiophenes (Figure A4-109).

There is no indication of biodegradation from the evaluation of aromatic compounds. For example, 1,2,4-trimethylbenzene is the largest peak in the *m/z* 120 mass chromatogram (Figure A6-131b), whereas in biodegraded oils, C₃ alkylbenzenes are either removed entirely or may be dominated by 1,2,3-trimethylbenzene (George et al., 2002).

The parameter [log (1,2,7-TMN/1,3,7-TMN)] is -0.7 which is below the benchmark value of -0.4, above which an angiosperm higher plant contribution would be suspected (Strachan et al., 1988). This is consistent with high abundances of C₂₇ steranes. Cadalene, eluting immediately after 1,3,6,7-TeMN, is present in low abundances in the *m/z* 183 mass chromatogram and 6-isopropyl-1-isohexylmethyl-2-methylnaphthalene (IP-iHMN) could not be detected (Figure A6-137a). Retene is present but also at low abundance (Figure A6-141b). Other aromatic biomarker ratios indicative of coniferous higher plant input, such as log (1-MP/9-MP) and log (Retene/9-MP), are low (Table A4-35), provide no evidence that the source rock contained significant amounts of *Araucariacean* higher plant organic matter (Alexander et al., 1988, 1992). The FI oil has a very low sulfur content indicated by low dibenzothiophene/phenanthrene (DBT/P) ratio. In a cross plot of DBT/P versus Pr/Ph, the FI oil falls in "Zone 3", as defined by Hughes et al. (1995), a zone typical for oils derived from "marine shale/other lacustrine settings". Hence marine shale is more probable over a lacustrine setting because of low abundances of C₂₆ tricyclic terpanes.

The methylbiphenyls, ethylnaphthalene, dimethylbiphenyls and trimethylnaphthalene distributions indicate highly variable maturities for the Gnarlyknots-1A FI oil. The aromatic hydrocarbon maturity parameters MNR, DNR-1 and MPR suggest the generation at a late oil to early gas window of 1.2-1.3% VRE. In contrast, the widely used maturity parameter MPI-1 gives a much lower calculated maturity value of 0.79% VRE, similar to the maturity based on MDR. Maturity based on TNR-2 gives a value of 0.96% VRE.

Diamondoid Hydrocarbons

Diamondoids were monitored in SIM mass chromatograms, and annotated mass chromatograms with corresponding blank levels are provided in Figure A6-149 and Figure A6-151. Abbreviations for diamondoid hydrocarbons are given in Table A5-44. Diamondoid hydrocarbons, previously identified in a number of crude oils and source rock samples (e.g. Petrov et al., 1974; Wingert, 1992 and Chen et al., 1996), have been suggested as indicators of thermal maturity (Chen et al., 1996), natural cracking (Dahl et al., 1999), biodegradation (Grice et al., 2000) and source rock facies (Schulz et al., 2001). Selected parameters derived from the diamondoid hydrocarbon distributions of the Gnarlyknots-1A FI oil is presented in Table A4-36.

The methyladamantane index (MAI) and the methyldiadamantane index (MDI) values for the Gnarlyknots-1A FI oil are 67 and 45 which, based on the relationship proposed by Chen et al. (1996), corresponds to VRE values of around 1.3%. This level of maturity is similar to VRE based on MNR, DNR-1 and MPR described previously.

The ratio of MA/A was found to increase with increasing levels of biodegradation and has been suggested as a tool for distinguishing different levels of biodegradation (Grice et al., 2000). The ratio of MA/A is 2, which is lower than the reported value of $MA/A \geq 6.0$ for biodegraded Australian crude oils (Grice et al., 2000). Schulz et al. (2001) defined the Ethyladamantane index (EAI) and Dimethyldiadamantane index 1 (DMDI-1) as indicators of source rock facies. DMDI-1 and EAI values (64 and 54) are comparable to the type II marine Spekk Formation from the Norwegian continental shelf (Schulz et al., 2001).

On-line MCI

Low molecular weight, gasoline range, hydrocarbons were studied by crushing and thermally extracting cleaned grains containing the oil inclusions. Selected chromatograms from the on-line crushing and thermal extraction are presented in Figure A7-153 to Figure A7-158. Abbreviations and structures for gasoline range hydrocarbons are defined in Table A5-45. Areas in the mass chromatograms were converted to TIC-equivalent data using response factors before calculating ratios, including the C₆-C₇ Thompson ratios that describe processes affecting light hydrocarbons (Table A4-37).

Toluene is the most abundant compound in the low molecular weight hydrocarbon range. The abundances of methylfuran and benzene are also much higher than the *n*-alkanes such as *n*-C₅, *n*-C₆, *n*-C₇, *n*-C₈ and *n*-C₉ (Figure A4-111). These compounds are relatively water soluble and most likely originated, in part, from coeval aqueous inclusions trapped in the rock grains (Ruble et al., 1998). As such, Thompson parameters (Thompson, 1987) based on these water soluble compounds, such as toluene/*n*-heptane (aromaticity ratio, "B"), are likely to be overestimated.

The Gnarlyknots-1A FI oil has a heptane value "H", $(100 \times n\text{-heptane})/(\Sigma \text{ cyclohexane} + C_7 \text{ HCs})$, of 47 and an "F" value, $n\text{-heptane}/\text{methylcyclohexane}$, of 2.4 (Table A4-37), falling in the "superature oils" category when applying Thompson's criteria with a VRE of around 1.6-1.8% (Thompson, 1987). Based on the paraffinicity ratio "I" $(2MH+3MH)/(C_{13}DMCP+t_{13}DMCP+t_{12}DMCP)$, however, the Gnarlyknots-1A FI oil was generated within the peak oil window with a VRE of 1.2%.

The dominance of 6 ring preference (methylcyclohexane+toluene) compared to 5 ring preference (alkylcyclopentanes) and 3 ring preference (iso-alkanes) among the C₇ hydrocarbons (Table A4-37) is

very strong and is likely a consequence of the incorporation of toluene from aqueous inclusions as discussed above. As such, these parameters cannot be used to infer source according to ring preference (ten Haven, 1996).

Carbon isotopes of fluid inclusion gases

The bulk carbon isotopic composition of FI gases in the Gnarlyknots-1A (4410-4415m) sample was analysed twice to assess variability in the data (Table A4-38; Figure 54).

The gasses CH₄ (methane), C₂H₆ (ethane) and CO₂ (carbon dioxide) were detected and the carbon isotopic compositions ($\delta^{13}\text{C}$) determined as; methane -28.4‰ and -28.6‰, ethane -17.6‰ and -18.1‰ and carbon dioxide -3.9‰ and -4.4‰. The carbon isotopic composition of higher molecular weight hydrocarbon gases were not obtained due to their low concentration.

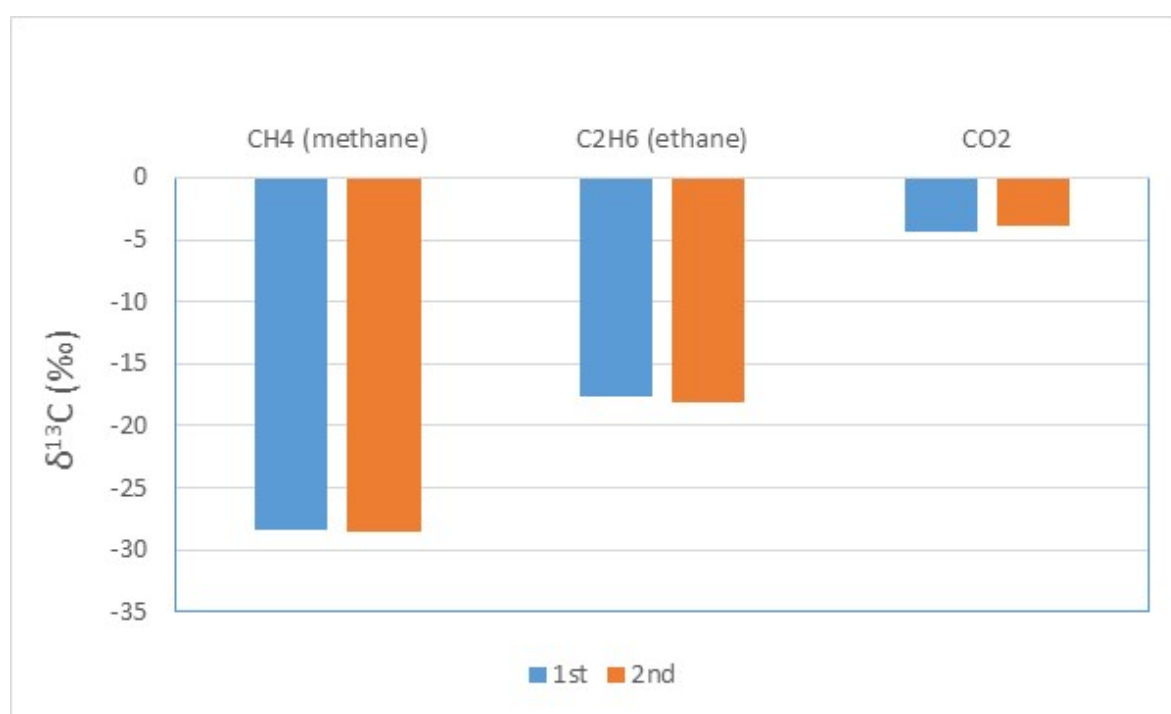


Figure 54: Carbon isotopic composition of FI gases from Gnarlyknots-1A (4410-15 mMD) showing reproducibility of the duplicates.

Greenly-1

A sand-rich cuttings interval from the Upper Cretaceous (Cenomanian) White Pointer Supersequence in Greenly-1, eastern Ceduna/Duntroon sub-basins, was selected for off-line MCI analysis only (Table 11; Figure 55).

- Off-line MCI sample: 4,806 m to 4,818 mMD (4 consecutive cuttings samples combined).

The Greenly-1 sample combined four cuttings intervals, two of which had confirmed anomalous GOI abundance (1.1% @ 4,809-12 m and 0.7% @ 4,812-15 m; Lisk et al., 2001). Due to the nature of the sample it was pre-prepared for MCI as two fractions; a disaggregated detrital sand fraction and a rock aggregate fraction. The rock aggregate fraction comprised carbonate-cemented sandstone with oil inclusions located in both detrital quartz and carbonate. After extensive treatment by the MCI method, a clean outside rinse of the rock aggregate fraction was successfully obtained.

This was not the case for the disaggregated sand fractions. Further mineral separation was required to separate the sample into two further fractions—one with clean quartz grains (non-magnetic) and one comprising quartz grain/carbonate cement (magnetic). After MCI cleaning, a clean outside rinse was obtained for the clean quartz grains but not the quartz grain/carbonate cement fraction. This was attributed to extraction of oil from inclusions in the softer carbonate cement during the cleaning process.

The aggregates and clean quartz fraction were combined for crushing as one sample (<15 g) for off-line MCI. The quartz grain/carbonate cement fraction was crushed separately. After comparing the results, and noting similarity, the data from both extracts was combined.

Table 11: MCI sample information – Greenly-1.

Well	Depth (mMD)	GOI (%)	Off-line MCI	On-line MCI	Gas isotopes
Greenly-1	4806-09 m	Not analysed	134522	-	-
Greenly-1	4809-12 m	GOI-1.1%	134603	-	-
Greenly-1	4812-15 m	GOI-0.7%	134523	-	-
Greenly-1	4815-18m	Not analysed	134604	-	-

Off-line MCI

Geochemical parameters obtained from the Greenly-1 FI oil are shown in Appendix 4. Mass chromatograms and the associated system blanks are shown in Appendix 8, with peak assignment nomenclature shown in Appendix 5.

n-Alkane and Branched Alkanes

The *m/z* 85 mass chromatogram (Figure A6-112) was used to calculate the abundances of *n*-alkanes and isoprenoids in the Greenly-1 FI oil. The quantitative data were derived from comparison of the area of the internal standard Squalane, with the *n*-alkanes, taking into account the response factor for the instrument used. Yields of *n*-alkanes of the Greenly-1 FI oil and system blank are provided in Table A4-31. Various *n*-alkane and isoprenoid ratios are provided in Table A4-32. Normalised distributions of *n*-alkanes in the Greenly-1 FI oil and system blank are shown in Figure A4-106.

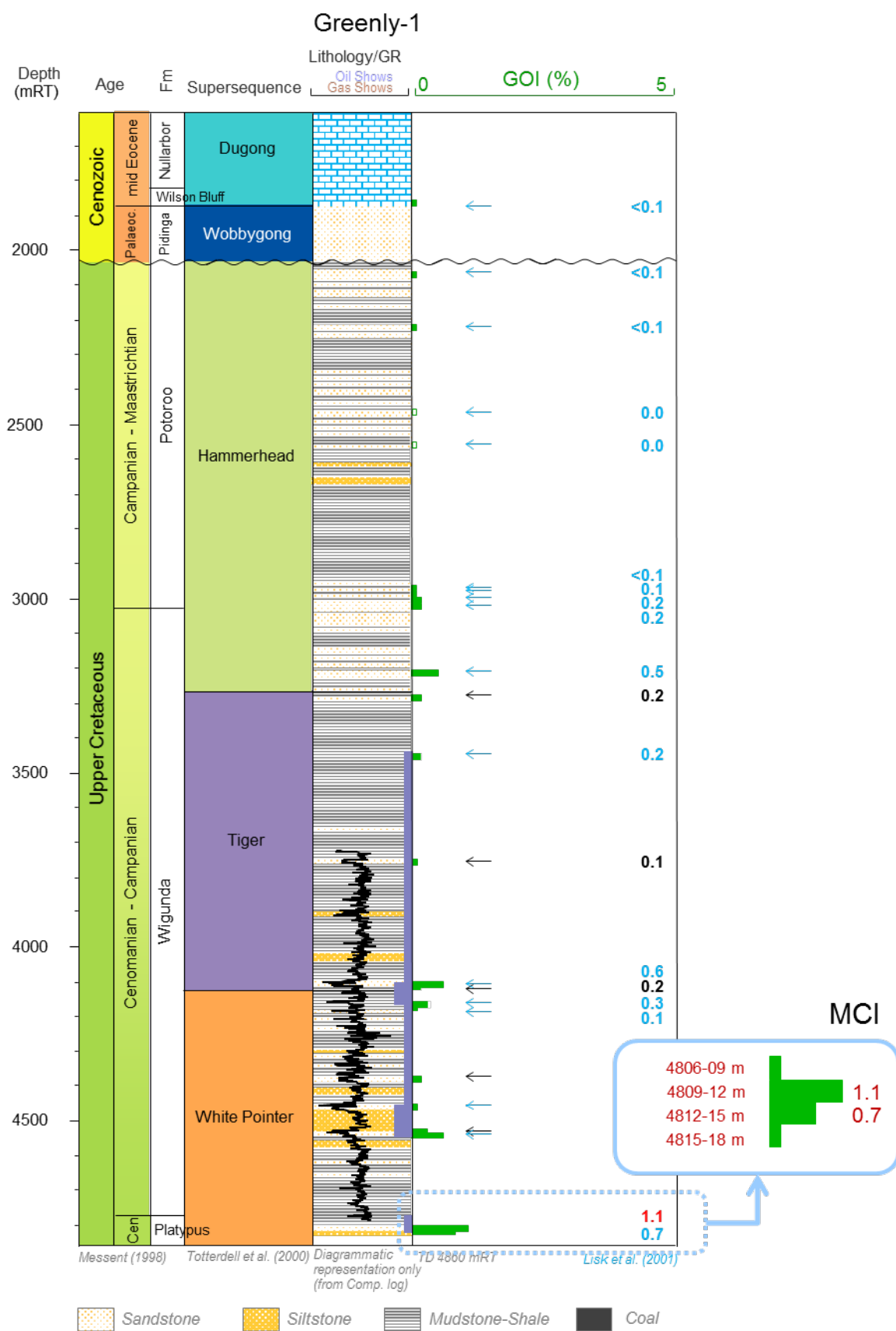


Figure 55: Greenly-1 — samples for MCI (off-line only).

n-Alkane recovery in the range of *n*-C₁₂ to *n*-C₃₂ from the Greenly-1 FI oil is 10,592.6 ng, which is 658 times more than that of the system blank and 145 times more than that of the final outside rinse (Table A4-31). Therefore, the results presented in this study can be interpreted with a high degree of confidence.

The *m/z* 85 mass chromatogram shows a unimodal distribution of *n*-alkanes with a maxima at *n*-C₂₅, which results in a high wax index (1.9) and indicates that the source of the Greenly-1 FI oil was derived from terrestrial organic matter input. A Pr/Ph ratio of 3 indicates an oxic depositional environment (Peters et al., 2005). Carbon preference indices (CPI) for C₂₂₋₃₂ show a slight odd-over-even predominance (Table A4-32). Based on a plot of Pr/*n*-C₁₈ versus Pr/*n*-C₁₇ (Figure A4-108), the source rock contains type III kerogen deposited in relatively oxic conditions.

Terpanes

Terpanes were monitored using four SIM mass chromatograms and also by MRM chromatograms. The *m/z* 123 mass chromatogram (Figure A8-163a) shows that C₁₄ to C₁₆ bicyclic sesquiterpanes are present in the Greenly-1 FI oil. Diterpane are either absent or below the limits of detection (Figure A8-163b). This indicates that the source rocks that generated the Greenly-1 FI oil contain no, or only minor amounts of, coniferous organic matter (Noble et al., 1985a, 1985b, 1986).

Hopanes, moretanenes (Figure A8-163c) and the tricyclic and tetracyclic terpanes (Figure A8-165a) were monitored using the *m/z* 191 mass chromatograms. The presence of dimethylhopanes was evaluated using the *m/z* 177 mass chromatogram (Figure A8-165b), whereas methylhopanes were analysed using the *m/z* 205 mass chromatogram (Figure A8-165c). Peak annotations are defined in Table A5-39. Mass chromatograms of the system blank scaled to the same extent by using the internal standard (Squalane) demonstrate that the Greenly-1 FI oil data can be interpreted with confidence. Ratios based on terpanes are shown in Table A4-33.

The relative abundances of tricyclic terpanes are very low, dominated by C₁₉ and C₂₀ tricyclic and C₂₄ tetracyclic terpane ((C₁₉+C₂₀)/C₂₃ tricyclic terpane = 10; C₂₄ tetracyclic/C₂₃ tricyclic terpane = 2.3), indicating terrestrial organic matter input (Philp and Gilbert, 1986; Preston and Edwards, 2000; Grice et al., 2001; Peters et al., 2005). The abundances of C₂₆ tricyclic terpanes are similar to that of C₂₅ tricyclic terpanes (C₂₆/C₂₅ tricyclic terpane = 1.02), indicating that the source rock of the Greenly-1 FI oil had little contribution from a lacustrine source (Peters et al., 2005).

Hopanes in the Greenly-1 FI oil are dominated by C₃₀ αβ hopane. The relatively high abundances of C₂₉Ts and diahopane (C₃₀*) (C₂₉Ts/C₂₉ αβ hopane = 0.33; C₃₀*/C₃₀ αβ hopane = 0.28) may indicate the source rock of the Greenly-1 FI oil was deposited under oxic conditions which is consistent with Pr/Ph ratio. Low C₂₉ αβ hopane/C₃₀ αβ hopane (0.59) and absence of C₃₀ 30-norhopane indicate the source rock of the Greenly-1 FI oil is not calcareous (Subroto et al., 1991). This is supported by low abundances of methylhopanes, peaks that tend to be more abundant in oils derived from calcareous source rock rich in prokaryotic organic matter (Summons et al., 1999). However, a series of C₃₂-C₃₄ 2α-methylhopanes probably indicate input of oxygen-producing cyanobacteria (Summons and Jahnke, 1990). A series of C₃₁- C₃₂ 3β methylhopanes indicate a methanotrophic bacteria source (Burhan et al., 2002; Farrimond et al., 2004). Oleanane, the biomarker for angiosperm higher plants that evolved during the Early Cretaceous- Late Jurassic, could not be detected. Gammacerane, a

biomarker suggesting water column stratification under a saline depositional environment or hypersalinity for the source rock (Sinninghe Damsté et al., 1995), is present in low abundance.

The lower abundance of rearranged hopane Ts relative to Tm ($T_s/T_m = 0.69$) may be due to relatively low thermal maturity. The $C_{31} 22S/(22S+22R)$ hopane ratio (0.52) is close to the equilibrium value (0.55), typical for most oils in the early oil generation window.

Steranes and Diasteranes

Steranes and diasteranes were monitored by SIM analyses using the m/z 217 and m/z 218 mass chromatograms (Figure A8-170), while the diasteranes were monitored using the m/z 217 and m/z 259 mass chromatograms (Figure A8-170a and Figure A8-172a). Peak annotations are defined in Table A5-40. An MRM experiment was also acquired to examine the distribution of C_{27} - C_{30} steranes, diasteranes and methylsteranes in greater detail (Figure A8-174 and Figure A8-175).

The commonly occurring series of C_{27} to C_{29} $\alpha\beta\beta$ steranes and $\beta\alpha$ diasteranes were detected in the Greenly-1 FI oil. The sterane distribution is characterised by higher abundances of C_{29} steranes compared to C_{27} steranes with $C_{27}:C_{28}:C_{29}$ sterane distribution of 29:13:59, indicating predominant inputs from terrestrial higher plant derived organic matter (Huang and Meinschein, 1979). The diasterane distribution is also dominated by C_{29} diasteranes ($C_{27}:C_{28}:C_{29}$ $\beta\alpha$ diasterane = 19:17:64). The diasterane/sterane ratio is relatively high (1.02), indicating the source rock of the Greenly-1 FI oil is clay-rich and not calcareous (Mello et al., 1988; Peters et al., 2005). Steranes with carbon number C_{26} or C_{30} could not be detected in the MRM chromatograms and these compounds are either absent or below detection limits. Therefore, it was not possible to assess; (i) the geological age of the probable source rock from the distribution of C_{26} steranes (Holba et al., 1998a, 1998b), (ii) verify the input of marine organic matter from the presence of *n-propyl* cholestanes (Moldowan et al., 1990) and (iii) the distribution of C_{30} methylsteranes (Summons et al., 1987).

Thermal maturity parameters determined from the distribution of steranes suggests an early oil window thermal maturity of the source rock that generated the Greenly-1 FI oil. The C_{29} sterane $\alpha\alpha\alpha$ 20S/(20S+20R) ratio for the Greenly-1 FI oil is 0.38 which is significantly lower than their empirical end values (0.52-0.55) reached at a VRE of ca. 0.8%. A correlation of C_{29} sterane $\alpha\alpha\alpha$ 20S/20R with vitrinite reflectance according to Sofer (1993) provides a VRE value of ca. 0.65%. This low maturity is supported by the C_{29} $\alpha\beta\beta/(\alpha\beta\beta+\alpha\alpha\alpha)$ sterane ratio of 0.5 which is lower than the theoretical endpoint of 0.7 reached at peak oil window maturity (Seifert and Moldowan, 1986).

Aromatic Hydrocarbons

Eight major classes of aromatic hydrocarbons were monitored to assess variations in thermal maturity and source characteristics of the Greenly-1 FI oil. These compound classes include alkylbenzenes, alkylnaphthalenes, alkylphenanthrenes, alkylbiphenyls, alkylfluorenes, alkylpyrenes, alkylfluoranthrenes and alkyldibenzothiophenes. All chromatograms are shown in Figure A8-178 to Figure A8-194. A wide variety of source and maturity related parameters were determined from the integrated SIM mass chromatograms, and selected ratios are reported in Table A4-35. Abbreviations for aromatic hydrocarbons are defined in Table A5-43.

The distribution of aromatic compound classes for the Greenly-1 FI oil is characterised by relatively high abundances of C_1 - C_3 alkylnaphthalenes, phenanthrene and alkylphenanthrenes (Figure A4-110). The predominance of alkyl-aromatics indicate a higher degree of alkylation.

There is no indication of biodegradation from the evaluation of aromatic compounds. For example, 1,2,4-trimethylbenzene is the largest peak in the m/z 120 mass chromatogram (Figure A8-178b), whereas in biodegraded oils, C3 alkylbenzenes are either removed entirely or may be dominated by 1,2,3-trimethylbenzene (George et al., 2002).

The parameter $[\log (1,2,7\text{-TMN}/1,3,7\text{-TMN})]$ is -0.74 which is below the benchmark value of -0.4, above which an angiosperm higher plant contribution would be suspected (Strachan et al., 1988). Cadalene, eluting immediately after 1,3,6,7-TeMN, is present in relatively low abundance in the m/z 183 mass chromatogram and 6-isopropyl-1-isohexylmethyl-2-methylnaphthalene (IP-iHMN) could not be detected (Figure A8-184a). Retene is also present at relatively low abundance (Figure A8-188b). Other aromatic biomarker ratios indicative of coniferous higher plant input, such as $\log (1\text{-MP}/9\text{-MP})$ and $\log (\text{Retene}/9\text{-MP})$, are low (Table A4-35) and do not provide evidence that the source rock contained significant amounts of *Araucariacean* higher plant organic matter (Alexander et al., 1988, 1992). The Greenly-1 FI oil contains very low sulfur content, as indicated by the low dibenzothiophene/phenanthrene ratio. In a cross plot of DBT/P versus Pr/Ph, the Greenly-1 FI oil falls between “Zone 3” and “Zone 4” (Hughes et al., 1995), and, while not specific, refers to oils derived from marine shale/other lacustrine settings or fluvial/deltaic settings.

The methylbiphenyls, ethylnaphthalene, dimethylbiphenyls and trimethylnaphthalene distributions indicate variable maturities for the Greenly-1 FI oil. The aromatic hydrocarbon maturity parameters MNR, TNR-2, MPR and MDR suggest the generation at peak oil window of 0.9-1.1%. In contrast, the widely used maturity parameter MPI-1 gives a much lower calculated maturity value of 0.8%, similar to the maturity based on DNR-1 (0.77% VRE).

Diamondoid Hydrocarbons

Diamondoids were monitored in SIM mass chromatograms, and annotated mass chromatograms with corresponding blank levels are provided in Figure A8-196 to Figure A8-199. Abbreviations for diamondoid hydrocarbons are given in Table A5-44. Diamondoid hydrocarbons, previously identified in a number of crude oils and source rock samples (e.g. Petrov et al., 1974; Wingert, 1992; Chen et al., 1996), have been suggested as indicators of thermal maturity (Chen et al., 1996), natural cracking (Dahl et al., 1999), biodegradation (Grice et al., 2000) and source rock facies (Schulz et al., 2001). Some selected parameters derived from the diamondoid hydrocarbon distributions of the Greenly-1 FI oil is presented in Table A4-36.

The methyladamantane index (MAI) and the methyldiadmantane index (MDI) values for the Greenly-1 FI oils are 55 and 50 which, based on the relationship proposed by Chen et al. (1996), corresponds to VRE values of a wide range from 1.1% to 1.6%. This level of maturity is higher than VRE values based on aromatic hydrocarbons described previously for the Gnarlyknots-1A FI oil.

The ratio of MA/A was found to increase with increasing levels of biodegradation and has been suggested as a tool for distinguishing different levels of biodegradation (Grice et al., 2000). The ratios of MA/A for the Greenly-1 FI oil is 1.4, which is lower than the reported value of $\text{MA}/\text{A} \geq 6.0$ for biodegraded Australian crude oils (Grice et al., 2000). Schulz et al. (2001) defined the Ethyladamantane index (EAI) and Dimethyldiamantane index 1 (DMDI-1) as indicators of source rock facies. DMDI-1 and EAI values (78 and 66) are comparable to possible mixed type II marine Spekk Formation and type III terrestrial Åre Formation from the Norwegian continental shelf (Schulz et al., 2001).

DISCUSSION

Potential Source Rocks in the Bight Basin

The thick sedimentary succession in the Ceduna and Duntroon sub-basins contains a number of source intervals of marine and non-marine carbonaceous shale, coal and oil shale. They were deposited in a variety of lacustrine (lake), deltaic and marine environments that have the potential to form good to excellent quality source rocks capable of generating hydrocarbons (Blevin et al., 2000; Totterdell et al., 2000; Stuckmeyer et al., 2001; Totterdell et al., 2008).

Six potential petroleum systems have been identified as a result of sequence stratigraphic analysis (Totterdell et al., 2000). From youngest to oldest these include:

- Hammerhead system: Santonian-Campanian marine deltaic system,
- White Pointer-Tiger system: Cenomanian-Santonian marine system,
- Blue Whale system: mid-Albian marine system,
- Upper Bronze Whaler system: Aptian marine system,
- Southern Right system: Berriasian, lacustrine system,
- Sea Lion-Minke system: Late Jurassic, syn-rift, lacustrine system.

While the Jurassic–Lower Cretaceous non-marine source rocks are important in the shallower, more proximal parts of the basin (Eyre and Duntroon Sub-basins), the key to the petroleum prospectivity of the Ceduna Sub-basin resides in marine shales of the Blue Whale and Tiger supersequences and coaly facies of the upper Bronze Whaler and White Pointer supersequences (Figure 61).

Tiger Supersequence

The Turonian–Santonian Tiger Supersequence comprises marine shales. While historic well data suggested the sequence had overall poor to fair source potential (Totterdell et al., 2009, 2010), deposition was at a time of high global sea levels, and potentially coincident with the Bonarelli Event (or Ocean Anoxia Event, OAE 2) at the Cenomanian–Turonian boundary (Arthur et al., 1990). Totterdell et al. (2000) and Struckmeyer et al. (2001) postulated that this unit in the Bight Basin could contain good quality marine source rocks. This was tested by dredging a number of samples from rocks outcropping on the seafloor (Totterdell et al., 2008; Totterdell and Mitchell, 2009) and those dated as latest-Cenomanian-to-Turonian (11 samples) had high amounts of extractable organic matter that was deposited in a marine environment under reducing conditions. These rocks have good to excellent generative potential for oil and is mature for oil and gas across the greater part of the depocentre and immature along the basin margins (Totterdell et al., 2008).

White Pointer Supersequence

The Cenomanian White Pointer Supersequence comprises deltaic to shallow marine shales, with a considerable proportion of organic matter being coal comprising Type III kerogen (Struckmeyer et al., 2001). TOC values from shales and siltstones are consistently above 1% and mostly above 2% and contain Type II/III kerogen. The succession has good to excellent source potential for both oil and gas (Totterdell et al., 2009, 2010). The lower part of this thick succession is typically gas mature

throughout the basin, except for the basin margins. The upper White Pointer Supersequence lies within the oil window and wet gas window in the greater part of the basin (Totterdell et al., 2008).

Blue Whale Supersequence

The Albian–Cenomanian Blue Whale Supersequence comprises marine shales. The proximal end-members of the Blue Whale Supersequence have been sampled in several wells and organic matter content is high (Struckmeyer et al., 2001), with TOC values ranging from 0.5% to 62%, typically comprising Type II/III kerogen. Rock-Eval and TOC data show that, overall, the Blue Whale Supersequence has good potential for the generation of both oil and gas (Totterdell et al., 2009, 2010). The depositional framework suggests that the supersequence was deposited in more open marine conditions further basinward, indicating source potential is likely to increase in more distal facies.

Upper Bronze Whaler Supersequence

The Valanginian–Albian Bronze Whaler Supersequence comprises coastal plain to marginal marine mudstones and coal. The supersequence has differing source richness for its upper and lower sections. High TOCs of up to 57% are largely due to the presence of coals in the upper part of the succession. This part of the supersequence is characterised by Type II/III to Type II kerogen, whereas the lower part contains mostly Type III kerogen and is more similar to the underlying Southern Right Supersequence (Struckmeyer et al., 2001). While the upper, more marine-influenced part has good to excellent potential for both oil and gas, the lower and dominantly non-marine section has moderate potential for mainly gas.

Fluid Inclusion Source Characteristics and Palaeo-depositional Conditions

Biomarkers are a group of compounds, primarily hydrocarbons, found in oils, rock extracts, recent sediment extracts and soil extracts. What distinguish biomarkers from other compounds in oil is that biomarkers can reasonably be called “molecular fossils”. Biomarkers are structurally similar to, and are diagenetic alteration products of specific natural products (compounds produced by living organisms). Hence biomarkers such as diterpanes, terpanes, hopanes and steranes can provide information on the organic matter type in the source, rock mineralogy (lithology), the depositional environment, age and thermal maturity.

The key source-environment biomarker information for the Gnarlyknots-1A and Greenly-1 FI oils is shown in Table 12. Comparisons of selected biomarker ratios for the Gnarlyknots-1A and Greenly-1 FI oils are shown in Figure 56 (*n*-alkanes), Figure 57 (pristane/*n*-C₁₇ versus phytane/*n*-C₁₈ ratios), Figure 58 (C₂₄ tetracyclic/C₂₃ tricyclic terpanes versus (C₁₉+C₂₀)/C₂₃ tricyclic terpane ratios), Figure 59 (C₂₇:C₂₈: C₂₉ sterane ratios) and Figure 60 (DBT/P versus pristane/phytane ratios).

Table 12: Summary of biomarker related source indicators in the Gnarlyknots-1A and Greenly-1 fluid inclusion oil.

Source information	Biomarker parameters	Comments	Distribution in FI oils
Terrigenous organic matter inputs	Oleanane, Lupanes	Present indicating higher plant input to source rock (Moldowan et al., 1994)	Absent in both FI oils
	Bicadinanes	Derived from Dipterocarpaceae tree resins (Cox et al., 1986; van Aarssen et al., 1990)	Absent in both FI oil
	Retene, Cadalene	Biomarkers indicating conifer input to source rock (Noble et al., 1985a, b)	Relatively higher in Greenly-1 FI oil
	C ₂₉ steranes	High relative to total C ₂₇ -C ₂₉ steranes (Huang and Meinschein, 1979; Moldowan et al., 1985)	Low in Gnarlyknots-1A FI oil and high in Greenly-1 FI oil
	C ₂₄ tetracyclic and C ₁₉ tricyclic terpanes	Biomarkers indicating higher plant inputs to source	Low in Gnarlyknots-1A FI oil and high in Greenly-1 FI oil
	<i>n</i> -C ₂₇ , <i>n</i> -C ₂₉ , <i>n</i> -C ₃₁	High indicating higher plant inputs (Eglinton and Hamilton, 1967)	High in both FI oils
Lacustrine source rock	3β-mehtylhopanes	High in lacustrine source indicating methanotrophic bacteria input (Colliser et al., 1992; Farrimond et al., 2004)	Present in Greenly-1 FI oil but absent in Gnarlyknots-1A FI oil
	C ₂₆ /C ₂₅ tricyclic terpanes	>1 in lacustrine-shale-sourced oils (Schiefelbein et al., 1999)	>1 in Greenly-1FI oil and <1 in Gnarlyknots-1A FI oil
	β-Carotane	Present indicating lacustrine source (Jiang and Flower, 1986)	Absent in both FI oils
	Tetracyclic polyprenoids	High in oils from lacustrine sources (Holba et al., 2000, 2003)	Absent in both FI oils
	Botryococcane	Present indicating lacustrine source (Moldowan et al., 1980)	Absent in both FI oils
Marine organic matter inputs	24- <i>n</i> -propycholestanes	Present indicating marine organic matter (Moldowan et al., 1990)	Absent in both FI oils
	Sterane/Hopane	≥1 indicating marine organic matter (Moldowan et al., 1985)	Less than 1 in both FI oils
	<i>n</i> -C ₁₅ , <i>n</i> -C ₁₇ , <i>n</i> -C ₁₉	High incidating algal inputs (Gelpi et al., 1970)	High in Gnarlyknots-1A and low in Greenly-1 FI oils
	C ₂₇ steranes	High indicating algal inputs (Peters et al., 2005)	High in Gnarlyknots-1A and low in Greenly-1 FI oils
Lithology of source rocks	2α-methylhopane	High in calcareous source rocks with high cyanobacterial input (Summons et al., 1999)	Present but not in high abundances in both FI oils
	C ₂₉ /C ₃₀ αβ hopane	≥1 indicating carbonate source rocks (ten Haven et al., 1988)	Less than 1 for both FI oils
	Diasteranes/steranes	High in clay-rich source rocks (Peters et al., 2005)	High in Greenly FI oil but moderate in Gnarlynots-1A FI oil
	Rearranged hopanes	High in clay-rich source rocks (Moldowan et al., 1991)	Relatively low in both FI oils
	Dibenzothiophene/pheanthrene	>1 in oils from high sulfur carbonate (Hughes et al., 1995)	Less than 1 in both FI oils
Depositional age of source rocks	Oleanane	Present indicating Late Cretaceous or younger source rocks (Moldowan et al., 1994)	Absent in both FI oils
	24-norcholestane and 24-nordiacholestane	high in source rocks containing diatoms (Cretaceous or younger, Holba et al., 1998)	Absent in both FI oil

	4 α -methylsteranes	Presence indicating evidence for Mesozoic or younger source rocks (Summons and Capon, 1988)	Absent in both FI oil
	C ₁₁ -C ₁₉ <i>n</i> -alkanes	Odd-carbon-number predominance in oil from many Ordovician sources (Douglas et al., 1991; Folwer, 1992)	No odd-carbon-predominance for both FI oils
Hypersaline depositional environment	Pr/Ph	<0.5 indicating hypersaline depositional condition (ten Haven et al., 1987; 1988)	>0.5 for both FI oils
	Gammacerane	High relative to C ₃₁ hopanes in oils derived from sources deposited under hypersaline depositional conditions. High values indicate stratified water column during source deposition (Sinninghe Damsté et al., 1995)	Low in both FI oils
Anoxic depositional environment	C ₃₅ homohopanes	High relative to total hopanes in oils from source rocks deposited under anoxic conditions (Peters and Moldowan, 1991)	Low in both FI oils
	Pr/Ph	< 1 indicates anoxic conditions (Didyk et al., 1978)	>1 for both FI oils
	28,30-bisnorhopane	High in certain reducing environment (Schoell et al., 1992; Moldowan et al., 1984)	Low in both FI oils

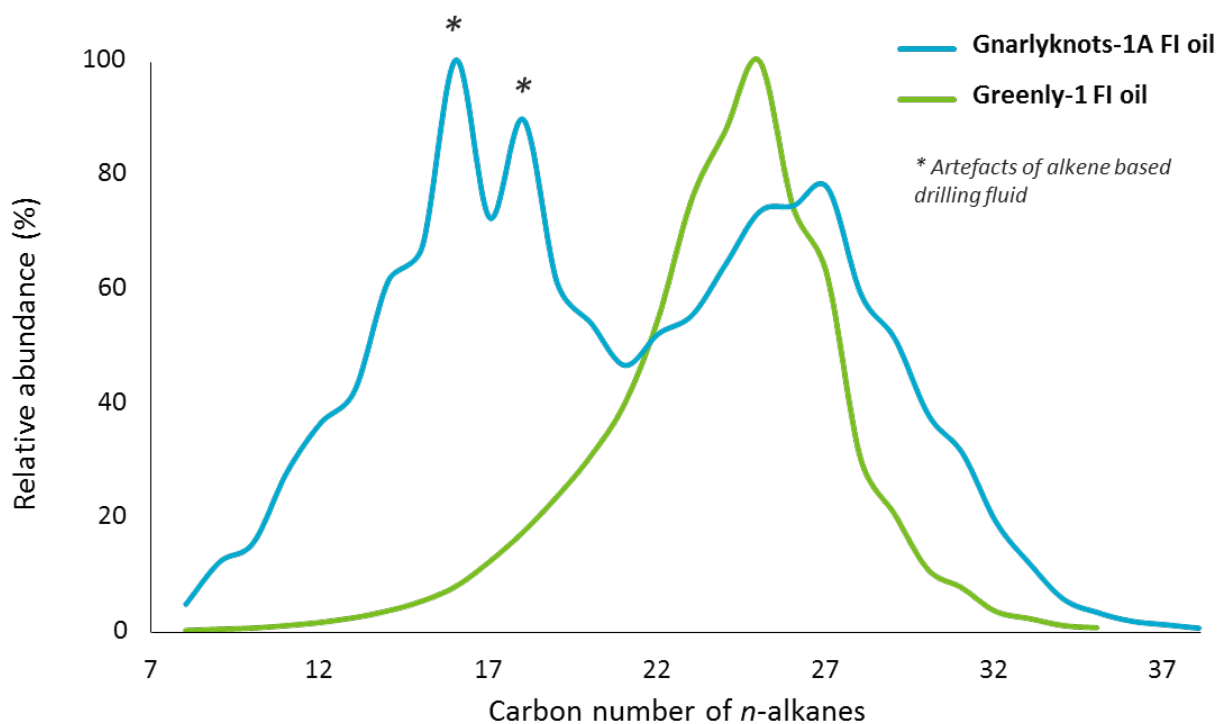


Figure 56: Comparison of normalized *n*-alkane distributions in the Gnarlyknots-1A and Greenly-1 FI oils.

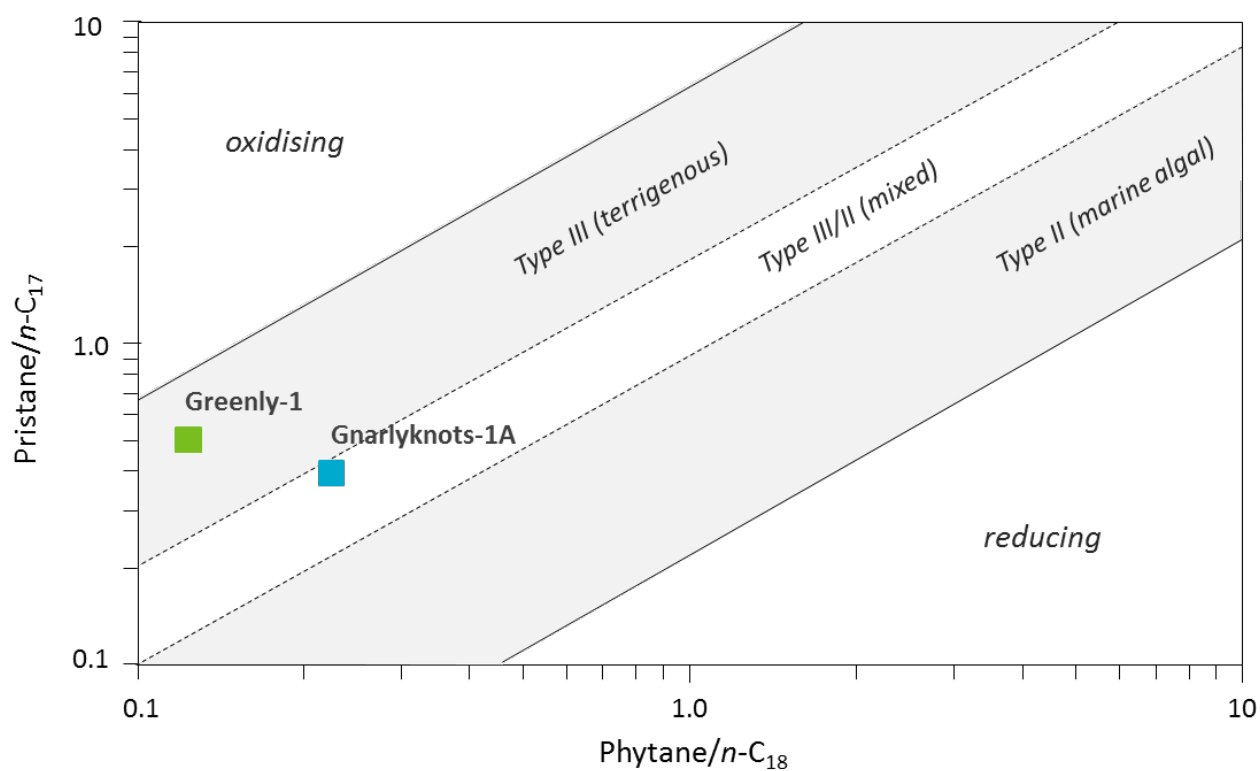


Figure 57: Comparison of pristane/ $n\text{-C}_{17}$ versus phytane/ $n\text{-C}_{18}$ ratios in the Gnarlyknots-1A and Greenly-1 FI oils.

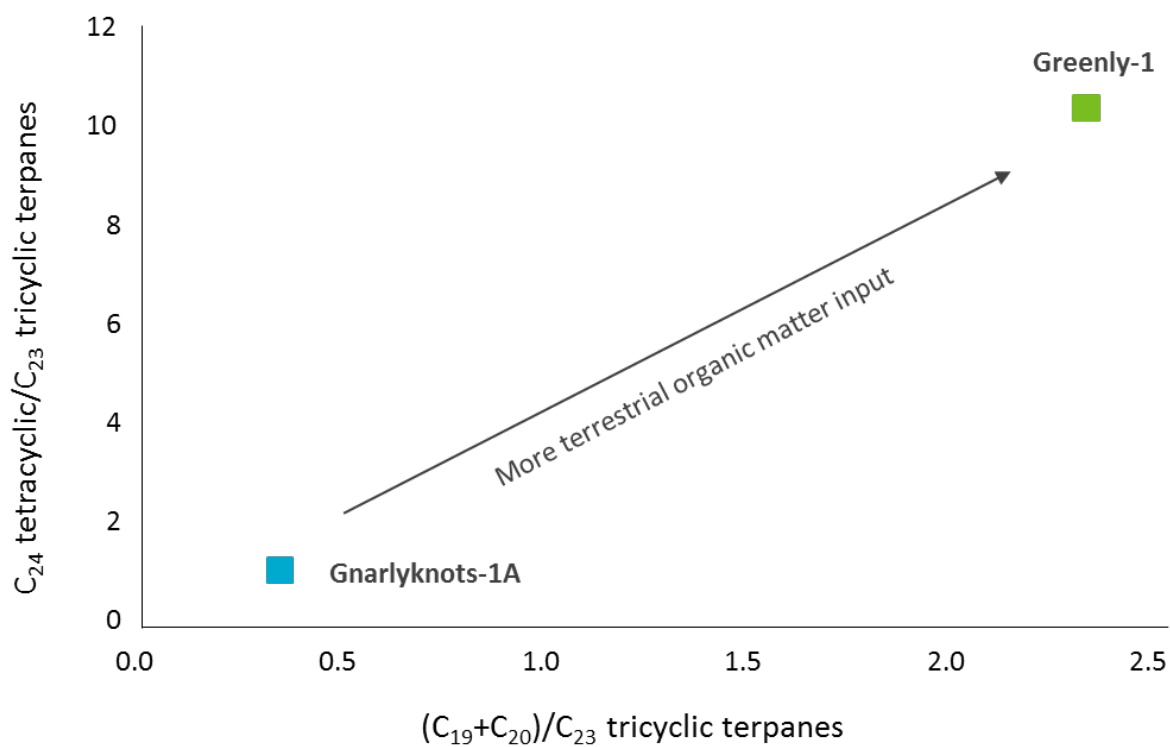


Figure 58: Comparison of C_{24} tetracyclic/ C_{23} tricyclic terpanes versus $(\text{C}_{19} + \text{C}_{20})/\text{C}_{23}$ tricyclic terpanes in the Gnarlyknots-1A and Greenly-1 FI oils.

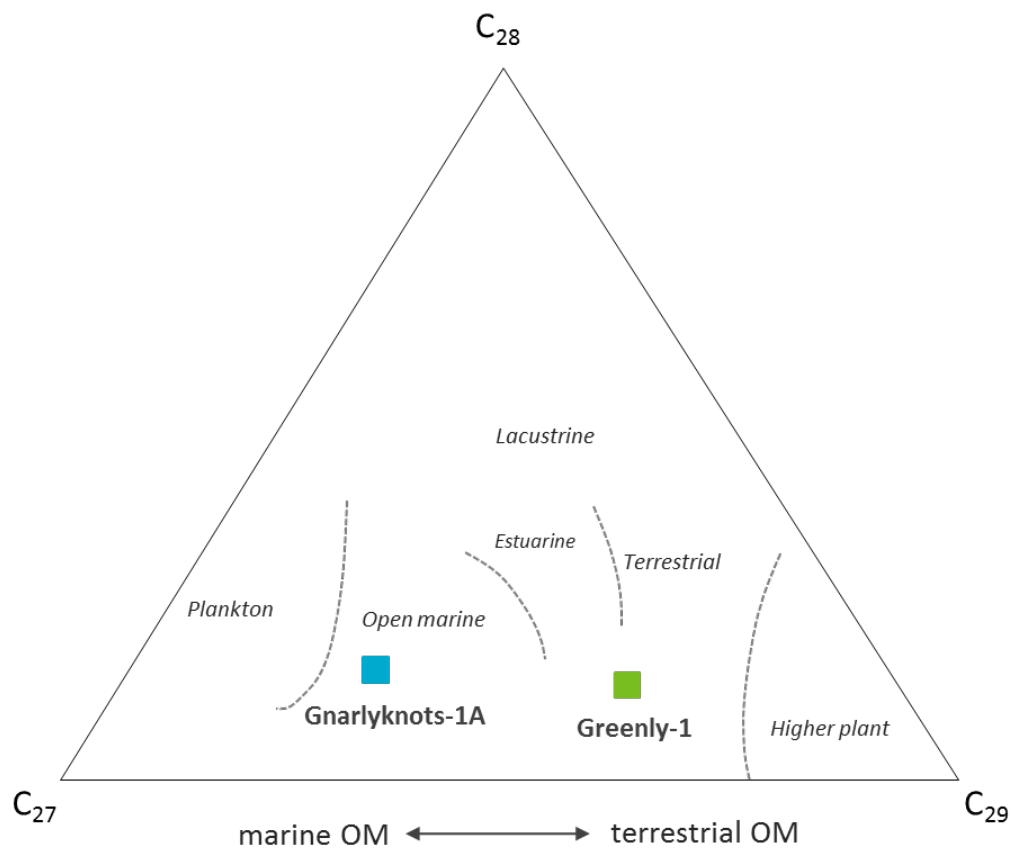


Figure 59: Comparison of C_{27} , C_{28} , C_{29} steranes in the Gnarlyknots-1A and Greenly-1 FI oils.

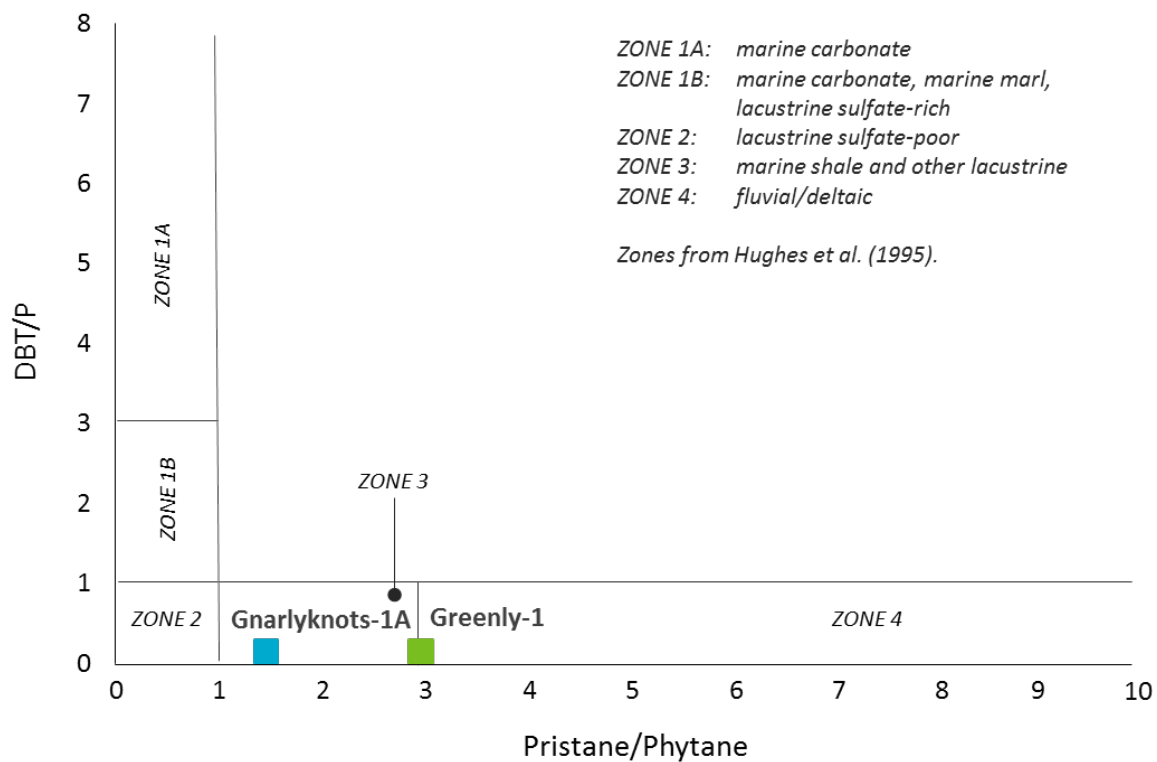


Figure 60: Comparison of dibenzothiophene/phenanthrene (DBT/P) versus pristane/phytane ratios in the Gnarlyknots-1A and Greenly-1 FI oils.

Gnarlyknots-1A FI Oil

The FI oil extracted from the Late Cretaceous (intra-Coniacian) Tiger Supersequence in Gnarlyknots-1A (4390 m to 4425 m) is a bulk extract derived from multiple detrital grains. While this FI oil may have been trapped at the same time, given the variability in assemblage composition of both oil and gas rich inclusions (Figure 13; Figure 33), it would seem more probable that the extract represents a mixture of different hydrocarbon generations.

The geochemical results show that the Gnarlyknots-1A FI oil was probably generated from marine shale deposited in a sub-oxic to oxic environment with mixed organic matter inputs including both algae and terrestrial plants indicated by bimodal *n*-alkane distribution (Figure 56), relatively low Pr/Ph ratio, mixed type II/III kerogen (Figure 57), and relatively high abundances of C₂₃ tricyclic terpanes (Figure 58) and C₂₇ steranes (Figure 59). The significance is that this represents the first geochemical evidence in the basin for hydrocarbons generated from at least some algal organic matter.

The Blue Whale and Tiger supersequences (Figure 61) are considered potential sources of marine algal organic matter in the Ceduna Sub-basin and co-sourcing from either one of these is a possibility for the FI oil in Gnarlyknots-1A. Similarly the White Pointer Supersequence is a potential source of terrigenous organic matter. Whether the Gnarlyknots-1A FI oil was derived from single or multiple source(s) is, however, not known because source rocks have not been cored for oil-source correlations. If, for instance, the White Pointer Sequence was considered a single source of the FI oil, then perhaps a paralic facies containing interfingered marine algal and terrigenous sediments might exist.

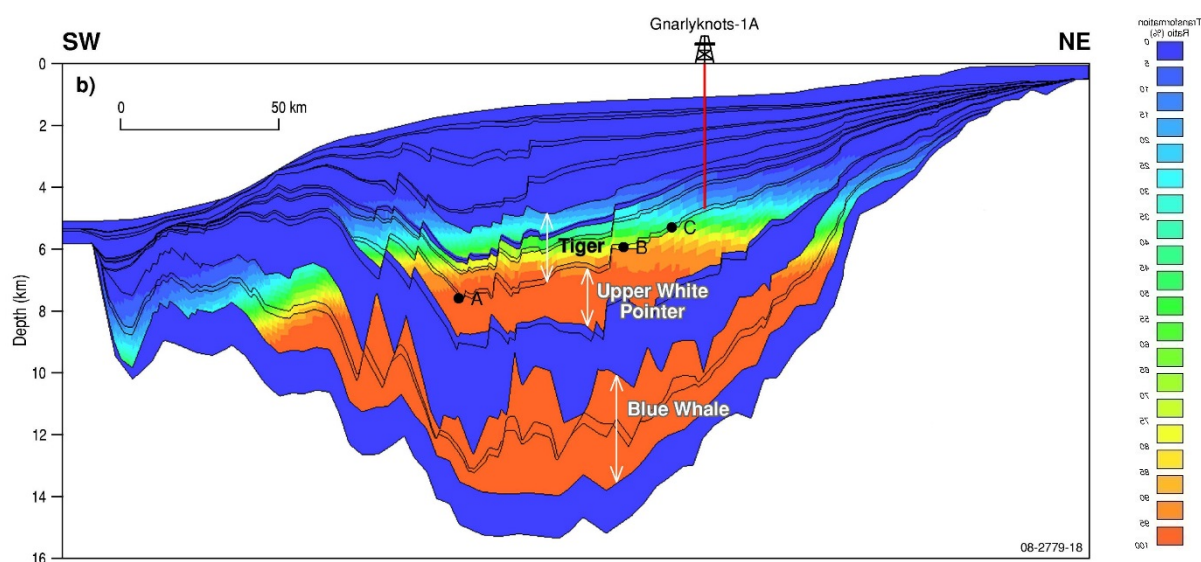


Figure 61: Modelled present-day transformation ratios of three potential source rock units within the Blue Whale, upper White Pointer and Tiger supersequences in the Ceduna Sub-basin.

The critical moment occurs in the range of 50 to 90% transformation ratio, which is the relative conversion of source-rock organic matter to hydrocarbons. © Commonwealth of Australia (Geoscience Australia) 2016.

Greenly-1 FI Oil

The FI oil extracted from the Late Cretaceous (Cenomanian) White Pointer Supersequence in Greenly-1 (4,806 m to 4,818 m) was probably generated from a source rock deposited in an oxic depositional environment with significant organic matter input from terrestrial plants, and a minor contribution from bacteria, as indicated by a unimodal *n*-alkane distribution (maxima *n*-C₂₅; Figure 56), high Pr/Ph ratio, type III keogen (Figure 57), high C₂₆/C₂₅ tricyclic terpane ratios, high wax index, high abundances of C₂₄ tetracyclic terpane (Figure 58), C₂₉Ts, C₃₀* and C₂₉steranes (Figure 59) and a series of 2 α and 3 β methyhopanes (Figure A8-165c). Based on this evidence, and on the DBT/P versus Pr/Ph (Figure 60; Hughes et al., 1995) plot and high diasteranes/steranes ratio, the source rock of the Greenly-1 FI oil may be clay-rich fluvial-deltaic source rocks.

Previous oil show extracts from 4,815 m and 4,817.5 m were interpreted by Edwards et al. (1999) as being from Upper Jurassic–Lower Cretaceous lacustrine source rocks of the Echidna Formation (Minke Supersequence). While no such correlation was referenced in the Smith and Donaldson (1995) paper, the biomarker results from the Greenly FI oil (this study) do not support this. Smith and Donaldson (1995) interpreted RFT oil (4,209 mMD) and oil show extracts (3,430–4,524 mMD), both from shallower intervals in the the Wigunda Formation, as having a mixed organic source with input from higher land plant waxes deposited in an oxic environment. Edwards et al. (1999) interpreted the same RFT oil as having a mixture of algal and land-plant organic matter from a source preserved within a calcareous marine source facies. This was tentatively correlated with the Upper Borda Formation (Bronze Whaler Supersequence) in Duntroon-1.

Strong terrigenous/deltaic source characteristics are indicated in the Greenly-1 FI oil, with no algal input. Because the FI oil is uncontaminated by organic matter, that might be present in the rock, it represents a more pristine oil sample compared to any of the oil show extracts from this well. While the Bronze Whaler and White Pointer are possible source sequences with type III terrestrial organic matter (Figure 62), the upper Bronze Whaler also contains type II organic matter. This is not a source characteristic present in the Greenly-1 FI oil and, in this regard, the White Pointer might be a better source candidate for the FI oil.

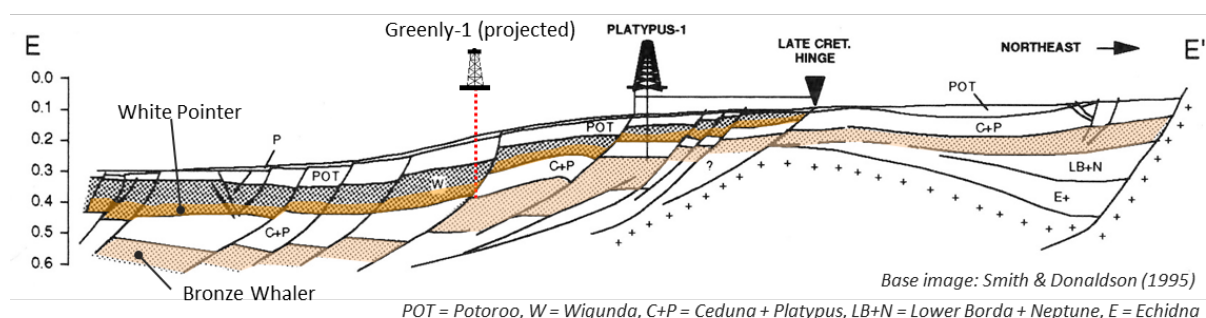


Figure 62: Schematic cross section (NE-SW) showing potential type III terrigenous source rocks (Bronze Whaler and White Pointer) for the Greenly-1 FI oil.

Molecular Thermal Maturity

Gnarlyknots-1A FI oil

The Gnarlyknots-1A FI oil has maturity variations from 0.65% to 1.3% VRE based on different maturity related parameters calculated from both aliphatic and aromatic hydrocarbons. The wide range of maturities suggests either that the Gnarlyknots-1A FI oil was a mixture of oils generated from the same source rock at different maturity stages or from different source rocks. The wide range of maturity is consistent with the variability observed in the oil inclusion assemblages, including the gas-condensate inclusions, which implies maturities within the gas window.

Greenly-1 FI oil

The Greenly FI oil has maturity ratios ranging from 0.8% to 1.1% VRE, based on different maturity related parameters calculated from aliphatic and aromatic hydrocarbons, suggesting the Greenly-1 FI oil was generated from source rocks within the early to peak oil window. It has a narrower maturity range compared to the Gnarlyknots-1A FI oil, which is consistent with the uniformity of oil inclusion assemblages.

Fluid Inclusion Gases in Gnarlyknots-1A

There are a number of sources of methane in the subsurface environment and these can be classified as either biotic or abiotic in origin. Biotic methane (CH_4), produced by microbial processes or by thermogenic degradation of organic matter in sedimentary rocks, is widespread on Earth and forms the major commercial natural gas reservoirs. Abiotic sources of methane, from chemical reactions that do not directly include organic matter (e.g. magmatic processes in volcanic and geothermal areas or low-temperature gas-water-rock reactions), produce much smaller amounts on a global scale (Etiope and Lollar, 2013). This abiotic methane is usually a minute constituent of fluid inclusions (Larsen et al., 1992). Ethane and the other light hydrocarbon gases such as propane and butane are primarily regarded as having a biotic origin only.

The stable carbon isotopic signature of methane is one of the main diagnostic methods used for provenance information on the source of hydrocarbon gas, and can be used to differentiate microbial decay in shallow environments (biogenic) from thermal alteration of organic matter (thermogenic). Biogenic gases are characterised by $\delta^{13}\text{C}$ values more depleted than -60‰, while thermogenic gases usually have more enriched $\delta^{13}\text{C}$ values between -50‰ and -20‰.

Methane and Ethane

Methane in the Gnarlyknots-1A sample is most likely derived from biotic sources given the occurrence of gas-bearing inclusions in association with liquid oil. The bulk $\delta^{13}\text{C}$ isotopic composition of methane extracted from the inclusions is around -28‰ (Figure 63). This isotopic value points to a thermogenic origin for the gas.

The likely type of kerogen for the methane can be inferred by comparison to Bernard et al. (1978) interpretative diagram combining molecular and isotope compositional information. Although gas compositions were not determined, a $\delta^{13}\text{C}_{\text{methane}}$ isotopic value of -28‰ would suggest derivation from possible type III (humic) kerogen (Figure 64), assuming methane from biotic sources only. Kerogen type III is formed from terrestrial plant matter that is lacking in lipids or waxy matter. If mixing with methane derived from abiotic sources was considered (which would be significantly

enriched in ^{13}C by comparison), then the relative ^{13}C component of the thermogenic gas would be more depleted than -28‰ and trend toward, and overlap with, Type II (planktonic) kerogen.

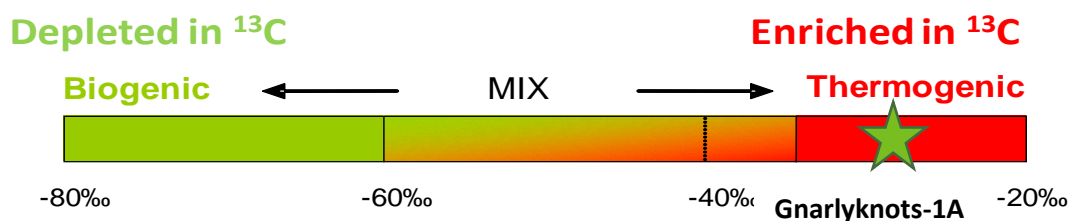


Figure 63: End member values for stable carbon isotopes of methane and the potential for mixing between these two sources. Base image from Stalker (2013).

Ethane and the other light hydrocarbon gases (propane and butane) are primarily regarded as biotic in origin and it can be reasonably inferred that the ethane extracted from the fluid inclusions in Gnarlyknots-1A was derived from similar sources. The $\delta^{13}\text{C}$ isotopic composition of ethane is around -18 ‰, which would suggest gas, or cracked gas, derived largely from humic-derived coaly facies (Figure 65). This is based on numerous studies of the Sichuan Basin, China, where a cut-off point of -28 ‰ for $\delta^{13}\text{C}_{\text{ethane}}$ was suggested for differentiating the origin of the thermogenic gases, with greater values (enriched in ^{13}C) indicating coal-derived gases sourced from terrestrial humic organic matter and lower values (depleted in ^{13}C) for oil-associated gases or oil-cracked gas sourced from marine sapropelic organic matter (Gang et al., 1997; Dai et al., 2005; Xiao et al., 2008; Ni et al., 2013).

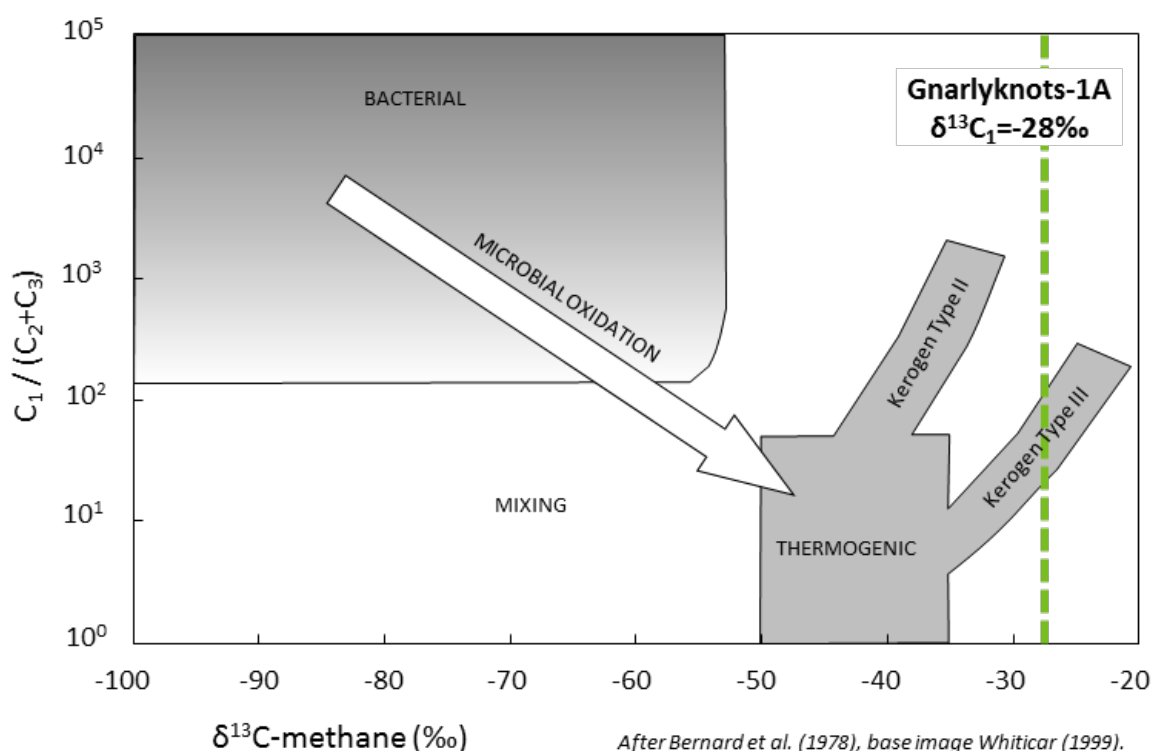


Figure 64: Natural gas interpretative diagram showing carbon isotopic composition of methane in Gnarlyknots-1A FI gases.

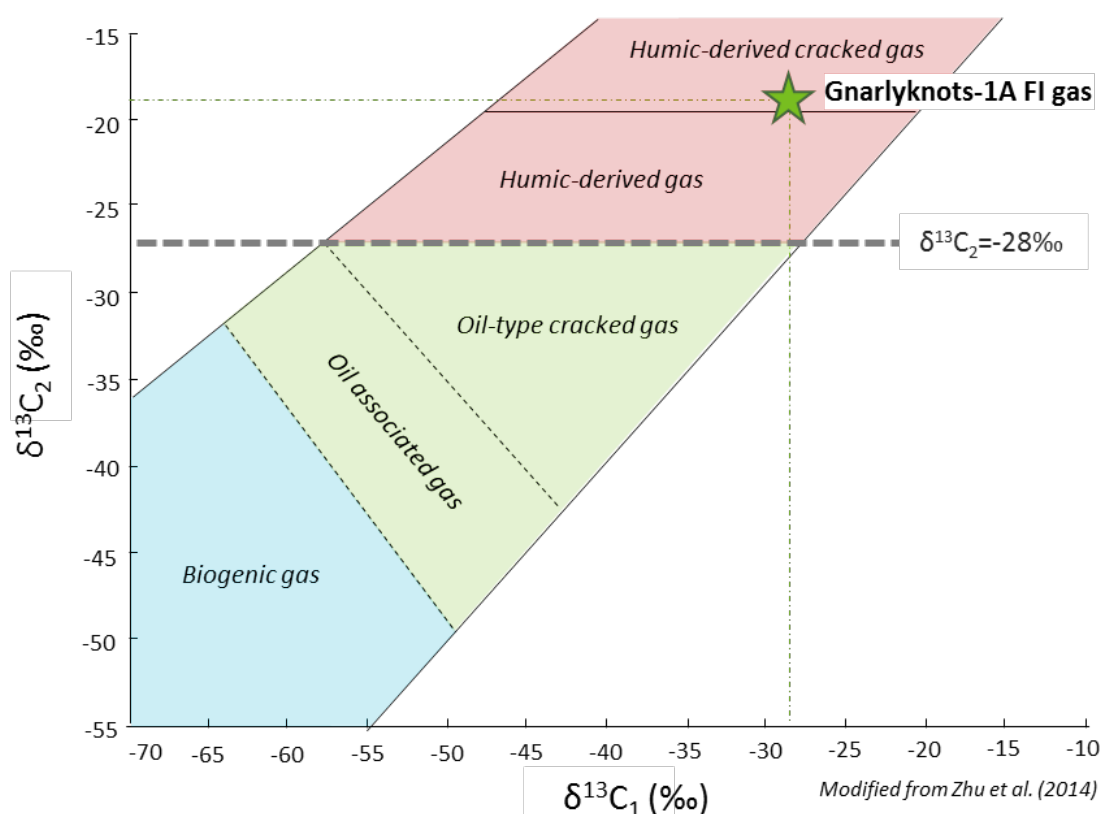


Figure 65: Natural gas interpretative diagram showing carbon isotopic compositions of methane and ethane in the Gnarlyknots-1A FI gases.

Carbon Dioxide

Carbon dioxide is common in the Earth's crust and is sourced from a wide variety of processes that extend back to the provenance of the rock (Table 13; Wycherley et al., 1999 and associated references cited therein). Generally, the carbon isotope ratios for CO₂ derived from organic carbon are generally depleted in ¹³C relative to carbon dioxide from inorganic origins. Although highly variable, the carbon isotopes of mantle/crustal-derived inorganic CO₂ are generally less depleted in ¹³C than -7 ± 2 ‰ (Gould et al., 1981), whereas δ¹³C_{CO2} for organic gases range from -10 ‰ to -20 ‰ (Shen and Xu, 1991).

Table 13: Sources of CO₂ in petroleum basins and carbon isotopic values.

Origin	δ ¹³ C _{CO2} PDB	Sources
Magmatic origin/mantle degassing	-4 to -7 ‰.	Inorganic
Regional metamorphism	0 to -10 ‰	
Contact metamorphism of carbonates	-2 to -12 ‰	
Marine carbonates	+2 to -2 ‰	
Biogenic decay	+15 to -30 ‰	Organic
Breakdown of coaly kerogen type III	-10 to -25 ‰	
Contact metamorphism of coals	-10 to -20 ‰	

A $\delta^{13}\text{C}$ value of around -4 ‰ for the bulk CO_2 extracted from fluid inclusion gases in Gnarlyknots-1A would suggest an inorganic origin from magma-related processes or from metamorphic reactions at depth. The precise distinction between average mantle-derived CO_2 and bulk crustal CO_2 is somewhat ambiguous, because both have similar $\delta^{13}\text{C}_{\text{CO}_2}$ values from -3 to -8 ‰ PDB (Wycherley et al., 1999).

While CO_2 from inclusions that were inherited from the provenance of the grain are likely to dominate the inclusion record in Gnarlyknots-1A, ^{13}C is not more depleted than -4 ‰ and this implies that organic sources did not contribute as much CO_2 by comparison.

Part II PVTx modelling & timing of hydrocarbon migration

Lead author

Julien Bourdet

INTRODUCTION

Overview

From CSIROs *Grains with Oil Inclusion (GOI)* method a total of four intervals were selected for pressure-volume-temperature-composition (PVTx) modelling from Gnarlyknots-1A and Potoroo-1, in the central Ceduna Sub-basin and Greenly-1 and Duntroon-1, in the eastern Ceduna/Duntoon sub-basins.

This work presents the results of various microscope-based techniques, with the objective to derive the pressure and temperature conditions (*PT*) at which fluids, both hydrocarbons and formation water, were trapped, as well as constraining their compositions. This is compared to independently calibrated burial history models, supplied by BP, to derive an approximate age of entrapment.

Data acquisition consisted of measuring (or deriving):

- the temperature of fluid phase changes using a thermometric heating stage;
- oil-gas ratios in hydrocarbon fluid inclusions using laser confocal microscopy techniques;
- water salinities in co-existing water inclusions using a thermometric freezing stage and Raman spectroscopy;
- the amount of dissolved methane in water inclusions using Raman spectroscopy.

Thermodynamic modelling tools, including Petroleum Inclusion Thermodynamic (PIT), were used to derive fluid compositions and calculate bubble point curves, dew point curves and isochores. The approach of locating intersecting isochores of contemporaneous hydrocarbon and aqueous fluids more accurately constrains the pressure and temperature of entrapment over homogenisation temperature alone which is only a minimum estimation of entrapment temperature.

Previous temperature studies

Fluid Inclusion Technologies Inc. previously undertook microthermometry on two cuttings (2,745 m and 3,950 m) and two sidewall core samples (4,467 m and 4,593 m) from Gnarlyknots-1A for the evaluation of trapping temperatures of petroleum fluids (Well completion report, 2004). The homogenisation temperature data were reported follows:

1. "Petroleum inclusions from the target section (the deeper two samples) have homogenization temperatures (T_h) predominantly in the 35-55°C range, and probably reflect trapping of a volatile oil or gas-condensate from a system at P-T conditions above bubble-point or dew-point. Consequently, actual trapping temperatures are likely to have been higher than measured T_h ".
2. "Petroleum inclusions from shallower samples have homogenisation temperatures that are again low (dominantly 30-65°C) and do not constrain trapping temperatures appreciably".

The measured T_h clearly do not adequately constrain the trapping temperatures of the petroleum fluids, which are likely to have been higher than those recorded. The Petroleum Inclusion Thermodynamic (PIT) fluid modelling technique of Thiéry et al. (2000, 2002), in combination with modelling of co-existing aqueous inclusions, allows for both temperature and pressure to be more accurately determined, thus offering a methodology to constrain the true trapping conditions. Such information, by reference to burial history models, can, in turn, be used to constrain the timing of petroleum migration and accumulation.

Samples

A total of four samples were selected from Gnarlyknots-1A, Greenly-1, Duntroon-1 and Potoroo-1 for PVT analysis based on GOI oil inclusion abundances. Generally higher raw counts of grains with oil inclusion yield better outcomes for PVT and samples were selected on this basis while attempting to give good geographical coverage of the Bight Basin.

Samples were prepared as double polished 100 µm thick sections glued on a petrographic glass slide using acetone-dissolvable superglue. For microthermometric analysis the rock wafer must be removed from the glass slide in order to fit on a 6 mm quartz disc within the heating/cooling stage. While still on the glass slides, the rock wafers were cut into 5 mm squares using a Dremel drill and diamond saw. The rock wafers were separated from the glass slides by dissolving in acetone for three hours. Each wafer was then cleaned using methanol and optical tissues.

Table 14: Sample information.

Well	CSIRO No	Depth	Rationale for sampling
Greenly-1	134513	4809-12 m	GOI of 1.1% – 16 gwoi in 1,425 grains
Gnarlyknots-1A	134524	4410-15 m	GOI of 0.4% – 29 gwoi in 7,027 grains Primary well objective: FIS WG-GC PTPL
Duntroon 1	134504	2505-10	GOI of 0.4% – 12 gwoi in 3,316 grains
Potoroo 1	134721+134722	1778-86	GOI of 0.2% – 34 gwoi in 21,384 grains

Note: all cuttings sample depths referred to in this report are in metres (m) measured relative to the drilling datum (RT or KB). FIS = Fluid Inclusion Stratigraphy, WG = wet gas, GC = gas condensate, PTPL = proximity to pay liquids.

Methods

The PVTx (pressure-volume-temperature-composition) methodology is an integrated approach using independent techniques to provide data that constrain the calculation of bubble point curves, dew point curves and isochores of contemporaneous hydrocarbon and aqueous fluids trapped in fluid inclusions. Fluid inclusions within the same assemblage are considered as contemporaneous. The following data inputs were required for the PVT modelling of each hydrocarbon-bearing assemblage:

- water inclusion homogenisation temperatures, salinities and methane contents;
- hydrocarbon inclusion homogenisation temperatures and vapour-volume fractions at room temperature.

Microthermometry

Temperature of phase transitions provide important information such as the minimum temperature of oil charge in a reservoir, the inference of gas-saturation of the oil and associated formation water and its salinity. Thermometric data are temperature measurements at phase transition in hydrocarbon and water inclusions. Measurements include homogenisation temperature (T_h) of oil, gas and water inclusions as well as the ice melting temperature of water inclusions (T_{mice}) (Figure 66).

Fluid inclusions are closed chambers with fixed volume. Their densities are constant, identical to the density of the ambient pore fluid at trapping. The pressures within the inclusions change with changing temperature, following an isochore (or iso-density curve) (Figure 67). At a temperature

below the T_h , the fluid inclusion comprises at least two phases; liquid and vapour. At temperatures equal to the T_h , the trapped fluid reaches its bubble point (oil or water inclusions) or dew point (gas inclusion). Consequently as one phase homogenises in the other, the vapour bubble disappears in oil inclusions and in water inclusions, while in gas inclusions the rim of oil around a gas phase disappears.

For oil or water having a small amount of dissolved methane, the homogenisation temperature is less than the true temperature of trapping (T_t), which is somewhere along the isochore of the fluid in the single phase domain. In this case the T_h can be used as minimum estimate of the trapping temperature. The slope of the isochores for water inclusions is steeper than hydrocarbon inclusions. Consequently, homogenisation temperatures of oil inclusions are generally less than the homogenisation temperature of co-located aqueous inclusions. The water inclusion T_h is a closer estimate of the trapping conditions than hydrocarbon inclusions.

If methane is abundant (gas saturated oil or water, or liquid saturated gas) the trapping temperature is on the bubble point curve and the T_h is the true trapping temperature. If however, free gas was present in the pore space as well as liquid, then co-entrapment of gas and liquid can occur. The resulting inclusions have homogenisation temperatures exceeding the temperature of trapping. This phenomenon is designated as two-phase trapping.

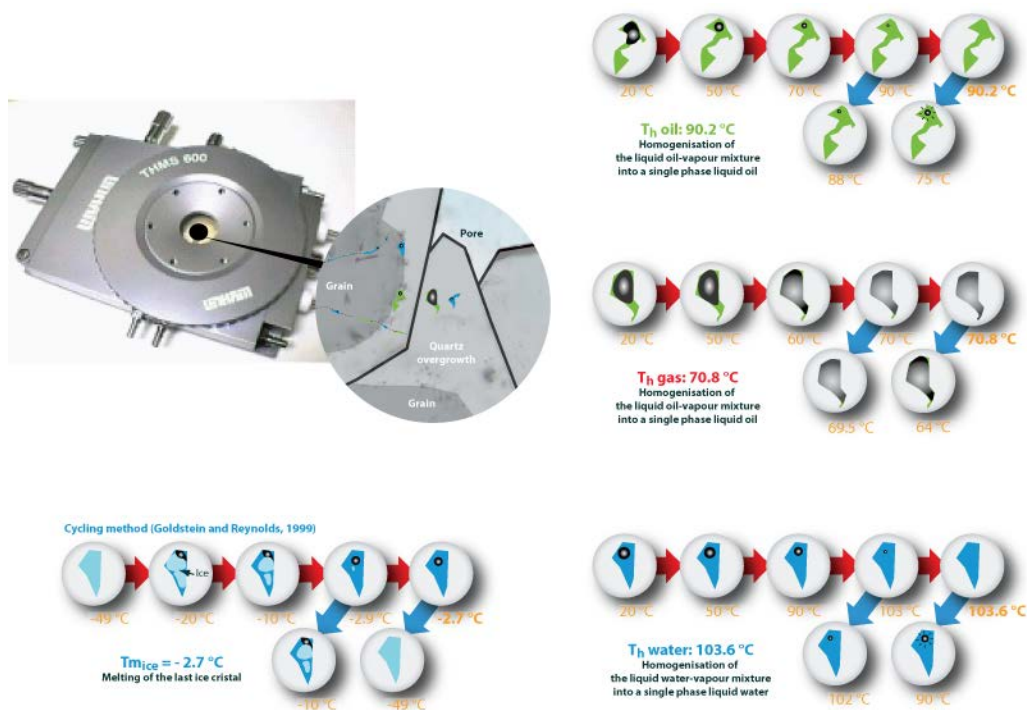


Figure 66: Thermometric observations and measurements acquired in the laboratory from oil inclusions, water inclusions or gas inclusions.

Salinity of water in a fluid inclusion can be derived using microthermometric techniques by recording the temperature of final ice melting ($T_{m,ice}$) after freezing of the fluid inclusion. Figure 66 and Figure 67 show a schematic representation of how $T_{m,ice}$ is determined using the cycling method of Goldstein and Reynolds (1994). This method guarantees reliable ice melting measurements that can

be bracketed to within 0.1 degree Celsius. First, the water inclusion is frozen. When frozen, the vapour bubble shrinks or disappears and ice and/or salt hydrate(s) fill the inclusion chamber. For low and moderately saline formation water (below 230,000 ppm NaCl equivalent), heating of the inclusion makes hydrohalite melts first, leaving salty water, ice and vapour in the inclusion. Slight cooling before the total melting of the ice will re-grow the ice instantaneously. Further heating melts the ice, and intense cooling will be necessary to re-freeze the inclusion.

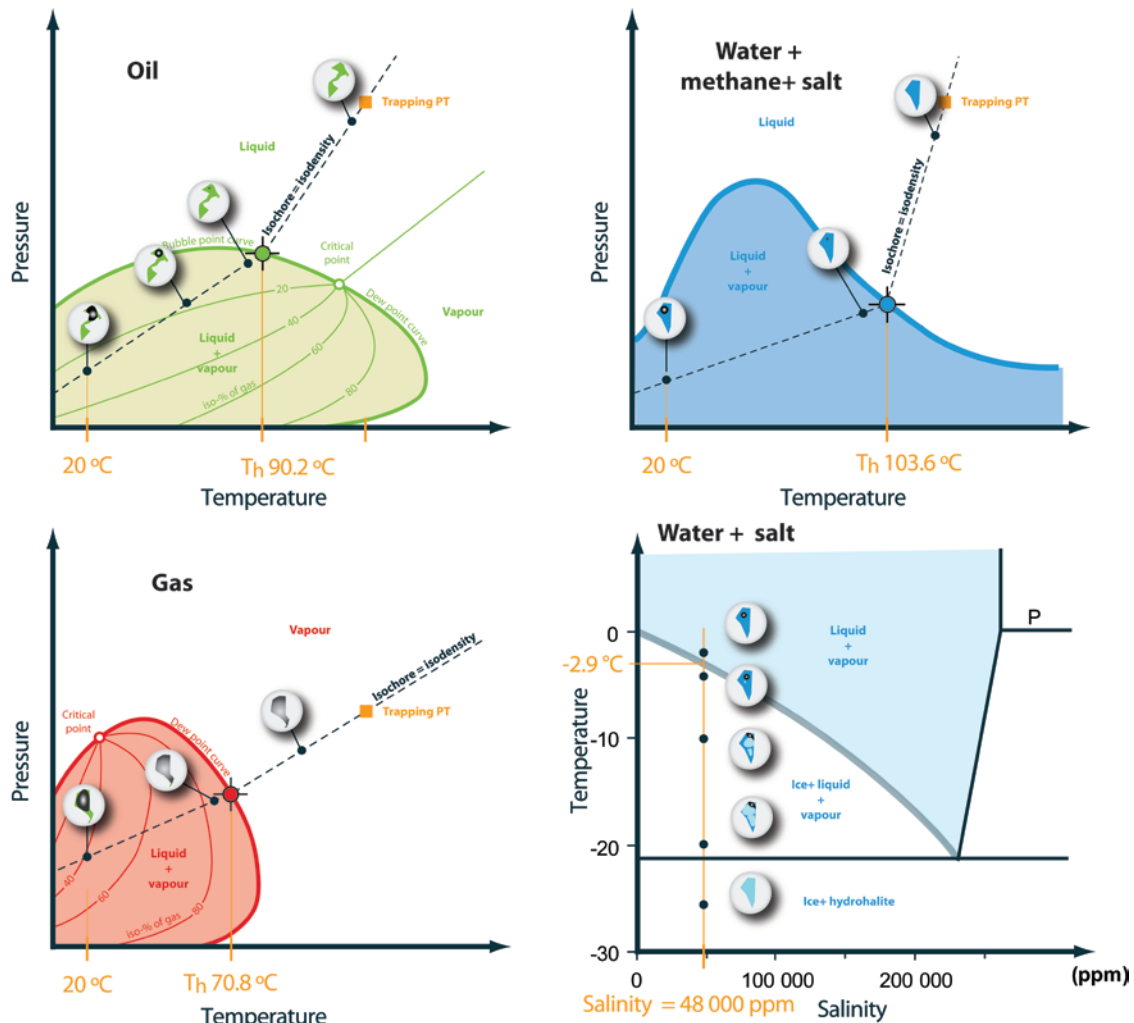


Figure 67: Phase diagrams illustrating the thermometric observations and measurements acquired in the laboratory from oil inclusions, water inclusions or gas inclusions.

The vapor bubble is sometimes absent during heating and at $T_{m\text{ ice}}$. In this case $T_{m\text{ ice}}$ must be ignored for deriving salinity. The absence of a vapor bubble during $T_{m\text{ ice}}$ measurement is a recurrent problem, reported by Roedder (1984) and Goldstein and Reynolds (1994) due to the metastable behaviour of water after freezing. Possible causes for the absence of a bubble in the inclusion during the melting of ice can be due to: (1) the surface tension of water inside the inclusion is preventing the bubble to nucleate and (2) ice and hydrates, having a lower density than liquid water, occupy a larger volume than water, preventing the formation of a contraction bubble.

Raman Spectroscopy

The Raman spectrometer at CSIRO is a Horiba LabRam HR Evolution using a 532 nm single frequency 100 mW diode laser, providing 12 mW at the focus point through a 100X objective. Grating settings were 600 grooves/mm for salinity measurements and 1,800 grooves/mm for gas detection. The signal was collected using a 1024x256 pixels Peltier cooled CCD Synapse detector, sensitive in the 300-1,050 nm range.

Salinity derivation

Raman microscopy can be used for salinity calculation of water, based on the vibration of water molecules excited by a laser beam. Molecular vibrations of liquid water molecules are perturbed by solutes and the perturbation in the spectrum due to the presence of salts is calibrated by measuring spectra for pure water and for standard salt solutions.

The vibration of the water molecules gives a characteristic O-H vibration (stretching) between 2,800 cm^{-1} and 3,800 cm^{-1} called the water band. The shape of the water band is partly dependent of the ionic environment of the water molecules. The changes in the shape of the water spectrum, with increasing salinity, correlates with the concentration of Chloride ions (Cl^-) (Georgiev et al., 1984; Mernagh and Wilde; 1989; Dubessy et al., 2002; Sun et al., 2010).

Applied to solutions, this technique is reliable and gives an adequate accuracy; applied to fluid inclusions trapped in quartz, measurements at different angles of polarisation are necessary (Dubessy et al., 2002; Baumgartner and Bakker, 2009; Sun et al., 2010). Indeed, the polarisation of quartz affects the laser and the Raman water band. This effect can be controlled by a series of measurements at different quartz orientations using a petrographic stage or by performing measurements at the crystallographic extinction position of the quartz grain (Baumgartner and Bakker, 2009; Bourdet and Kempton, 2014).

The salinity derivation method of Bourdet and Kempton (2014) was used in this study. For each spectrum, a derivative function was fitted between 3,360 and 3,460 cm^{-1} to calculate the position (ω_{max}) of the maximum Raman spectral intensity. A first order function was fitted between 3,248 and 3,280 cm^{-1} to calculate the intensity value at 3,260 cm^{-1} and to derive a ratio (I_{3260}/I_{max}) of the Raman signal intensity at 3,260 cm^{-1} to the maximum Raman intensity. The ω_{max} and I_{3260}/I_{max} values can be converted into salinities using the calibration equations derived from the same spectrometer. Salinity values from the Raman should be close to those derived from conventional thermometric techniques. However, it appears that the Raman signal of water can be affected by a background signal of the quartz crystal. This background signal will not affect the two parameters in the same way and large differences between the two derived salinity values are indicative of quartz background effect. In such a situation the salinity results are regarded with low confidence.

Methane detection and quantification

The presence of methane (CH_4) and other gasses such as CO_2 , H_2S and N_2 in the vapour phase of water inclusions at room temperature was detected using Raman spectroscopy. Methane at low pressure has a peak position at 2,917.6 cm^{-1} (Lin et al., 2005) and this peak position is dependent of the methane density. Therefore the peak position changes with the pressure inside the bubble and calibration curves have been calculated to derive the pressure in the bubble from the methane peak position (Lin et al., 2005; Lu et al., 2007). A methane standard in a fused silica tube, with an internal pressure below 1 bar, was used as reference for the methane peak position. The calculation

procedure developed by Becker et al. (2010) was used for deriving bulk methane concentration in the water inclusions from salinity, methane peak position at room temperature and homogenisation temperature.

In some cases, the vapour bubble movements prevented the methane peak to be detected at room temperature. In this case, the methane quantification method at homogenisation reported in Guillaume et al. (2003) and Caumon et al. (2014) was used.

Fluid Modelling

The CH₄-H₂O-NaCl fluid model of Duan and Mao (2006) was used to calculate the bubble point curves for water inclusions with available bulk methane, T_h and salinity data (described above). The pressure at homogenisation temperature (P_h) can also be calculated using this model and provides, on its own, an estimation of the minimum pressure condition at the fluid entrapment.

The bubble point curve, dew point curve and isochore of individual oil and gas inclusions are calculated using Petroleum Inclusion Thermodynamics software (PIT; Montel, 1993; Thiéry et al., 2000, 2002) developed by the Centre de Recherches sur la Géologie des Matières Premières Minérales et Énergétiques (CREGU) and TOTAL. The input data are the measured homogenisation temperature and the vapour volume fraction in the hydrocarbon fluid inclusion at room temperature. The PIT modelling calculates a range of matching compositions. By selecting one composition, the program calculates the bubble point curve, dew point curve and isochore. The vapour volume fraction at room temperature of hydrocarbon inclusions is measured, following the method of Pironon et al. (1998) using a confocal laser scanning microscope (CLSM) to reconstruct a 3D volume of the liquid oil creating a series of stacked images of the fluorescent oil. The image processing and volume calculations were undertaken with open source image program ImageJ. The bubble volume was calculated by measuring the dimension of the vapour bubble and assuming a sphere or an ellipsoid. This procedure is limited to the hydrocarbon inclusions with spherical, cylindrical or ellipsoidal and non-moving bubbles. Therefore, for hydrocarbon inclusions with a moving bubble or with a complex shape, the vapour volume fraction could not be measured.

The calculated bubble point curves, dew point curves and isochores of contemporaneous hydrocarbon and aqueous inclusions are assembled to interpret the palaeo-pressure and temperature conditions of entrapment. The PT trapping condition of contemporaneous immiscible fluids is located at the intersection of their isochores (Roedder and Bodnar, 1980; Pironon, 2004). Three general cases can be distinguished based on the gas richness of the fluids (Pironon, 2004):

- A. The water and contemporaneous oil can be gas under-saturated (Figure 68A). This implies that, if present, more methane could be dissolved in the fluids. In this case, no free gas can be present when the fluids were trapped. The entrapment PT conditions occur along each isochores, at their intersection. The T_h of the water inclusions and oil inclusions are lower than the trapping palaeo-temperature, and the T_h values of the water inclusions are closer to the trapping temperature than the T_h of oil inclusions.
- B. Due to gas solubility differences between oil and water, the water can be gas saturated, while the contemporaneous oil can be gas under-saturated (Figure 68B). In this case, the entrapment PT conditions occur along the oil isochores and at the bubble point of the water. The T_h values of the water inclusions are equal the trapping temperature.

- C. The water and contemporaneous oil can be gas saturated (Figure 68C). This implies that no more methane could be dissolved in the fluids; the fluids are at their bubble point. Free gas can be present when the fluids were trapped. The T_h values of oil inclusions are equal to the T_h of the water inclusions. Two-phase trapping might occur.

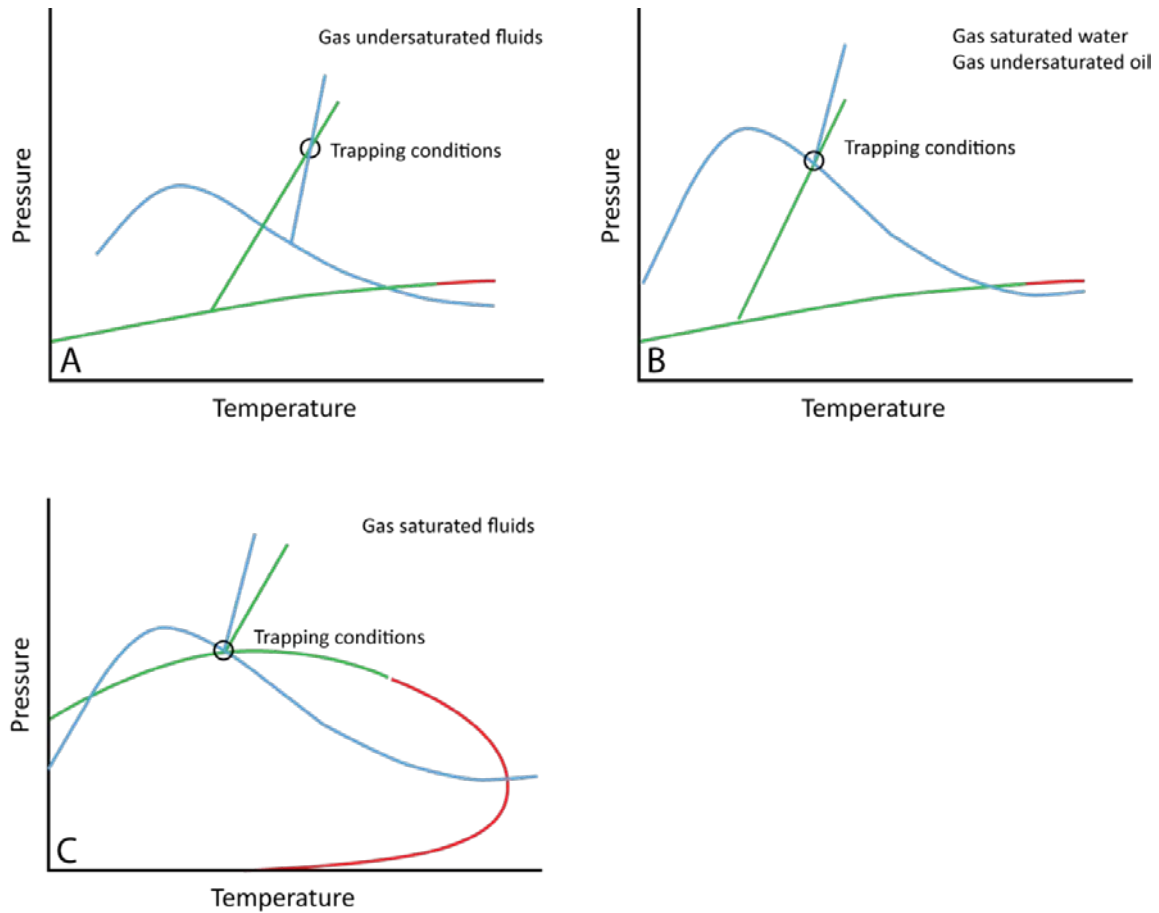


Figure 68: Phase envelopes of aqueous and petroleum fluids at different scenarios of gas saturation in liquid at entrapment.

RESULTS

Gnarlyknots-1A (4410-15 mMD)

A sand-rich cutting sample from the Upper Cretaceous (Coniacian) Tiger Supersequence at 4,410-15 mMD central Ceduna Sub-basin, was investigated for detailed *PVTx* analysis of the hydrocarbon fluid inclusions, and associated water inclusions, trapped in quartz.

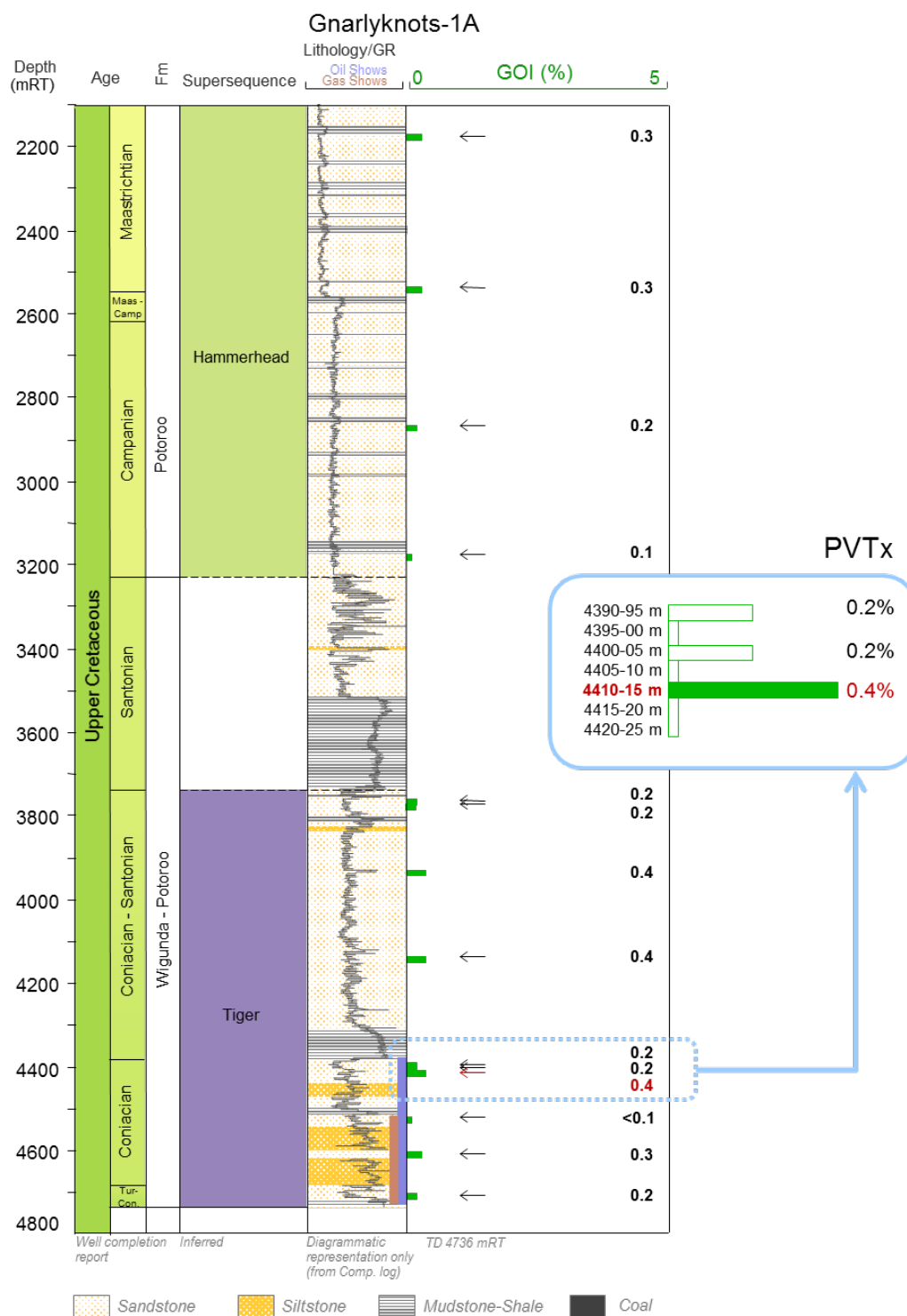


Figure 69: GOI log for Gnarlyknots-1A showing location of sample for PVT analysis.

Fluid Inclusion Assemblages

Fluid inclusion assemblages were investigated in 16 different grains from Gnarlyknots-1A (Table 15). Amongst those, 13 assemblages contained hydrocarbon fluids (some with associated water inclusions) and 3 contained only water inclusions.

At room temperature, the petroleum inclusions are dominantly 2-phase, comprising a volumetrically dominant liquid oil phase and a small to medium-sized vapour phase ($L_{oil}-V$; Figure 70). Other types of fluid inclusion assemblages include:

- 2-phase inclusions ($L_{oil}-V$) comprising a volumetrically large vapour/gas bubble and liquid oil;
- 3-phase inclusions ($L_w-L_{oil}-V$) comprising liquid water, liquid oil and a small to medium-size vapour bubble. The bubble is systematically contained in the oil phase;
- 3-phase inclusions ($L_w-L_{oil}-V$) comprising liquid water, liquid oil and a volumetrically large vapour bubble. The bubble is systematically contained within the oil phase;
- 1-phase inclusions (monophase), comprising a fluorescing hydrocarbon phase without a vapour bubble at room temperature.

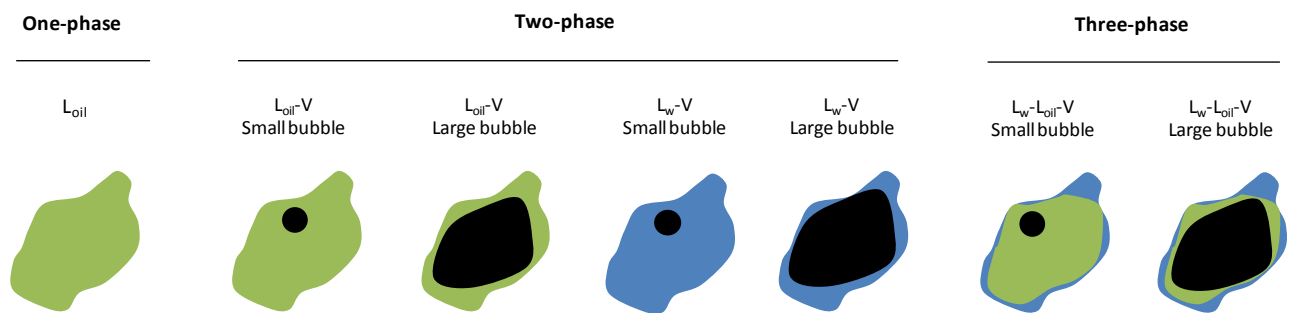


Figure 70: Fluid inclusions types observed in Gnarlyknots-1A sample (at room temperature).

At room temperature, the water inclusions encountered in Gnarlyknots-1A were mostly 2-phase comprising a volumetrically dominant liquid water phase and a small vapour phase (L_w-V). Only one assemblage had water inclusions with large vapour bubbles.

The range of fluid inclusions assemblages are shown in Figure 70 and described as having either uniform or variable fluorescence colour of oil under UV-illumination, and uniform or variable bubble size at room temperature. Vapour bubbles are classified as small (<10%), medium (<20%), medium-large (<35%) or large (>50%). The oil inclusions exhibit mostly white fluorescence, but blue and yellow fluorescence was also observed, mainly in assemblages with variable fluorescence colour. Uniform yellow fluorescence assemblages were observed in oil inclusions assemblages (OIAs) 6 and 11.

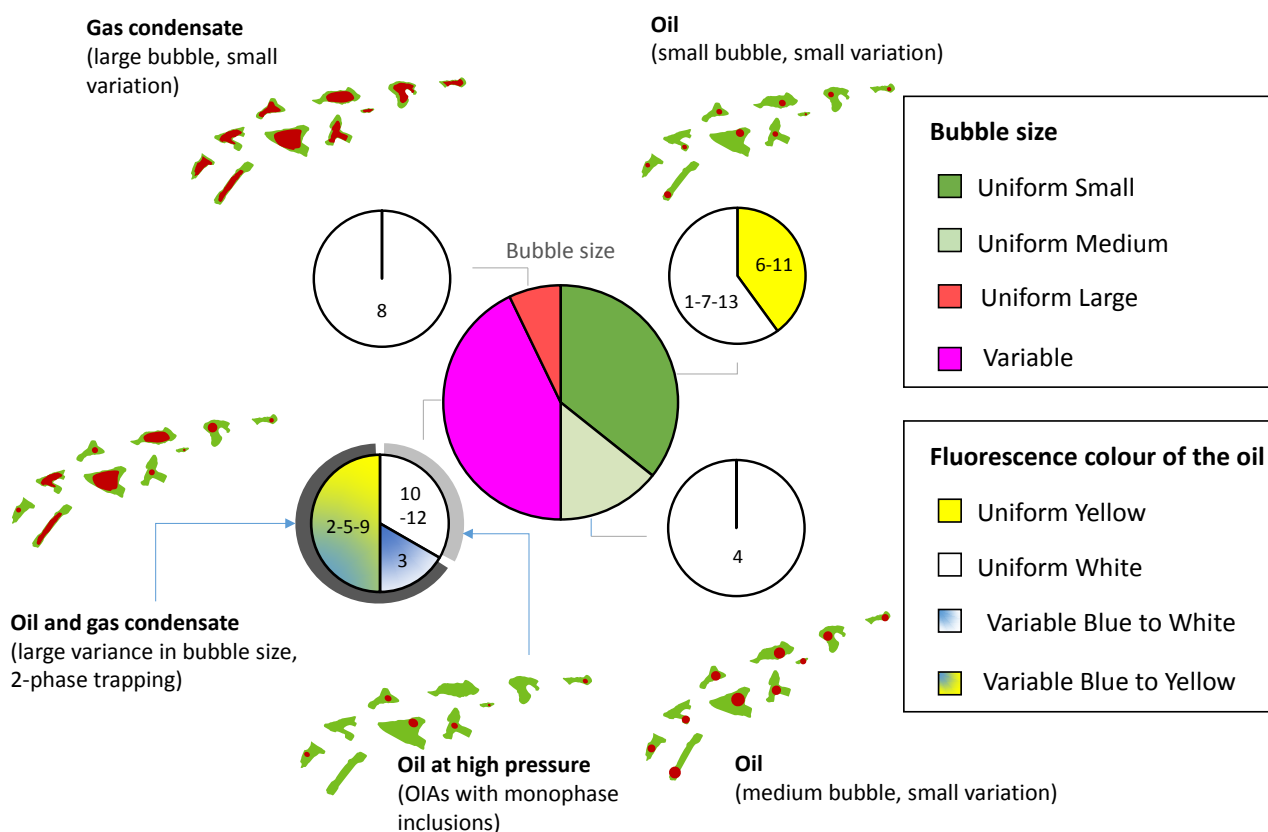


Figure 71 Petroleum fluid inclusion assemblages observed from 4410-15 mMD in Gnarlyknots-1A
Numbers within the pie charts refer to the assemblage numbers in Table 15.

Microthermometry

The homogenization temperatures (T_h) measured on hydrocarbon and aqueous inclusions have a large spread (Figure 72). For presenting the results these assemblages are grouped into:

OIAs with uniform small to medium vapour bubbles

- Uniformly yellow fluorescent oil with uniformly small vapour bubbles (OIAs 6 and 11). The T_h of the oil inclusions are between 72 and 86°C with one T_h at 106°C. The fluid was trapped as liquid oil. The fluorescence colour suggests this oil might have low maturity (George et al., 2001). No water inclusions were measurable for T_h or salinity.
- Uniformly white fluorescent oil with uniformly small or medium vapour bubbles (OIAs 1, 4, 7 and 13). The difference in bubble size between these assemblages indicates differences in density and/or gas content. The oil inclusions have T_h between 39.5 and 65°C and the fluid was trapped as liquid oil. Water inclusions have T_h values between 56.9 and 62°C. No salinity could be determined.

OIAs with uniformly large vapour bubbles

- Uniformly white fluorescent oil with uniformly large bubbles at room temperature (OIA 8). The T_h range from 45.2 and 54.0°C and the liquid homogenises into the gas phase. This indicates that the fluid was trapped in the vapour (gas) phase. No water inclusions were measurable for T_h or salinity.

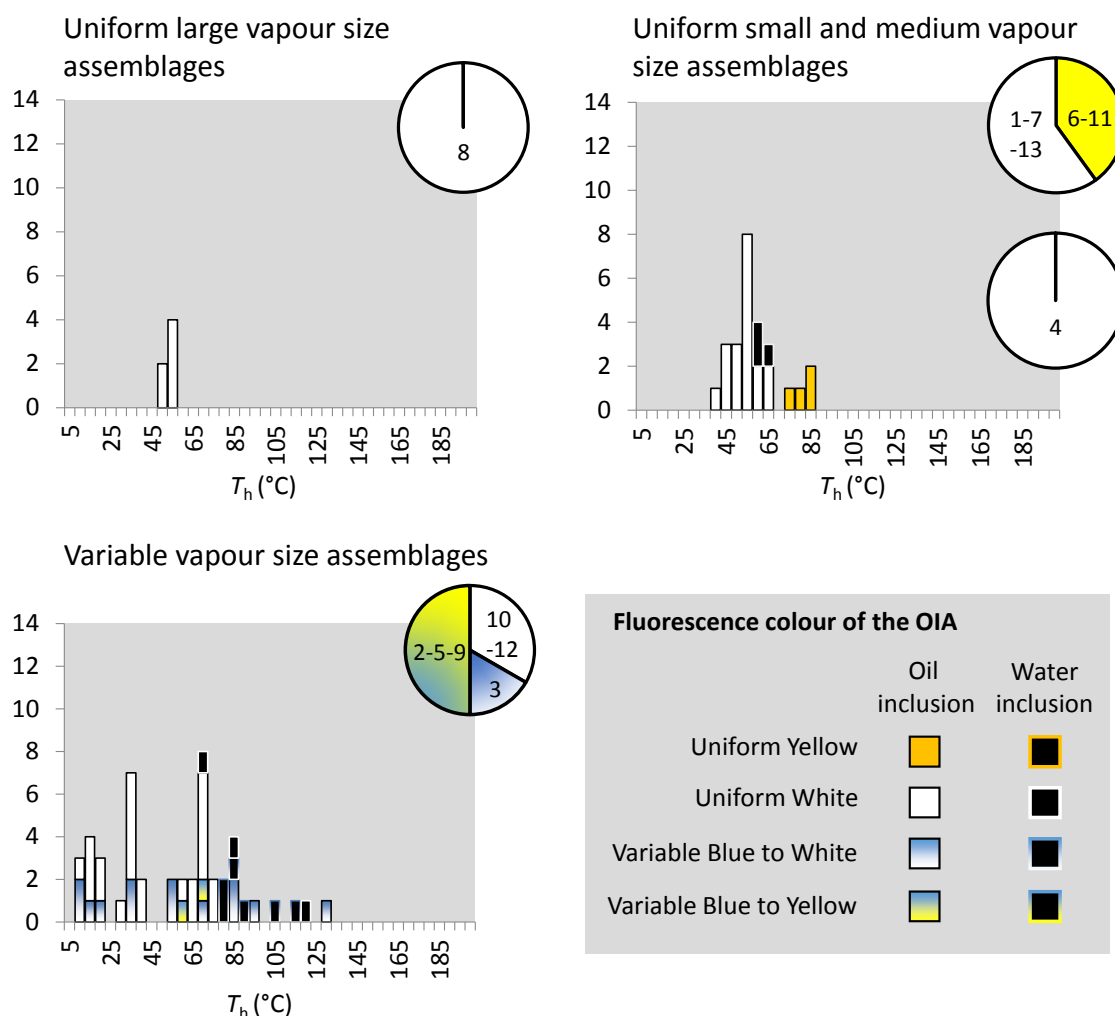


Figure 72: Homogenisation temperatures of oil and associated water inclusion from 4410-15 mMD in Gnarlyknots-1A. Inclusions separated into 3 groups of assemblages.

OIAs with variably-sized vapour bubbles

- Uniformly white fluorescent two-phase oil (small vapour) inclusions with monophasic oil inclusions at room temperature. This includes OIAs 10 and 12. The measured T_h values are between 6 and 41.0°C. No water inclusions were identified for T_h or salinity.
- Variable blue to white fluorescent oil with monophasic and two-phase oil inclusions (OIA 3). The white fluorescent oil inclusions have medium sized bubbles and the blue fluorescing inclusions do not have a bubble at room temperature (1-phase). The 2-phase white fluorescent inclusions have T_h of 31.7 and 34.2°C. During cooling to -40°C, a second liquid fluorescent yellow oil appears as a rim around a larger liquid phase with no fluorescence. A vapour bubble also appears in the larger liquid phase. Those inclusions have two T_h , at the homogenisation of the vapour bubble into the larger liquid phase and the homogenisation of the second liquid into the main phase.
- Variable blue to yellow fluorescent oil inclusions with variable small to large bubbles (OIAs 2, 5 and 9). The oil inclusions have T_h between 35.1 and 110.1°C, the gas inclusions have T_h of 88 and 125°C and water inclusions have T_h ranging from 69.2 and 115°C.

Water inclusion assemblages

In rare occurrences of quartz cement, water inclusion assemblages were observed at the quartz-overgrowth boundary (no oil) and their T_h values are between 76.5 and 137.5°C (Figure 73).

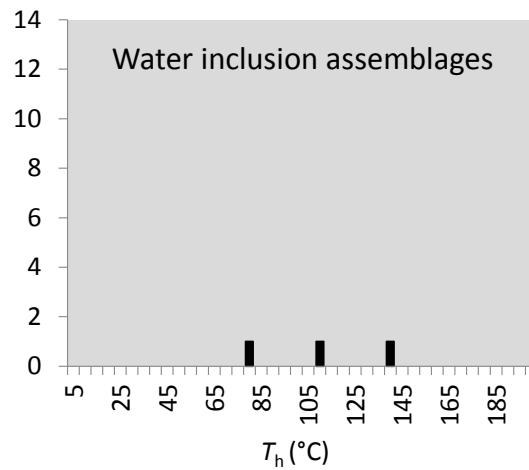


Figure 73: Homogenisation temperatures of water inclusion assemblages at the quartz overgrowth boundary from 4410-15 mMD in Gnarlyknots-1A.

Table 15: Gnarlyknots-1A thermometric results.

OIA	Fluo. variability	Bubble size variability	Location	FI No	Inclusion type	Fluo. colour	Bubble size	T_h (°C)	Phase transition	T_h (°C)	Phase transition	$T_{m\ ice}$ (°C)	Salinity eq. NaCl (wt%)
1	Uniform	Uniform	FTQG	1	L _{oil} -V	White	S	44.9	L _{oil} -V → L _{oil}	-	-	-	-
				2	L _{oil} -V			52.1	L _{oil} -V → L _{oil}	-	-	-	-
				3	L _{oil} -V			50.2	L _{oil} -V → L _{oil}	-	-	-	-
				4	L _{oil} -V			50.8	L _{oil} -V → L _{oil}	-	-	-	-
				5	L _{oil} -V			46.4	L _{oil} -V → L _{oil}	-	-	-	-
				6	L _{oil} -V			51.0	L _{oil} -V → L _{oil}	-	-	-	-
				7	L _{oil} -V			63.5	L _{oil} -V → L _{oil}	-	-	-	-
				8	L _{oil} -V			59.5	L _{oil} -V → L _{oil}	-	-	-	-
				9	L _{oil} -V			55.2	L _{oil} -V → L _{oil}	-	-	-	-
				10	L _w -L _{oil} -V			55.8	L _w -L _{oil} -V → L _w -L _{oil}	-	-	-	-
				11	L _{oil} -V			51.1	L _{oil} -V → L _{oil}	-	-	-	-
2	Variable	Variable	FTQG	11b	L _w -V	-	S	62.0	L _w -V → L _w	-	-	-	-
				11c	L _{oil} -V	-	-	48.6	L _{oil} -V → L _{oil}	-	-	-	-
				12	L _{oil} -V	White	S	67.1	L _{oil} -V → L _{oil}	-	-	-	-
				13	L _{oil} -V	White	S	82.3	L _{oil} -V → L _{oil}	-	-	-	-
				14	L _{oil} -V	White	M	90.3	L _{oil} -V → L _{oil}	-	-	-	-
				15	L _w -L _{oil} -V	White	M	110.1	L _w -L _{oil} -V → L _w -L _{oil}	-	-	-	-
				16	L _w -V	-	S	80.0*	L _w -V → L _w	-	-	-	-
				16b	L _w -V	-	S	88	L _w -V → L _w	-	-	7.2*	-
				16c	L _w -V	-	S	80-85	L _w -V → L _w	-	-	-	47500
				17	L _{oil} -V	Blue	L	125.5	L _{oil} -V → V	-	-	-	-
				18	L _w -L _{oil} -V	Blue	L	88.4	L _w -L _{oil} -V → L _w -V	-	-	-	-
				19	L _w -V	-	L	-	-	-	-	-	-
				20	L _w -V	-	S	115.0	L _w -V → L _w	-	-	-	51500
				20b	L _w -V	-	S	78.0*	L _w -V → L _w	-	-	-	44000
				21	L _{oil} -V	White	S	81.8	L _{oil} -V → L _{oil}	-	-	-	-
				22	L _{oil} -V	White	S	50.8	L _{oil} -V → L _{oil}	-	-	-	-
				23	L _{oil} -V	White	S	54.7	L _{oil} -V → L _{oil}	-	-	-	-
3	Variable	Variable	FTQG	24	L	Blue	-	13.0	L _{oil} -L _H C → L _{oil}	-22.6	L _{oil} -L _H C-V → L _{oil} -L _H C	-	-
				25	L	Blue	-	7.0	L _{oil} -L _H C → L _{oil}	-33.8	L _{oil} -L _H C-V → L _{oil} -L _H C	-	-
				26	L _{oil} -V	White	M	34.2	L _{oil} -V → L _{oil}	-	-	-	-
				27	L	Blue	-	-	L _{oil} -L _H C → L _{oil}	-48.4	L _{oil} -L _H C-V → L _{oil} -L _H C	-	-
				28	L	Blue	-	8.0	L _{oil} -L _H C → L _{oil}	-29.6	L _{oil} -L _H C-V → L _{oil} -L _H C	-	-
				29	L	Blue	-	20.0	L _{oil} -L _H C → L _{oil}	-19.5	L _{oil} -L _H C-V → L _{oil} -L _H C	-	-
				30	L _{oil} -V	White	M	31.7	L _{oil} -V → L _{oil}	-	-	-	-
				31	L _w -V	-	S	102.0	L _w -V → L _w	-	-	2.3*	-
4	Uniform	Uniform	FTQG	32	L _{oil} -V	White	M	65.0	L _{oil} -V → L _{oil}	-	-	-	-
				33	L _{oil} -V			54.0	L _{oil} -V → L _{oil}	-	-	-	-

OIA	Fluo. variability	Bubble size variability	Location	FI No	Inclusion type	Fluo. colour	Bubble size	T_h (°C)	Phase transition	Other T_h (°C)	Phase transition	$T_{m\text{ Ice}}$ (°C)	Salinity eq. NaCl (wt%)
5	Variable	Variable	FTQG	34	$L_{oil}-V$	Yellow	S	56.4	$L_{oil}-V \rightarrow L_{oil}$	-	-	-	-
				35	$L_{oil}-V$		M	71.6	$L_{oil}-V \rightarrow L_{oil}$	-	-	-	-
				36	$L_w-L_{oil}-V$		S	84.5	$L_w-L_{oil}-V \rightarrow L_w-L_{oil}$	-	-	-	-
				37	$L_{oil}-V$	Blue	M	67.2	$L_{oil}-V \rightarrow L_{oil}$	-	-	-	-
				38	$L_{oil}-V$	Blue	M	66.7	$L_{oil}-V \rightarrow L_{oil}$	-	-	-	-
				39	$L_{oil}-V$		S	35.1	$L_{oil}-V \rightarrow L_{oil}$	-	-	-	-
				40	$L_{oil}-V$		M-L	69.1	$L_{oil}-V \rightarrow L_{oil}$	-	-	-	-
				41	$L_{oil}-V$		M-L	70.1	$L_{oil}-V \rightarrow L_{oil}$	-	-	-	-
				42	$L_{oil}-V$		M-L	64.2	$L_{oil}-V \rightarrow L_{oil}$	-	-	-	-
				43	$L_{oil}-V$		M-L	64.2	$L_{oil}-V \rightarrow L_{oil}$	-	-	-	-
				44	$L_{oil}-V$		M-L	67.2	$L_{oil}-V \rightarrow L_{oil}$	-	-	-	-
				45	$L_{oil}-V$		M-L	68.1	$L_{oil}-V \rightarrow L_{oil}$	-	-	-	-
				45b	L_w-V	-	S	69.2	$L_w-V \rightarrow L_w$	-	-	1.5*	-
6	Uniform	Uniform	FTQG	46	$L_w-L_{oil}-V$	Yellow	S	73	$L_w-L_{oil}-V \rightarrow L_w-L_{oil}$	-	-	-	-
				47	$L_w-L_{oil}-V$			86	$L_w-L_{oil}-V \rightarrow L_w-L_{oil}$	-	-	-	-
				48	$L_w-L_{oil}-V$			85	$L_w-L_{oil}-V \rightarrow L_w-L_{oil}$	-	-	-	-
7	Uniform	Uniform	FTQG	49	$L_{oil}-V$	White	S	46.3	$L_{oil}-V \rightarrow L_{oil}$	-	-	-	-
				50	$L_{oil}-V$			52.5	$L_{oil}-V \rightarrow L_{oil}$	-	-	-	-
				51	$L_{oil}-V$				$L_{oil}-V \rightarrow L_{oil}$	-	-	-	-
				52	$L_{oil}-V$			43.3	$L_{oil}-V \rightarrow L_{oil}$	-	-	-	-
8	Uniform	Uniform	FTQG	53	$L_{oil}-V$	White	L	54	$L_{oil}-V \rightarrow V$	-	-	-	-
				54	$L_{oil}-V$			54	$L_{oil}-V \rightarrow V$	-	-	-	-
				55	$L_{oil}-V$			53	$L_{oil}-V \rightarrow V$	-	-	-	-
				56	$L_{oil}-V$			47	$L_{oil}-V \rightarrow V$	-	-	-	-
				57	$L_{oil}-V$			50.2	$L_{oil}-V \rightarrow V$	-	-	-	-
				58	$L_{oil}-V$			45.2	$L_{oil}-V \rightarrow V$	-	-	-	-
9	Variable	Variable	FTQG	59	$L_{oil}-V$	White	M-L	65.4	$L_{HC}-V \rightarrow L_{HC}$	58	$L_{oil}-L_{HC}-V \rightarrow L_{HC}-V$	-	-
				60	$L_{oil}-V$	White	M	58.8	$L_{oil}-V \rightarrow L_{oil}$	-	-	-	-
				61	$L_w-L_{oil}-V$	Blue	M	43.5	$L_w-L_{oil}-V \rightarrow L_w-L_{oil}$	-	-	-	-
				62	$L_w-L_{oil}-V$	Yellow	L	70	$L_w-L_{oil}-V \rightarrow L_w-V$	-	-	-	-
10	Uniform	Uniform	FTQG	63	L_w-V		S	-	$L_w-V \rightarrow L_w$	-	-	2.3*	-
				64	L_{oil}	White		33.8	$L_{oil}-V \rightarrow L_{oil}$	-	-	-	-
				65	L_{oil}			33.5	$L_{oil}-V \rightarrow L_{oil}$	-	-	-	-
				66	L_{oil}			31.9	$L_{oil}-V \rightarrow L_{oil}$	-	-	-	-
				67	L_{oil}			6.0	$L_{oil}-V \rightarrow L_{oil}$	-	-	-	-
				68	L_{oil}			15.0	$L_{oil}-V \rightarrow L_{oil}$	-	-	-	-
				69	L_{oil}			27.0	$L_{oil}-V \rightarrow L_{oil}$	-	-	-	-
				70	L_{oil}			33.0	$L_{oil}-V \rightarrow L_{oil}$	-	-	-	-

OIA	Fluo. variability	Bubble size variability	Location	FI No	Inclusion type	Fluo. colour	Bubble size	T_h (°C)	Phase transition	T_h (°C)	Phase transition	$T_{m\text{ Ice}}$ (°C)	Salinity eq. NaCl (wt%)
11	Uniform	Uniform	FTQG	71	$L_{oil}-V$	Yellow	S	72	$L_{oil}-V \rightarrow L_{oil}$	-	-	-	-
				72	$L_{oil}-V$			82	$L_{oil}-V \rightarrow L_{oil}$	-	-	-	-
				73	$L_w-L_{oil}-V$			106	$L_w-L_{oil}-V \rightarrow L_w-L_{oil}$	-	-	-	-
				74	$L_w-L_{oil}-V$			86*	$L_w-L_{oil}-V \rightarrow L_w-L_{oil}$	-	-	-	-
				75	$L_{oil}-V$			79.9	$L_{oil}-V \rightarrow L_{oil}$	-	-	-	-
				76	$L_{oil}-V$			81.9	$L_{oil}-V \rightarrow L_{oil}$	-	-	-	-
12	Uniform	Variable	FTQG	77	L_{oil}	White	S	12.5	$L_{oil}-V \rightarrow L_{oil}$	-	-	-	-
				78	L_{oil}			19	$L_{oil}-V \rightarrow L_{oil}$	-	-	-	-
				79	L_{oil}			10.5	$L_{oil}-V \rightarrow L_{oil}$	-	-	-	-
				80	$L_w-L_{oil}-V$			41	$L_w-L_{oil}-V \rightarrow L_w-L_{oil}$	-	-	-	-
				81	$L_{oil}-V$			34	$L_{oil}-V \rightarrow L_{oil}$	-	-	-	-
				82	L_{oil}			16.1	$L_{oil}-V \rightarrow L_{oil}$	-	-	-	-
13	Uniform	Uniform	FTQG	83	$L_{oil}-V$	White	S	35.7	$L_{oil}-V \rightarrow L_{oil}$	-	-	-	-
				87	$L_w-L_{oil}-V$			56.9	$L_w-L_{oil}-V \rightarrow L_w-L_{oil}$	-	-	0.6*	-
				88	$L_{oil}-V$			43.5	$L_{oil}-V \rightarrow L_{oil}$	-	-	-	-
				89	$L_{oil}-V$			39.5	$L_{oil}-V \rightarrow L_{oil}$	-	-	-	-
				90	$L_{oil}-V$			55	$L_{oil}-V \rightarrow L_{oil}$	-	-	-	-
14	None	Variable	QOB	91	$L_w-L_{oil}-V$		S	58.5	$L_w-L_{oil}-V \rightarrow L_w-L_{oil}$	-	-	2.2*	-
				92	L_w-V				$L_w-V \rightarrow L_w$	-	-	-2.0	33721
15	None	Variable	QOB	93	L_w-V		S	76.5	$L_w-V \rightarrow L_w$	-	-	2.0*	35000
				84	L_w-V		S	109	$L_w-V \rightarrow L_w$	-	-	-	-
16	None	Variable	QOB	85	L_w-V			-	$L_w-V \rightarrow L_w$	-	-	-1.8	30319
				86	L_w-V			137.5	$L_w-V \rightarrow L_w$	-	-	2.5*	-

*Non cycled temperature.

Table 16: Gnarlyknots-1A Raman results for gas detection.

Inclusion No	Inclusion type at room temperature	Bubble size	T_h (°C)	Salinity eq. NaCl (wt%)	ν_1 CH ₄ peak shift (cm ⁻¹)	[CH ₄]m (mol/kg)	[CH ₄]m (ppm)	Ph (bar)	P vap (bar)	CO ₂ (mol.%)	CH ₄ (mol.%)
16	L_w-V	Small	80	47500	2916.15	0.131	2090	314	80	30	70
16b	L_w-V	Small	88		2915.94	0.154	2457	408	78		
16c	L_w-V	Small	80		2916.28	0.123	1971	285	64		
16c	L_w-V	Small	85		2916.28	0.130	2081	308	64		
18	$L_w-L_{oil}-V$	Large	88.4	51500	2911.98	0.144	2308	370	184*	30	70
19	L_w-V	Large			2911.82				218*		
20	L_w-V	Small	115		2915.33				102		
20b	L_w-V	Small	78		2915.86				82		
92	L_w-V	Small		33500	2917.59	0.001	20	2	0		
93	L_w-V	Small	76.5		2917.51	0.016	257	23	5		

*Calculation using Seitz et al. 1996 dataset for the system CH₄-CO₂.

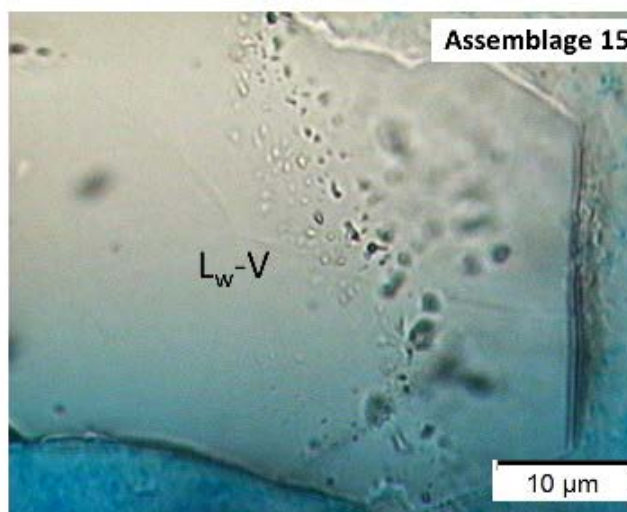
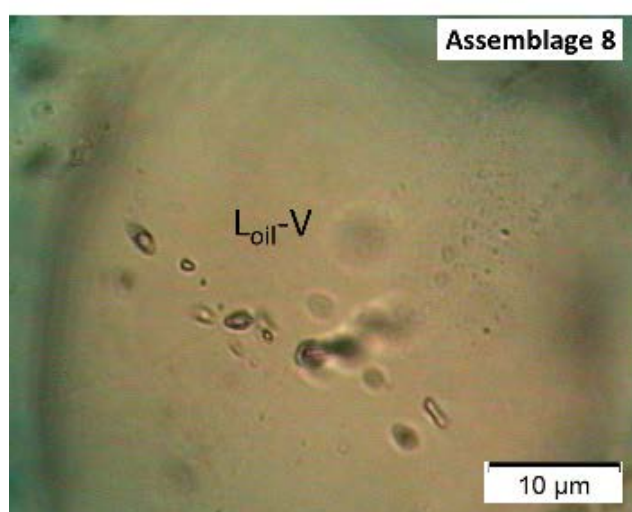
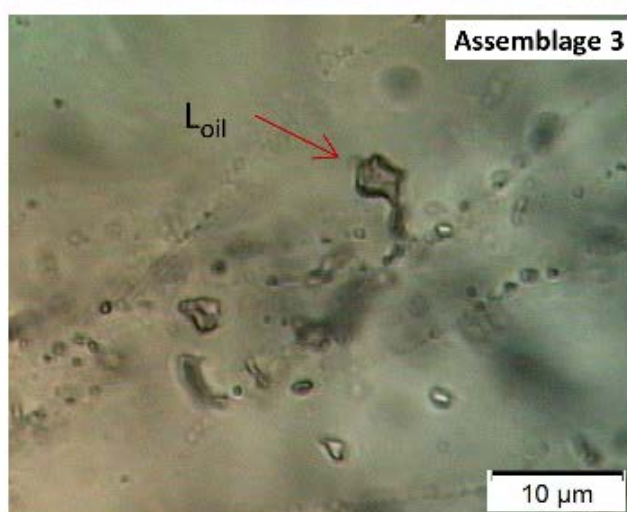
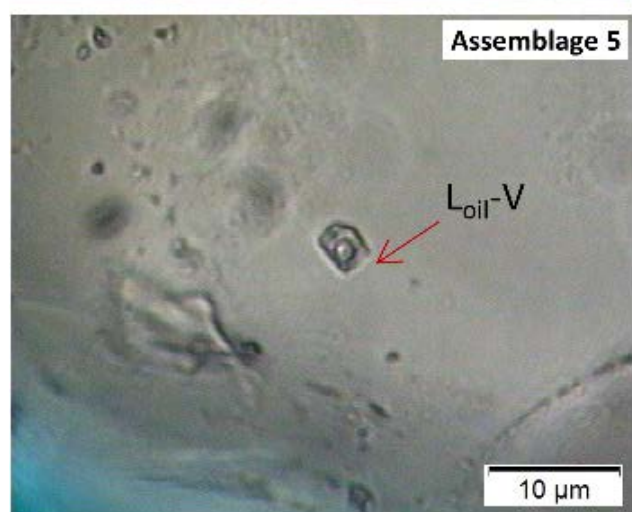
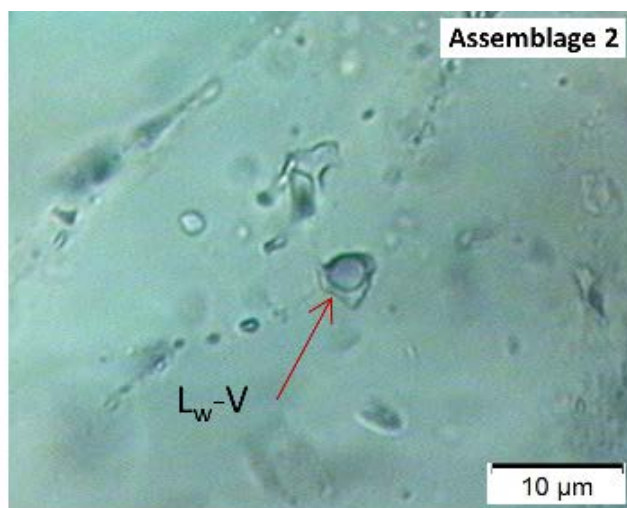
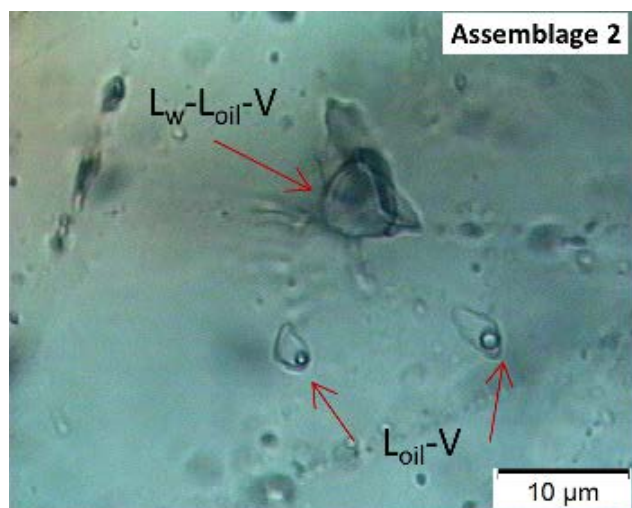


Figure 74: Transmitted light photomicrographs of Gnarlyknots-1A oil inclusion assemblages 2, 3, 5, 8, 15.

PVT Analysis

Each fluid inclusion assemblage with hydrocarbon fluids represents a record of the fluids that migrated through the rock over time. The *PVT* analysis then allows their trapping pressure and temperature to be constrained. Phase envelopes and isochores for both oil and associated water inclusions, that are used to derive entrapment pressures and temperatures, are shown separately in Appendix 9.

Assemblage 5 comprises mostly oil inclusions with variable, but mostly medium-sized vapour bubbles. Inclusions 37, 38 and 43 have a T_h values between 64.2 and 67.2°C and measured vapour volume fractions ranging from 14.9 and 28.5 %. PIT modelling gives a range of compatible compositions corresponding of light oil (Table 17). Phase envelopes and isochores for oil inclusion 43 are shown in Appendix 9, which represent the range of possible compositions. An aqueous inclusion belonging to the same assemblage has a T_h of 69.2 °C. Salinity and methane content data could not be acquired due to background fluorescence. However, as the T_h of the water is the same as the T_h of the oil, it is assumed that the water is gas saturated and therefore the T_h of the water inclusions equals the entrapment temperature. The oil inclusion isochores intersect this temperature of 69.2°C at pressures between 240 and 270 bars.

Assemblage 2 comprises water, oil and gas inclusions with variability in oil fluorescence colour and bubble size. The T_h have a large spread in temperature. These features together suggest the co-existence of oil, gas and water when the fluid inclusion assemblage formed, and consequently the water inclusions were trapped at gas saturation. Water inclusion 16c has a T_h between 80-85°C, a salinity of 47,500 ppm and a methane concentration of about 2,000 ppm. The calculated pressures are 285 bars at 80°C and 308 bars at 85°C. Oil inclusion 12, 13 and 14 have T_h of 67.1 to 90.3°C and a measured vapour volume fraction between 1.3 to 8.9%. PIT modelling gives a range of compatible compositions corresponding to gas depleted black oils to regular black oils. The phase envelopes and isochores shown in Appendix 9 represent the range of possible compositions for each of those three inclusions. Inclusion 15 has a higher T_h and larger vapour phase above 30% volume. The calculated composition corresponds to a light oil. The presence of light oil, gas depleted black oil and gas-rich inclusions suggest that the variability in vapour bubble size and composition might be due to a gas-oil de-mixing process generated from reaching of the bubble point curve of a light oil. The minimum oil inclusion T_h value for this assemblage is 50.8°C and was measured from a small vapour phase inclusion. It was assumed to correspond to the same black oil composition present at the intersection of isochores between black oil and water at 285-308 bar and 80-85°C.

In the same grain containing assemblage 2, an assemblage of both water and gas/water-rich inclusions were also observed. Water inclusions 20b has a T_h of 78°C and a calculated pressure at the T_h of 370 bars and inclusion 16b has a T_h of 88°C and a calculated pressure at the T_h of 408 bars. Raman analysis of the associated 2-phase gas-water inclusion with large vapour bubble indicates that the gas is composed of 70 mol% CH₄ and 30 mole% CO₂ (Table 16). No N₂ or H₂S was detected. Given some degree of uncertainty in the gas inclusion isochore calculation, the best estimation of trapping conditions are constrained by the water inclusion P_h and T_h between 370-408 bars at temperatures between 78 to 88°C, however, the trapping PT space on Figure 75 is extended to where the gas inclusion isochore sits.

Assemblage 8 comprises oil inclusions with large-sized vapour bubbles. Inclusion 57 and 58 have T_h values of 50 and 45°C, respectively, and vapour volume fractions, estimated by confocal microscopy reconstruction, of 35 to 20%, respectively. PIT modelling gives a range of compatible compositions that corresponds to gas condensate. No aqueous inclusion belonging to the same assemblage could be identified and there is no constraint on where, along the isochore, the gas inclusions were entrapped.

These isochores do, however, cross the independently modelled *PT* curve from BP at around at 80°C, corresponding to pressures of 350 to 410 bars.

Assemblage 3 comprises 1-phase dull fluorescent (blue) inclusions, and white fluorescent 2-phase oil inclusions. The T_h of the 2-phase inclusions is in the range of 30-35°C and homogenization is into the liquid phase. Within the 1-phase inclusions, a thin irregular rim of yellow fluorescent oil appeared during cooling, with the main liquid phase showing no sign of visible fluorescence. With further cooling, the main liquid phase nucleated a bubble. The vapour bubbles homogenise back into the main liquid phase between -48.4 and -19.5°C. The thin rims of yellow fluorescent oil homogenise back into the dull fluorescent blue liquid between 7 and 20°C. This type of phase behaviour cannot be directly simulated with PIT modelling. It is suspected that the thin yellow fluorescent rim is a condensation product, at low temperature and low internal pressure, of heavy poly-aromatic hydrocarbons (i.e. aromatic, resin and asphaltene molecules) un-mixing from a non-fluorescent paraffinic mixture. This is similar to the asphaltene precipitation when production fluids pass the upper asphaltene onset pressure (upper AOP; refer to Appendix 13).

Table 17: Oil inclusions compositions calculated for Gnarlyknots-1A using PIT.

OIA	Inc	ϕ_{vap} (20°C)	T_h (°C)	Alpha	Beta	C ₁	C ₂	C ₃	iC ₄	nC ₄	iC ₅	nC ₅	nC ₆	C ₇₊
2	15	32.2	110.1	0.847	0.553	54.8	9.6	6.7	1.3	2.9	1.7	2.7	2.9	25.0
	15	33.7	110.1	0.847	0.565	56.0	9.6	6.6	1.3	2.8	1.7	2.7	2.8	24.7
	12	1.3	67.1	0.975	0.268	6.8	0.7	1.3	0.4	0.8	0.7	1.1	2.5	5.0
	12	3.0	67.1	0.949	0.405	20.9	3.3	4.1	1.0	2.2	1.6	2.6	3.7	14.7
	14	6.9	90.3	0.926	0.420	27.7	5.0	5.4	1.3	2.8	2.0	3.2	4.1	19.6
	14	8.9	90.3	0.911	0.441	32.8	6.2	6.1	1.4	3.1	2.1	3.4	4.1	22.3
	13	3.3	82.3	0.955	0.364	16.3	2.4	3.3	0.8	1.9	1.4	2.2	3.6	12.0
	13	4.5	82.3	0.941	0.389	21.6	3.6	4.4	1.1	2.4	1.7	2.8	4.0	16.0
5	37	22.8	67.2	0.849	0.583	57.9	9.6	6.4	1.2	2.7	1.6	2.5	2.6	15.4
	37	28.5	67.2	0.834	0.594	61.0	9.7	6.2	1.1	2.6	1.5	2.3	2.5	13.1
	43	14.9	64.2	0.869	0.56	52.5	9.2	6.6	1.3	2.9	1.8	2.8	3.0	20.0
	43	16.6	64.2	0.857	0.59	54.9	9.1	6.3	1.2	2.8	1.6	2.6	2.7	18.7
	39	6.5	35.1	0.829	0.51	52.6	9.8	7.1	1.4	3.1	1.8	3.0	3.3	17.9
	39	6.5	35.1	0.8128	0.54	57.6	10.0	6.7	1.3	2.8	1.6	2.6	3.0	14.4
	38	16.1	66.7	0.8767	0.58	53.6	9.1	6.4	1.3	2.8	1.7	2.7	2.8	19.6
8	57	34.8	50.2	0.8521	0.67	67.2	9.0	5.3	1.0	2.1	1.2	1.9	1.8	10.5
	57	34.8	50.2	0.7887	0.6	66.2	9.7	5.9	1.0	2.3	1.2	1.9	2.2	9.5
	57	29.9	50.2	0.8474	0.65	65.5	9.2	5.6	1.0	2.3	1.2	2.0	2.0	11.2
	57	29.9	50.2	0.7961	0.59	64.5	9.8	6.1	1.1	2.4	1.3	2.1	2.4	10.5
	58	21	45.2	0.8482	0.63	63.1	9.4	5.9	1.1	2.4	1.3	2.2	2.2	12.5
	58	21	45.2	0.7993	0.57	62.1	10.0	6.3	1.1	2.6	1.4	2.3	2.6	11.7
10	64	2.5	33.8	0.8812	0.46	40.1	8.0	6.9	1.5	3.3	2.2	3.5	4.0	30.5

Assemblage 10 comprise oil inclusions with small, or absent, vapour bubbles. Inclusion 66 has a T_h of 31.9°C and a vapour volume fraction of 2.5%. PIT modelling gives a range of compatible compositions that corresponds to a black oil. The isochores representing the range of possible PT entrapment conditions are shown in Appendix 9 (and displayed in Figure 75). Only one aqueous inclusion with a T_h of 118°C was measured, however, this temperature is considered too elevated (possibly due to two-phase trapping) relative to other T_h data. Therefore, there is no constraint on where, along the PIT isochores for inclusion 66, the oil inclusions were entrapped. The isochore does, however, cross the independently modelled PT curve from BP at a pressure of 400 bars (at 80°C).

Summary of *PT* Trapping Conditions

The oil and gas-bearing assemblages observed at 441-15 mMD in Gnarlyknots-1A record a variety of fluid compositions and *PT* conditions (Table 18). Inclusion oils generally have consistent white fluorescence colour, however the variability of T_h values indicates that trapping occurred at a range of *PT* conditions that track a hydrocarbon maturation profile as follows;

- The earliest oil entrapment constrained by PVTx, light oil, took place at a minimum temperature of 69°C. Earlier oil migration is likely to have taken place at lower minimum temperatures between 58 to 62°C (OIA 1 and 13), but their compositions, and therefore pressures, is not constrained.
- Phase separation of light oil into gas-rich inclusions and gas-depleted black oil is constrained, by the latter, at temperatures of 80-85°C and pressures of 285-308 bar.
- Gas-condensate was then trapped, most probably between 350-410 bars @ 80°C, but the temperature is not well constrained.
- Free gas (70 mol% CH₄ and 30 mol% CO₂) is estimated to have been trapped between 370-408 bars at temperatures between 78 to 88°C.
- Some low T_h oil inclusions indicate that some black oil was still migrating at more elevated pressure conditions of 400 bar @ 80°C.

Table 18: Summary of *PT* entrapment conditions in Gnarlyknots-1A.

Assemblage	Temperature (°C)	Pressure (bar)	Composition
1, 13	58-62 (min)	-	Oil (not modelled)
5	69.2	240-270	Light oil
2	80-85	285-308	Gas depleted black oils to regular black oils
8	-	350-410 (@80°C)	Gas-condensate
10	-	400 (@80°C)	Black oil
2	78-88	370-408	Gas + CO ₂

Min = minimum PT estimation only. Estimated = temperature constraint from 1D burial history curve.

These palaeo-*PT* conditions recorded by the fluid inclusion assemblages closely follow the independently modelled Pressure-Temperature-time (*PT-t*) curve provided by BP from a 3D burial history model at this approximate sample depth (Figure 75). This suggests that the burial history model is well calibrated in this location, assuming that the temperature constraints represent fluid in equilibrium with the rock.

A limited number of water inclusion salinities, from inclusions associated with the presence of hydrocarbon, were measured. These salinities of 30,000-50,000 ppm are lower than the interpreted resistivity log-derived formation water salinity of 70,000 ppm. The lowest salinities measured, from water inclusions at the quartz overgrowth boundary (and not associated with hydrocarbon fluids), were about 30,000 ppm. A minimum T_h of 76.5°C, from a range of generally higher values, is consistent with crystallisation of at least some quartz overgrowth after the first oil migration event. In support of this, some fractures with oil inclusions in Gnarlyknots-1A were observed to terminate at the quartz overgrowth boundary (Figure 26C). Those hydrocarbon-bearing assemblages with T_h higher than this suggest they were trapped after the onset of quartz cementation.

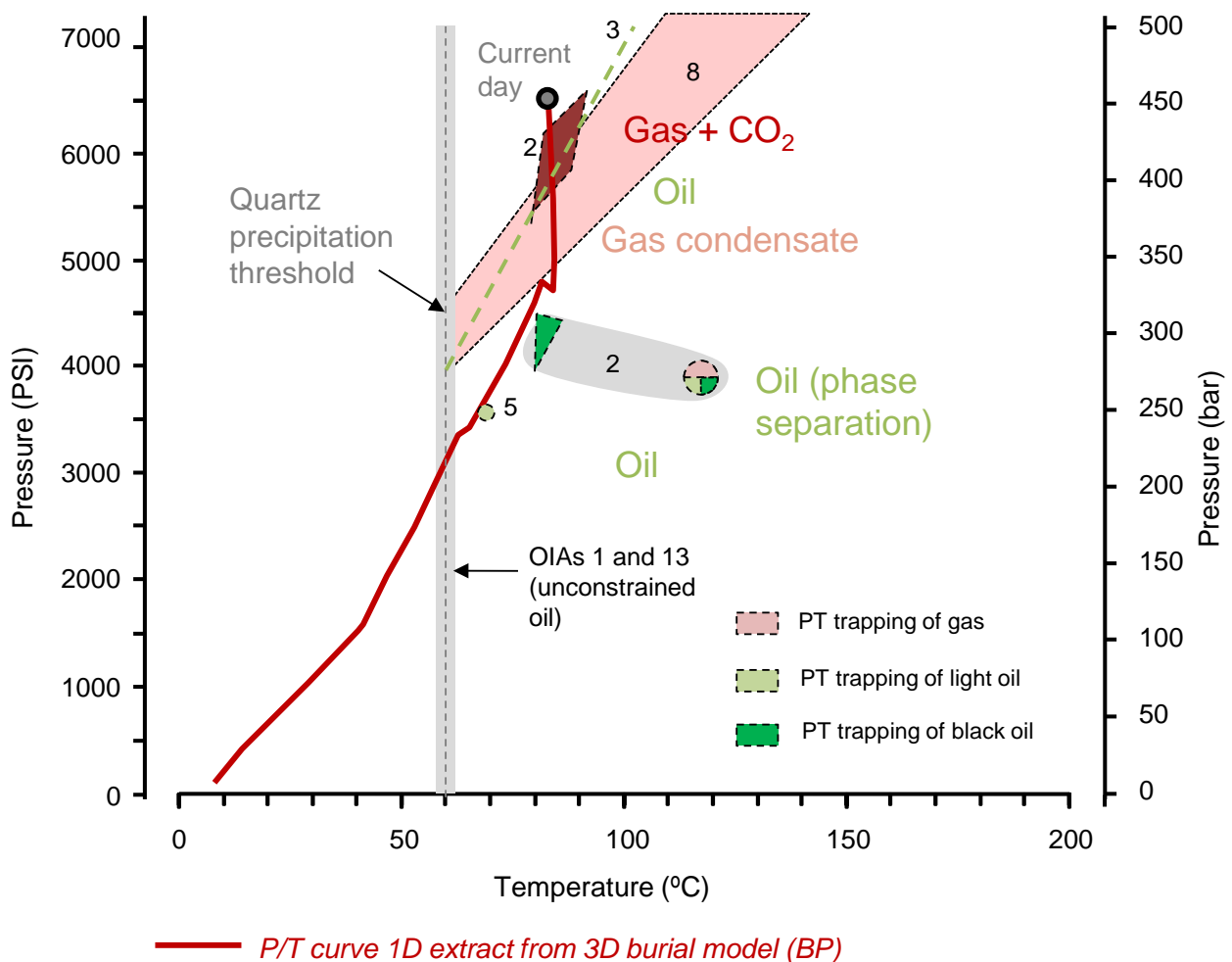


Figure 75: Trapping conditions at 4410-15 mMD in Gnarlyknots-1A derived from PVTx modelling of gas, oil and water fluid inclusion assemblages. Red line is the estimated PT curve at the closest depth of 4380 mTVDKB from gridding constraints provided by BP (extracted from 3D burial history model).

Greenly-1 (4809-12 mMD)

A sand-rich cutting sample from the Upper Cretaceous (Cenomanian) White Pointer Supersequence at 4,809-12 mMD, eastern Ceduna/Dunroon sub-basins, was investigated for detailed PVTx analysis of the hydrocarbon fluid inclusions trapped in quartz.

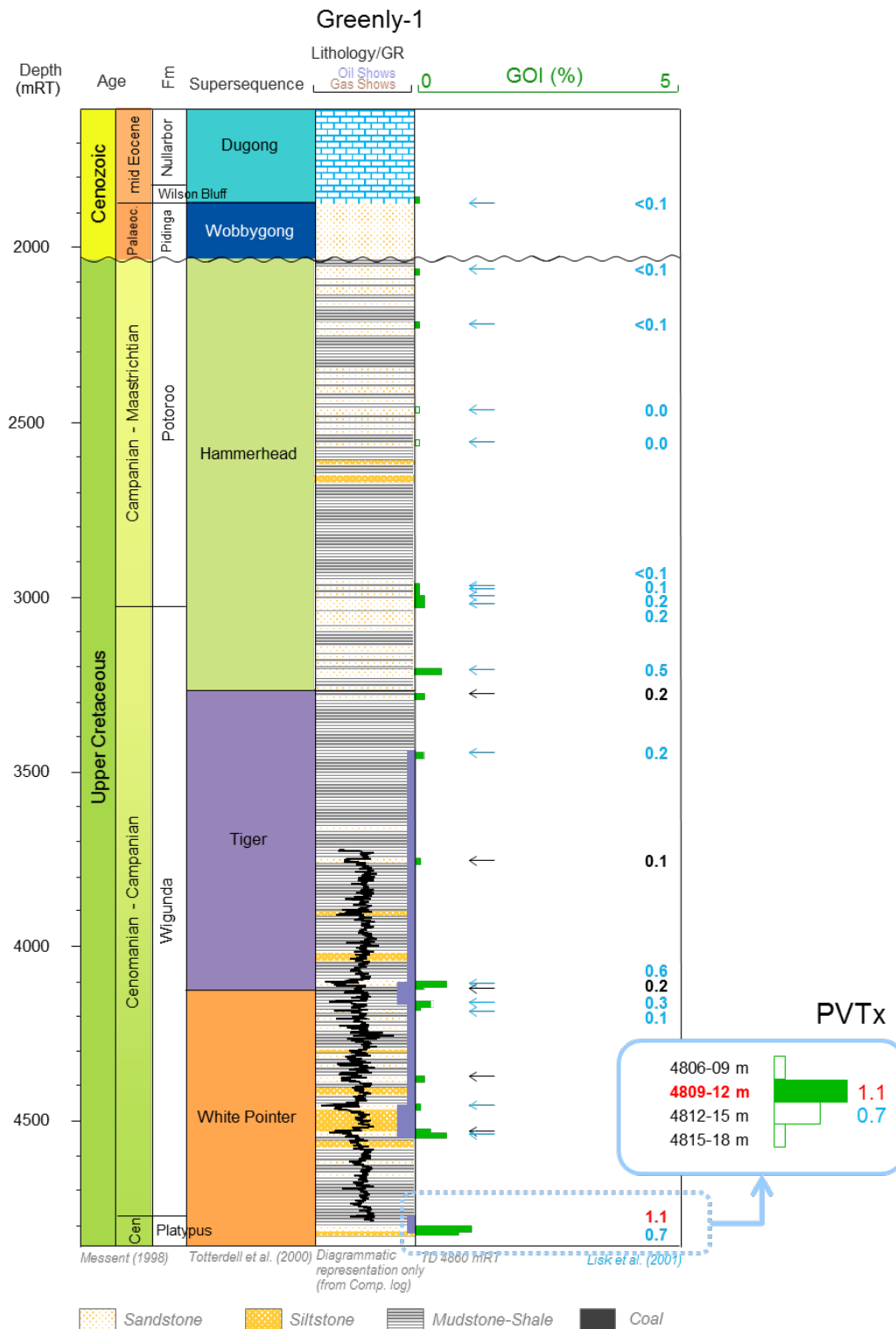


Figure 76: GOI log for Greenly-1 showing location of sample for PVT analysis.

Fluid Inclusion Assemblage Descriptions

Fluid inclusion assemblages were investigated in 11 different grains from Greenly 1 (Table 19). Amongst those, 7 assemblages contained associated hydrocarbon and water inclusions.

At room temperature, the petroleum inclusions are dominantly 2-phase, comprising a volumetrically dominant liquid oil phase and a small sized vapour phase (L_{oil} -V; Figure 77). The oil has dominantly white fluorescence colour, but near-blue fluorescence oil inclusions were also observed (OIAs 4 and 9). Other types of fluid inclusion assemblages include:

- 3-phase inclusions, comprising liquid oil, liquid water and a small-sized bubble (L_w - L_{oil} -V). The bubble is systematically contained within the oil phase;
- 4-phase inclusions, comprising bitumen (solid), liquid oil, liquid water and a small to medium-sized bubble (L_w - L_{oil} -V- S_B).

At room temperature, the water inclusions were systematically 2-phase comprising a volumetrically dominant liquid water phase and a small vapour bubble phase (L_w -V).

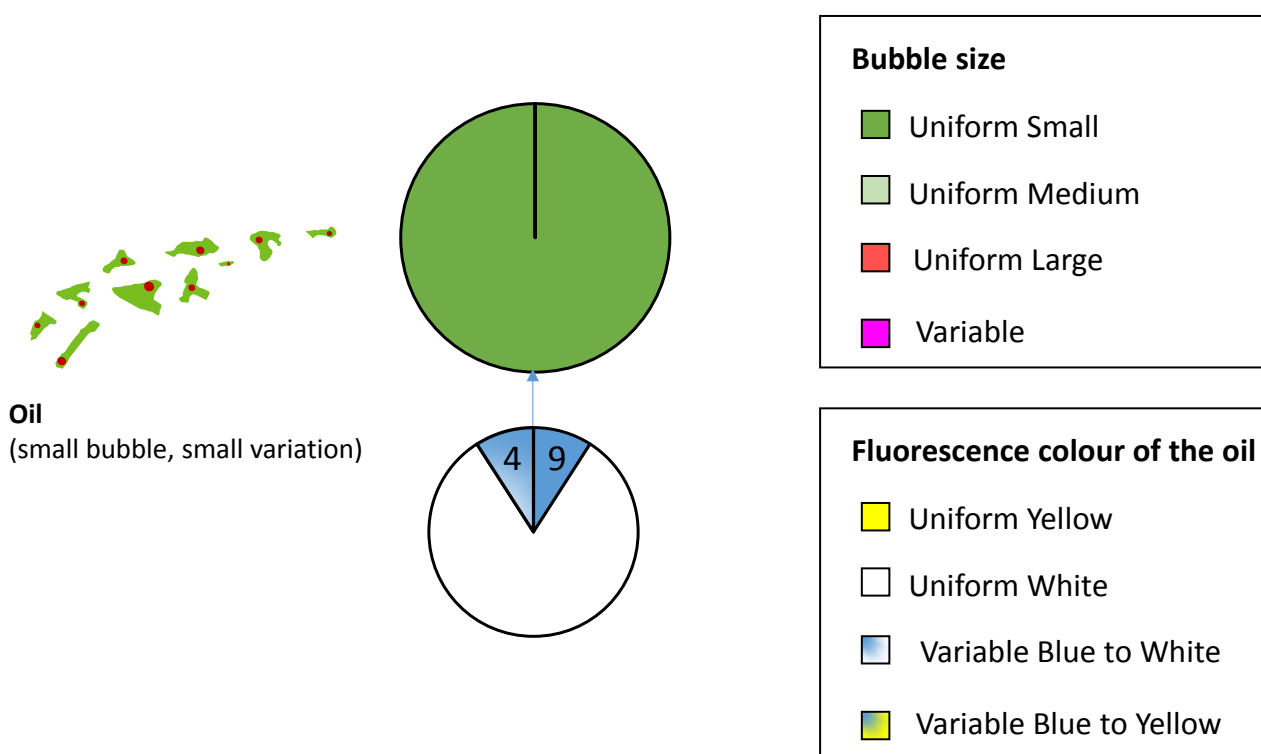


Figure 77 Petroleum fluid inclusion assemblages observed from 4809-12 mMD in Greenly 1,. Numbers within the pie charts refer to the assemblage numbers in Table 5.

Microthermometry

The homogenisation temperatures, acquired on both hydrocarbon and aqueous inclusions, have a narrow spread and, compared to Gnarlyknots-1A, are consistent with the uniformity in attributes observed in many of the inclusion assemblages (Figure 78).

OIAs with uniformly small and medium vapour bubbles

- Uniform white fluorescent oil with uniformly small vapour bubbles (OIAs 1, 2, 3, 6, 7, 8, 10 and 11). The T_h of the oil inclusions are mostly between 80.2 and 99.8°C, with two outliers at 127.8°C and 122.6°C. The fluid was trapped as liquid oil. The associated water inclusions have T_h values of 113 to 133°C and were measured from OIAs 1, 6, 8, 10 and 11. Salinities were obtained from OIAs 1, 8, 10 and 11. No water inclusions were measurable for T_h from OIAs 2, 3 and 7.
- Uniform blue fluorescent oil with uniformly small vapour bubbles (OIA 9). The T_h of the one oil inclusion was 87°C and the fluid was trapped as liquid oil. The associated water inclusion had a T_h of 122°C.
- Variable blue to white fluorescent oil with uniformly small vapour bubbles (OIA 4). The T_h of the oil inclusions are between 80.4 and 98.4°C and the fluid was trapped as liquid oil. The associated water inclusions had T_h values of 125.1 and 127.3°C.

Water inclusion assemblages

No water inclusion assemblages from quartz overgrowth or carbonate cements were measured.

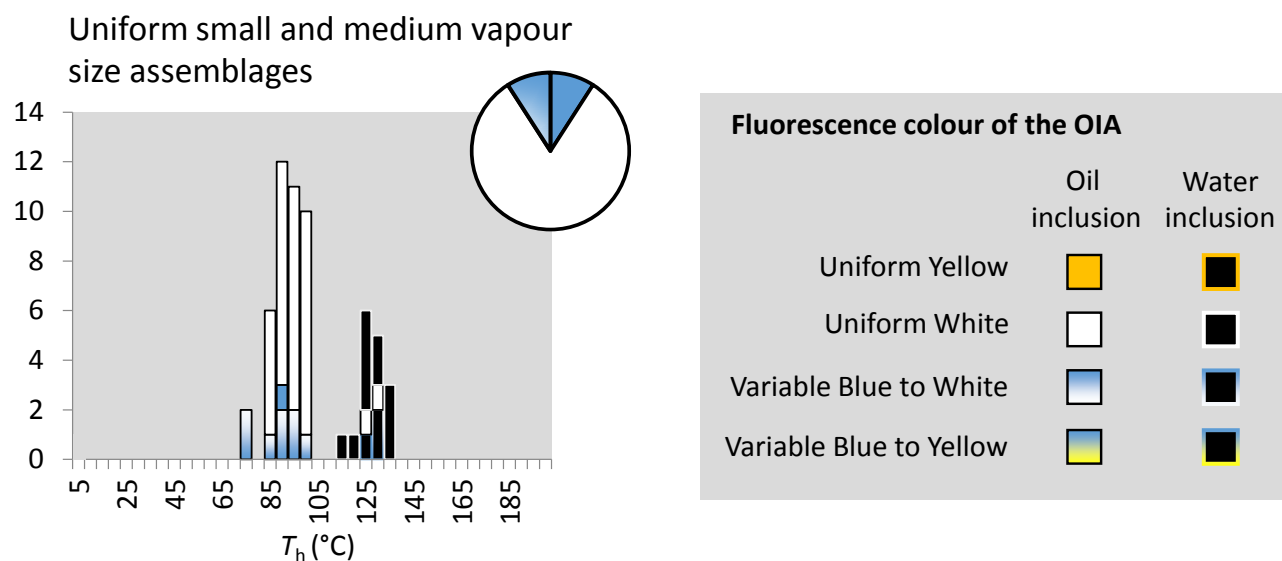


Figure 78: Homogenisation temperatures of oil and associated water inclusions from 4809-12 mMD in Greenly-1.

Table 19: Greenly-1 thermometric results

OIA	Fluo. variability	Bubble size variability	Location	FI No	Inclusion type	Fluro. colour	Bubble size	T_h (°C)	Phase transition	$T_{m\text{ Ice}}$ (°C)	Salinity eq. NaCl (wt%)
1	Uniform	Uniform	FTQG	1	L _w -L _{oil} -V	White	S	89.1	L _w -L _{oil} -V → L _w -L _{oil}	-	-
				2	L _w -L _{oil} -V	White	S	93.6	L _w -L _{oil} -V → L _w -L _{oil}	-	-
				3	L _w -L _{oil} -V	White	S	93.7	L _w -L _{oil} -V → L _w -L _{oil}	-	-
				4	L _{oil} -V	White	S	99.2	L _{oil} -V → L _{oil}	-	-
				5	L _w -V	-	S	116.9	L _w -V → L _w	0*	140000
				6	L _w -V	-	S	120.4	L _w -V → L _w	0*	-
				7	L _{oil} -V	White	S	90.8	L _{oil} -V → L _{oil}	-	-
				8	L _{oil} -V	White	S	127.8	L _{oil} -V → L _{oil}	-	-
				9	L _w -V	White	S	132.4	L _w -V → L _w	-	-
				10	L _{oil} -V	White	S	90.3	L _{oil} -V → L _{oil}	-	-
				11	L _{oil} -V	White	S	80.2	L _{oil} -V → L _{oil}	-	-
				12	L _{oil} -V	White	S	90.25	L _{oil} -V → L _{oil}	-	-
2	Uniform	Uniform	FTQG	13	L _{oil} -V	White	S	94.0	L _{oil} -V → L _{oil}	-	-
				14	L _{oil} -V	White	S	96.0	L _{oil} -V → L _{oil}	-	-
3	Uniform	Uniform	FTQG	15	L _{oil} -V	White	S	93.9	L _{oil} -V → L _{oil}	-	-
				16	L _{oil} -V	White	S	95.4	L _{oil} -V → L _{oil}	-	-
				17	L _{oil} -V	White	S	96	L _{oil} -V → L _{oil}	-	-
4	Variable	Uniform	FTQG	18	L _{oil} -V	White	S	72.6	L _{oil} -V → L _{oil}	-	-
				19	L _{oil} -V	White	S	87.1	L _{oil} -V → L _{oil}	-	-
				20	L _{oil} -V	White	S	98.4	L _{oil} -V → L _{oil}	-	-
				21	L _w -L _{oil} -V-Sbitumen	White	S	73.8	L _{oil} -V → L _{oil}	-	-
				22	L _w -L _{oil} -V-Sbitumen	Near-blue	S	88	L _{oil} -V → L _{oil}	-	-
				23	L _w -V	-	S	125.1	L _w -V → L _w	-7.8	116478
				23bis	L _w -V	-	S	127.3	L _w -V → L _w	-6.9	105506
				24	L _{oil} -V	White	S	80.4	L _{oil} -V → L _{oil}	-	-
				25	L _{oil} -V	White	S	90.8	L _{oil} -V → L _{oil}	-	-
				26	L _{oil} -V	White	S	92.8	L _{oil} -V → L _{oil}	-	-
6	Uniform	Uniform	FTQG	29	L _w -V	-	S	133	L _w -V → L _w	-0.3*	-
				30	L _w -L _{oil} -V	White	S	84.1	L _w -L _{oil} -V → L _w -L _{oil}	-	-
				31	L _{oil} -V	White	S	83.7	L _{oil} -V → L _{oil}	-	-
				32	L _{oil} -V	White	S	84.6	L _{oil} -V → L _{oil}	-	-
				32 bis	L _{oil} -V	White	S	89.8	L _{oil} -V → L _{oil}	-	-
7	Uniform	Uniform	FTQG	33	L _{oil} -V	White	S	99.8	L _{oil} -V → L _{oil}	-	-
				34	L _{oil} -V	White	S	95.2	L _{oil} -V → L _{oil}	-	-
				35	L _{oil} -V	White	S	85.7	L _{oil} -V → L _{oil}	-	-

OIA	Fluo. variability	Bubble size variability	Location	FI No	Inclusion type	Fluro. colour	Bubble size	T _h (°C)	Phase transition	T _{m Ice} (°C)	Salinity eq. NaCl (wt%)
8	Uniform	Uniform	FTQG	36	L _w -L _{oil} -V	White	S	85.2	L _w -L _{oil} -V → L _w -L _{oil}	-	-
				37	L _w -L _{oil} -V	White	S	87.8	L _w -L _{oil} -V → L _w -L _{oil}	-	-
				38	L _w -L _{oil} -V	White	S	89.5	L _w -L _{oil} -V → L _w -L _{oil}	-	-
				39	L _w -L _{oil} -V-S _{bitumen}	White	S	90.4	L _w -L _{oil} -V → L _w -L _{oil}	-	-
				40	L _w -V	-	S	125	L _w -V → L _w	1*	22000
				41	L _w -V	-	S		L _w -V → L _w	-	-
				42	L _w -V	-	S		L _w -V → L _w	-	-
9	Uniform	Uniform	FTQG	43	L _w -V	-	S	123	L _w -V → L _w	-	-
				44	L _{oil} -V	Near blue	S	87	L _{oil} -V → L _{oil}	-	-
				45	L _w -V	-	S	122	L _w -V → L _w	3.7*	-
10	Uniform	Uniform	FTQG	46	L _w -V	-	S	131	L _w -V → L _w	-10.4	141000
				47	L _w -V	-	S		L _w -V → L _w	-10.4	141000
				48	L _{oil} -V	White	S	96.9	L _{oil} -V → L _{oil}	-	-
				49	L _w -V	-	S	121	L _w -V → L _w	-	24000
				50	L _{oil} -V	White	S	96.7	L _{oil} -V → L _{oil}	-	-
11	Uniform	Uniform	FTQG	51	L _w -V	-	S	112	L _w -V → L _w	-	62000
				52	L _w -L _{oil} -V	White	S	122.6	L _w -L _{oil} -V → L _w -L _{oil}	-	29000
				53	L _w -V	-	S	130	L _w -V → L _w	-	62000
				54	L _{oil} -V	White	S	83.5	L _{oil} -V → L _{oil}	-	-
				55	L _{oil} -V	White	S	85.3	L _{oil} -V → L _{oil}	-	-
				56	L _{oil} -V	White	S	85.9	L _{oil} -V → L _{oil}	-	-
				57	L _w -V	-	S	126	L _w -V → L _w	-	-

* Temperature not cycled.

Table 20: Greenly-1 Raman results for gas detection.

Inclusion No	Inclusion type at room temperature	Bubble size	T_h (°C)	Salinity eq. NaCl (wt%)	ν_1 CH ₄ peak shift (cm ⁻¹)	[CH ₄]m (mol/kg)	[CH ₄]m (ppm)	Ph (bar)	P vap (bar)	CO ₂ (mol.%)	CH ₄ (mol.%)
29	L_w-V	Small	133	30000	2916.36	0.183	2927	523	64	0	100
29	L_w-V	Small	133	96000	2916.36	0.221	3529	453	64	0	100
40	L_w-V	Small	125	21500	2916.87	0.138	2212	229	38	0	100
49	L_w-V	Small	121	24000	2916.92	0.125	1998	207	35	-	-
53	L_w-V	Small	130	62000	2916.96	0.123	1973	210	34	-	-

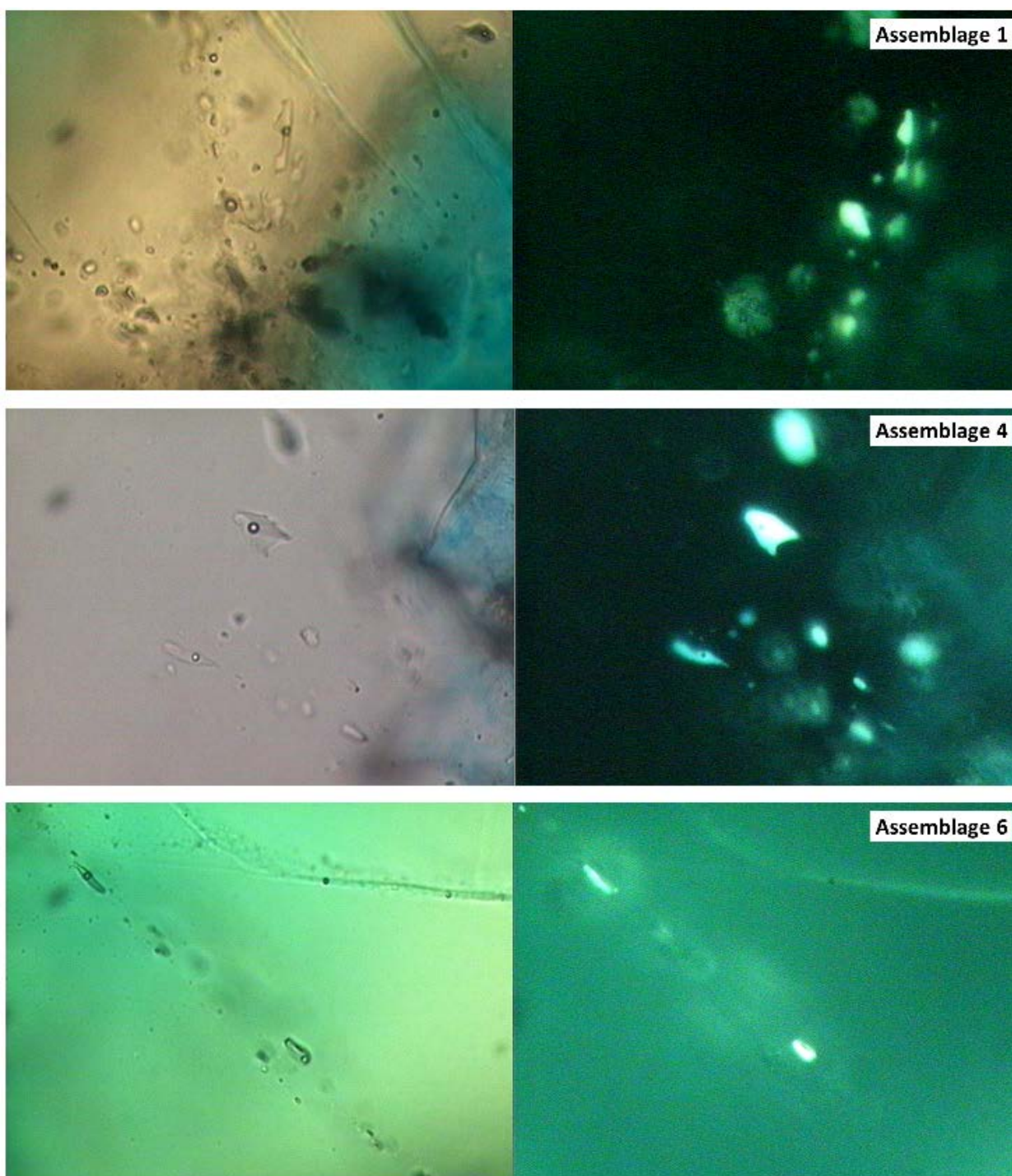


Figure 79: Paired transmitted light and UV photomicrographs of Greenly-1 oil inclusion assemblages 1, 4, 6.

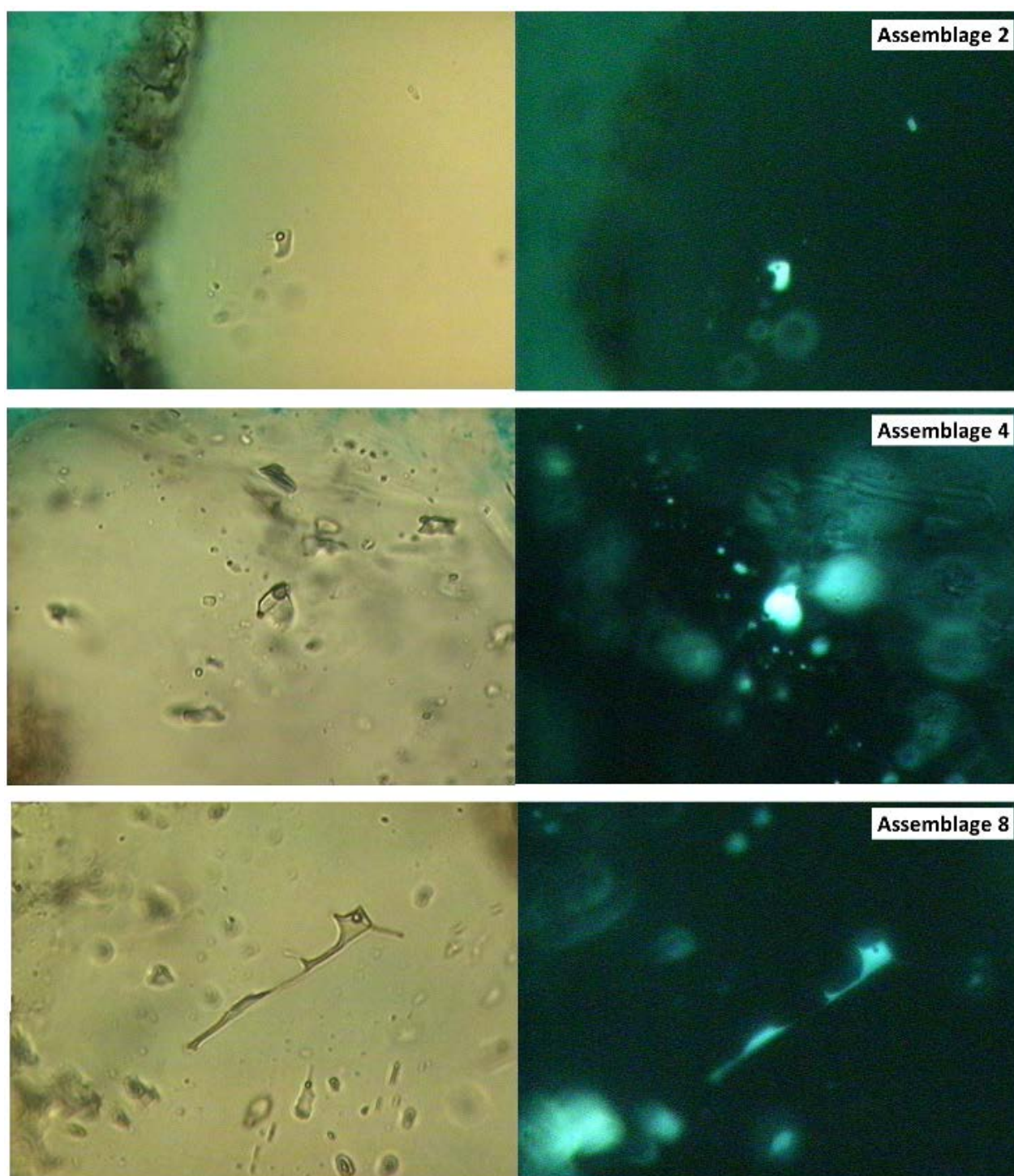


Figure 80: Paired transmitted light and UV photomicrographs of Greenly-1 oil inclusion assemblages 2, 4, 8.

PVT Analysis

Phase envelopes and isochores for both oil and associated water inclusions, that are used to derive entrapment pressures and temperatures, are shown in Appendix 10.

Assemblage 1 has uniform white fluorescent oil inclusions, uniform small vapour bubbles and a narrow spread of T_h values with a mode at 90-95°C. Inclusion 1 and 3 have a T_h of 89.1 and 93.7°C and estimated vapour volume fractions of 4.8 to 6.3% (Table 21). PIT modelling provided a range of compatible compositions corresponding to black oils. An aqueous inclusion belonging to the same assemblage has a T_h of 116.9°C. A salinity of 140,000 ppm was derived from Raman spectroscopy and no gas was detected. The intersection of the hydrocarbon and water isochores gives compatible trapping conditions of 130°C and pressures between 270 and 330 bars (Appendix 10).

Assemblage 4 has mostly uniform white fluorescent oil inclusions (with only one inclusion with near-blue fluorescence). The bubbles are small, with some minor variability. The T_h range from 72.6 to 98.4°C. Two water inclusions were measured from the same assemblage, both with high salinities (106,000 and 116,000 ppm) and no methane. Their T_h values are 125.1 and 127.3°C respectively. Oil inclusions 18, 19, 20 and 22 were used for PIT modelling and give a range of compatible compositions corresponding to black oils. The water isochore intersects these oil isochores at temperatures of between 140 to 148°C and over a wide range of pressures between 300 and 460 bars (Appendix 10).

Assemblage 6 has uniform white fluorescent oil inclusions and uniform small vapour bubbles with a narrow spread in T_h from 84.7 and 89.8°C. Inclusion 32, 32b and 32c provide PIT modelling compatible compositions corresponding to black oils. An aqueous inclusion belonging to the same assemblage has a T_h of 133 °C. Methane was detected and quantified (Table 20) but, as no salinity could be derived, the bubble point curve and isochores for salinities of 30,000 ppm and 96,000 ppm (current salinity) were calculated and used instead. The intersection of the oil and water isochores provides compatible trapping conditions in the range 133-135°C and 305 to 340 bars (Appendix 10).

Assemblage 8 has uniform white fluorescent oil inclusions and uniform small vapour bubbles with T_h ranging from 85.2 to 90.4°C. PIT modelling of Inclusions 36 and 38 provided a range of compatible compositions corresponding to slightly gas depleted black oil. Aqueous inclusions belonging to the same assemblage have T_h values of 123 and 125°C. A salinity of 22,000 ppm was derived from the Raman spectrum and methane was detected at a concentration of 2,212 ppm for calculating the bubble point curve and isochore of water. The intersection of the hydrocarbon and water isochores gives compatible trapping conditions of 130°C and 290 to 340 bars (Appendix 10).

Assemblage 11 has uniform white fluorescent oil inclusions and uniform small vapour bubbles. PIT modelling of inclusion 55 provided a range of compatible compositions corresponding to black oil. An aqueous inclusion belonging to the same assemblage (inclusion 53), with dissolved methane at a concentration of 1,998 ppm, has T_h of 130°C. A salinity of 62,000 ppm was derived from Raman spectrum and used for calculating the bubble point curve and isochore of water. The intersection of the oil and water isochores gives compatible trapping conditions around 135°C and 340 bars. At the lower limit, an aqueous inclusion with a T_h of 112°C (inclusion 51) did not contain methane and the calculated isochore crosses the oil inclusion isochores at around 127°C and 290-300 bars.

Table 21: Oil inclusion compositions calculated in Greenly-1 using PIT.

OIA	Inc	φ_{vap} (20°C)	T_h (°C)	Alpha	Beta	C ₁	C ₂	C ₃	iC ₄	nC ₄	iC ₅	nC ₅	nC ₆	C ₇₊
1	1	5	89.1	0.943	0.408	23	4	4	1	2	2	3	4	58
	1	6.5	89.1	0.927	0.407	26	5	5	1	3	2	3	4	50
	3	4.8	93.7	0.949	0.413	21	3	4	1	2	2	3	4	61
	3	5.5	93.7	0.943	0.424	24	4	5	1	2	2	3	4	56
4	22	8.2	88	0.905	0.390	29	6	6	1	3	2	4	5	44
	18	5.5	72.6	0.914	0.380	27	5	6	1	3	2	3	5	48
	19	9.1	87.1	0.897	0.400	32	6	6	1	3	2	4	5	40
	20	9.7	98.4	0.906	0.400	30	6	6	1	3	2	4	4	43
6	32c	6.3	89.8	0.924	0.360	23	4	5	1	3	2	3	4	53
	32c	8.8	89.8	0.903	0.400	31	6	6	1	3	2	4	4	42
	32b	6.7	84.1	0.915	0.380	27	5	6	1	3	2	3	5	48
	32b	7.2	84.1	0.909	0.380	28	5	6	1	3	2	4	5	46
	32	5.7	84.6	0.922	0.330	22	4	5	1	3	2	3	5	55
8	36	5.1	85.2	0.939	0.411	24	4	5	1	3	2	3	4	55
	36	7.2	85.2	0.914	0.400	29	5	6	1	3	2	3	4	46
	38	4.4	89.5	0.949	0.391	20	3	4	1	2	2	3	4	62
	38	5.1	89.5	0.943	0.403	23	4	4	1	2	2	3	4	57
11	55	3.8	85.3	0.949	0.340	16	3	3	1	2	2	2	4	67
	55	6.1	85.3	0.924	0.380	25	5	5	1	3	2	3	4	51

Summary of *PT* Trapping Conditions

The physical properties of hydrocarbon inclusions contained in grains from 4,809-12 mMD in Greenly-1 are all very consistent. PIT-derived compositions are all compatible with black oil. No associated gas or gas-condensate inclusions were identified.

The entrapment conditions for the oil is also very consistent. Modelled pressures and temperatures from each assemblage fall in a narrow range of 127-148°C and 270-340 bar, with outlier pressures up to 460 bar (Table 22; Figure 81). This suggests that all of the oil in Greenly-1 was trapped under the same *PT* conditions and, therefore, at the same time. In comparison to Gnarlyknots-1A, the modelled *PT* conditions do not sit on the independently modelled *PT* curve (supplied by BP). Changing the input parameters in the basin model by increasing heat flow does not give a better fit to the data points obtained in this study, at least with geologically sensible conditions. This either suggests that; (1) the temperatures are correct and the pressures are lower than they should be or, (2) the pressures are correct and the temperatures are higher than they should be. The former would suggest entrapment of oil at temperatures equivalent to current day, with the latter suggesting entrapment at some point in the geologic past.

Table 22: Summary of PT entrapment conditions in Greenly-1.

Assemblage	Temperature (°C)	Pressure (bar)	Composition
1	130	270-330	Black oil
4	140-148	300-460	Black oil
6	133-135	305-340	Black oil
8	130	290-340	Black oil
11	135	340	Black oil
	127	290-300	Black oil

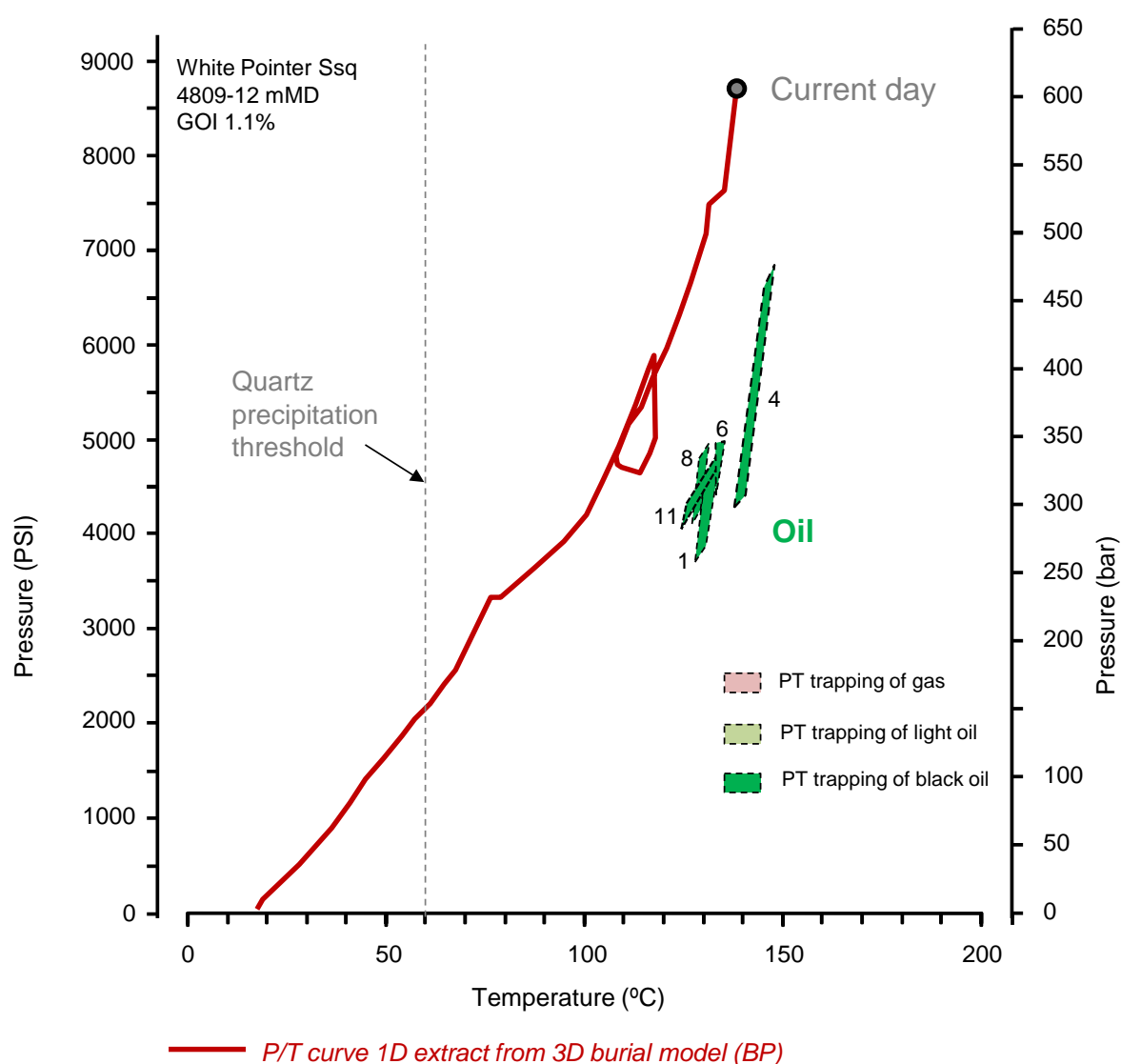


Figure 81: Trapping conditions at 4809-12 mMD in Greenly-1 derived from PVTx modelling of oil and water fluid inclusion assemblages. Red line is the estimated PT curve at the closest depth of 4818 mTVDKB from gridding constraints provided by BP (extracted from 3D burial history model). Loop in PT model is an erosion event (rapid drop in pressure and slower thermal response).

Duntroon-1 (2505-10 mMD)

A sand-rich cutting sample of Upper Cretaceous (Turonian-Santonian) Tiger Supersequence at 2,505-2,510 mMD in Duntroon-1, eastern Ceduna/Duntroon sub-basins, was investigated for detailed *PVT_x* analysis of the hydrocarbon fluid inclusions trapped in quartz (Figure 82).

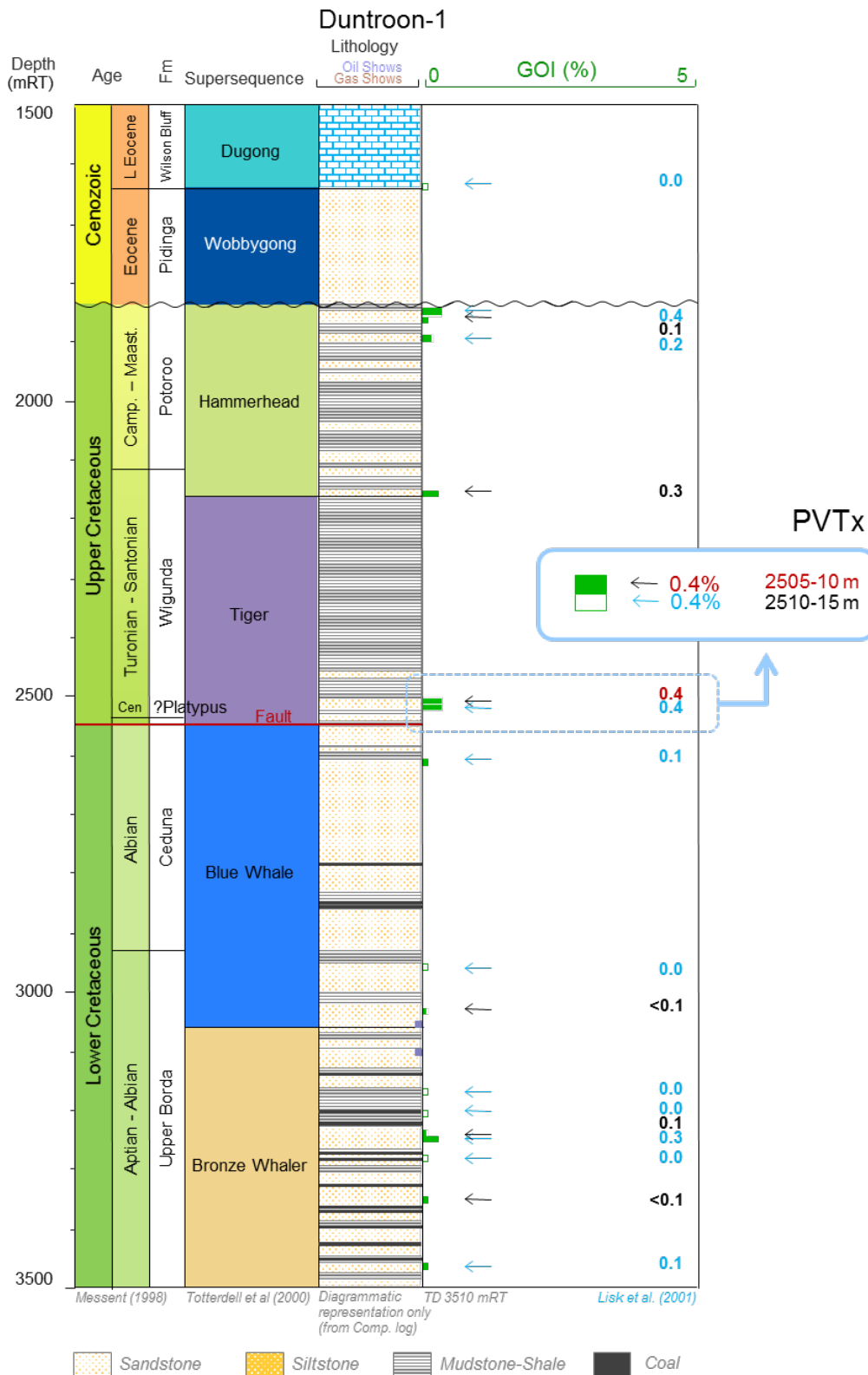


Figure 82: GOI log for Duntroon-1 showing location of sample for *PVT_x* analysis.

Fluid Inclusion Assemblage Descriptions

In Duntroon-1, petroleum-bearing inclusion assemblages (oil, gas and water) were investigated from 14 different grains (Table 23). Six additional grains were examined for water inclusion assemblages in quartz cements only.

At room temperature, the petroleum inclusions observed were dominantly 2-phase, comprising a volumetrically dominant liquid oil phase and a small to medium-size vapour phase (L_{oil} -V; Figure 83). Other types of fluid inclusion assemblages include:

- 2-phase inclusions (L_{oil} -V) comprising a volumetrically large vapour/gas bubble and liquid oil;
- 3-phase inclusions (L_w - L_{oil} -V) comprising liquid water, liquid oil and a small to medium-size vapour bubble. The bubble is systematically contained in the oil phase;
- 3-phase inclusions (L_w - L_{oil} -V) comprising liquid water, liquid oil and a volumetrically large vapour bubble. The bubble is systematically contained within the oil phase;
- 1-phase inclusions (monophase), comprising a fluorescing hydrocarbon phase without a vapour bubble at room temperature.

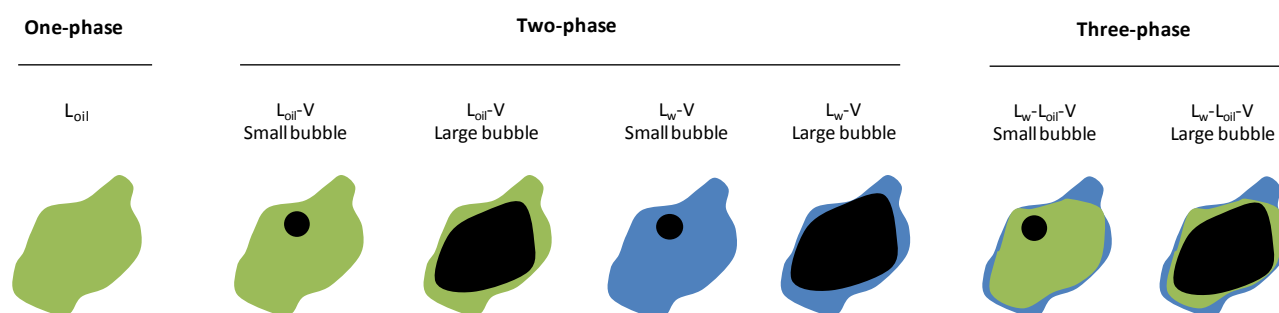


Figure 83. Fluid inclusions types observed at room temperature in the sample from Duntroon-1.

The oil inclusion assemblages (OIA) are classified primarily by the uniformity, or variability, of the vapour phase size in the inclusions populating the assemblages (Figure 84). The assemblages were also classified by fluorescence colour under UV-illumination, and the degree of uniformity or variability. Assemblages with uniform yellow, uniform white, variable blue to yellow and variable blue to white fluorescence were encountered in the sample from Duntroon-1.

Six OIAs have uniform small or medium vapour bubbles. Of these, four have small vapour bubbles (Figure 84) and include OIAs 9 and 12 with uniform yellow fluorescence, and OIAs 4 and 11 with uniform white fluorescence. Two OIAs have uniform medium-sized vapour bubbles (OIAs 6 and 14) with uniform white fluorescence. Three assemblages have uniform large vapour bubbles (gas condensate); OIA 3 has uniform white fluorescence and OIAs 5 and 7 have uniform yellow fluorescence.

Five OIAs have variable size vapour bubbles (small to large), with some including monophase inclusions. OIA 1 has uniform yellow fluorescence with both monophase and two-phase oil inclusions (small vapour bubble) at room temperature. OIA 8 has uniform white fluorescing two-phase oil inclusions with small to medium vapour bubbles at room temperature. OIA 13 has variable blue to yellow fluorescing oil inclusions with both monophase and two-phase oil inclusions (variable small to

large vapour bubbles) at room temperature. OIAs 2 and 10 have variable blue to white fluorescing two-phase oil inclusions with variable small to large vapour bubbles at room temperature.

Water inclusions encountered in Duntroon-1 were all 2-phase comprising a volumetrically dominant aqueous phase and a small vapour phase (L_w -V).

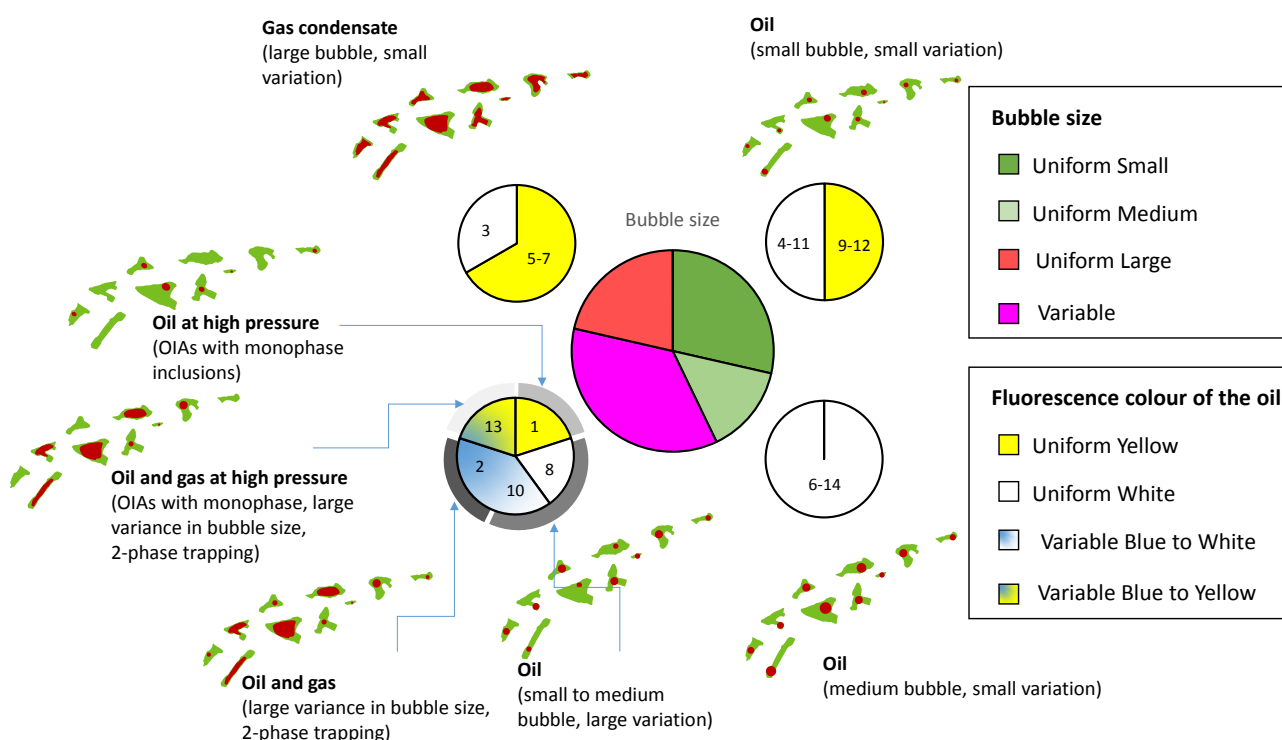


Figure 84: Petroleum fluid inclusion assemblages observed from 2505-10 mMD in Duntroon 1. Numbers within the pie charts refer to the assemblage numbers in Table 19.

Microthermometry

The T_h measured on hydrocarbon and associated aqueous inclusions have a large spread of values (Table 23; Figure 85). These assemblages are grouped into:

OIAs with uniform small and medium vapour bubbles:

- Uniform yellow fluorescence fluorescing oil with uniform small vapour bubbles (OIAs 9 and 12). The T_h of the oil inclusions are between 69.7 and 91°C. The fluorescence colour suggests this oil might have low maturity (George et al., 2001). Two water inclusions provided T_h values of 86 and 90°C. No salinity could be determined due to metastable behaviour of ice melting.
- Uniform white fluorescence oil with uniform small or medium sized vapour bubbles (OIAs 4, 6, 11 and 14). The oil inclusions have T_h between 66 and 123.9°C. The water inclusions in those assemblages have T_h values between 88.9 and 114°C. No salinity could be determined due to the metastable behaviour of ice melting.

OIAs with uniformly large vapour bubbles:

- Uniform white fluorescence oil with large bubbles at room temperature (OIA 3). The T_h values range from 104 and 135°C with homogenisation into the liquid phase. The water inclusion in this assemblage has a T_h value of 119.6°C. No salinity could be determined due to the metastable behaviour of ice melting.
- Uniform yellow fluorescence oil with uniform large vapour bubbles (OIAs 5 and 7). The T_h values range from -75 to -54°C with homogenisation into gas phase. The water inclusions in those assemblages have T_h values between 83 and 92.2°C. No salinity could be determined due to the metastable behaviour of ice melting.

OIAs with variably-sized vapour bubbles:

- Uniform yellow fluorescence oil with monophasic and two-phase oil inclusions, with small vapour bubbles, at room temperature (OIA 1). The monophasic inclusions nucleate a bubble by lowering the temperature below 20°C. The T_h values of the oil inclusions range from 19.3 to 78.3°C, with homogenisation into the liquid phase. The water inclusions in this assemblage have T_h values between 81 and 84.8°C. No salinity could be determined due to metastable behaviour of the ice melting.
- Variable blue to yellow fluorescence oil with monophasic and two-phase oil inclusions, with small to large vapour bubbles, at room temperature (OIA 13). The monophasic inclusions nucleate a bubble by lowering the temperature below 20°C. The T_h values of the oil inclusions range from 19 to 85°C, with homogenisation into the liquid phase. The water inclusions in this assemblage have T_h values between 88 and 88.5°C. No salinity could be determined due to the metastable behaviour of ice melting.
- Uniform white fluorescence two-phase oil inclusions, with small to medium vapour bubbles, at room temperature (OIA 8). The T_h values of the oil inclusions range from 86.4 to 102°C, with homogenisation into the liquid phase. One water inclusion in those assemblages has a T_h value of 86.7°C. No salinity could be determined due to the metastable behaviour of ice melting.
- Variable blue to white fluorescence two-phase oil inclusions, with small to large vapour bubbles, at room temperature (OIA 2 and 10). The T_h values of the oil inclusions range from 51 to 136°C, with homogenisation into either the liquid or gas phase. One water inclusion in those assemblages has a T_h value of 126°C. No salinity could be determined due to the metastable behaviour of ice melting.

Water inclusion assemblages

Water inclusion assemblages were observed at the quartz overgrowth boundary and within quartz overgrowth cement. Their T_h values range from 87.5 to 138°C (Figure 86).

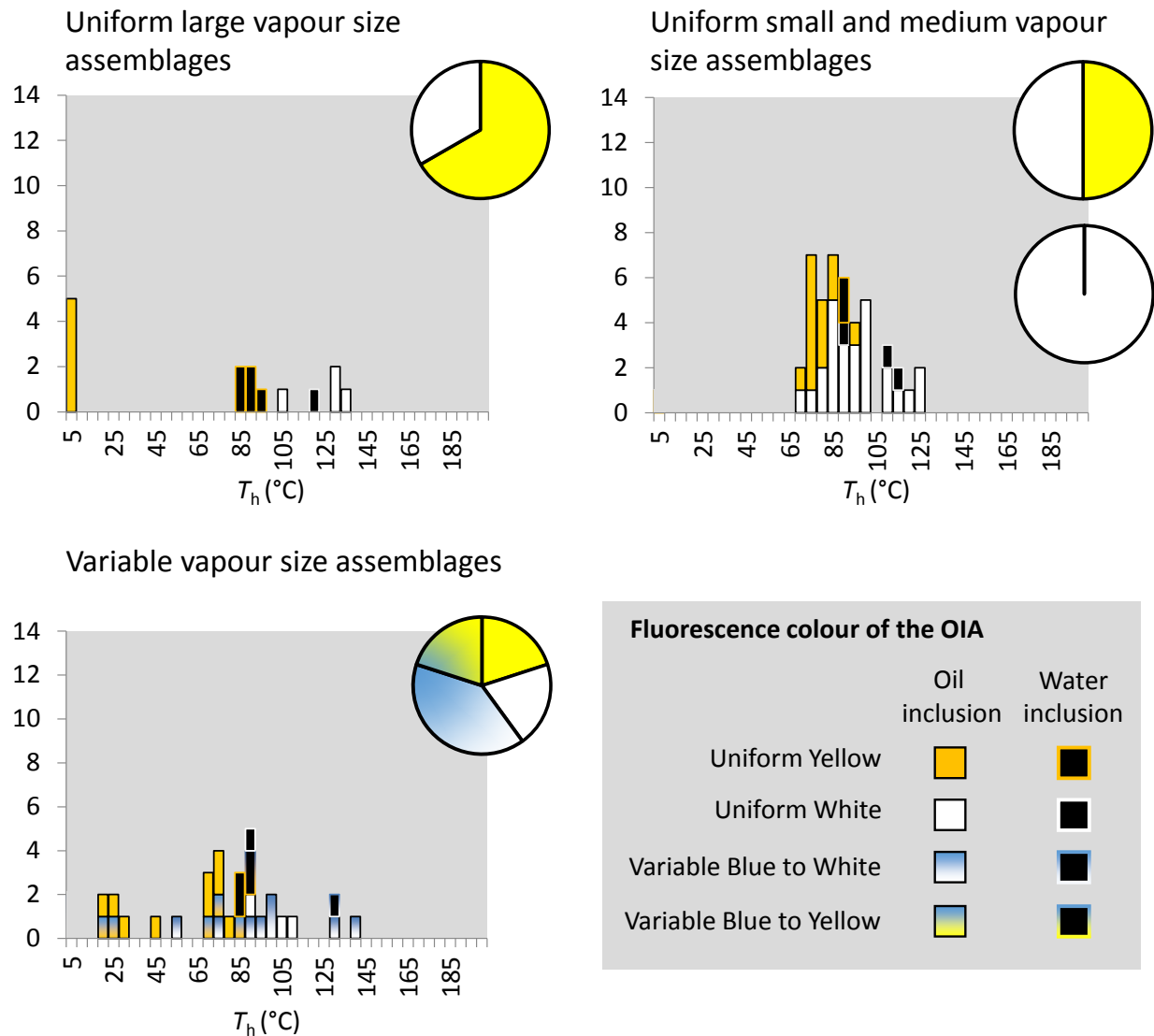


Figure 85: Homogenisation temperatures of petroleum and associated water inclusion assemblages from 2505-10 mMD in Duntroon-1.

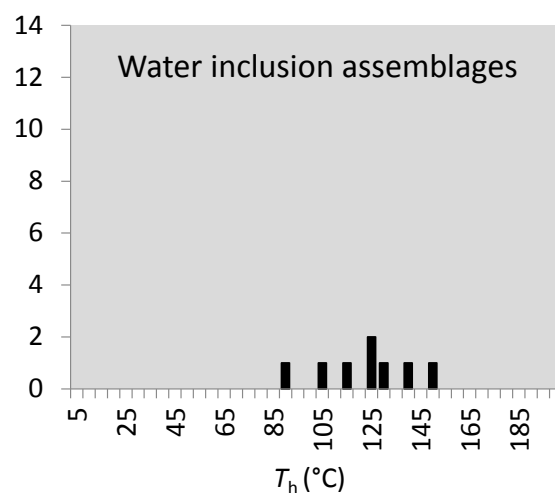


Figure 86: Homogenisation temperatures of water inclusions from 2505-10 mMD in Duntroon-1.

Table 23: Duntroon-1 thermometric results.

OIA	Vapor-size variability	Fluo. variability	Location	FI No	Inclusion type at 20°C	Fluo. Colour	vapor size at 20°C	T _h (°C)	Phase transition	T _m (°C)	T _m -derived salinity CH ₄ -H ₂ O-NaCl (ppm)
1	Variable None-small	Uniform Yellow	FTQG	1	L _{oil}	Y	None	20.8	L _{oil} -V → L _{oil}	1.8*	
				2	L _{oil}	Y	None	19.3	L _{oil} -V → L _{oil}		
				3	L _{oil} -L _w -V	Y	S	69.5	L _w -L _{oil} -V → L _w -L _{oil}		
				4	L _{oil} -L _w -V	Y	S	71.4	L _w -L _{oil} -V → L _w -L _{oil}		
				5	L _w -V	None	S	84.8	L _w -V → L _w		
				6	L _{oil} -L _w -V	Y	S	70.3	L _w -L _{oil} -V → L _w -L _{oil}		
				7	L _{oil}	Y	S	27	L _{oil} -V → L _{oil}		
				8	L _{oil} -V	Y	S	44	L _{oil} -V → L _{oil}		
				9	L _{oil} -V	Y	S	68.7	L _{oil} -V → L _{oil}		
				10	L _{oil} -L _w -V	Y	S	78.3	L _w -L _{oil} -V → L _w -L _{oil}	1.2*	
				11	L _w -V	None	S	81	L _w -V → L _w	1.2*	
2	Variable Medium-large	Variable Blue to White	FTQG	12	L _{oil} -V	W	M	136	L _{oil} -V → L _{oil}		
				13	L _{oil} -V	W	L	128	L _{oil} -V → V		
				14	L _w -V	None	L		L _w -V → L _w		
3	Uniform Large	Uniform White	FTQG	15	L _{oil} -V	W	L	125.5	L _{oil} -V → L _{oil}		
				16	L _{oil} -V	W	L	128	L _{oil} -V → L _{oil}		
				17	L _{oil} -V	W	L	135	L _{oil} -V → L _{oil}		
				18	L _w -V	None	S	119.6	L _w -V → L _w		
				19	L _{oil} -V	W	L	104	L _{oil} -V → L _{oil}		
4	Uniform Small	Uniform White	FTQG	20	L _{oil} -V	W	S	87	L _{oil} -V → L _{oil}		
				21	L _{oil} -L _w -V	W	S	118	L _w -L _{oil} -V → L _w -L _{oil}		
				23	L _{oil} -V	W	S	82	L _{oil} -V → L _{oil}		
				24	L _{oil} -V	W	S	82	L _{oil} -V → L _{oil}		
				25	L _{oil} -V	W	S	83.5	L _{oil} -V → L _{oil}		
				26	L _{oil} -V	W	S	82.3	L _{oil} -V → L _{oil}		
				27	L _w -V	None	S	110*	L _w -V → L _w		
				28	L _{oil} -V	W	S	66	L _{oil} -V → L _{oil}		
5	Uniform Small	Uniform Yellow	FTQG	29	L _w -V	None	S	92.2	L _w -V → L _w	0.8*	
				29 _{gas}	V	None	L				
				30	L _w -V	None	S	83	L _w -V → L _w		
6	Uniform Medium	Uniform White	QOB	31	L _{oil} -V	W	M	89.9	L _{oil} -V → L _{oil}		
				32	L _{oil} -V	W	M	123.9	L _{oil} -V → L _{oil}		
				33	L _{oil} -V	W	M	93.8	L _{oil} -V → L _{oil}		
				34	L _{oil} -V	W	M	121.7	L _{oil} -V → L _{oil}		
				35	L _w -V	None	S	88.9	L _w -V → L _w		
				36	L _{oil} -V	W	M	110.4	L _{oil} -V → L _{oil}		

OIA	Vapor-size variability	Fluo. variability	Location	FI No	Inclusion type at 20°C	Fluo. Colour	vapor size at 20°C	T _h (°C)	Phase transition	T _m (°C)	T _m -derived salinity CH ₄ -H ₂ O-NaCl (ppm)
7	Uniform Large	Uniform Yellow	FTQG	37	L _{oil} -V	Y	L	-75	L _{oil} -V → V	22	
				38	L _w -V	None	S	87	L _w -V → L _w		
				39	L _w -V	None	S	87	L _w -V → L _w		
				40	L _w -V	None	S	83	L _w -V → L _w		
				41	L _{oil} -V	Y	L		L _{oil} -V → V		
				42	L _{oil} -V	Y	L	-60	L _{oil} -V → V		
				43	L _{oil} -V	Y	L	-55	L _{oil} -V → V		
8	Variable Small-Medium	Uniform White	FTQG	44	L _{oil} -V	Y	L	-54	L _{oil} -V → V	1.8*	
				45	L _w -V	None	S	86.7	L _w -V → L _w		
				46	L _{oil} -V	W	S	86.4	L _{oil} -V → L _{oil}		
				47	L _{oil} -V	W	M	107	L _{oil} -V → L _{oil}		
9	Uniform Small	Uniform Yellow	FTQG	48	L _{oil} -V	W	M	102	L _{oil} -V → L _{oil}	1.6*	
				49	S _B -L _{oil} -V	Y	S	71	L _{oil} -V → L _{oil}		
				50	S _B -L _{oil} -V	Y	S	71.8	L _{oil} -V → L _{oil}		
				51	S _B -L _{oil} -V	Y	S	73.5	L _{oil} -V → L _{oil}		
				52	L _w -V	None	S	86	L _w -V → L _w		
				53	S _B -L _{oil} -V	Y	S	71.7	L _{oil} -V → L _{oil}		
				54	S _B -L _{oil} -V	Y	S	75.1	L _{oil} -V → L _{oil}		
				55	S _B -L _{oil} -V	Y	S	70.9	L _{oil} -V → L _{oil}		
10	Variable Small-Medium	Variable Blue to White	FTQG	56	S _B -L _{oil} -V	Y	S	70.6	L _{oil} -V → L _{oil}	1.2* 2*	
				57	S _B -L _{oil} -V	Y	S	69.7	L _{oil} -V → L _{oil}		
				58	L _{oil} -V	W	S	75	L _{oil} -V → L _{oil}		
				59	L _{oil} -V	W	M	95.9	L _{oil} -V → L _{oil}		
				60	L _{oil} -V	W	S	51	L _{oil} -V → L _{oil}		
				61	L _{oil} -V	W	M	92	L _{oil} -V → L _{oil}		
				62	L _{oil} -V	W	M	96	L _{oil} -V → L _{oil}		
11	Uniform Small	Uniform White	FTQG	63	L _w -V	None	S	126	L _w -V → L _w		
				64	L _w -V	None	S		L _w -V → L _w		
				65	L _{oil} -V	W	S	86	L _{oil} -V → L _{oil}		
				66	L _{oil} -V	W	S	95.7	L _{oil} -V → L _{oil}		
				67	L _{oil} -V	W	S	108.1	L _{oil} -V → L _{oil}		
				68	L _{oil} -V	W	S	95.1	L _{oil} -V → L _{oil}		
				69	L _{oil} -V	W	S	92.5	L _{oil} -V → L _{oil}		
				70	L _{oil} -V	W	S	95.5	L _{oil} -V → L _{oil}		

OIA	Vapor-size variability	Fluo. variability	Location	FI No	Inclusion type at 20°C	Fluo. Colour	vapor size at 20°C	T _h (°C)	Phase transition	T _m (°C)	T _m -derived salinity H ₂ O-NaCl or CH ₄ -H ₂ O-NaCl (ppm)
12	Uniform Small	Uniform Yellow	FTQG	71	L _{oil} -L _w -V	Y	S	82	L _w -L _{oil} -V → L _w -L _{oil}	1* 2*	
				72	L _{oil} -V	Y	S	78.3	L _{oil} -V → L _{oil}		
				73	L _{oil} -V	Y	S	91	L _{oil} -V → L _{oil}		
				74	L _{oil} -L _w -V	Y	S	76.1	L _w -L _{oil} -V → L _w -L _{oil}		
				75	L _w -V	None	S	90	L _w -V → L _w		
				76	L _w -V	None	S		L _w -V → L _w		
				77	L _{oil} -V	Y	S	81.2	L _{oil} -V → L _{oil}		
13	Variable Small-Large	Variable Blue to Yellow	FTQG	78	L _{oil} -L _w -V	Y	S	68.4	L _w -L _{oil} -V → L _w -L _{oil}		
				79	L _w -V	None	S	88	L _w -V → L _w		
				80	L _{oil} -V	B	S	19	L _{oil} -V → L _{oil}		
				81	L _{oil} -V	B	M	23	L _{oil} -V → L _{oil}		
				82	L _w -V	None	S	88.5	L _w -V → L _w		
				83	L _{oil} -V	B	L	85	L _{oil} -V → L _{oil}		
				84	L _{oil} -V	B	L	75	L _{oil} -V → L _{oil}		
14	Uniform Medium	Uniform White	FTQG	85	L _{oil} -V	W	M	92.2	L _{oil} -V → L _{oil}	3.2*	
				86	L _{oil} -L _w -V	W	M	105.8	L _{oil} -V → L _{oil}		
				87	L _{oil} -V	W	M	96.2	L _{oil} -V → L _{oil}		
				88	L _{oil} -V	W	M	96.3	L _{oil} -V → L _{oil}		
				89	L _{oil} -V	W	M	74	L _{oil} -V → L _{oil}		
				90	L _{oil} -V	W	M	88.4	L _{oil} -V → L _{oil}		
				91	L _{oil} -V	W	M	75.3	L _{oil} -V → L _{oil}		
				92	L _w -V	None	S	114	L _w -V → L _w		
				92bis	L _w -V	None	S		L _w -V → L _w		
				93	L _{oil} -V	W	M	79	L _{oil} -V → L _{oil}		
WIA	Uniform Small	None	QOB	95	L _w -V	None	S	123	L _w -V → L _w	-1.5	29993
			WQO	96	L _w -V	None	S	138	L _w -V → L _w	-1.5	26001
			QOB	97	L _w -V	None	S	87.5	L _w -V → L _w	1.3*	
			QOB	98	L _w -V	None	S	148	L _w -V → L _w	-1.5	29993
			QOB	99	L _w -V	None	S	124.6	L _w -V → L _w	-1.7	33237
			QOB	100	L _w -V	None	S	128.7	L _w -V → L _w	-1.8	34847
			QOB	101	L _w -V	None	S	104.7	L _w -V → L _w	0.7*	
			QOB	102	L _w -V	None	S	115	L _w -V → L _w	-1.0	17824

(* temperature not cycled)

Table 24: Duntroon-1 Raman-derived pressure and fluid compositions.

OIAs	Inclusion No	Inclusion type at room temp.	Bubble size	T _h (°C)	Salinity eq. NaCl (wt%)	CH ₄ Raman peak position (cm ⁻¹)	[CH ₄]m (mol/kg)	[CH ₄]m (ppm)	P _h (bar)	P vap (bar)	Vapour CO ₂ (mol%)	Vapour CH ₄ (mol%)	Vapour N ₂ (mol%)	Vapour C ₂ H ₆ (mol%)	Vapour C ₃ H ₈ (mol%)
1	5	Lw-V	S	84.8		2913.21			353	236					
	11	Lw-V	S	81		2916.37	0.143	2293	327	74					
3	18	Lw-V	S	119.				2042							
4		Lw-V	S	110		2916.49	0.159	2542	332	55					
	29	Lw-V	S	92.2		2917.04	0.108	1737	203	44					
5	29gas bis	V	L			2914.56			255	170					
	29gas	V	L			2913.56			255	170	3	96		3	
	30	Lw-V	S	83											
6	35	Lw-V	S	88.9		2916.77	0.124	1992	253	54					
	37	Loil-V	L	-75		2914.03			354	250	6	61	26	6	1
	38	Lw-V	S	87		2917.22	0.063	1014	100	26					
	39	Lw-V	S	87		2917.41	0.034	550	49	14					
	40	Lw-V	S	83											
7	41	Lw-Loil-V	L												
	42	Loil-V	L	-60		2912.98			358	246					
	43	Loil-V	L	-55											
	44	Loil-V	L	-54		2912.82				267					
	45	Lw-V	S	86.7		2916.87	0.105	1679	196	45					
9	52	Lw-V	S	86		2916.62	0.126	2015	259	57					
10	63	Lw-V	S	126											
	64	Lw-V	S												
12	75	Lw-V	S	90		2916.96	0.129	2059	265	54					
	76	Lw-V	S												
13	79	Lw-V	S	88											
	82	Lw-V	S	88.5											
	86	Loil-Lw-V	M	105.		2914.76				164	27	32	33		
14	92	Lw-V	S	114		2917.33	0.141	2263	268	46					
	92bis	Lw-V	S			2915.94					69	7	25		
	95	Lw-V	S	123	25727	2918.06	0.044	704	61	12					
	96	Lw-V	S	138	21768	2917.7	0.126	2010	188	31					
	97	Lw-V	S	87.5		2917.07	0.092	1468	161	38					
	98	Lw-V	S	148	29993	2917.65	0.078	1243	99	17					
	99	Lw-V	S	124.	29014	2917.46	0.069	1111	101	19					
	100	Lw-V	S	128.	30645										
	101	Lw-V	S	104.		2917.32	0.095	1525	162	33					
	102	Lw-V	S	115	13513	2916.91	0.146	2336	262	45	4	96			

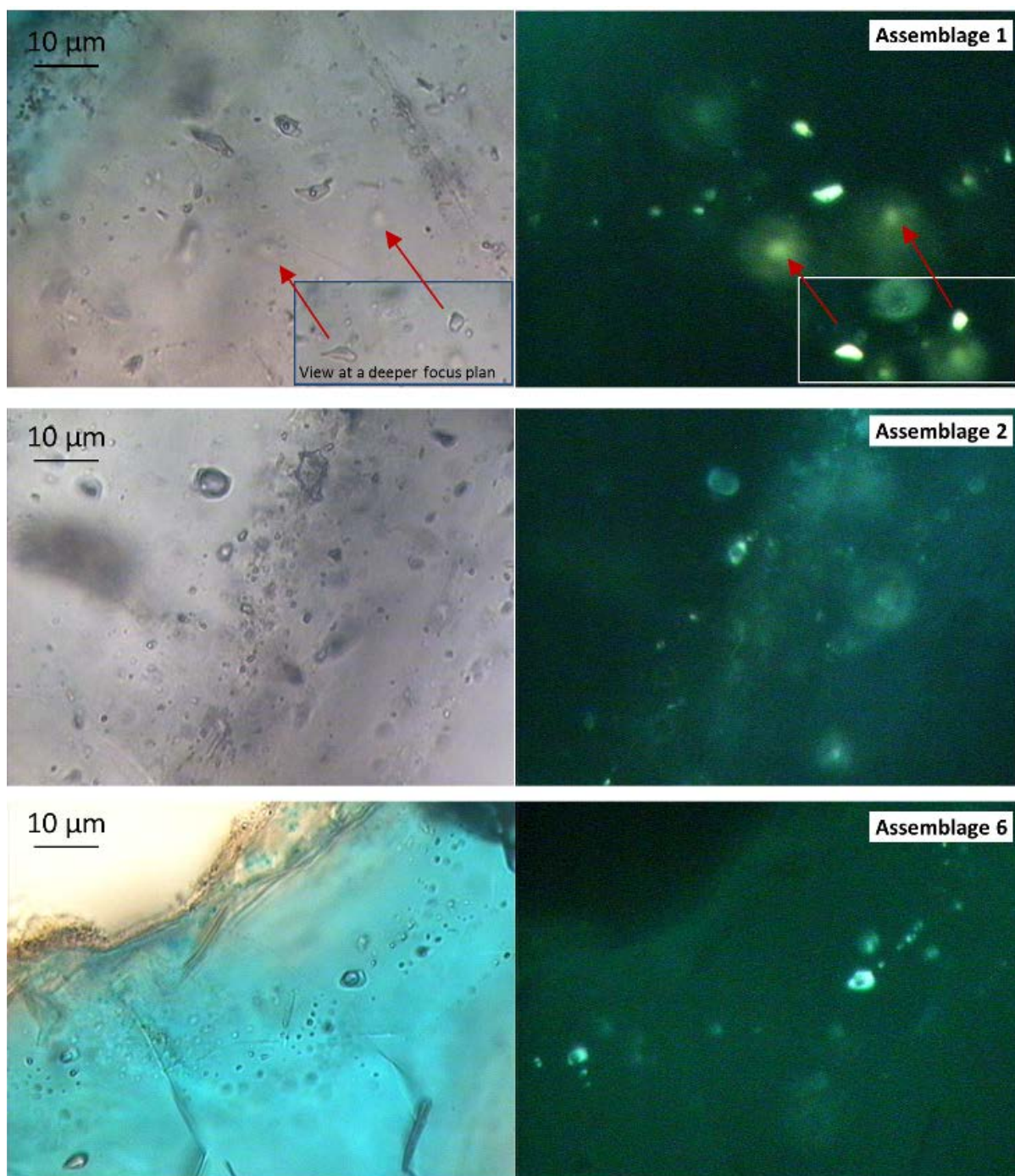


Figure 87: Paired transmitted light and UV photomicrographs of Duntroon-1 oil inclusion assemblages 1, 2, 6.

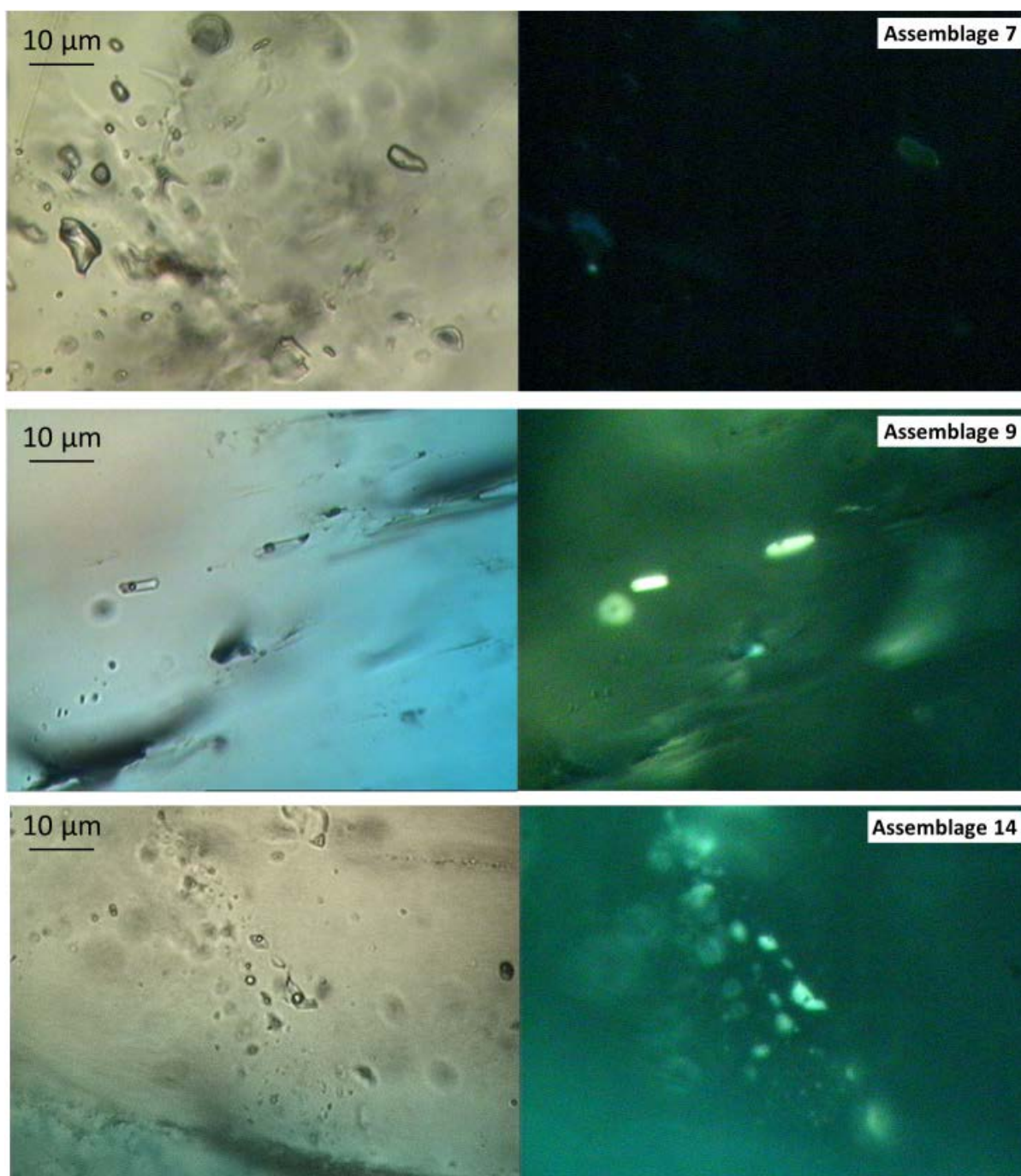


Figure 88: Paired transmitted light and UV photomicrographs of Duntroon-1 oil inclusion assemblages 2, 4, 8.

PVT analysis

Phase envelopes and isochores for both oil and associated water inclusions, that are used to derive entrapment pressures and temperatures, are shown in Appendix 11. Raman spectroscopy on water and gas inclusions and *PVTx* modelling using PIT software on oil inclusions provide composition data shown in Table 24 and Table 25.

OIAs with uniform small and medium vapour bubbles

Oil inclusions from assemblage 9 have uniform yellow fluorescence and small vapour size. The vapour volume was estimated for inclusion 50b at between 4.7 and 6.4 %. PIT modelling gives a range of compatible compositions consistent with black oil. Methane was detected in the associated water inclusions but the resulting isochores do not cross the oil inclusion isochores (Appendix 11). As a minimum *PT* constraint, the bubble point pressure of water inclusion 52 from OIA 9, modelled directly from the $\text{H}_2\text{O}-\text{CH}_4$ -salt system, is 259 bars at a T_h of 86°C.

Assemblage 6 comprises uniform white fluorescent oil inclusions with uniform medium sized vapour bubbles, and T_h values of between 89.9 and 123.9°C. The PIT compositions are compatible with light oil. The one water inclusion in the same assemblage has a T_h of 88.9°C, contains dissolved methane and its modelled bubble point curve reaches 253 bar at homogenisation temperature. The proximity in the *PT* diagram of the oil and water bubble point curves, as well as the similar minimum T_h values are indicative of gas saturation in both the oil and the water inclusions. While the oil and water inclusion isochores do not cross, they can be reasonably interpreted as indicative of entrapment at *PT* in the range 85-90°C and 240-255 bars and at gas saturation. The higher T_h recorded in some oil inclusions may have been generated by two-phase trapping and do not necessarily reflect the *PT* conditions at which trapping occurred.

Oil inclusions from assemblage 14 have uniform white fluorescence and medium vapour size, estimated between 14.8 to 22.9 %. The PIT compositions are compatible with light oil. Nitrogen and CO_2 was also detected, along with methane, in the vapour phase of the oil inclusions. Methane was also detected in the associated water inclusion. Some oil inclusion isochores cross the bubble point curve of water close to the measured T_h of 114°C, giving a minimum estimate for the pressure of 268 bar. Other oil inclusion isochore cross the water isochore at slightly higher temperatures but at pressures up to around 320 bars.

OIAs with variably sized vapour bubbles

Assemblage 1, with uniform yellow fluorescent monophase and two-phase (small bubble) oil inclusions, has a wide spread of T_h . The lowest T_h of 20.8°C, from inclusion 1, has a vapour volume fraction of 8.1% at 6°C and PIT compatible compositions that match black oil. Several additional isochores, corresponding to more elevated T_h values in this assemblage, were calculated using this same composition and are shown as dashed lines in Appendix 11. Methane was detected in aqueous inclusion 11 from this assemblage and, as a minimum *PT* constraint, the bubble point pressure, modelled directly from the $\text{H}_2\text{O}-\text{CH}_4$ -salt system, is 320 bars at a T_h of 81°C. The water inclusion isochore crosses the oil inclusion isochores at various other locations on the *PT* diagram up to 90°C and 540 bar.

Assemblage 8 comprises uniformly white fluorescing oil inclusions with variably medium to small vapour bubbles. Inclusion 48 from this assemblage has a vapour fraction of 22.3% and a T_h of 102°C that is compatible with light oil. The minimum oil inclusion isochore (inclusion 46) did not yield a

vapour fraction for PIT modelling, however has been used here for *PT* constraints assuming the same composition as inclusion 48 (Table 25). Water inclusion 45, in the same assemblage, contains dissolved methane and its isochore crosses the oil inclusion isochore at about 87°C and 205-220 bars (Appendix 11).

Table 25: Duntroon-1 oil inclusion compositions calculated using PIT.

OIA	Inc	φ_{vap} (20°C)	T_h (°C)	Alpha	Beta	C ₁	C ₂	C ₃	iC ₄	nC ₄	iC ₅	nC ₅	nC ₆	C ₇₊
1	1	1.1	20.8	0.929	0.429	27.7	4.9	5.3	1.2	2.8	1.9	3.1	4.0	49.0
3	16	26	128	0.874	0.520	47.4	8.8	6.8	1.4	3.1	1.9	3.1	3.4	24.0
	16	26	128	0.891	0.570	50.2	8.7	6.4	1.3	2.9	1.8	2.8	2.9	23.1
	16	26	128	0.864	0.490	45.8	8.9	7.0	1.5	3.3	2.0	3.3	3.7	24.5
	19	6.8	104	0.932	0.350	21.0	3.7	4.6	1.2	2.6	1.9	3.0	4.4	57.6
	19	8.9	104	0.917	0.390	27.1	5.1	5.6	1.3	3.0	2.1	3.4	4.4	47.9
	19	8.9	104	0.926	0.450	30.4	5.4	5.5	1.3	2.8	2.0	3.1	3.9	45.5
6	31	19.4	89.9	0.873	0.543	50.0	9.0	6.7	1.3	3.0	1.8	3.0	3.2	22.0
	31	24.2	89.9	0.858	0.557	53.7	9.4	6.7	1.3	2.9	1.7	2.8	3.0	18.5
	34	19.3	121.7	0.894	0.510	42.9	8.0	6.6	1.4	3.1	2.0	3.2	3.5	29.3
	34	23.8	121.7	0.876	0.520	46.6	8.7	6.8	1.4	3.1	2.0	3.2	3.4	24.7
8	48	22.6	102	0.867	0.530	49.6	9.1	6.8	1.4	3.1	1.9	3.0	3.3	21.9
	48	22.6	102	0.859	0.510	48.6	9.2	7.0	1.4	3.2	2.0	3.1	3.5	22.1
9	50b	4.7	71.8	0.926	0.390	25.2	4.6	5.2	1.2	2.8	2.0	3.2	4.3	51.5
	50b	6.4	71.8	0.902	0.390	30.1	6.0	6.2	1.4	3.2	2.3	3.6	4.6	42.5
14	85	15.2	92.2	0.887	0.512	44.5	8.3	6.7	1.4	3.1	2.0	3.2	3.5	27.3
	85	21	92.2	0.871	0.550	51.0	9.1	6.7	1.3	3.0	1.8	2.9	3.1	21.1
	87	14.8	96.2	0.894	0.513	43.3	8.0	6.6	1.4	3.1	2.0	3.2	3.5	28.9
	87	20.5	96.2	0.875	0.542	49.6	9.0	6.7	1.3	3.0	1.9	3.0	3.2	22.4
	90	9.2	88.2	0.910	0.460	34.8	6.6	6.2	1.4	3.1	2.1	3.3	3.9	38.6
	90	22.9	88.2	0.859	0.550	52.9	9.4	6.7	1.3	3.0	1.8	2.8	3.0	19.0

OIAs with uniformly large vapour bubbles

Assemblage 3 has uniform white fluorescent oil trapped in two-phase inclusions with large vapour bubbles. The PIT composition matching the vapour volume fraction and T_h values correspond to light oil. Due to bubble movement in the associated water inclusion, methane was quantified at homogenisation and two sets of isopleths-isochores were calculated based on an upper and lower concentration. The *PT* conditions compatible with the trapping of these fluids, by crossing of isochores, are in the range 119.6-125°C and 200-260 bar.

Assemblage 5 comprises gas and water inclusions, with the minor liquid oil component in the gas having yellow fluorescence. The Raman spectra measured in gas inclusion 29bis indicates a composition of CH₄ (84 mol%), C₂H₆ (13 mol%) and CO₂ (3 mol%) with the presence of other heavier hydrocarbons that could not be quantified. The pressure, at room temperature, was derived from the methane peak shift using the closest experimental data of Brunsgaard et al. (2001) for the

mixture $\text{CH}_4\text{-C}_2\text{H}_6$ (85-15 mol%). The density and pressure at 92.2°C, corresponding to the measured T_h of water inclusion 29, was derived using the pure methane system to draw the petroleum isochore of inclusion 29bis. The isochores of these water and gas inclusions cross at 95°C and 255 bar, which corresponds to the current *PT* conditions in the well at this depth.

Assemblage 7 contains gas inclusions that enclose some minor low intensity yellow fluorescence oil (Figure 88). It is not clear if this yellow fluorescence correspond to an oil rim or a low intensity fluorescence from the whole inclusion. The gas inclusions nucleate a vapour phase at low temperature (between -70 to -100°C) that homogenise between -75 and -54°C. Good quality Raman spectra indicated the presence of CH_4 (61 mol%), N_2 (26 mol%), C_2H_6 (6 mol%), CO_2 (6 mol%) and C_3H_8 (1 mol%) in inclusion 37. High fluorescence background in the other gas inclusions prevented the detection of gases other than methane. Methane was detected in the water inclusions from the same assemblage and their T_h are 83 and 87° C. The pressure, at room temperature, of gas inclusion 37 was calculated using the Raman peak position of methane for the gas system $\text{CH}_4\text{-N}_2$ (Seitz et al., 1993) and deriving a density and a pressure at 83°C using the equation of state of Thiéry et al. (1994). The crossing of the gas and water inclusion isochores constrains the *PT* conditions to 95°C and 365 bars.

Summary of *PT* Trapping Conditions

A range of hydrocarbon fluid compositions were modelled by PIT as black oil and light oil (oil rim in gas-rich inclusion (OIA 2) indicates the presence of gas condensate) and Raman spectroscopy specified a range of gas compositions. The *PT* trapping conditions are variable, with temperatures above 81°C and pressures in excess of 200 bar (Table 26; Figure 89).

The modelled *PT* conditions do not conform, in the main, to the independently modelled *PT* curve supplied by BP and only a few assemblages lie on or close to the *PT* curve. OIAs 1, 5, 6, 7, 8 and 9 all fall in a temperature range close to that of current day for this depth interval in Duntroon-1. Of these, OIAs 5, 6 and 9 are consistent with close to current-day pressures and therefore plot close to the *PT* curve.

The BP *PT* curve is well calibrated from vitrinite reflectance data and the non-conformance of modelled *PT* conditions to this independent curve may indicate transient episodes of; (1) hotter fluids (>114°C) in disequilibrium with the rock (OIAs 3 and 14) or, (2) overpressure (OIAs 1 and 7). While overpressure is suggested in OIAs 1 and 7, those approaching 540 bar in OIA 1 are unlikely and the water inclusion minimum pressure constraint of 81°C and 320 bar from the $\text{H}_2\text{O-CH}_4\text{-salt}$ system is a minimum.

Table 26: Summary of PT entrapment conditions in Duntroon-1.

Assemblage	Temperature (°C)	Pressure (bar)	Composition
1	81 (min up to 90)	320 (min up to 540)	Black oil
3	119.6-125	200-260	Light oil
5	95	255	Gas and water (+CO ₂)
6	85-90	240-255	Light oil
7	95	365	Gas (oil) and water (+CO ₂ , N ₂)
8	87	205-220	Light oil
9	86 (min)	259 (min)	Black oil
14	114 (min)	268 (min up to 320)	Light oil (+CO ₂ , N ₂)

Min = minimum PT estimation only.

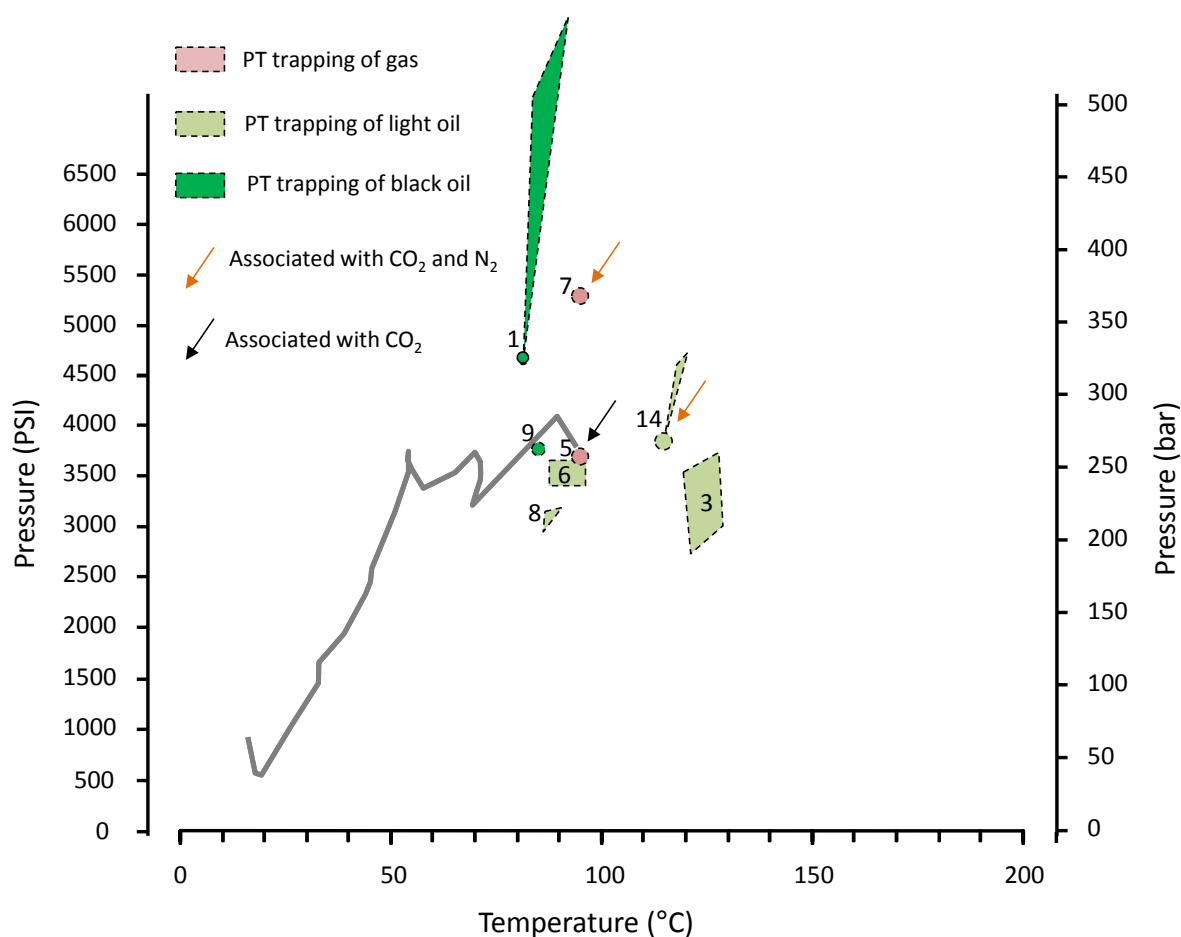


Figure 89: Trapping conditions at 2505-10 mMD in Duntroon-1 derived from PVTx modelling of gas, oil and water fluid inclusion assemblages.

Grey line is the estimated PT curve at the sample depth provided by BP (extracted from 3D burial history model).

Potoroo-1 (2505-10 mMD)

A silt-rich cutting sample of Upper Cretaceous (Cenomanian-Santonian) Tiger Supersequence at 1,778-1,786 mMD in Potoroo 1, central Ceduna Sub-basin, was investigated for detailed PVTx analysis of the hydrocarbon fluid inclusions trapped in quartz.

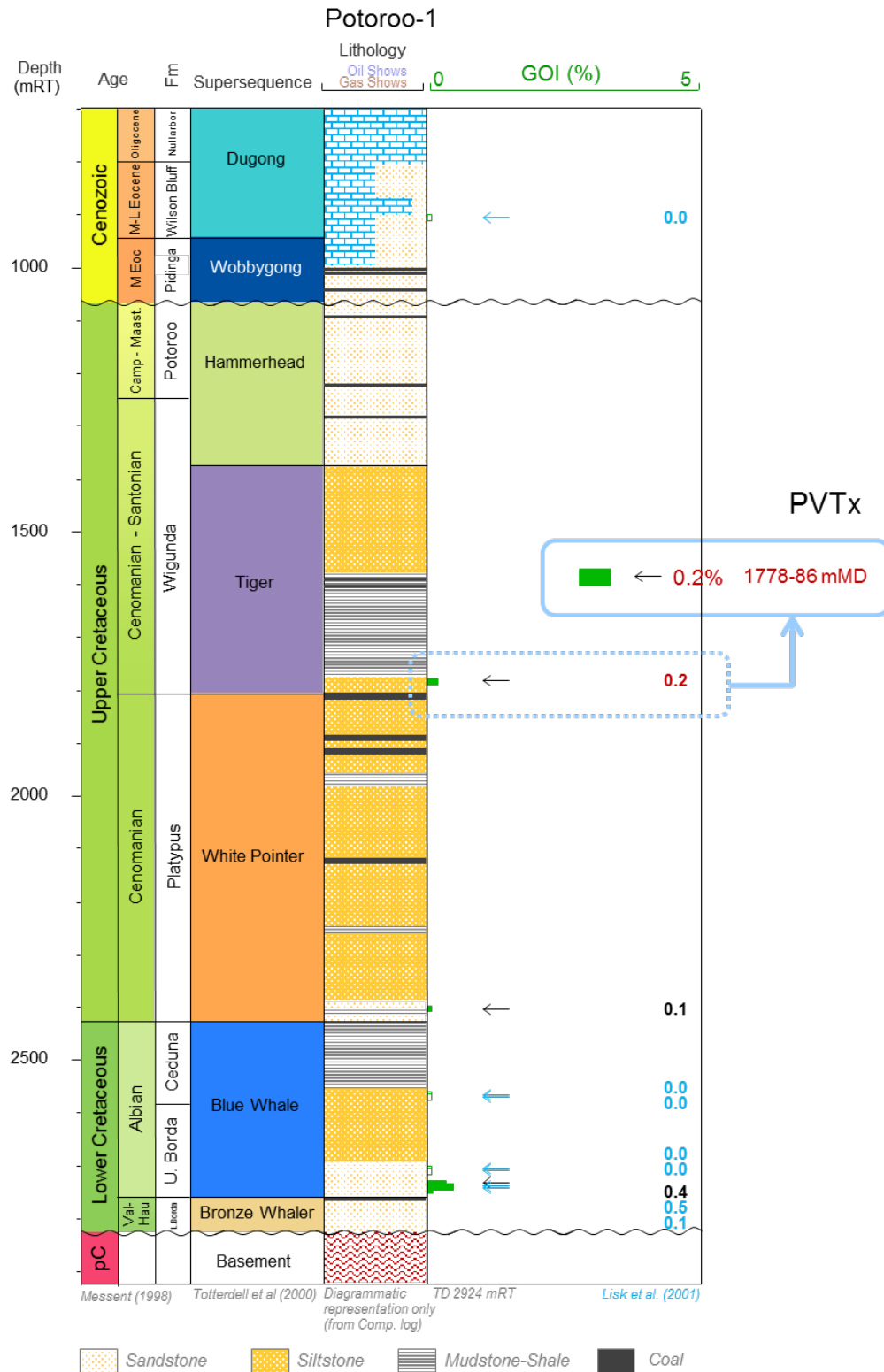


Figure 90: GOI log for Potoroo-1 showing location of sample for PVT analysis.

Fluid Inclusion Assemblage Descriptions

At Potoroo 1, petroleum inclusion assemblages (oil, gas and water) were investigated in 15 different grains (Table 27). One additional grain was examined for water inclusion assemblage in quartz cement.

At room temperature, the petroleum inclusions observed were dominantly 2-phase, comprising a volumetrically dominant liquid oil phase and a small to medium-size vapour phase ($L_{oil}-V$). Other types of fluid inclusion assemblages include:

- 2-phase inclusions ($L_{oil}-V$) comprising a volumetrically large vapour/gas bubble and liquid oil;
- 3-phase inclusions ($L_w-L_{oil}-V$) comprising liquid water, liquid oil and a small to medium-size vapour bubble. The bubble is systematically contained in the oil phase.
- 3-phase inclusions ($S_B-L_{oil}-V$) comprising a solid bitumen, liquid oil and a vapour bubble. The bubble is systematically contained in the oil phase.

The assemblages are classified based on the uniformity or variability of the vapour phase (i.e. size of the bubble) in the inclusions populating the assemblages (Figure 91). The assemblages were also described as having uniform or variable fluorescence colours under UV-illumination. Assemblages with uniform white, uniform yellow and variable blue to yellow fluorescence were encountered in the grains from Potoroo-1.

Only one OIA has uniformly small vapour bubbles (OIA 12) and the oil has uniform yellow fluorescence. Two assemblages have uniformly large vapour bubbles, both associated with white fluorescing oil (OIAs 6 and 14).

Most of the OIAs have variability in the size of the vapour phase and are dominated by uniformly white fluorescent oil. The variability in the vapour phase includes small to medium (OIAs 1, 3, 4, 9 and 11), small to large (OIA 8), medium to large (OIAs 5 and 7) bubble sizes. Two assemblages have variably small to medium vapour bubbles associated with yellow fluorescence (OIAs 2 and 10) and one assemblage has variably small to large vapour bubbles with blue to yellow fluorescent oil (OIAs 15).

One assemblage with variably sized vapour bubbles (OIA 9) also includes monophasic inclusions. Some of the oil inclusions in this assemblage also enclose a small amount of solid bitumen.

The water inclusions in Potoroo-1 were all 2-phase comprising a volumetrically dominant liquid water phase and a small vapour phase (L_w-V).

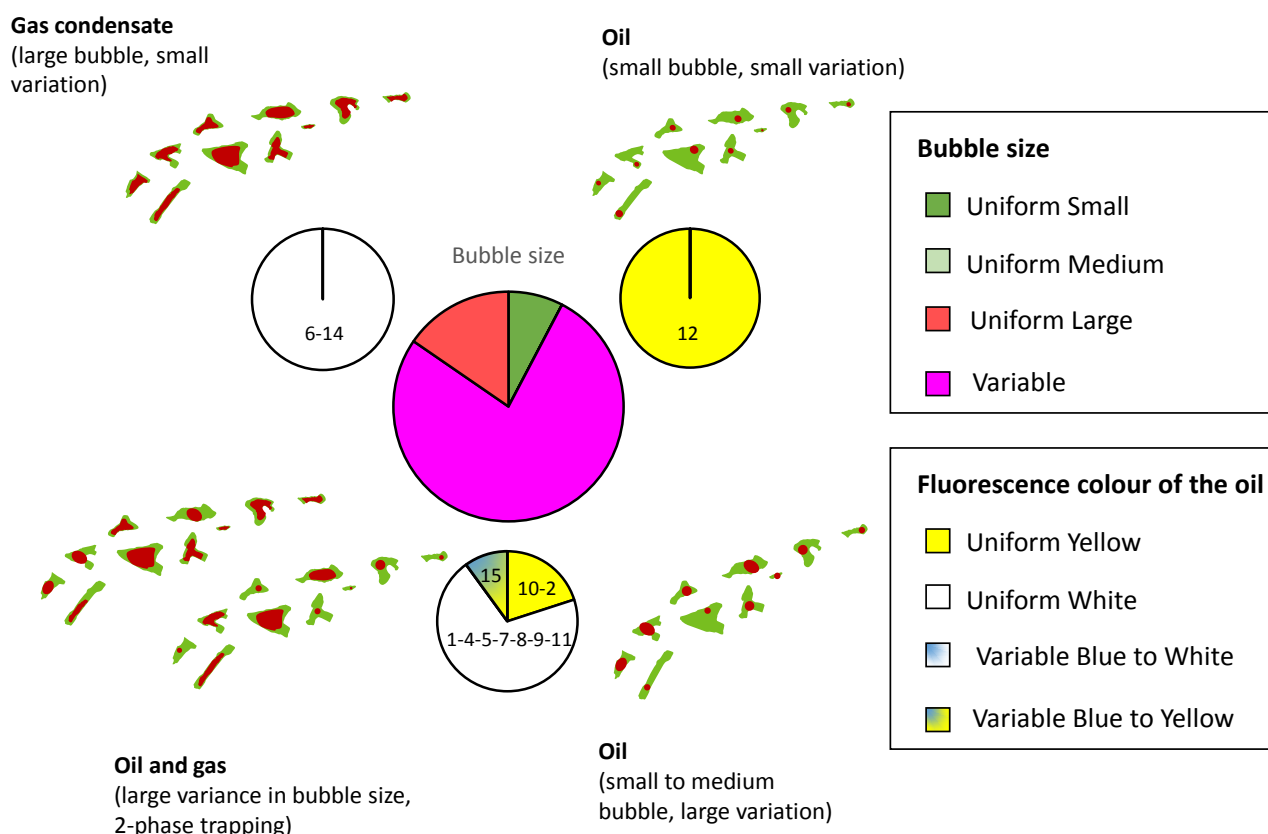


Figure 91: Petroleum fluid inclusion assemblages observed from 1778-86 mMD in Potoroo-1. Numbers within the pie charts refer to the assemblage numbers in Table 23.

Microthermometry

The T_h measured on hydrocarbon and associated aqueous inclusions are summarised in Table 27 and Figure 92. These assemblages are grouped into:

OIAs with uniformly small vapour bubbles

OIA 12 has uniformly small vapour bubbles, with uniform yellow fluorescent oil. The T_h of the oil inclusions are between 39.6 and 44°C, with homogenisation into the liquid phase. Water inclusion T_h could not be obtained.

OIAs with uniformly large vapour bubbles

OIAs 6 and 14 have uniformly large bubbles with white fluorescent oil. Only one gas inclusion in each OIA provided measurable T_h , of 45°C (OIA 6) and 75°C (OIAs 14), respectively. The vapour bubbles homogenise into the gas phase. Water inclusion T_h could not be obtained.

OIAs with variably sized vapour bubbles

The T_h for the OIAs with variably sized vapour bubbles show a wide spread in values:

- OIAs 2 and 10, with yellow fluorescent oil and small to medium vapour bubbles, have oil inclusion T_h values of 32.5 to 81°C, with homogenisation into the liquid phase. Water inclusion T_h could not be obtained for either OIA.

- White fluorescing oil inclusion assemblages with small to medium (OIAs 1, 3 and 11), medium to large (OIAs 4, 5 and 7) and small to large (OIAs 8) vapour bubbles have oil inclusion T_h values of 65 to more than 200°C, with homogenisation into the liquid phase. Water inclusion in associated assemblages have T_h values between 69 to 108.6°C.
- OIA 9 has uniform white fluorescent oil, with both monophasic and two-phase oil inclusions with small to medium vapour bubble at room temperature. The monophasic inclusions nucleate a bubble by lowering the temperature below 20°C. The T_h values of oil inclusions range from 6.5 to 77.5°C, with homogenisation into the liquid phase. Water inclusions in assemblage have T_h of 94 and 109°C.
- OIA 15, with variable Blue to Yellow fluorescent two-phase oil inclusions with small to large vapour bubbles, have T_h values ranging from 65.2 to 86.7°C, which homogenise into the liquid phase. The only water inclusion in this assemblage has a T_h of 88.3°C.

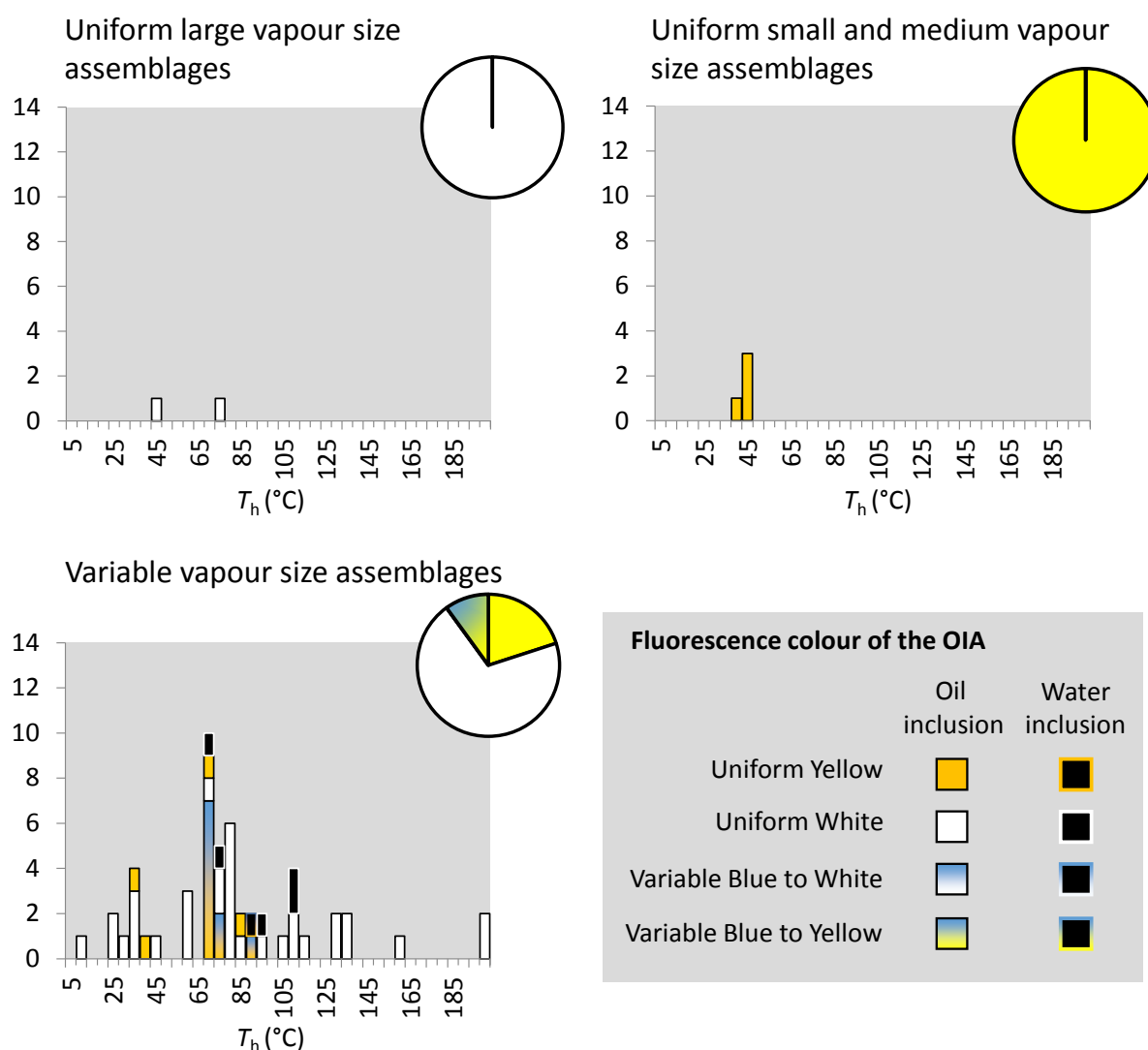


Figure 92 Homogenisation temperatures of petroleum and associated water inclusion assemblages from 1778-86mMD in Potoroo-1.

Water Inclusion Assemblages

Water inclusion assemblage 13, located at the quartz overgrowth boundary, had only one measurable T_h of 105°C (Table 27, Figure 93).

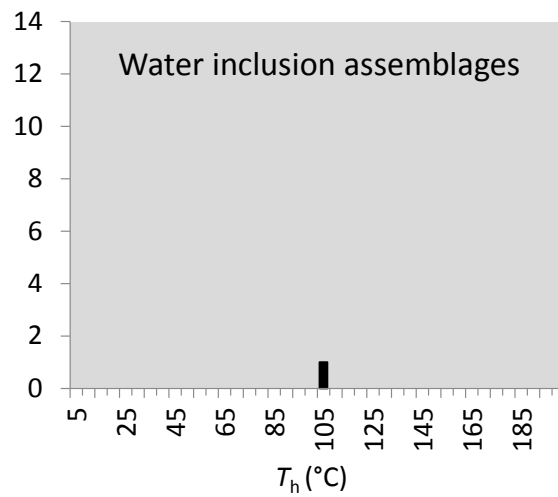


Figure 93: Homogenisation temperatures of water inclusions from 1778-86mMD in Potoroo-1.

Table 27: Potoroo-1 thermometric results.

OIA	Vapour-size variability	Fluo. variability	Location	FI No	Inclusion type at 20°C	Fluo. Colour	vapor size at 20°C	T _h (°C)	Phase transition	T _m (°C)	Raman-derived or T _m -derived salinity CH ₄ -H ₂ O-NaCl (ppm)
1	Variable Small to Medium	Uniform white	FTQG	1	Loil-V	W	S	93.6	Loil-V → Loil		
				2	Loil-V	W	S	103.5	Loil-V → Loil		
				3	Loil-V	W	M-L	126	Loil-V → Loil		
				4	Loil-V	W	M-L	129	Loil-V → Loil		
				5	Loil-V	W	S	77.8	Loil-V → Loil		
2	Variable Small to Medium	Uniform Yellow	FTQG	6	Loil-V	Y	S	35.4	Loil-V → Loil		
				7	Loil-V	Y	S	32.5	Loil-V → Loil		
				8	Loil-V	Y	S	81	Loil-V → Loil		
3	Variable Small to Medium	Uniform white	QOB	9	Lw-V	None	S	73.1	Lw-V → Lw	0.2*	38862
				10	Lw-V	None	S	69	Lw-V → Lw	2.2*	
4	Variable Small to Medium	Uniform White	FTQG	11	Lw-V	None	S	108.6	Lw-V → Lw	5*	
				12	Loil-Lw-V	W	M	84.3	Lw-Loil-V → Lw-Loil		
				13	Loil-V	W	M	200	Loil-V → V		
5	Variable Medium to Large	Uniform White	FTQG	14	Loil-V	W	M	65.6	Loil-V → Loil		
				15	Loil-V	W	M	79.5	Loil-V → Loil		
				17	Loil-V	W	M	79	Loil-V → Loil		
				18	Loil-V	W	M	75.7	Loil-V → Loil		
6	Uniform Large	Uniform White	FTQG	19	Loil-V	W	L	41.5	Loil-V → V		
7	Variable Medium to Large	Uniform White	FTQG	20	Loil-Lw-V	W	M	75.5	Loil-V → Loil		
				20bis	Loil-V	W	M-L	110	Loil-V → Loil		
				20ter	Loil-V	W	L	160	Loil-V → Loil		
8	Variable small to Large	Uniform White	FTQG	21	Loil-V	W	L	113	Loil-V → Loil		
9	Variable Small to Medium	Uniform White	FTQG	22	Loil-V	W	M	77.5	Loil-V → Loil		
				23	Loil-V	W	S	34.7	Loil-V → Loil		
				24	Loil-V	W	M-L	56.6	Loil-V → Loil		
				25	S _B -Loil-V	W	S	32.7	S _B -Loil-V → S _B -Loil		
				26	S _B -Loil-V	W	M	43.7	S _B -Loil-V → S _B -Loil		
				27	Loil-V	W	M	55.6	Loil-V → Loil		
				28	S _B -Loil-V	W	M	58.1	S _B -Loil-V → S _B -Loil		

OIA	Vapour-size variability	Fluo. variability	Location	FI No	Inclusion type at 20°C	Fluo. Colour	vapor size at 20°C	T _h (°C)	Phase transition	T _m (°C)	Raman-derived or T _m -derived salinity CH ₄ -H ₂ O-NaCl (ppm)
9	Variable Small to Medium	Uniform White	FTQG	29	S _B -Loil-V	W	S	23.7	S _B -Loil-V → S _B -Loil	2.3*	
				30	Loil-V	W	S	32.4	Loil-V → Loil		
				31	Loil-V	W	S	26.3	Loil-V → Loil		
				32	S _B -Loil-V	W	S	22.6	S _B -Loil-V → S _B -Loil		
				33	S _B -Loil-V	W	S	6.5	S _B -Loil-V → S _B -Loil		
				34	Lw-V	None	S	94	Lw-V → Lw		
10	Variable Small	Uniform	FTQG	35	Lw-V	None	S	109	Lw-V → Lw		
				36.0	Loil-V	Y	S	70	Loil-V → Loil		
11	Variable Small to Medium	Uniform White	FTQG	37	Loil-V	W	S	106.6	Loil-V → Loil		
				38	Loil-V	W	S	74	Loil-V → Loil		
				39	Loil-V	W	M-L	134	Loil-V → Loil		
				40	Loil-V	W	M-L	134.5	Loil-V → Loil		
				41	Loil-V	W	S	72.5	Loil-V → Loil		
				42	Loil-V	W	M-L	200	Loil-V → Loil		
12	Uniform Small	Uniform Yellow	FTQG	43	Loil-V	Y	S	44	Loil-V → Loil		
				44	Loil-V	Y	S	43	Loil-V → Loil		
				45	Loil-V	Y	S	39.6	Loil-V → Loil		
				46	Loil-V	Y	S	43	Loil-V → Loil		
WIA-13	Uniform small	None	QOB	47	Lw-V	None	S	105	Lw-V → Lw		
14	Uniform	Uniform	FTQG	48	Loil-V	W	L	75	Loil-V → V		
15	Variable Small to Large	Variable Blue to Yellow	FTQG	49	Loil-V	B	S	67.6	Loil-V → Loil	2.9*	
				50	Loil-V	B	S	65.2	Loil-V → Loil		
				51	Loil-V	B	S	68	Loil-V → Loil		
				52	Loil-V	B	S	68	Loil-V → Loil		
				53	Loil-V	Y	S	72.5	Loil-V → Loil		
				54	Lw-V	None	S	88.3	Lw-V → Lw		
				55	Loil-V	B	M	69.3	Loil-V → Loil		
				56	Loil-V	B	L	86.7	Loil-V → Loil		
				57	Loil-V	B	M	67.9	Loil-V → Loil		
				58	Loil-V	B	M	67.9	Loil-V → Loil		
				59	Loil-V	B	M	71.3	Loil-V → Loil		

(* temperature not cycled).

Table 28: Potoroo-1 Raman-derived pressure and fluid compositions.

OIA	Inc	Inclusion type at room temperature	Bubble size	T_h (°C)	Salinity eq. NaCl (wt%)	CH ₄ Raman peak position (cm ⁻¹)	[CH ₄]m (mol/kg)	[CH ₄]m (ppm)	P_h (bar)	P vap (bar)	Vapour CO ₂ (mol.%)	Vapour CH ₄ (mol.%)	Vapour N ₂ (mol.%)	Vapour C ₂ H ₆ (mol.%)	Vapour C ₃ H ₈ (mol.%)
3	9	Lw-V	S	73.1	38862	2916.63	0.095	1518	178	49	-	-	-	-	-

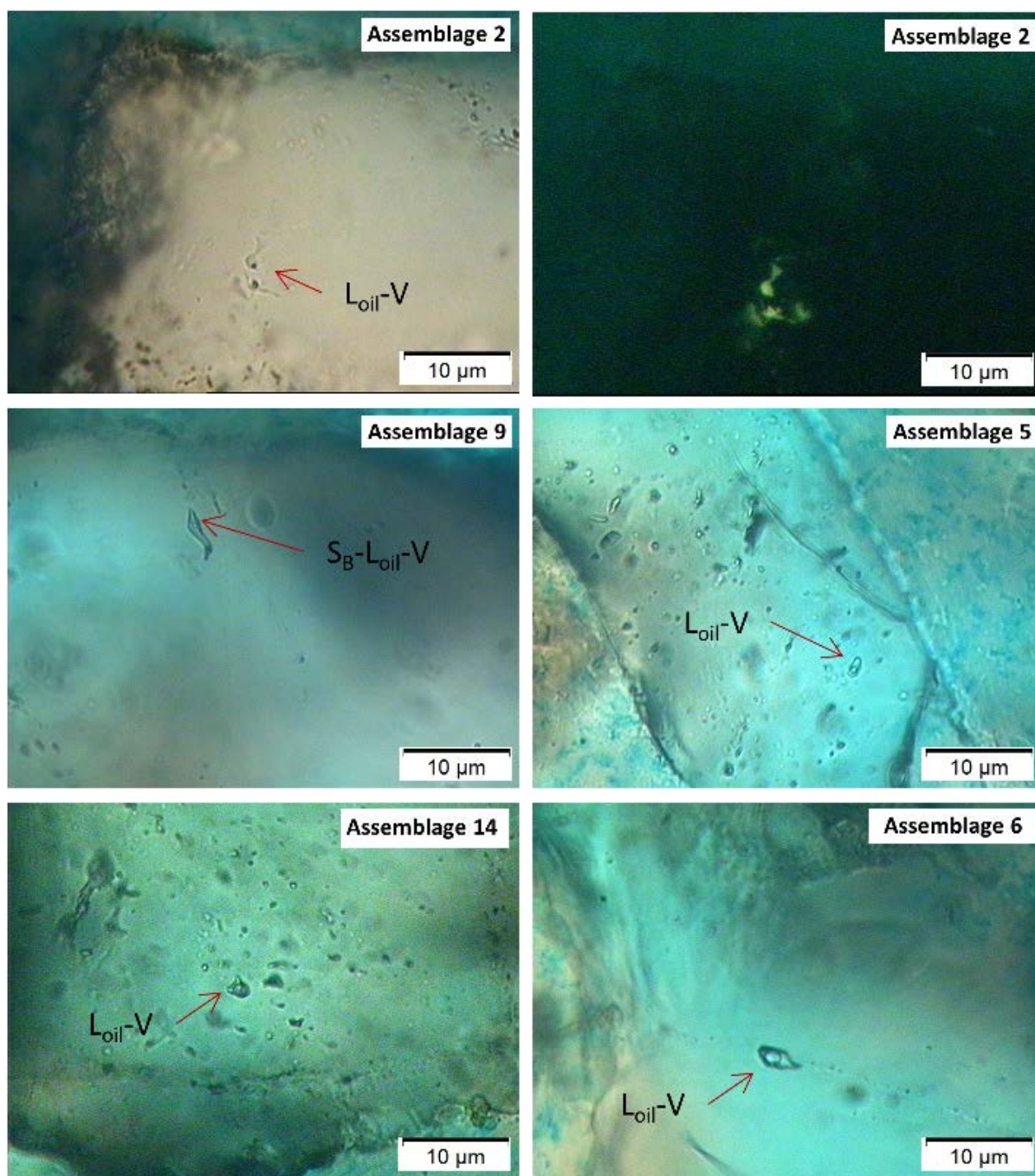


Figure 94: Paired transmitted light and UV photomicrographs of Potoroo-1 oil inclusion assemblages 2, 5, 6, 9 and 14.

PVT Analysis

The *PVTx* results of the Potoroo 1 sample are limited, mainly due to the low temperatures expected at 1,778-86 mMD. Most quartz cementation models estimate that the minimum temperature for quartz to precipitate in sedimentary basins is about 60°C. Two *PT* curves for the depth of the sample at Potoroo-1 were provided by BP; (1) a *PT* curve that reaches 56.5°C at present time (maximum burial) and, (2) a “hotter” scenario with higher heat-flow and a *PT* curve that reaches 70°C.

Phase envelopes and isochores for both oil and associated water inclusions, that are used to derive entrapment pressures and temperatures, are shown in Appendix 12. Raman spectroscopy on water and gas inclusions and *PVTx* modelling using PIT software on oil inclusions provide composition data shown in Table 28 and Table 29.

Table 29: Potoroo-1 oil inclusion compositions calculated using PIT.

OIA	Inc	ϕ_{vap} (20°C)	T_h (°C)	Alpha	Beta	C ₁	C ₂	C ₃	iC ₄	nC ₄	iC ₅	nC ₅	nC ₆	C ₇₊
5	14	9.2	65.6	0.874	0.46	41.3	8.2	7.0	1.5	3.4	2.2	3.5	4.0	29.0
	14	9.7	65.6	0.876	0.48	42.9	8.4	6.9	1.5	3.3	2.1	3.4	3.8	27.7
6	19	38.7	41.5	0.792	0.63	68.9	9.4	5.5	0.9	2.1	1.1	1.8	2.0	8.4
	19	39.9	41.5	0.792	0.62	69.2	9.3	5.4	0.9	2.1	1.1	1.7	1.9	8.3
9	22	6	77.5	0.924	0.44	29.9	5.4	5.6	1.3	2.9	2.0	3.2	4.0	45.8
	22	7.7	77.5	0.9121	0.47	35.3	6.6	6.1	1.4	3.0	2.0	3.3	3.8	38.4
	24	5.4	56.6	0.9067	0.48	37.4	7.0	6.3	1.4	3.1	2.1	3.3	3.8	35.6
	24	5.6	56.6	0.904	0.48	38.0	7.2	6.4	1.4	3.1	2.1	3.3	3.8	34.8
	24	5.6	56.6	0.8906	0.43	35.7	7.2	6.7	1.5	3.3	2.2	3.6	4.3	35.6
15	50	2.4	65.2	0.9547	0.38	17.3	2.5	3.4	0.9	1.9	1.4	2.3	3.6	66.7
	50	2.8	65.2	0.9474	0.38	19.3	3.0	3.9	1.0	2.2	1.6	2.6	3.8	62.6
	49	4.2	67.6	0.9301	0.41	25.9	4.6	5.1	1.2	2.7	1.9	3.1	4.1	51.3
	49	5.1	67.6	0.9217	0.44	30.4	5.6	5.7	1.3	2.9	2.0	3.2	4.0	44.9

OIAs with variably sized vapour bubbles

Assemblage 5 (inclusion 14) has white fluorescent oil with a T_h of 65.6°C and vapour volume fraction estimated between 9.2 and 9.7%. The modelled PIT compositions are compatible with light oil.

Water inclusions were not observed in this assemblage and are therefore unable to constrain the *PT* trapping conditions by crossing of isochores. The bubble point pressure of oil inclusion 14 at a T_h of 65.6°C is 160-175 bar and these can be considered minimum *PT* conditions for entrapment of this fluid.

Assemblage 3 has white fluorescent oil in water-rich inclusions that did not provide measureable T_h . However, two associated water inclusions homogenised at 69°C (inclusion 10) and 73.1°C (inclusion 9). Water salinity from Raman analysis of inclusion 9 was about 39,000 ppm, with a methane content of 1,820 ppm. Fluid modelling indicates a minimum pressure of 178 bars at T_h .

Various oil inclusions in assemblages 9 and 15 have heavier PIT modelled oil compositions and all are compatible with black oil. The associated water inclusions in both assemblages have minimum temperatures of 94°C and 88.3°C, respectively, but their bubble point curves could not be modelled. The minimum *PT* conditions of entrapment, at a T_h of 88.3°C, is around 200 bars for assemblage 15

and 210 bars, at a T_h of 94°C, for assemblage 9 (extending up to 300 bars if a T_h of 109°C from inclusions 35 is used instead).

OIAs with uniformly large vapour bubbles

Inclusion 19 from OIA 6 has weak whitish fluorescence, a large vapour volume fraction estimated between 38.7 and 39.9% and homogenises into the vapour phase at 41.5°C. PIT modelling failed to provide a composition compatible with these parameters. The high liquid content at room temperature, together with homogenisation into the gas phase does, however, suggest a gas condensate. If this were the case, the minimum trapping conditions can only be constrained by the T_h of 41.5°C, but the entrapment temperature is likely to be higher than this and above the minimum threshold for quartz precipitation of around 60°C.

Summary of *PT* Trapping Conditions

A range of hydrocarbon fluid compositions were modelled by PIT as black oil and light oil, with gas-condensate being inferred from phase behaviour in one other inclusion. The *PT* trapping conditions are all minimum constraints, with temperatures above 65.6°C and pressures in excess of 160 bar (Table 30; Figure 95).

In reference to the independently modelled *PT* curve from BP, assemblages 3, 5, 9 and 15 all fall in a temperature range greater than this, including that of current day (approximately 59°C). However, the minimum temperatures and pressures for OIAs 3 and 5 are closer to the upper end of temperatures for the “hotter” *PT* curve. The minimum temperatures for OIAs 9 and 15 are not readily explained by either burial model, however the minimum pressures are compatible with the current day sample depth.

*Table 30: Summary of *PT* entrapment conditions in Potoroo-1.*

Assemblage	Temperature (°C)	Pressure (bar)	Composition
5	65.6 (min)	160-175 (min)	Light oil
3	73.1 (min)	178 (min)	Water (+oil)
9	94 (min)	210 (min)	Black oil
15	88.3 (min)	200 (min)	Black oil
6	-	-	Gas-condensate

Min = minimum *PT* estimation only.

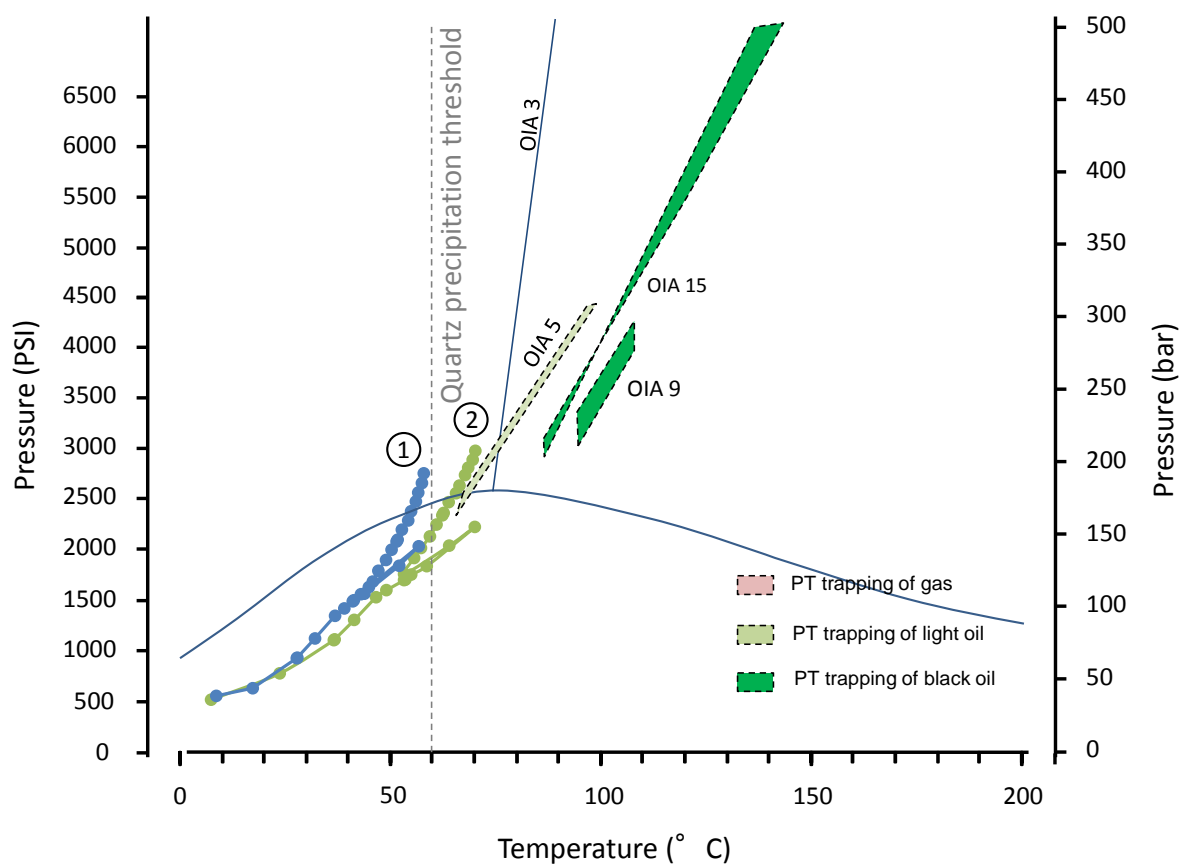


Figure 95: Trapping conditions at 1178-86 mMD in Potoroo-1 derived from PVTx modelling of oil and water fluid inclusion assemblages.

Blue line is the estimated PT curve at the sample depth provided by BP (extracted from 3D burial history model). Green line is the "hotter" PT curve allowable by the model. Shown are the Th data for all petroleum and associated water inclusions (refer to Figure 85 for explanation) and the bubble-point/isochore for water inclusions in OIA 3.

DISCUSSION

Timing of Hydrocarbon Entrapment in the Central Ceduna Sub-basin

Gnarlyknots-1A

From *PVTx* analysis, the intra-Coniacian interval at 4,410-15 mMD appears to have been a migration pathway for a variety of hydrocarbon fluid compositions over an extended period of time (Figure 96). The measured *PT* conditions derived from each assemblage (Figure 75), when translated onto independently modelled Pressure-time (*Pt*) and Temperature-time (*Tt*) plots, show that the earliest phase of hydrocarbon entrapment in Gnarlyknots-1A was light oil (constrained from OIA 5). From both *Pt* and *Tt* constraints, this occurred at end of the Cretaceous around 70-75 Ma (Campanian). Potentially some oil of unconstrained composition (OIAs 1, 13) may have been entrapped earlier than this, closer to 80 Ma, on minimum temperature constraints.

Phase separation of light oil, and entrapment of both gas-rich phases and gas-depleted black oil, is constrained from *Pt* and *Tt* to around 70 Ma (Maastrichtian) and at the end of the Cretaceous.

After deposition of the Hammerhead Supersequence, thermal sag combined with lower sedimentation rates, led to increasing water depths from the Palaeocene onwards. The consequence was a gradual rise in pressure with burial, but with very little increase in temperature. The *Tt* plot is thus less reliable at this point, as similar temperatures persisted over a long period of geologic time. Using the *Pt* curve instead, entrapment of gas-rich assemblages occurred later in Gnarlyknots-1A, with gas-condensate from about 35-15 Ma in the Oligocene to Early Miocene, followed by gas and CO₂ from about 27-15 Ma in the Late Oligocene to Early Miocene. Note that the timing of gas-condensate is less well constrained and only pressures are estimated where the isochore crosses the BP model at approximately 80°C.

The entrapment history of these fluids and gases in Gnarlyknots-1A, with light oil giving way to gas condensate, is suggestive of the manner in which organic matter matures through time as a result of increasing temperatures with greater burial depth. While source rocks form oil and gas at different rates, depending on its kerogen content and type, increasing temperature and maturity causes initially complex petroleum compounds to undergo structural simplification—typically starting with oil, then wet gas and ending at dry gas (Figure 97). A simple explanation for this apparent sequence of hydrocarbon entrapment in Gnarlyknots-1A might be generation from a single source rock.

There is some indication for late black oil entrapment in Gnarlyknots-1A, at about 18 Ma in the Miocene from pressure constraints where the isochore intersects the independent *PT* model at approximately 80°C (i.e. less well constrained). This oil might possibly arise from a different source rock that entered the oil window at a later time in the basin history.

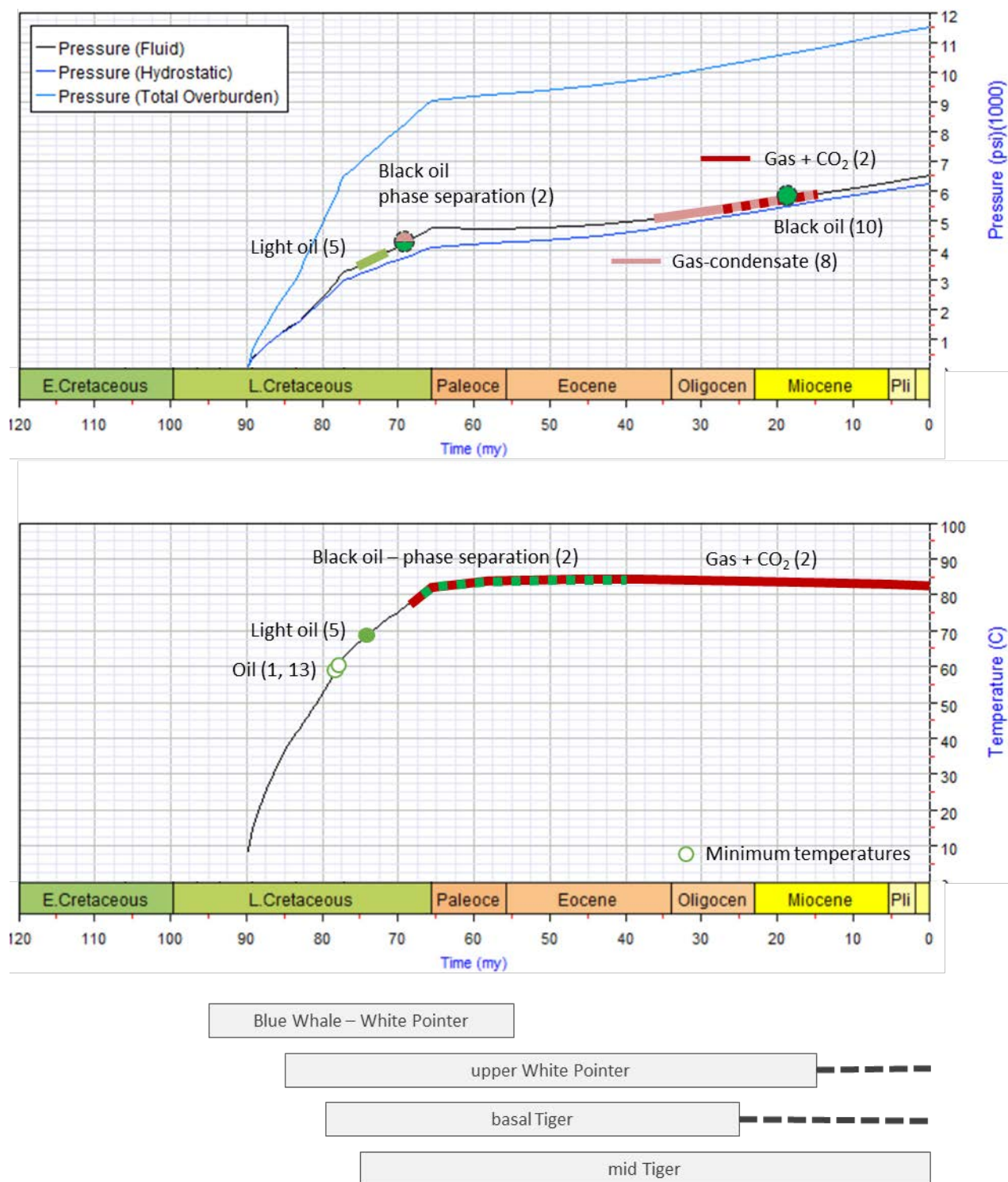


Figure 96: Pressure-time and Temperature-time plots for entrapment of oil and gas bearing inclusion assemblages at 4410-15 mMD in Gnarlyknots-1A. Pt and Tt data provided by BP at the closest depth of 4380 mTVDKB. Modelled timing of generation from several potential source rocks from Struckmeyer (2009).

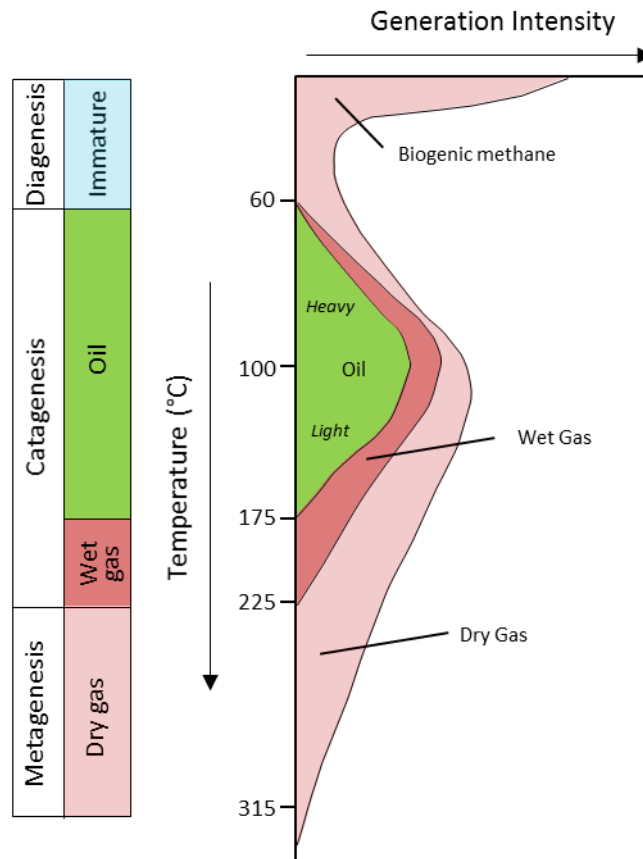


Figure 97: Maturation of organic matter.

Potoroo-1

From PVTx analysis, the 1,778-86 mMD in Potoroo-1 appears to have been a migration pathway for mostly light and black oil. Some gas-condensate was inferred from phase behaviour.

The measured *PT* data are from only a few oil inclusion assemblages and are minimum constraints only. Given their higher temperatures and pressures, they are compared to the “hotter” *Pt* and *Tt* plots supplied by BP for constraining the time of entrapment. With regard to this, entrapment of oil and light oil (OIA 3, 5) in Potoroo-1 occurred from as early as the Oligocene (~32 Ma), from *Pt* constraints, and from the Early Miocene (~25 Ma) to Recent from *Tt* constraints (Figure 98). Black oil (OIA 9, 15) appears to have been entrapped at a later time, from the Pliocene (~5 Ma), however the corresponding temperatures are higher than even the “hotter” burial model predicts.

In a comparison between Gnarlyknots-1A and Potoroo-1, the fluid inclusion record shows that during Cenozoic trapping, Gnarlyknots-1A records mainly gaseous entrapment while in Potoroo-1 there is mainly liquid oil entrapment.

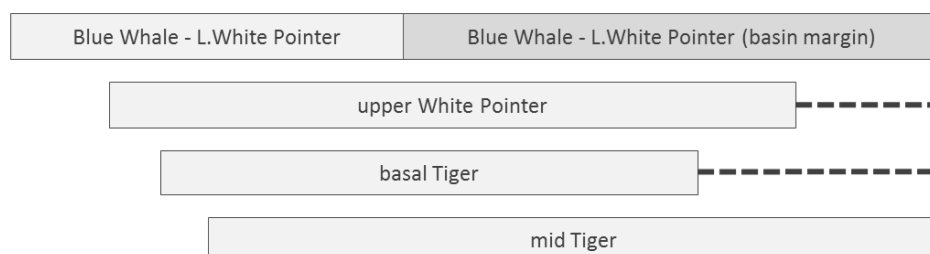
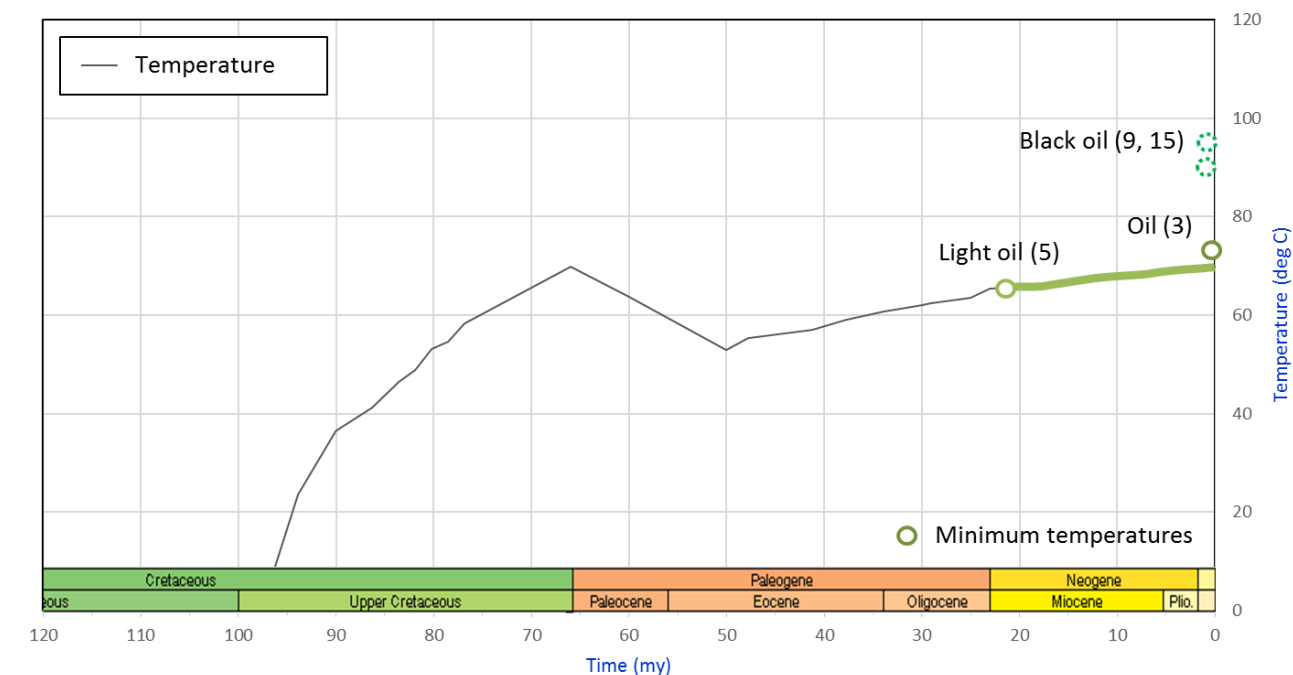
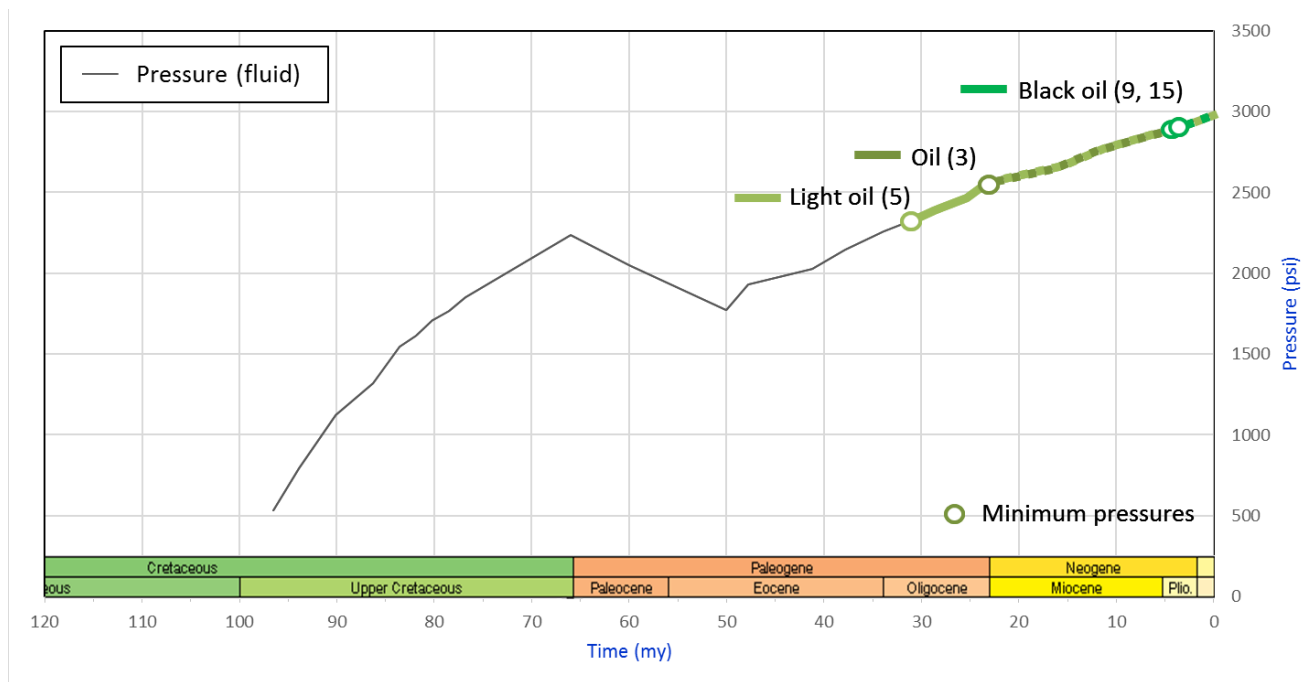


Figure 98: Pressure-time and Temperature-time plots for entrapment of oil and gas bearing inclusion assemblages at 1778-86 mMD in Potoroo-1 (hotter PT modelled conditions). Pt and Tt data provided by BP at an unspecified depth in proximity to the sample. Modelled timing of generation from several potential source rocks from Struckmeyer (2009).

Generation-Expulsion Modelling (Literature)

Two-dimensional petroleum systems modelling (Totterdell et al., 2008) and three-dimensional modelling (Struckmeyer, 2009) of the Ceduna Sub-basin was previously undertaken to constrain the timing of generation and expulsion of hydrocarbons from three modelled source units; the Blue Whale, White Pointer and Tiger supersequences. Although not comprehensive, these three modelled units were considered to have the highest potential of having sourced hydrocarbons that are preserved in traps. For all three potential source rock units, the results from the 2D models described in Totterdell et al. (2008) were confirmed by the 3D models of Struckmeyer (2009), with generation and expulsion as summarised as follows:

- Tiger (marine source rock): mid Campanian to Recent
 - Middle Tiger (Turonian-Coniacian) - predicted expulsion from these younger source rocks would have occurred from about 75 Ma in the deepest part of the depocentre.
 - Potential source rocks of this unit are modelled to be oil mature only and in the deepest part of the basin.
 - Basal Tiger (Cenomanian-Turonian) - predicted expulsion from this source rock occurred from about 80 Ma to 25 Ma in the central basin depocentre.
 - Potential source rocks of this unit are modelled to be oil and gas mature over a large area of the Ceduna Sub-basin.
- Upper White Pointer (deltaic source rock): early Campanian to Recent.
 - Expulsion from the coaly source rocks probably occurred from about 85 Ma onwards, but the significant phase of expulsion in the central basin is likely to have occurred between 80 and 15 Ma.
 - Potential source rocks of this unit are modelled to be both oil to gas mature over a large area of the Ceduna Sub-basin.
- Blue Whale to lower White Pointer (marine source rock): Turonian-Santonian to Recent.
 - Predicted timing of expulsion is likely to have occurred between 95 to about 55 Ma in the basin depocentre and from 55 Ma to Recent along the basin margins.
 - Potential source rocks of this unit are modelled to be oil to gas mature over a large area of the Ceduna Sub-basin.

Implications for Gnarlyknots-1A

The number of input parameters to petroleum systems models is typically large (geological model, source rock properties, heat flow, maturity etc) and, for frontier basins like the Ceduna, the choice of inputs is compromised by the lack of available data. While these models have caveats, they do provide a framework in which the timing of hydrocarbon entrapment, measured directly from fluid inclusions, can be compared. Comparing the timing of entrapment from the *Pt* data with the modelled timings of generation (Figure 96), the Blue Whale, White Pointer and Tiger source sequences are all possible sources of the FI oil in Gnarlyknots-1A.

Because the FI oil is a bulk mixture of all fluid inclusion assemblages that were trapped over an extended period of time, it may have origins from either single or multiple sources. Perhaps the simplest explanation for the apparent sequence of hydrocarbon entrapment in Gnarlyknots-1A (Figure 96) might be generation from a single source rock, where increasing temperatures cause oil

to form first, followed by wet-gas or gas-condensate. Because the FI oil in Gnarlyknots-1A contains a mixture of both algal and terrestrial organic matter, with thermogenic gas (methane and ethane) from type III humic matter, the same mixture of organic matter types would be required in the source. None of the potential source rocks currently identified have this, but these do not consider possible facies variations. There is a possibility of an, as yet unidentified, paralic facies of the White Pointer Supersequence containing inter-fingered marine (algal) and terrestrial sediments. Less likely would be significant terrestrial input to the marine Tiger and Blue Whale source sequences, particularly in distal basin settings further from the source of input.

If the FI oil in Gnarlyknots-1A was generated from multiple sources, then any one of the Blue Whale, White Pointer and Tiger source sequences are potentially compatible. In this scenario, timing of generation from the Blue Whale/lower White Pointer source could explain the late Cretaceous oil, but not gas-condensate in the Oligocene-Miocene. The upper White Pointer (terrestrial) and basal-Tiger (marine algal) are potentially better placed to explain both oil and gas generation over a range of possible timings. Indeed, Totterdell et al. (2008) predicted oil accumulations in the central Ceduna sourced by both White Pointer and Tiger source units to approximately equal proportions (Figure 99). The mid-Tiger is oil mature only in the deepest part of the basin and, while this could be a source of the late black oil, could not be a source of the gas-condensate.

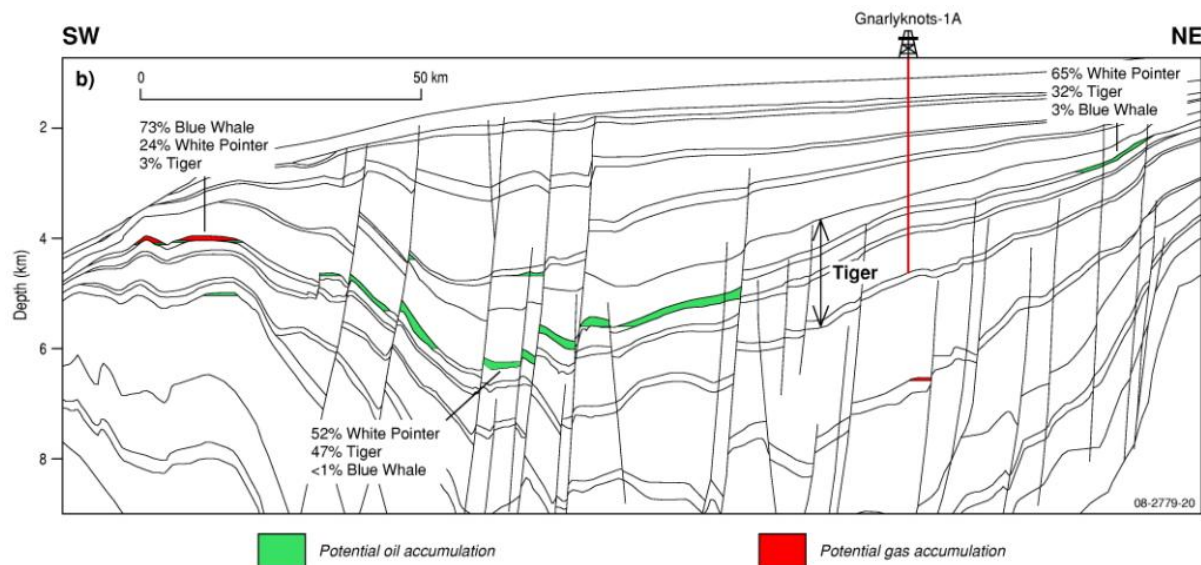


Figure 99: Predicted accumulations and the percentage of liquids contribution from three potential source units in the central Ceduna transect.

In either source scenario, there is a gap in the entrapment history between oil-rich assemblages in the latest Cretaceous and gas-rich inclusions, plus late stage oil, in the Oligocene to Miocene (Figure 96). While sediment loading of the Upper Cretaceous succession and, in particular, the Hammerhead Supersequence, was the critical event for generation of the earlier oil, the PT time constraints suggests some additional control for generation of later gas and oil. While Tertiary progrades are a key control for late stage maturation in the eastern Ceduna/Duntroon sub-basins (Bight Petroleum, 2016), the lack of significant Tertiary cover outboard—only 300 in the Gnarlyknots-1A—potentially limits this as a mechanism in the central Ceduna Sub-basin.

Implications for Potoroo-1

Measured *PT* entrapment of light oil in Potoroo-1, which is located along the inboard margin of the Ceduna Sub-basin, appears relatively late and from the Oligocene (~32 Ma), with black oil from the Pliocene (~5 Ma). Based on potential source sequences proximal to Potoroo-1, only the Blue Whale/lower White Pointer reached thermal maturities capable of generating this oil. Totterdell et al. (2008), however, modelled potential oil accumulations sourced from the White Pointer, but with a significant contribution from the Tiger, along basin margin (Figure 99). As indicated by Struckmeyer (2009), earlier oil and gas from these potential source sequences in the Ceduna depocentre may have spilled/re-migrated to the basin margin following the Late Cretaceous break-up event. While the thermal input parameters for the burial model were increased to satisfy the minimum measured *PT* data at Potoroo-1, the fluid entrapment temperatures are still higher compared to the predicted rock temperatures from basin models (Figure 95). This potentially supports the concept of fluid migration from deeper and hotter parts of the basin depocentre toward the shallower basin margins and for thermal disequilibrium between fluids and rock.

Timing of Hydrocarbon Entrapment in the Eastern Ceduna/Duntroon Sub-basins **Greenly-1**

In Greenly-1 the measured *PT* conditions for the entrapment of oil do not lie on the independently modelled *PT* curve supplied by BP (Figure 81). As previously stated, this would suggest that; (1) the temperatures reflect the entrapment conditions but the pressures were lower or, (2) the pressures reflect the entrapment conditions and the temperatures were higher. Given that the *PT* trapping conditions of oil in Greenly-1 are remarkably similar, and all of the same fluid composition (black oil), this would suggest that both the *P* and *T* constraints are correct.

If the temperatures reflect the entrapment conditions, then from the *Tt* constraint this would suggest trapping of black oil sometime from the Early Miocene (~23-5 Ma; Figure 100), and at pressures roughly 200 bars less than modelled (~2km shallower). This pressure difference might not be as large if current day overpressure is factored. One consideration is late Tertiary burial from a thick wedge of Tertiary sediments that formed at the present day shelf edge, and which recently prograded across the older Late Cretaceous deltas. This Tertiary burial rate peaked around 15 million years ago with the main source rocks in the Platypus (White Pointer) and Wigunda (Tiger) formations only recently being pushed through the oil window (Bight Petroleum, 2016). Perhaps FI oil entrapment in Miocene (~23 Ma in Greenly-1), as a result of generation from Tertiary progradation, occurred at pressures prior to rapid burial of the Late Cretaceous sediments from 15 Ma onwards. Around 1.8 km of Oligocene to Recent carbonate sediment is indicated in BP's burial history model, which would go some way to explain the pressure difference. This scenario is perhaps more favoured, because the MCI data from Greenly-1 indicates a more likely terrestrial White Pointer source for the FI oil, which can only have been generated from Tertiary loading.

If, however, the pressures reflect the entrapment conditions, then from the *Pt* constraint this would suggest earlier trapping sometime from the Campanian, in the Late Cretaceous (~75 Ma), to the early Eocene (~52 Ma; Figure 100). If this is considered, then temperatures about 30°C higher than modelled are required. One explanation might be a transient period of hotter fluids that were in thermal disequilibrium with the rock, perhaps migrating from depth along faults or permeable carrier beds. Without additional constraints, the precise timing of oil entrapment in Greenly-1 remains somewhat equivocal.

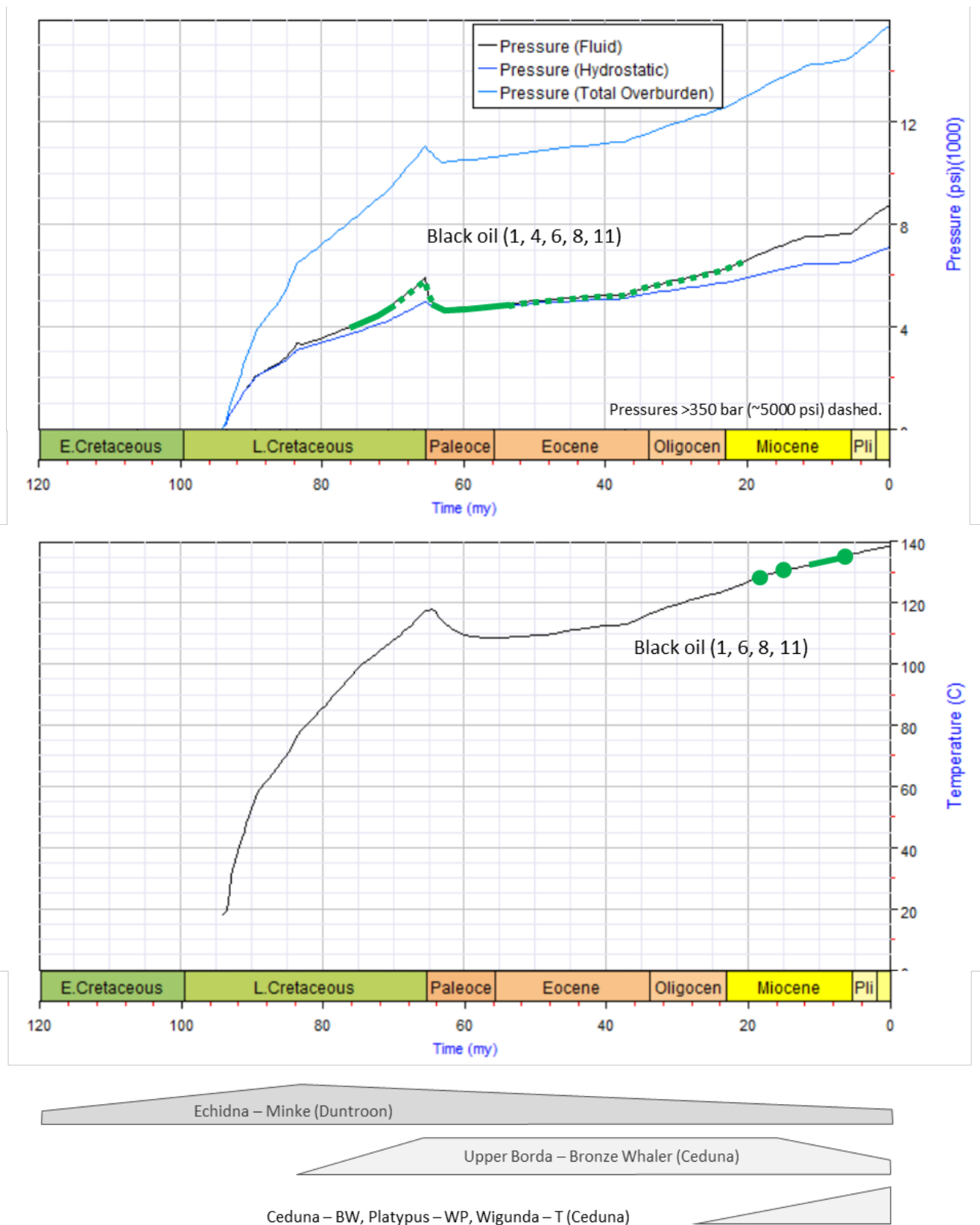


Figure 100: Pressure-time and Temperature-time plots for entrapment of oil bearing inclusion assemblages at 4809-12 mMD in Greenly-1.
 Pt and Tt data provided by BP at a depth of 4818 mTVDKB. Modelled timing of generation from several potential source rocks from Smith and Donaldson (1995). BW = Blue Whale, WP = White Pointer, T = Tiger.

Duntroon-1

In Duntroon-1 the measured *PT* conditions for the entrapment of oil and gas do not conform, in the main, to the independently modelled *PT* curve supplied by BP (Figure 89). Only a few assemblages (OIAs 5, 6 and 9) lie on or close to the *PT* curve at conditions approaching those of current day.

When considering the *Pt* and *Tt* evolution to constrain timing, both data sets need to be considered together (Figure 101). The measured temperatures are all above 81°C on the *Tt* plot and this suggests entrapment from about 17 Ma in the mid Miocene, onwards. The pressures of entrapment for black oil (OIA 9) and gas (OIA 5) are also consistent with this timing on the corresponding *Pt* plot, as would be expected given that they also lie on the independently modelled *PT* curve. Because pressure evolution in Duntroon-1 was essentially static over the Cenozoic, there are non-unique times in the *Pt* history for entrapment of the light oil assemblages (OIAs 3, 6, 8) that would otherwise suggest entrapment in the Late Cretaceous. This is considered less likely as the corresponding inclusion temperatures are much higher (50°C) than those indicated by the burial model indicates for this period.

In considering only those OIAs from the *Tt* plot, an evolution in composition over time is apparent:

- Earliest oil entrapment as black oil at 81-86°C and, in OIA 9, at a minimum of 259 bar (mid-Miocene).
- Light oil entrapment over a temperature window of 85-90°C (OIAs 6, 8) and corresponding pressures from OIA 6 of 240-255 bar (Late Miocene).
- Later stage entrapment of gas (Holocene), in association with CO₂ and N₂, at temperatures and pressures close to present day of 95°C and 255 bar (OIAs 5, 7).

Like Greenly-1, 40 km to the east of Duntroon-1, entrapment of both black and light oil appears to have occurred in the Miocene. Therefore, generation from the White Pointer, or even the Tiger, via Tertiary loading, might be the sources of these hydrocarbons (Figure 101). Because no MCI was attempted on the Duntroon-1 FI oil sample, no further distinction can be made based on source-specific biomarker information.

The source of gas (CH₄, C₂H₆, C₃H₈) in the fluid inclusions at Duntroon-1 is not well constrained, however they are associated with abundant CO₂ and N₂ and a low amount of liquid oil (weak yellow fluorescence) indicative of heavier aromatic compounds. McKirdy and Chivas (1992) described aromatic condensate associated with volcanic CO₂ produced by the Caroline-1 well in the southeast Otway Basin to the east. They argued that CO₂ from a magmatic origin, linked to Holocene volcanism in the area, circulated in the sedimentary succession and stripped hydrocarbons from marginally mature disseminated kerogen. While the volcanics extrusions in the Ceduna Sub-basin have been dated to a short-lived period during the Middle Eocene (Schofield and Totterdell, 2008), a similar magmatic origin could be envisaged for the presence of these non-hydrocarbon gases in Duntroon-1. This has potential implications for thermal history evolution and petroleum systems modelling.

At Duntroon-1, some hotter fluid entrapment temperatures are encountered compared to the predicted rock temperatures from basin models (Figure 89). This potentially supports the concept of

fluid migration from deeper and hotter parts of the basin depocentre toward the shallower basin margins and for thermal disequilibrium between fluids and rock.

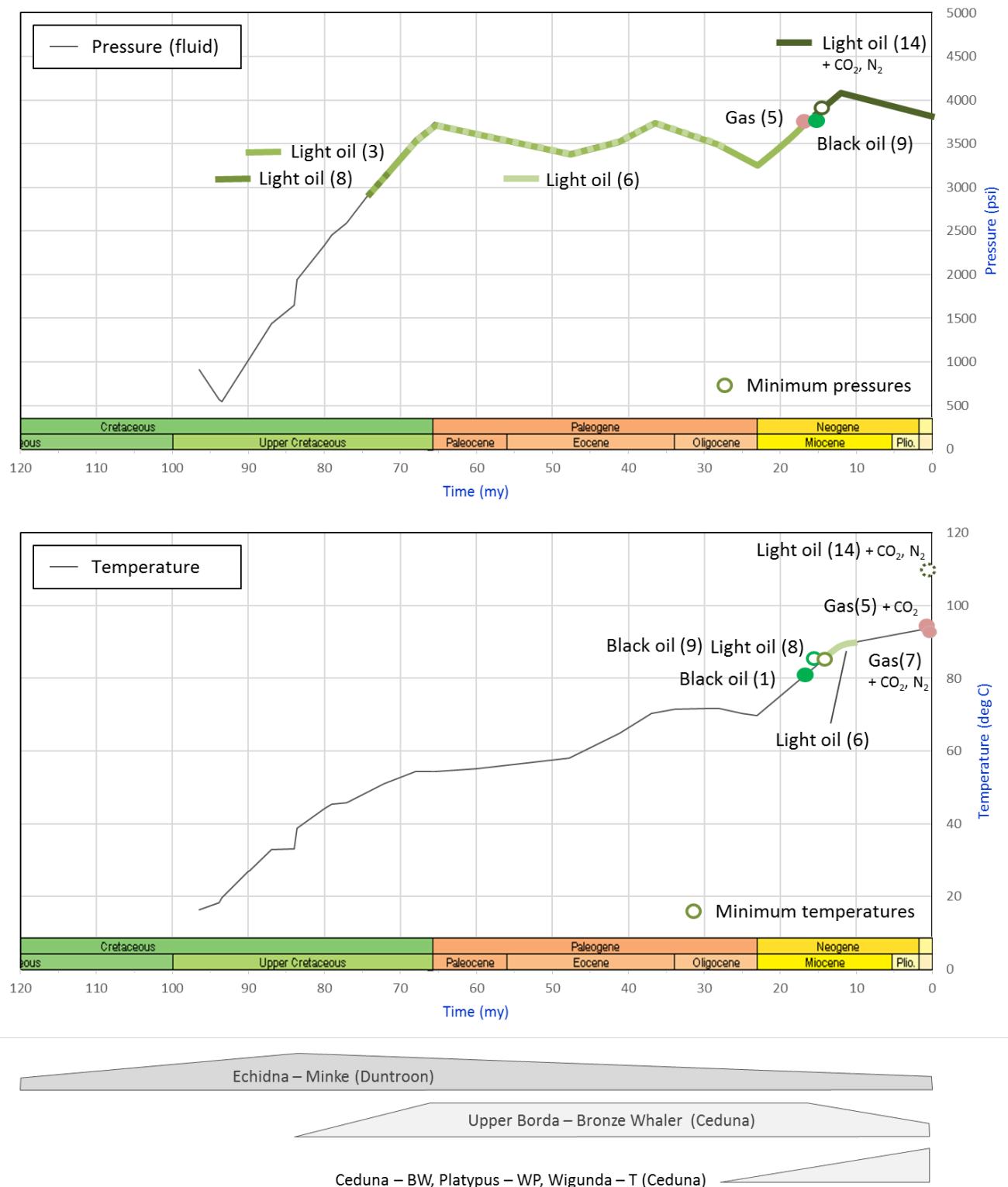


Figure 101: Pressure-time and Temperature-time plots for entrapment of oil bearing inclusion assemblages at 2505-10 mMD in Duntroon-1.

Pt and Tt data provided by BP at unspecified depth in proximity to sample. Modelled timing of generation from several potential source rocks from Smith and Donaldson (1995). BW = Blue Whale, WP = White Pointer, T = Tiger.

Consequences of Entrapment in Quartz for Understanding Migration

This fluid inclusion study was carried out on a limited number of wells and choices for samples were restricted to cuttings. As the target lithologies were all sandstones, and sample preparation concentrated the detrital grains of quartz, fluid inclusions measured in the present study were limited to those trapped in quartz only. Fluid inclusions commonly form at moderate depths of burial in diagenetic cements—that is, after consolidation of the rock where mechanical stresses cause intra-grain fracturing and temperatures are suitable for cements to form. In the case of quartz cement, this temperature is at a minimum of around 60°C (McBirde, 1989). Therefore, at temperatures below this threshold, no fluid record exists in quartz, and hydrocarbon migration is potentially not detected by fluid inclusion techniques. In the case of Gnarlyknots-1, oil inclusion entrapment at palaeo-temperatures as low as about 60°C are recorded, indicating entrapment during Late Cretaceous (80-75 Ma) in the Ceduna Sub-Basin. Earlier hydrocarbon migration might have occurred but remains undetected by fluid inclusion techniques in quartz. Similarly, at Potoroo 1, the temperatures predicted by the basin model at the sample depth reach a maximum of 70°C at the present day. According to the quartz models, only migrations from the Oligocene might be recorded by fluid inclusion entrapment in quartz (noting that temperatures >60°C also existed in the Late Cretaceous to Palaeocene as well; Figure 98). In the eastern Ceduna/Duntroon sub-basins, Greenly-1 and Duntroon-1 have inclusion assemblages that indicate entrapment significantly above the quartz cement threshold temperature. In the case of Greenly-1, temperatures >60°C were reached from the Late Cretaceous and migration from this time might be recorded by fluid inclusion entrapment in quartz. In Duntroon-1, 60°C was reached only from the mid-Eocene onwards.

CONCLUSIONS

Contributions to Petroleum Systems Knowledge in the Bight Basin

The Bight Basin, and the prospective Ceduna Sub-basin, are frontier areas for hydrocarbon exploration and this region has seen a significant uptake of permits since BP Developments Australia acquired EPP 37, EPP 38, EPP 39 and EPP 40 in 2011. The only direct indications for oil are limited to those in the Greenly-1 well, together with reports of coastal bitumen strandings along the southern coastline of Australia that date back to the mid-1800s.

Grains containing Oil Inclusions (GOI)

To screen the Bight Basin for hidden oil indications, 36 samples were analysed from 7 historic exploration wells, including the previously untested Gnarlyknots-1A well, using CSIRO's *Grains with Oil Inclusions (GOI™)* technique.

Project 5.3 was successful in detecting hidden hydrocarbons, trapped in fluid inclusions, over multiple intervals in both Gnarlyknots-1A and in supplementary wells where new intervals were revealed and the continuity of previous GOI tested. The key contributions to petroleum systems knowledge are summarised as follows:

- Widespread evidence for hydrocarbon migration in both the central Ceduna and eastern Ceduna/Duntroon sub-basins. Possible small palaeo-oil accumulation at 4,209-15 mMD in Greenly-1.
- Improvement on conventional oil show/indications from Greenly-1 only.
- Hydrocarbon inclusions are more frequent in intervals from the Late Cretaceous White Pointer, Tiger and Hammerhead supersequences, but could be biased by drilling targets and sampling strategy.
- Indications for oil and gas-condensate in the fluid inclusion record.
- Light crude oil has inferred API gravities between 37° to about 45°.
- Presence of hydrocarbon inclusions implies generation/expulsion and direct evidence for petroleum systems, most significantly in the deepwater Ceduna Sub-basin.
- This, in turn, implies effective source rocks that are beyond the reach of existing well intersections.
- Previous interpretations of palaeo-oil zones in Jerboa-1, Eyre Sub-basin, are not supported by repeat GOI measurements.

Molecular Composition of Oil Inclusions (MCI)

To characterise the fluid inclusion oils and gases within the rocks of the Bight Basin, CSIRO's *Molecular Composition of Inclusions (MCI)* method was attempted on Gnarlyknots-1A (Tiger Supersequence) and Greenly-1 (White Pointer Supersequence).

Project 5.3 was successful in extracting minute quantities of hydrocarbons for analysis from these low GOI samples and this represents a step change in the applicability of the technique to characterising migration intervals. The key contributions to petroleum systems knowledge are summarised as follows:

Gnarlyknots-1A

- The *n*-alkane and biomarker characteristics show that Gnarlyknots-1A fluid inclusion (FI) oil (4,390 m to 4,425 mMD), has mixed organic matter input from both algae and terrestrial plants and was generated from source rock(s) deposited in suboxic-oxic marine environment(s).
- The wide range of maturities, 0.65% to 1.3% VRE, suggests that this FI oil is either a mixture of oils generated from different source rocks or from the same source rock, at different maturity stages.
- The Blue Whale and Tiger are potential source sequences of algal organic matter (marine environment), while the White Pointer is a potential source of terrestrial organic matter. If a single source is considered, an unrecognised paralic facies of the White Pointer, containing both algal and terrestrial organic matter, is plausible.
- Algal input to the FI oil is the first direct evidence for generation from rocks containing type II kerogen and this significantly improves prospectivity in the deepwater Ceduna Sub-basin.
- Toluene dominates the gasoline range hydrocarbons in the FI oil (4,410-15 mMD) and originated, in part, from coeval aqueous inclusions.
- Methane and ethane in the FI oil (4,410-15 mMD) have carbon isotopic values that indicate a thermogenic origin for these hydrocarbon gases, possibly sourced from type III (humic) organic matter. Carbon dioxide has a wholly inorganic origin from inherited inclusions of probable magmatic or metamorphic sources.

Greenly-1

- The bulk FI oil (4,806-4,818 mMD) has significant organic matter input from terrestrial plants and a minor contribution from a lacustrine source and was generated from a source rock deposited in an oxic, clay-rich fluviodeltaic depositional environment.
- The FI oil was generated at the early to peak oil window (0.8% to 1.1% VRE).
- The FI oil represents a more pristine oil sample compared to oil show extracts that are potentially contaminated by organic matter in the rock.
- While previous correlations of oil show extracts with the Bronze Whaler have been made, the lack of algal input to the FI oil suggests this is incorrect and that the White Pointer may be a better source candidate.

Timing of Hydrocarbon Entrapment (PVT)

To constrain the composition and timing of hydrocarbon entrapment in the Bight Basin, unique thermometric modelling methods were attempted on samples from the Tiger Supersequence in Gnarlyknots-1A, Duntroon-1 and Potoroo-1, and the White Pointer Supersequence in Greenly-1.

It was found that in the deepwater Ceduna Sub-basin, there was a high degree of concordance between measured *PT* entrapment conditions from fluid inclusions in Gnarlyknots-1A, with independently modelled *PT* conditions from burial models. This differs from *PT* entrapment conditions in wells located along the basin margin such as Potoroo-1, Duntroon-1 and Greenly-1, where hotter fluid entrapment temperatures are encountered compared to predicted rock temperatures from basin models. The key contributions to petroleum systems knowledge are summarised as follows:

Gnarlyknots-1A

- The intra-Coniacian interval (4,410-15 mMD) was a migration pathway for a variety of hydrocarbon fluid compositions—black oil, light oil, gas-condensate and gas+CO₂—over an extended period of time.
- The sequence of hydrocarbon entrapment from fluid inclusions:
 - The earliest phase of hydrocarbon entrapment was light oil and this occurred at *PT* conditions (240-270 bar; 69.2°C) consistent with the end of the Cretaceous at around 70-75 Ma (Campanian). Potentially some oil may have been entrapped earlier than at temperature conditions (58-62°C minimum), closer to 80 Ma.
 - Phase separation of light oil, and entrapment of both gas-rich phases and gas-depleted black oil, occurred at *PT* conditions (285-308 bar; 80-85°C) consistent with the end of the Cretaceous at around 70 Ma (Maastrichtian).
 - Entrapment of later stage gas-rich phases, with gas- condensate at pressure conditions (350-410 bar @ 80°C) equivalent to 35-15 Ma (Oligocene to Early Miocene), followed by gas and CO₂ at *PT* conditions (370-408 bar; 78-88°C) equivalent to 27-15 Ma (Late Oligocene to Early Miocene).
 - Late black oil entrapment at about 18 Ma in the Miocene from pressure constraints (400 bar @ 80°C) where the isochore intersects the independent *PT* model.
- The apparent sequence of hydrocarbon entrapment from oil to gas might simply be explained by generation from a single source rock over a range of thermal maturity stages. Mixed organic input from an unrecognised paralic facies of the White Pointer might be a possibility, otherwise more complex charge scenarios involving marine shales of the Blue Whale and Tiger supersequences, and the deltaic White Pointer, are options.
- The earlier oil-rich assemblages are readily explained by sediment loading of the Upper Cretaceous succession by the Hammerhead Supersequence, but a mechanism for generation of later stage gas-rich inclusions, plus late stage oil, in the Miocene is less clear.

Greenly-1

- The Cenomanian interval (4,808-12 mMD) trapped hydrocarbon assemblages consistently modelled as black oil.
- The measured *PT* conditions of entrapment are also consistent (270-340 bar; 127-135°C: excluding OIA 4 as an outlier), however do not intersect the independently modelled *PT* curve.
- If the temperatures reflect entrapment conditions, then this constrains oil charge from the Early Miocene (~23-5 Ma) and at a depth equivalent to about 2 km less than that modelled. Tertiary progrades, and rapid late burial peaking around 15 Ma, is one explanation for this pressure difference, with a White Pointer source favoured from the MCI result.
- If the pressures reflect entrapment conditions, then this constrains oil charge to the Campanian to early Eocene (~75-52 Ma) and temperatures about 30°C higher. One explanation might be a transient period of hotter fluids that were in thermal disequilibrium with the rock.

Duntroon-1

- The Turonian-Santonian interval (2,505-10 mMD) was a migration pathway for a variety of hydrocarbon fluid compositions—black oil, light oil and gas (+N₂ and CO₂).

- The sequence of hydrocarbon entrapment from fluid inclusions:
 - The earliest phase of hydrocarbon entrapment was black oil and this occurred at *PT* conditions (259 bar minimum; 81-86°C) consistent with the mid-Miocene.
 - Entrapment of light oil was later and this occurred at *PT* conditions (240-255 bar; 85-90°C) consistent with the Late Miocene.
 - Late stage gas entrapment, in association with CO₂ and N₂, occurred at *PT* conditions (255 bar; 95°C) consistent with current day conditions (Holocene).
- Miocene entrapment of both black and light oil, via Tertiary loading mechanisms, would constrain generation to the White Pointer, or even the Tiger, source sequences.
- Gas, and associated N₂ and CO₂, in the Holocene may be linked to the effects of volcanics extrusions, as they are in the Otway Basin.

Potoroo-1

- The Cenomanian-Santonian interval (1,778-86 mMD) was a migration pathway for mostly light oil and black oil, with some minor gas-condensate inferred.
- Minimum *PT* constraints from fluid inclusions are all higher than the independent *PT* curve, with better alignment achieved using higher heat flows in the burial model.
- The earliest phase of hydrocarbon entrapment was light oil (and an unconstrained oil) and this occurred from Oligocene (~32 Ma) at pressure conditions of 160-178 bar, or from the Early Miocene (~25 Ma) at temperature conditions of 65.6-73.1°C.
- Black oil appears to have been trapped later, and this occurred from the Pliocene (~5 Ma) at pressure conditions of 200-210 bar.
- Only the Blue Whale/lower White Pointer source sequence reached thermal maturities capable of generating this oil locally.
- Re-migrated oil and gas from various sources in the Ceduna depocentre are also likely.

Implications for natural Bitumen Strandings in South Australia ([Link to Project 5.2](#))

Strandings of asphaltites (4-18 °API) and waxy bitumen has been recovered over the last 100 years from numerous locations along the southern margin of Australia, including the Eyre Peninsula and the South Australian and Victorian coastlines from Kangaroo Island to Cape Otway (Edwards et al., 1998; Edwards et al., 2016). They are widely regarded as artefacts of submarine oil seepage.

The less common asphaltite is postulated to be a product of low-intensity seepage from tar mats exposed by the incision of submarine canyons into Australia's southern continental slope. This includes the Morum Sub-basin, offshore from the Limestone Coast and southern Kangaroo Island where the highest concentration of historical strandings is recorded (Hall et al., 2014), and the Ceduna Sub-basin, where suitable mid-Cretaceous potential marine source rocks have been identified. Based on their source-dependent molecular and isotopic signatures and their remarkably uniform composition, no distinction could be made between the stranded asphaltites implying a common source (Edwards et al., 1998; Hall et al., 2014): marine shale containing sulfur-rich type II kerogen, probably deposited during an Early Cretaceous oceanic anoxic event.

Waxy bitumens account for 90% of the strandings, and are thought to originate from oil seeps within the Indonesian Archipelago and are transported into southern Australian waters as flotsam by a complex system of surface ocean currents (Mckirdy et al., 1986, 1994; Currie et al., 1992; Summons

et al., 1993; Alexander et al., 1994; Dowling et al., 1995; Padley, 1995). Whilst diagnostic biomarkers of Indonesia crude oils have been identified in most of the tar ball families, they are not present in all tar ball families, however previous publications have inferred a similar source for the materials.

The comparison analysis between the Gnarlyknots-1A and Greenly-1 FI oils, with naturally stranded asphaltites and waxy bitumens along the South Australian coast, was assessed here by hierarchical cluster analysis (HCA) of 26 source variables derived from the molecular distribution of hopanes, steranes and various aromatic parameters (Figure 102). Geochemical analysis of asphaltites and waxy bitumens, acquired on archived material from the DMITRE (now Department of State Development) core library in South Australia, was undertaken by Weatherfords (the analysis funded through a separate contract between BP and CSIRO, and due to SA government's reporting requirements for archived materials the data has been transmitted to them for public domain release). Based on this multivariate statistical analysis it is concluded that; (1) the Gnarlyknots-1A and Greenly-1 FI oils have different source origins; (2) neither the Gnarlyknots-1A nor Greenly-1 FI oils are closely related to the asphaltites, which are recognised as having a local southern margin origin (Edwards et al., 1998; Totterdell et al., 2008; Hall et al., 2014); and (3) the Greenly-1 FI oil is not closely related to any type of waxy bitumen, whereas the Gnarlyknots-1A FI oil is related to some of the waxy bitumens with similarity value of >0.6.

While all the waxy bitumens are reported to originate from Indonesia, there are key differences in the types of waxy bitumens starting to emerge from more detailed geochemical investigations of waxy bitumens collected from Project 5.2 beach surveys. The Gnarlyknots-1A FI oil is also a bulk oil extract containing evidence for both terrestrial and algal organic matter. While this could be a mixture from several different sources, it would be intriguing to know if the algal source input to the FI oil, at least, bore any correlation to the asphaltites and their suggested source from marine shale containing sulfur-rich type II kerogen.

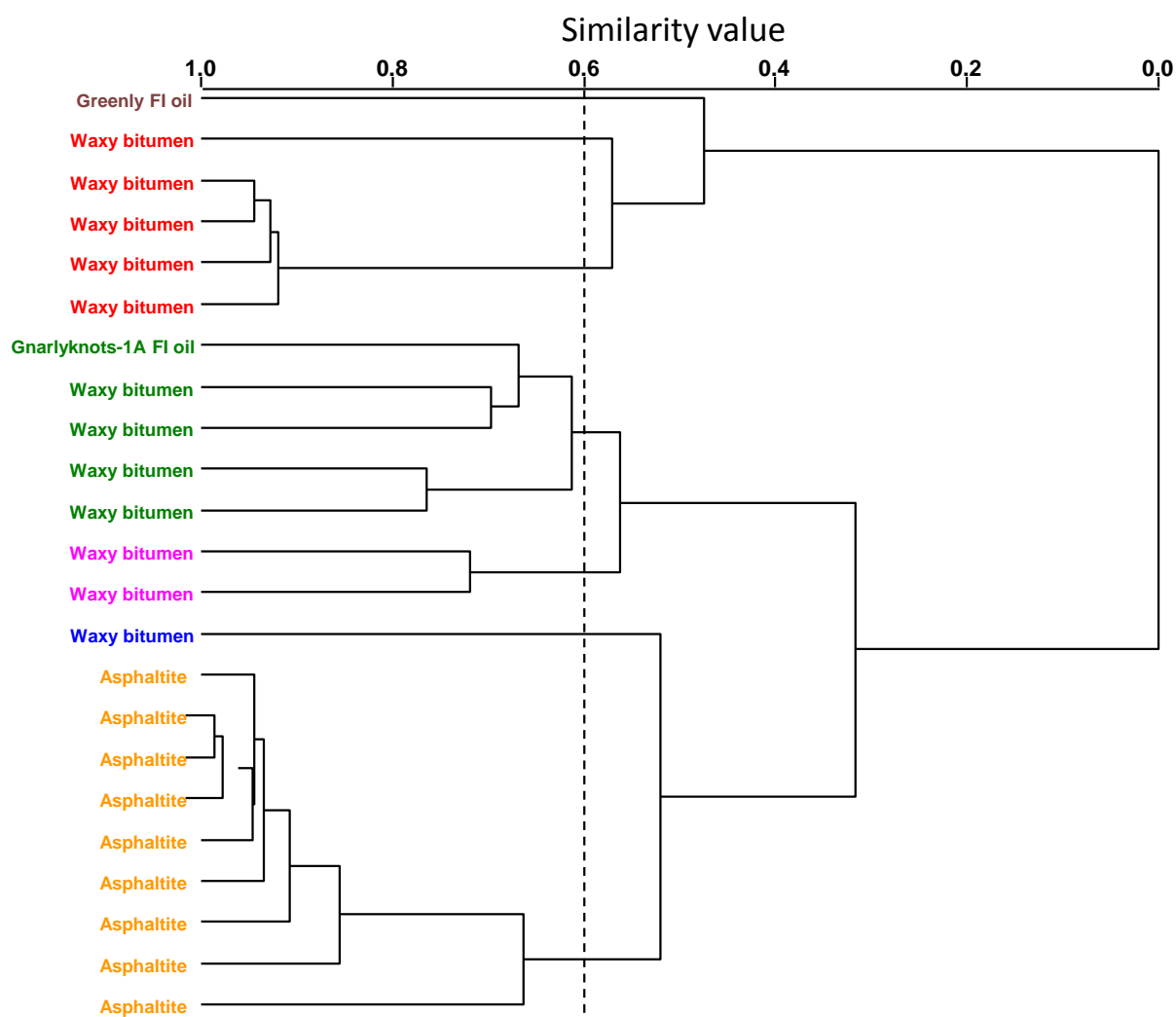


Figure 102: Dendrogram of the hierarchical cluster analysis (HCA) of 26 source variables showing similarity and dissimilarity between Gnarlyknots-1A and Greenly-1 FI oils and asphaltites and waxy bitumens from the GAB.

Asphaltite and waxy bitumen data from Weatherfords (analysis funded through a separate contract between BP and CSIRO, and due to SA governments reporting requirements for archived materials the data has been transmitted to them for public domain release).

The source variables used for calculation of Euclidean distance (autoscale preprocessing, incremental linkage) are : **1.** $C_{30}^*/C_{29}Ts$, **2.** $C_{30}^*/C_{30} \alpha\beta$ hopane, **3.** Homohopanes/ $C_{30} \alpha\beta$ hopane, **4.** Oleanane/ $C_{30} \alpha\beta$ hopane, **5.** Gammarcerance/ $C_{30} \alpha\beta$ hoapne, **6.** C_{30} 30-norhopane/ $C_{30} \alpha\beta$ hopane, **7.** $C_{29} \alpha\beta$ hopane/ $C_{30} \alpha\beta$ hopane, **8.** C_{26}/C_{25} tricyclic terpanes, **9.** C_{23}/C_{21} tricyclic terpanes, **10.** C_{24} tetracyclic/ C_{26} tricyclic terpanes, **11.** C_{24} tetracyclic/(C_{24} tetracyclic + C_{23} tricyclic terpane), **12.** $C_{19}/(C_{19}+C_{23}$ tricyclic terpanes), **13.** C_{29} steranes/ $C_{29} \alpha\beta$ hopane, **14.** $C_{29} \alpha\beta\beta$ steranes 20 S+R / $C_{27} \alpha\beta\beta$ steranes 20 S+R, **15.** $C_{27} \alpha\beta\beta$ steranes 20 S+R / $C_{29} \alpha\beta\beta$ steranes 20 S+R, **16.** (C_{27} steranes+diasteranes) / (C_{29} steranes+diasteranes), **17.** C_{27} regular steranes (%), **18.** C_{28} regular steranes (%), **19.** C_{29} regular steranes (%), **20.** $C_{29} / C_{27}\beta\alpha$ diasteranes, **21.** $C_{27}+C_{28}+C_{29} \beta\alpha$ diasteranes/($\alpha\alpha\alpha+\alpha\beta\beta$ steranes), **22.** Log (1,2,5-TMN/1,3,6-TMN), **23.** Log (1,2,7-TMN/1,3,7-TMN), **24.** Log 1-MP/9-MP, **25.** Log (Retene/9-MP), **26.** DBT/Phenanthrene.

REFERENCES

- Ahmed, M., & George, S.C. (2004). Changes in the molecular composition of crude oils during their preparation for GC and GC-MS analyses. *Organic Geochemistry*, 35(2), 137–155.
- Alexander, R., Currie, T.J., & Kagi, R.I. (1994). The origin of coastal bitumens from Western Australia. *The APEA Journal*, 34(1), 787-798.
- Alexander, R., Larcher, A.V., Kagi, R.I., & Price, P.L. (1988). The use of plant-derived biomarkers for correlation of oils with source rocks in the Cooper/Eromanga Basin System, Australia. *Australian Petroleum Exploration Association Journal*, 28, 310-324.
- Alexander, R., Larcher, A.V., Kagi, R.I., & Price, P.L. (1992). An oil-source correlation study using age-specific plant-derived aromatic biomarkers. In: J.M. Moldowan, P. Albrecht, Philp, R.P. (Eds.), *Biological markers in sediments and petroleum* (Ed. by J.M. Moldowan, P. Albrecht, Philp, R.P.), pp. 201-221. Prentice Hall, New Jersey.
- Aquino Neto, F.R., Trendel, J.M., Restle, A., Connan, J., & Albrecht, P.A. (1983). Occurrences and formation of tricyclics and tetracyclic terpanes in sediments and petroleum. In: Bjorøy, M. et al. (Eds.), *Advances in Organic Geochemistry*. Wiley, Chichester, 659-667.
- Arthur, M.A., Jenkyns, H.C., Brumsack, H.J., & Schlanger, S.O. (1990). Stratigraphy, geochemistry, and paleoceanography of organic carbon-rich Cretaceous sequences. In: Ginsburg, R.N., and Beaudoin, B. (Eds.), *Cretaceous Resources, Events and Rhythms: Background and Plans for Research*. NATO ASI Ser., Ser. C, 304, 75–119.
- Baumgartner, M., & Bakker, R.J. (2009). Raman spectroscopy of pure H₂O and NaCl- H₂O containing synthetic fluid inclusion in quartz – a study of polarization effects. *Mineral Petrol.*, 95, 1-15.
- Becker, S.P., Eichhulb, P., Laubach, S.E., Reed, R.M., Lander, R.H., & Bodnar, R.J. (2010). A 48 m.y. history of fracture opening, temperature and fluid pressure: Cretaceous Travis Peak Formation, East Texas basin. *Geological Society of America Bulletin*, 122(7/8), 1081-1093.
- Bein, J., & Taylor, M.L. (1981). The Eyre Sub-basin: recent exploration results. *The APEA Journal*, 21 (1), 91–98.
- Bernard, B.B., Brooks, J.M., & Sackett, W.M., (1978). Light hydrocarbons in recent Texas continental shelf and slope sediments. *Journal of Geophysical Research*, 83, 4053-4061.
- Bight Petroleum (2016). Overview of the Bight Basin. Website accessed 13 July 2015. <http://www.bightpetroleum.com/pages/14829/Overview-Of-The-Bight-Basin.htm>.
- Blevin, J.E., Totterdell, J.M., Logan, G.A., Kennard, J.M., Struckmeyer, H.I.M., & Colwell, J.B. (2000). Hydrocarbon prospectivity of the Bight Basin—petroleum systems analysis in a frontier basin. In: 2nd Sprigg Symposium—Frontier Basins, Frontier Ideas, Adelaide, 29-30 June, 2000. Geological Society of Australia. Abstracts 60, 24-29.
- Bourdet, J., & Kempton, R. (2014). Novel approach to measuring irreducible water salinity in gas reservoirs. *Offshore Technology Conference, OTC-25064-MS*, Kuala Lumpur, Malaysia, 25-28 March 2014..
- Bourdet, J., Burruss, R.C., Chou, I-M., Kempton, R., Liu, K., & Hung, N.V. (2014). Evidence for a palaeo-oil column and alteration of residual oil in a gas-condensate field: Integrated oil inclusion and experimental results. *Geochimica et Cosmochimica Acta*, 142, 362-385.
- Bradshaw, B.E., Rollet, N., Totterdell, J.M., & Borissova, I. (2003). A revised structural framework for frontier basins on the southern and southwestern Australian continental margin. *Geoscience Australia Record* 2003/03.

- Burhan, R.Y.P., Trendel, J.M., Adam, P., Wehrung, P., & Nissenbaum, A. (2002). Fossil bacterial ecosystem at methane seeps: Origin of organic matter from Be'eri sulfur deposit, Israel. *Geochimica et Cosmochimica Acta*, 66(23), 4085-4101.
- Dutkiewicz, A. & Ridley, J. (2003). Hydrocarbon pseudo-inclusions in barite: how to recognize and avoid artifacts. *Journal of Sedimentary Research*, 73 (2), 171–176.
- Caumon, M.-C., Dubessy, J., Robert, P., & Tarantola, A. (2014). Determination of methane content in aqueous fluid inclusions by Raman spectroscopy. Application to the external part of the Central Alps (Switzerland). *Chemical Geology*, 378-379, 52-61.
- Chen, J., Fu, J., Sheng, G., Liu, D., & Zhang, J., (1996). Diamondoid hydrocarbon ratios: novel maturity indices for highly mature crude oils. *Organic Geochemistry*, 25, 179-190.
- Collister, J.W., Summons, R.E., Lichtfouse, E., & Hayes, J.M. (1992). An isotopic biogeochemical study of the Green River oil shale. *Organic Geochemistry*, 19, 265–276.
- Cox, H.C., de Leeuw, J.W., Schenck, P.A., van Koningsveld, H., Jansen, J.C., van de Graaf, B., van Geerestein, V.J., Kanters, J.A., Kruk, C., & Jans, A.W.H. (1986). Bicaninane, a C30 pentacyclic isoprenoid hydrocarbon found in crude oil. *Nature*, 319, 316-318.
- Currie, T.J., Alexander, R., & Kagi, R.I. (1992). Coastal bitumens from Western Australia — long distance transport by ocean currents. *Organic Geochemistry*, 18, 595-601.
- Dahl, J.E., Moldowan, J.M., Peters, K.E., Claypool, G.E., Rooney, M.A., Michael, G.E., Mello, M.R., & Kohnen, M.L., (1999). Diamondoid hydrocarbons as indicators of natural oil cracking. *Nature*, 399, 54-57.
- Dai, J.X., Qin, S., Tao, S., Zhu, G., & Mi, J., (2005). Development trends of natural gas industry and the significant progress on natural gas geological theories in China. *Natural Gas Geoscience*, 16(2), 127-142.
- Didyk, B.M., Simoneit, B.R.T., & Brassell, S.C. (1978). Organic Geochemical indicators of palaeoenvironmental conditions of sedimentation. *Nature*, 272, 216-22.
- Douglas, A.G., Damste J.S.S., Fowler, M G., Eglinton, T.I., & de Leeuw J.W. (1991). Unique distributions of hydrocarbons and sulphur compounds released by flash pyrolysis from the fossilized alga *Gloecapsomorpha prisca*, a major constituent in one of four Ordovician kerogens: *Geochimica et Cosmochimica Acta*, 55, 275-291.
- Dowling, L.M., Boreham, C.J., Hope, J.M., Murray, A.P., & Summons, R.E. (1995). Carbon isotopic composition of hydrocarbons in ocean-transported bitumens from the coastline of Australia. *Organic Geochemistry*, 23, 729-737.
- Duan, Z., & Mao, S. (2006). A thermodynamic model for calculating methane solubility, density and gas phase composition of methane- bearing aqueous fluids from 273 to 523 K and from 1 to 2000 bar. *Geochimica et Cosmochimica Acta*, 70, 3369–3386.
- Dubessy, J., Lhomme, T., Boiron, M.C., & RUII, F. (2002). Determination of chlorinity in aqueous fluids using Raman spectroscopy of the stretching band of water at room temperature: application to fluid inclusions. *Applied Spectroscopy*, 56, 99–106.
- Eadington, P.J., Lisk, M., & Krieger, F.W. (1996). Identifying oil well sites. Patent No. 5,543,616, United States.
- Edwards, D., McKirdy, D.M., & Summons, R.E. (1998). Enigmatic asphaltites from the southern Australian margin: molecular and carbon isotopic composition. *PESA Journal*, 26, 106-129.

- Edwards, D.S., Struckmeyer, H.I.M., Bradshaw, M.T., & Skinner, J.E. (1999). Geochemical characteristics of Australia's Southern Margin petroleum systems. *The APEA Journal*, 39, 297-321.
- Edwards, D.S., Vinall, D.R., Corrick, A.J., & McKirdy, D.M. (2016). Natural bitumen stranding on the ocean beaches of Southern Australia: a historical and geospatial review. *Transactions of the Royal Society of South Australia*, 140(2), 152-185.
- Eglinton, G., & Hamilton, R.J. (1967). Leaf epicuticular waxes. *Science*, 156, 1322-1335.
- Elias, V.O., Simoneit, B.R.T., & Cardoso, J.N. (1997). Even n-alkanes predominance on the Amazon Shelf and a Northeast Pacific hydrothermal system. *Naturwissenschaften*, 84, 415-420.
- Etioppe, G., & Lollar, B.S., (2013). Abiotic methane on Earth. *Reviews of Geophysics*, 51, 276-299
- Farrimond, P., Talbot, H.M., Watson, D.F., Schulz, L.K., & Wilhelms, A. (2004). Methylhopanoids: molecular indicators of ancient bacteria and a petroleum correlation tool. *Geochimica et Cosmochimica Acta*, 68(19), 3873-3882.
- Feary, D.A., & James, N.P. (1998). Seismic stratigraphy and geological evolution of the Cenozoic, cool-water Eucla Platform, Great Australian Bight. *AAPG Bulletin*, 82, 792-816.
- Fowler, M.G. (1992). The influence of *Gloeocapsomorpha prisca* on the organic geochemistry of oils and organic rich rocks of Late Ordovician age from Canada. In M. Schidlowski, and et al. (eds.), *Early Organic Evolution: Implications for Mineral and Energy Resources*: Berlin, Springer-Verlag, 336-356.
- Fraser, A.R., & Tilbury, L.A. (1979). Structure and stratigraphy of the Ceduna Terrace region, Great Australian Bight. *The APEA Journal*, 19(1), 53-65.
- Gang, W., Gao, G., Hao, S., & Zhu, L. (1997). Carbon isotope of ethane applied in the analyses of genetic types of natural gas. *Petroleum Exploration and Development*, 19(2), 164-167.
- Garrigues, P., Connan, J., Parlanti, E., Bellocq, J., & Ewald, M. (1988). Relationship between rank and distribution of methylaromatic hydrocarbons for condensates of different origins. *Organic Geochemistry*, 13, 1115-1121.
- Gelpi, E., Schneider, H., Mann, J., & Oró, J. (1970). Hydrocarbons of geochemical significance in microscopic algae. *Phytochemistry*, 9(3), 603-612.
- George, S.C., Boreham, C.J., Minifie, S.A., & Teerman, S.C. (2002). The effect of minor to moderate biodegradation on C5 to C9 hydrocarbons in crude oils. *Organic Geochemistry*, 33(12), 1293-1317.
- George, S.C., Volk, H., & Ahmed, M. (2007). Geochemical analysis techniques and geological applications of oil-bearing fluid inclusions, with some Australian case studies. *Journal of Petroleum Science and Engineering*, 57(1-2), 119-138.
- Georgiev, G.M., Kalkanjev, T.K., Petrov, V.P., & Nickolov, Z.H. (1984). Determination of salts in water solutions by a skewing parameter of the water Raman band. *Applied Spectroscopy*, 38, 593-595.
- Gnarlyknots-1 & 1A (2003). Well completion report, EPP-29, Cedina Sub-basin – basic data.
- Gnarlyknots-1 & 1A (2004). Well completion report, EPP-29, Cedina Sub-basin – interpretive data.
- Goldstein, R.H., & Reynolds, T.J. (1994). Systematics of fluid inclusions in diagenetic minerals. *SEPM (Society for Sedimentary Geology)*, Short Course 31, Tulsa, Oklahoma.

- Gould, K.W., Hart, G.N., & Smith, J.W. (1981). Technical note: carbon dioxide in the southern coalfields N.S.W.: a factor in the evaluation of natural gas potential. *Proceedings of the Australasian Institute of Mining and Metallurgy*, 279, 41-42.
- Grice, K., Alexander, R., & Kagi, R.I. (2000). Diamondoid hydrocarbon ratios as indicators of biodegradation in Australian crude oils. *Organic Geochemistry*, 31(1), 67-73.
- Grice, K., Audino, M., Boreham, C.J., Alexander, R., & Kagi, R.I. (2001). Distributions and stable carbon isotopic compositions of biomarkers in torbanites from different palaeogeographical locations. *Organic Geochemistry*, 32, 1195-1120.
- Guillaume, D., Teinturier, S., Dubessy, J., & Pironon, J. (2003). Calibration of methane analysis by Raman spectroscopy in H₂O–NaCl–CH₄ fluid inclusions. *Chem. Geol.* 194, 41-49.
- Hadley, M., Hall, D., Sterner, M., & Shentwu, W. (1997). Hydrocarbon pay delineation and product characterization with fluid inclusions: examples from East Coast of Canada and Western Canada Sedimentary Basin. In: *Site* (Canadian Well Logging Society), 1, 2-4.
- Hall, A.P., McKirdy, D.M., Grice, K., & Edwards, D.S. (2014). Australasian asphaltite strandings: Their origin reviewed in light of the effects of weathering and biodegradation on their biomarker and isotopic profiles. *Marine and Petroleum Geology*, 57, 572-593.
- Hill, A.J. (1995). Bight Basin. In: Drexel, J.F. and Preiss, W.V. (Editors), *The Geology of South Australia, Vol.2, The Phanerozoic*. Geological Survey of South Australia Bulletin, 54, 133-149.
- Holba, A.G., Dzou, L.I.P., Masterson, W.D., Hughes, W.B., Huizinga, B.J., Singletary, M.S., Moldowan, J.M., Mello, M.R., & Tegelaar, E., (1998a). Application of 24-norcholestanes for constraining source age of petroleum. *Organic Geochemistry*, 29(5-7), 1269-1283.
- Holba, A.G., Dzou, L.I., Wood, G.D., Ellis, L., Adam, P., Schaeffer, P., Albrecht, P., Greene, T., & Hughes, W.B. (2003). Application of tetracyclic polyprenoids as indicators of input from fresh-brackish water environments. *Organic Geochemistry*, 34, 441-469.
- Holba, A.G., Tegelaar, E., Ellis, L., Singletary, M.S., & Albrecht, P. (2000). Tetracyclic polyprenoids: Indicators of freshwater (lacustrine) algal input. *Geology*, 28, 251-254.
- Holba, A.G., Tegelaar, E.W., Huizinga, B.J., Moldowan, J.M., Singletary, M.S., McCaffrey, M.A., & Dzou, L.I.P., (1998b). 24-Norcholestanes as age-sensitive molecular fossils. *Geology*, 26, 783-786.
- Huang, W.Y., & Meinshein, W.G. (1979). Sterols as ecological indicators. *Geochimica et Cosmochimica Acta*, 43, 739-745.
- Hughes, W.B., Holba, A.G., & Dzou, L.I. (1995). The ratios of dibenzothiophene to phenanthrene and pristane to phytane as indicators of depositional environment and lithology of petroleum rocks. *Geochimica et Cosmochimica Acta*, 59, 3581-3598.
- Jiang Z., & Fowler, M. G. (1986). Carotenoid-derived alkanes in oils from northwestern China, in D. Leythaeuser, and J. Rullkötter, eds., *Advances in Organic Geochemistry 1985*, *Organic Geochemistry*, 10, 831-839.
- Larsen, R.B. Brooks, C.K., & Bird, D.K. (1992). Methane-bearing, aqueous, saline solutions in the Skaergaard intrusion, east Greenland. *Contrib. Mineral Petrol.*, 112, 428-437.
- Lin, F., Sum, A.K., & Bodnar, R.J. (2007). Correlation of methane Raman ν_1 band position with fluid density and interactions at the molecular level. *Journal of Raman Spectroscopy*, 38, 1510-1515.

- Lisk, M., Hall, D., Ostby, J., & Brincat, M.P. (2001). Addressing the oil migration risks in the Great Australian Bight. PESA Eastern Australasian Basins Symposium, 25-28 November 2001, Melbourne, Australia, 553-562.
- Lisk, M., O'Brien, G.W. & Eadington, P.J. (2002). Quantitative evaluation of the oil-leg potential in the Oliver gas field, Timor Sea, Australia. AAPG Bulletin, 86(9), 1531-1542.
- Liu, K., & Eadington, P.E. (1998). Hydrocarbon petrography of Jerboa-1, Eyre Sub-basin, the Great Australian Bight. CSIRO Petroleum Confidential Report, 98-031, Australia (unpublished).
- Liu, K., Fenton, S. Bastow, T., van Aarssen, B., & Eadington, P. (2005). Geochemical evidence of multiple hydrocarbon charge and long distance oil migration in the Vulcan Sub-basin, Timor Sea. APPEA Journal, 45(1), 493-509.
- Lu, W., Chou, I.M., Burruss, R.C., & Song, Y. (2007). A unified equation for calculating methane vapor pressures in the CH₄–H₂O system with measured Raman shifts. *Geochimica et Cosmochimica Acta*, 71, 3969-3978.
- MacDonald, J.D., Holford, S.P., Green, P.F., Duddy, I.R., King, R.C. & Backé, G. (2013). Detrital zircon data reveal the origin of Australia's largest delta system. *Journal of the Geological Society*, 170, 3-6.
- McBirde E.F. (1989). Quartz cement in sandstones: a review. *Earth Science Reviews*, 26, 69-112.
- McKirdy, D.M., & Chivas, A.R. (1992). Nonbiodegraded aromatic condensate associated with volcanic supercritical carbon dioxide, Otway Basin: implications for primary migration from terrestrial organic matter. *Organic Geochemistry*, 18, 611-627.
- McKirdy, D.M., Cox, R.E., Volkman, J.K., & Howell, V.J. (1986). Botryococcane in a new class of Australian non-marine crude oils. *Nature*, 320, 57-59.
- McKirdy, D.M., Summons, R.E., Padley, D., Serafini, K.M., Boreham, C.J., & Struckmeyer, H.I.M. (1994). Molecular fossils in coastal bitumens from southern Australia: signatures of precursor biota and source rock environments. *Organic Geochemistry*, 21, 265-286.
- Mello, M.R., Koutsoukos, E.A.M., Hart, M.B., Brassell, S.C., & Maxwell, J.R. (1990). Late Cretaceous anoxic events in the Brazilian continental margin. *Organic Geochemistry*, 14, 529-542.
- Mello, M.R., Telnaes, N., Gaglianone, P.C., Cheicarelli, M.I., Brassell, S.C., & Maxwell, J.R. (1988). Organic geochemical characterisation of depositional palaeoenvironments of source rocks and oils in Brazilian marginal basins. *Organic Geochemistry*, 13, 31-45.
- Mernagh, T.P. & Wilde, A.R. (1989). The use of laser Raman microprobe for the determination of salinity in fluid inclusions. *Geochimica et Cosmochimica Acta*, 53, 765–771.
- Messent, B.E.J. (1998). Great Australian Bight: well audit. Australian Geological Survey Organization Record 1998/37.
- Messent, B.E.J., Wilson, C., & Flynn, K. (1996). Assessment of the seal potential of Tertiary carbonates, Duntroon Basin, South Australia. *The APPEA Journal*, 36, 233-247.
- Moldowan, J.M., Dahl, J., Huizinga, B.J., Fago, F.J., Hickey, L.J., Peakman, T.M., & Taylor, D.W (1994). The molecular fossil record of oleanane and its relation to angiosperms. *Science*, 265, 758-771.
- Moldowan, J.M., Fago, F.J., Carlson, R.M.K., Young, D.C., Van Duyne, G., Clardy, J., Schoell, M., Pillinger, C.T., & Watt, D.S. (1991). Rearranged hopanes in sediments and petroleum. *Geochimica et Cosmochimica Acta*, 55, 3333-3353.

- Moldowan, J. M., Seifert, W. K., Arnold, E., & Clardy, J. (1984). Structure proof and significance of stereoisomeric 28, 30-bisnorhopanes in petroleum and petroleum source rocks: *Geochimica et Cosmochimica Acta*, 48, 1651-1661.
- Moldowan, J. M., Seifert, W. K., & Gallegos, E. J. (1985). Relationship between petroleum composition and depositional environment of petroleum source rocks: *AAPG Bulletin*, 69, 1255-1268.
- Moldowan, J.M., Fago, F.J., Lee, C.Y., Jacobson, S.R., Watt, D.S., Slougui, N. E., Jeganathan, A., & Young, D.C., (1990). Sedimentary 24-n-propylcholestanes, molecular fossils diagnostic of marine algae. *Science*, 247, 309-312.
- Moldowan, J.M., & Seifert, W.K. (1980). First discovery of botryococcane in petroleum. *Journal of Chemical Society, Chemical Communications*, 912-914.
- Moldowan, J. M., Dahl, J., Huizinga, B. J., Fago, F. J., Hickey, L. J., Peakman, T. M., & Taylor, D. W. (1994). The molecular fossil record of oleanane and its relation to angiosperms. *Science*, 265, 768 - 771.
- Montel, F. (1993). Phase Equilibria needs for petroleum exploration and production industry. *Fluid Phase Equilibria*, 84, 343-367.
- Ni, Y., Dai, J., Zhu, G., Zhang, S., Zhang, D., Su, J., Tao, X., Liao, F., Wu, W., Gong, D., & Liu, D. (2013). Stable hydrogen and carbon isotopic ratios of coal-derived and oil-derived gases: A case study in the Tarim basin, NW China. *International Journal of Coal Geology* 116-117, 302-313.
- Noble, R.A., Alexander, R., Kagi, R.I., & Knox, J. (1985b). Tetracyclic diterpenoid hydrocarbons in some Australian, coals, sediments and crude oils. *Geochimica et Cosmochimica Acta*, 49, 2141-2147.
- Noble, R.A., Alexander, R., Kagi, R.I., Knox, J., Leythaeuser, D.E., & Rullkötter, J.E. (1986). Identification of some diterpenoid hydrocarbons in petroleum. In: *Advances in organic geochemistry 1985; Part II, Molecular and general organic geochemistry*, 10, 825-829. Pergamon, Oxford-New York, International.
- Noble, R., Knox, J., Alexander, R., & Kagi, R.I. (1985a). Identification of tetracyclic diterpene hydrocarbons in Australian crude oils and sediments. *Organic Geochemistry*, 10(4-6), 825-829.
- Norvick, M.S., & Smith, M.A. (2001). Mapping the plate tectonic reconstruction of southern and southeastern Australia and implications for petroleum systems. *The APPEA Journal*, 41(1), 15–35.
- O’Neil, B.J. (2003). History of Petroleum Exploration. In: O’Brien, G.W., Paraschivoiu, E. and Hibburt, J.E. (eds), *Petroleum Geology of South Australia*, Vol. 5: Great Australian Bight.
- Padley, D. (1995). Petroleum geochemistry of the Otway Basin and the significance of coastal bitumen strandings on adjacent southern Australian beaches, Ph.D. Thesis, Department of Geology and Geophysics, The University of Adelaide (Unpublished).
- Peters, K. E., & Moldowan J. M. (1991). Effects of source, thermal maturity and biodegradation on the distribution and isomerization of homohopanes in petroleum: *Organic Geochemistry*, 17, 47-61.
- Peters, K.E., Walters, C., & Moldowan, J.M., (2005). *The Biomarker Guide*, Cambridge University Press, Cambridge.
- Petrov, A.A., Arefjev, O.A., & Yakubson, Z.V. (1974). Hydrocarbons of adamantane series as indices of petroleum catagenesis process. In: B. Tissot, F. Biennet (Eds.), *Advances in Organic Geochemistry*, Editions Technip, Paris, 517-522.

- Philp, R.P., & Gilbert, T.D., (1986). Biomarker distributions in oils predominantly derived from terrigenous source material. In: D. Leythaeuser, J. Rullkötter (eds.), *Advances in Organic Geochemistry 1985*, Pergamon Press, Jülich, 73-84.
- Pironon, J. (2004). Fluid inclusions in petroleum environments: analytical procedure for PTX reconstruction: *Acta Petrologica Sinica*, 20(6), 1333-1342.
- Pironon, J., Canals, M., Dubessy, J., Walgenwitz, F., & Laplace-Builhe, C. (1998). Volumetric reconstruction of individual oil inclusions by confocal scanning laser microscopy. *European Journal of Mineralogy*, 10, 1143-1150.
- Preston, J.C., & Edwards, D.S. (2000). The petroleum geochemistry of oils and source rocks from the northern Bonaparte Basin, offshore northern Australia. *The APPEA Journal*, 40(1), 257-282.
- Radke, M. (1988). Application of aromatic compounds as maturity indicators in source rocks and crude oils. *Marine and Petroleum Geology*, 5, 224-236.
- Radke, M., Leythaeuser, D., & Teichmüller, M. (1984). Relationship between rank and composition of aromatic hydrocarbons from coals of different origins. *Organic Geochemistry*, 6, 423-430.
- Radke, M., Rullkötter, J., & Vriend, S. P. (1994). Distribution of naphthalenes in crude oils from the Java Sea: source and maturation effects. *Geochimica et Cosmochimica Acta*, 58, 3675-3689.
- Radke, M., & Welte, D.H. (1983). The methylphenanthrene index (MPI): a maturity parameter based on aromatic hydrocarbons. In: (M. Bjørøy et al. (eds.), *Advances in Organic Geochemistry*, John Wiley, Chichester, 504-512.
- Roedder, E. (1984). Fluid inclusions. *Mineralogical Society of America, Reviews in Mineralogy*, 12.
- Roedder, E., & Bodnar, R.J. (1980). Geological pressure determination from fluid inclusion studies. *Annu. Rev. Earth Planet. Sci.*, 8, 263-301.
- Ruble, T.E., George, S.C., Lisk, M., & Quezada, R.A. (1998). Organic compounds trapped in aqueous fluid inclusions. *Organic Geochemistry*, 29, 195-205.
- Ruble, T.E., Logan, G.A., Blevin, J.E., Struckmeyer, H.I.M., Liu, K., Ahmed, M., Eadington, P.J., & Quezada, R.A. (2001). Geochemistry and charge history of a palaeo-oil column: Jerboa-1, Eyre Sub-basin, Great Australian Bight. In: Hill, K.C. and Bernecker, T. (Eds), *Eastern Australasian Basins Symposium: a refocused energy perspective for the future*. Petroleum Exploration Society of Australia, Special Publication, 521-530.
- Schaefer, R.G. (1992). Zur Geochemie niedrigmolekularer Kohlenwasserstoffe im Posidonienschiefer der Hilsmulde. *Erdöl und Kohle. Erdgas, Petrochemie* 45, 73-78.
- Schiefelbein, C.F., Zumberge, J.E., Cameron, N.R., & Brown, S.W. (1999). Petroleum systems in the South Atlantic margins. In: N.R. Cameron, R.H. Bate and V.S. Clure (Eds), *The oil and gas habitats of the South Atlantic*, Geological Society of London Special Publication, 169-179.
- Schoell, M., McCaffery, M.A., Fago, F.J., & Moldowan, J.M. (1992). Carbon isotope compositions of 28, 30-bisnorhopanes and other biological markers in a Monterey crude oil. *Geochimica et Cosmochimica Acta*, 56, 1391-1399.
- Schofield, A., & Totterdell, J.M. (2008). Distribution, timing and origin of magmatism in the Bight and Eucla Basins. *Geoscience Australia, Record 2008/24*, 19 p.
- Schulz, L.K., Wilhelms, A., Rein, E., & Steen, A.S. (2001). Application of diamondoids to distinguish source rock facies. *Organic Geochemistry*, 32(3), 365-375.
- Seifert, W.K., & Moldowan, J.M. (1986). Use of biological markers in petroleum exploration. In: R.B. Johns (Ed.), *Methods in geochemistry and geophysics*, 24, 261-290.

- Seitz, J.C., Pasteris J.D., & Chou, I.M. (1993). Raman spectroscopic characterization of gas mixtures. I. Quantitative composition and density determination of CH₄, N₂, and their mixtures. *Am. J. Sci.* 293, 297–321.
- Seitz, J.C., Pasteris J.D., & Chou I.M. (1996). Raman spectroscopic characterization of gas mixtures. II. Quantitative composition and pressure determination of the CO₂–CH₄ system. *Am. J. Sci.*, 296, 577–600.
- Shen, P., & Xu, Y. (1991). *Geochemical characteristics of gas source rocks and natural gas genesis*. Gansu Science and Technology Press, Lanzhou.
- Sinninghe Damsté, J.S., Kenig, F., Koopmans, M.P., Köster, J., Schouten, S., Hayes, J.M., & Leeuw, J.W.D. (1995). Evidence for gammacerane as an indicator of water column stratification. *Geochimica et Cosmochimica Acta*, 59, 1895–1900.
- Smith, M.A., & Donaldson, I.F. (1995). The hydrocarbon potential of the Duntroon Basin. *The APEA Journal*, 35(1), 203–219.
- Sofer, Z. (1993). Distribution of genetic oil families in West Africa based on biomarker ratios. In: M. R. Mello and L. A. F. Trindade (eds.), *Third Latin American Congress on Organic Geochemistry, ALAGO*, Oxford, 134–137.
- Stalker, L. (2013). *Methane origins and behaviour*. CSIRO Report EP1310665, Australia.
- Strachan, M.G., Alexander, R., & Kagi, R.I. (1988). Trimethylnaphthalenes in crude oils and sediments: effects of source and maturity. *Geochimica et Cosmochimica Acta*, 52, 1255–1264.
- Stasiuk, L.D., & Snowdon, L.R. (1997). Fluorescence micro-spectrometry of synthetic and natural hydrocarbon fluid inclusions: crude oil chemistry, density and application to petroleum migration. *Applied Geochemistry*, 12, 229–241.
- Struckmeyer, H.I.M. (2009). Ceduna Sub-basin, Bight Basin: results of 3D petroleum systems modelling. Geoscience Australia, Geocat no. 69485.
- Struckmeyer, H.I.M., Totterdell, J.M., Blevin, J.E., Logan, G.A., Boreham, C.J., Deighton, I., Krassay, A.A., & Bradshaw, M.T. (2001). Character, maturity and distribution of potential Cretaceous oil source rocks in the Ceduna Sub basin, Bight Basin, Great Australian Bight. In: Hill, K.C. and Bernecker, T. (eds), *Eastern Australian Basin Symposium: a refocused energy perspective for the future*. Petroleum Exploration Society of Australia, Special Publication, 543–552.
- Subroto, E.A., Alexander, & R., Kagi, R.I. (1991). 30-Norhopanes: their occurrence in sediments and crude oils. *Chemical Geology*, 93, 179–192.
- Summons, R.E., Bradshaw, J., Burchardt, D.M., Goody, A.K., Murray, A.P., & Foster, C.B. (1993). Hydrocarbon composition and origins of coastal bitumens from the Northern Territory. *The APEA Journal*, 21(1), 31–42.
- Summons, R.E., & Capon, R.J. (1988). Fossil steranes with unprecedented methylation in ring A. *Geochimica et Cosmochimica Acta*, 52, 2733–2736.
- Summons, R.E., & Jahnke, L.L. (1990). Identification of the methylhopanes in sediments and petroleum. *Geochimica et Cosmochimica Acta*, 54, 247–251.
- Summons, R.E., Jahnke, L.L., Hope, J.M., & Logan, G.A. (1999). 2-Methylhopanoids as biomarkers for cyanobacterial oxygenic photosynthesis. *Nature*, 400, 554–557.
- Summons, R.E., Volkman, J.K., & Boreham, C.J. (1987). Dinosterane and other steroidal hydrocarbons of dinoflagellate origin in sediments and petroleum. *Geochimica et Cosmochimica Acta*, 51, 3075–3082.

- Sun, Q., Zhao, L., Li, N., & Liu, J. (2010). Raman spectroscopic study for the determination of Cl⁻ concentration (molarity scale) in aqueous solutions: Application to fluid inclusions. *Chemical Geology*, 272, 55–61.
- Tapley, D., Mee, B.C., King, S.J., Davis, R.C., & Leischner, K.R. (2005). Petroleum potential of the Ceduna Sub-basin: impact of Gnarlyknots-1A. *The APPEA Journal*, 45(1), 365–380.
- Teasdale, J.P., Pryer, L.L., Stuart-Smith, P.G., Romine, K.K., Etheridge, M.A., Loutit, T.S., & Kyan, D.M. (2003). Structural framework and basin evolution of Australia's southern margin. *The APPEA Journal*, 43 (1), 13–37.
- ten Haven, H.L. (1996). Application and limitations of Mango's light hydrocarbon parameters in petroleum correlation studies. *Organic Geochemistry*, 24, 957-976.
- ten Haven, H.L., de Leeuw, J.W., Rullkötter, J., & Sinninghe Damste, J.S. (1987). Restricted utility of the pristane/phytane ratio as a paleoenvironmental indicator: *Nature*, 330, 641-643.
- ten Haven, H.L., de Leeuw, J.W., Sinninghe Damste, J.S., Schenck, P.A., Palmer, S.E. & Zumberge, J.E. (1988). Application of biological markers in the recognition of palaeo-hypersaline environments, In: K. Kelts, A. Fleet, and M. Talbot (eds.), *Lacustrine Petroleum Source Rocks: Geological Society Special Publication*, 40, Blackwell, 123-130.
- Thiéry, R., Pironon, J., Walgenwitz, F., & Montel, F. (2000). PIT (Petroleum Inclusion Thermodynamics): a new modelling tool for the characterisation of hydrocarbon fluid inclusions from volumetric and microthermometric measurements. *Journal of Geochemical Exploration*, 69-70, 701-704.
- Thiéry, R., Pironon, J., Walgenwitz, F., & Montel, F. (2002). Individual characterisation of petroleum fluid inclusions (composition and P-T trapping conditions) by microthermometry and confocal laser scanning microscopy: inferences from applied thermodynamics of oils. *Marine and Petroleum Geology*, 19, 847-859.
- Thiéry, R., van den Kerkhof, A.M., & Dubessy, J. (1994) v_X properties of CH₄-CO₂ and CO₂-N₂ fluid inclusions: modelling for T < 31°C and P < 400 bar. *European Journal of Mineralogy*, 6, 753–771.
- Tikku, A., & Cande, S.C. (1999). The oldest magnetic anomalies in the Australian-Antarctic Basin. *Journal of Geophysical Research*, 104(1), 661-677.
- Thompson, K.F.M. (1979). Light hydrocarbons in subsurface sediments. *Geochimica et Cosmochimica Acta*, 43, 657-672.
- Thompson, K.F.M. (1987). Fractured aromatic petroleum and the generation of gas-condensate. *Organic Geochemistry*, 11, 573-590.
- Totterdell, J.M., Blevin, J.E., Struckmeyer, H.I.M., Bradshaw, B.E., Colwell, J.B., & Kennard, J.M. (2000). A new sequence framework for the Great Australian Bight: starting with a clean slate. *The APPEA Journal*, 40(1), 95–117.
- Totterdell, J.M., & Bradshaw, B.E. (2004). The structural framework and tectonic evolution of the Bight Basin. In: Boulton, P.J., Johns, D.R. and Lang, S.C. (eds), *Eastern Australasian Basins Symposium II. Petroleum Exploration Society of Australia, Special Publication*, 41–61.
- Totterdell, J.M., & Mitchell, C. eds (2009). Bight Basin geological sampling and seepage survey, R/V Southern Surveyor Survey SS01/2007: post-survey report. *Geoscience Australia Record* 2009/24.
- Totterdell, J.M., Struckmeyer, H.I.M., Boreham, C.J., Mitchell, C.H., Monteil, E., & Bradshaw, B.E. (2008). Mid–Late Cretaceous organic-rich rocks from the eastern Bight Basin: implications for prospectivity. In: Blevin, J.E., Bradshaw, B.E. and Uruski, C. (eds), *Eastern Australasian Basins Symposium III, Petroleum Exploration Society of Australia, Special Publication*, 137–158.

- Totterdell, J.M., Struckmeyer, H.I.M., & Stacey, A.R. (2010). Bight Basin acreage release-new exploration opportunities in a deep water frontier. *PESA News*, December/January 2009/2010.
- Totterdell and Bradshaw, 2009 Basin Evolution and Tectonostratigraphic Framework –does this exist or is the referwence wrong???
- van Aarssen, B.G.K., Cox, H.C., Hoogendoorn, P., & de Leeuw, J.W. (1990). A cadinene biopolymer present in fossil and extant dammar resins as a source for cadinanes and bicadinanes in crude oils from South East Asia. *Geochemica et Cosmochimica Acta*, 58(1), 223-229.
- Walderhaug, O. (1994). Precipitation rates for quartz cement in sandstones determined by fluid-Inclusion microthermometry and temperature-history modeling: *Journal of Sedimentary Research*, A64, p. 324-333.
- Whiticar, M.J. (1999). Carbon and hydrogen isotope systematics of bacterial formation and oxidation of methane. *Chemical Geology*, 161, 291–314.
- Willcox, J.B., & Stagg, H.M.J. (1990). Australia's southern margin: a product of oblique extension. *Tectonophysics*, 173, 269–281.
- Wingert, W.S., (1992). GS-MS analysis of diamondoid hydrocarbons in Smackover petroleums. *Fuel*, 71, 37-43.
- Wycherley, H., Fleet, A., & Shaw, H. (1999). Some observations on the origins of large volumes of carbon dioxide accumulations in sedimentary basins. *Marine and Petroleum Geology*, 16, 489-494.
- Xiao, Z., Xie, Z., Li, Z., & Ma, C. (2008). Isotopic characteristics of natural gas of Xujiache Formation in southern and middle of Sichuan basin. *Geochimica*, 37(3), 245-250.
- Zheng, S.L., & Wang, X. (2010). An Undercover Angiosperm from the Jurassic of China. *Acta Geologica Sinica-English Edition*, 84(4), 895-902.
- Zhu, G., Wang, Z., Dai, J., & Su, J. (2014). Natural gas constituent and carbon isotopic composition in petroliferous basins, China. *Journal of Asian Earth Sciences*, 80, 1-17.

APPENDIX 1: DATA MANAGEMENT

Raw Datasets Created

Grains containing Oil Inclusions (GOI)

- GOI % – the proportion of oil-bearing inclusions divided by the total number of grains.
- Description of oil-bearing inclusions used to calculate GOI.
- Assemblage attributes:
 - Fluorescence color.
 - Location in grain.
 - Bubble size and variability.

Molecular Composition of oil Inclusions (MCI) – Offline

- Aliphatic hydrocarbon concentrations.
- Partial mass chromatograms and peak identifications: m/z 85, m/z 113.13, m/z 123.12, m/z 191.18, m/z 177.16, m/z 205.20, m/z 370 → 191, m/z 384 → 191, m/z 398 → 191, m/z 412 → 191, m/z 426 → 191, m/z 440 → 191, m/z 454 → 191, m/z 468 → 191, m/z 482 → 191, m/z 217, m/z 218, m/z 259.24, m/z 231.21, m/z 372 → 217, m/z 386 → 217, m/z 400 → 217, m/z 358 → 217, m/z 414 → 217, m/z 414 → 231, m/z 253.2, m/z 231.12, m/z 106.08, m/z 120.09, m/z 134.11, m/z 128.06, m/z 142.08, m/z 156.09, m/z 170.11, m/z 184.13, m/z 198.14, m/z 197.13, m/z 183.12, m/z 198.14, m/z 178.08, m/z 192.09, m/z 206.11, m/z 220.13, m/z 234.14, m/z 154.08, m/z 168.09, m/z 182.11, m/z 166.08, m/z 180.09, m/z 202.08, m/z 216.09, m/z 184.03, m/z 198.05, m/z 212.07, m/z 136.1, m/z 135.1, m/z 149.1, m/z 163.1, m/z 177.1, m/z 188.2, m/z 187.1, m/z 201.2 and m/z 215.2 chromatograms.

Molecular Composition of oil Inclusions (MCI) – On-line

- Partial mass chromatograms and peak identifications: m/z 57, m/z 70, m/z 71, m/z 85, m/z 56, m/z 68, m/z 78, m/z 82, m/z 55, m/z 91, m/z 97, m/z 99, m/z 57, m/z 57, m/z 97, m/z 106.
- TIC partial mass chromatograms and peak identifications: m/z 57, m/z 55.

Carbon isotopic composition of fluid inclusion gases:

- $\delta_{13}\text{C}_{\text{CH}_4}$ (‰)
- $\delta_{13}\text{C}_{\text{C}_2\text{H}_6}$ (‰)
- $\delta_{13}\text{C}_{\text{CO}_2}$ (‰)

PVT

- Homogenisation temperatures (Th) – oil and water inclusions.
- Vapour volume fraction at 20°C (confocal microscopy) – oil inclusions.
- Salinity (Tm ice or Raman) – water inclusions.
- Methane pressure (Raman) – water inclusions.

Data Processing and Derived Datasets

Offline MCI – parameters and ratios:

- Aliphatic hydrocarbon parameters.
- Terpane parameters.
- Sterane and diasterane parameters.
- Aromatic hydrocarbon parameters.
- Diamondoid hydrocarbon parameters.
- Aliphatic hydrocarbon distributions.

Low molecular weight hydrocarbon parameters

- $i\text{-C}_5/n\text{-C}_5$
- A; Benzene/ $n\text{-C}_6$
- B; Toluene/ $n\text{-C}_7$
- C: $(n\text{-C}_6+n\text{-C}_7)/(\text{CH}+\text{MCH})$
- Heptane value (H)
- Isoheptane value (I)
- F: $n\text{-C}_7/\text{MCH}$
- U: CH/MCP
- R: $n\text{-C}_7/2\text{-MH}$
- $n\text{-C}_7/\text{MCP}$
- 3-MP/Benzene
- MCH/Toluene
- CH/Benzene
- 3-MP/ $n\text{-C}_6$
- Benzene/toluene
- MCP/MCH
- Toluene/*o*-xylene
- *m*-+*p*-xylene/ $n\text{-C}_8$
- $K_1: (2\text{-MH}+23\text{-DMP})/(3\text{-MH}+24\text{-DMP})$
- 2-MH/3-MH
- $n\text{-C}_7$ (% of total C_7 hydrocarbons)
- 3 ring preference % (DMP+MH)
- 5 ring preference % (DMCP+ECP)
- 6 ring preference % (MCH+toluene)
- $(2\text{MH}+3\text{MH})/(c13\text{DMCP}+t13\text{DMCP}+t12\text{DMCP})$
- Rc (J)

PVT

- Bubble/dew point curves and isochors for oil (PIT modelling).
- Oil compositions (PIT modelling).
- Bubble point curves and isochors for aqueous fluids.

Data Curation and Archive

Data files (raw data, derived datasets, working files, reports) relating to the project are currently stored CSIRO's network in secure locations only accessible to personnel listed in the GAB Research Program - Project Plan 5.3.

Data Access, Use Agreements and Licensing

None required.

Publication of Datasets

National Offshore Petroleum Data & Core Repository (NOPDCR) Approval No: N00074 (and ext.).

- Kempton, R (2015) GOI™ results from petroleum wells in the Great Australian Bight. CSIRO report EP155295 (open file), 1 July 2015, 30p. Statutory report to NOPDCR.
- Gong, S (2015) MCI geochemistry from Gnarlyknots-1A & Greenly-1, Great Australian Bight. CSIRO report EP155315 (open file), 4 September 2015, 127p. Statutory report to NOPDCR.
- Bourdet, J (2015) Pressure/temperature constraints of hydrocarbon migration in Gnarlyknots-1A & Greenly-1, Great Australian Bight. CSIRO report EP155317 (open file), 10 September 2015, 36p. Statutory report to NOPDCR.

National Offshore Petroleum Data & Core Repository (NOPDCR) Approval No: N00335.

- Yet to be finalised.

APPENDIX 2: PROJECT PUBLICATIONS

Papers

Kempton, R.*, Bourdet, J, Gong, S., Ross, R. and Pironon, J. (2017). Petroleum migration in the Bight Basin: a fluid inclusion approach to constraining source, composition and timing. The APPEA Journal 2017, 57, 762–766. <http://dx.doi.org/10.1071/AJ16222>.

Presentations

1. Geofluids VIII 2016: June 23-25 2016, Wuhan, China.

Bourdet, J*, Kempton, R., Ross, R. and Pironon, J. “Petroleum migration in the Bight Basin: a fluid inclusion approach to constraining composition and timing”. Abstract and oral presentation (*presenter).

2. Australian Earth Sciences Convention (AESC); 26-30 June 2016, Adelaide.

Kempton, R.*, Bourdet, J, Gong, S., Ross, R. and Pironon, J. “Petroleum migration in the Bight Basin: a fluid inclusion approach to constraining source, composition and timing”. Abstract and oral presentation (*presenter).

3. The Geological Society, Petroleum Group conference; “Application of Analytical Techniques to Petroleum Systems Problems”; 28 Feb-1 March 2017, London.

Kempton, R.*, Bourdet, J, Gong, S., Ross, R. and Pironon, J. “Using fluid inclusions to trace petroleum systems – a integrated case study of oil and gas migration in the Bight Basin to constrain source, composition and timing”. Abstract and oral presentation (*presenter).

Patents

None

Media Releases

None

APPENDIX 3: INTELLECTUAL PROPERTY

Unique discoveries

The results of Project 5.3 would be of commercial interest to other parties with interests in the Great Australian Bight. It is, however, a statutory requirement of the National Offshore Petroleum Data & Core Repository (NOPDCR), on behalf of the Commonwealth Government, that results data be made available 6 months from the date of sampling.

Action plan

None required

APPENDIX 4: Molecular Composition of oil Inclusions (MCI) – Tables & Figures

Table A4-31: Aliphatic hydrocarbon concentrations of the FI oil, associated system blank and final outside rinse.

Compound	Gnarlyknots- 1A FI oil/ng	BLK_MB/ng	OR-3/ng	Greenly- 1 FI oil/ng	BLK_ME/ng	OR-5/ng
<i>n</i> -C ₈	3.4	0.4	0.2	1.4	0.0	0.1
<i>n</i> -C ₉	8.8	0.4	0.4	4.8	0.0	0.2
<i>n</i> -C ₁₀	11.2	0.2	0.5	8.3	0.0	0.2
<i>n</i> -C ₁₁	20.2	0.2	0.2	15.2	0.0	0.4
<i>n</i> -C ₁₂	26.4	0.0	0.1	23.7	0.0	0.3
<i>n</i> -C ₁₃	30.5	0.0	0.0	37.0	0.0	1.1
<i>n</i> -C ₁₄	44.4	0.0	0.3	55.8	0.0	0.8
<i>n</i> -C ₁₅	48.7	0.0	0.5	82.5	0.0	1.4
<i>n</i> -C ₁₆	72.3	0.0	0.8	122.9	0.0	2.6
<i>n</i> -C ₁₇	52.4	1.2	2.0	191.4	0.0	3.7
<i>n</i> -C ₁₈	64.8	1.4	1.0	273.2	1.1	5.6
<i>n</i> -C ₁₉	44.1	0.7	0.5	371.1	0.2	4.1
<i>n</i> -C ₂₀	39.0	0.2	0.6	483.0	0.9	4.7
<i>n</i> -C ₂₁	33.7	0.1	0.4	626.8	0.6	3.6
<i>n</i> -C ₂₂	37.7	0.6	1.2	862.5	1.9	8.0
<i>n</i> -C ₂₃	40.1	0.6	1.1	1193.6	0.7	3.9
<i>n</i> -C ₂₄	46.6	1.1	1.9	1384.4	1.4	7.4
<i>n</i> -C ₂₅	53.2	1.2	1.9	1577.0	1.8	5.1
<i>n</i> -C ₂₆	53.9	1.4	1.9	1173.5	1.7	4.6
<i>n</i> -C ₂₇	56.2	1.3	0.0	987.7	2.1	0.0
<i>n</i> -C ₂₈	42.7	0.8	1.9	477.6	1.7	5.0
<i>n</i> -C ₂₉	37.0	0.5	1.4	324.7	1.5	4.2
<i>n</i> -C ₃₀	27.4	0.2	0.9	170.2	0.7	2.6
<i>n</i> -C ₃₁	22.6	0.0	0.5	119.6	0.8	1.9
<i>n</i> -C ₃₂	13.8	0.0	0.1	54.5	0.2	1.2
<i>n</i> -C ₃₃	8.5	0.0	0.0	34.4	0.1	0.3
<i>n</i> -C ₃₄	4.1	0.0	0.0	15.2	0.0	0.0
<i>n</i> -C ₃₅	2.4	0.0	0.0	9.1	0.0	0.0
<i>n</i> -C ₃₆	1.3	0.0	0.0	0.0	0.0	0.0
Σ ng alkanes <i>n</i> -C ₁₂ to <i>n</i> - C ₃₂	887.4	11.6	19.2	10592.6	17.4	73.0

Table A4-32: Aliphatic hydrocarbon parameters.

Parameter	Gnarlyknots-1A FI oil	Greenly-1 FI oil
Pr/Ph	1.5	3.0
Pr/ <i>n</i> -C ₁₇	0.40	0.51
Ph/ <i>n</i> -C ₁₈	0.22	0.12
CPI ₂₂₋₃₂	1.1	1.1
CPI ₂₄₋₃₂	1.1	1.2
CPI ₂₆₋₃₂	1.1	1.1
CPI ₂₆₋₃₀	1.1	1.1
CPI 2 ₂₆₋₂₈	1.2	1.2
CPI 2 ₂₈₋₃₀	1.1	1.0
CPI 2 ₂₀₋₂₂	0.88	0.93
<i>n</i> -C ₃₁ / <i>n</i> -C ₁₉	0.51	0.32
Wax index (<i>n</i> -C ₂₁₊₂₂ / <i>n</i> -C ₂₈₊₂₉)	0.90	1.9
Fractionation index (<i>n</i> -C ₁₀ / <i>n</i> -C ₁₆₊₂₅)	0.09	0.00

$$CPI_{22-32} = \left[\frac{2 * (C_{23} + C_{25} + C_{27} + C_{29} + C_{31})}{C_{22} + 2 * (C_{24} + C_{26} + C_{28} + C_{30}) + C_{32}} \right]$$

$$CPI_{24-32} = \left[\frac{2 * (C_{25} + C_{27} + C_{29} + C_{31})}{C_{24} + 2 * (C_{26} + C_{28} + C_{30}) + C_{32}} \right] \quad CPI_{26-32} = \left[\frac{2 * (C_{27} + C_{29} + C_{31})}{C_{26} + 2 * (C_{28} + C_{30}) + C_{32}} \right]$$

$$CPI_{26-30} = \left[\frac{2 * (C_{27} + C_{29})}{C_{26} + 2 * C_{28} + C_{30}} \right]$$

$$CPI \ 2_{26-28} = \left[\frac{2 \times C_{27}}{C_{26} + C_{28}} \right] \quad CPI \ 2_{28-30} = \left[\frac{2 \times C_{29}}{C_{28} + C_{30}} \right] \quad CPI \ 2_{20-22} = \left[\frac{2 \times C_{21}}{C_{20} + C_{22}} \right]$$

$$Wax \ Index = \left[\frac{C_{21} + C_{22}}{C_{28} + C_{29}} \right] \quad Fractionation \ Index = \left[\frac{C_{10}}{C_{16} + C_{25}} \right]$$

Table A4-33: Terpane parameters.

Parameter	Gnarlyknots-1A FI	Transition	Greenly-1 FI	Transition
	oil		oil	
Drimane/homodrimane	0.68	M191	0.43	M191
Ts/Tm	0.97	M191	0.69	MRM
Ts/(Ts+Tm)	0.49	M191	0.41	MRM
C ₂₉ Ts/C ₂₉ αβ hopane	0.23	M191	0.33	MRM
C ₂₉ Ts/(C ₂₉ Ts+C ₂₉ αβ hopane)	0.19	M191	0.25	MRM
C ₃₀ */C ₂₉ Ts	0.43	M191	1.78	M191
C ₂₉ */C ₂₉ αβ hopane	n.d.	MRM	0.14	MRM
C ₃₀ */C ₃₀ αβ hopane	0.08	MRM	0.07	MRM
C ₂₉ 25-norhopane/C ₂₉ αβ hopane	0.34	M191	n.d.	MRM
C ₂₉ αβ/(αβ+βα) hopanes	0.83	M191	0.82	M191
C ₃₀ αβ/(αβ+βα) hopanes	0.82	M191	0.86	M191
C ₃₁ αβ 22S/(22S+22R) hopanes	0.53	MRM	0.58	MRM
% C ₃₁ of total αβ homohopanes	50	M191	48	M191
% C ₃₂ of total αβ homohopanes	26	M191	27	M191
% C ₃₃ of total αβ homohopanes	13	M191	13	M191
% C ₃₄ of total αβ homohopanes	11	M191	9	M191
% C ₃₅ of total αβ homohopanes	n.d.	M191	3	M191
Homohopanes/C ₃₀ αβ hopane	1.3	M191	1.5	M191
Gammacerane/C ₃₀ αβ hopane	0.13	M191	0.08	M191
Ts/C ₃₀ αβ hopane	0.27	M191	0.15	M191
C ₂₇ hopanes/C ₃₀ αβ hopane	0.56	M191	0.41	M191
28,30-BNH/C ₃₀ αβ hopane	n.d.	MRM	0.03	MRM
28,30-BNH/Ts	n.d.	MRM	0.11	MRM
C ₂₉ αβ hopane/C ₃₀ αβ hopane	0.79	M191	0.59	M191
C ₃₁ αβ hopanes/C ₃₀ αβ hopane	0.65	M191	0.74	M191
C ₂₆ /C ₂₅ tricyclic terpanes	0.73	M191	1.02	M191
C ₂₃ tricyclic terpane/C ₃₀ αβ hopane	0.87	M191	0.07	M191
C ₂₄ tetracyclic terpane/C ₃₀ αβ hopane	0.30	M191	0.16	M191
C ₂₃ /C ₂₁ tricyclic terpanes	1.2	M191	0.90	M191
C ₂₃₋₂₆ /C ₁₉₋₂₁ tricyclic terpanes	0.95	M191	0.19	M191
C ₂₄ tetracyclic/C ₂₆ tricyclic terpanes	2.2	M191	7	M191
C ₂₄ tetracyclic/C ₂₃ tricyclic terpanes	0.35	M191	2.3	M191
(C ₁₉ +C ₂₀)/C ₂₃ tricyclic terpanes	1.0	M191	10	M191
C ₂₄ tetracyclic/(C ₂₄ tetracyclic + C ₂₃ tricyclic terpane)	0.26	M191	0.70	M191
C ₁₉ /(C ₁₉ + C ₂₃ tricyclic terpanes)	0.23	M191	0.63	M191
C ₂₉ steranes/C ₂₉ αβ hopane	0.56	M191	0.44	M191
C ₃₂ 2α Me/(C ₃₂ 2α Me+C ₃₁ αβ hopanes)	0.27	M205	0.14	M205
C ₃₃ 2α Me/(C ₃₃ 2α Me+C ₃₂ αβ hopanes)	n.d.	M205	0.45	M205

M: Multiple Ion Detection, MRM: Metastable Reaction Monitoring

Table A4-34: Sterane and diasterane parameters.

Parameter	Gnarlyknots- 1A FI oil	Greenly- 1 FI oil	Transition
C ₂₇ ααα 20R (% of total C ₂₇ to C ₂₉ ααα 20R steranes)	67	37	M217
C ₂₈ ααα 20R (% of total C ₂₇ to C ₂₉ ααα 20R steranes)	13	12	M217
C ₂₉ ααα 20R (% of total C ₂₇ to C ₂₉ ααα 20R steranes)	20	51	M217
C ₂₉ ααα 20R/C ₂₇ ααα 20R steranes	0.30	1.4	M217
C ₂₈ ααα 20R/C ₂₉ ααα 20R steranes	0.62	0.23	M217
C ₂₇ αββ steranes 20S+R (% of C ₂₇ to C ₂₉ αββ 20R steranes)	21	16	MRM
C ₂₈ αββ steranes 20S+R (% of C ₂₇ to C ₂₉ αββ 20R steranes)	25	12	MRM
C ₂₉ αββ steranes 20S+R (% of C ₂₇ to C ₂₉ αββ 20R steranes)	53	72	MRM
C ₂₇ αββ steranes 20S+R (% of C ₂₇ to C ₂₉ αββ 20R steranes)	29	23	M218
C ₂₈ αββ steranes 20S+R (% of C ₂₇ to C ₂₉ αββ 20R steranes)	21	15	M218
C ₂₉ αββ steranes 20S+R (% of C ₂₇ to C ₂₉ αββ 20R steranes)	50	62	M218
C ₂₉ αββ steranes 20S+R /C ₂₇ αββ steranes 20S+R	2.5	4.7	M218
C ₂₇ αββ steranes 20S+R /C ₂₉ αββ steranes 20S+R	0.40	0.21	M218
(C ₂₇ steranes+diasteranes) / (C ₂₉ steranes+diasteranes)	1.5	0.38	MRM
C ₂₇ steranes (% of total C ₂₇ to C ₂₉ regular steranes)	57	29	MRM
C ₂₈ steranes (% of total C ₂₇ to C ₂₉ regular steranes)	14	13	MRM
C ₂₉ steranes (% of total C ₂₇ to C ₂₉ regular steranes)	29	59	MRM
C ₂₇ βα diasterane 20S+R (% of C ₂₇ to C ₂₉ βα 20S+R diasteranes)	34	19	MRM
C ₂₈ βα diasterane 20S+R (% of C ₂₇ to C ₂₉ βα 20S+R diasteranes)	30	17	MRM
C ₂₉ βα diasterane 20S+R (% of C ₂₇ to C ₂₉ βα 20S+R diasteranes)	35	64	MRM
C ₂₉ / C ₂₇ βα diasteranes	1.0	3.3	MRM
C ₂₇ βα diasterane 20S+R (% of C ₂₇ to C ₂₉ βα 20S+R diasteranes)	32	n.d.	M259
C ₂₈ βα diasterane 20S+R (% of C ₂₇ to C ₂₉ βα 20S+R diasteranes)	34	n.d.	M259
C ₂₉ βα diasterane 20S+R (% of C ₂₇ to C ₂₉ βα 20S+R diasteranes)	33	n.d.	M259
C ₂₇ βα diasteranes/(ααα+αββ steranes)	0.36	0.68	MRM
C ₂₈ βα diasteranes/(ααα+αββ steranes)	1.3	1.4	MRM
C ₂₉ βα diasteranes/(ααα+αββ steranes)	0.73	1.10	MRM
C ₂₇ +C ₂₈ +C ₂₉ βα diasteranes/(ααα+αββ steranes)	0.60	1.02	MRM
C ₂₉ ααα 20S/(20S+20R)	0.38	0.50	MRM
C ₂₉ ααα 20S/20R	0.60	1.01	MRM
% Rc from C ₂₉ ααα 20S/20R (Sofer <i>et al.</i> , 1993)	0.65	0.86	MRM
C ₂₉ αββ/(αββ+ααα)	0.50	0.56	MRM
C ₂₇ βα diasterane 20S/(20S+20R)	0.65	0.64	MRM
C ₂₈ βα diasterane 20S/(20S+20R)	0.59	0.59	MRM
C ₂₉ βα diasterane 20S/(20S+20R)	0.58	0.59	MRM

M: Multiple Ion Detection, MRM: Metastable Reaction Monitoring

Table A4-35: Aromatic hydrocarbon parameters.

Parameter	Gnarlyknots-1A FI oil	Greenly-1 FI oil
Methylnaphthalene ratio (MNR: 2-MN/1-MN)	2.4	1.4
%Rc from MNR	1.2	1.1
Naphthalene/ Σ methylnaphthalenes	1.3	0.40
Ethylnaphthalene ratio (ENR: 2-EN/1-EN)	0.97	1.19
DNR-1 ([2,6-+2,7-DMN]/1,5-DMN)	7.3	3.1
% Rc from DNR-1	1.2	0.77
TNR-1 (2,3,6-TMN/[1,4,6-+1,3,5-TMN])	1.1	0.86
TNR-2 ([2,3,6-+1,3,7-TMN]/[1,4,6-+1,3,5-+1,3,6-TMN])	0.93	0.84
%Rc from TNR-2	0.96	0.91
Log (1,2,5-TMN/1,3,6-TMN)	-0.32	-0.08
Log (1,2,7-TMN/1,3,7-TMN)	-0.71	-0.74
TeMNR-1 (2,3,6,7-TeMN/1,2,3,6-TeMN)	0.75	1.3
(1,2,5,6+1,2,3,5-TeMN)/1,2,3,6-TeMN	3.3	4.1
TMNr (1,3,7-TMN/[1,3,7-+1,2,5-TMN])	0.63	0.49
TeMNr (1,3,6,7-TeMN/[1,3,6,7+1,2,5,6-TeMN])	0.55	0.58
PMNr (1,2,4,6,7-PMN/[1,2,4,6,7+1,2,3,5,6-PMN])	0.33	0.33
MPI-1 =1.5*[3-MP+2-MP]/[P+9-MP+1-MP])	0.65	0.67
%Rc (MPI-1)	0.79	0.80
MPDF =(3-MP+2-MP)/ Σ MPs)	0.64	0.47
Log (1-MP/9-MP)	-0.01	-0.02
MPR = 2-MP/1-MP	2.2	1.1
%Rc (MPR)	1.3	0.98
DPR = (3,5-+2,6-DMP+2,7-DMP)/ (1,3-+3,9-+2,10-+3,10-DMP+1,6-+2,9-+2,5-DMP)	0.58	0.26
Log (1,7-DMP/1,3-+3,9-+2,10-+3,10-DMP)	-0.30	-0.11
DPR-x (1,7-DMP/1,7-+1,3-+3,9-+2,10-+3,10-DMP)	0.33	0.44
Log (Retene/9-MP)	-0.94	-1.15
Fluoranthene/(fluoranthene + pyrene)	0.50	0.41
MPyI2=2-MPy/1-+4-Mpy	0.52	0.32
3-MBp/Bp	0.55	0.80
MBp = 3-MBp/2-MBp	22	38
3-MBp/4-MBp	2.7	2.2

Table A4-33 (continued): Aromatic hydrocarbon parameters.

Parameter	Gnarlyknots-1A FI oil	Greenly-1 FI oil
DMBpR-x = 3,5-DMBp/2,5-DMBp	22	23
DMBpR-y= 3,3'-DMBp/2,3'-DMBp	34	38
Dibenzothiophene/phenanthrene	0.15	0.08
MDR= 4-MDBT/1-MDBT	3.6	7.7
% Rc(MDR)	0.78	1.1
DMDR = 4,6-DMDBT/3,6-+2,6-DMDBT	0.73	0.63
Dibenzothiophene/1,3,6,7-TeMN	4.7	1.7
Dibenzothiophene/1,2,5,6-+1,2,3,5-TeMN	5.7	2.4
%Rc from MNR ((0.17*MNR)+0.82), from Radke et al. 1984		
% Rc from DNR-1 (0.49+(0.09xDNR-1)), from Radke et al. 1994		
%Rc from TNR-2 (0.4+(0.6xTNR-2)), from Radke et al., 1994		
MPI: Methylphenanthrene index		
%Rc (MPI-1) 0.6*MPI-1+0.4 (for Ro <1.35), from Radke and Welte, 1983		
MPDF: Methylphenanthrene distribution fraction		
MPR: Methylphenanthrene ratio		
%Rc from (MPR) 0.99*log MPR+0.94, from Radke et al., 1984		
DPR: Dimethylphenanthrene ratio		
MPyI2: Methylpyrene index, from Garrigues et al., 1988		
MBp: Methylbiphenyl ratio		
DMBpR-x: Dimethylbiphenyl ratio-x		
DMBpR-y: Dimethylbiphenyl ratio-y		
MDR: Methyl dibenzothiophene ratio		
%Rc from (MDR) 0.073*MDR+0.51, from Radke, 1988		
DMDR Dimethyldibenzothiophene ratio		

Table A4-36: Diamondoid hydrocarbon parameters.

Parameters	Gnarlyknots-1A FI oil	Greenly-1 FI oil
$MAI = 1-MA/(1-MA+2-MA) \text{ (%)}$	67	55
$MDI = 4-MD/(1-MD+3-MD+4-MD) \text{ (%)}$	45	50
$(1-MA + 2-MA)/A$	2.0	1.4
$(1-MD+3-MD+4-MD)/D$	5.6	3.7
$DMDI-1 = 3,4-DMD/(3,4-DMD + 4,9-DMDA) \text{ (%)}$	64	78
$DMDI-2 = 4,8-DMD/(4,8-DMD + 4,9-DMDA) \text{ (%)}$	50	71
$EAI = 2EA/(2EA + 1EA) \text{ (%)}$	54	66

A=Admantane, MA=Methyladamantane, D=Diamantane

DMDI=Dimethyldiamantane, EA=Ehtyladamantane

MAI: Methyl adamantane index

MDI: Methyl diamantane index

DMDI-1: Dimethyl diamantane index 1

DMDI-2: Dimethyl diamantane index 2

EAI: Ethyl adamantane index

Table A4-37: Low molecular weight hydrocarbon parameters (on-line).

Parameters	Gnarlyknots-1A FI oil
A: Benzene/ n -C ₆	1.91
B: Toluene/ n -C ₇	6.3
C: (n -C ₆ + n -C ₇)/(CH+MCH)	3.3
Heptane value (H; Thompson, 1979)	47
Isoheptane value (I; Thompson, 1987)	2.3
F: n -C ₇ /MCH	2.4
U: CH/MCP	0.7
R: n -C ₇ /2-MH	6
n -C ₇ /MCP	2.7
3-MP/Benzene	0.1
MCH/Toluene	0.06
CH/Benzene	0.11
3-MP/ n -C ₆	0.2
Benzene/toluene	0.36
MCP/MCH	0.9
Toluene/o-xylene	20
m-+p-xylene/ n -C ₈	0.54
K1: (2-MH+23-DMP)/(3-MH+24-DMP)	1.9
2-MH/3-MH	1.9
n -C ₇ (% of total C7 hydrocarbons)	12
3 ring preference % (DMP+MH)	4
5 ring preference % (DMCP+ECP)	3
6 ring preference % (MCH+toluene)	93
(2MH+3MH)/(c13DMCP+t13DMCP+t12DMCP) (modified from Schaefer, 1992)	2.2
Rc (J) (Schaefer, 1992)	1.2

Table A4-38: Carbon isotopic composition of fluid inclusion gases.

Well	Depth (mMD)	$\delta^{13}\text{C}_{\text{CH}_4}$ (‰)	$\delta^{13}\text{C}_{\text{C}_2\text{H}_6}$ (‰)	$\delta^{13}\text{C}_{\text{CO}_2}$ (‰)
Gnarlyknots-1A	4410-4415	-28.4	-17.6	-4.4
Gnarlyknots-1A	4410-4415	-28.6	-18.1	-3.9

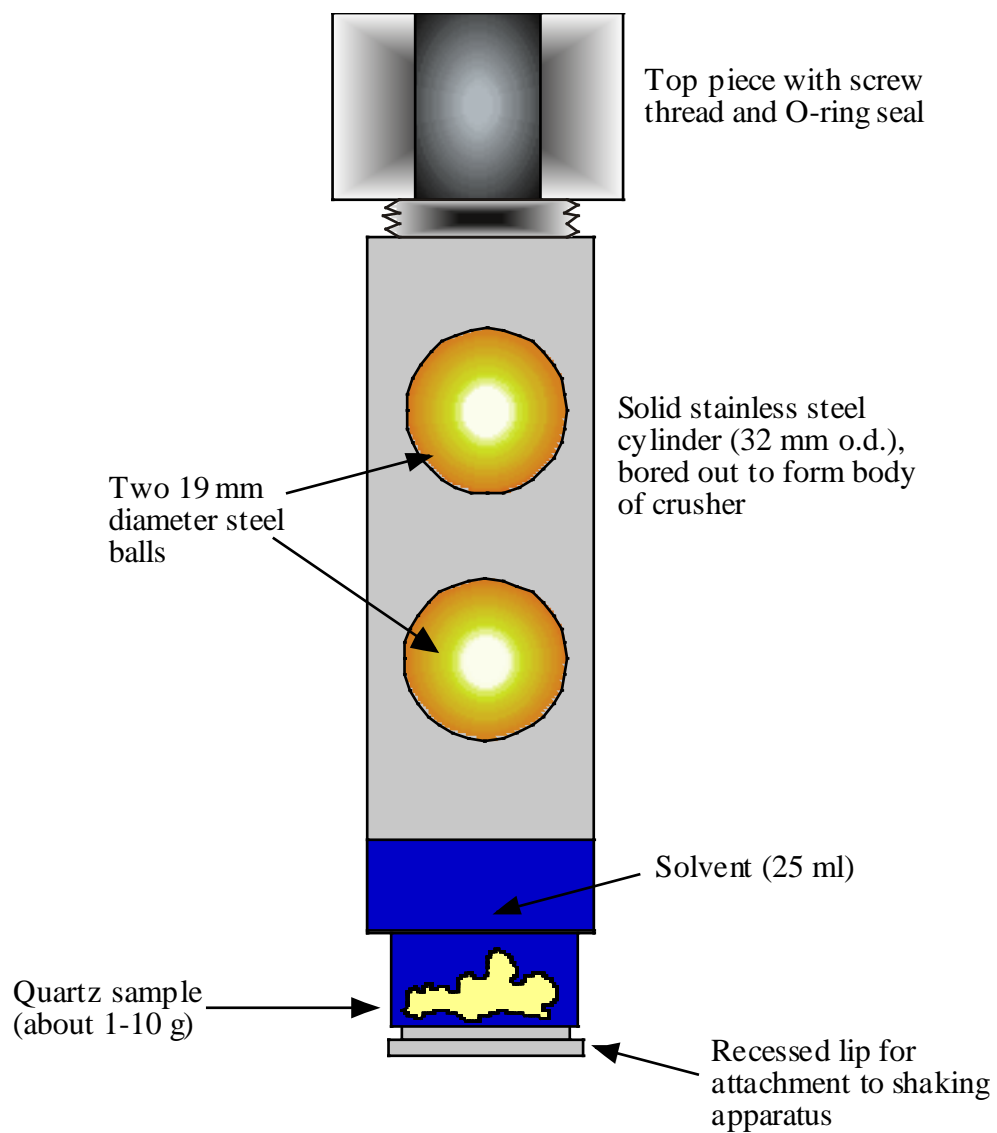


Figure A4-103: Diagram of the 55 mL stainless steel crushing cylinder used for off-line analyses of FI oils.

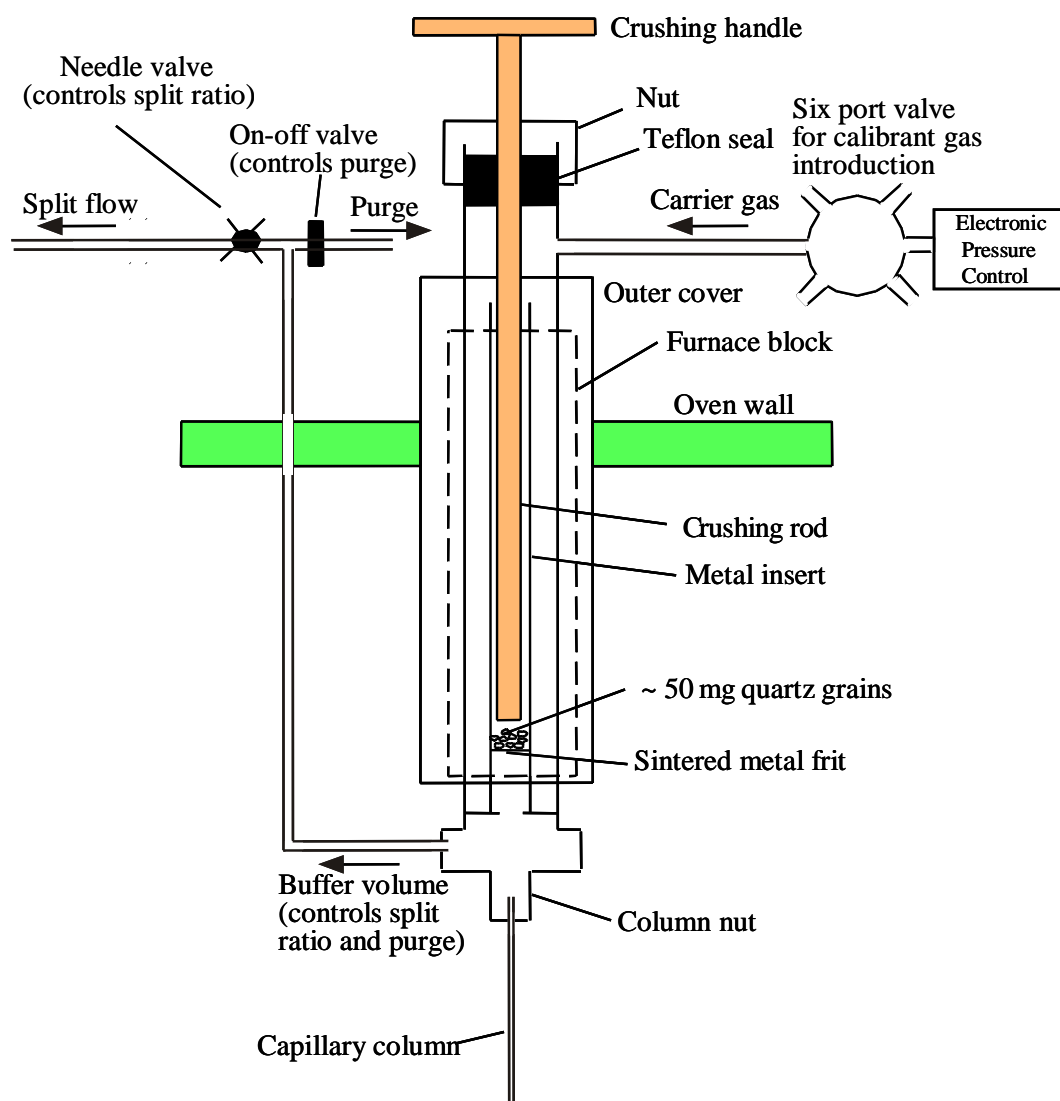


Figure A4-104: Schematic diagram of the Quantum MSSV1B Thermal Analysis System used for the on-line crushing of quartz grains containing oil-bearing fluid inclusions directly onto a GC-MS capillary column

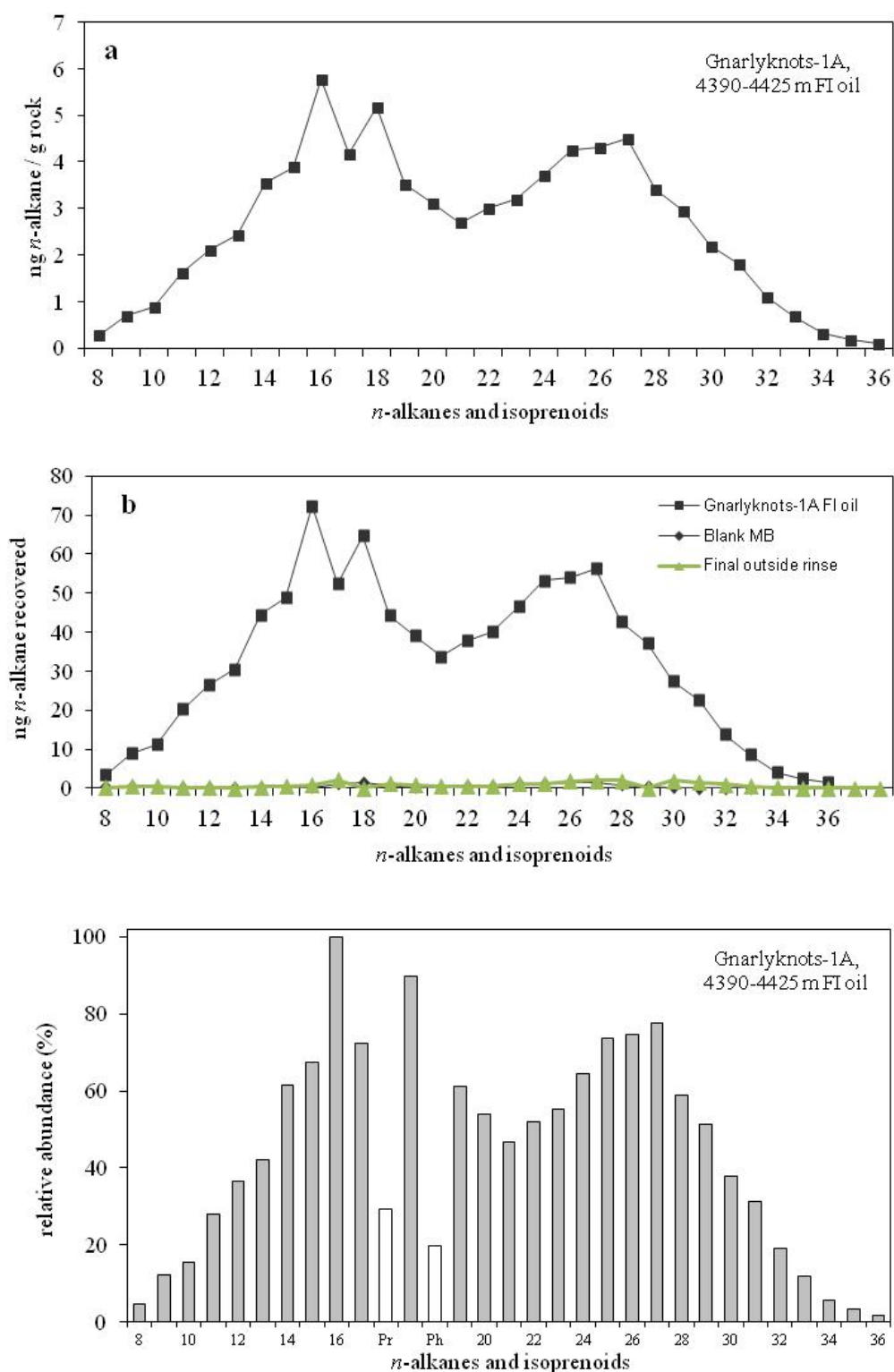


Figure A4-105: Aliphatic hydrocarbon distributions in the Gnarlyknots-1A (4390-4425 m) MCI sample. Showing (a) the amounts of *n*-alkanes recovered /g of rock, (b) absolute amounts recovered compared to those in the associated blank and final outside rinse, and (c) the relative abundance of *n*-alkanes and regular isoprenoids pristane (Pr) and phytane (Ph). The graphs are derived from *m/z* 85 mass chromatograms.

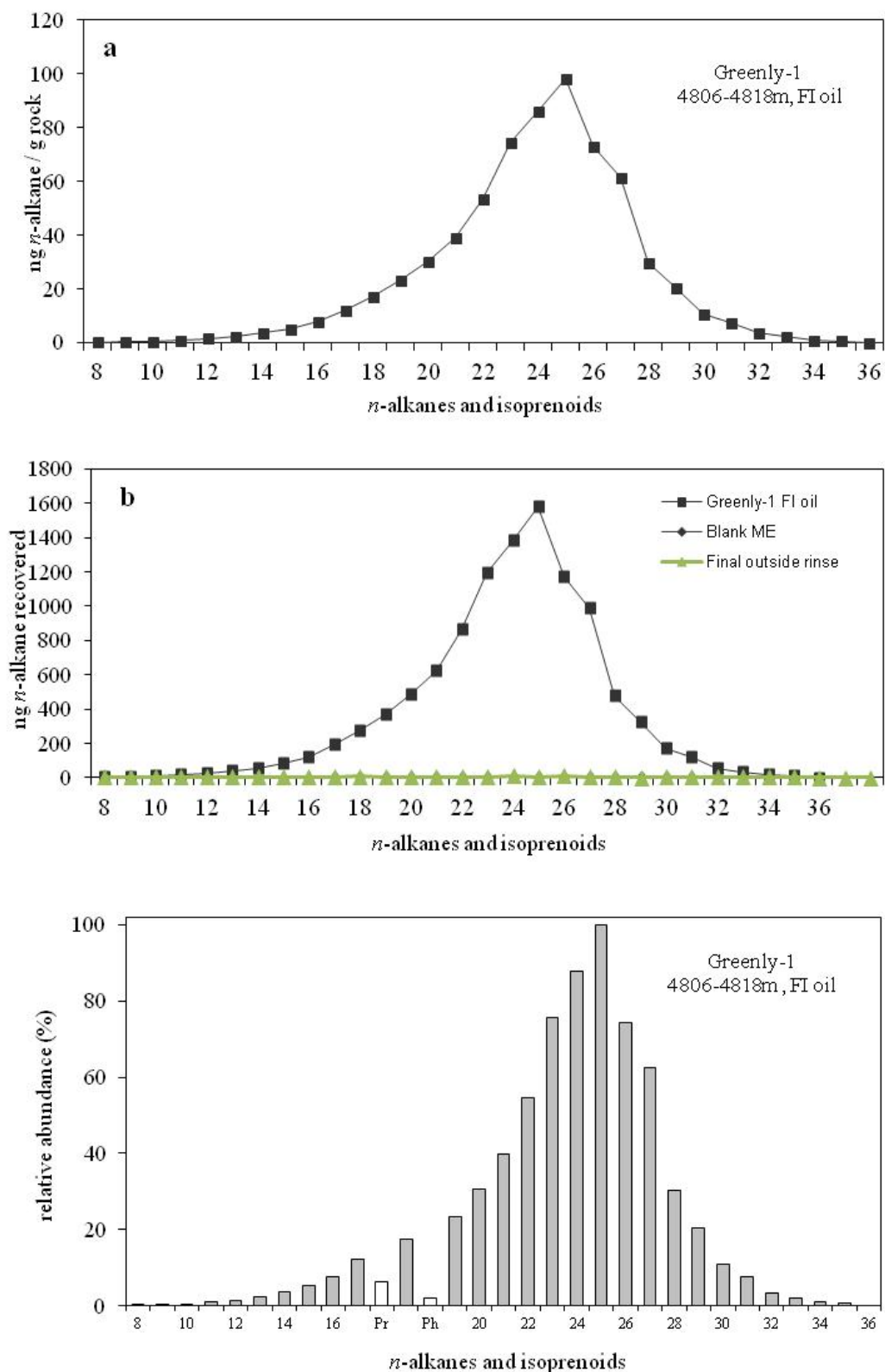


Figure A4-106: Aliphatic hydrocarbon distributions in the Greenly-1 (4806-4818 m) MCI sample. Showing (a) the amounts of *n*-alkanes recovered /g of rock, (b) absolute amounts recovered compared to those in the associated blank and final outside rinse, and (c) the relative abundance of *n*-alkanes and regular isoprenoids pristane (Pr) and phytane (Ph). The graphs are derived from *m/z* 85 mass chromatograms.

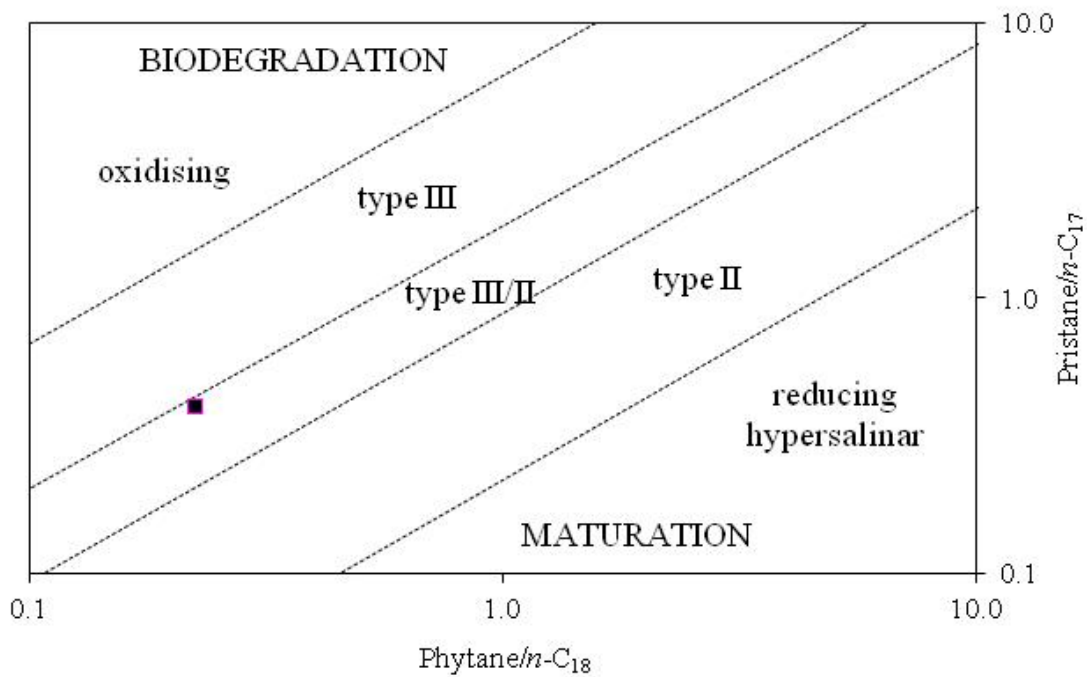


Figure A4-107: Plot of Ph/ n -C₁₈ versus Pr/ n -C₁₇ ratios of Gnarlyknots-1A (4390-4425 m) FI oil.

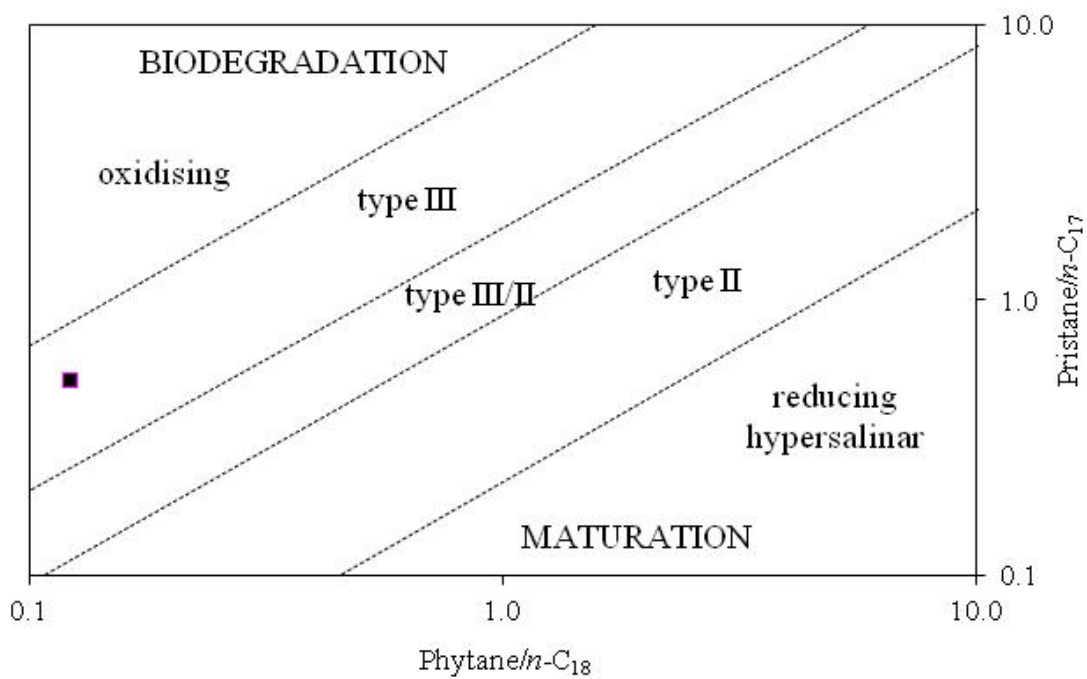


Figure A4-108: Plot of Ph/ n -C₁₈ versus Pr/ n -C₁₇ ratios of Greenly-1 (4806-4818 m) FI oil.

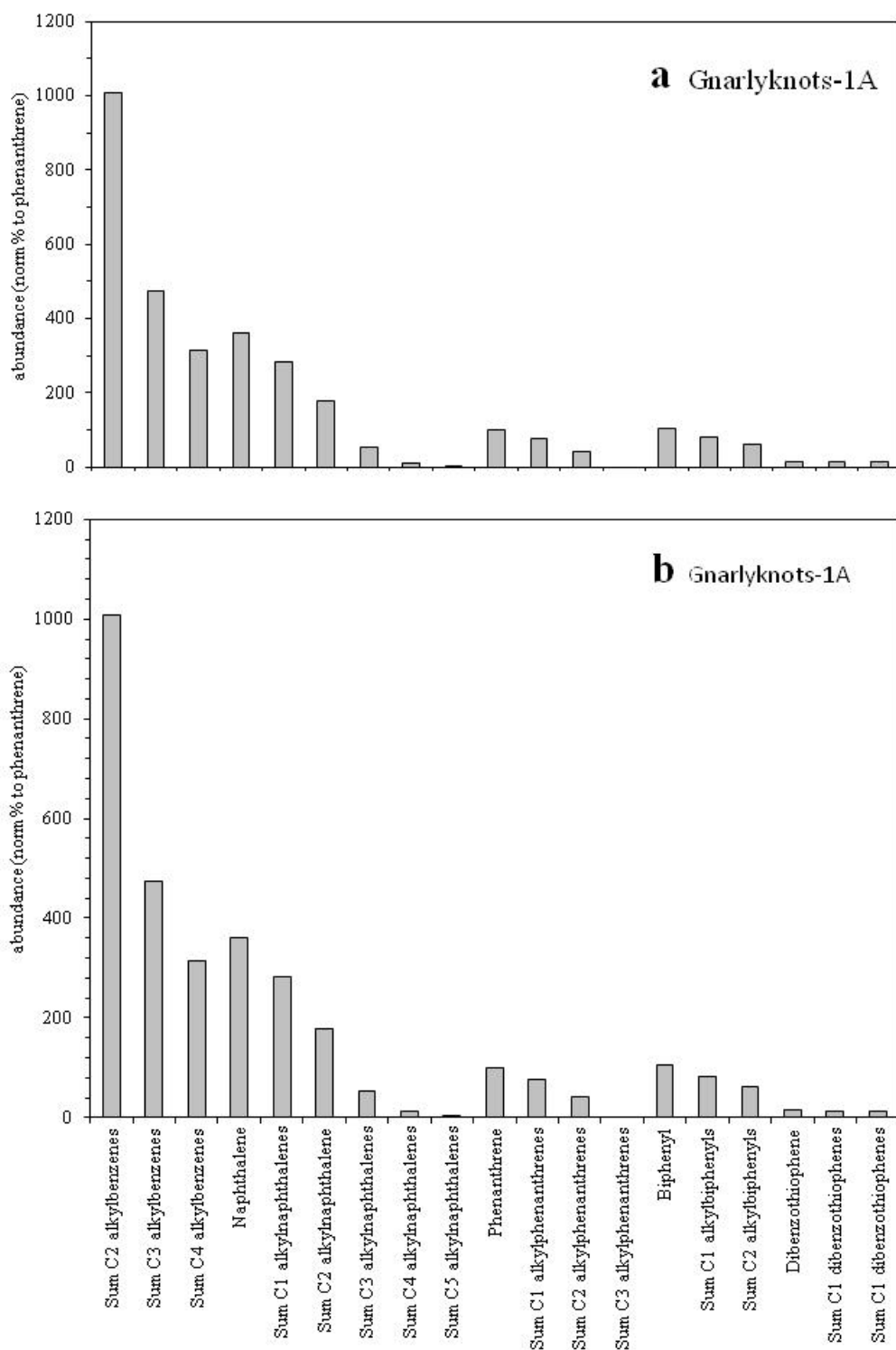


Figure A4-109: Distribution of alkylbenzenes, naphthalene, phenanthrene, biphenyl, dibenzothiophene and alkylated homologues of Gnarlyknots-1A (4390-4425 m) FI oil. Scaled to show (a) overall distributions and (b) less abundant compound classes. Values calculated from the responses in the m/z 106, 120, 134, 128, 142, 156, 170, 184, 178, 192, 206, 154, 168, 182, 184, 198 and 212 mass chromatograms.

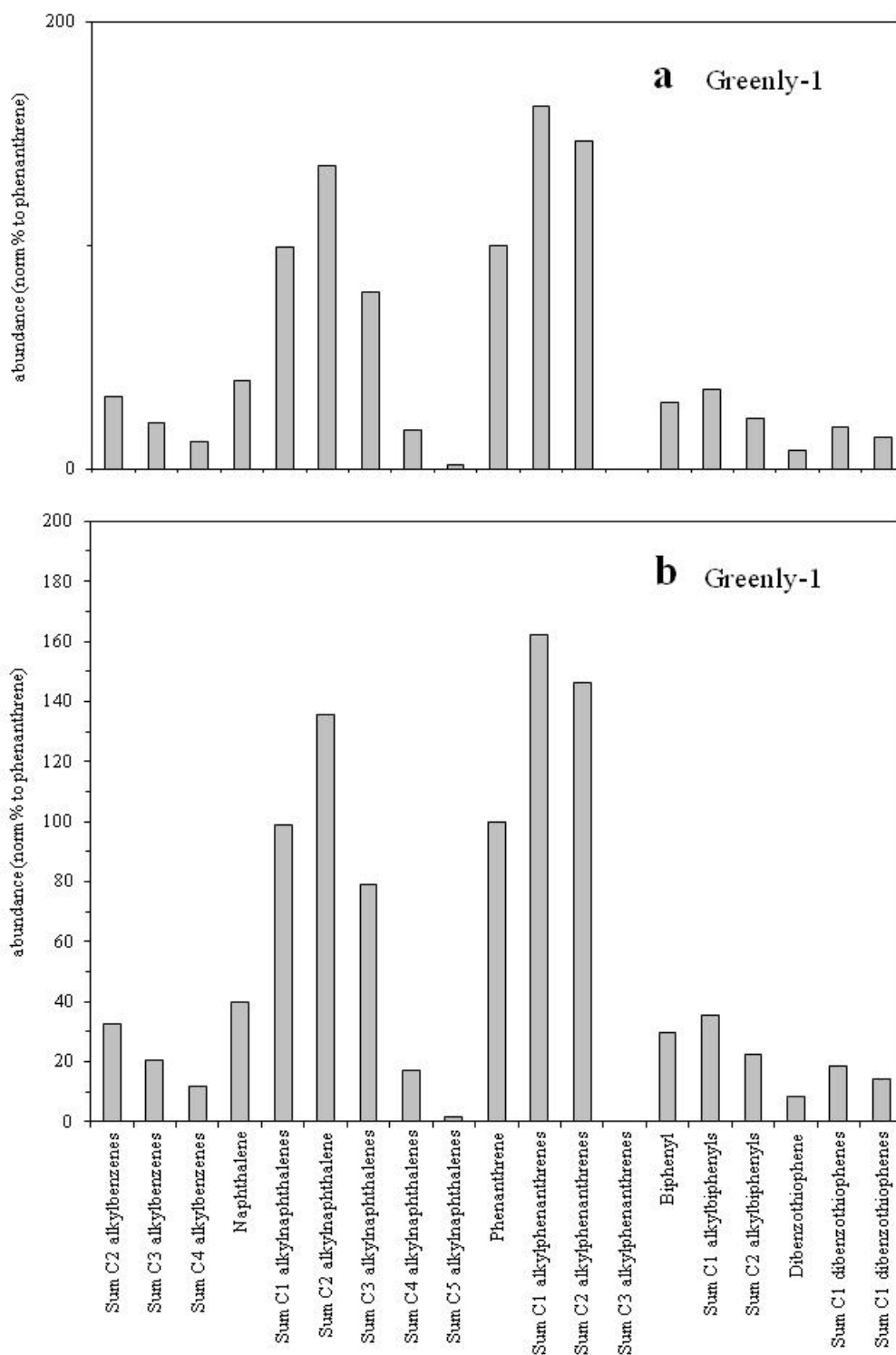


Figure A4-110: Distribution of alkylbenzenes, naphthalene, phenanthrene, biphenyl, dibenzothiophene and alkylated homologues of Greenly-1 (4806-4818 m) FI oil.

Scaled to show (a) overall distributions and (b) less abundant compound classes. Values calculated from the responses in the m/z 106, 120, 134, 128, 142, 156, 170, 184, 178, 192, 206, 154, 168, 182, 184, 198 and 212 mass chromatograms.

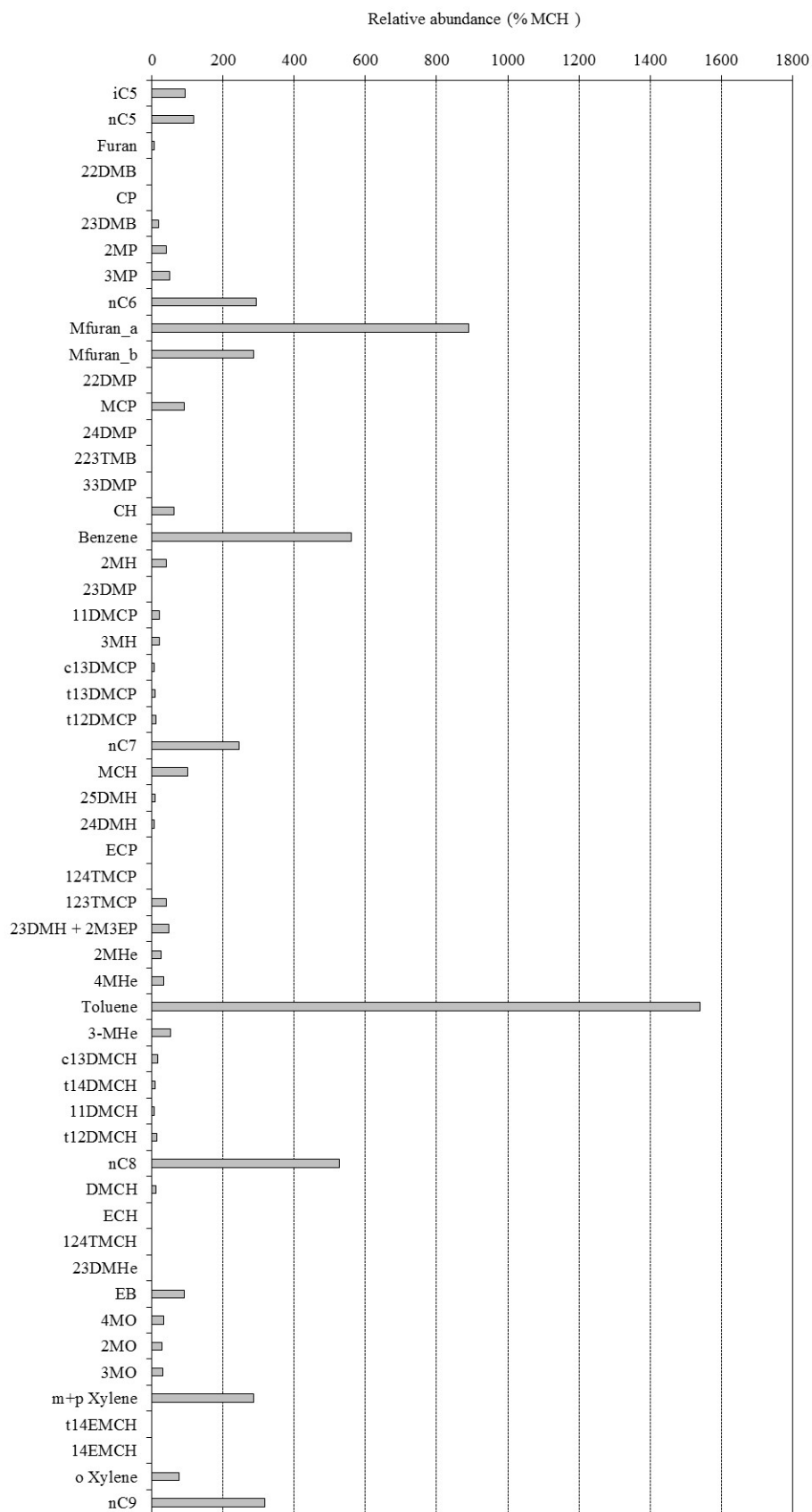


Figure A4-111: Normalised distribution of low molecular weight compounds in the Gnarlyknots-1A FI oil. Measured using the on-line thermal extraction method. Abbreviation for components are listed in Appendix Table B7. Note that all abundances are FID-equivalent data.

APPENDIX 5: MCI – Peak Assignments & Abbreviations

Table A5-39: Peak assignments for terpanes in the *m/z* 191, 177 and 205 mass chromatograms and MRM chromatograms.

Peak	Terpane assignments
Ts	C ₂₇ 18 α (H),22,29,30-trisnorneohopane
TNH	C ₂₇ 25,28,30 -trisorhopane
C ₂₉ §	C ₂₉ rearranged triterpane
C ₃₀ §	C ₃₀ rearranged triterpane
Tm	C ₂₇ 17 α (H),22,29,30-trisorhopane
C ₂₇ β	C ₂₇ 17β(H),22,29,30-trisorhopane
25,30-BNH	C ₂₈ 25,30-bisorhopane
29,30-BNH	C ₂₈ 29,30-bisorhopane
28,30-BNH	C ₂₈ 28,30-bisorhopane
25-nor	C ₂₉ 25-nor-17 α (H)-hopane
C ₂₉ *	C ₂₉ 17 α (H)-diahopane
C ₂₉ αβ	17 α (H),21β(H)-30-norhopane
C ₂₉ Ts	18 α (H)-30-norneohopane
C ₃₀ *	C ₃₀ 17 α (H)-diahopane
C ₂₉ βα	17β(H),21 α (H)-30-norhopane
C ₃₀ 25-nor <i>S</i>	C ₃₀ 25-nor-17 α (H)-hopane (22 <i>S</i>)
C ₃₀ 25-nor <i>R</i>	C ₃₀ 25-nor-17 α (H)-hopane (22 <i>R</i>)
Oleanane	18 α (H)-oleanane (+ 18β(H)-oleanane)
C ₃₀ αβ	17 α (H),21β(H)-hopane
30-nor	C ₃₀ to C ₃₄ 30-nor-17 α (H)-hopanes
C ₃₀ βα	17β(H),21 α (H)-hopane
C ₃₁ *	C ₃₁ 17 α (H)-diahopane
C ₃₁ αβ 22 <i>S</i>	17 α (H),21β(H)-homohopane (22 <i>S</i>)
C ₃₁ αβ 22 <i>R</i>	17 α (H),21β(H)-homohopane (22 <i>R</i>)
G	Gammacerane
C ₃₁ βα 22 <i>S</i> + <i>R</i>	17β(H),21 α (H)-homohopane (22 <i>S</i> and 22 <i>R</i>)
C ₃₂ *	C ₃₂ 17 α (H)-diahopane
C ₃₂ αβ 22 <i>S</i>	17 α (H),21β(H)-bishomohopane (22 <i>S</i>)
C ₃₂ αβ 22 <i>R</i>	17 α (H),21β(H)-bishomohopane (22 <i>R</i>)
C ₃₃ αβ 22 <i>S</i>	17 α (H),21β(H)-trishomohopane (22 <i>S</i>)
C ₃₃ αβ 22 <i>R</i>	17 α (H),21β(H)-trishomohopane (22 <i>R</i>)
C ₃₄ αβ 22 <i>S</i>	17 α (H),21β(H)-tetrakishomohopane (22 <i>S</i>)
C ₃₄ αβ 22 <i>R</i>	17 α (H),21β(H)-tetrakishomohopane (22 <i>R</i>)
C ₃₅ αβ 22 <i>S</i>	17 α (H),21β(H)-pentakishomohopane (22 <i>S</i>)
C ₃₅ αβ 22 <i>R</i>	17 α (H),21β(H)-pentakishomohopane (22 <i>R</i>)
2 α (Me)	2 α -methylhopane
3 β (Me)	3 β -methylhopane
T, T1 and R	C ₃₀ bicadinanes of proven or inferred <i>trans-trans-trans</i> configuration
W	C ₃₀ bicadinane of proven <i>cis-cis-trans</i> configuration
MeW, MeT and MeT1	C ₃₁ methylbicadinanes
dO, dL and dU	A-ring degraded oleanane, lupane and ursane
BNO	18 α (H)-24,28-bisnoroleanane
α-BNL	17 α (H)-24,28-bisnorlupane
β-BNL	17β(H)-24,28-bisnorlupane

Table A5-40: Peak assignments for steranes, diasteranes and methylsteranes in the m/z 217, 218, 259 and 231 mass chromatograms and MRM chromatograms.

Peak	Sterane, diasterane and methylsterane assignments	Abbreviation
1	13 β (H),17 α (H)-24-nordiacholestane (20 <i>S</i>)	C ₂₆ $\beta\alpha$ 20 <i>S</i> 24-nor-dia
2	13 β (H),17 α (H)-24-nordiacholestane (20 <i>R</i>)	C ₂₆ $\beta\alpha$ 20 <i>R</i> 24-nor-dia
3	13 β (H),17 α (H)-27-nordiacholestane (20 <i>S</i>)	C ₂₆ $\beta\alpha$ 20 <i>S</i> 27-nor-dia
4	13 β (H),17 α (H)-27-nordiacholestane (20 <i>R</i>)	C ₂₆ $\beta\alpha$ 20 <i>R</i> 27-nor-dia
5	5 α (H),14 α (H),17 α (H)-24-norcholestane (20 <i>S</i>)	C ₂₆ $\alpha\alpha\alpha$ 20 <i>S</i> 24-nor-ster
6	5 α (H),14 β (H),17 β (H)-24-norcholestane (20 <i>R</i>)	C ₂₆ $\alpha\beta\beta$ 20 <i>R</i> 24-nor-ster
7	5 α (H),14 β (H),17 β (H)-24-norcholestane (20 <i>S</i>)	C ₂₆ $\alpha\beta\beta$ 20 <i>S</i> 24-nor-ster
8	5 α (H),14 α (H),17 α (H)-24-norcholestane (20 <i>R</i>)	C ₂₆ $\alpha\alpha\alpha$ 20 <i>R</i> 24-nor-ster
9	5 α (H),14 α (H),17 α (H)-21-norcholestane + 5 α (H),14 β (H),17 β (H)-21-norcholestane	C ₂₆ $\alpha\alpha\alpha$ + $\alpha\beta\beta$ 21-nor-steranes
10	5 α (H),14 α (H),17 α (H)-27-norcholestane (20 <i>S</i>)	C ₂₆ $\alpha\alpha\alpha$ 20 <i>S</i> 27-nor-ster
11	5 α (H),14 β (H),17 β (H)-27-norcholestane (20 <i>R</i>)	C ₂₆ $\alpha\beta\beta$ 20 <i>R</i> 27-nor-ster
12	5 α (H),14 β (H),17 β (H)-27-norcholestane (20 <i>S</i>)	C ₂₆ $\alpha\beta\beta$ 20 <i>S</i> 27-nor-ster
13	5 α (H),14 α (H),17 α (H)-27-norcholestane (20 <i>R</i>)	C ₂₆ $\alpha\alpha\alpha$ 20 <i>R</i> 27-nor-ster
a	13 β (H),17 α (H)-diacholestane (20 <i>S</i>)	C ₂₇ $\beta\alpha$ 20 <i>S</i> diasterane
b	13 β (H),17 α (H)-diacholestane (20 <i>R</i>)	C ₂₇ $\beta\alpha$ 20 <i>R</i> diasterane
c	13 α (H),17 β (H)-diacholestane (20 <i>S</i>)	C ₂₇ $\alpha\beta$ 20 <i>S</i> diasterane
d	13 α (H),17 β (H)-diacholestane (20 <i>R</i>)	C ₂₇ $\alpha\beta$ 20 <i>R</i> diasterane
e	5 α (H),14 α (H),17 α (H)-cholestane (20 <i>S</i>)	C ₂₇ $\alpha\alpha\alpha$ 20 <i>S</i> sterane
f	5 α (H),14 β (H),17 β (H)-cholestane (20 <i>R</i>)	C ₂₇ $\alpha\beta\beta$ 20 <i>R</i> sterane
g	5 α (H),14 β (H),17 β (H)-cholestane (20 <i>S</i>)	C ₂₇ $\alpha\beta\beta$ 20 <i>S</i> sterane
h	5 α (H),14 α (H),17 α (H)-cholestane (20 <i>R</i>)	C ₂₇ $\alpha\alpha\alpha$ 20 <i>R</i> sterane
i	24-methyl-13 β (H),17 α (H)-diacholestane (20 <i>S</i>)*	C ₂₈ $\beta\alpha$ 20 <i>S</i> diasterane
j	24-methyl-13 β (H),17 α (H)-diacholestane (20 <i>R</i>)*	C ₂₈ $\beta\alpha$ 20 <i>R</i> diasterane
k	24-methyl-13 α (H),17 β (H)-diacholestane (20 <i>S</i>)	C ₂₈ $\alpha\beta$ 20 <i>S</i> diasterane
l	24-methyl-13 α (H),17 β (H)-diacholestane (20 <i>R</i>)*	C ₂₈ $\alpha\beta$ 20 <i>R</i> diasterane
m	24-methyl-5 α (H),14 α (H),17 α (H)-cholestane (20 <i>S</i>)*	C ₂₈ $\alpha\alpha\alpha$ 20 <i>S</i> sterane
n	24-methyl-5 α (H),14 β (H),17 β (H)-cholestane (20 <i>R</i>)	C ₂₈ $\alpha\beta\beta$ 20 <i>R</i> sterane
o	24-methyl-5 α (H),14 β (H),17 β (H)-cholestane (20 <i>S</i>)	C ₂₈ $\alpha\beta\beta$ 20 <i>S</i> sterane
p	24-methyl-5 α (H),14 α (H),17 α (H)-cholestane (20 <i>R</i>)	C ₂₈ $\alpha\alpha\alpha$ 20 <i>R</i> sterane
q	24-ethyl-13 β (H),17 α (H)-diacholestane (20 <i>S</i>)	C ₂₉ $\beta\alpha$ 20 <i>S</i> diasterane

Continued...

Table A5-38 (continued): Peak assignments for steranes, diasteranes and methylsteranes in the *m/z* 217, 218, 259 and 231 mass chromatograms and MRM chromatograms.

Peak	Sterane, diasterane and methylsterane assignments	Abbreviation
r	24-ethyl-13 β (H),17 α (H)-diacholestane (20 <i>R</i>)	C ₂₉ $\beta\alpha$ 20 <i>R</i> diasterane
s	24-ethyl-13 α (H),17 β (H)-diacholestane (20 <i>S</i>)	C ₂₉ $\alpha\beta$ 20 <i>S</i> diasterane
t	24-ethyl-13 α (H),17 β (H)-diacholestane (20 <i>R</i>)	C ₂₉ $\alpha\beta$ 20 <i>R</i> diasterane
u	24-ethyl-5 α (H),14 α (H),17 α (H)-cholestane (20 <i>S</i>)	C ₂₉ $\alpha\alpha\alpha$ 20 <i>S</i> sterane
v	24-ethyl-5 α (H),14 β (H),17 β (H)-cholestane (20 <i>R</i>)	C ₂₉ $\alpha\beta\beta$ 20 <i>R</i> sterane
w	24-ethyl-5 α (H),14 β (H),17 β (H)-cholestane (20 <i>S</i>)	C ₂₉ $\alpha\beta\beta$ 20 <i>S</i> sterane
x	24-ethyl-5 α (H),14 α (H),17 α (H)-cholestane (20 <i>R</i>)	C ₂₉ $\alpha\alpha\alpha$ 20 <i>R</i> sterane
y	24- <i>n</i> -propyl-13 β (H),17 α (H)-diacholestane (20 <i>S</i>)	C ₃₀ $\beta\alpha$ 20 <i>S</i> diasterane
z	24- <i>n</i> -propyl-13 β (H),17 α (H)-diacholestane (20 <i>R</i>)	C ₃₀ $\beta\alpha$ 20 <i>R</i> diasterane
A	24- <i>n</i> -propyl-5 α (H),14 α (H),17 α (H)-cholestane (20 <i>S</i>)	C ₃₀ $\alpha\alpha\alpha$ 20 <i>S</i> sterane
B	24- <i>n</i> -propyl-5 α (H),14 β (H),17 β (H)-cholestane (20 <i>R</i>)	C ₃₀ $\alpha\beta\beta$ 20 <i>R</i> sterane
C	24- <i>n</i> -propyl-5 α (H),14 β (H),17 β (H)-cholestane (20 <i>S</i>)	C ₃₀ $\alpha\beta\beta$ 20 <i>S</i> sterane
D	24- <i>n</i> -propyl-5 α (H),14 α (H),17 α (H)-cholestane (20 <i>R</i>)	C ₃₀ $\alpha\alpha\alpha$ 20 <i>R</i> sterane
E	2 α -methyl-24-ethylcholestane (20 <i>S</i>)	2 α -methyl 20 <i>S</i>
F	3 β -methyl-24-ethylcholestane (20 <i>S</i>)	3 β -methyl 20 <i>S</i>
G	2 α -methyl-24-ethylcholestane (14 β ,17 β (H), 20 <i>R</i>)	2 α -methyl $\beta\beta$ 20 <i>R</i>
H	2 α -methyl-24-ethylcholestane (14 β ,17 β (H), 20 <i>S</i>)	2 α -methyl $\beta\beta$ 20 <i>S</i>
I	3 β -methyl-24-ethylcholestane (14 β ,17 β (H), 20 <i>R</i>)	3 β -methyl $\beta\beta$ 20 <i>R</i>
J	3 β -methyl-24-ethylcholestane (14 β ,17 β (H), 20 <i>S</i>)	3 β -methyl $\beta\beta$ 20 <i>S</i>
K	4 α -methyl-24-ethylcholestane (20 <i>S</i>)	4 α -methyl 20 <i>S</i>
L	4 α -methyl-24-ethylcholestane (14 β ,17 β (H), 20 <i>R</i>)	4 α -methyl $\beta\beta$ 20 <i>R</i>
M	4 α -methyl-24-ethylcholestane (14 β ,17 β (H), 20 <i>S</i>)	4 α -methyl $\beta\beta$ 20 <i>S</i>
N	2 α -methyl-24-ethylcholestane (20 <i>R</i>)	2 α -methyl 20 <i>R</i>
O	3 β -methyl-24-ethylcholestane (20 <i>R</i>)	3 β -methyl 20 <i>R</i>
P	4 α , 23 <i>S</i> , 24 <i>S</i> -trimethylcholestane (20 <i>R</i>)	4 α ,23 <i>S</i> ,24 <i>S</i> dinost 20 <i>R</i>
Q	4 α , 23 <i>S</i> , 24 <i>R</i> -trimethylcholestane (20 <i>R</i>)	4 α ,23 <i>S</i> ,24 <i>R</i> dinost 20 <i>R</i>
R	4 α -methyl-24-ethylcholestane (20 <i>R</i>)	4 α -methyl 20 <i>R</i>
S	4 α , 23 <i>R</i> , 24 <i>R</i> -trimethylcholestane (20 <i>R</i>)	4 α ,23 <i>R</i> ,24 <i>R</i> dinost 20 <i>R</i>
T	4 α , 23 <i>R</i> , 24 <i>S</i> -trimethylcholestane (20 <i>R</i>)	4 α ,23 <i>R</i> ,24 <i>S</i> dinost 20 <i>R</i>
Ta	Tetracyclic polyprenoid Ta (Holba <i>et al.</i> , 2000)	TPP Ta
Tb	Tetracyclic polyprenoid Tb (Holba <i>et al.</i> , 2000)	TPP Tb

* = isomeric peaks (24*S* and 24*R*); dinost = dinosterane isomers.

Table A5-41: Peak assignments for monoaromatic (MA) and rearranged dia-monoaromatic (DMA) steroids in the *m/z* 253 mass chromatogram.

Peak	Name of sterane with the same side chain (X) structure
4	β 20 <i>S</i> C ₂₇ MA
5	β 20 <i>S</i> C ₂₇ DMA
6	β 20 <i>R</i> C ₂₇ DMA + β 20 <i>R</i> C ₂₇ MA + α 20 <i>S</i> C ₂₇ MA
7-8	β 20 <i>S</i> C ₂₈ MA + α 20 <i>R</i> C ₂₇ DMA + β 20 <i>S</i> C ₂₈ DMA + α 20 <i>S</i> C ₂₇ DMA
9-12	α 20 <i>R</i> C ₂₇ MA + α 20 <i>S</i> C ₂₈ MA + β 20 <i>R</i> C ₂₈ MA + β 20 <i>R</i> C ₂₈ DMA + β 20 <i>S</i> C ₂₉ MA + β 20 <i>S</i> C ₂₉ DMA
13-15	α 20 <i>S</i> C ₂₉ MA + α 20 <i>R</i> C ₂₉ MA + β 20 <i>R</i> C ₂₉ MA + β 20 <i>R</i> C ₂₉ DMA

Table A5-42: Peak assignments for triaromatic steroids in the *m/z* 231 mass chromatogram.

Peak	Name of sterane with the same side chain (X) structure	Carbon Number
1	pregnane (X = ethyl)	20
2	20-methylpregnane (X = 2-propyl)	21
3	20-ethylpregnanes (X = 2-butyl)*	22
4	cholestane (20 <i>S</i>)	26
5	cholestane (20 <i>R</i>) + ergostane (20 <i>S</i>)	26, 27
6	24-ethylcholestane (20 <i>S</i>)	28
7	24-methylcholestane (20 <i>R</i>)	27
8	24-ethylcholestane (20 <i>R</i>)	28
9	24- <i>n</i> -propylcholestane (20 <i>S</i>)**	29
10	24- <i>n</i> -propylcholestane (20 <i>R</i>)	29

* = epimeric peaks a and b at C₂₀.

** = epimeric peaks a and b at C₂₄.

Table A5-43: Peak abbreviations for the aromatic hydrocarbons, with diagnostic m/z ions.

Aromatic compound assignment	Abbreviation	Ion
Ethylbenzene	EB	106
<i>meta</i> - and <i>para</i> -Xylene	m-+p-xylene	106
<i>ortho</i> -Xylene	o-xylene	106
Isopropylbenzene	iPB	120
<i>n</i> -Propylbenzene	nPB	120
1-Methyl-3-ethylbenzene	1M3EB	120
1-Methyl-4-ethylbenzene	1M4EB	120
1,3,5-Trimethylbenzene	1,3,5-TMB	120
1-Methyl-2-ethylbenzene	1M2EB	120
1,2,4-Trimethylbenzene	1,2,4-TMB	120
1,2,3-Trimethylbenzene	1,2,3-TMB	120
Isobutylbenzene	iBB	134
<i>sec</i> -Butylbenzene	sBB	134
1-Methyl-3-isopropylbenzene	1M3IB	134
1-Methyl-4-isopropylbenzene	1M4IB	134
1-Methyl-2-isopropylbenzene	1M2IB	134
1,3-Diethylbenzene	1,3-DEB	134
1-Methyl-3-propylbenzene	1M3PB	134
1-Methyl-4-propylbenzene	1M4PB	134
1,4-Diethylbenzene	1,4-DEB	134
<i>n</i> -Butylbenzene	nBB	134
1,2-Diethylbenzene	1,2-DEB	134
1,3-Dimethyl-5-ethylbenzene	1,3-D5EB	134
1-Methyl-2-propylbenzene	1M2PB	134
1,4-Dimethyl-2-ethylbenzene	1,4-D2EB	134
1,3-Dimethyl-4-ethylbenzene	1,3-D4EB	134
1,2-Dimethyl-4-ethylbenzene	1,2-D4EB	134
1,3-Dimethyl-2-ethylbenzene	1,3-D2EB	134
1,2-Dimethyl-3-ethylbenzene	1,2-D3EB	134
1,2,4,5-Tetramethylbenzene	1,2,4,5-TeMB	134
1,2,3,5-Tetramethylbenzene	1,2,3,5-TeMB	134
1,2,3,4-Tetramethylbenzene	1,2,3,4-TeMB	134
Continued...		

Table A5-41 (continued): Peak abbreviations for the aromatic hydrocarbons, with diagnostic m/z ions.

Aromatic compound assignment	Abbreviation	Ion
Naphthalene	N	128
2-Methylnaphthalene	2-MN	142
1-Methylnaphthalene	1-MN	142
2-Ethylnaphthalene	2-EN	156
1-Ethylnaphthalene	1-EN	156
2,6-Dimethylnaphthalene	2,6-DMN	156
2,7-Dimethylnaphthalene	2,7-DMN	156
1,3- and 1,7-Dimethylnaphthalene	1,3- and 1,7-DMN	156
1,6-Dimethylnaphthalene	1,6-DMN	156
1,4- and 2,3-Dimethylnaphthalene	1,4- and 2,3-DMN	156
1,5-Dimethylnaphthalene	1,5-DMN	156
1,2-Dimethylnaphthalene	1,2-DMN	156
1,8-Dimethylnaphthalene	1,8-DMN	156
1,3,7-Trimethylnaphthalene	1,3,7-TMN	170
1,3,6-Trimethylnaphthalene	1,3,6-TMN	170
1,3,5- and 1,4,6-Trimethylnaphthalene	1,3,5- and 1,4,6-TMN	170
2,3,6-Trimethylnaphthalene	2,3,6-TMN	170
1,2,7-Trimethylnaphthalene	1,2,7-TMN	170
1,6,7-Trimethylnaphthalene	1,6,7-TMN	170
1,2,6-Trimethylnaphthalene	1,2,6-TMN	170
1,2,4-Trimethylnaphthalene	1,2,4-TMN	170
1,2,5-Trimethylnaphthalene	1,2,5-TMN	170
1,2,3-Trimethylnaphthalene	1,2,3-TMN	170
1,3,6,7-Tetramethylnaphthalene	1,3,6,7-TeMN	184
1,2,4,6-, 1,2,4,7- and 1,4,6,7-Tetramethylnaphthalene	1,2,4,6-, 1,2,4,7- and 1,4,6,7-TeMN	184
1,2,5,7-Tetramethylnaphthalene	1,2,5,7-TeMN	184
2,3,6,7-Tetramethylnaphthalene	2,3,6,7-TeMN	184
1,2,6,7-Tetramethylnaphthalene	1,2,6,7-TeMN	184
1,2,3,7-Tetramethylnaphthalene	1,2,3,7-TeMN	184
1,2,3,6-Tetramethylnaphthalene	1,2,3,6-TeMN	184
1,2,5,6- and 1,2,3,5-Tetramethylnaphthalene	1,3,6,7- and 1,2,3,5-TeMN	184

Continued...

Table A5-41 (continued): Peak abbreviations for the aromatic hydrocarbons, with diagnostic m/z ions.

Aromatic compound assignment	Abbreviation	Ion
1,2,4,6,7-Pentamethylnaphthalenes	1,2,4,6,7-PMN	198
1,2,3,5,7-Pentamethylnaphthalenes	1,2,3,5,7-PMN	198
1,2,3,6,7-Pentamethylnaphthalenes	1,2,3,6,7-PMN	198
1,2,3,5,6-Pentamethylnaphthalenes	1,2,3,5,6-PMN	198
Phenanthrene	P	178
3-Methylphenanthrene	3-MP	192
2-Methylphenanthrene	2-MP	192
9-Methylphenanthrene	9-MP	192
1-Methylphenanthrene	1-MP	192
3-Ethylphenanthrene	3-EP	206
9-, 2- and 1 + Ethylphenanthrene + 3,6-Dimethylphenanthrene	9-EP, 2-EP, 1-EP, 3,6-DMP	206
3,5- and 2,6-Dimethylphenanthrene	3,5- and 2,6-DMP	206
2,7-Dimethylphenanthrene	2,7-DMP	206
1,3-, 3,9-, 2,10- and 3,10-Dimethylphenanthrene	1,3-, 3,9-, 2,10- and 3,10-	206
1,6-, 2,9- and 2,5-Dimethylphenanthrene	1,6-, 2,9- and 2,5-DMP	206
1,7-Dimethylphenanthrene	1,7-DMP	206
2,3-, 1,9-, 4,9- and 4,10-Dimethylphenanthrene	2,3-, 1,9-, 4,9- and 4,10-DMP	206
1,8-Dimethylphenanthrene	1,8-DMP	206
1,2-Dimethylphenanthrene	1,2-DMP	206
Trimethylphenanthrenes	TMPs	220
Tetramethylphenanthrenes	TeMPs	234
1-Isohexyl-2-methyl-6-isopropylnaphthalene	i-HMN	197
Biphenyl	Bp	154
2-Methylbiphenyl	2-MBp	168
Diphenylmethane	DPM	168
3-Methylbiphenyl	3-MBp	168
4-Methylbiphenyl	4-MBp	168
Dibenzofuran	DBF	168
2,3'-Dimethylbiphenyl	2,3'-DMBp	182
2,5-Dimethylbiphenyl	2,5-DMBp	182
2,4- + 2,4'-Dimethylbiphenyl	2,4- + 2,4'-DMBp	182
2,3-Dimethylbiphenyl	2,3-DMBp	182
3-Methyldiphenylmethane	3-MDPM	182
4-Methyldiphenylmethane	4-MDPM	182
3-Ethylbiphenyl	3-EBp	182
3,5-Dimethylbiphenyl	3,5-DMBp	182

Continued...

Table A5-41 (continued): Peak abbreviations for the aromatic hydrocarbons, with diagnostic m/z ions.

Aromatic compound assignment	Abbreviation	Ion
3,3'-Dimethylbiphenyl	3,3'-DMBp	182
4-Ethylbiphenyl	4-EBp	182
3,4'-Dimethylbiphenyl	3,4'-DMBp	182
4,4'-Dimethylbiphenyl	4,4'-DMBp	182
Fluorene	Fl	166
2-Methylfluorene	2-MFl	180
3-Methylfluorene	3-MFl	180
1-Methylfluorene	1-MFl	180
4-Methylfluorene	4-MFl	180
Fluoranthene	Fa	202
Pyrene	Py	202
Methylfluoranthenes	MFa	216
2-Methylpyrene	2-MPy	216
4-Methylpyrene	4-MPy	216
1-Methylpyrene	1-MPy	216
Dibenzothiophene	DBT	184
4-Methyldibenzothiophene	4-MDBT	198
2-Methyldibenzothiophene	2-MDBT	198
3-Methyldibenzothiophene	3-MDBT	198
1-Methyldibenzothiophene	1-MDBT	198
4-Ethyldibenzothiophene	4-ETDBT	212
4,6-Dimethyldibenzothiophene	4,6-DMDBT	212
2,4-Dimethyldibenzothiophene	2,4-DMDBT	212
2,6-Dimethyldibenzothiophene	2,6-DMDBT	212
3,6-Dimethyldibenzothiophene	3,6-DMDBT	212
3,7-Dimethyldibenzothiophene	3,7-DMDBT	212
1,4-Dimethyldibenzothiophene	1,4-DMDBT	212
1,6-Dimethyldibenzothiophene	1,6-DMDBT	212
1,8-Dimethyldibenzothiophene	1,8-DMDBT	212
1,3-Dimethyldibenzothiophene	1,3-DMDBT	212
1,9-Dimethyldibenzothiophene	1,9-DMDBT	212
1,2-Dimethyldibenzothiophene	1,2-DMDBT	212

Table A5-44: Peak assignments for diamondoid hydrocarbons (adamantanes and diamantanes), with the diagnostic *m/z* ions.

Diamondoid compound assignment	Abbreviation	Ion
Adamantane	Ad	136
1-Methyladamantane	1-MAd	135
2-Methyladamantane	2-MAd	135
1-Ethyladamantane	1-EtAd	135
2-Ethyladamantane	2-EtAd	135
1,3-Dimethyladamantane	1,3-DMAd	149
<i>cis</i> -1,3-Dimethyladamantane	<i>cis</i> -1,4-DMAd	149
<i>trans</i> -1,3-Dimethyladamantane	<i>trans</i> -1,4-DMAd	149
1,2-Dimethyladamantane	1,2-DMAd	149
1-Ethyl, 3-Methyladamantane	1-Et,3-MAd	149
1,3,5-Trimethyladamantane	1,3,5-TMAd	163
1,3,6-Trimethyladamantane	1,3,6-TMAd	163
<i>cis</i> -1,3,4-Trimethyladamantane	<i>cis</i> -1,3,4-TMAd	163
<i>trans</i> -1,3,4-Trimethyladamantane	<i>trans</i> -1,3,4-TMAd	163
1-Ethyl, 3,5-Dimethyladamantane	1-Et,3,5-DMAd	163
1,3,5,7-Tetramethyladamantane	1,3,5,7-TeMAd	177
1,2,5,7-Tetramethyladamantane	1,2,5,7-TeMAd	177
Diamantane	DIA	188
4-Methyldiamantane	4-MDIA	187
1-Methyldiamantane	1-MDIA	187
3-Methyldiamantane	3-MDIA	187
4,9-Dimethyldiamantane	4,9-DMDIA	201
1,4- and 2,4-Dimethyldiamantane	1,4- + 2,4-DMDIA	201
4,8-Dimethyldiamantane	4,8-DMDIA	201
3,4-Dimethyldiamantane	3,4-DMDIA	201
Trimethyldiamantane	TMDIA	215

Table A5-45: Peak assignments for low molecular weight hydrocarbons, with structures.

Abbreviation	Identification	Structure
C1	Methane	CH ₄
C2	Ethane	
C3	Propane	
iC4	<i>iso</i> -Butane	
nC4	<i>n</i> -Butane	
22DMP	2,2-Dimethylpropane	
iC5	<i>iso</i> -Pentane	
nC5	<i>n</i> -Pentane	
F	Furan	
22DMB	2,2-Dimethylbutane	
CP	Cyclopentane	
23DMB	2,3-Dimethylbutane	
2MP	2-Methylpentane	
3MP	3-Methylpentane	
n=C6	<i>n</i> -Hexene	
nC6	<i>n</i> -Hexane	
MF	Methylfuran (2 isomers, a and b)	
22DMP	2,2-Dimethylpentane	
MCP	Methylcyclopentane	
24DMP	2,4-Dimethylpentane	
223TMB	2,2,3-Trimethylbutane	

Table A5-43 (continued): Peak assignments for low molecular weight hydrocarbons, with structures.




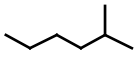
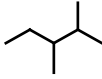
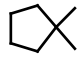
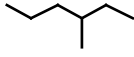
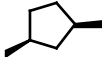
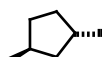
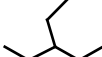
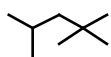
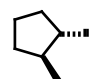


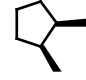
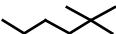
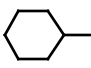
Abbreviation	Identification	Structure
33DMP	3,3-Dimethylpentane	
B	Benzene	
CH	Cyclohexane	
2MH	2-Methylhexane	
23DMP	2,3-Dimethylpentane	
11DMCP	1,1-Dimethylcyclopentane	
3MH	3-Methylhexane	
c13DMCP	1, <i>cis</i> -3-Dimethylcyclopentane	
t13DMCP	1, <i>trans</i> -3-Dimethylcyclopentane	
3EP	3-Ethylpentane	
224TMP	2,2,4-Trimethylpentane	
t12DMCP	1, <i>trans</i> -2-Dimethylcyclopentane	
n=C7	<i>n</i> -Heptene	
nC7	<i>n</i> -Heptane	
c12DMCP	1, <i>cis</i> -2-Dimethylcyclopentane	
22DMH	2,2-Dimethylhexane	
MCH	Methylcyclohexane	

Table A5-43 (continued): Peak assignments for low molecular weight hydrocarbons, with structures.


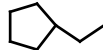
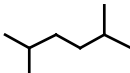
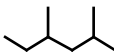
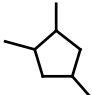

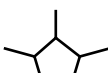
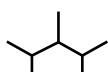
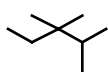
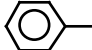
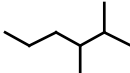
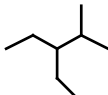
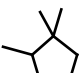
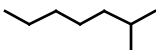
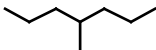
Abbreviation	Identification	Structure
113TMCP	1,1,3-Trimethylcyclopentane	
ECP	Ethylcyclopentane	
25DMH	2,5-Dimethylhexane	
24DMH	2,4-Dimethylhexane	
124TMCP	1,2,4-Trimethylcyclopentane	
33DMH	3,3-Dimethylhexane	
123TMCP	1,2,3-Trimethylcyclopentane	
234TMP	2,3,4-Trimethylpentane	
233TMP	2,3,3-Trimethylpentane	
T	Toluene	
23DMH	2,3-Dimethylhexane	
2M3EP	2-Methyl-3-ethylpentane	
112TMCP	1,1,2-Trimethylcyclopentane	
2MHe	2-Methylheptane	
4MHe	4-Methylheptane	

Table A5-43 (continued): Peak assignments for low molecular weight hydrocarbons, with structures.

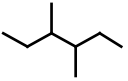
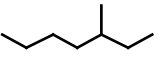
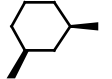
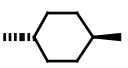
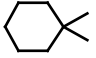
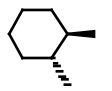
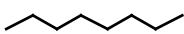
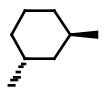
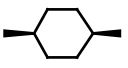
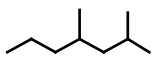
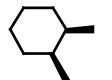
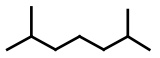
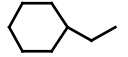
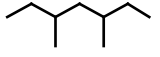
Abbreviation	Identification	Structure
34DMH	3,4-Dimethylhexane	
3MHe	3-Methylheptane	
c13DMCH	1, <i>cis</i> -3-Dimethylcyclohexane	
t14DMCH	1, <i>trans</i> -4-Dimethylcyclohexane	
11DMCH	1,1-Dimethylcyclohexane	
C3CP	C ₃ Cyclopentane	—
t12DMCH	1, <i>trans</i> -2-Dimethylcyclohexane	
C4CP	C ₄ Cyclopentane	—
nC8	<i>n</i> -Octane	
t13DMCH	1, <i>trans</i> -3-Dimethylcyclohexane	
c14DMCH	1, <i>cis</i> -4-Dimethylcyclohexane	
24DMHe	2,4-Dimethylheptane	
c12DMCH	1, <i>cis</i> -2-Dimethylcyclohexane	
26DMHe	2,6-Dimethylheptane	
ECH	Ethylcyclohexane	
35DMHe	3,5-Dimethylheptane	

Table A5-43 (continued): Peak assignments for low molecular weight hydrocarbons, with structures.

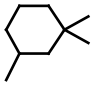
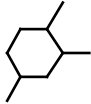
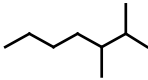
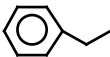
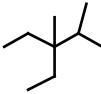
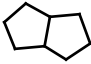
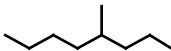
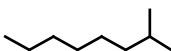
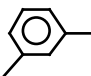
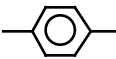
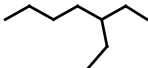
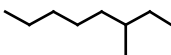
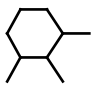
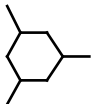
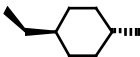
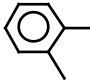
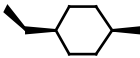

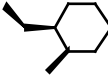
Abbreviation	Identification	Structure
113TMCH	1,1,3-Trimethylcyclohexane	
124TMCH	1,2,4-Trimethylcyclohexane	
23DMHe	2,3-Dimethylheptane	
EB	Ethylbenzene	
EDMP	3-Ethyl-2,3-dimethylpentane	
OHP	Octahydropentalene	
4MO	4-Methyloctane	
2MO	2-Methyloctane	
m-xylene	<i>meta</i> -Xylene	
p-xylene	<i>para</i> -Xylene	
3EHe	3-Ethylheptane	
3MO	3-Methyloctane	
123TMCH	1,2,3-Trimethylcyclohexane	
135TMCH	1,3,5-Trimethylcyclohexane	

Table A5-43 (continued): Peak assignments for low molecular weight hydrocarbons, with structures.

Abbreviation	Identification	Structure
t14EMCH	1, <i>trans</i> -4-Ethylmethylcyclohexane	
<i>o</i> -xylene	<i>ortho</i> -Xylene	
c14EMCH	1, <i>cis</i> -4-Ethylmethylcyclohexane	
nC9	<i>n</i> -Nonane	
c12EMCH	1, <i>cis</i> -2-Ethylmethylcyclohexane	

APPENDIX 6: OFF-LINE MCI – Gnarlyknots-1A

Fluid Inclusion Oil (4390-4425 mMD)

Mass Chromatograms and Peak Identifications

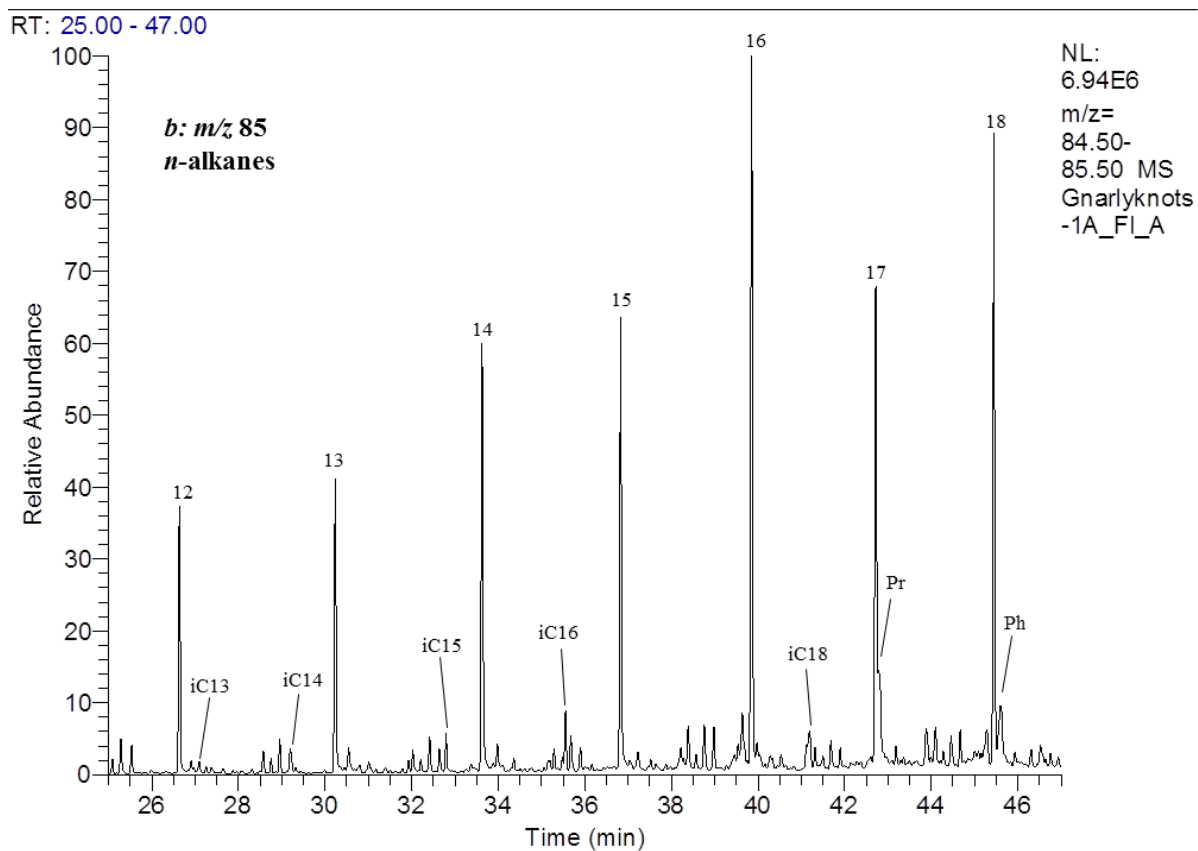
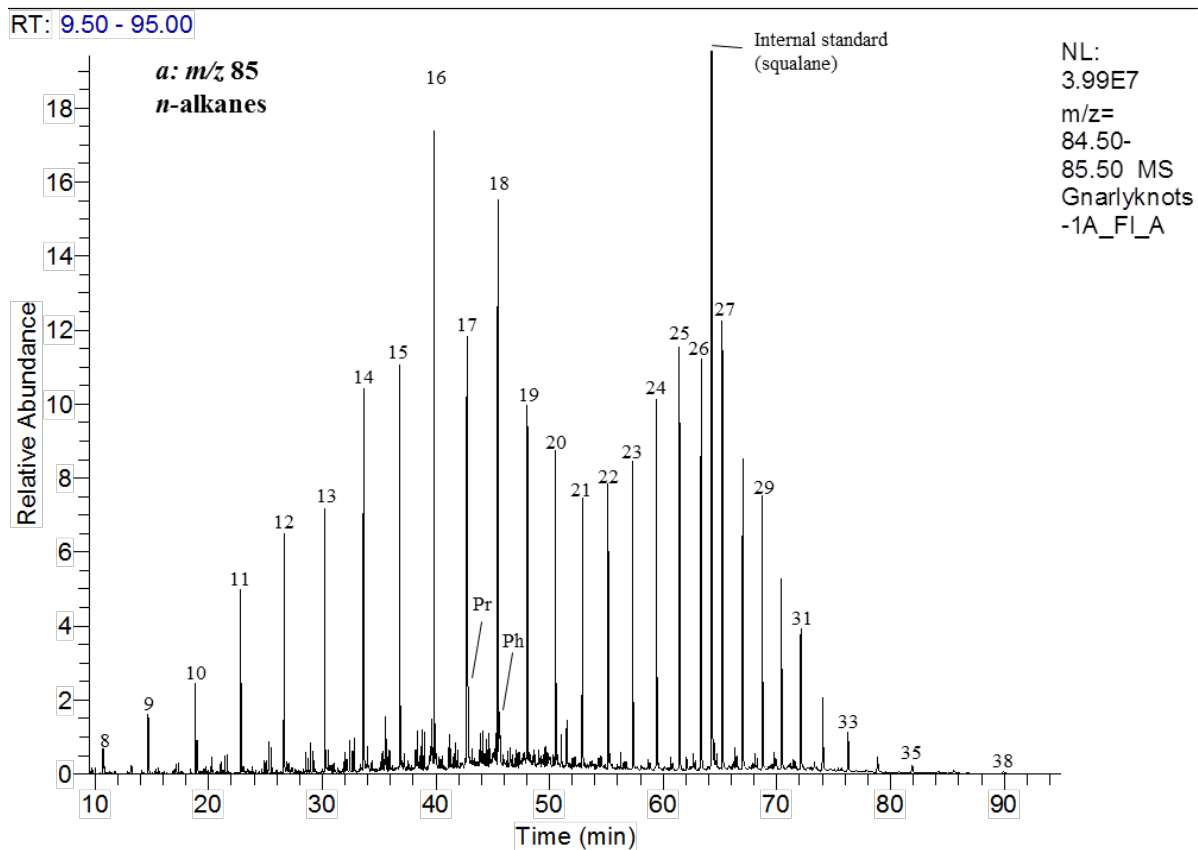


Figure A6-112: Partial m/z 85 mass chromatograms for the Gnarlyknots-1A (4390-4425m) FI oil. Showing the distribution of n-alkanes and isoprenoids. Numbers refer to n-alkane chain length, Pr = pristane, Ph = phytane, iC13 = C13 isoprenoid, etc.

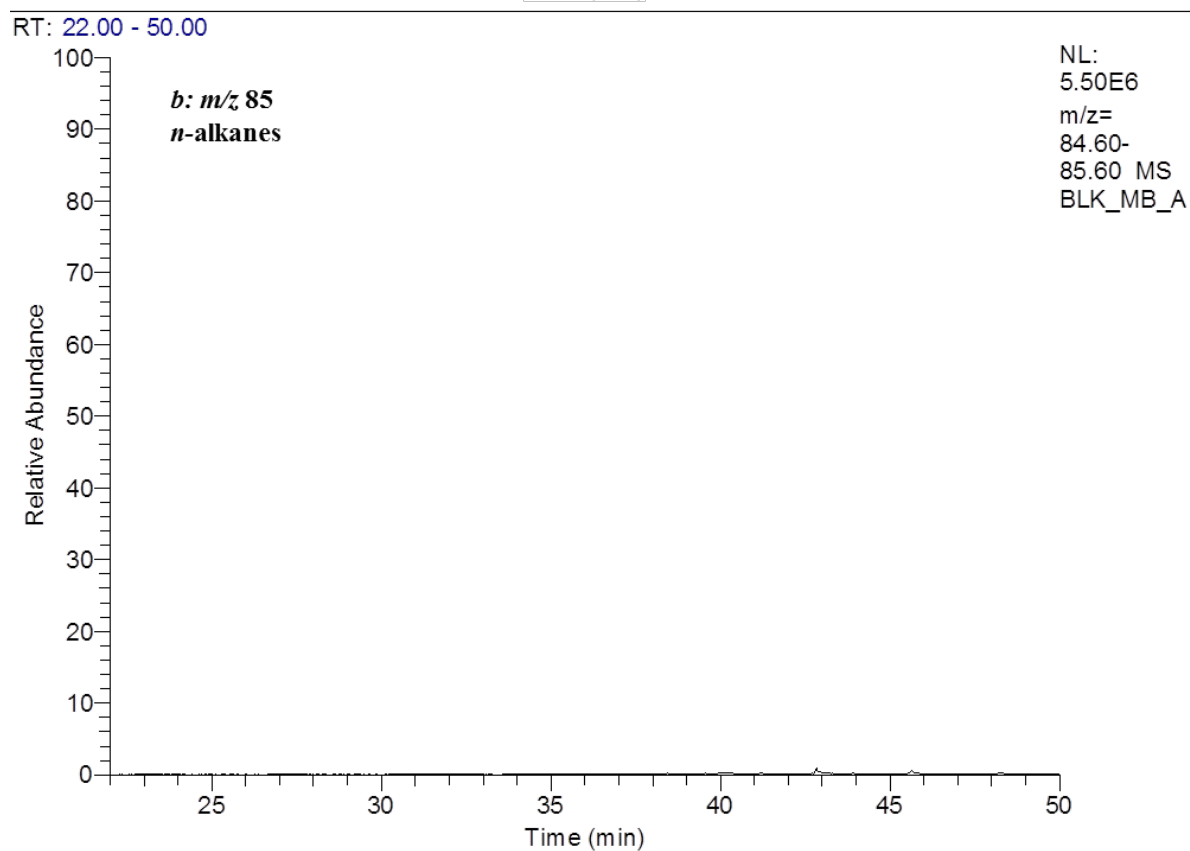
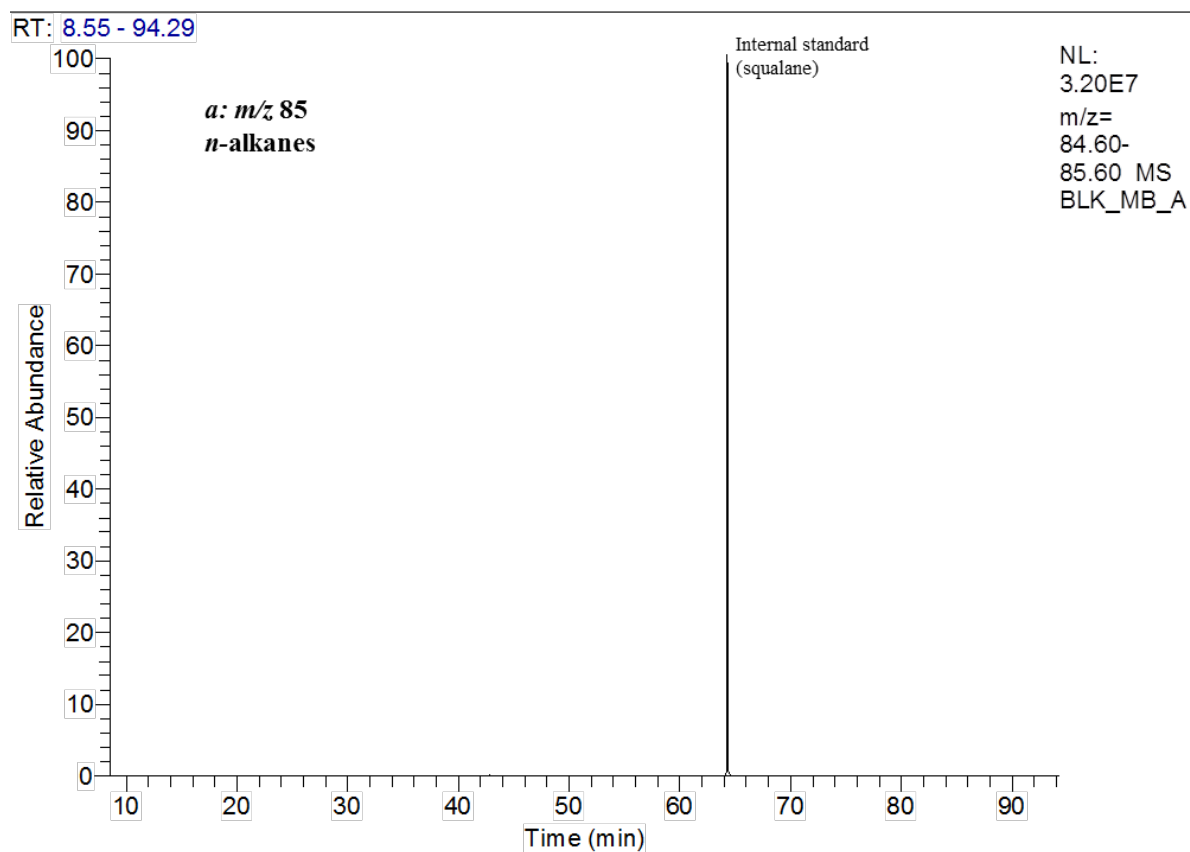


Figure A6-113: Partial m/z 85 mass chromatograms for the Gnarlyknots-1A (4390-4425m) FI system blank. Showing the distribution of *n*-alkanes, methylalkanes and isoprenoids. Numbers refer to *n*-alkane chain length, Pr = pristane, Ph = phytane, iC13 = C13 isoprenoid, etc.

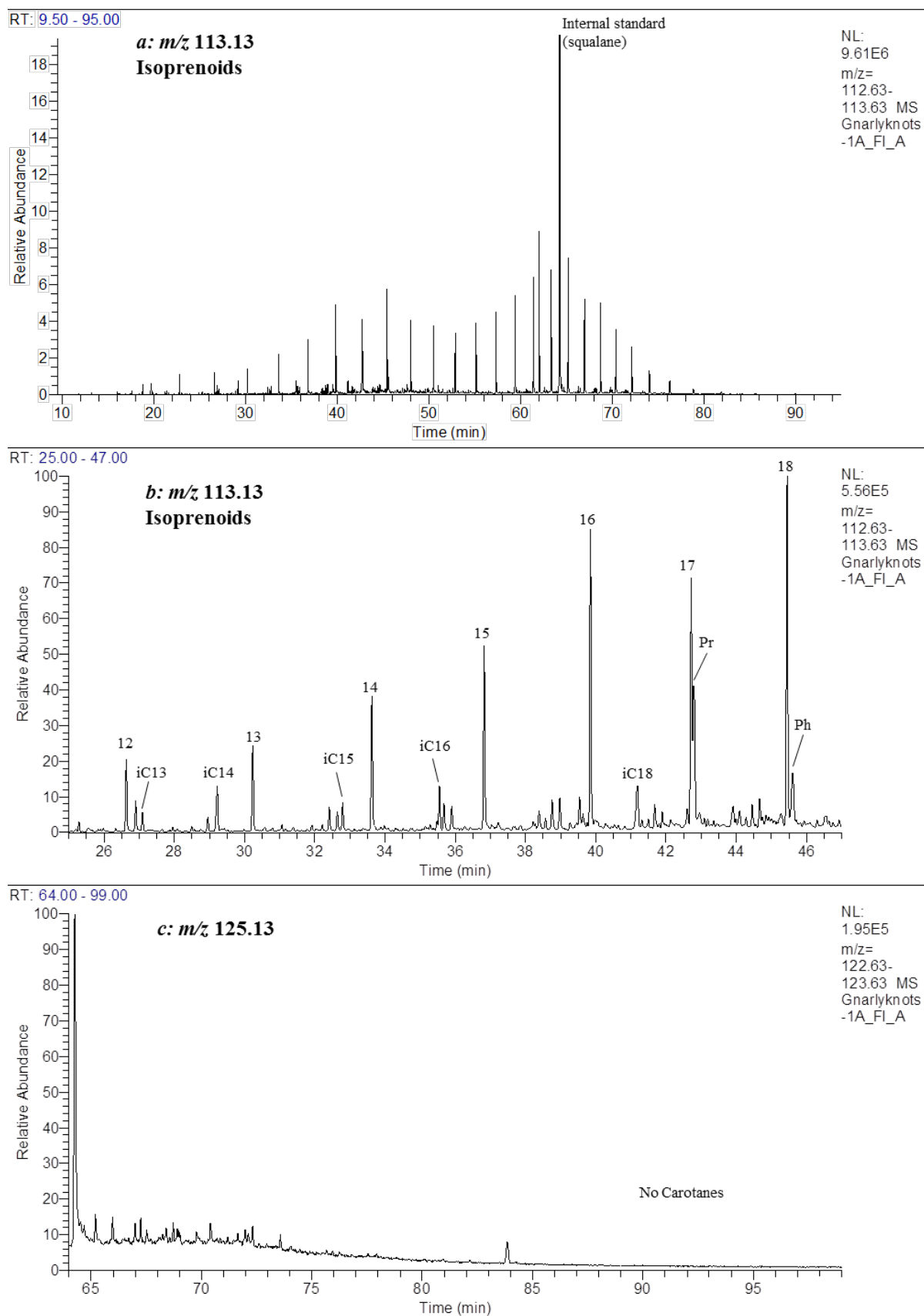


Figure A6-114: Partial m/z 113 and 125 mass chromatograms for the Gnarlyknots-1A (4390-4425m) FI oil. Showing the distribution of isoprenoids and β -carotene. Numbers refer to n -alkane chain length, Pr = pristane, Ph = phytane, iC13 = C13 isoprenoid, etc.

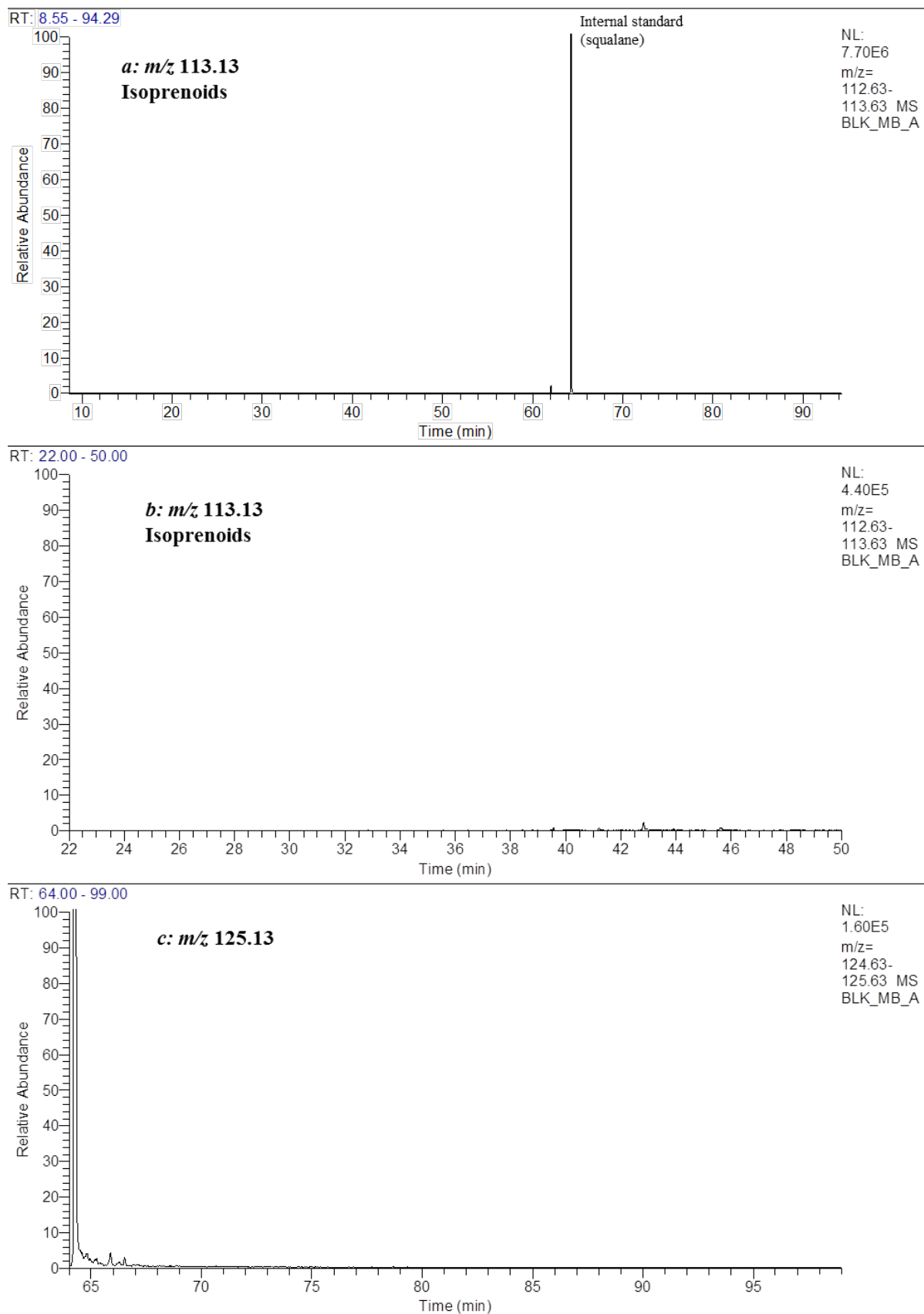


Figure A6-115: Partial m/z 113 and 125 mass chromatograms for the Gnarlyknots-1A (4390-4425m) FI system blank. Showing the distribution of isoprenoids and *b*-carotane. Numbers refer to *n*-alkane chain length, Pr = pristane, Ph = phytane, *i*C13 = C13 isoprenoid, etc

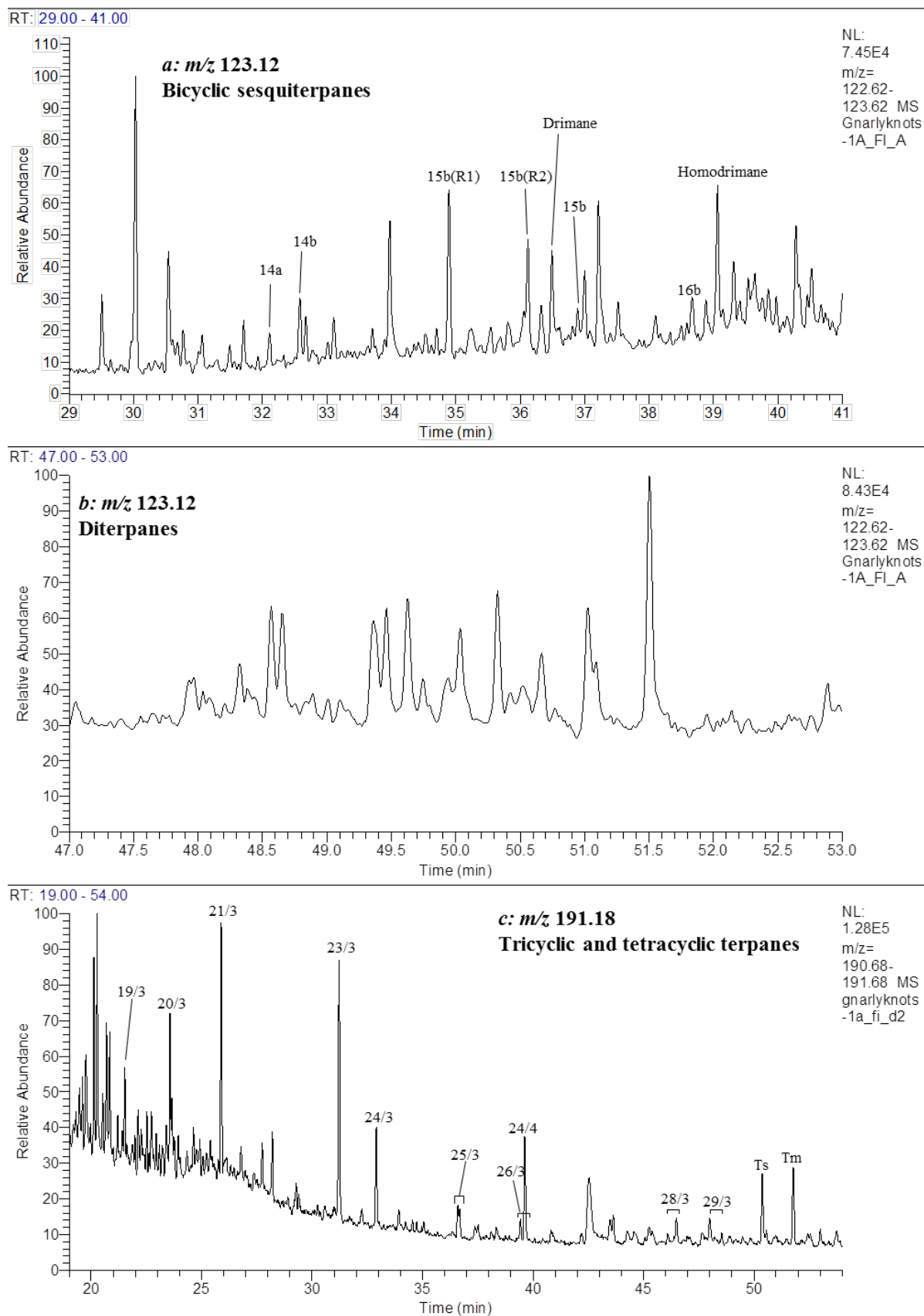


Figure A6-116: Partial m/z 123 and 191 mass chromatograms for the Gnarlyknots-1A (4390-4425m) FI oil. Showing the distribution of (a) C14 to C16 bicyclic sesquiterpanes, (b) diterpanes and (c) tricyclic/tetracyclic terpanes. 14b refers to C14 bicyclic sesquiterpanes, 19/3 refers to C19 tricyclic terpane, 24/4 refers to C24 tetracyclic terpane, and so on. dO, dL and dU refer to A-ring degraded oleanoids, lupane and ursane. Hopane abbreviations listed in Table A5-37.

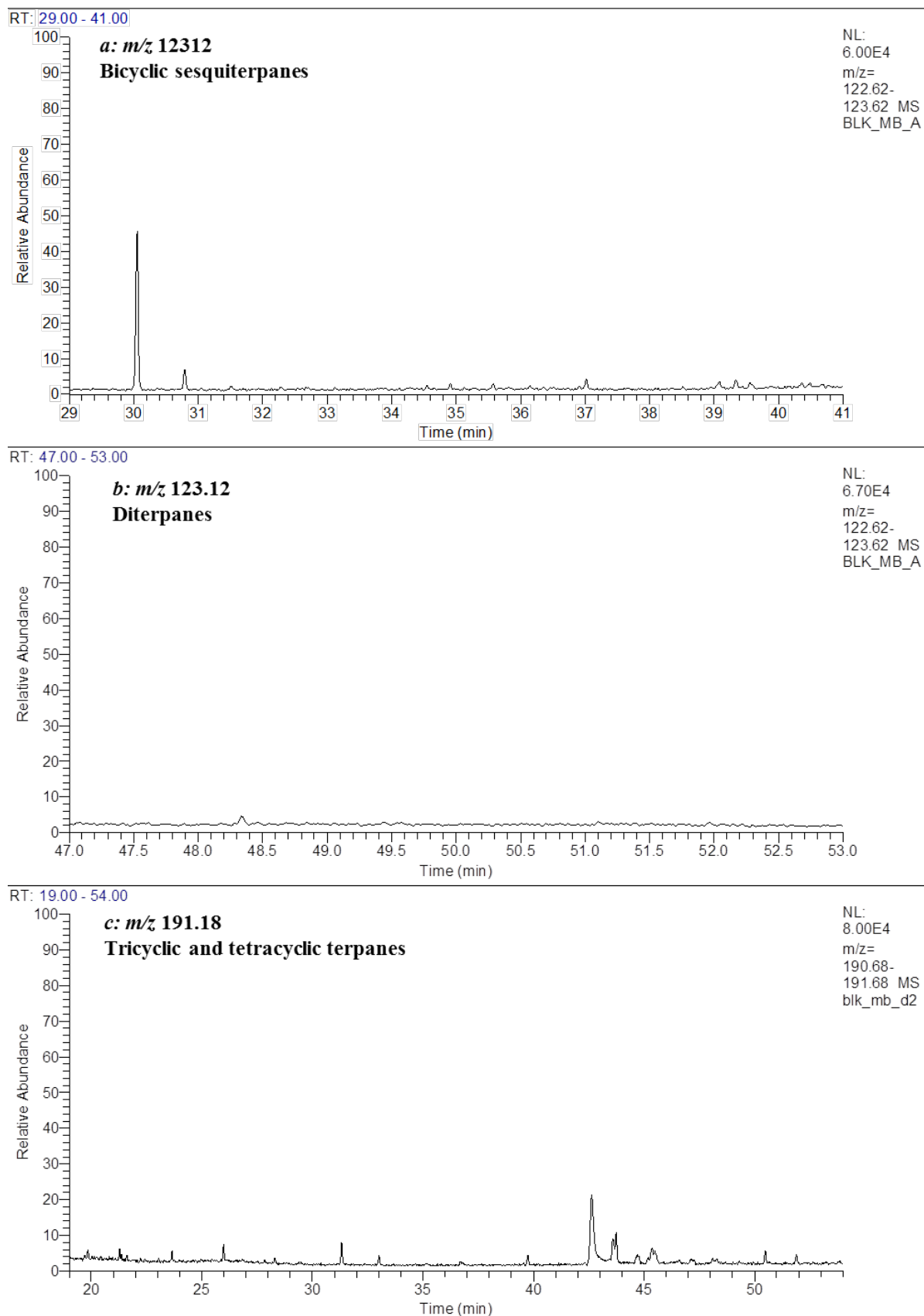


Figure A6-117: Partial m/z 123 and 191 mass chromatograms for the Gnarlyknots-1A (4390-4425m) FI system blank. Showing the distribution of (a) C14 to C16 bicyclic sesquiterpanes, (b) diterpanes and (c) tricyclic/tetracyclic terpanes. 14b refers to C₁₄ bicyclic sesquiterpanes, 19/3 refers to C₁₉ tricyclic terpane, 24/4 refers to C₂₄ tetracyclic terpane, and so on. dO, dL and dU refer to A-ring degraded oleanoids, lupane and ursane. Hopane abbreviations listed in Table A5-37.

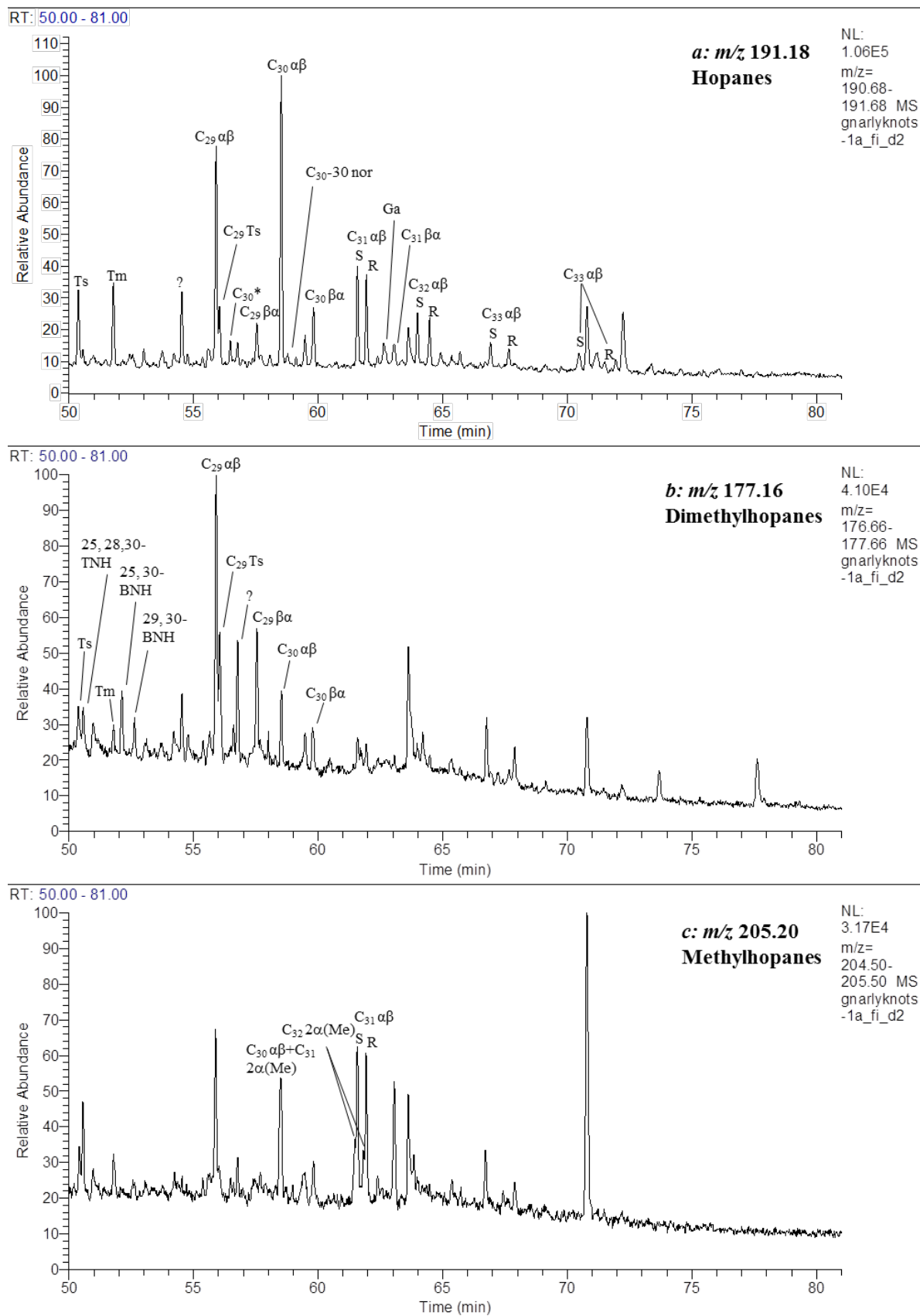


Figure A6-118: Partial m/z 191, 177 and 205 mass chromatograms for the Gnarlyknots-1A (4390-4425m) FI oil. Showing the distribution of (a) hopanes, (b) demethylhopanes and (c) methylhopanes, respectively. Hopane abbreviations are listed in Table A5-37.

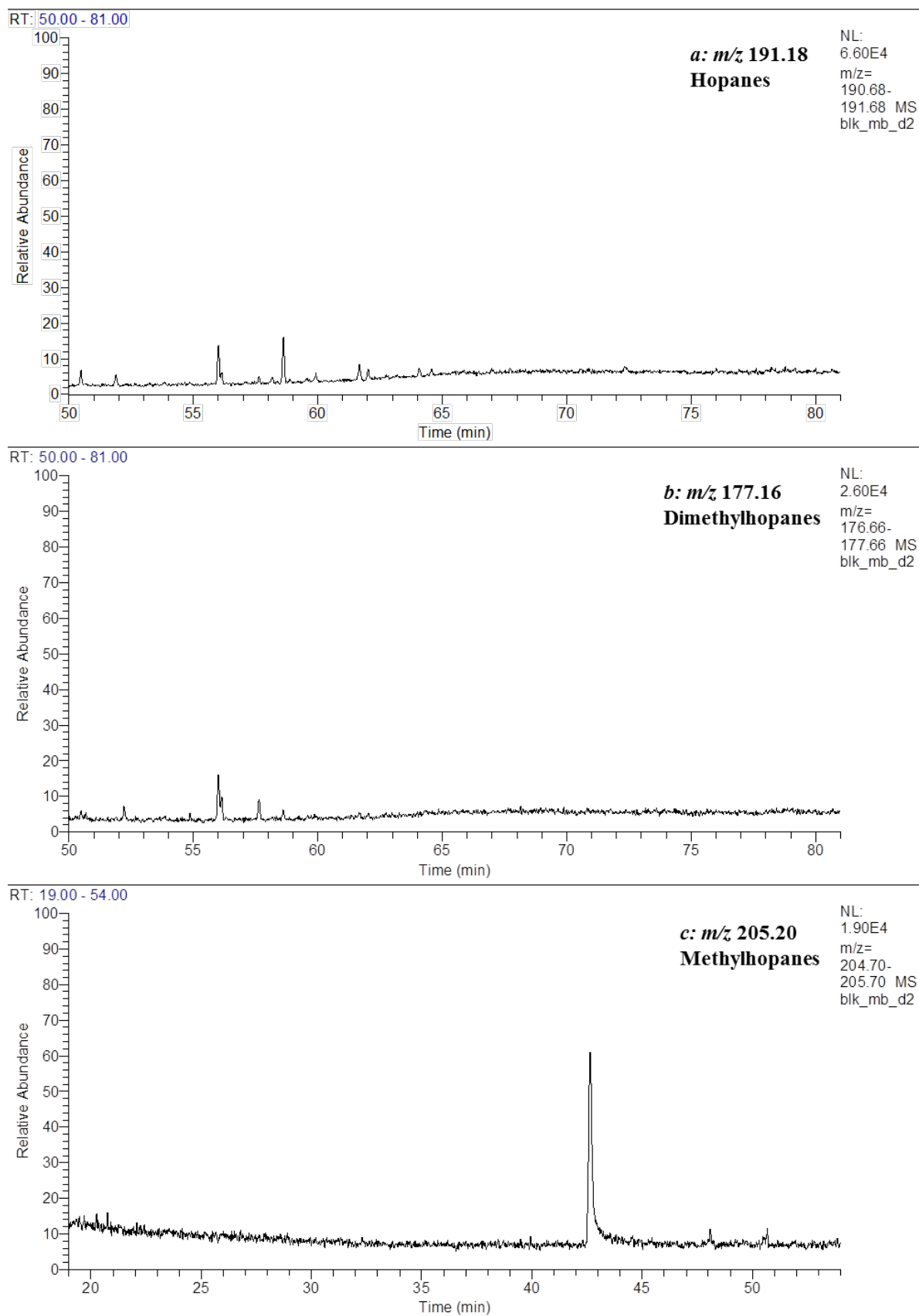


Figure A6-119: Partial m/z 191, 177 and 205 mass chromatograms for the Gnarlyknots-1A (4390-4425m) FI system blank. Showing the distribution of (a) hopanes, (b) demethylhopanes and (c) methylhopanes, respectively. Hopane abbreviations are listed in Table A5-37.

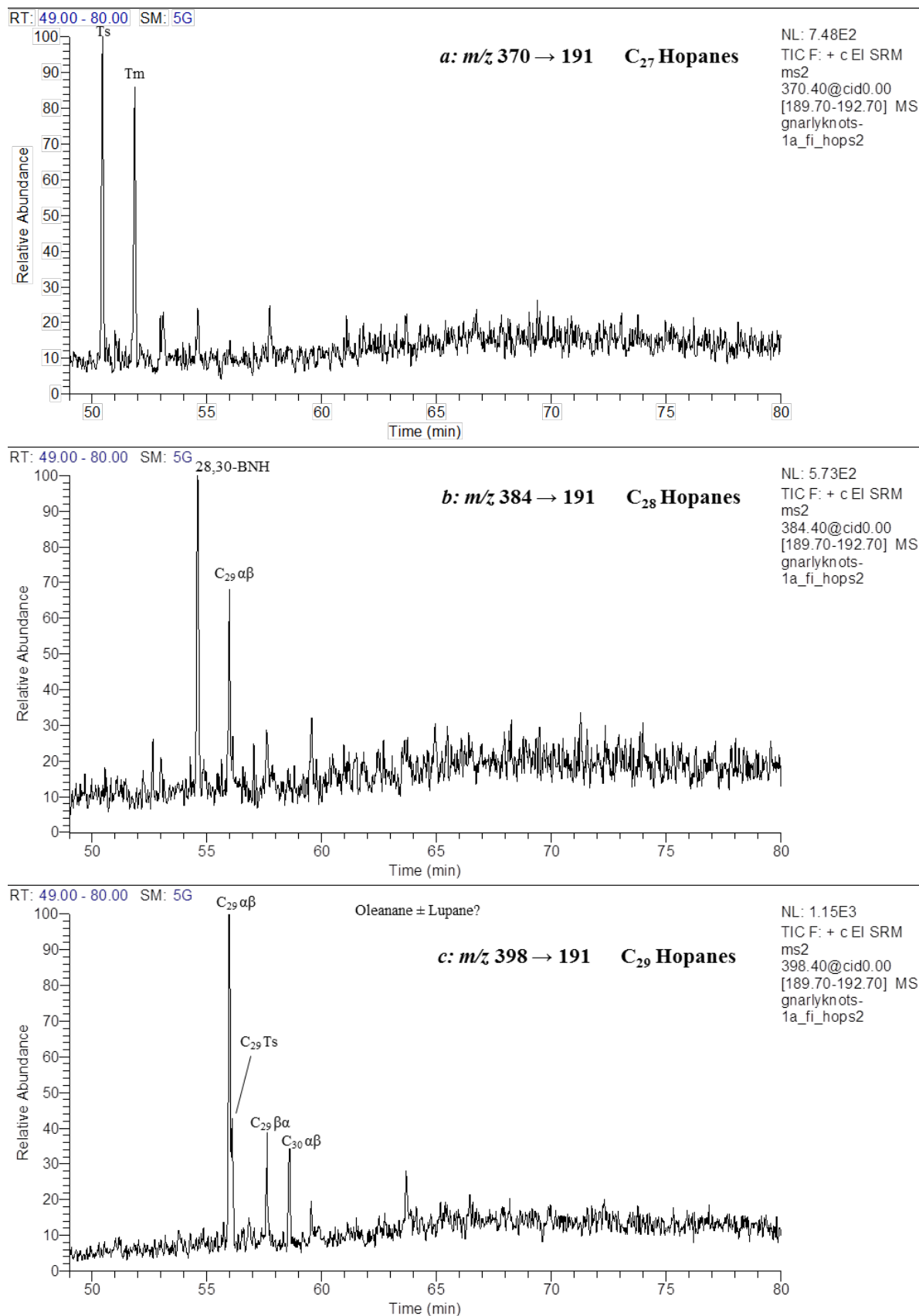


Figure A6-120: Partial MRM chromatograms (m/z 370.4, 398.4 and 398.4 \rightarrow 191.2) of the aliphatic hydrocarbons from the Gnarlyknots-1A (4390-4425m) FI oil.

Showing the distribution of (a) C_{27} (b) C_{28} and (c) C_{29} hopanes. Hopane abbreviations are listed in Table A5-37.

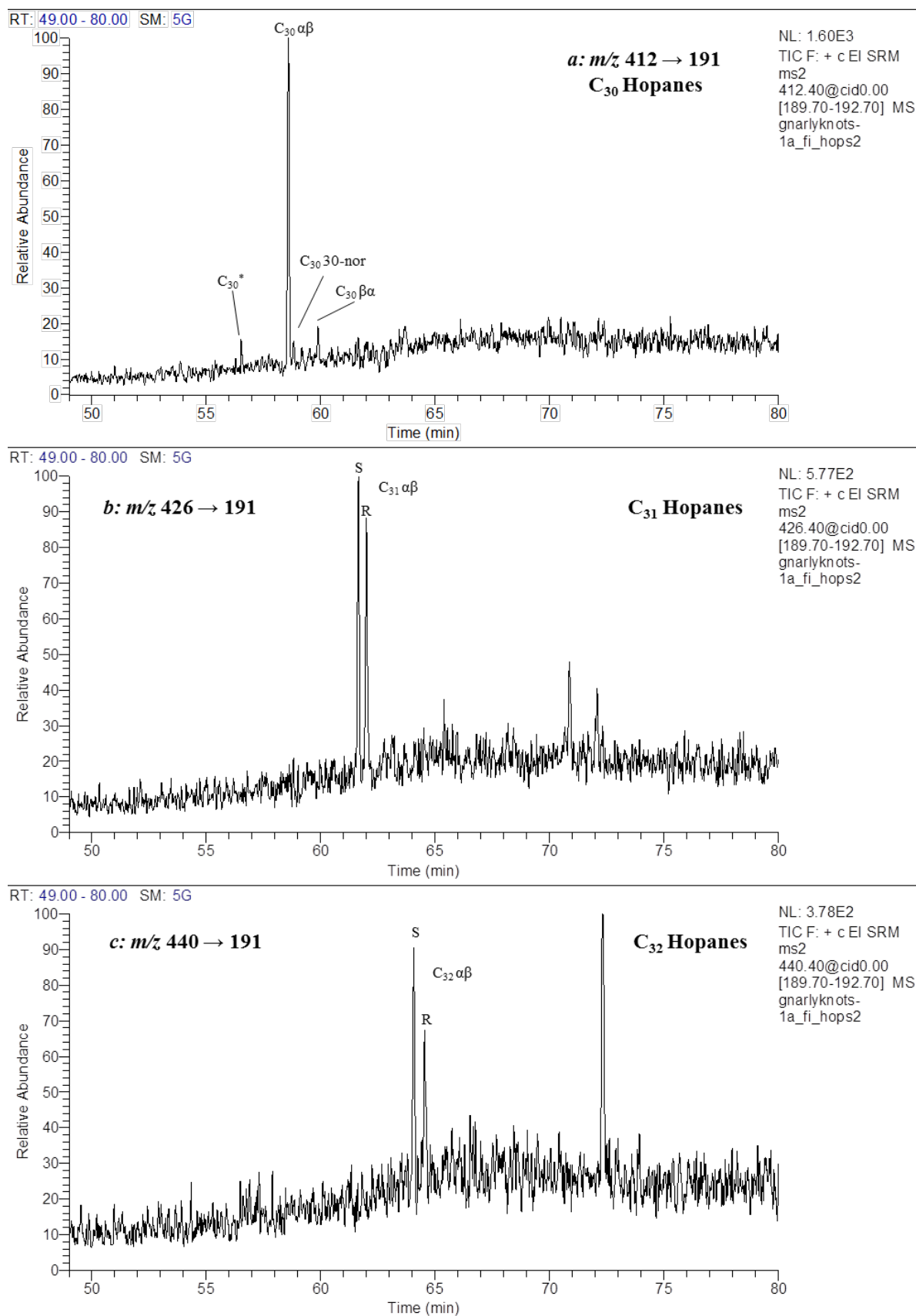


Figure A6-121: Partial MRM chromatograms (m/z 412.4, 426.4 and 440.4 \rightarrow 191.2) of the aliphatic hydrocarbons from the Gnarlyknots-1A (4390-4425m) FI oil.

Showing the distribution of (a) C₃₀ (b) C₃₁ and (c) C₃₂ hopanes. Hopane abbreviations are listed in Table A5-37.

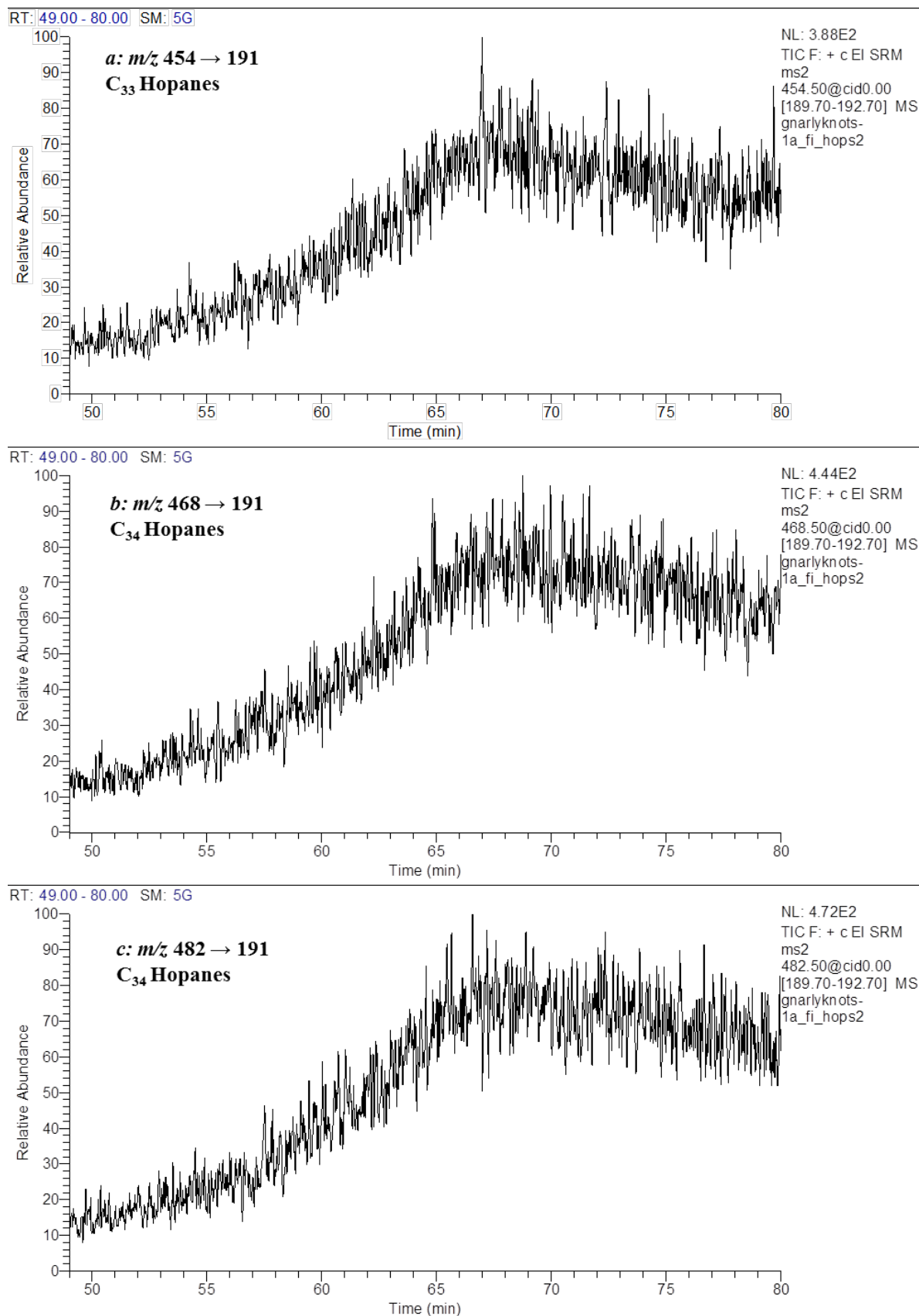


Figure A6-122: Partial MRM chromatograms (m/z 454.5, 468.5 and 482.5 \rightarrow 191.2) of the aliphatic hydrocarbons from the Gnarlyknots-1A (4390-4425m) FI oil.

Showing the distribution of (a) C₃₃ (b) C₃₄ and (c) C₃₅ hopanes. Hopane abbreviations are listed in Table A5-37.

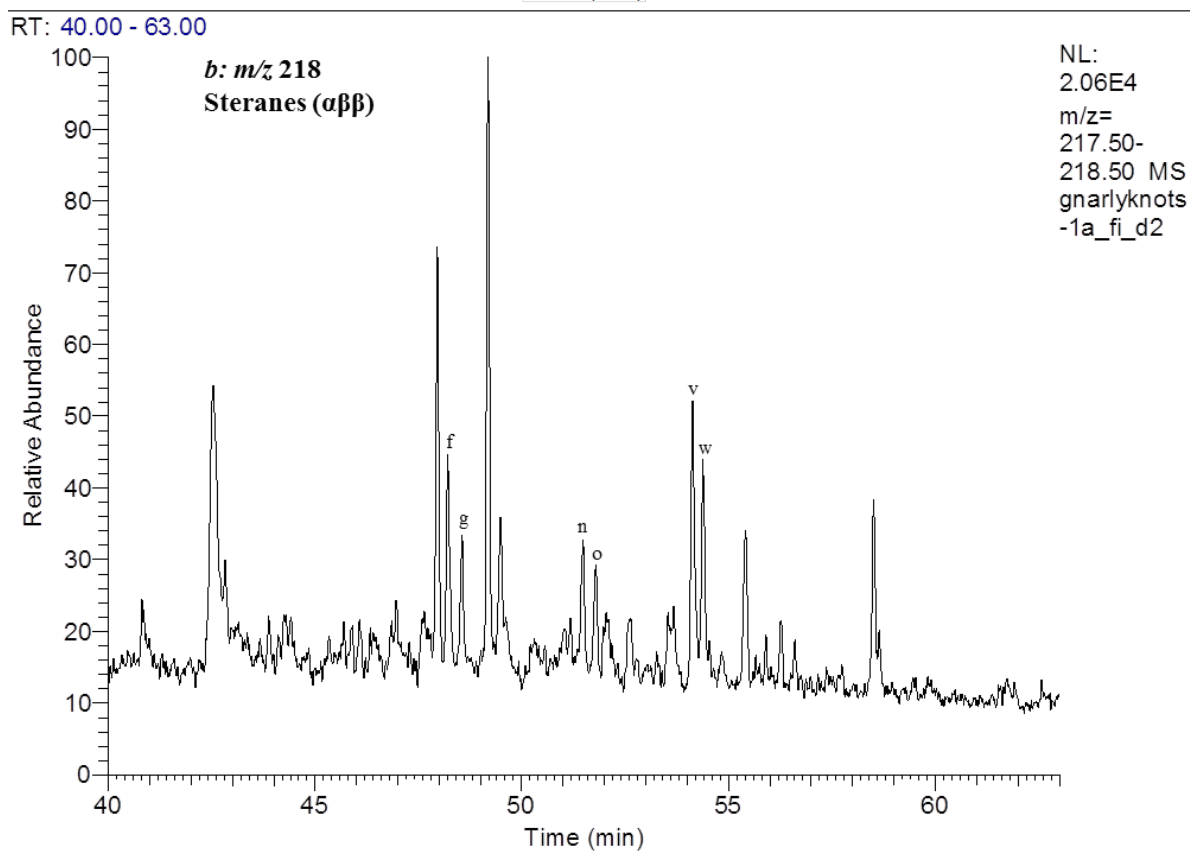
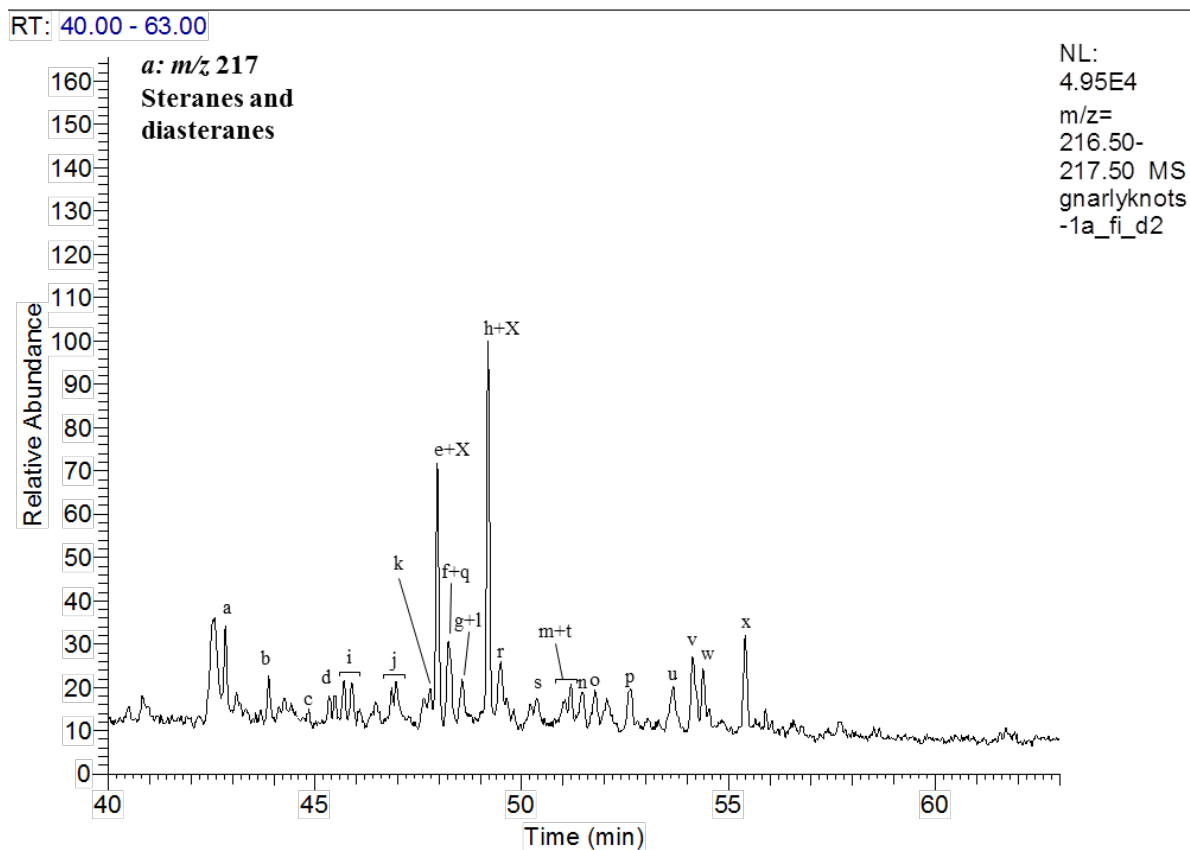


Figure A6-123: Partial m/z (a) 217 and (b) 218 mass chromatograms for the Gnarlyknots-1A (4390-4425m) FI oil. Showing the distribution of steranes and diasteranes. Sterane and diasterane abbreviations are listed in Table A5-38. Peaks labelled with X are unknown compounds.

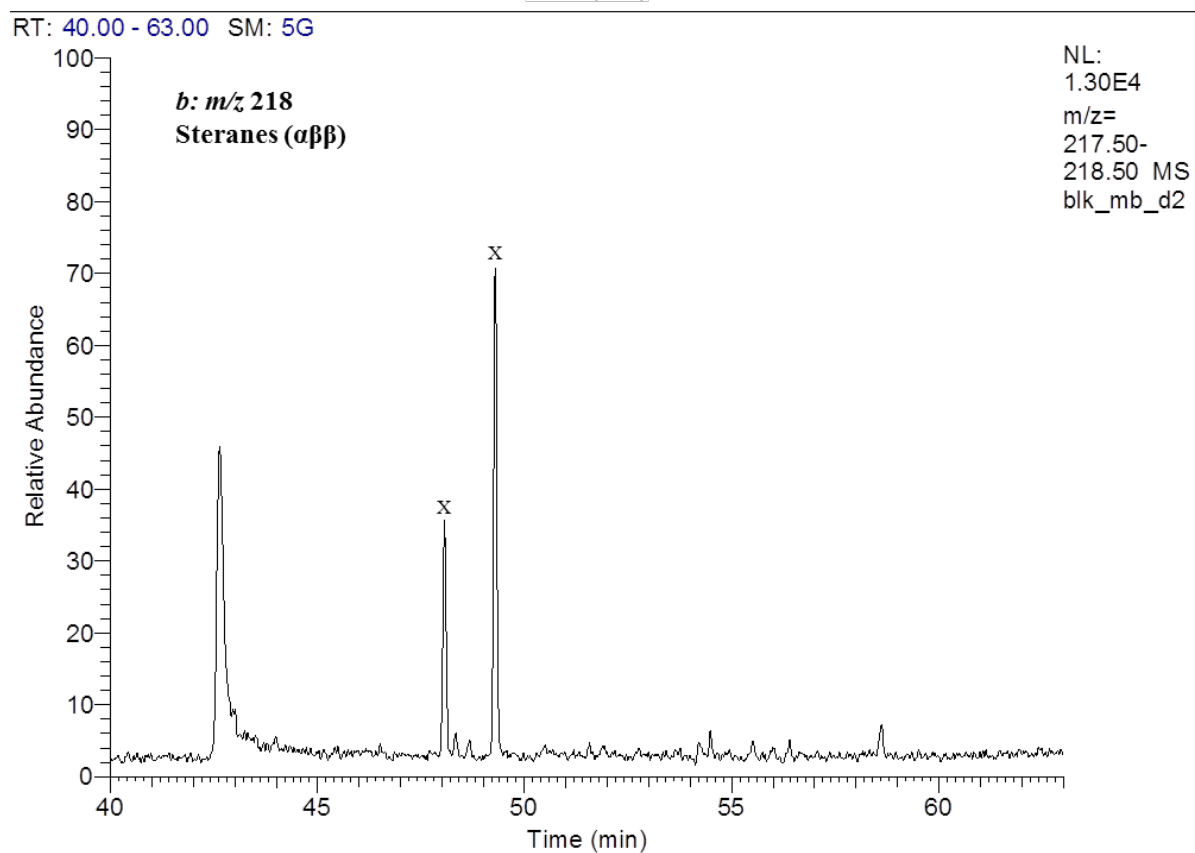
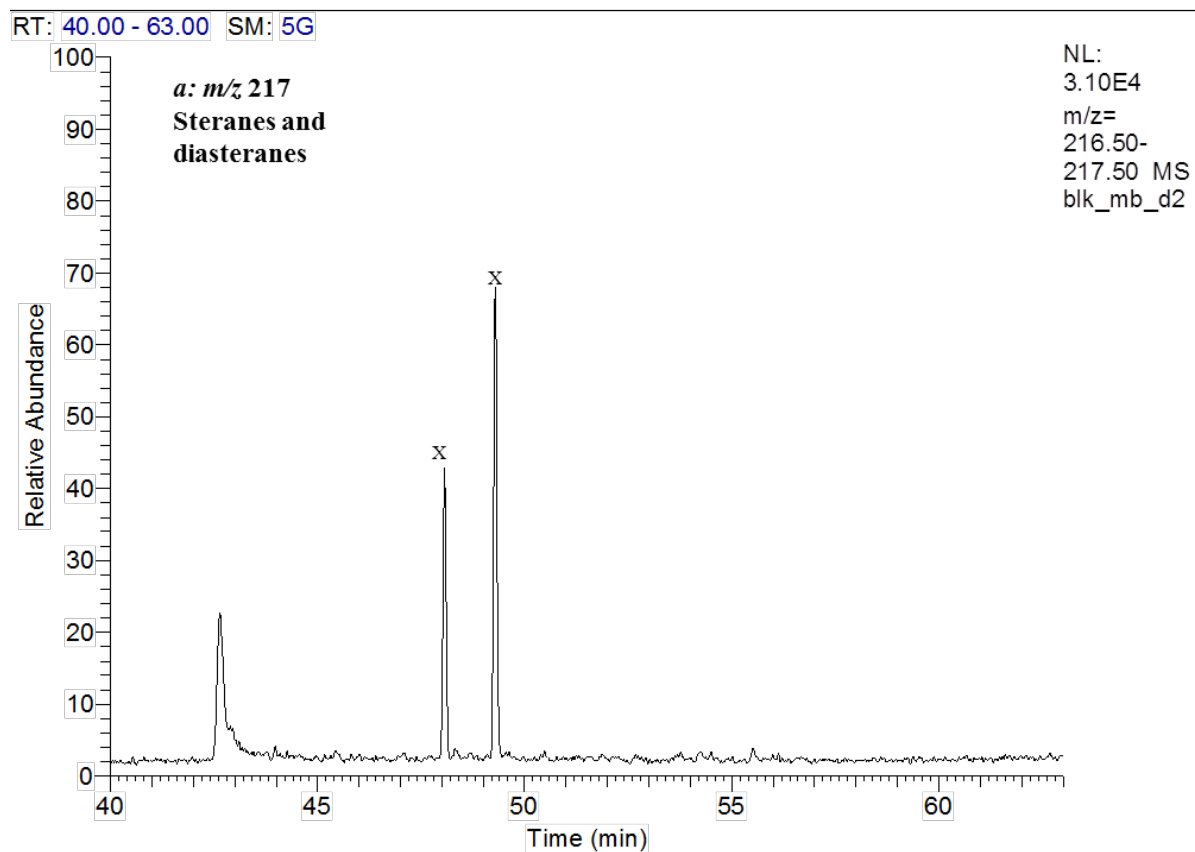


Figure A6-124: Partial m/z (a) 217 and (b) 218 mass chromatograms for the Gnarlyknots-1A (4390-4425m) FI system blank. Showing the distribution of steranes and diasteranes. Sterane and diasterane abbreviations are listed in Table A5-38. Peaks labelled with X are unknown compounds.

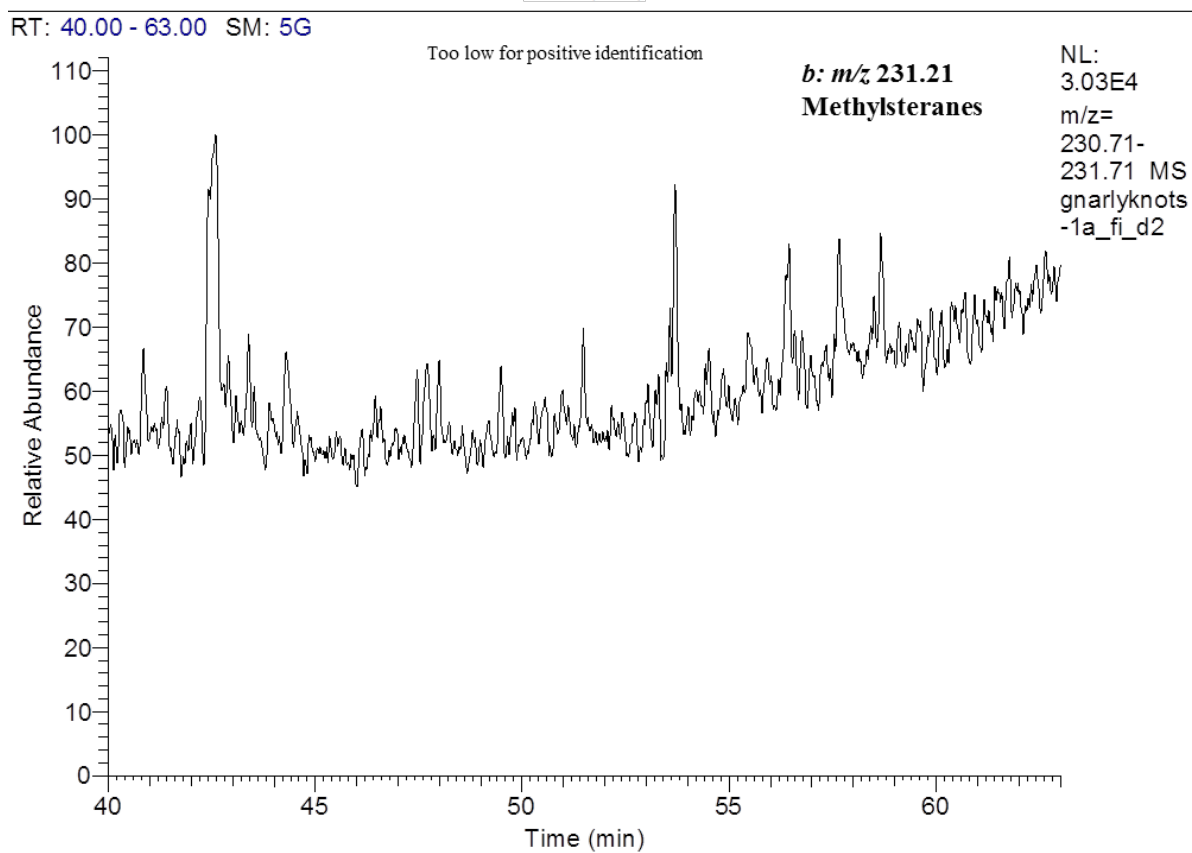
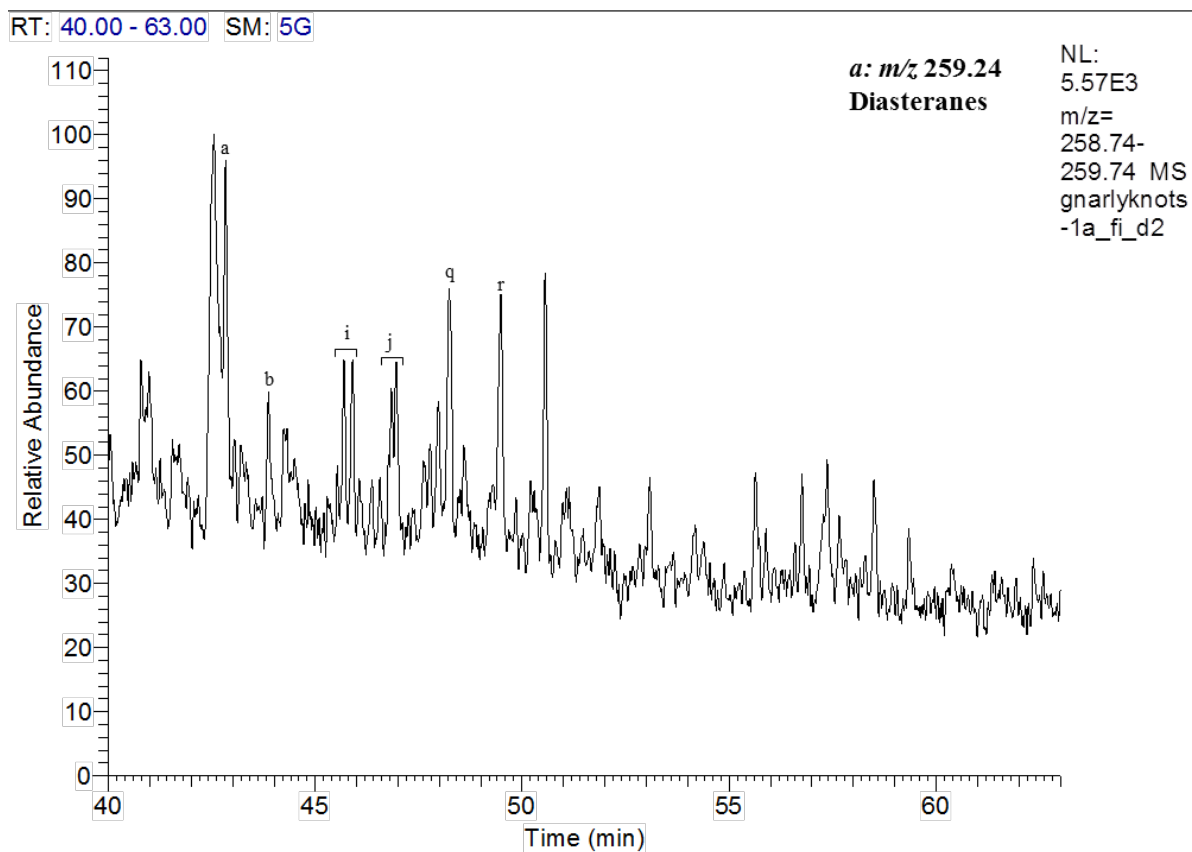


Figure A6-125: Partial m/z (a) 259 and (b) 231 mass chromatograms for the Gnarlyknots-1A (4390-4425m) FI oil. Showing the distribution of diasteranes and methylsteranes. Sterane and diasterane abbreviations are listed in Table A5-38.

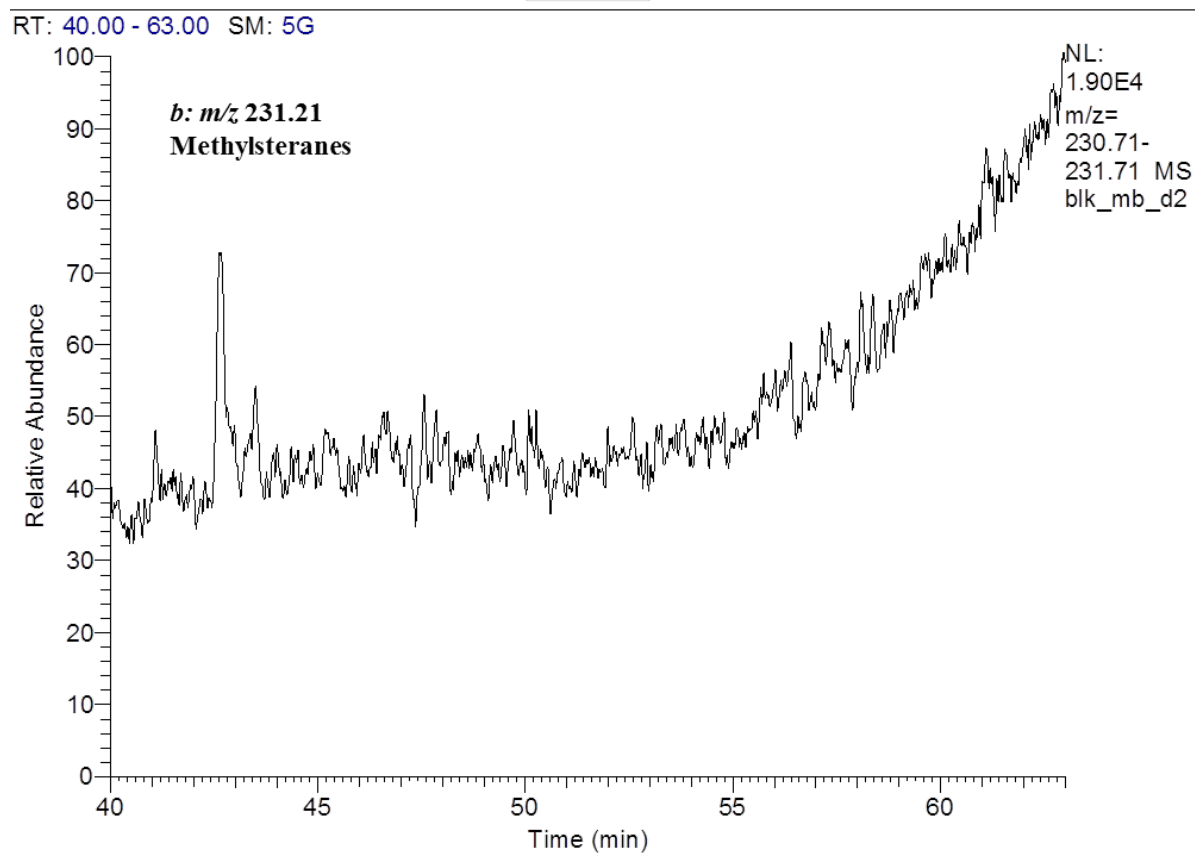
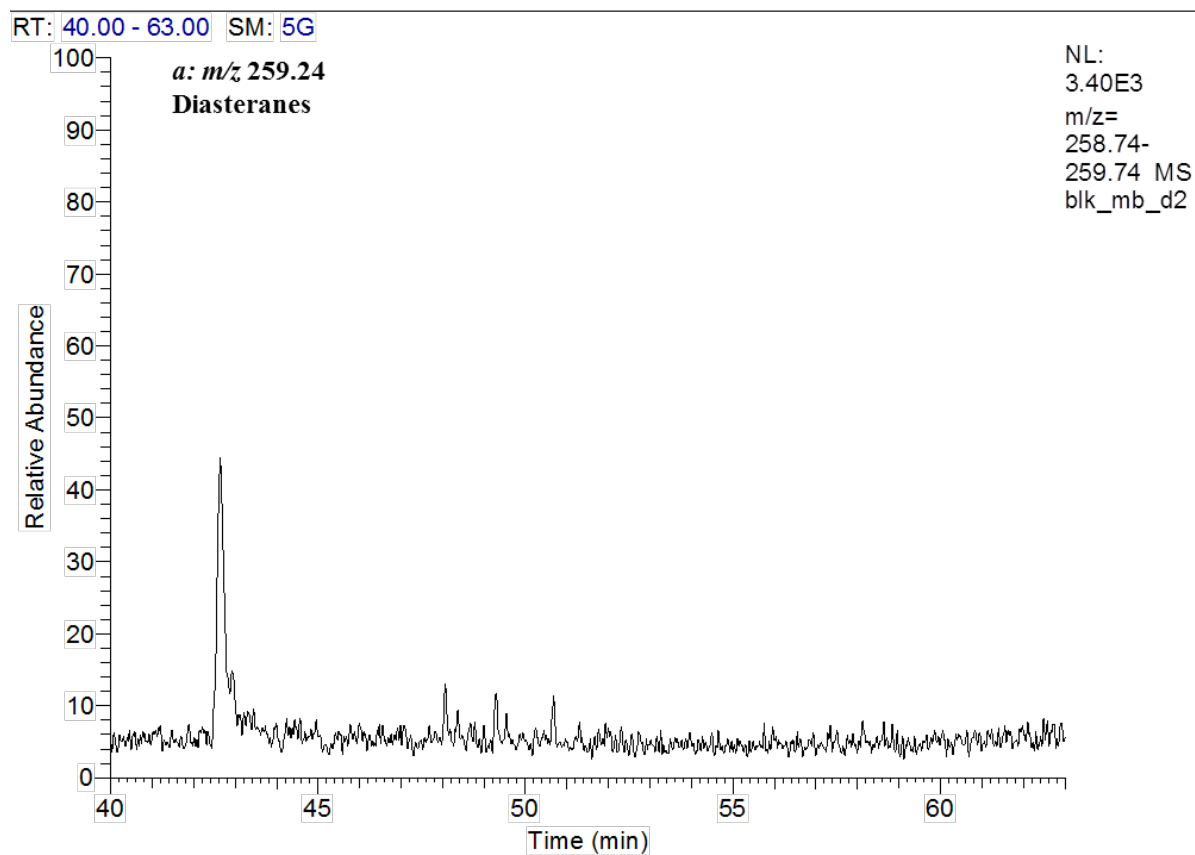


Figure A6-126: Partial m/z (a) 259 and (b) 231 mass chromatograms for the Gnarlyknots-1A (4390-4425m) FI system blank. Showing the distribution of diasteranes and methylsteranes. Sterane and diasterane abbreviations are listed in Table A5-38.

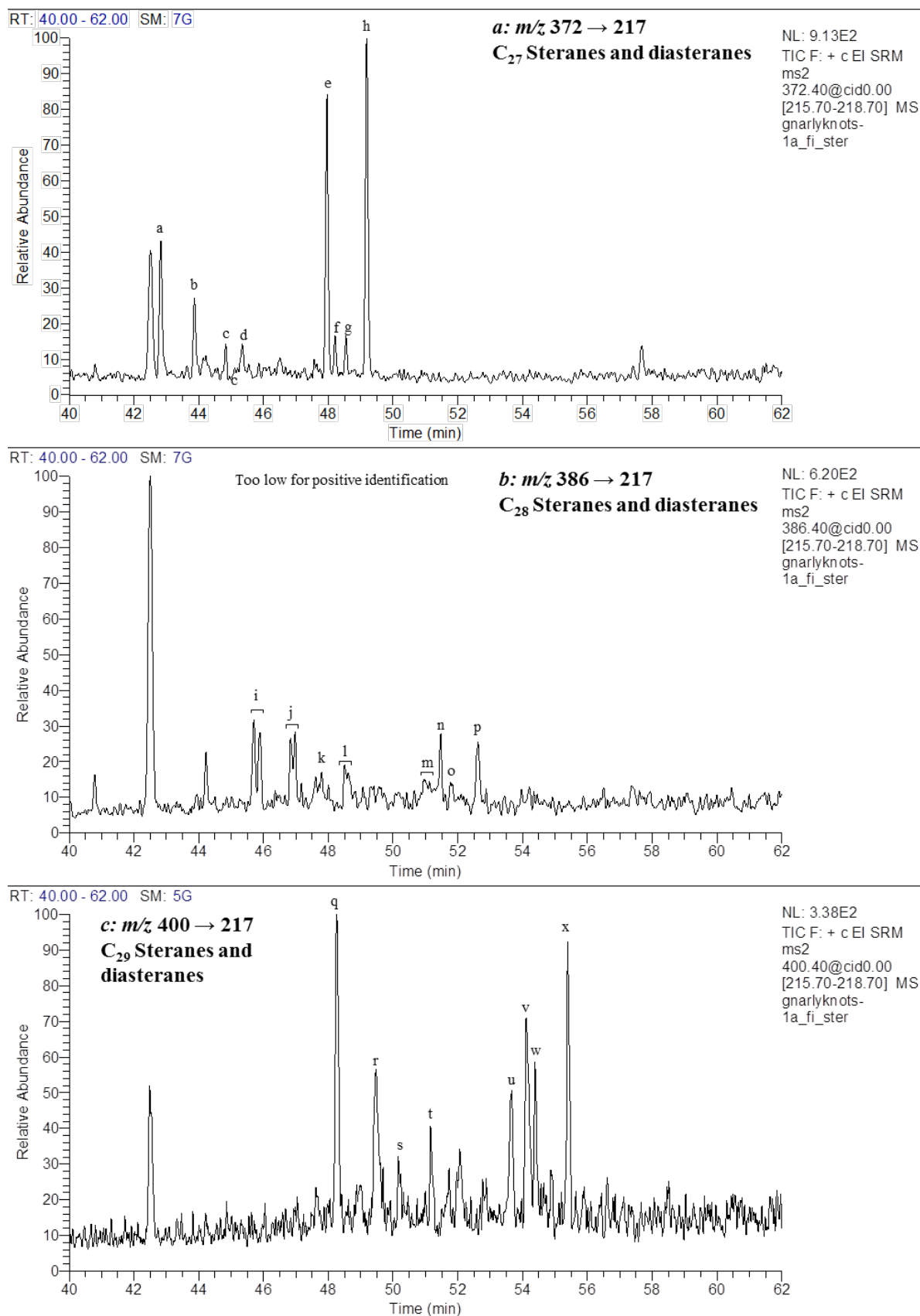


Figure A6-127: Partial MRM chromatograms (m/z 372.4, 386.4 and 400.4 \rightarrow 217.2) of the aliphatic hydrocarbons from the Gnarlyknots-1A (4390-4425m) FI oil.

Showing the distribution of (a) C₂₇ (b) C₂₈ and (c) C₂₉ steranes and diasteranes. Steranes and diasteranes abbreviations are listed in Table A5-38.

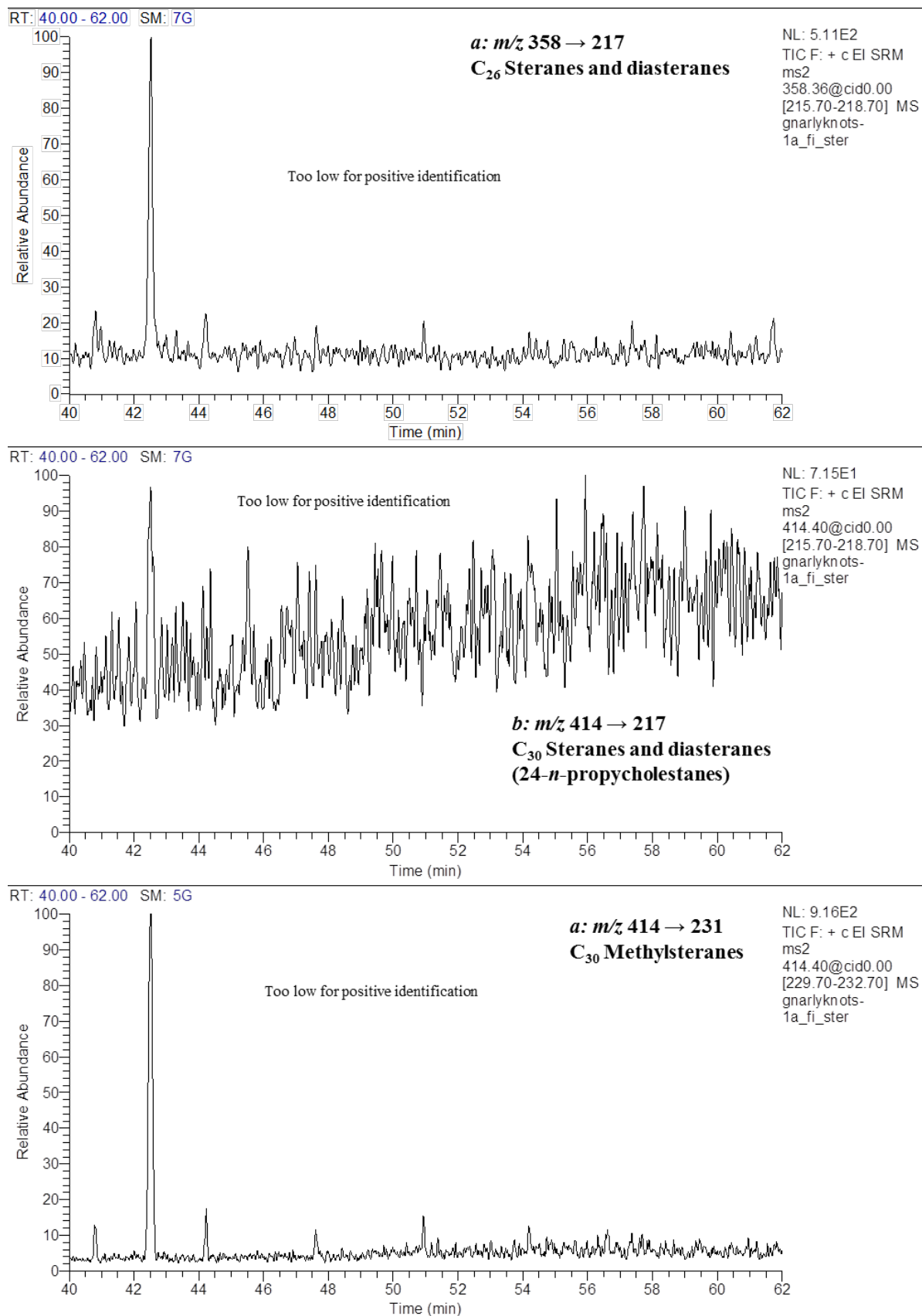


Figure A6-128: Partial MRM chromatograms (m/z 358.4 and 414.4 \rightarrow 217.2; 414.4 \rightarrow 231.2) of the aliphatic hydrocarbons from the Gnarlyknots-1A (4390-4425m) FI oil.

Showing the distribution of (a) C_{26} and (b) C_{30} steranes and diasteranes, and (c) C_{30} methylsteranes. Steranes, diasteranes and methylsteranes abbreviations are listed in Table A5-38.

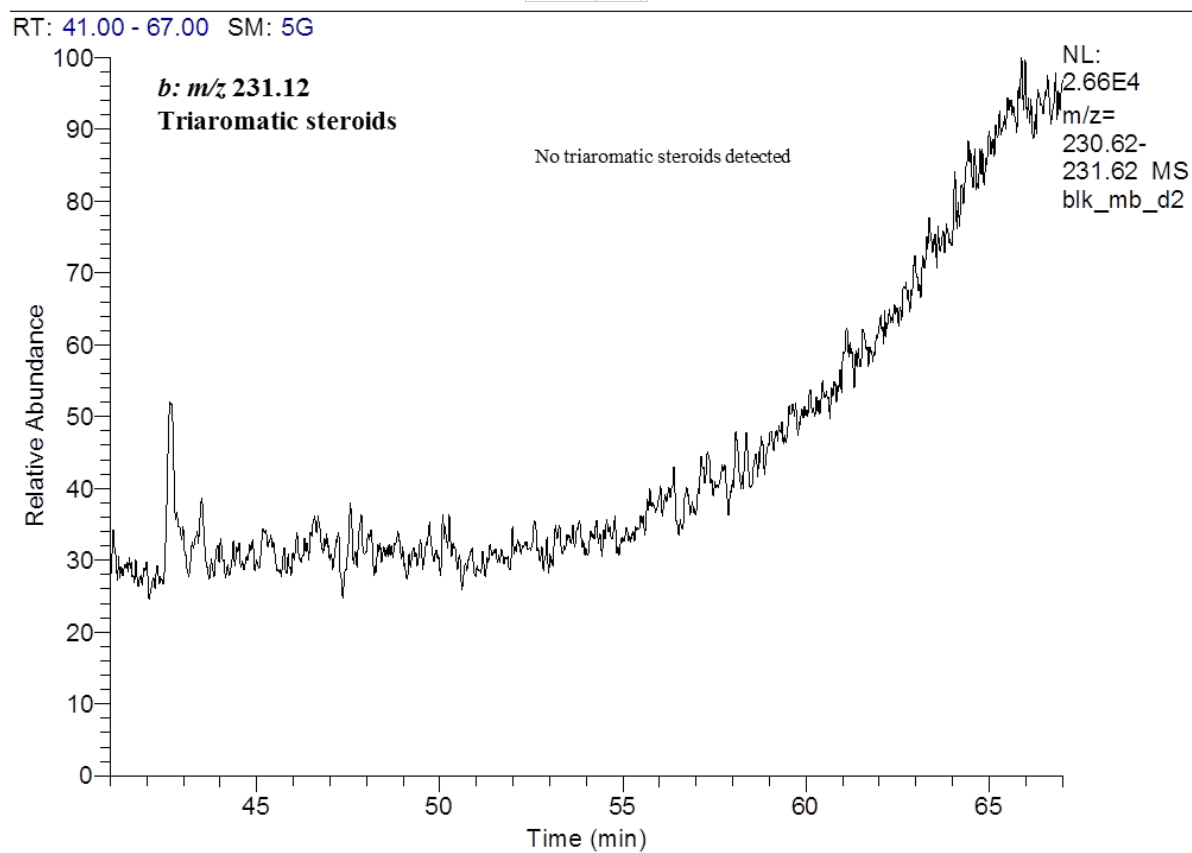
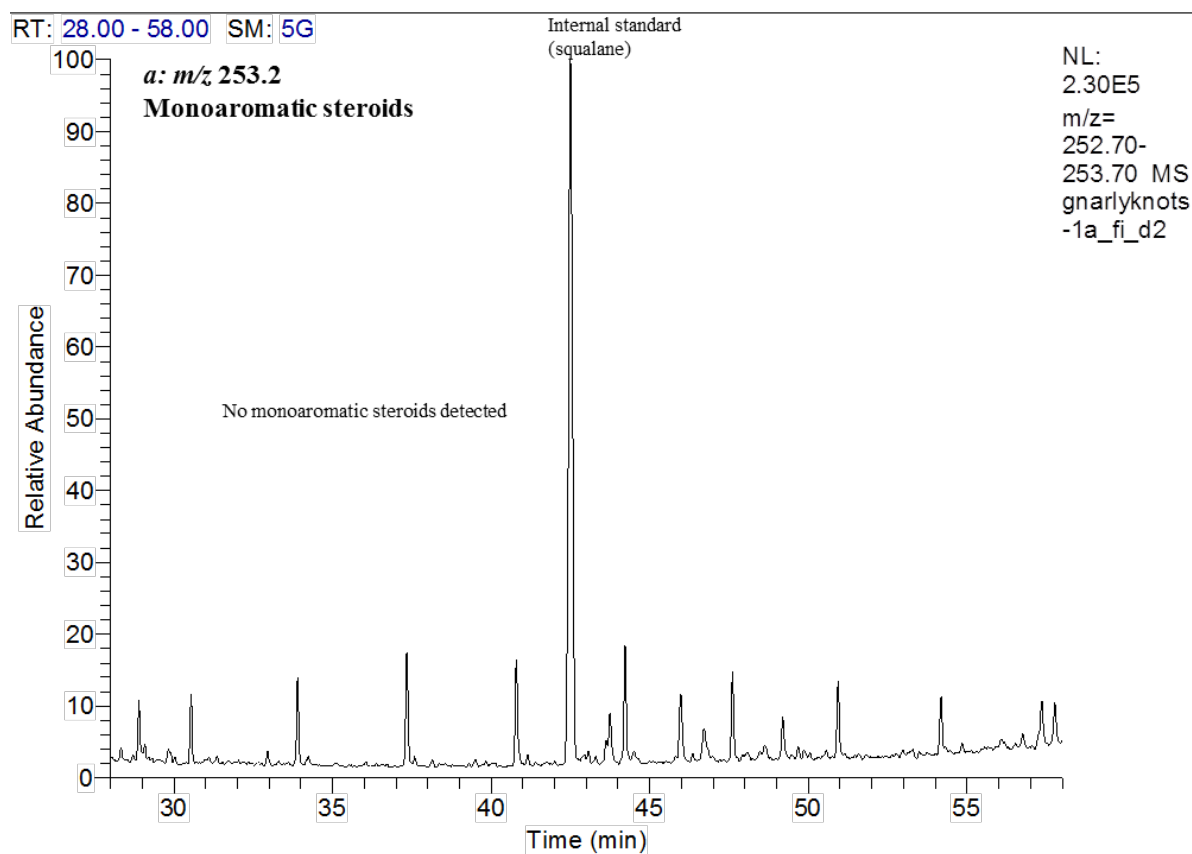


Figure A6-129: Partial m/z (a) 253.2 and (b) 231.12 mass chromatograms for the Gnarlyknots-1A (4390-4425m) FI oil. Showing the distribution of diasteranes and methylsteranes. Sterane and diasterane abbreviations are listed in Table A5-39, Table A5-40.

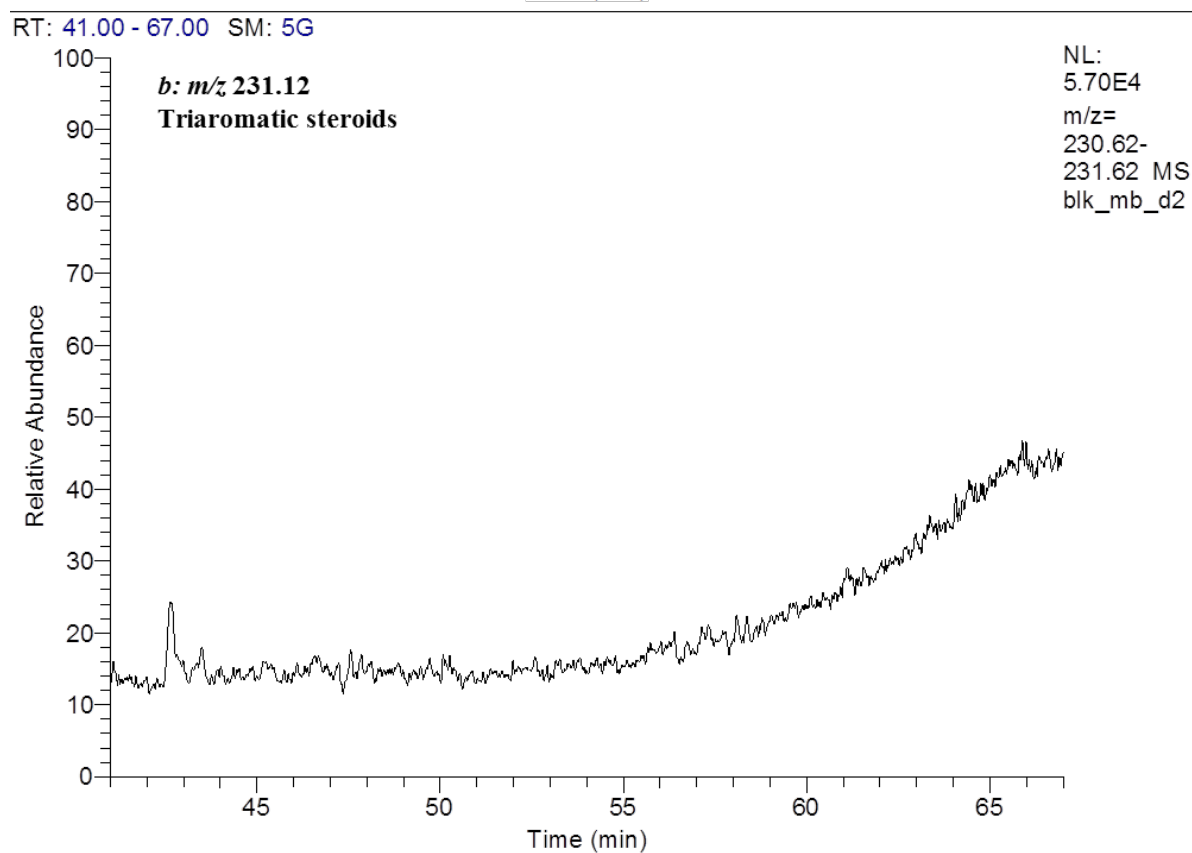
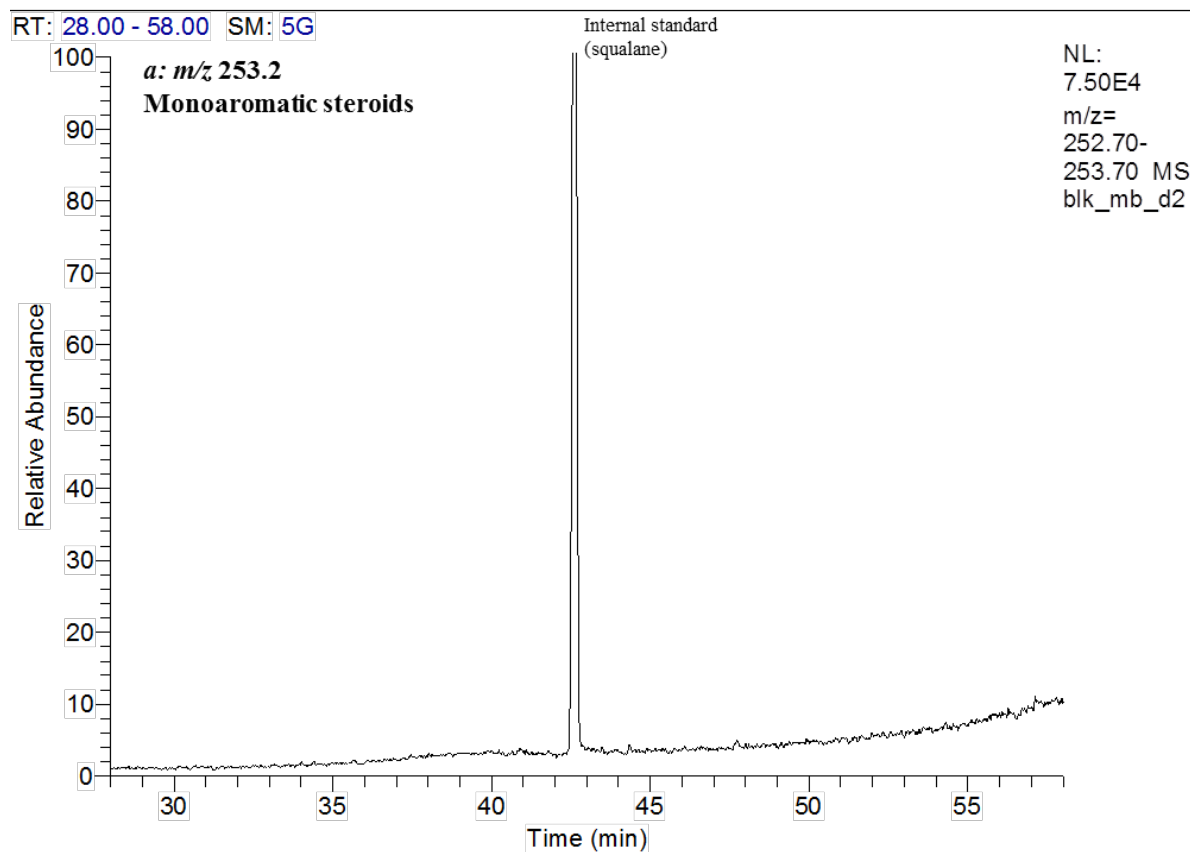


Figure A6-130: Partial m/z (a) 253.2 and (b) 231.12 mass chromatograms for the Gnarlyknots-1A (4390-4425m) FI oil. Showing the distribution of diasteranes and methylsteranes. Sterane and diasterane abbreviations are listed in Table A5-39, Table A5-40.

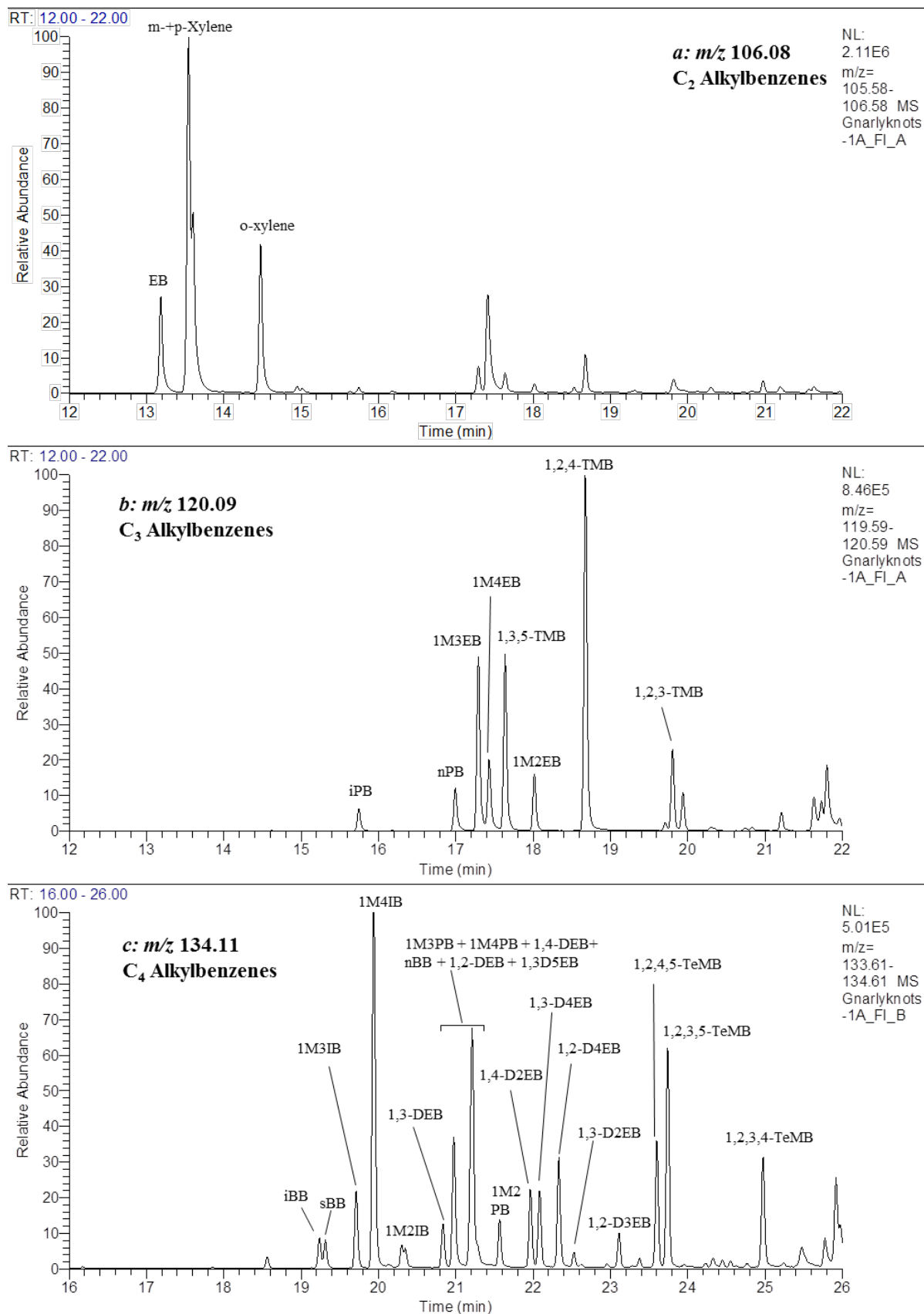


Figure A6-131: Partial m/z 106, 120 and 134 mass chromatograms for the Gnarlyknots-1A (4390-4425m) FI oil. Showing the distribution of (a) C₂ alkylbenzenes, (b) C₃ alkylbenzenes and (c) C₄ alkylbenzenes respectively. Peak abbreviations are listed in Table A5-41.

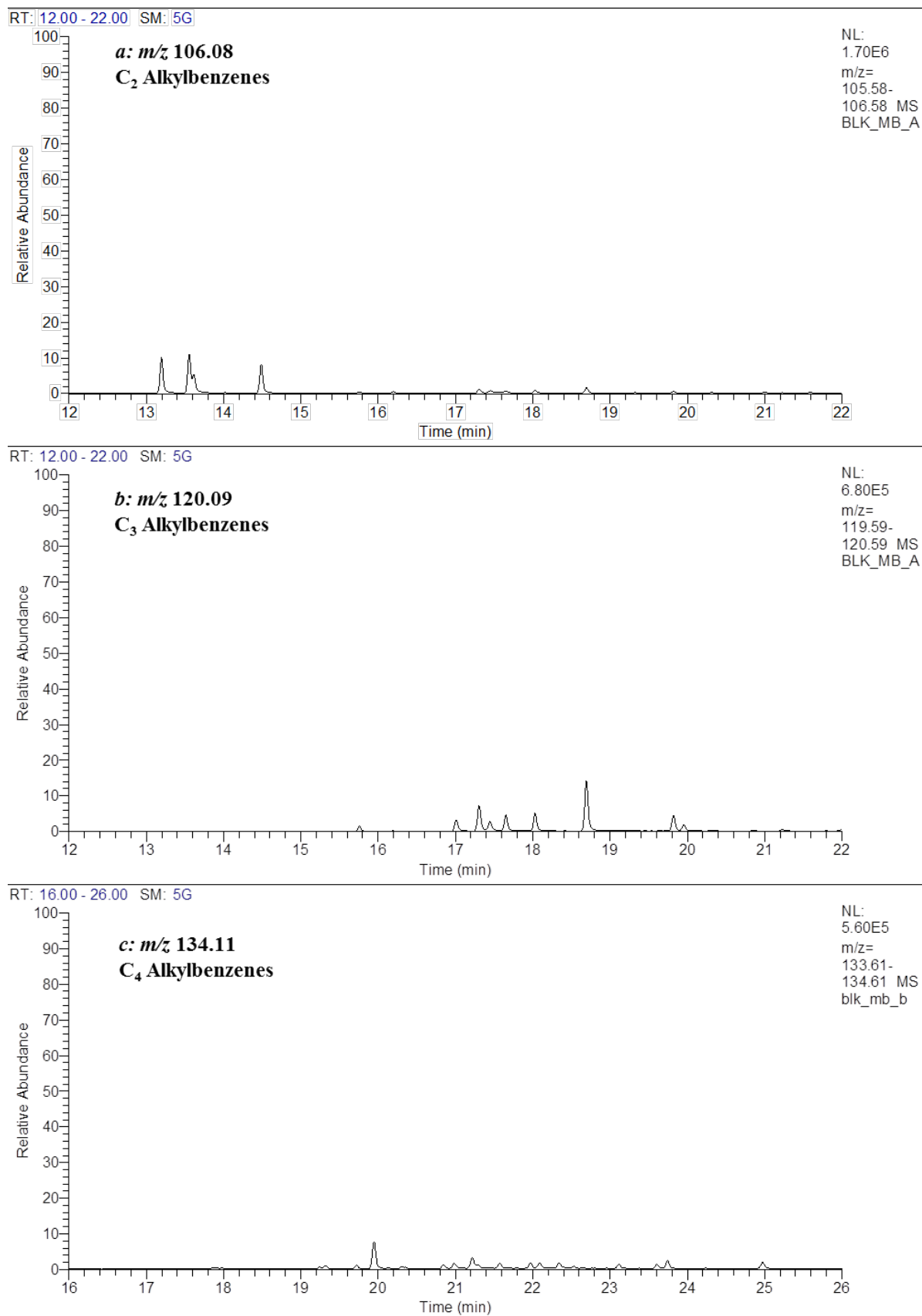


Figure A6-132: Partial m/z 106, 120 and 134 mass chromatograms for the Gnarlyknots-1A (4390-4425m) FI system blank. Showing the distribution of (a) C₂ alkylbenzenes, (b) C₃ alkylbenzenes and (c) C₄ alkylbenzenes respectively. Peak abbreviations are listed in Table A5-41.

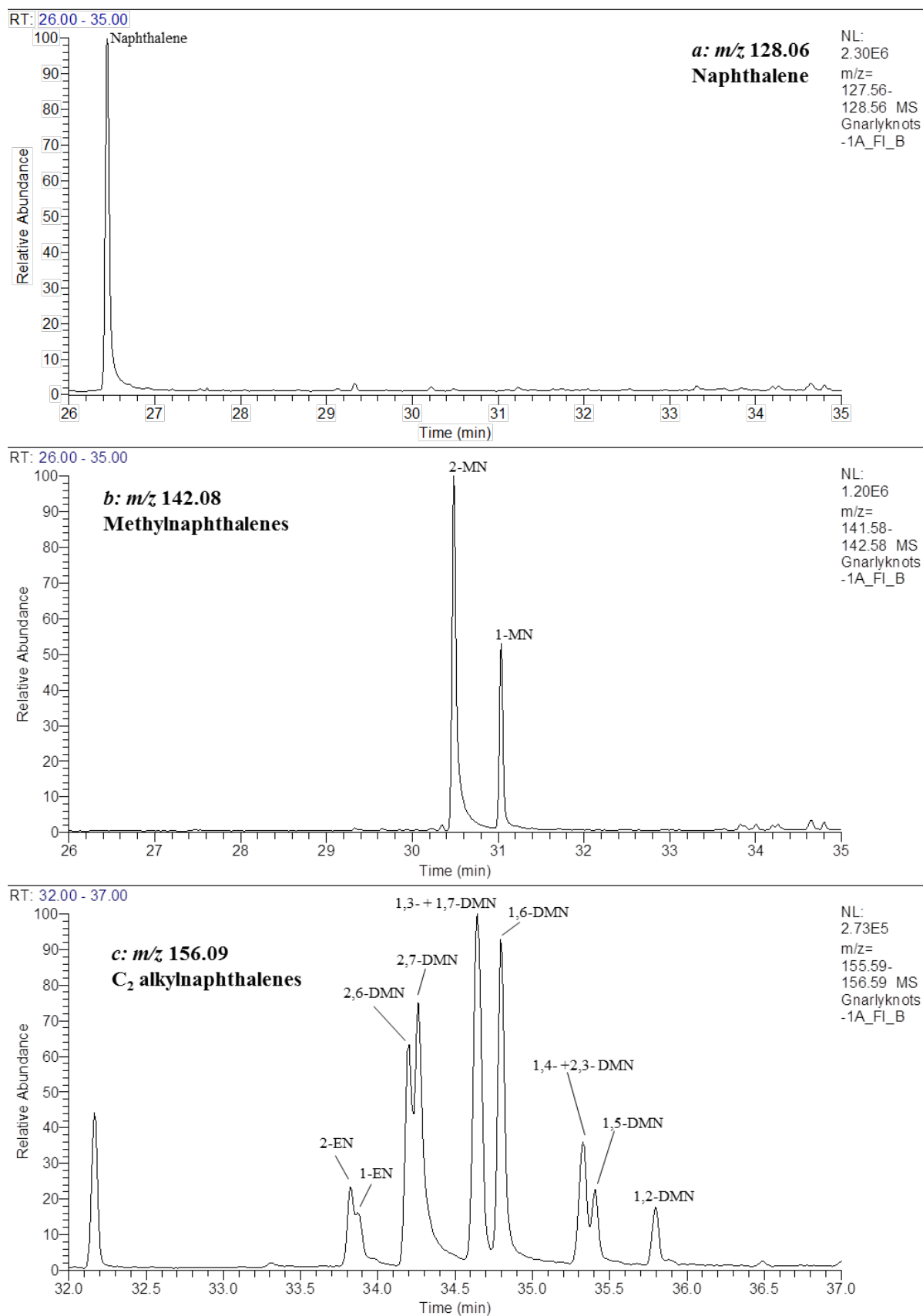


Figure A6-133: Partial m/z 128, 142 and 156 mass chromatograms for the Gnarlyknots-1A (4390-4425m) FI oil. Showing the distribution of (a) naphthalene, (b) methylnaphthalenes and (c) ethylnaphthalenes and dimethylnaphthalenes respectively. Peak abbreviations are listed in Table A5-41.

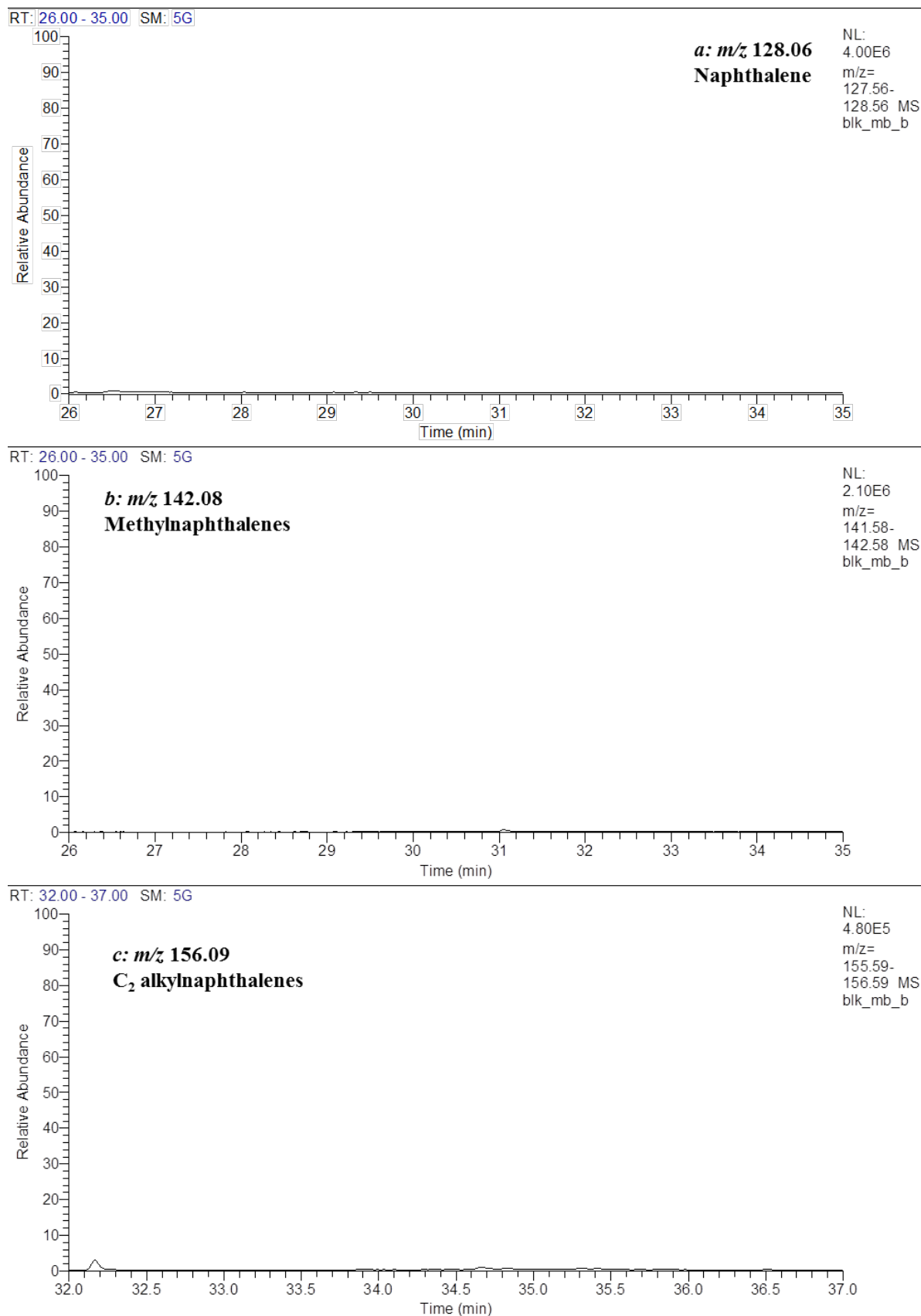


Figure A6-134: Partial m/z 128, 142 and 156 mass chromatograms for the Gnarlyknots-1A (4390-4425m) FI system blank. Showing the distribution of (a) naphthalene, (b) methylnaphthalenes and (c) ethylnaphthalenes and dimethylnaphthalenes respectively. Peak abbreviations are listed in Table A5-41.

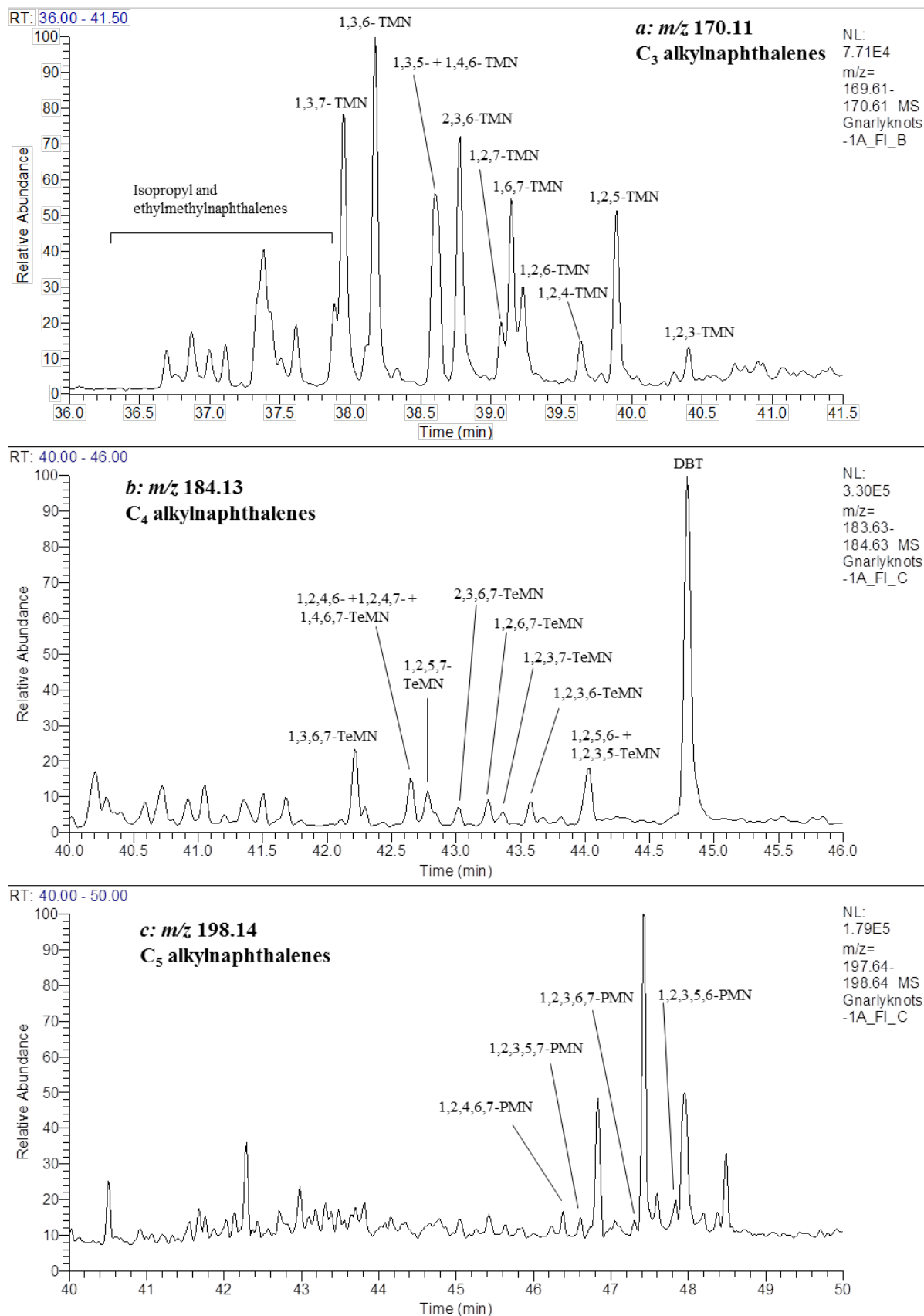


Figure A6-135: Partial m/z 170, 184 and 198 mass chromatograms for the Gnarlyknots-1A (4390-4425m) FI oil. Showing the distribution of (a) trimethylnaphthalenes, (b) tetramethylnaphthalenes and (c) pentamethylnaphthalenes respectively. Peak abbreviations are listed in Table A5-41.

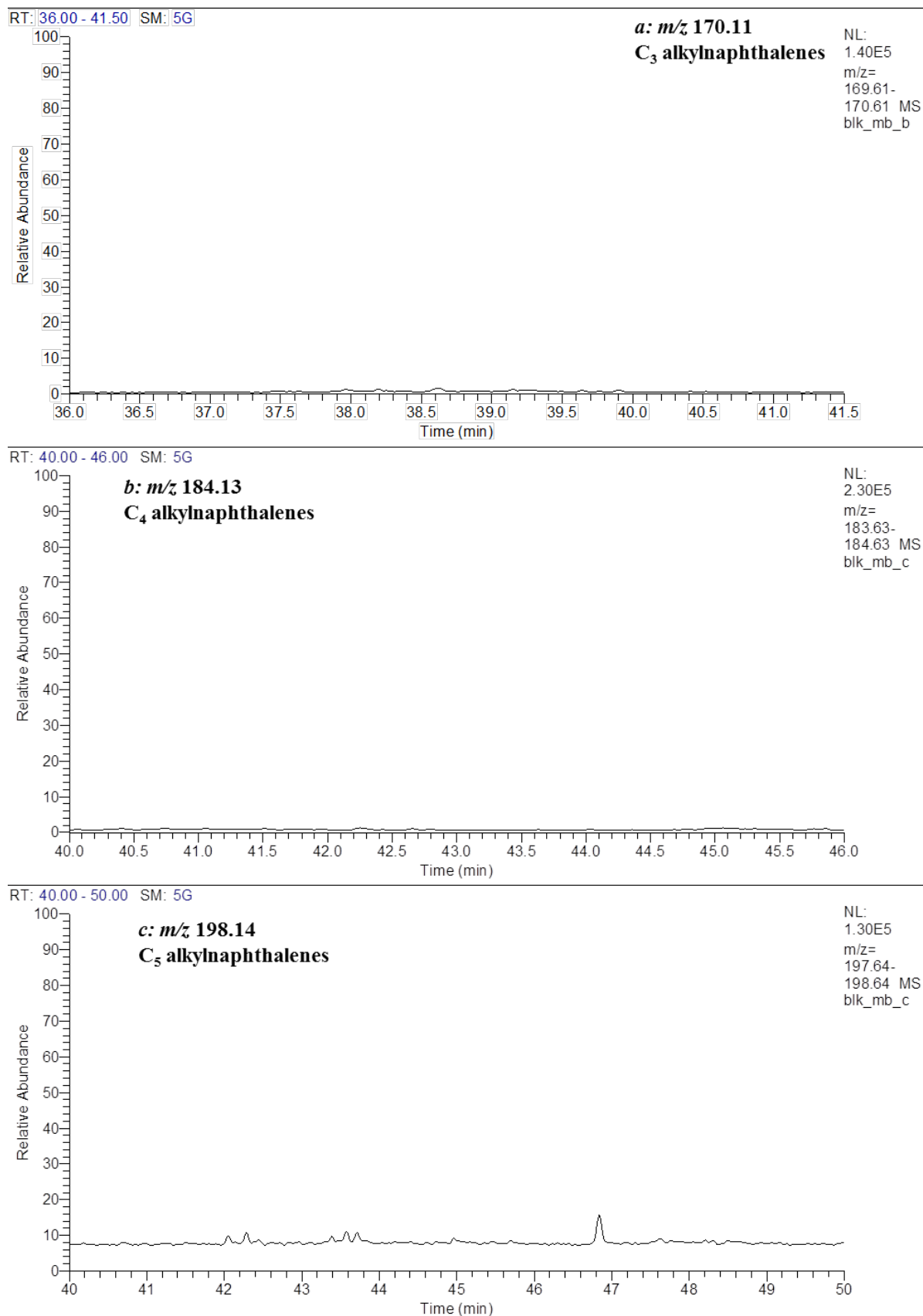


Figure A6-136: Partial m/z 170, 184 and 198 mass chromatograms for the Gnarlyknots-1A (4390-4425m) FI system blank. Showing the distribution of (a) trimethylnaphthalenes, (b) tetramethylnaphthalenes and (c) pentamethylnaphthalenes respectively. Peak abbreviations are listed in Table A5-41.

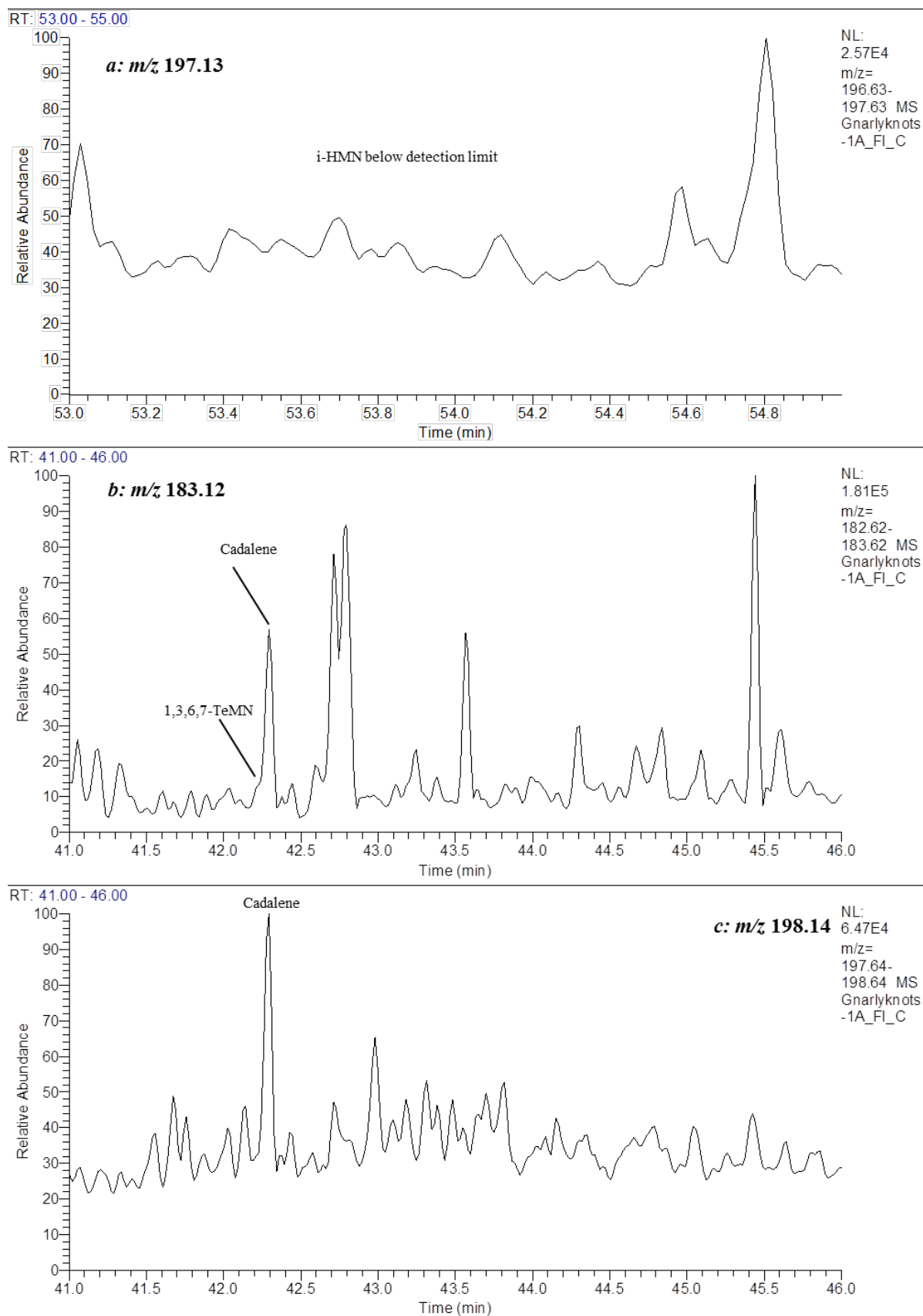


Figure A6-137: Partial m/z 197, 183 and 198 mass chromatograms for the Gnarlyknots-1A (4390-4425m) FI oil. Showing the distribution of (a) iso-hexylmethylnaphthalene, and (b) and (c) cadalene. Peak abbreviations are listed in Table A5-41.

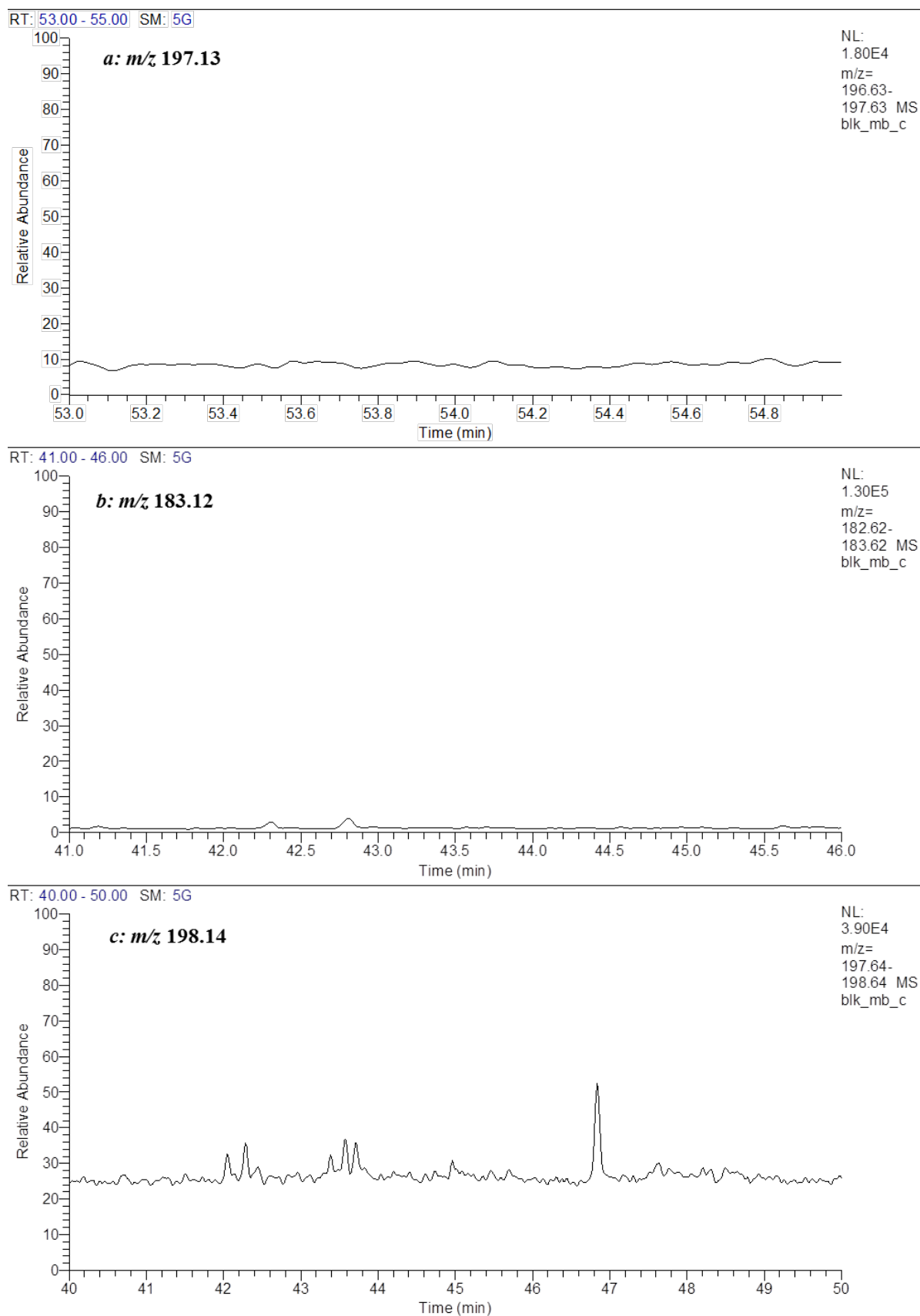


Figure A6-138: Partial m/z 197, 183 and 198 mass chromatograms for the Gnarlyknots-1A (4390-4425m) FI system blank. Showing the distribution of (a) iso-hexylmethylanthalene, and (b) and (c) cadalene. Peak abbreviations are listed in Table A5-41.

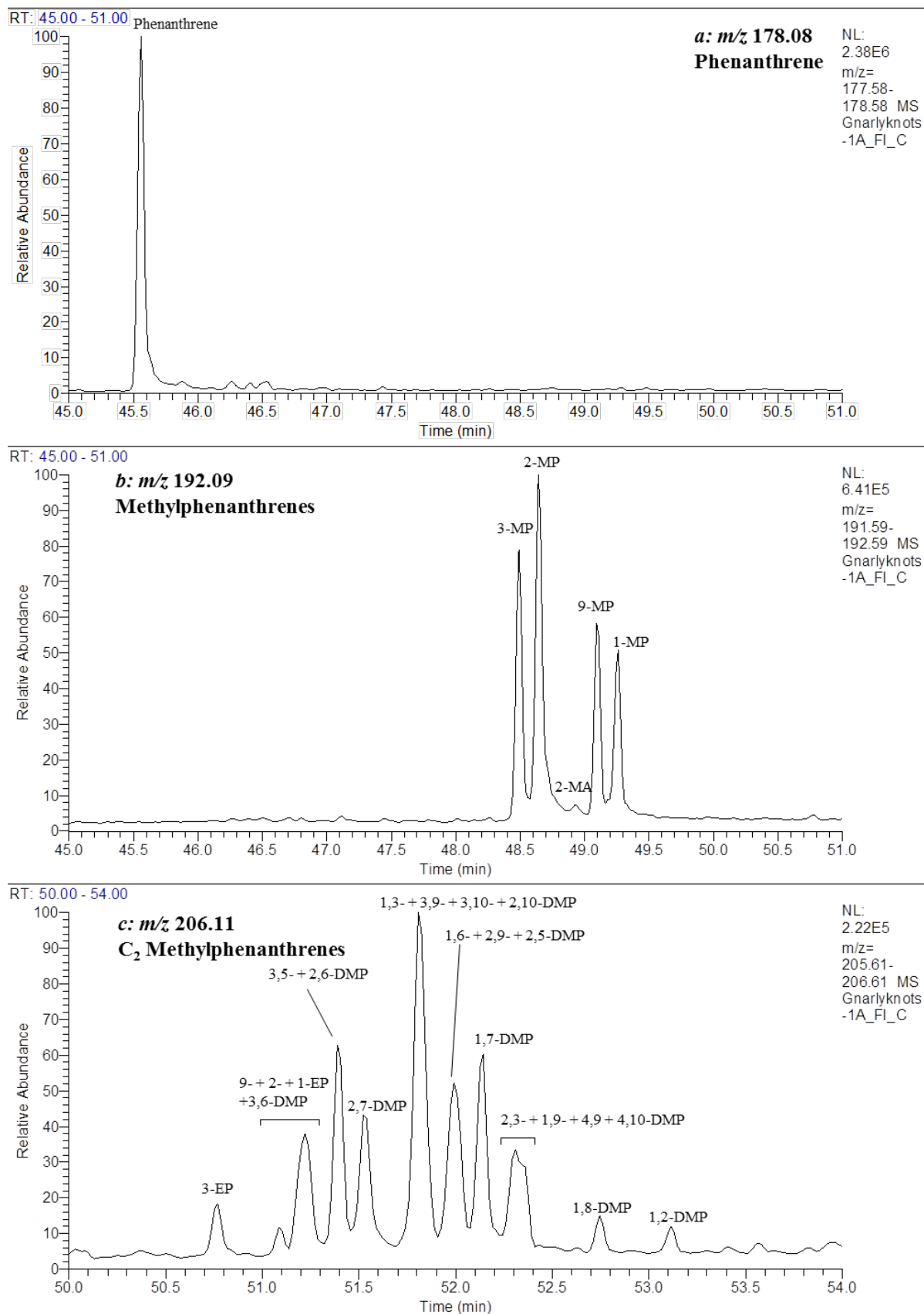


Figure A6-139: Partial m/z 178, 192 and 206 mass chromatograms for the Gnarlyknots-1A (4390-4425m) FI oil. Showing the distribution of (a) phenanthrene, (b) methylphenanthrenes and (c) ethylphenanthrenes and dimethylphenanthrenes respectively. Peak abbreviations are listed in Table A5-41.

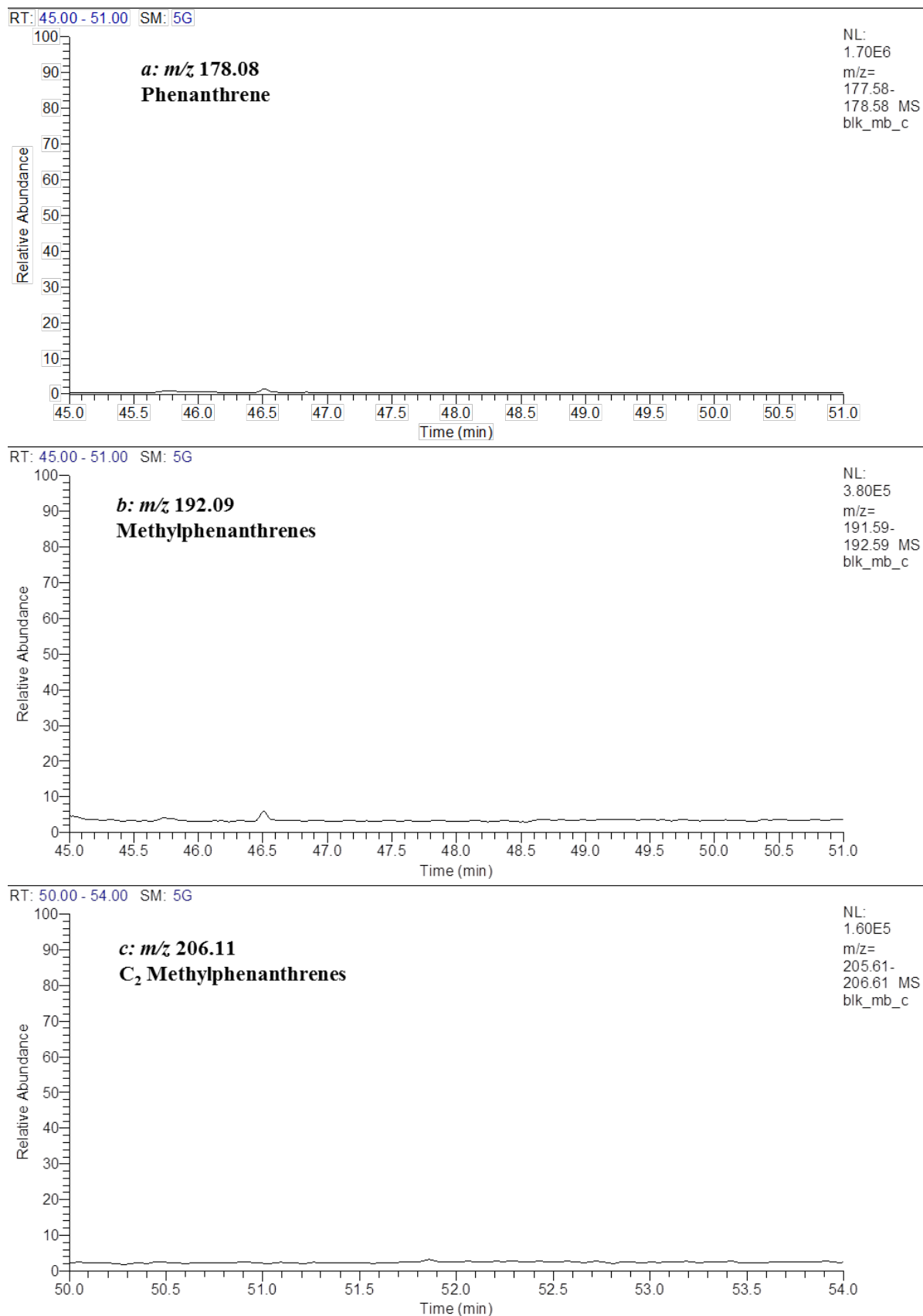


Figure A6-140: Partial m/z 178, 192 and 206 mass chromatograms for the Gnarlyknots-1A (4390-4425m) FI system blank. Showing the distribution of (a) phenanthrene, (b) methylphenanthrenes and (c) ethylphenanthrenes and dimethylphenanthrenes respectively. Peak abbreviations are listed in Table A5-41.

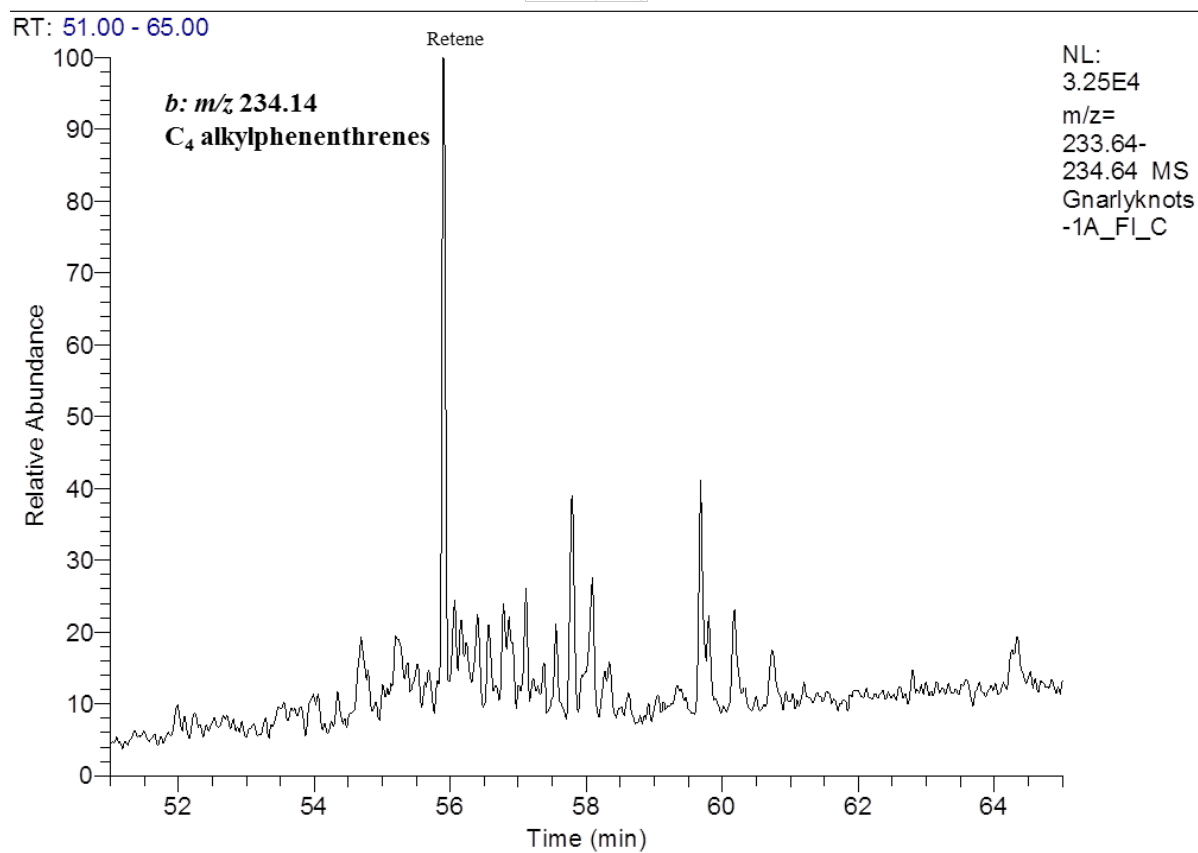
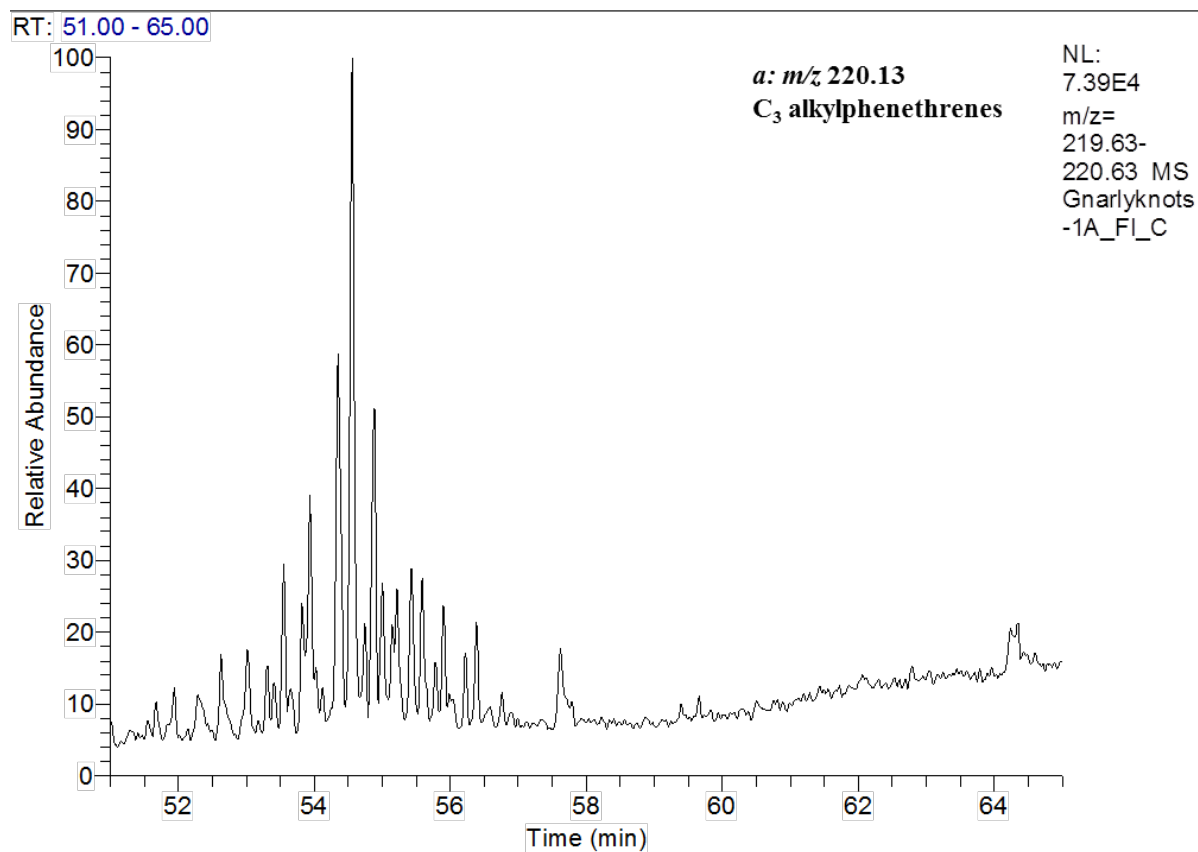


Figure A6-141: Partial m/z 220 and 234 mass chromatograms for the Gnarlyknots-1A (4390-4425m) FI oil. Showing the distribution of (a) trimethylphenanthrenes and (b) retene and tetramethylphenanthrenes. Peak abbreviations are listed in Table A5-41.

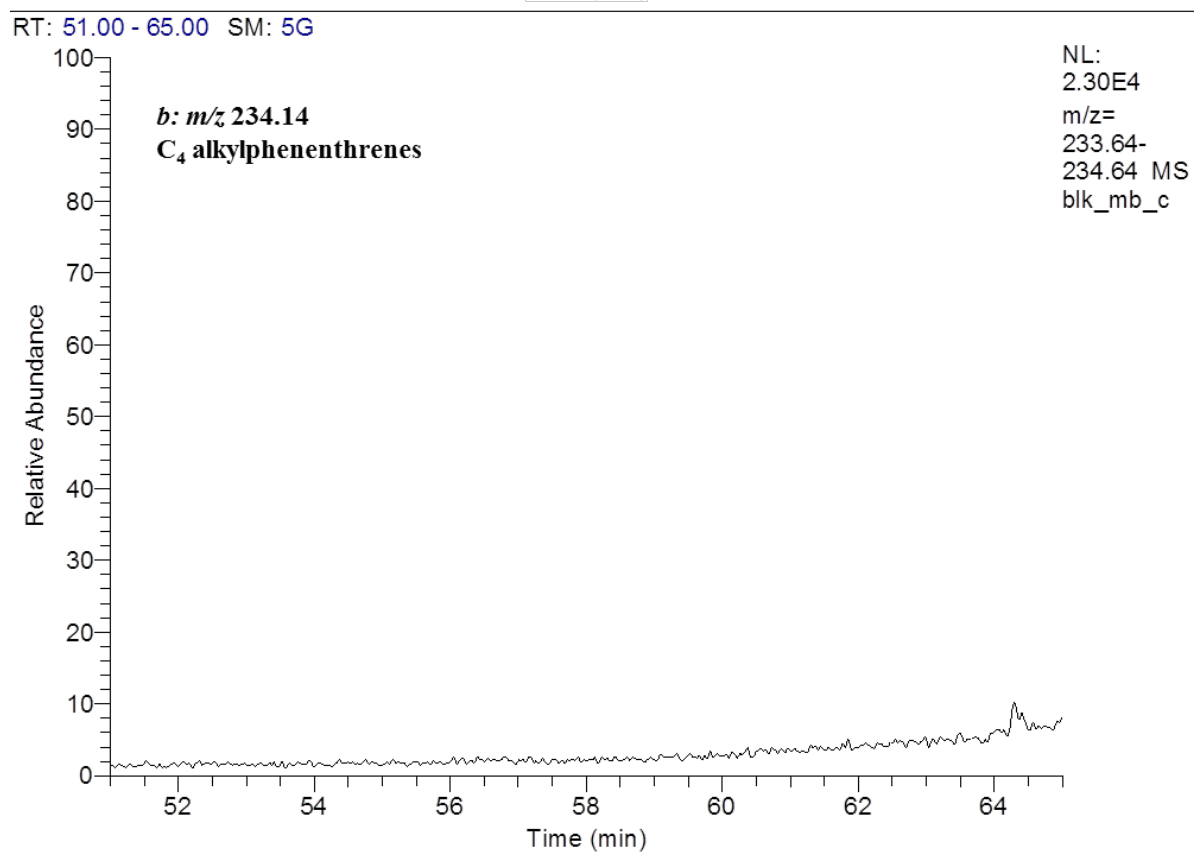
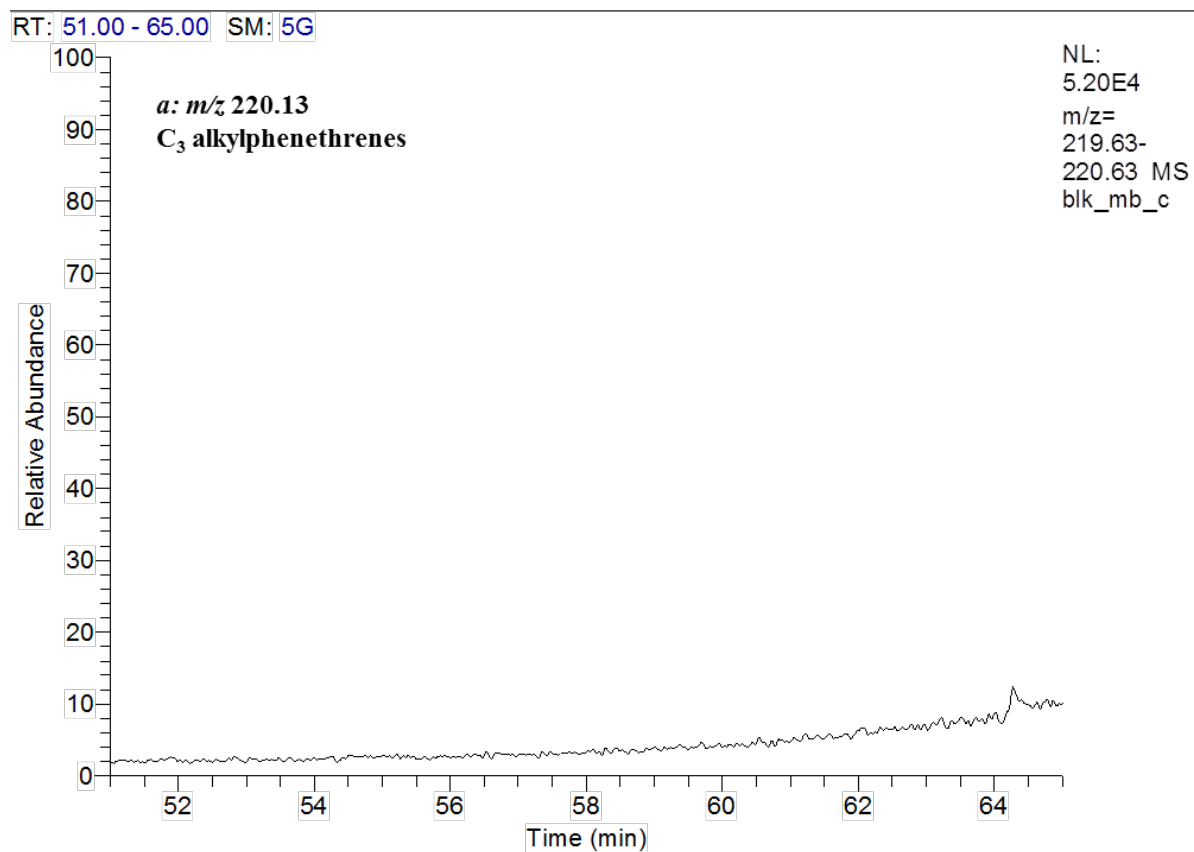


Figure A6-142: Partial m/z 220 and 234 mass chromatograms for the Gnarlyknots-1A (4390-4425m) FI system blank. Showing the distribution of (a) trimethylphenanthrenes and (b) retene and tetramethylphenanthrenes. Peak abbreviations are listed in Table A5-41.

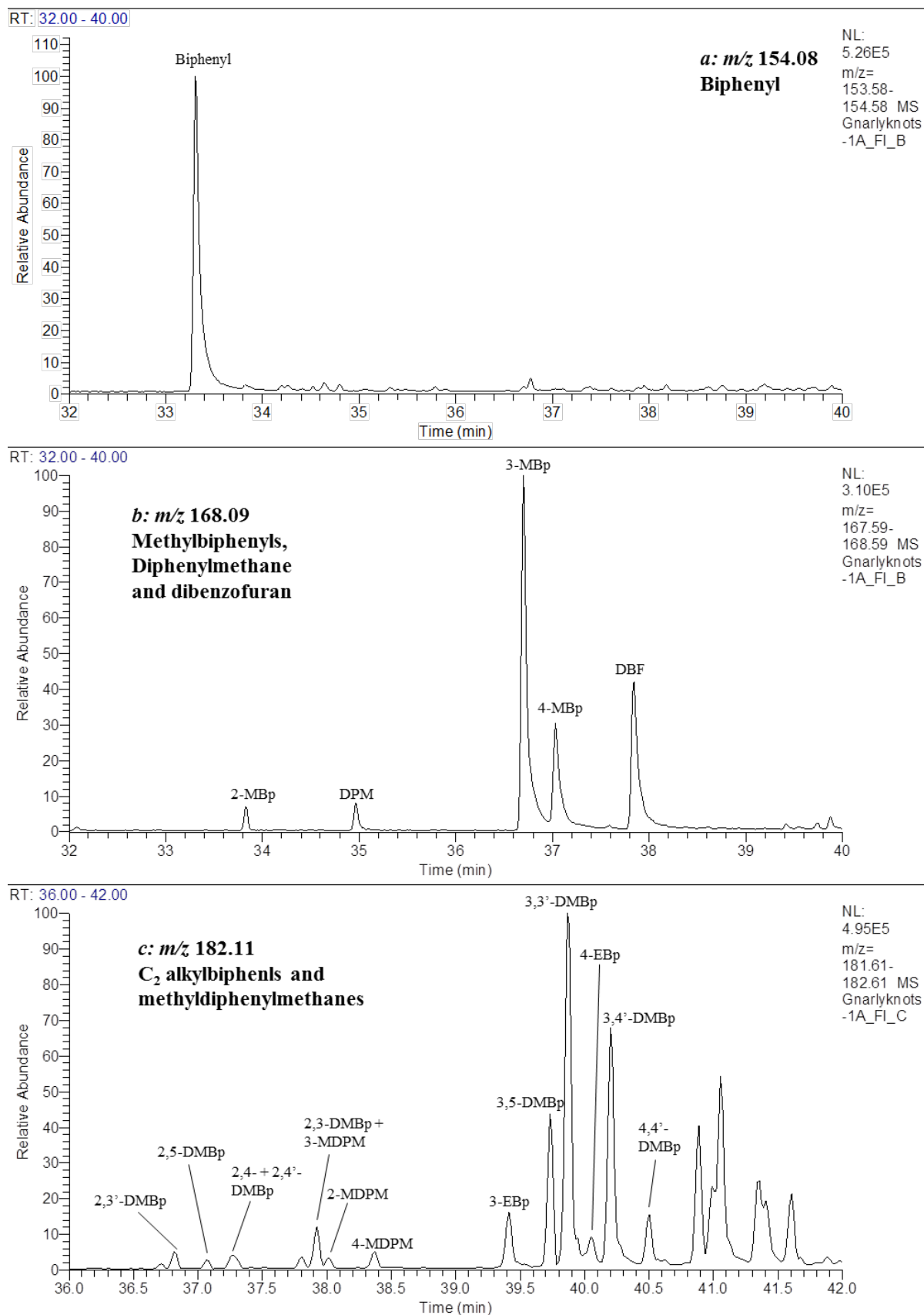


Figure A6-143: Partial m/z 154, 168 and 182 mass chromatograms for the Gnarlyknots-1A (4390-4425m) FI oil. Showing the distribution of (a) biphenyl, (b) methylbiphenyls, diphenylmethane and dibenzofuran, and (c) dimethylbiphenyls, ethylbiphenyls and methyldiphenylmethanes, respectively. Peak abbreviations are listed in Table A5-41.

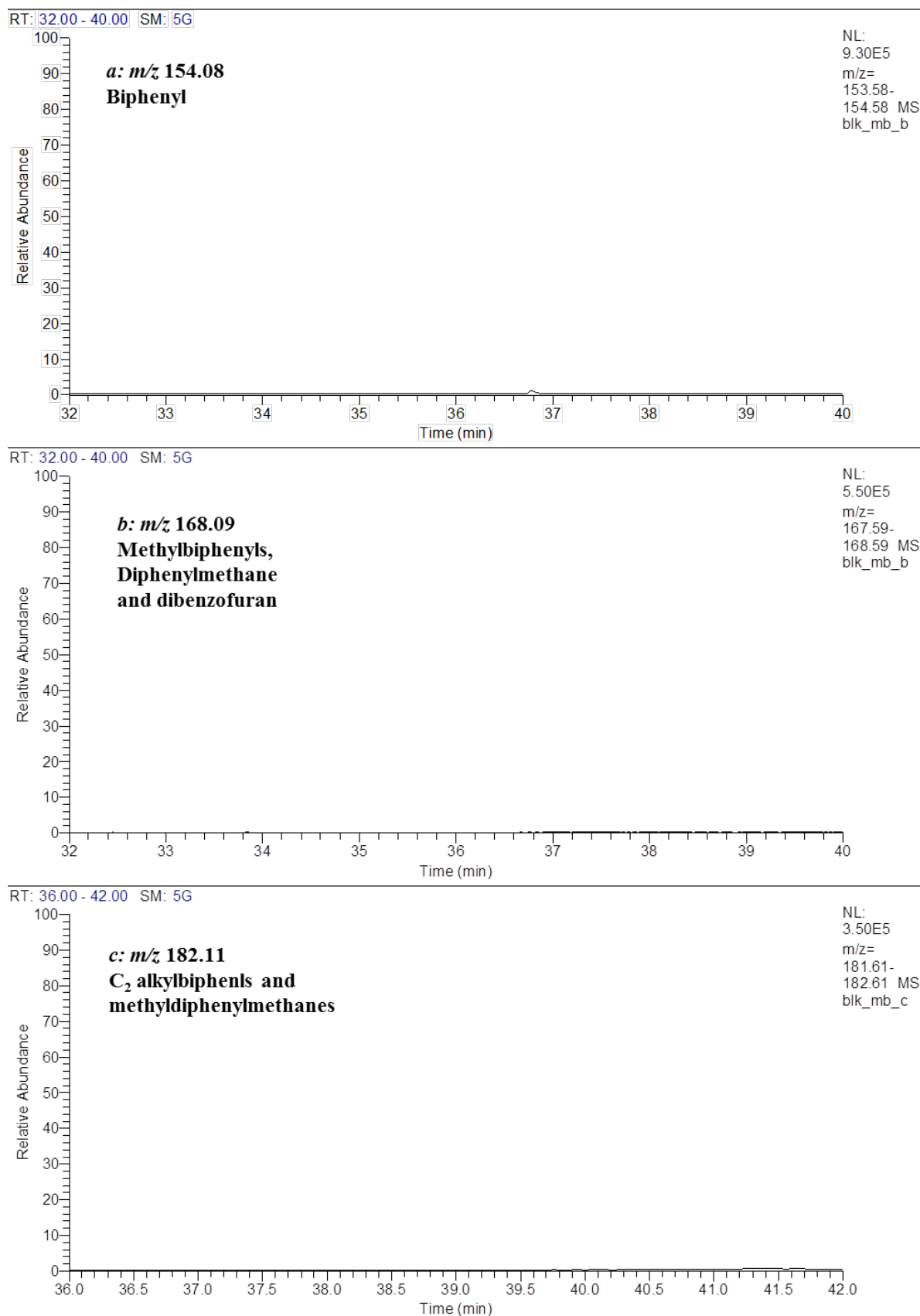


Figure A6-144: Partial m/z 154, 168 and 182 mass chromatograms for the Gnarlyknots-1A (4390-4425m) FI system blank. Showing the distribution of (a) biphenyl, (b) methylbiphenyls, diphenylmethane and dibenzofuran, and (c) dimethylbiphenyls, ethylbiphenyls and methyldiphenylmethanes, respectively. Peak abbreviations are listed in Table A5-41.

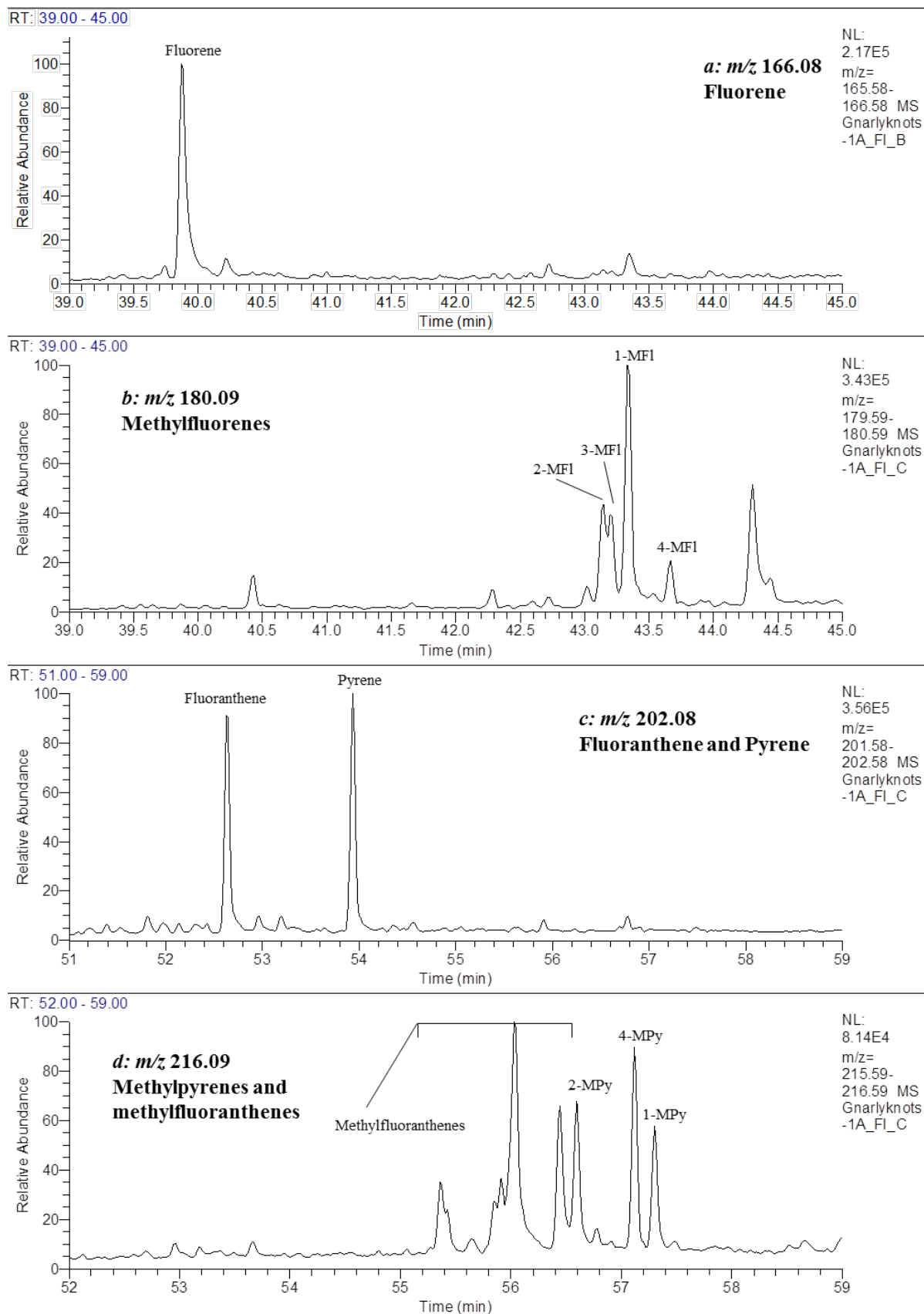


Figure A6-145: Partial m/z 166, 180, 202 and 216 mass chromatograms for the Gnarlyknots-1A (4390-4425m) FI oil. Showing the distribution of (a) fluorene, (b) methylfluorenes, (c) fluoranthene and pyrene, and (d) methylfluoranthenes and methylpyrenes respectively. Peak abbreviations are listed in Table A5-41.

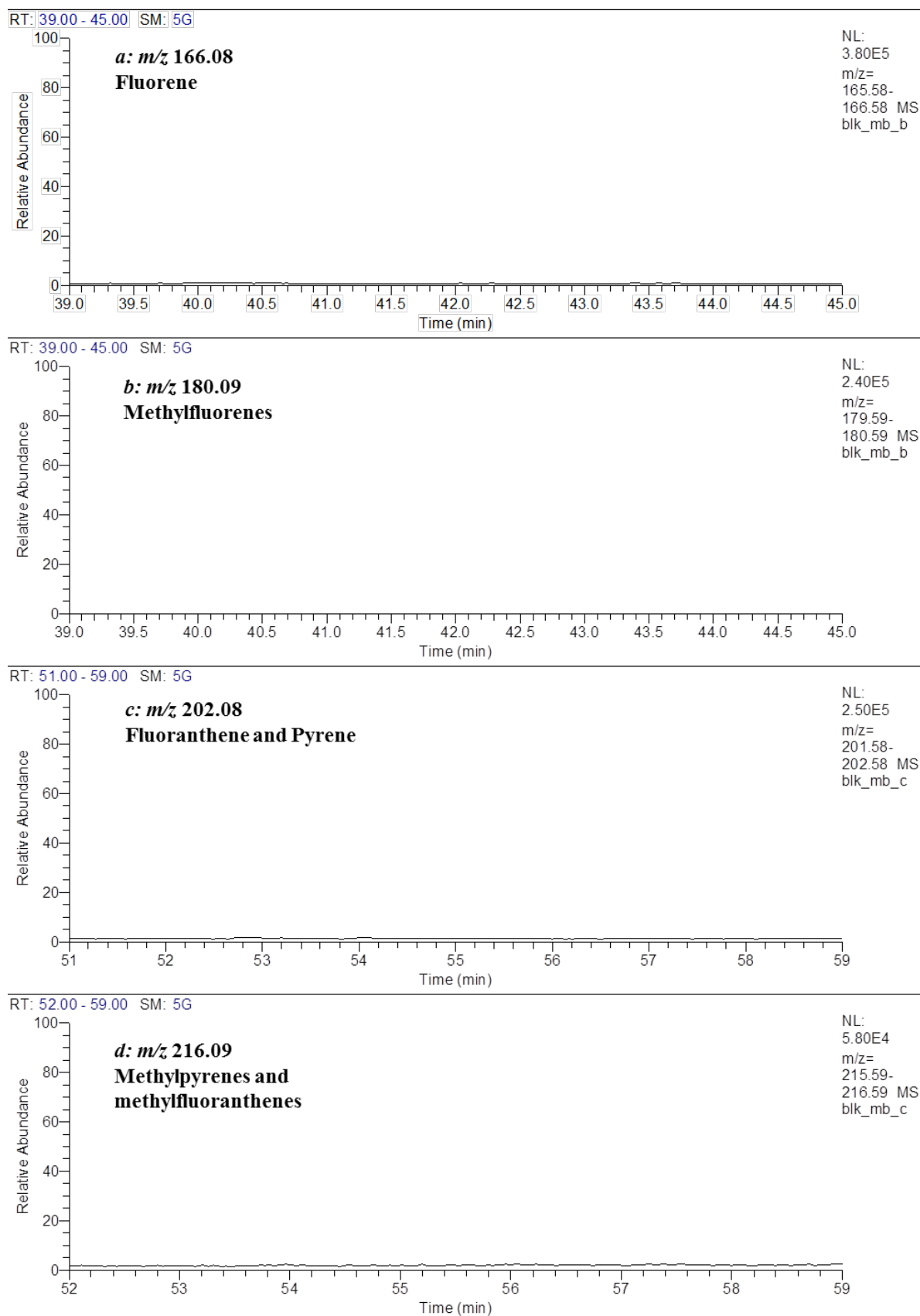


Figure A6-146: Partial m/z 166, 180, 202 and 216 mass chromatograms for the Gnarlyknots-1A (4390-4425m) FI system blank.

Showing the distribution of (a) fluorene, (b) methylfluorenes, (c) fluoranthene and pyrene, and (d) methylfluoranthenes and methylpyrenes respectively. Peak abbreviations are listed in Table A5-41.

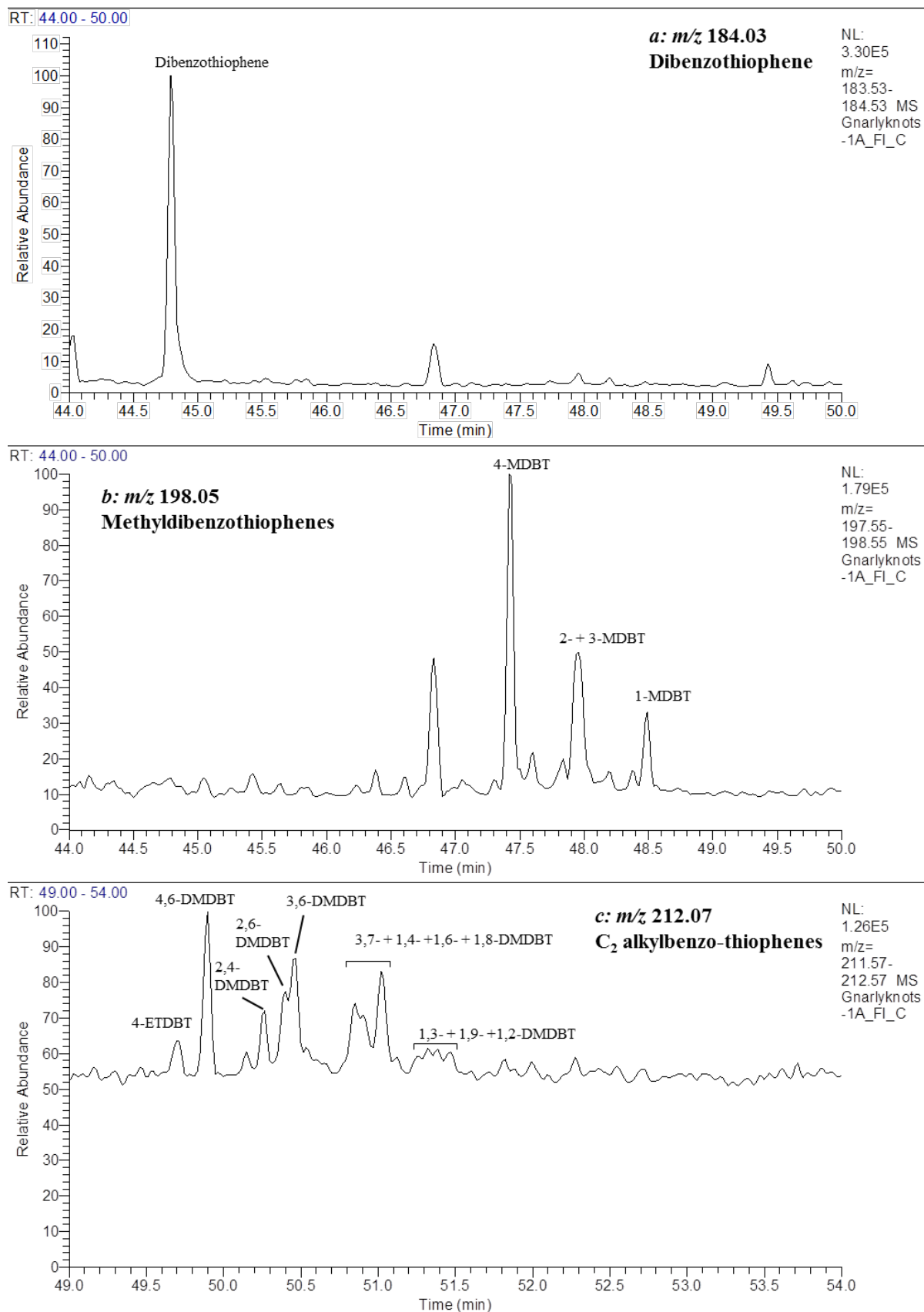


Figure A6-147: Partial m/z 184, 198 and 212 mass chromatograms for the Gnarlyknots-1A (4390-4425m) FI oil. Showing the distribution of (a) dibenzothiophene, (b) methyldibenzothiophenes and (c) dimethyldibenzothiophenes and ethyldibenzothiophenes respectively. Peak abbreviations are listed in Table A5-41.

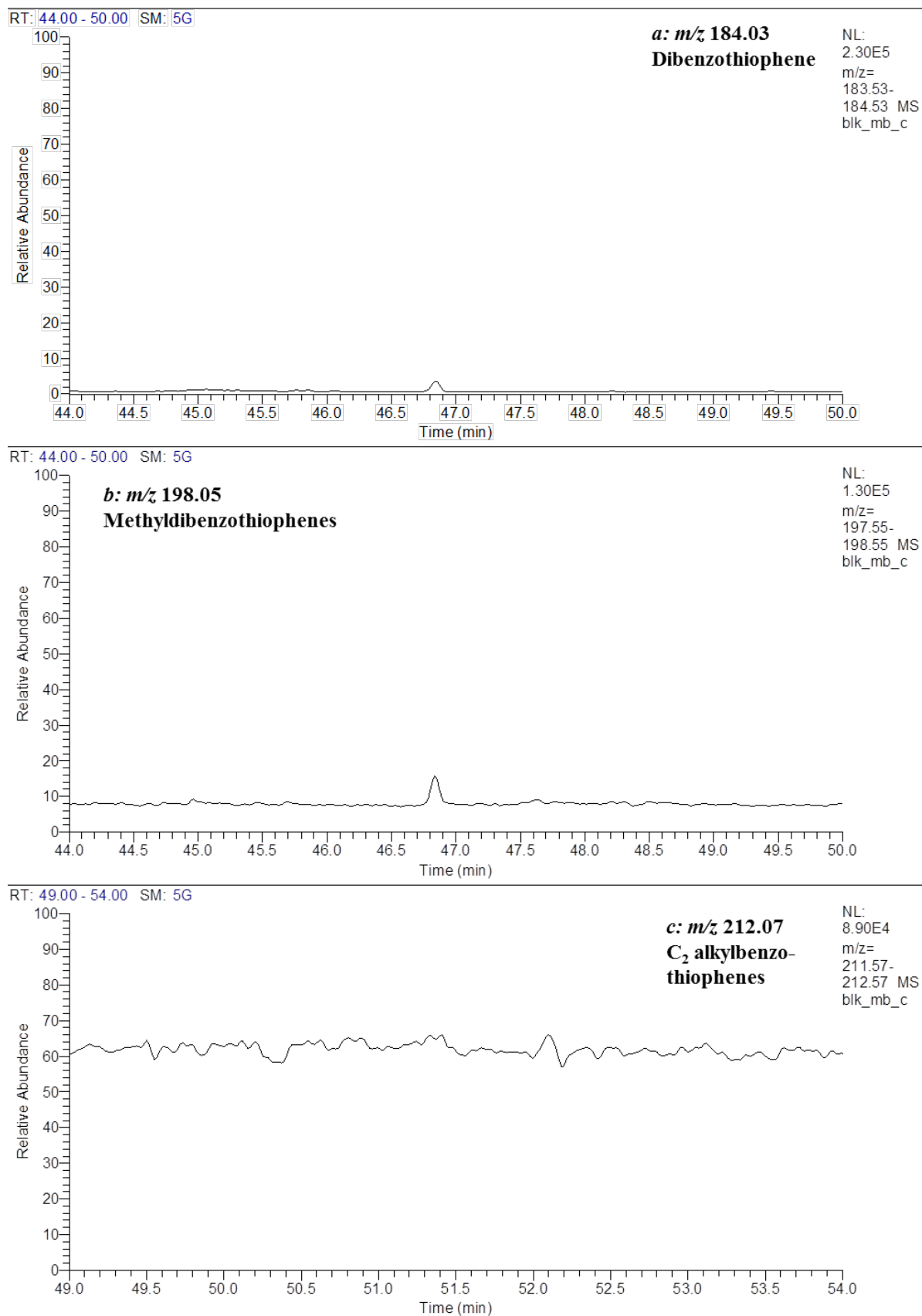


Figure A6-148: Partial m/z 184, 198 and 212 mass chromatograms for the Gnarlyknots-1A (4390-4425m) FI system blank. Showing the distribution of (a) dibenzothiophene, (b) methyldibenzothiophenes and (c) dimethyldibenzothiophenes and ethyldibenzothiophenes respectively. Peak abbreviations are listed in Table A5-41.

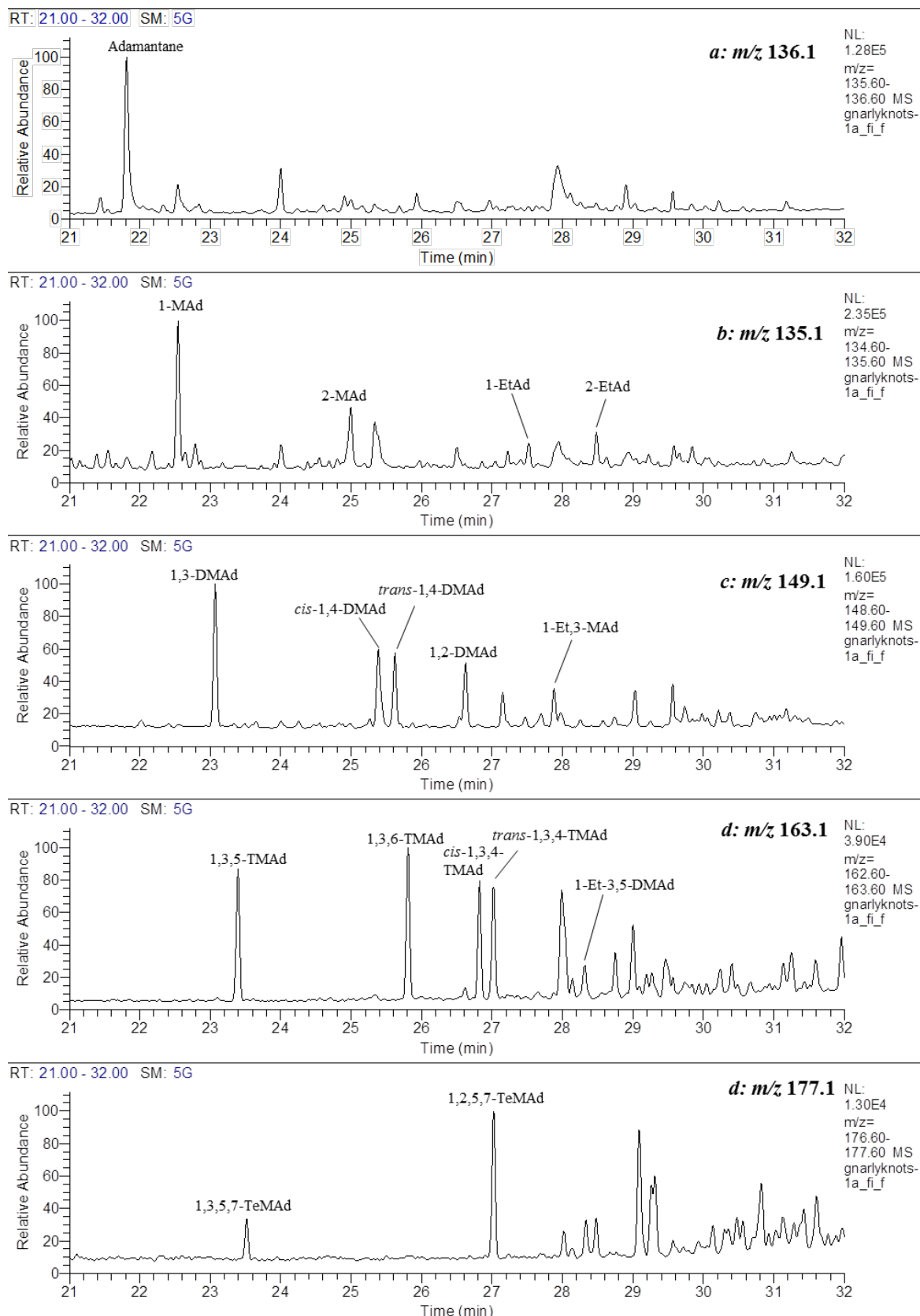


Figure A6-149: Partial m/z 136.1, 135.1, 149.1, 163.1 and 177.1 mass chromatograms for the Gnarlyknots-1A (4390-4425m) FI oil.

Showing the distribution of (a) adamantane, (b) methyladamantanes and ethyladamantanes, (c) dimethyladamantanes and ethylmethyladamantanes, (d) trimethyladamantanes and (e) tetramethyladamantanes. Peak abbreviations are listed in Table A5-B6.

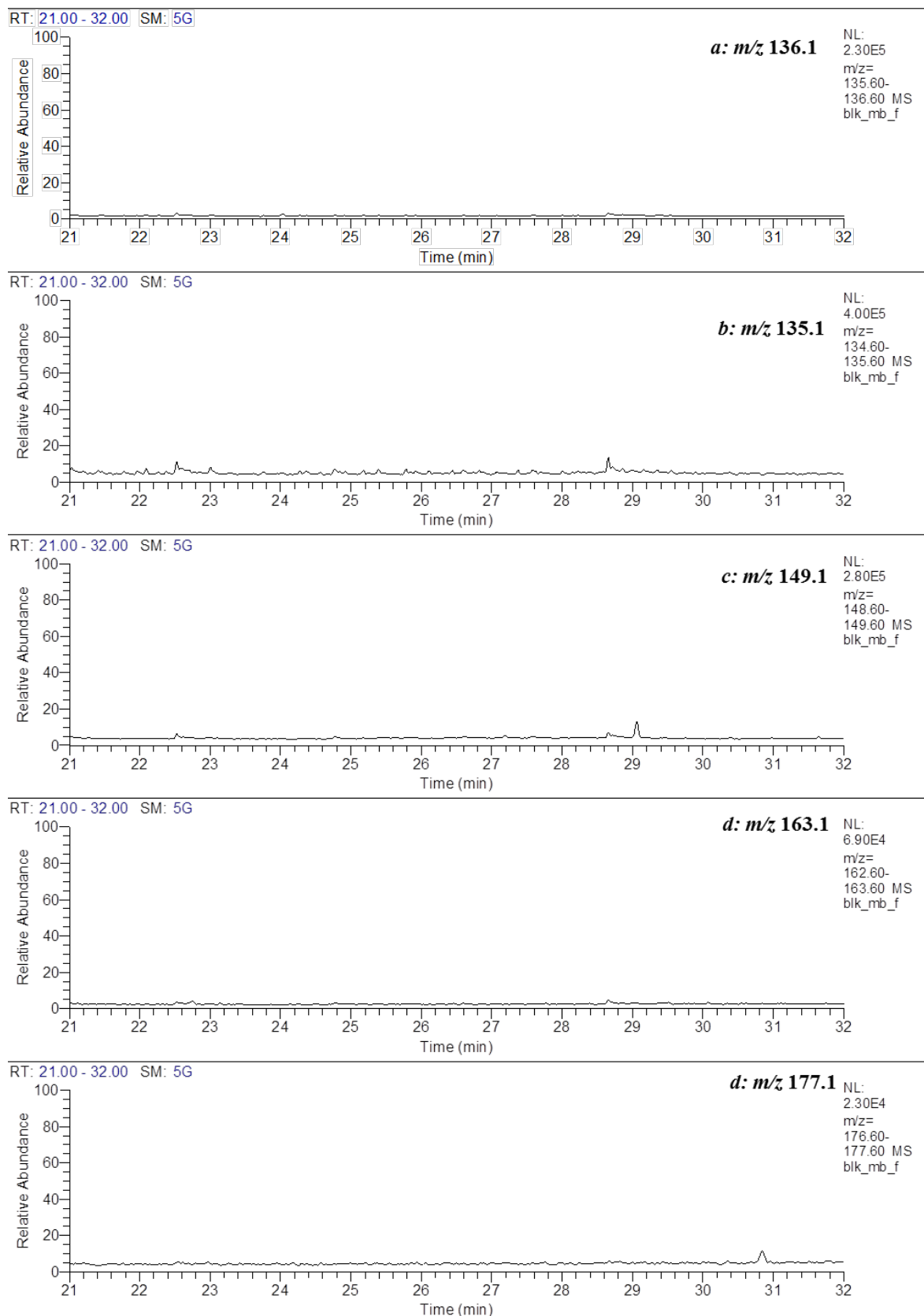


Figure A6-150: Partial m/z 136.1, 135.1, 149.1, 163.1 and 177.1 mass chromatograms for the Gnarlyknots-1A (4390-4425m) FI system blank.

Showing the distribution of (a) adamantane, (b) methyladamantanes and ethyladamantanes, (c) dimethyladamantanes and ethylmethyladamantanes, (d) trimethyladamantanes and (e) tetramethyladamantanes. Peak abbreviations are listed in Table A5-B6.

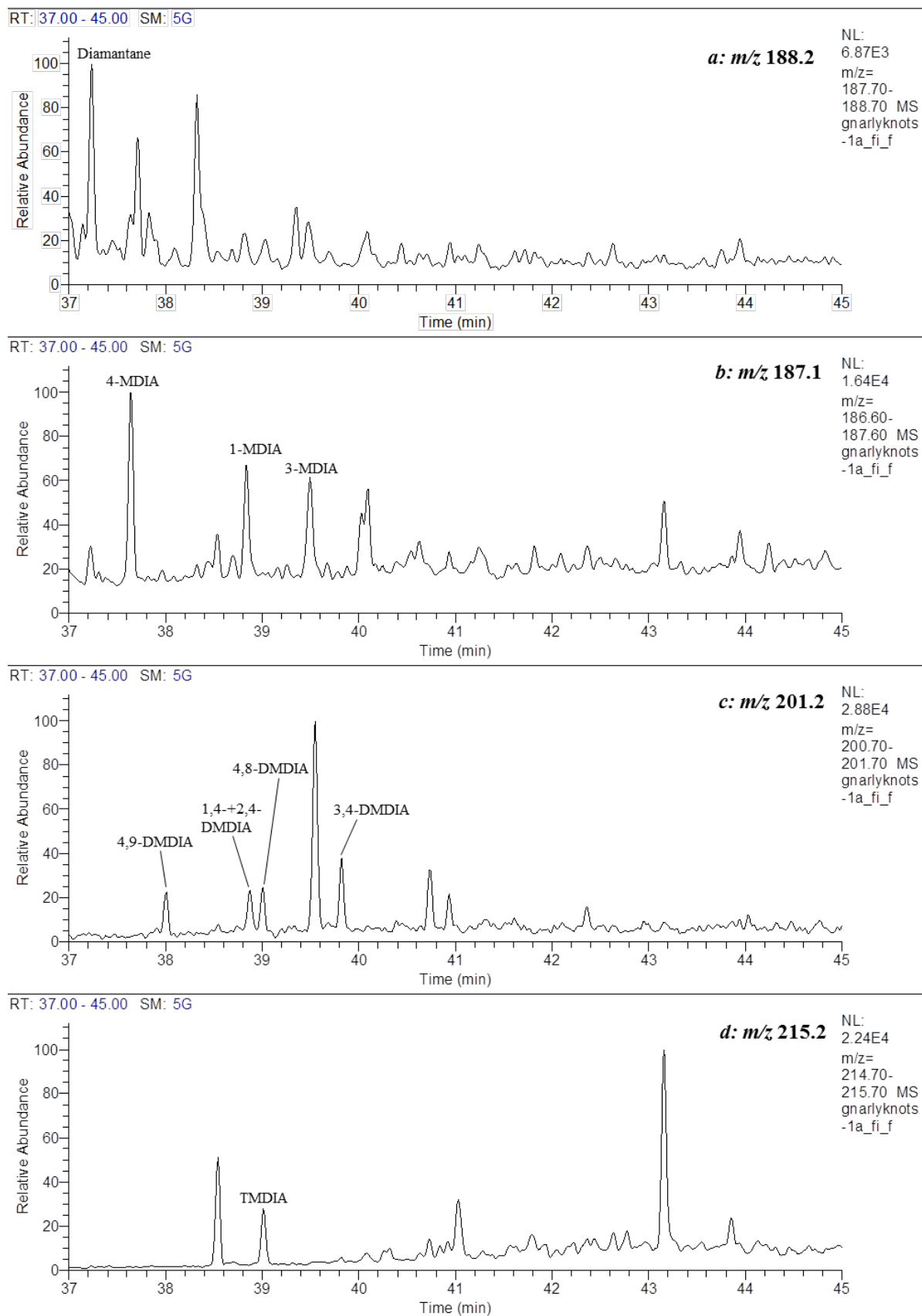


Figure A6-151: Partial m/z 188.2, 187.1, 201.2 and 215.2 mass chromatograms for the Gnarlyknots-1A (4390-4425m) FI oil. Showing the distribution of (a) diamantane, (b) methyldiamantanes, (c) dimethyldiamantanes and (d) trimethyldiamantanes respectively. Peak abbreviations are listed in Table A5-B6.

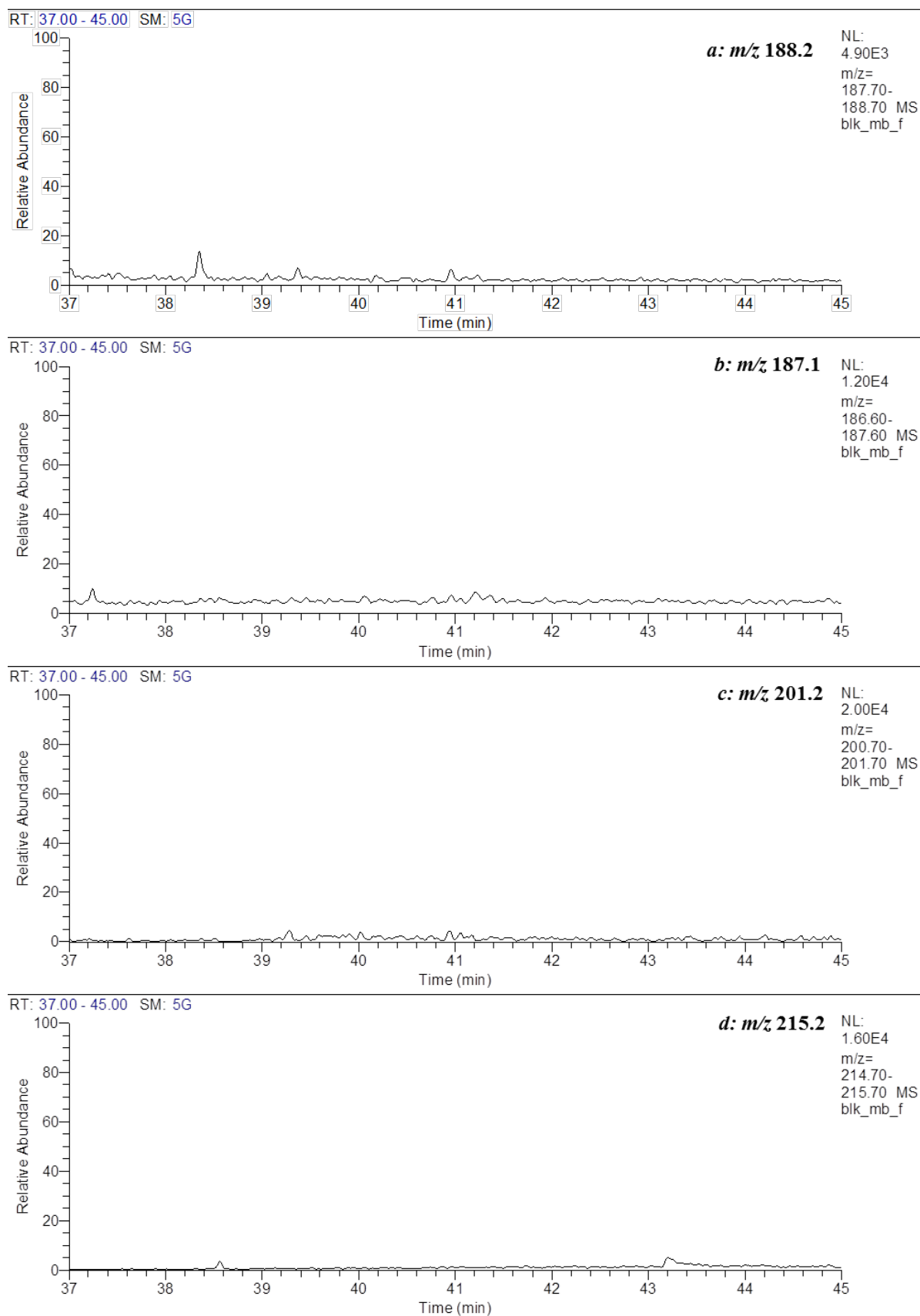


Figure A6-152: Partial m/z 188.2, 187.1, 201.2 and 215.2 mass chromatograms for the Gnarlyknots-1A (4390-4425m) FI system blank.

Showing the distribution of (a) diamantane, (b) methyldiamantanes, (c) dimethyldiamantanes and (d) trimethyldiamantanes respectively. Peak abbreviations are listed in Table A5-B6.

APPENDIX 7: ON-LINE MCI – Gnarlyknots-1A

Fluid Inclusion Oil (4390-4425 mMD)

Mass Chromatograms and Peak Identifications

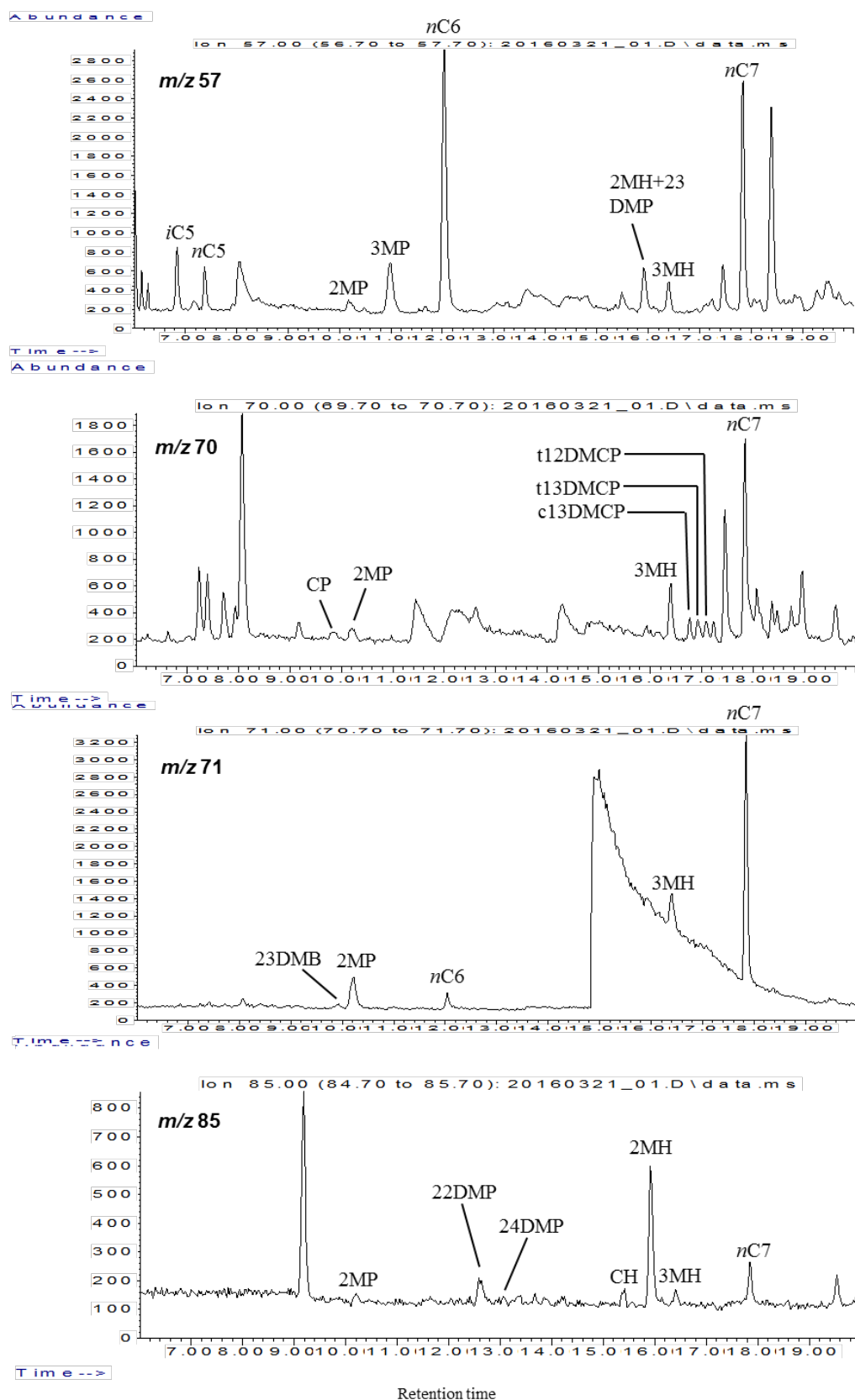


Figure A7-153: Partial m/z 57, 70, 71, 85 mass chromatograms for the Gnarlyknots-1A (4410-4415 m) FI oil (on-line crushing method). Showing the distribution of low molecular weight hydrocarbons in the C5 to C7 range. Peak identifications and structures are given in Table A5-B7.

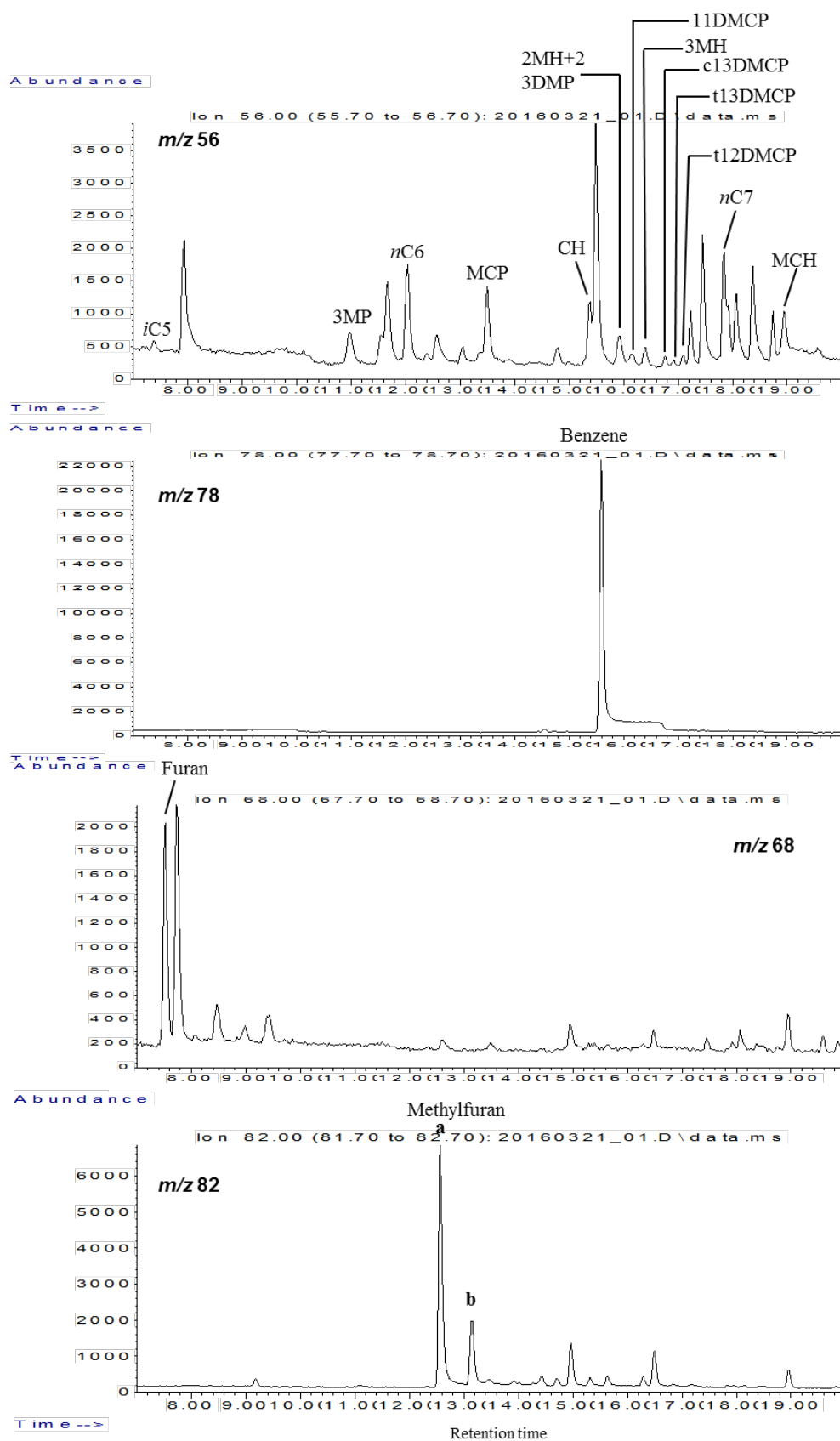


Figure A7-154: Partial m/z 56, 78, 68 and 82 mass chromatograms for Gnarlyknots-1A (4410-4415 m) FI oil (on-line crushing method). Showing the distribution of low molecular weight hydrocarbons in the C6 to C7 range. Peak identifications and structures are given in Table A5-B7.

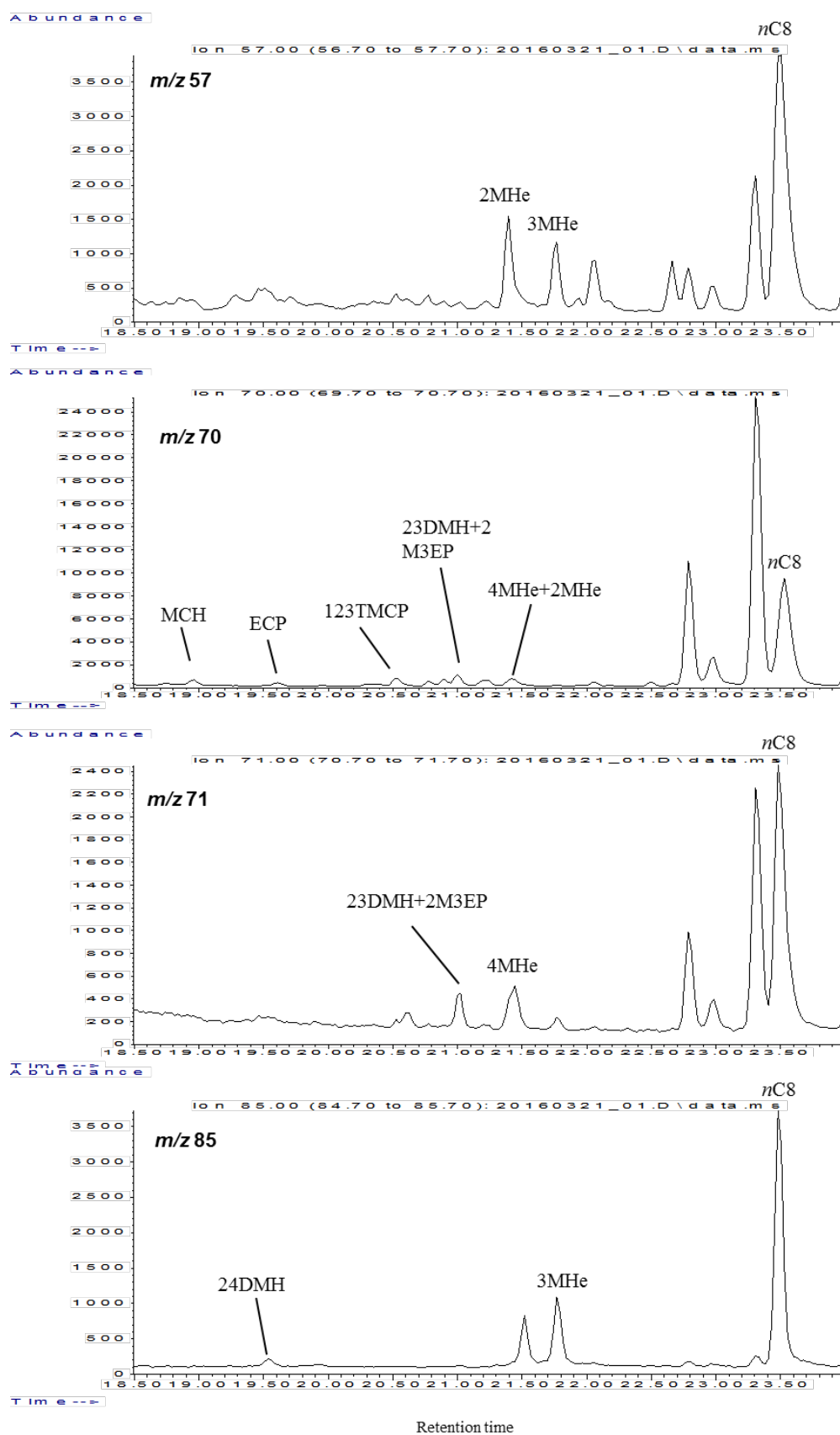


Figure A7-155: Partial m/z 57, 70, 71 and 85 mass chromatograms for the Gnarlyknots-1A (4410-4415 m) FI oil (on-line crushing method). Showing the distribution of low molecular weight hydrocarbons in the C7 to C8 range. Peak identifications and structures are given in Table A5-B7.

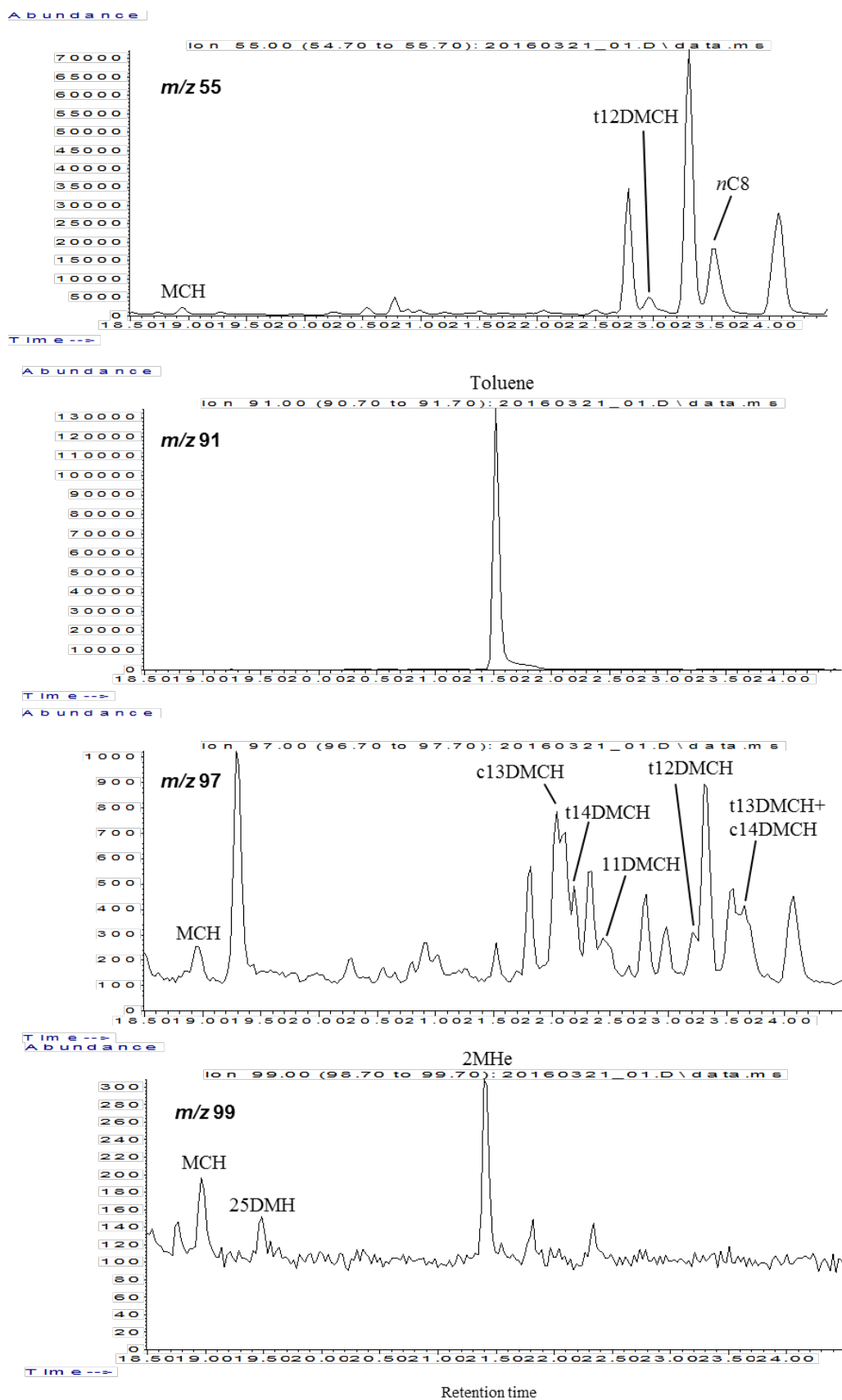


Figure A7-156: Partial m/z 55, 91, 97 and 99 mass chromatograms for the Gnarlyknots-1A (4410-4415 m) FI oil (on-line crushing method).
Showing the distribution of low molecular weight hydrocarbons in the C7 to C8 range. Peak identifications and structures are given in Table A5-B7.

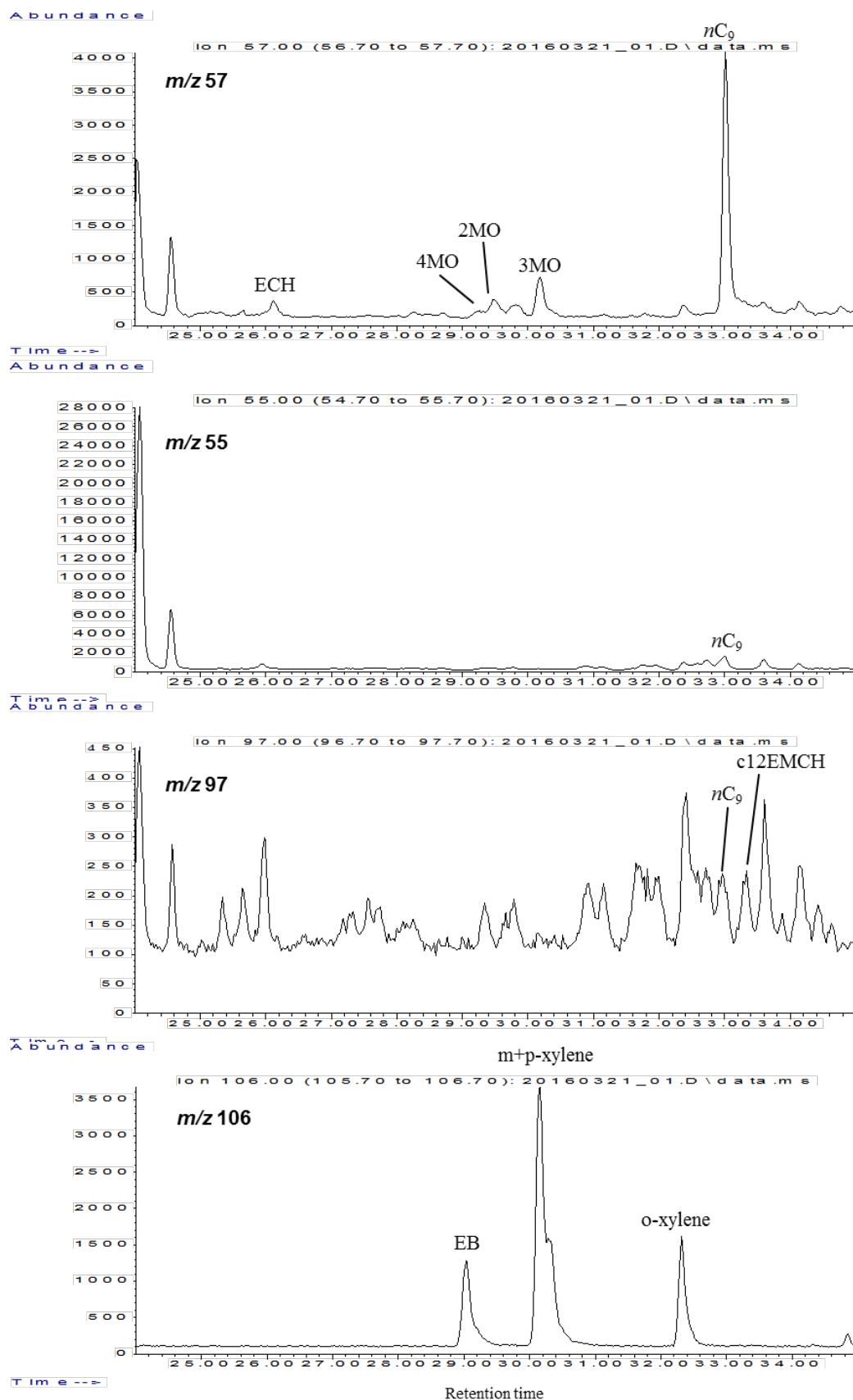
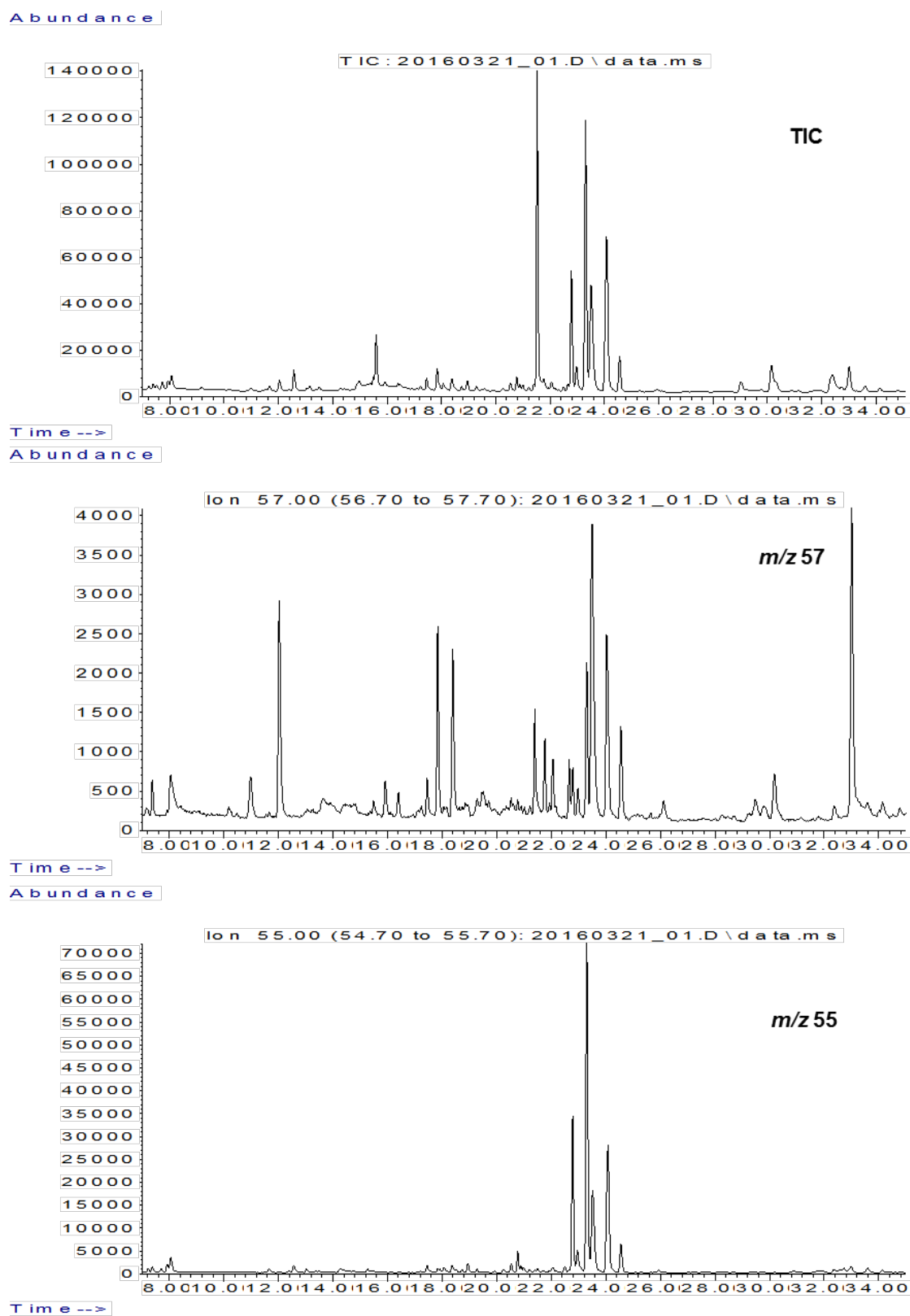


Figure A7-157: Partial m/z 57, 55, 97 and 106 mass chromatograms for the Gnarlyknots-1A (4410-4415 m) FI oil (on-line crushing method). Showing the distribution of low molecular weight hydrocarbons in the C8 to C9 range. Peak identifications and structures are given in Table A5-B7.



Retention time

Figure A7-158: TIC, partial m/z 57 and 55 mass chromatograms for the Gnarlyknots-1A (4410-4415 m) FI oil (on-line crushing method).
Showing the distribution of low molecular weight hydrocarbons in the C5 to C9 range. Peak identifications and structures are given in Table A5-B7.

APPENDIX 8: OFF-LINE MCI – Greenly-1

Fluid Inclusion Oil (4806-4818 mMD)

Mass Chromatograms and Peak Identifications

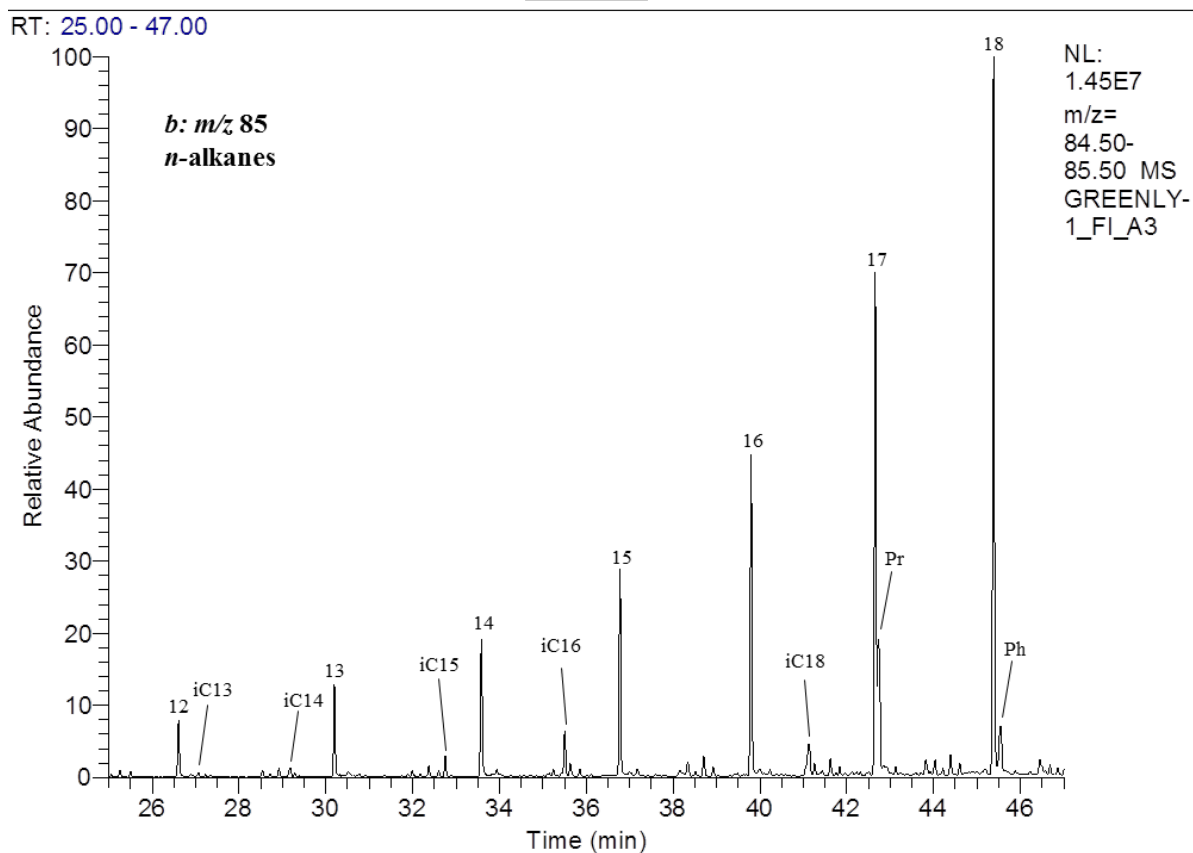
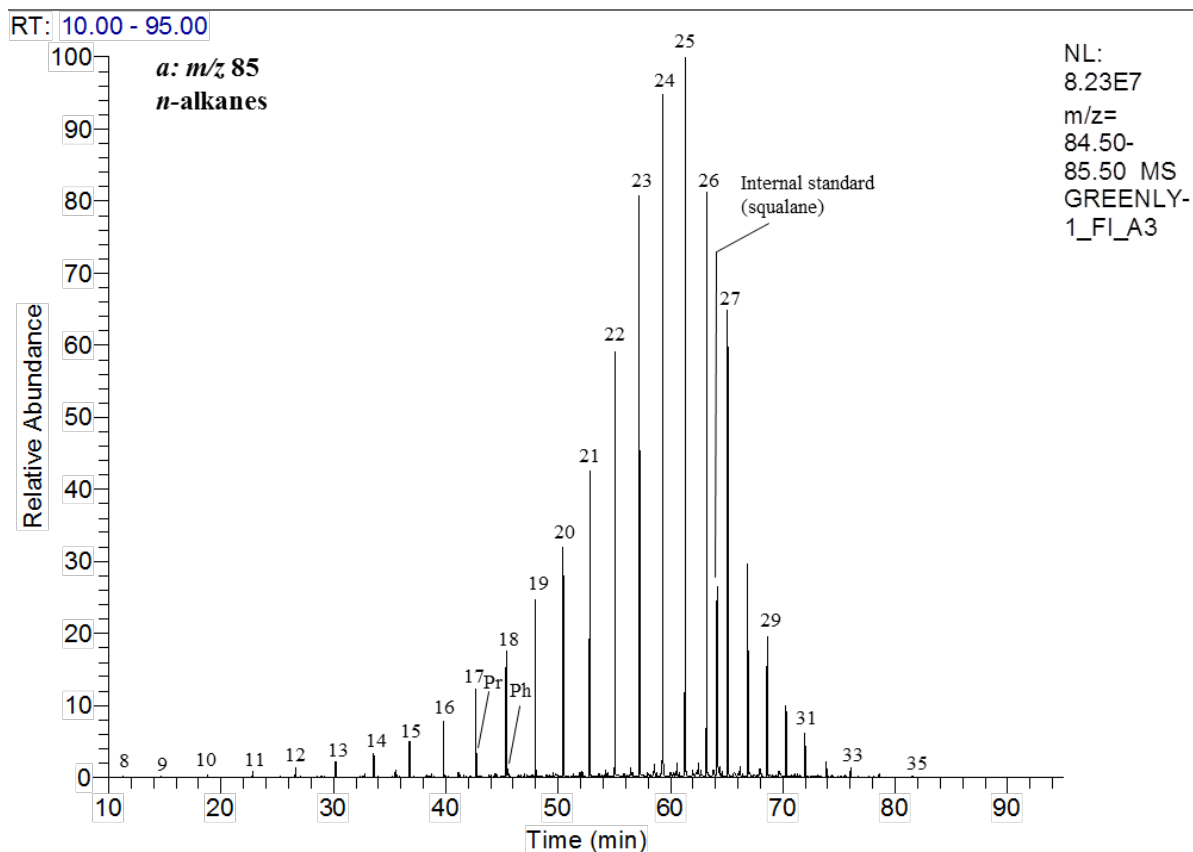


Figure A8-159: Partial m/z 85 mass chromatograms for the Greenly-1 (4806-4818 m) FI oil. Showing the distribution of n-alkanes and isoprenoids. Numbers refer to n-alkane chain length, Pr = pristane, Ph = phytane, iC13 = C13 isoprenoid, etc.

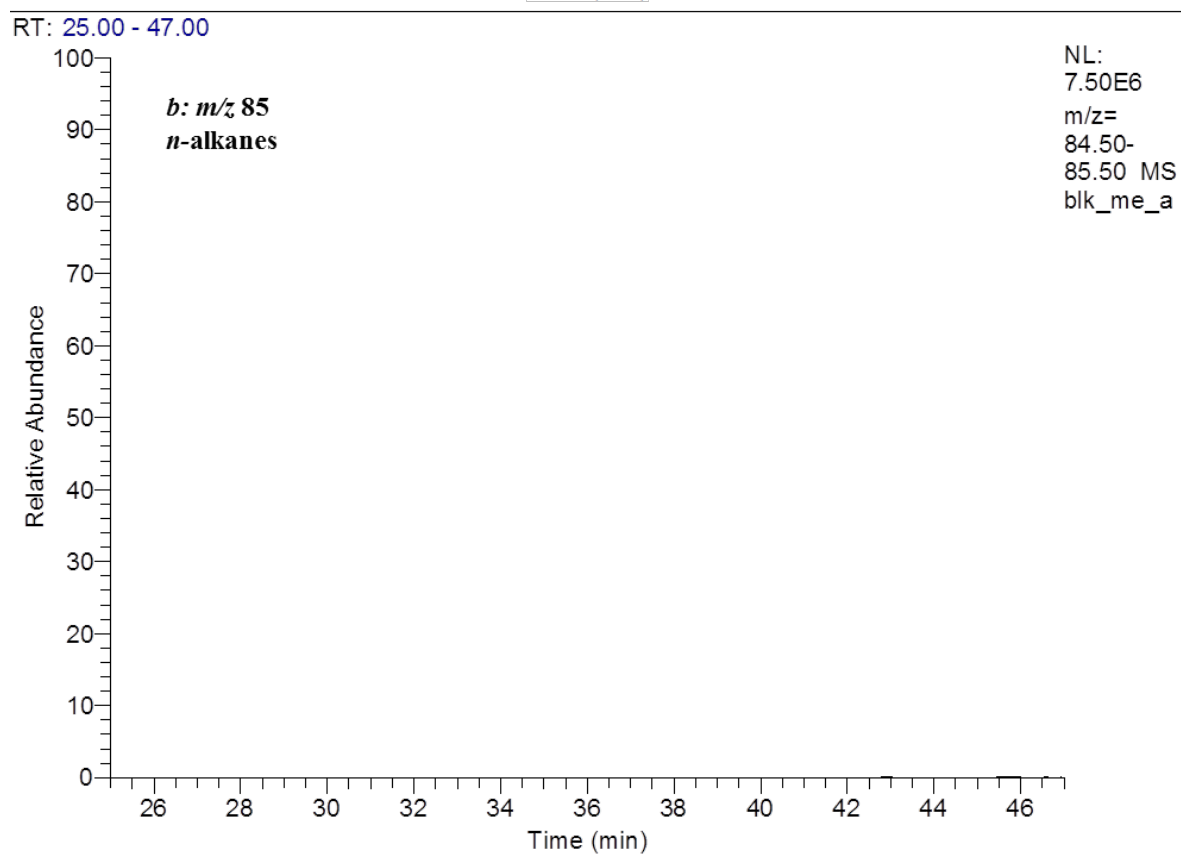
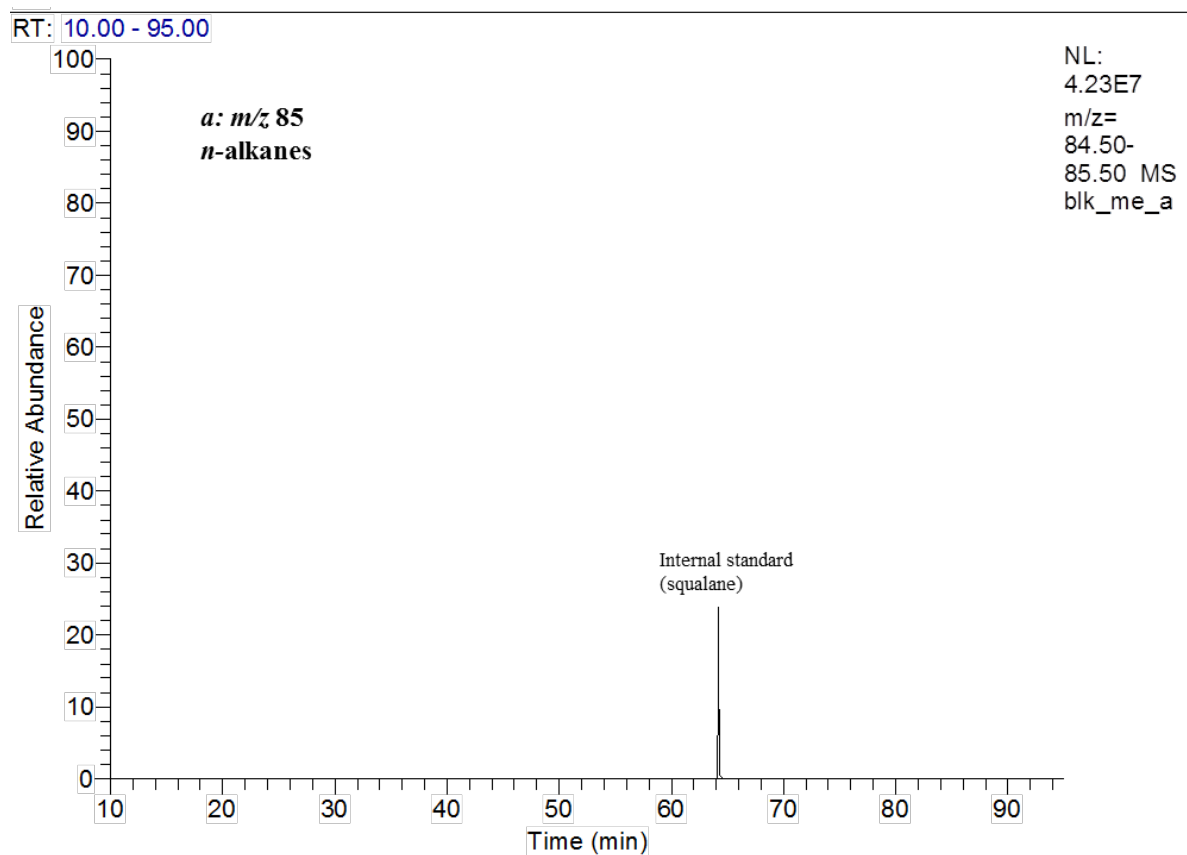


Figure A8-160: Partial m/z 85 mass chromatograms for the Greenly-1 (4806-4818 m) FI system blank. Showing the distribution of n-alkanes, methylalkanes and isoprenoids. Numbers refer to n-alkane chain length, Pr = pristane, Ph = phytane, iC13 = C13 isoprenoid, etc.

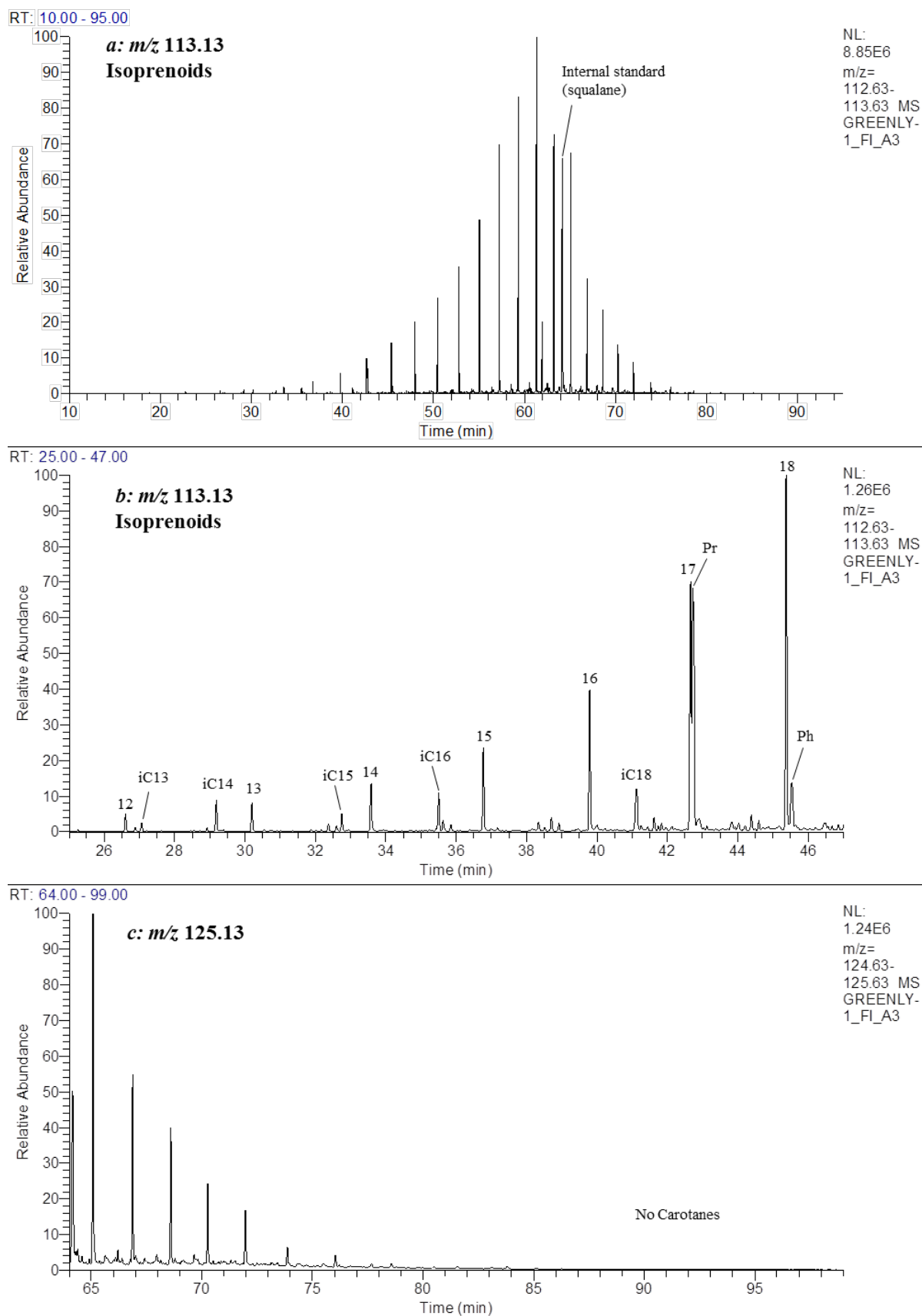


Figure A8-161: Partial m/z 113 and 125 mass chromatograms for the Greenly-1 (4806-4818 m) FI oil. Showing the distribution of isoprenoids and b-carotene. Numbers refer to n -alkane chain length, Pr = pristane, Ph = phytane, iC13 = C13 isoprenoid, etc.

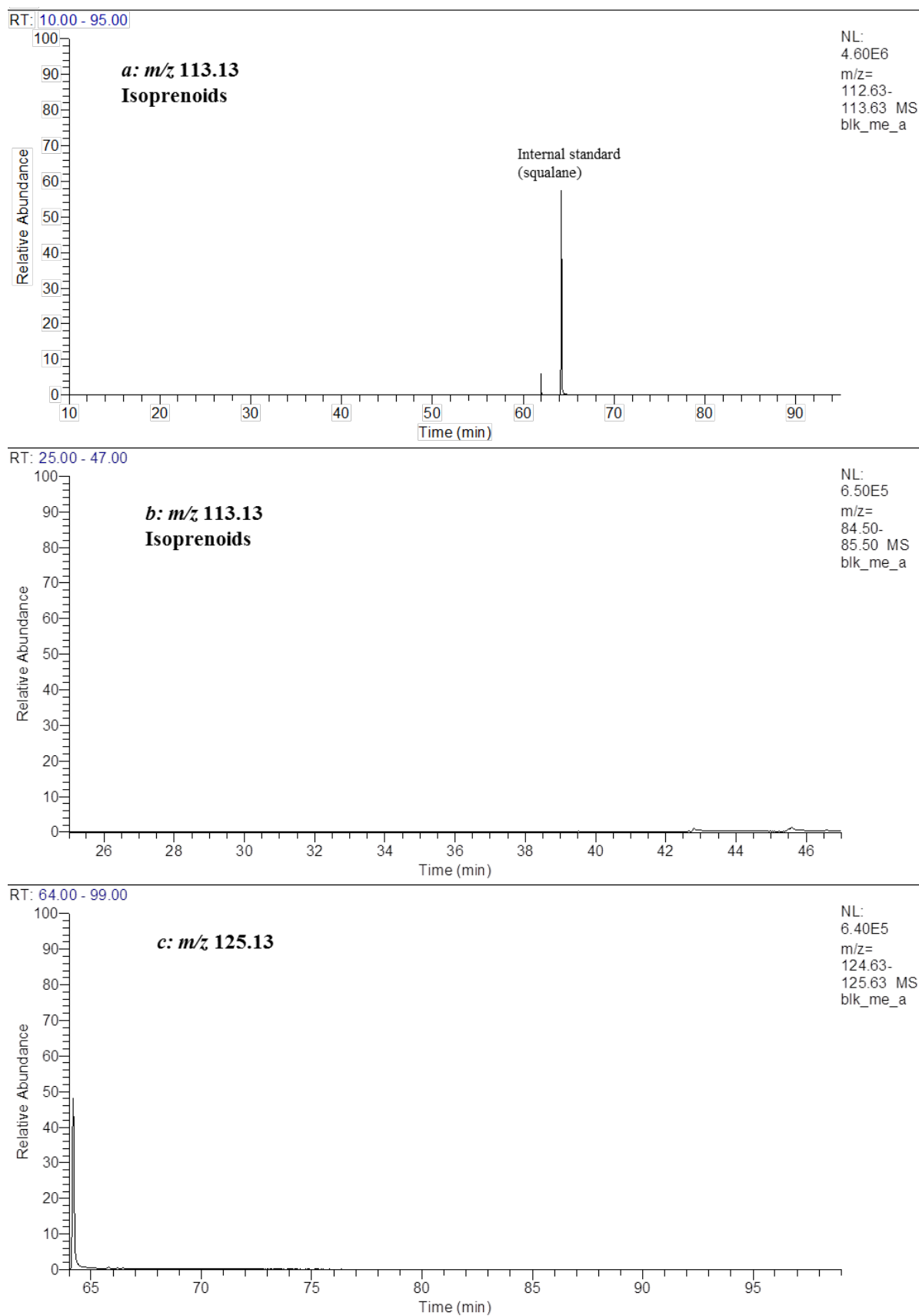


Figure A8-162: Partial m/z 113 and 125 mass chromatograms for the Greenly-1 (4806-4818 m) FI system blank. Showing the distribution of isoprenoids and b-carotane. Numbers refer to n-alkane chain length, Pr = pristane, Ph = phytane, iC13 = C13 isoprenoid, etc

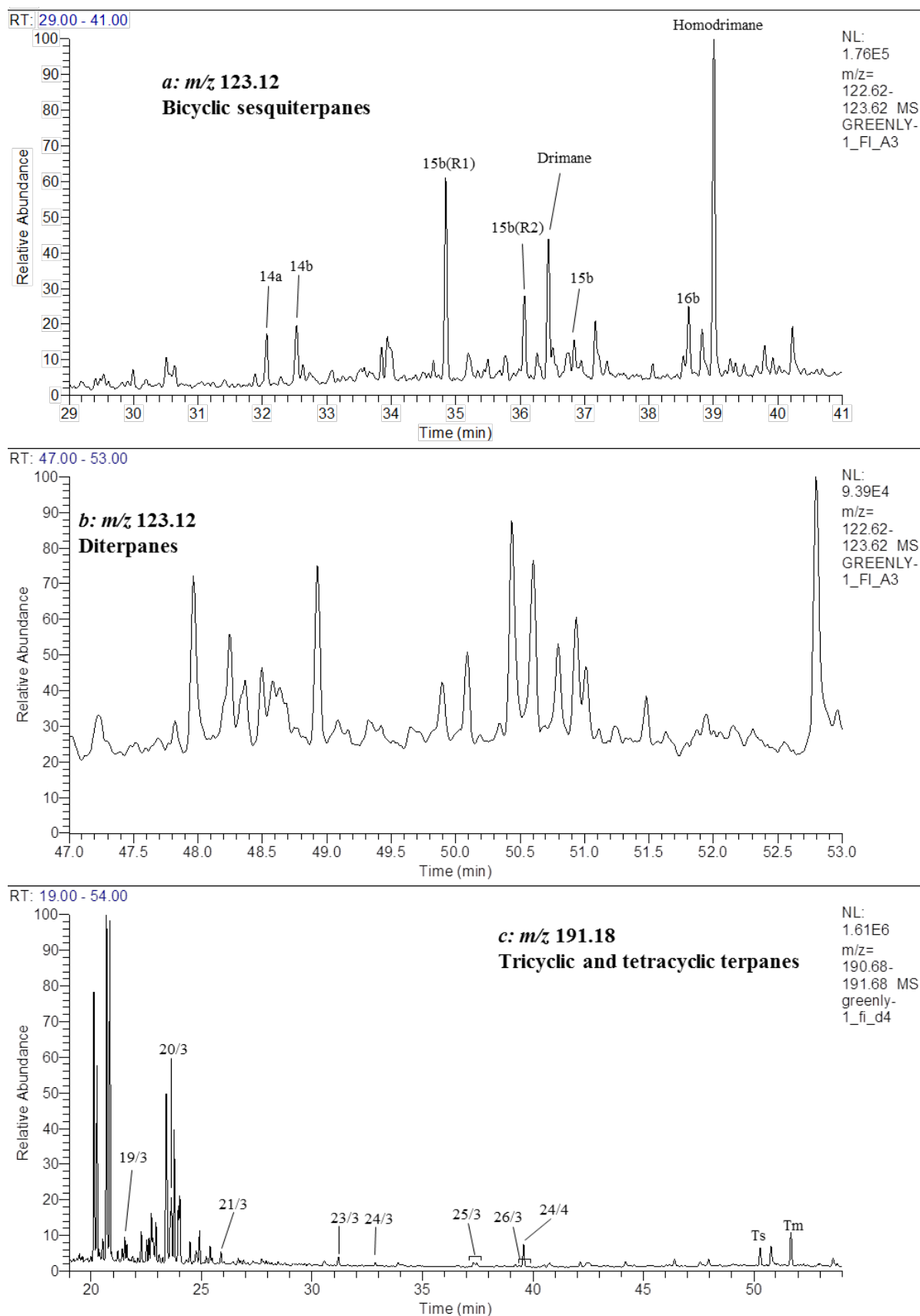


Figure A8-163: Partial m/z 123 and 191 mass chromatograms for the Greenly-1 (4806-4818 m) FI oil. Showing the distribution of (a) C_{14} to C_{16} bicyclic sesquiterpanes, (b) diterpanes and (c) tricyclic/tetracyclic terpanes. 14b refers to C_{14} bicyclic sesquiterpanes, 19/3 refers to C_{19} tricyclic terpane, 24/4 refers to C_{24} tetracyclic terpane, and so on. dO, dL and dU refer to A-ring degraded oleanoids, lupane and ursane. Hopane abbreviations listed in Table A5-37.

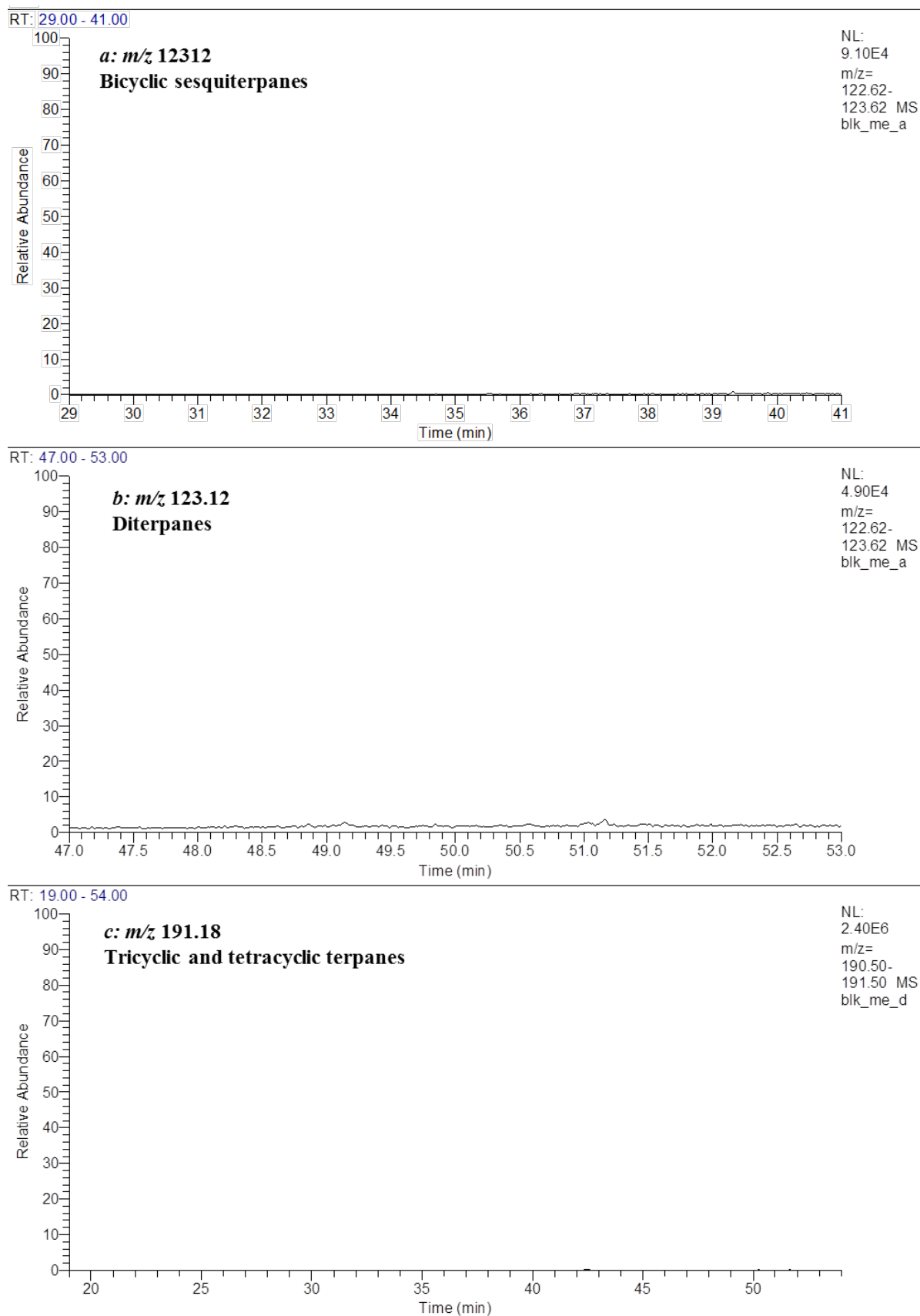


Figure A8-164: Partial m/z 123 and 191 mass chromatograms for the Greenly-1 (4806-4818 m) FI system blank. Showing the distribution of (a) C_{14} to C_{16} bicyclic sesquiterpanes, (b) diterpanes and (c) tricyclic/tetracyclic terpanes. 14b refers to C_{14} bicyclic sesquiterpanes, 19/3 refers to C_{19} tricyclic terpane, 24/4 refers to C_{24} tetracyclic terpene, and so on. dO, dL and dU refer to A-ring degraded oleanoids, lupane and ursane. Hopane abbreviations listed in Table A5-37.

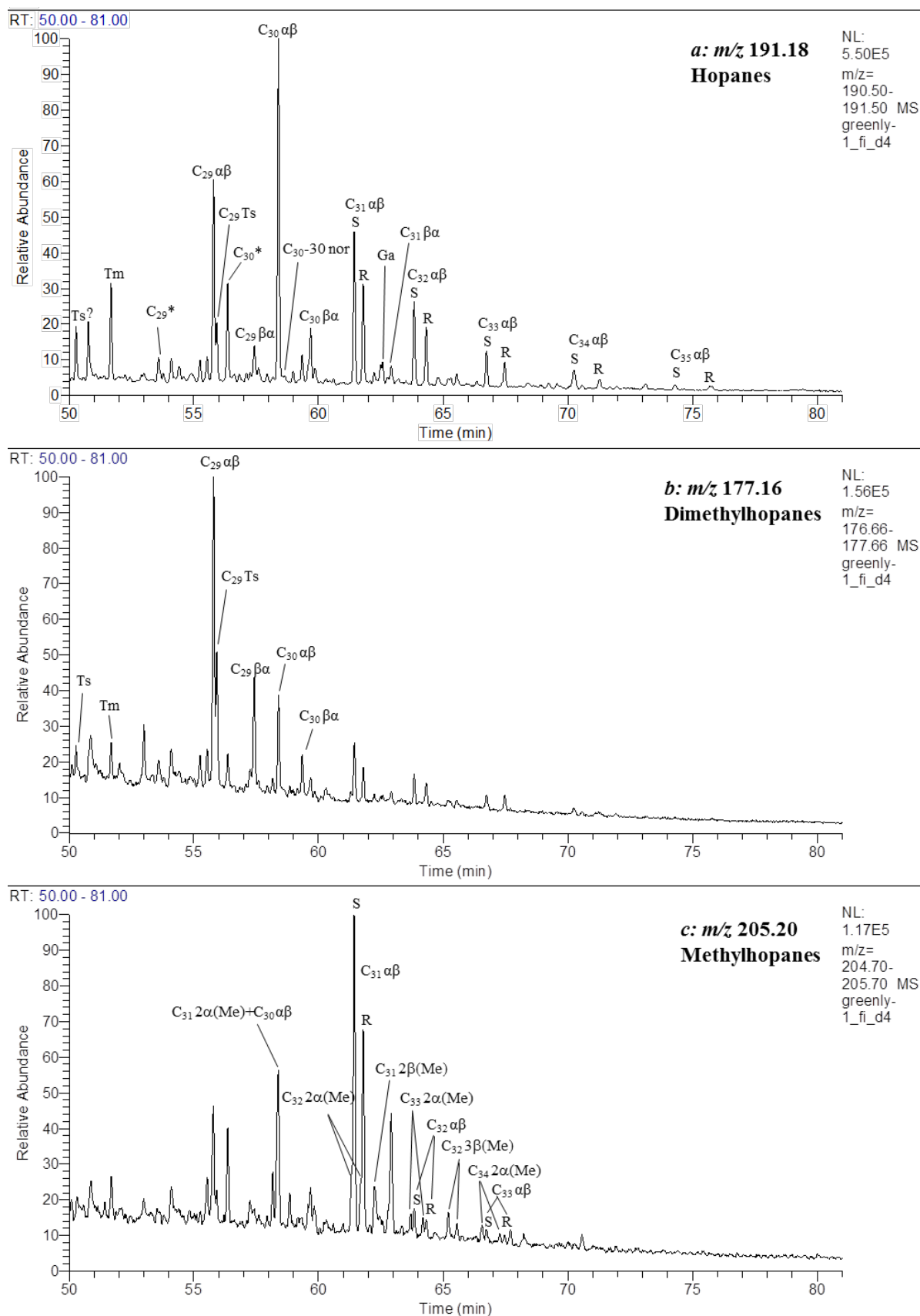


Figure A8-165: Partial m/z 191, 177 and 205 mass chromatograms for the Greenly-1 (4806-4818 m) FI oil. Showing the distribution of (a) hopanes, (b) demethylhopanes and (c) methylhopanes, respectively. Hopane abbreviations are listed in Table A5-37.

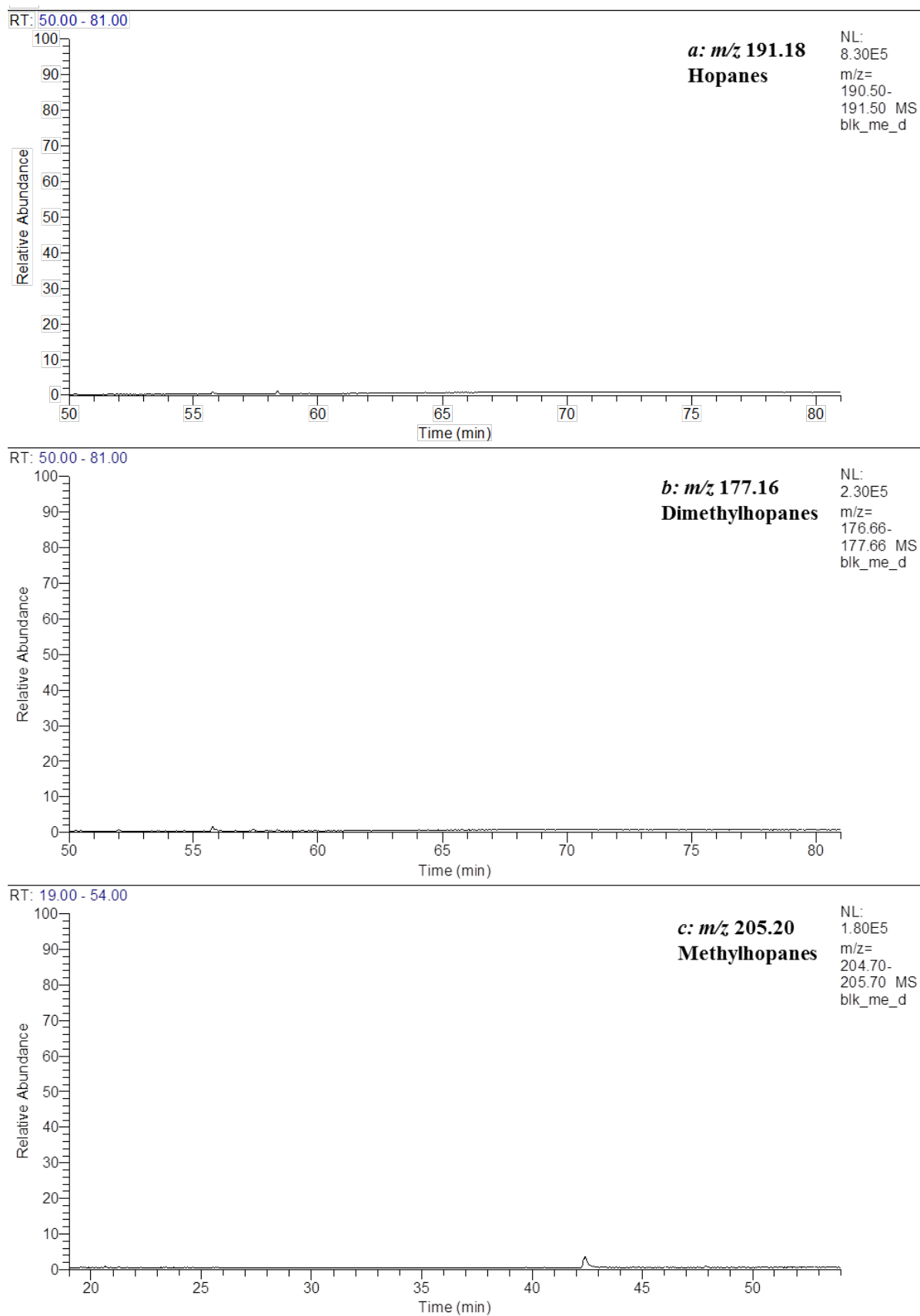


Figure A8-166: Partial m/z 191, 177 and 205 mass chromatograms for the Greenly-1 (4806-4818 m) FI system blank. Showing the distribution of (a) hopanes, (b) demethylhopanes and (c) methylhopanes, respectively. Hopane abbreviations are listed in Table A5-37.

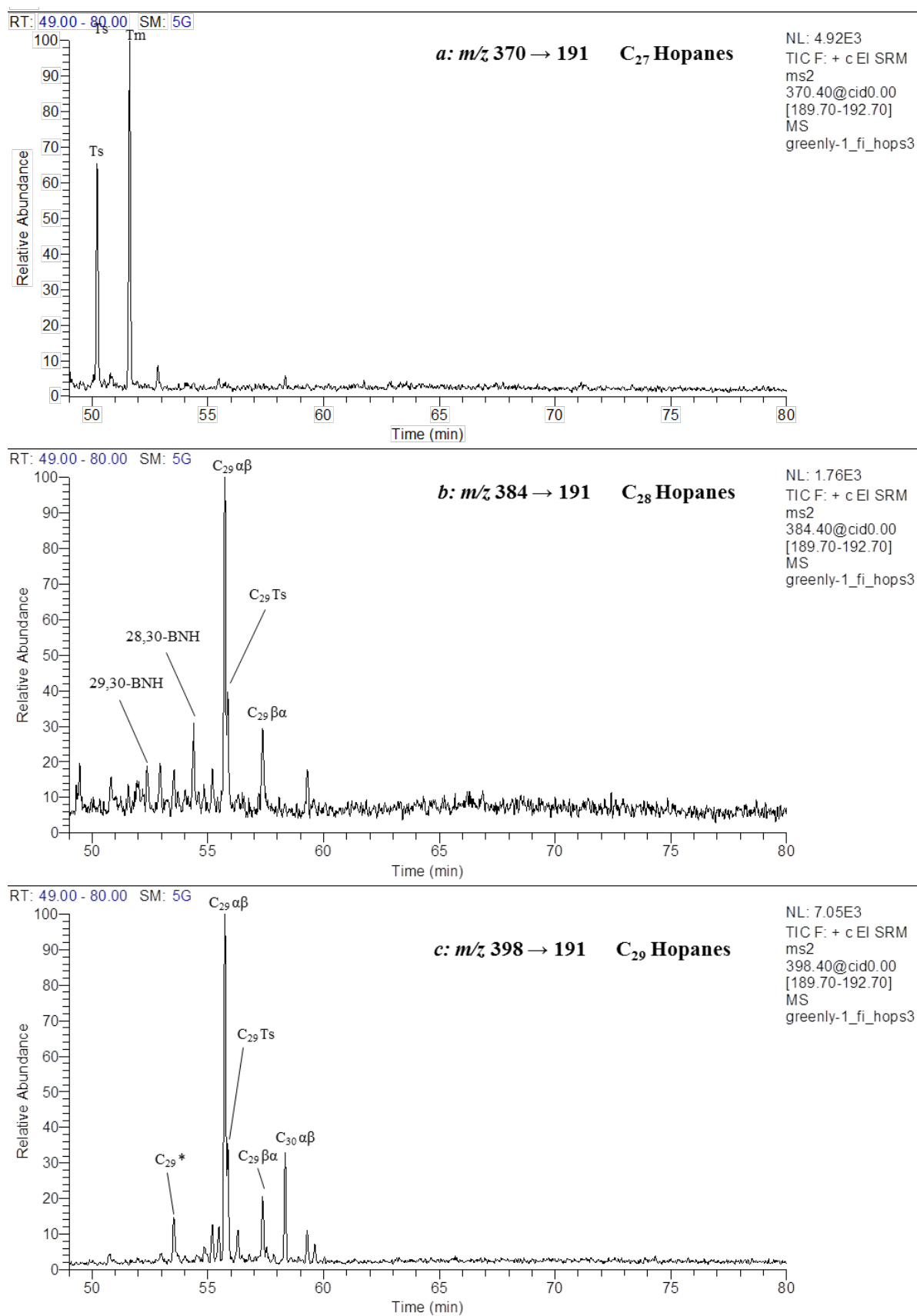


Figure A8-167: Partial MRM chromatograms (m/z 370.4, 398.4 and 398.4 \rightarrow 191.2) of the aliphatic hydrocarbons from the Greenly-1 (4806-4818 m) FI oil.

Showing the distribution of (a) C₂₇ (b) C₂₈ and (c) C₂₉ hopanes. Hopane abbreviations are listed in Table A5-37.

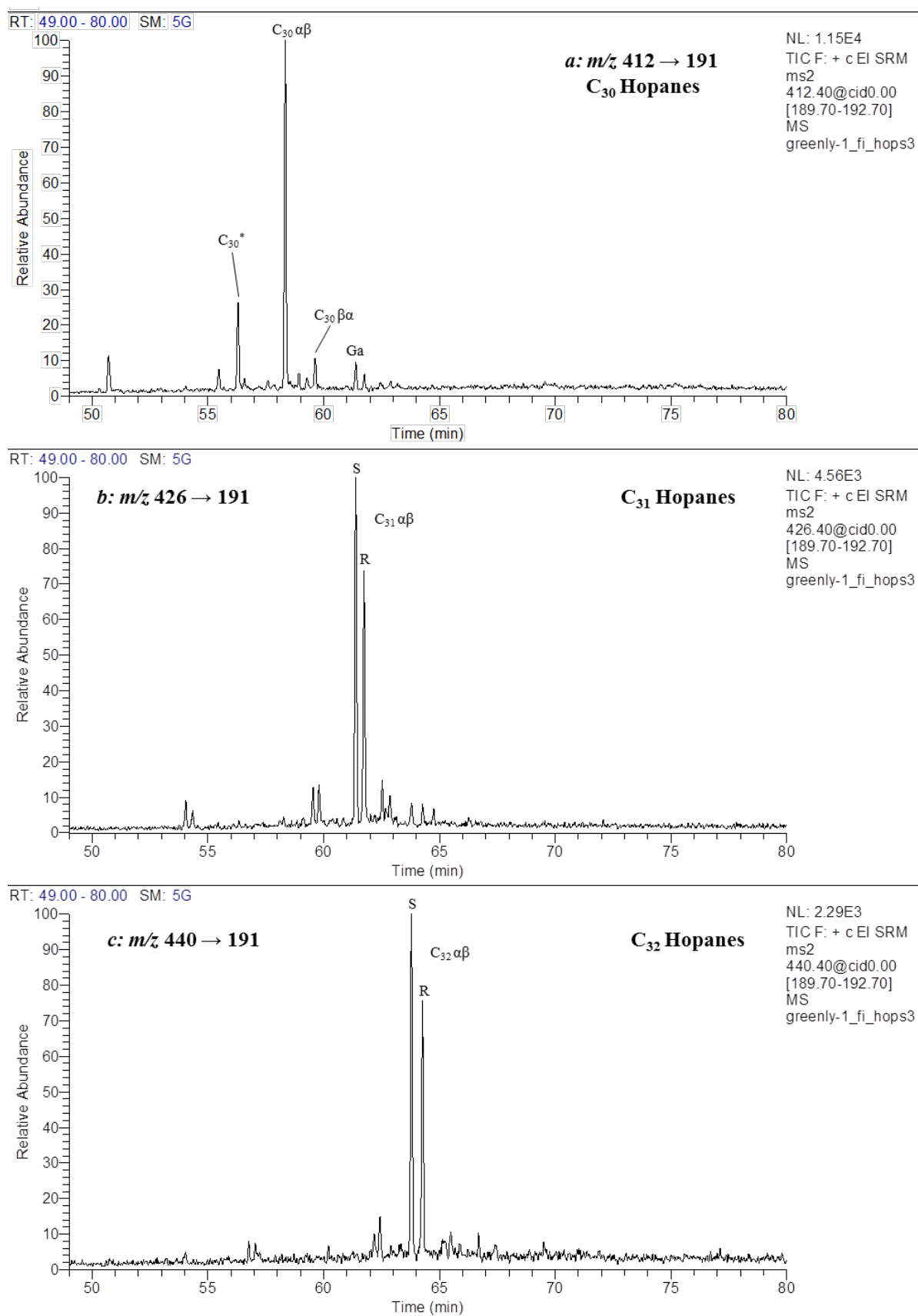


Figure A8-168: Partial MRM chromatograms (m/z 412.4, 426.4 and 440.4 \rightarrow 191.2) of the aliphatic hydrocarbons from the Greenly-1 (4806-4818 m) FI oil.

Showing the distribution of (a) C₃₀ (b) C₃₁ and (c) C₃₂ hopanes. Hopane abbreviations are listed in Table A5-37.

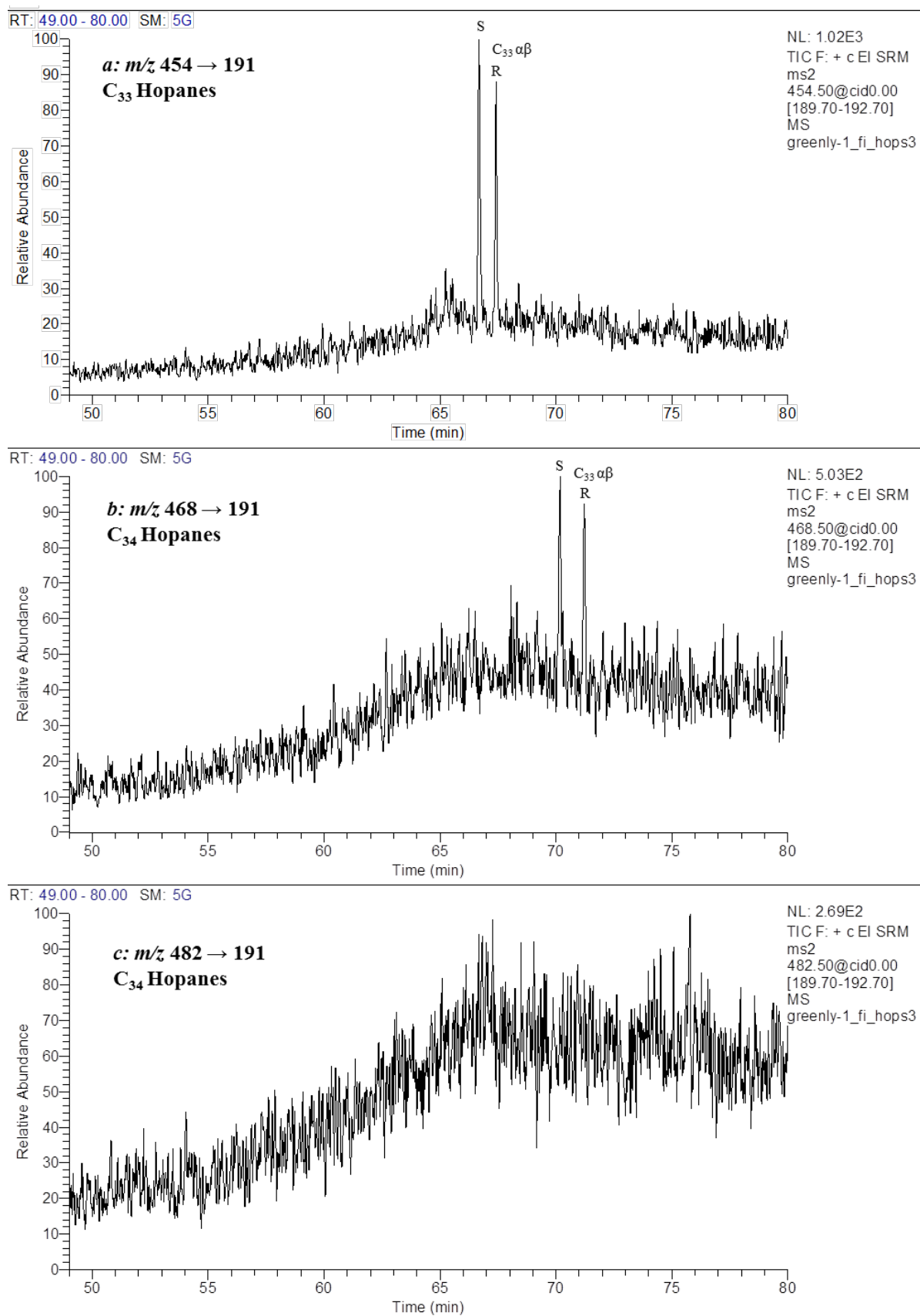


Figure A8-169: Partial MRM chromatograms (m/z 454.5, 468.5 and 482.5 \rightarrow 191.2) of the aliphatic hydrocarbons from the Greenly-1 (4806-4818 m) FI oil.

Showing the distribution of (a) C_{33} (b) C_{34} and (c) C_{35} hopanes. Hopane abbreviations are listed in Table A5-37.

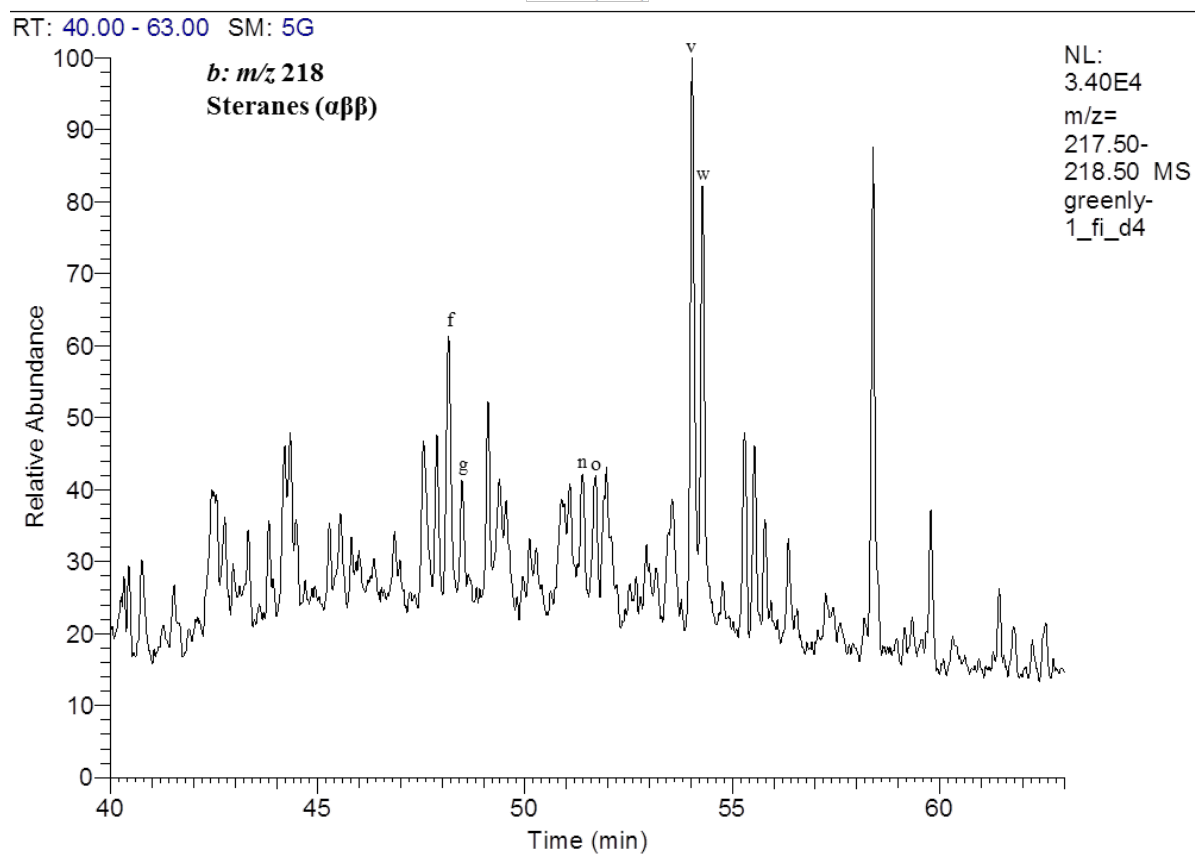
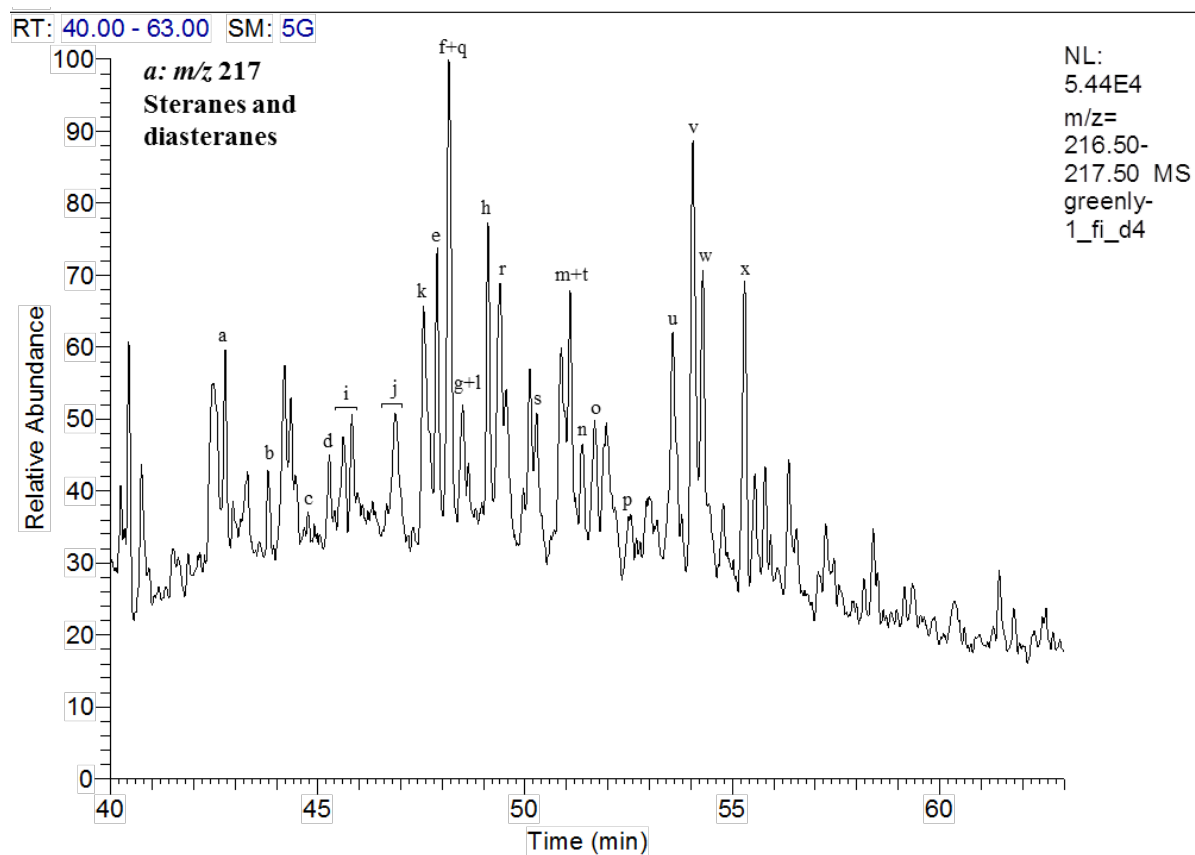


Figure A8-170: Partial m/z (a) 217 and (b) 218 mass chromatograms for the Greenly-1 (4806-4818 m) FI oil. Showing the distribution of steranes and diasteranes. Sterane and diasterane abbreviations are listed in Table A5-38. Peaks labelled with X are unknown compounds.

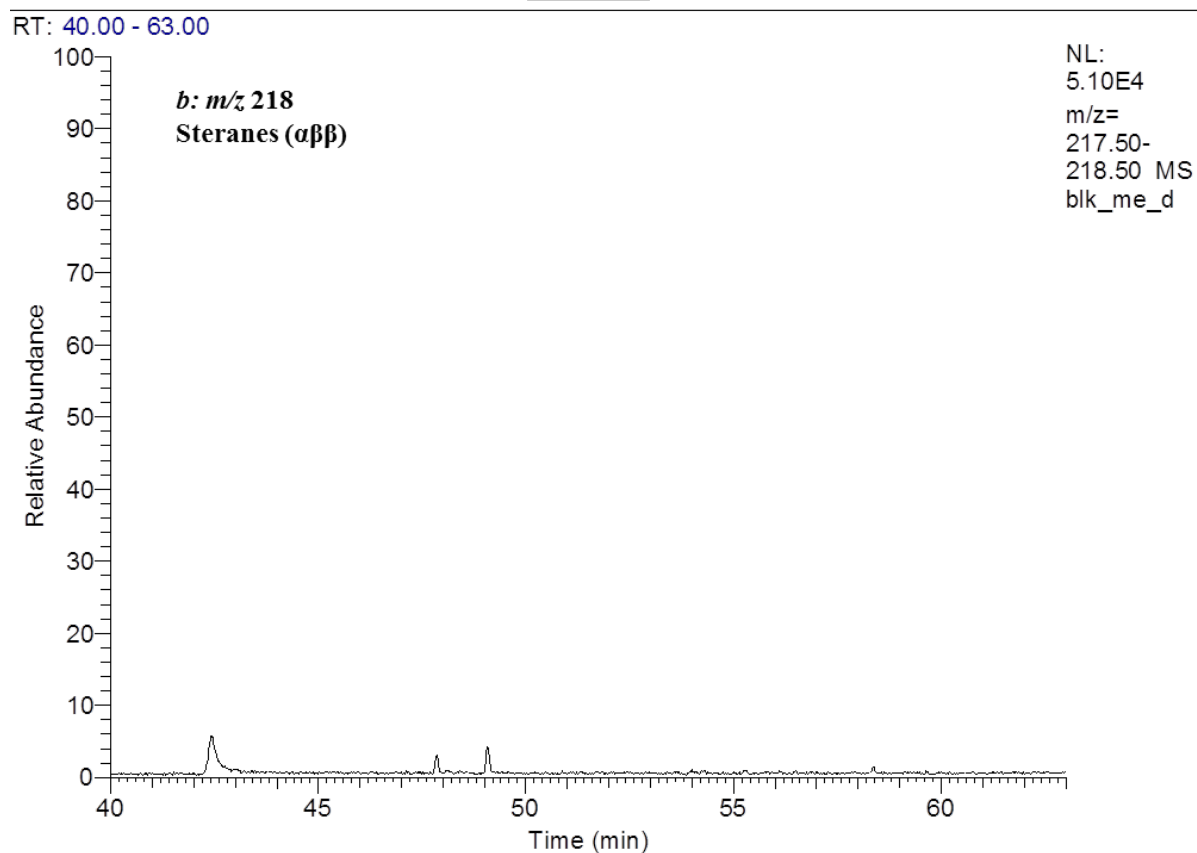
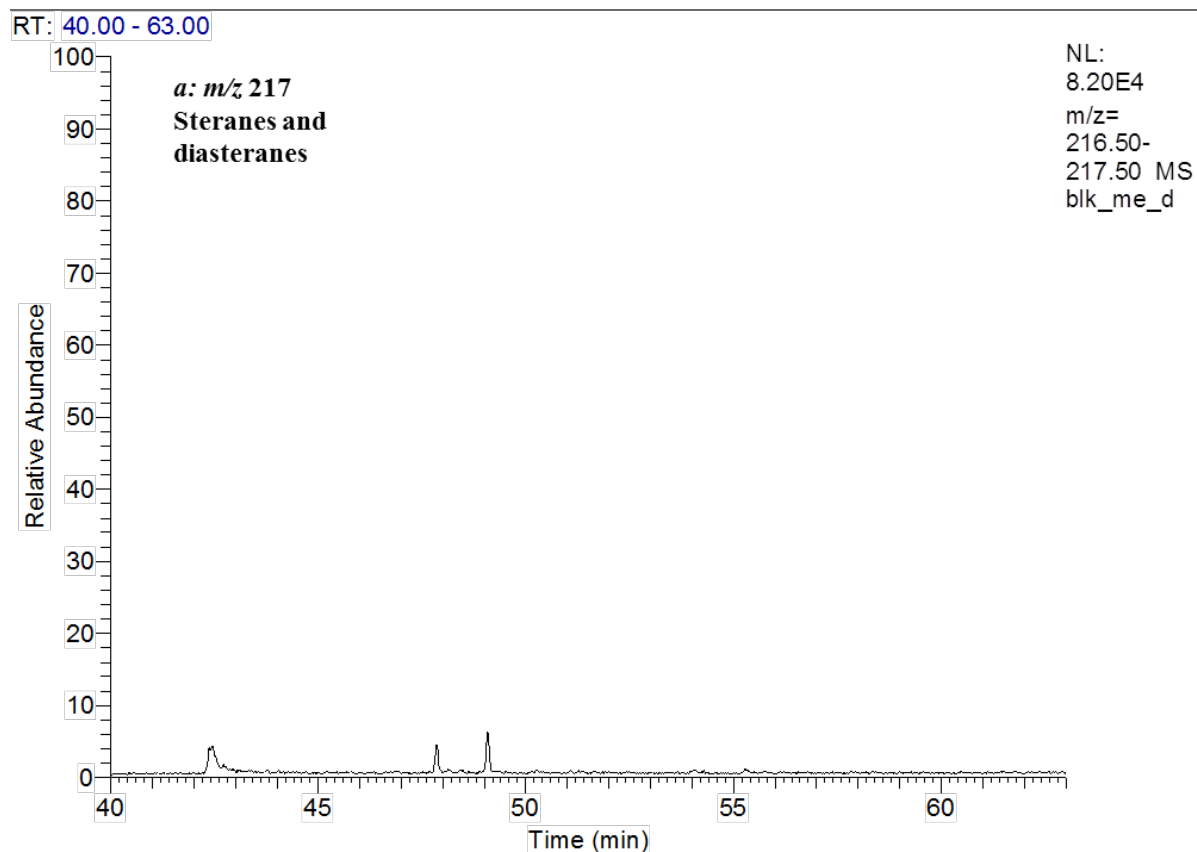


Figure A8-171: Partial m/z (a) 217 and (b) 218 mass chromatograms for the Greenly-1 (4806-4818 m) FI system blank. Showing the distribution of steranes and diasteranes. Sterane and diasterane abbreviations are listed in Table A5-38. Peaks labelled with X are unknown compounds.

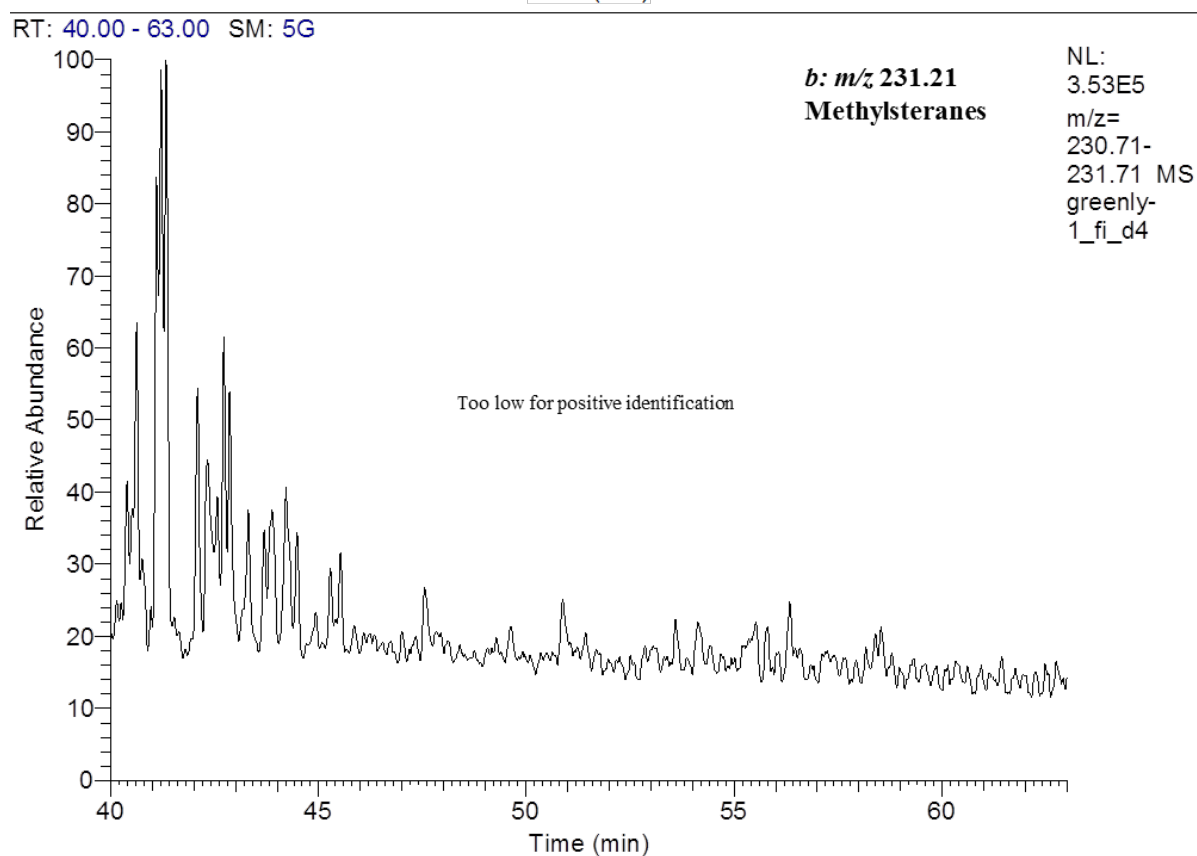
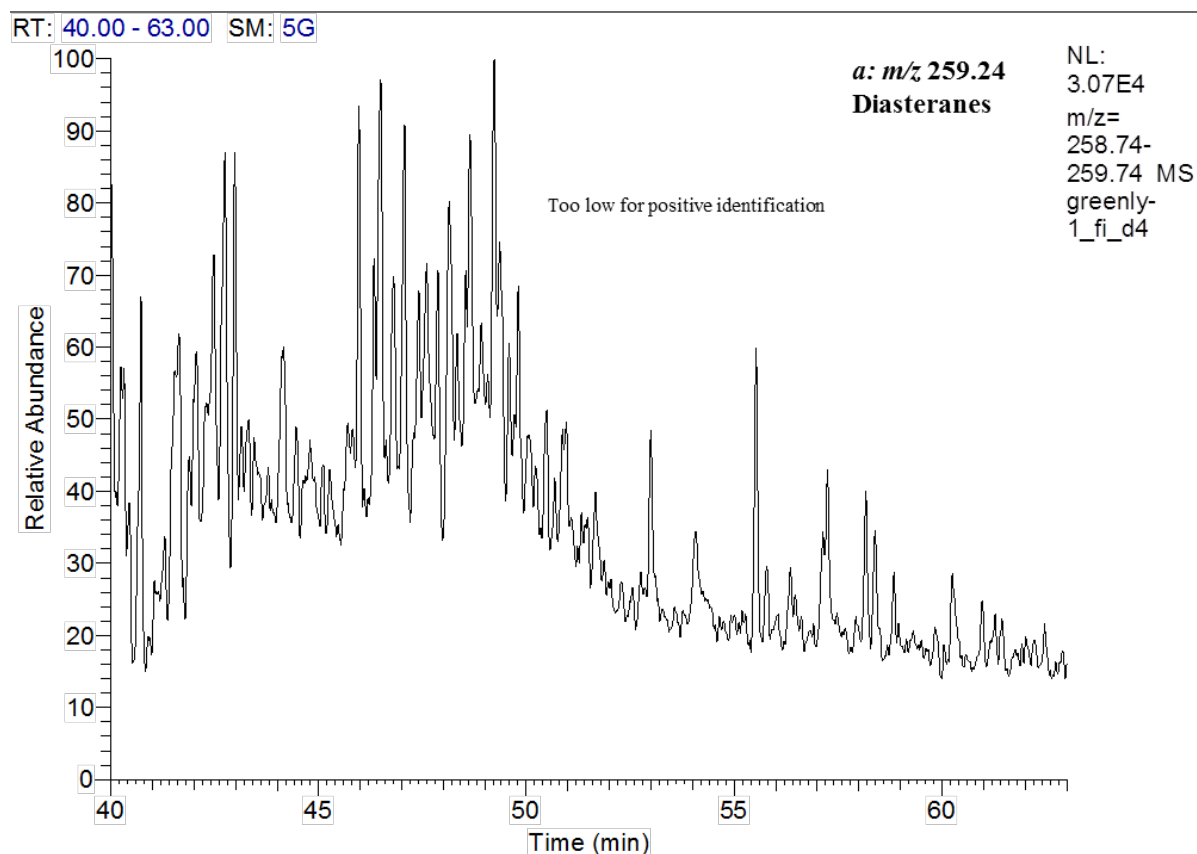


Figure A8-172: Partial m/z (a) 259 and (b) 231 mass chromatograms for the Greenly-1 (4806-4818 m) FI oil. Showing the distribution of diasteranes and methylsteranes. Sterane and diasterane abbreviations are listed in Table A5-38.

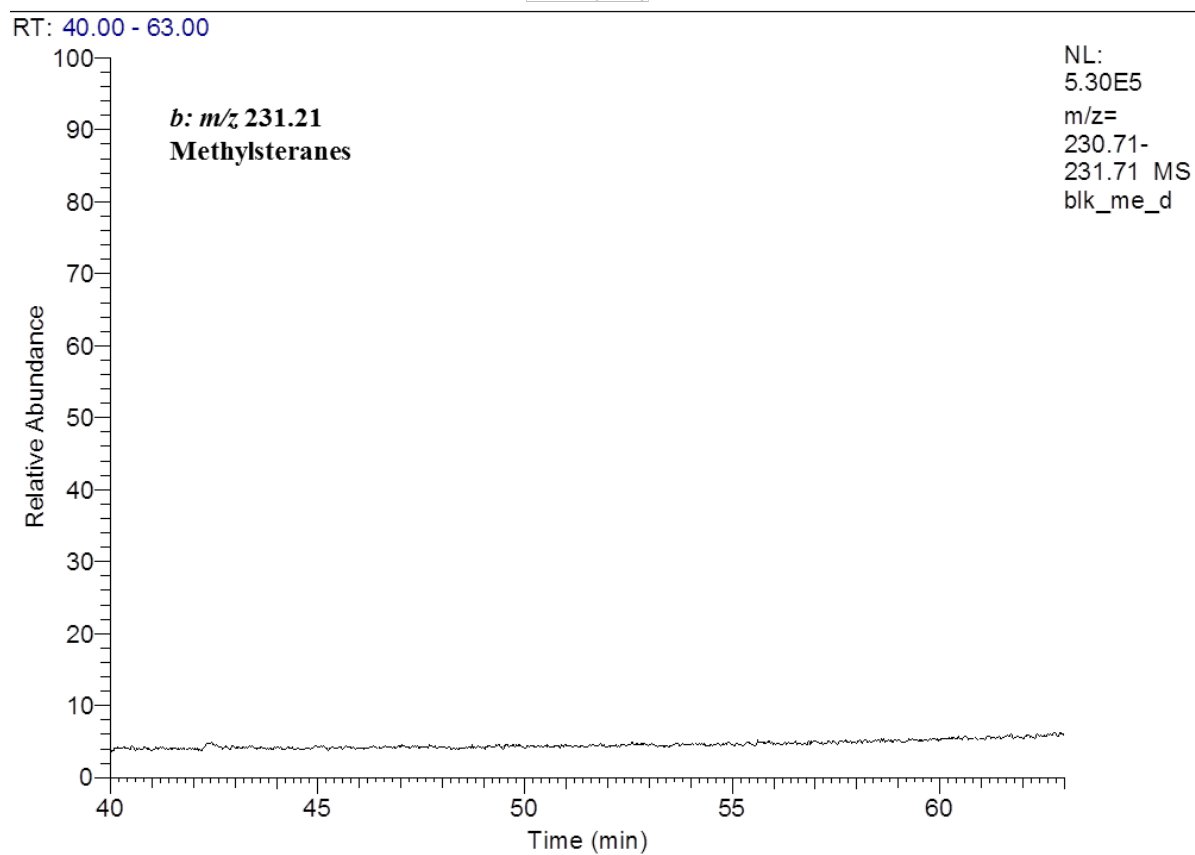
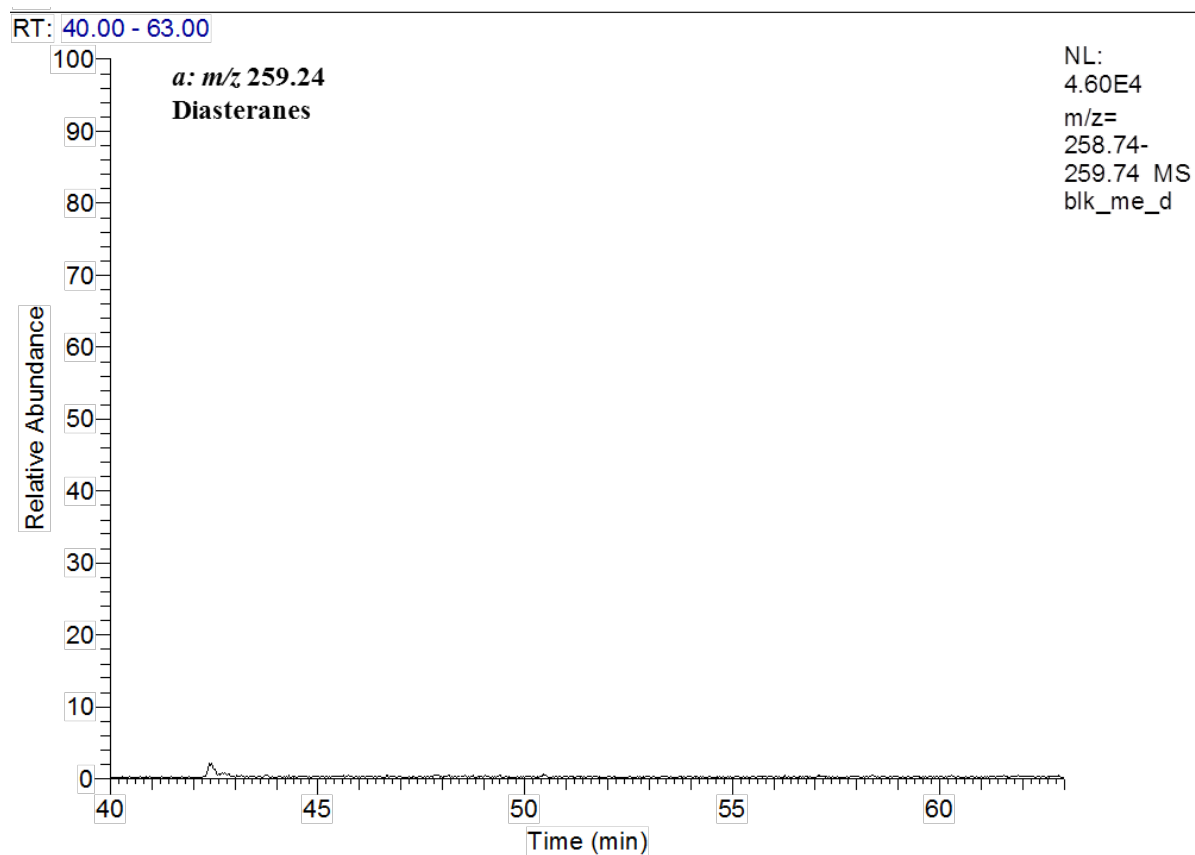


Figure A8-173: Partial m/z (a) 259 and (b) 231 mass chromatograms for the Greenly-1 (4806-4818 m) FI system blank. Showing the distribution of diasteranes and methylsteranes. Sterane and diasterane abbreviations are listed in Table A5-38.

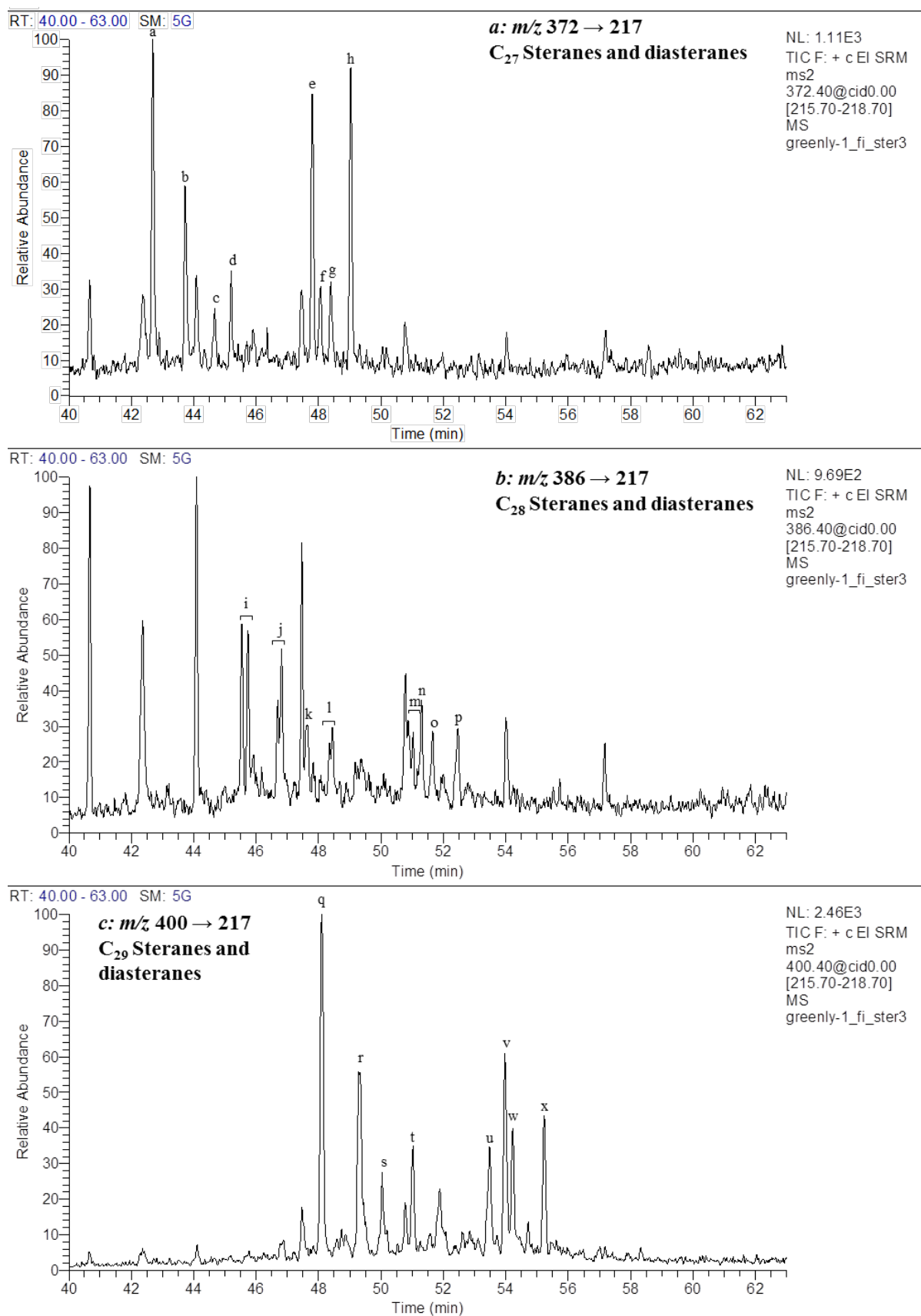


Figure A8-174: Partial MRM chromatograms (m/z 372.4, 386.4 and 400.4 \rightarrow 217.2) of the aliphatic hydrocarbons from the Greenly-1 (4806-4818 m) FI oil.

Showing the distribution of (a) C_{27} (b) C_{28} and (c) C_{29} steranes and diasteranes. Steranes and diasteranes abbreviations are listed in Table A5-38.

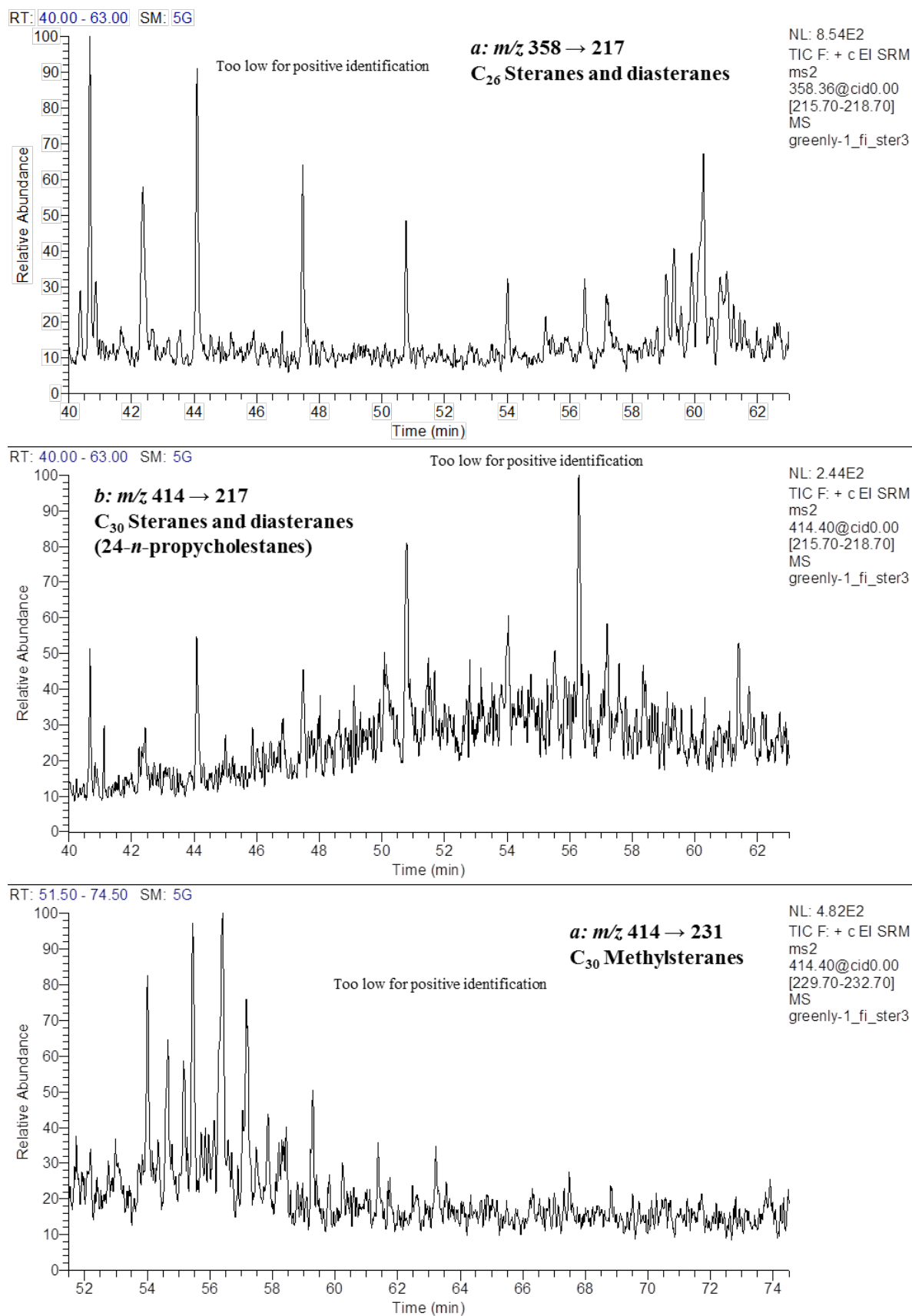
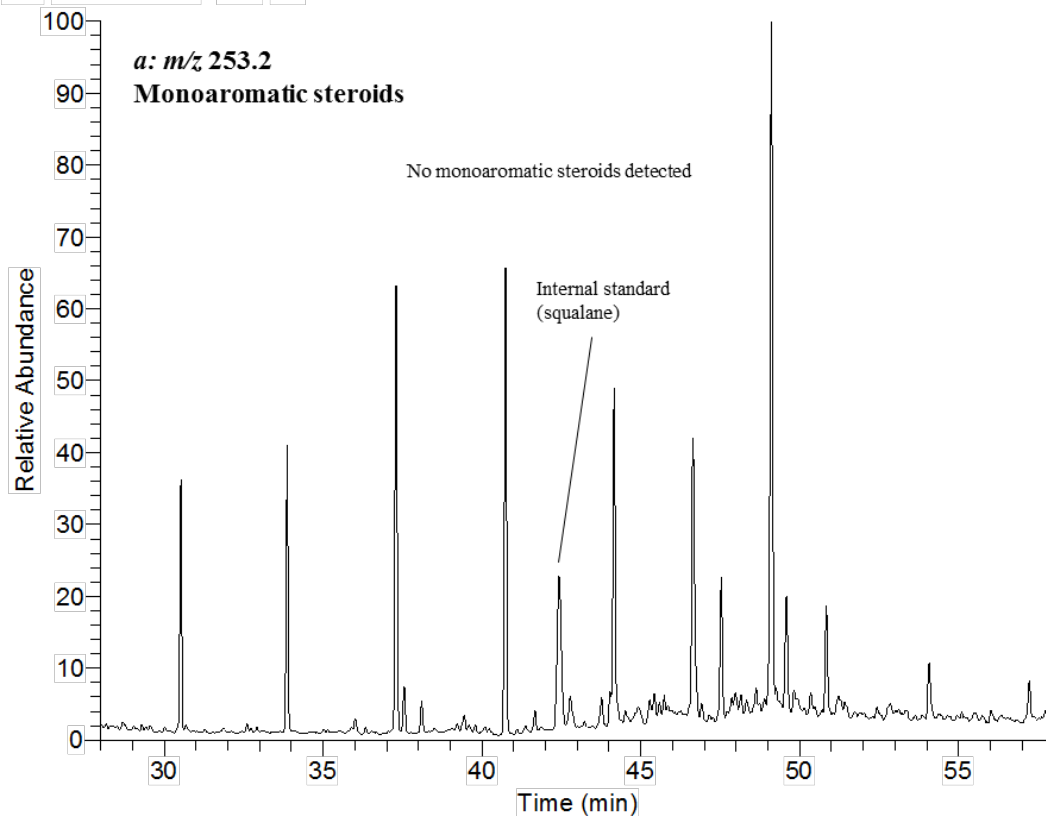


Figure A8-175: Partial MRM chromatograms (m/z 358.4 and 414.4 \rightarrow 217.2; 414.4 \rightarrow 231.2) of the aliphatic hydrocarbons from the Greenly-1 (4806-4818 m) FI oil.

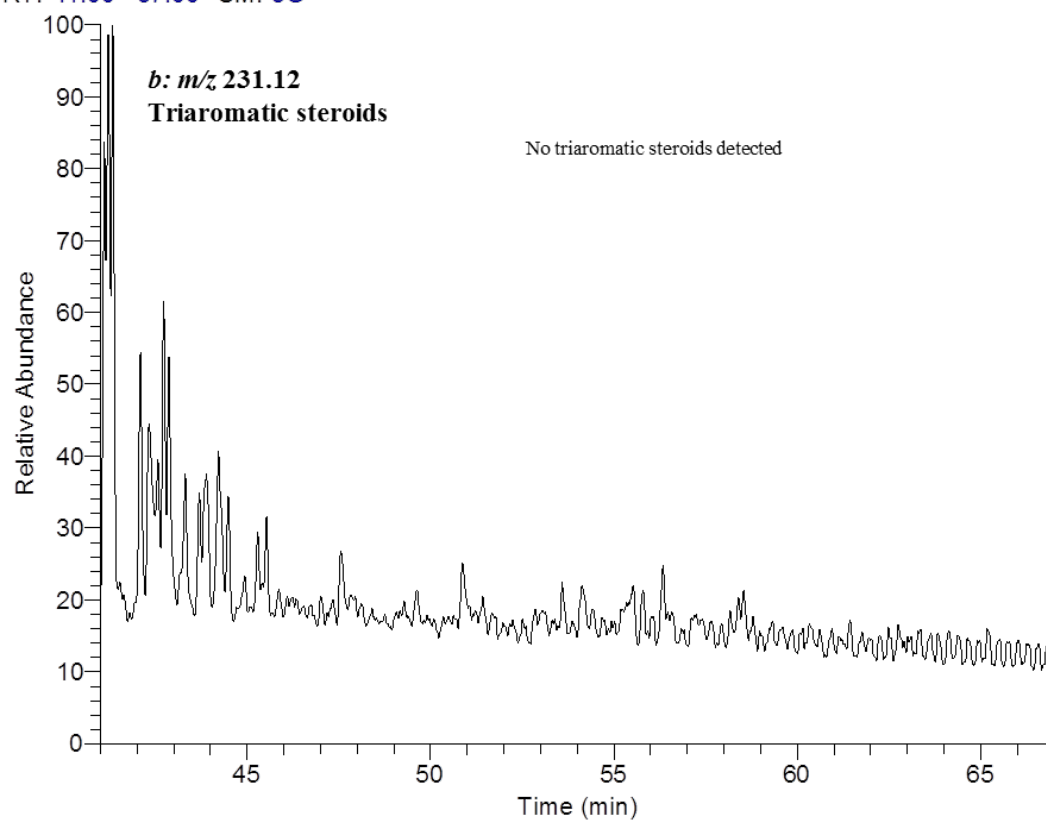
Showing the distribution of (a) C_{26} and (b) C_{30} steranes and diasteranes, and (c) C_{30} methylsteranes. Steranes, diasteranes and methylsteranes abbreviations are listed in Table A5-38.

RT: 28.00 - 58.00 SM: 5G



NL:
7.83E5
m/z=
252.70-
253.70 MS
greenly-
1_fi_d4

RT: 41.00 - 67.00 SM: 5G



NL:
3.53E5
m/z=
230.62-
231.62 MS
greenly-
1_fi_d4

Figure A8-176: Partial m/z (a) 253.2 and (b) 231.12 mass chromatograms for the Greenly-1 (4806-4818 m) FI oil. Showing the distribution of diasteranes and methylsteranes. Sterane and diasterane abbreviations are listed in Table A5-39, Table A5-40.

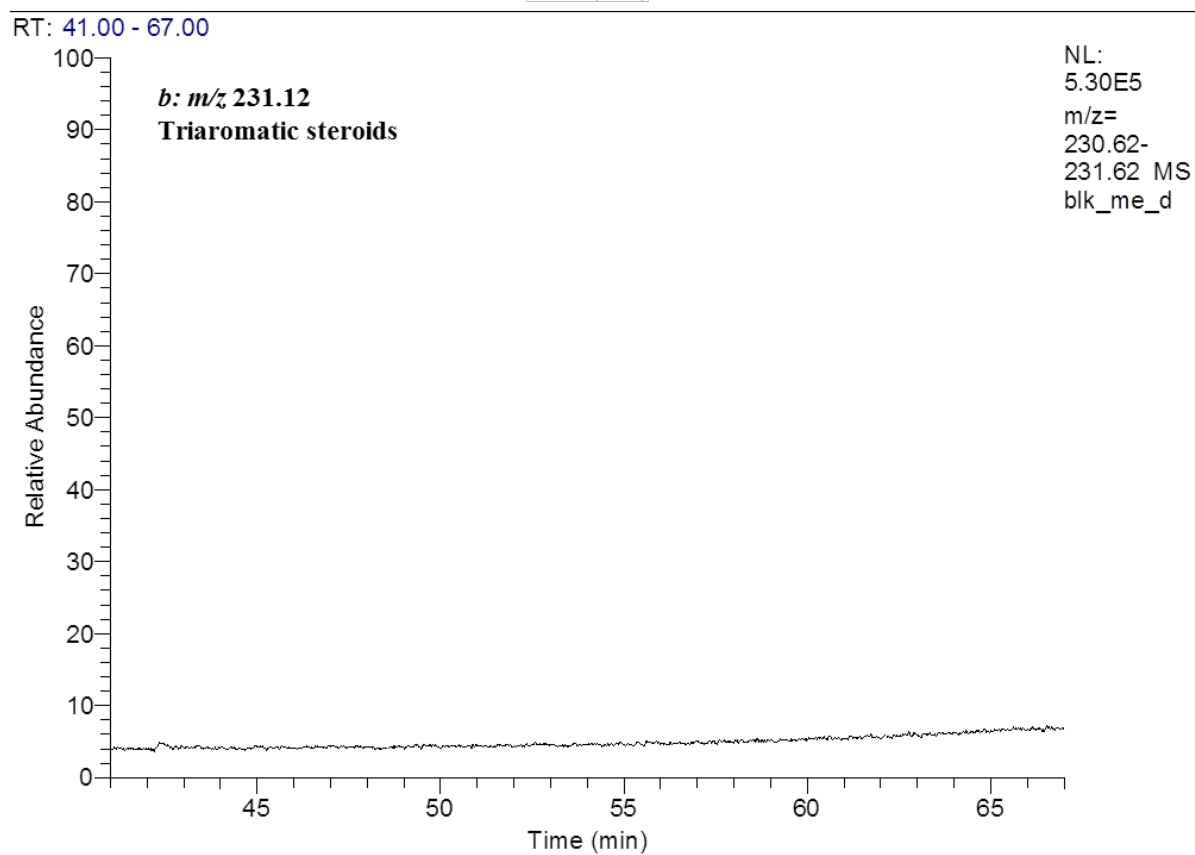
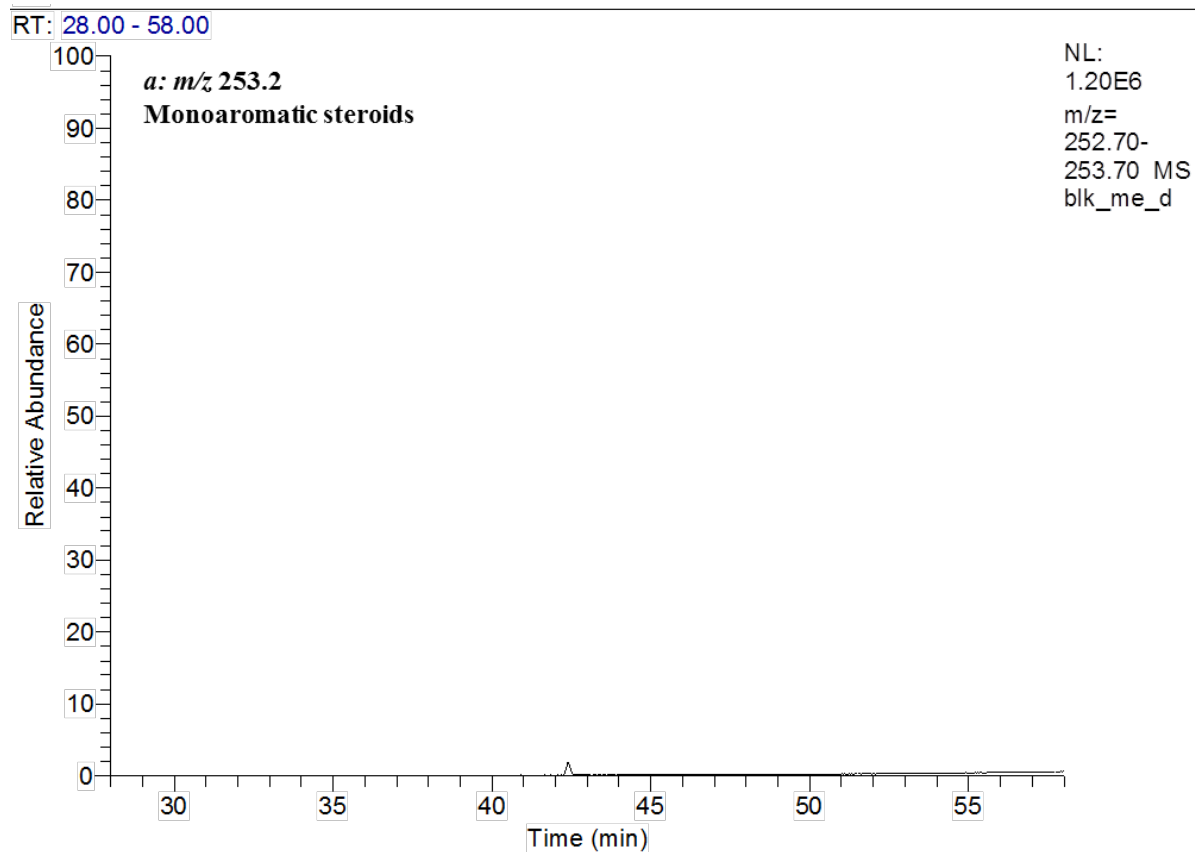


Figure A8-177: Partial m/z (a) 253.2 and (b) 231.12 mass chromatograms for the Greenly-1 (4806-4818 m) FI oil. Showing the distribution of diasteranes and methylsteranes. Sterane and diasterane abbreviations are listed in Table A5-39, Table A5-40.

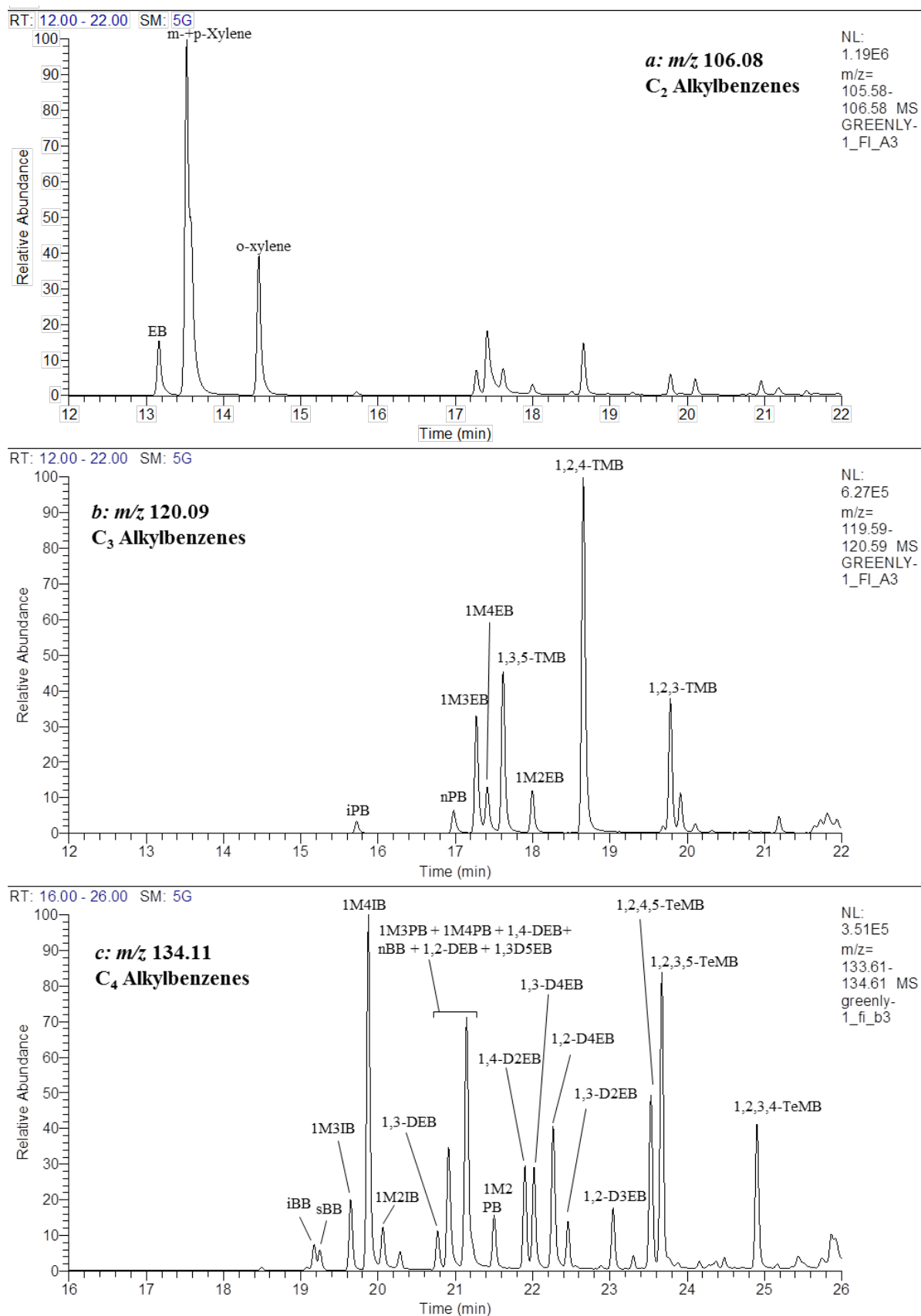


Figure A8-178: Partial m/z 106, 120 and 134 mass chromatograms for the Greenly-1 (4806-4818 m) FI oil. Showing the distribution of (a) C₂ alkylbenzenes, (b) C₃ alkylbenzenes and (c) C₄ alkylbenzenes respectively. Peak abbreviations are listed in Table A5-41.

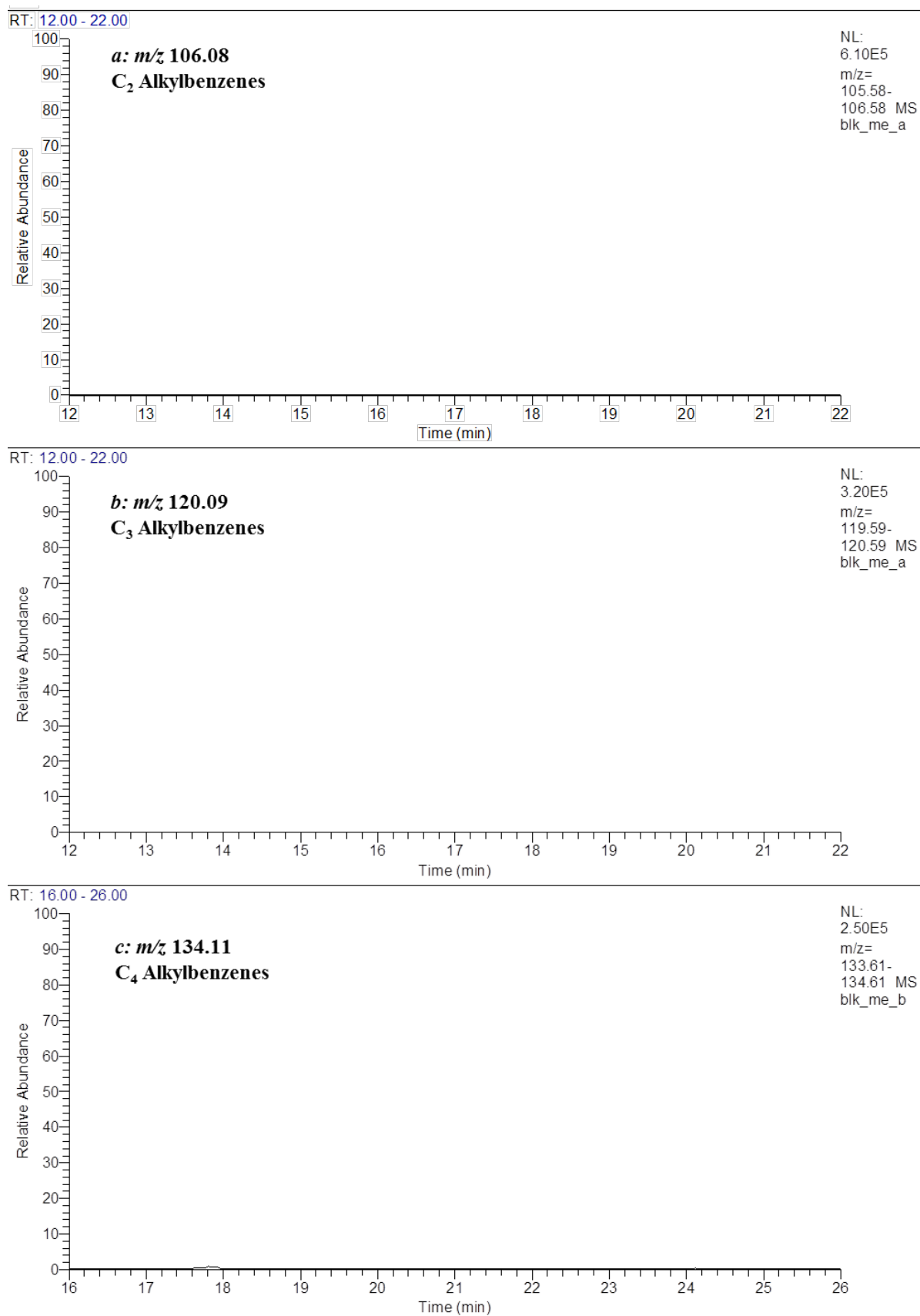


Figure A8-179: Partial m/z 106, 120 and 134 mass chromatograms for the Greenly-1 (4806-4818 m) FI system blank. Showing the distribution of (a) C₂ alkylbenzenes, (b) C₃ alkylbenzenes and (c) C₄ alkylbenzenes respectively. Peak abbreviations are listed in Table A5-41.

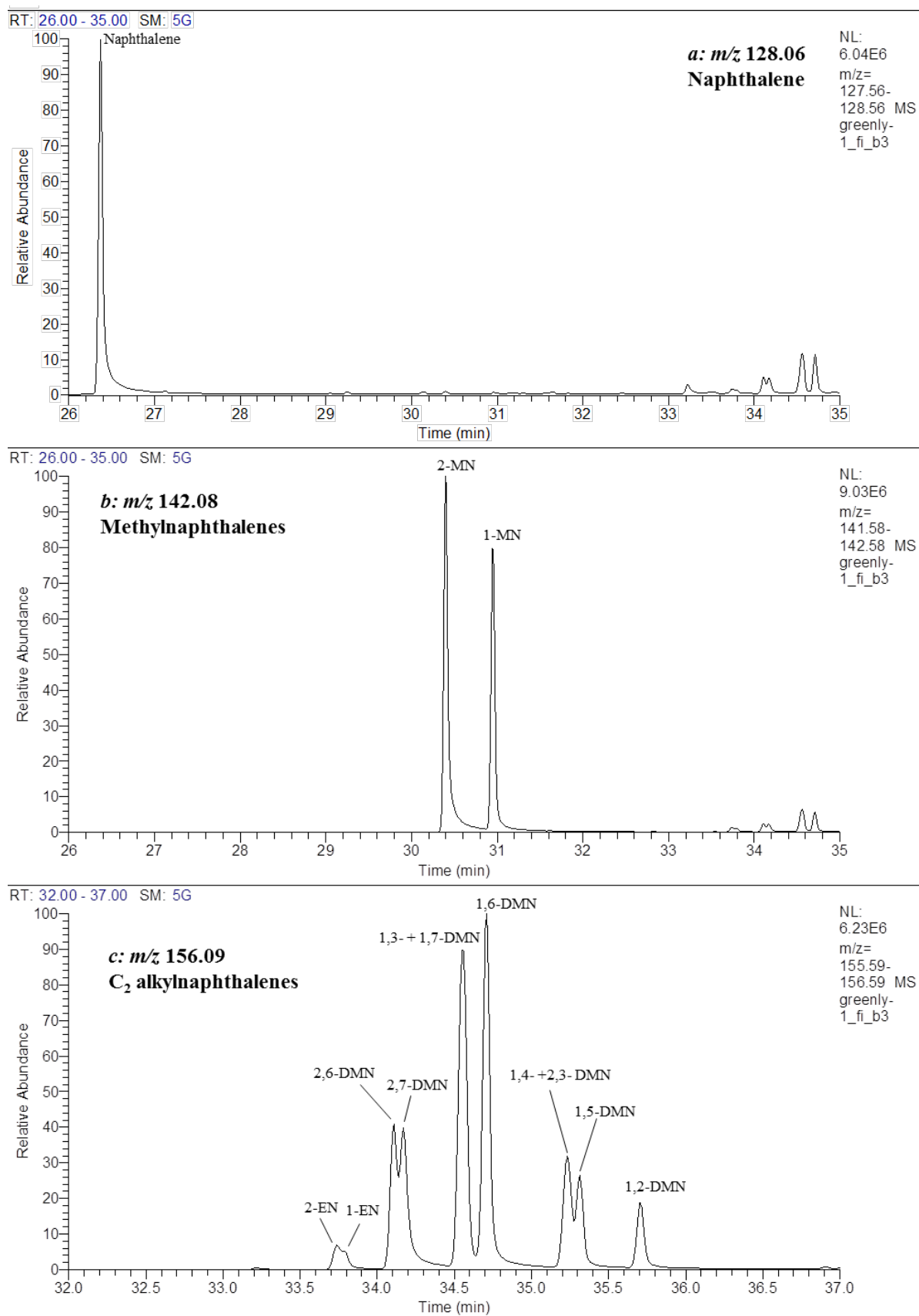


Figure A8-180: Partial m/z 128, 142 and 156 mass chromatograms for the Greenly-1 (4806-4818 m) FI oil. Showing the distribution of (a) naphthalene, (b) methylnaphthalenes and (c) ethylnaphthalenes and dimethylnaphthalenes respectively. Peak abbreviations are listed in Table A5-41.

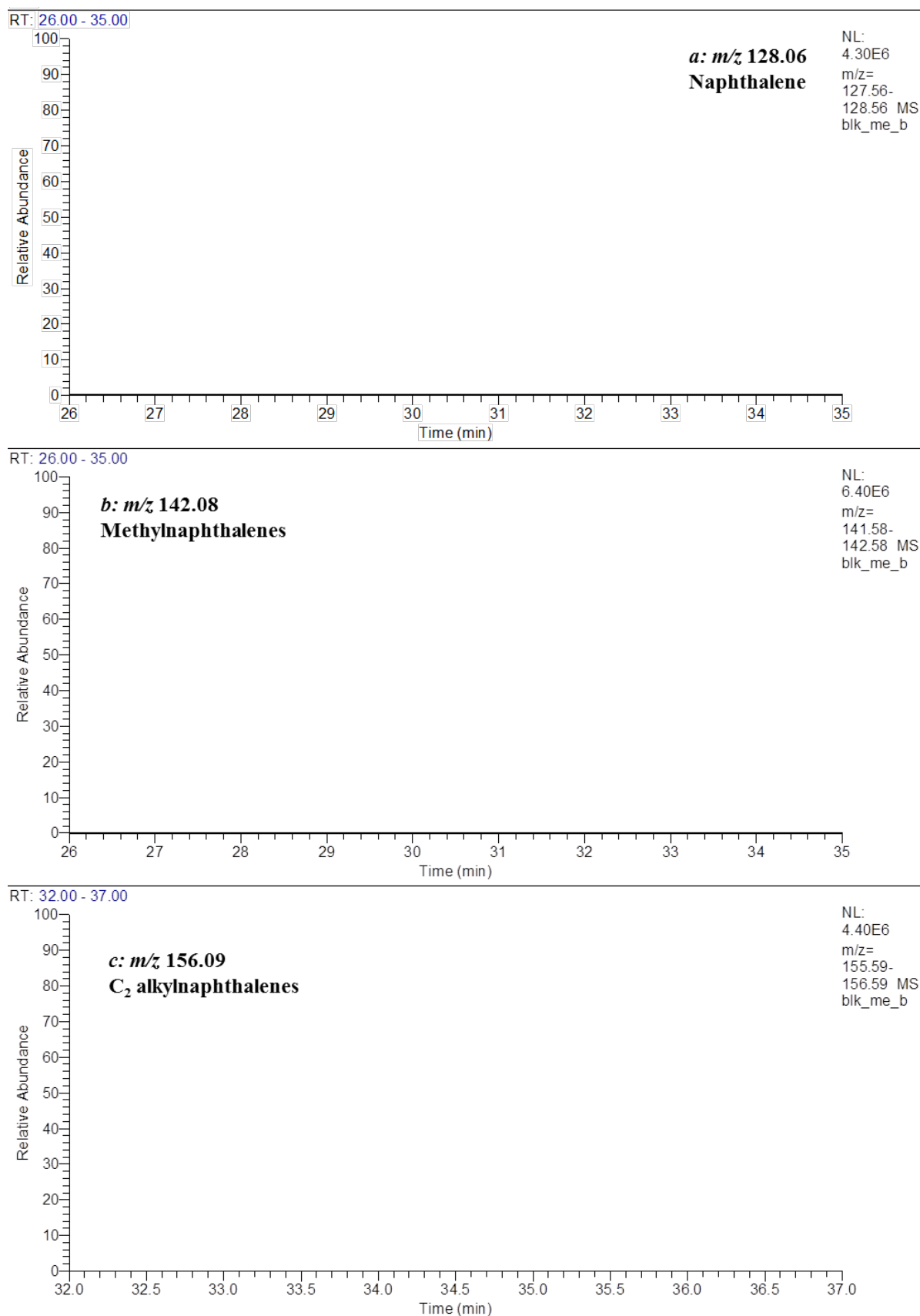


Figure A8-181: Partial m/z 128, 142 and 156 mass chromatograms for the Greenly-1 (4806-4818 m) FI system blank. Showing the distribution of (a) naphthalene, (b) methylnaphthalenes and (c) ethylnaphthalenes and dimethylnaphthalenes respectively. Peak abbreviations are listed in Table A5-41.

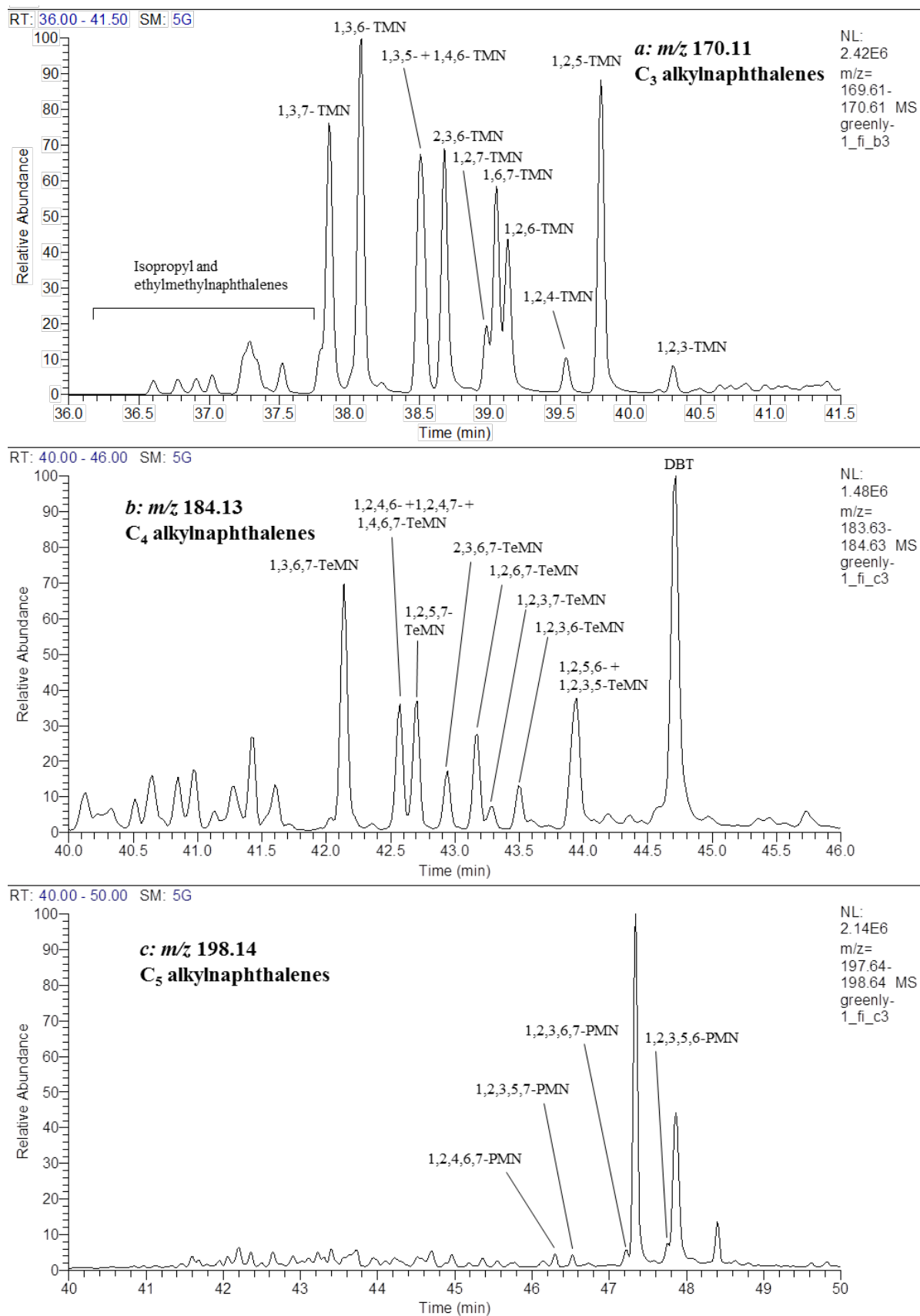


Figure A8-182: Partial m/z 170, 184 and 198 mass chromatograms for the Greenly-1 (4806-4818 m) FI oil. Showing the distribution of (a) trimethylnaphthalenes, (b) tetramethylnaphthalenes and (c) pentamethylnaphthalenes respectively. Peak abbreviations are listed in Table A5-41.

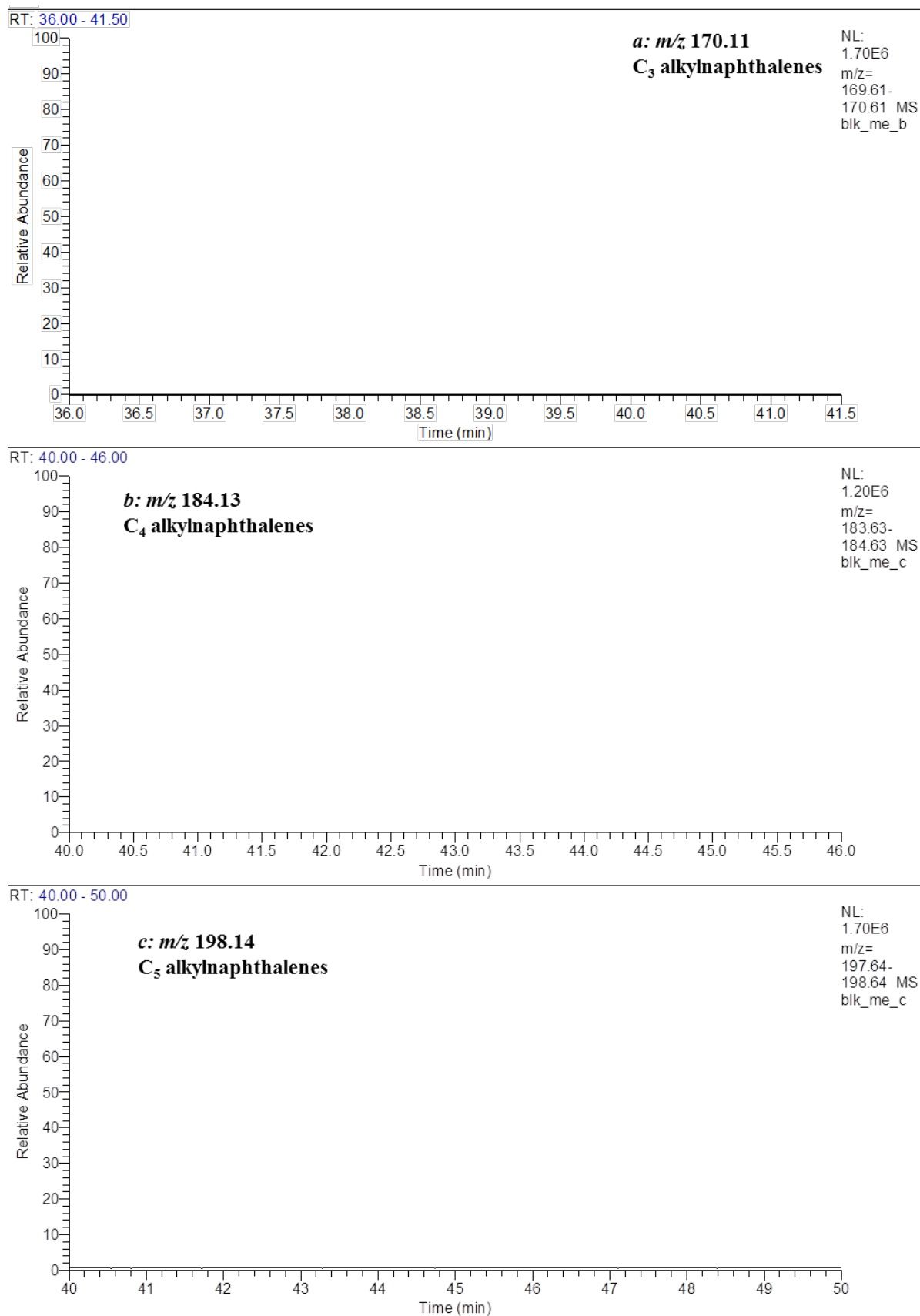


Figure A8-183: Partial m/z 170, 184 and 198 mass chromatograms for the Greenly-1 (4806-4818 m) FI system blank. Showing the distribution of (a) trimethylnaphthalenes, (b) tetramethylnaphthalenes and (c) pentamethylnaphthalenes respectively. Peak abbreviations are listed in Table A5-41.

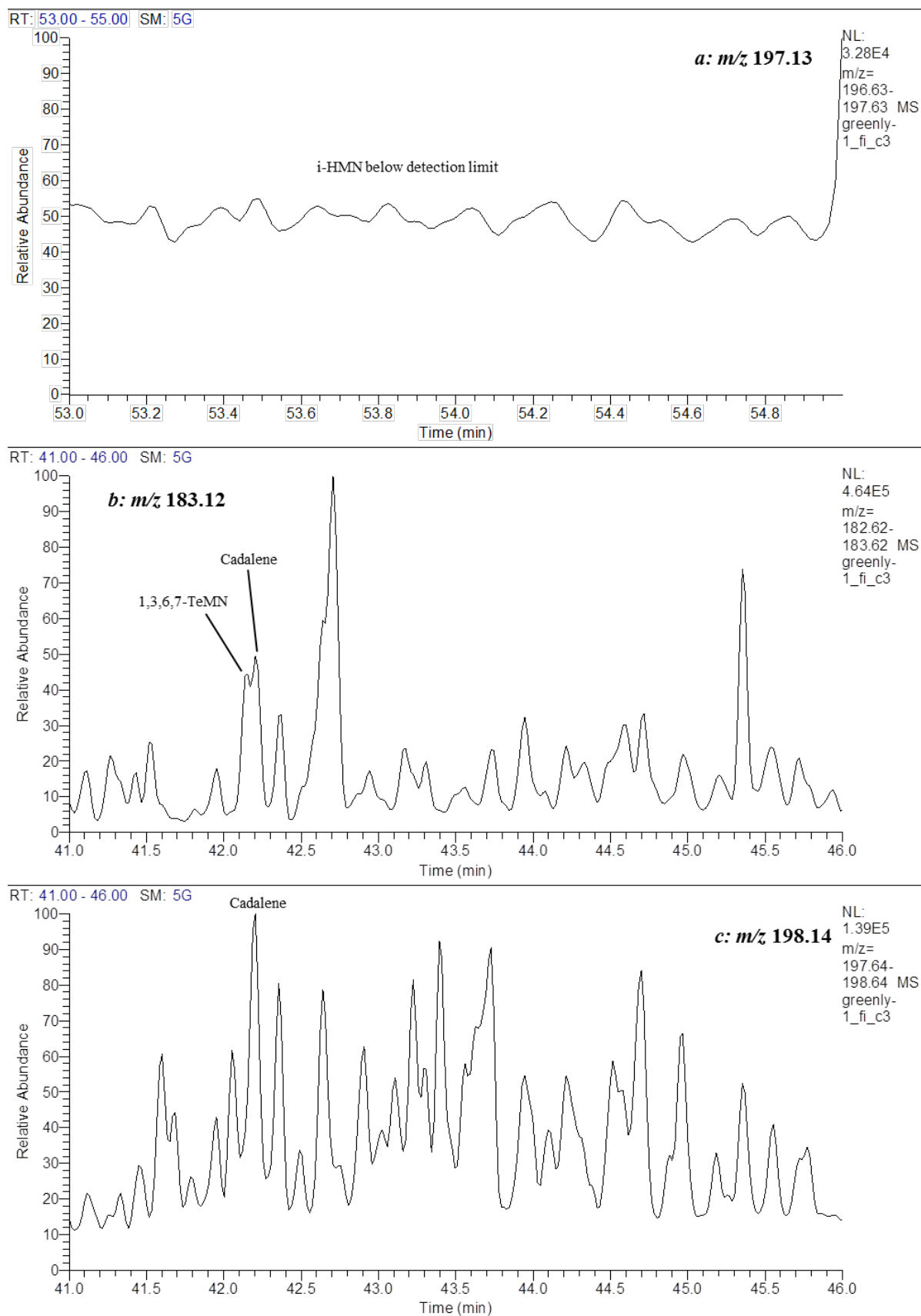


Figure A8-184: Partial m/z 197, 183 and 198 mass chromatograms for the Greenly-1 (4806-4818 m) FI oil. Showing the distribution of (a) iso-hexylmethylnaphthalene, and (b) and (c) cadalene. Peak abbreviations are listed in Table A5-41.

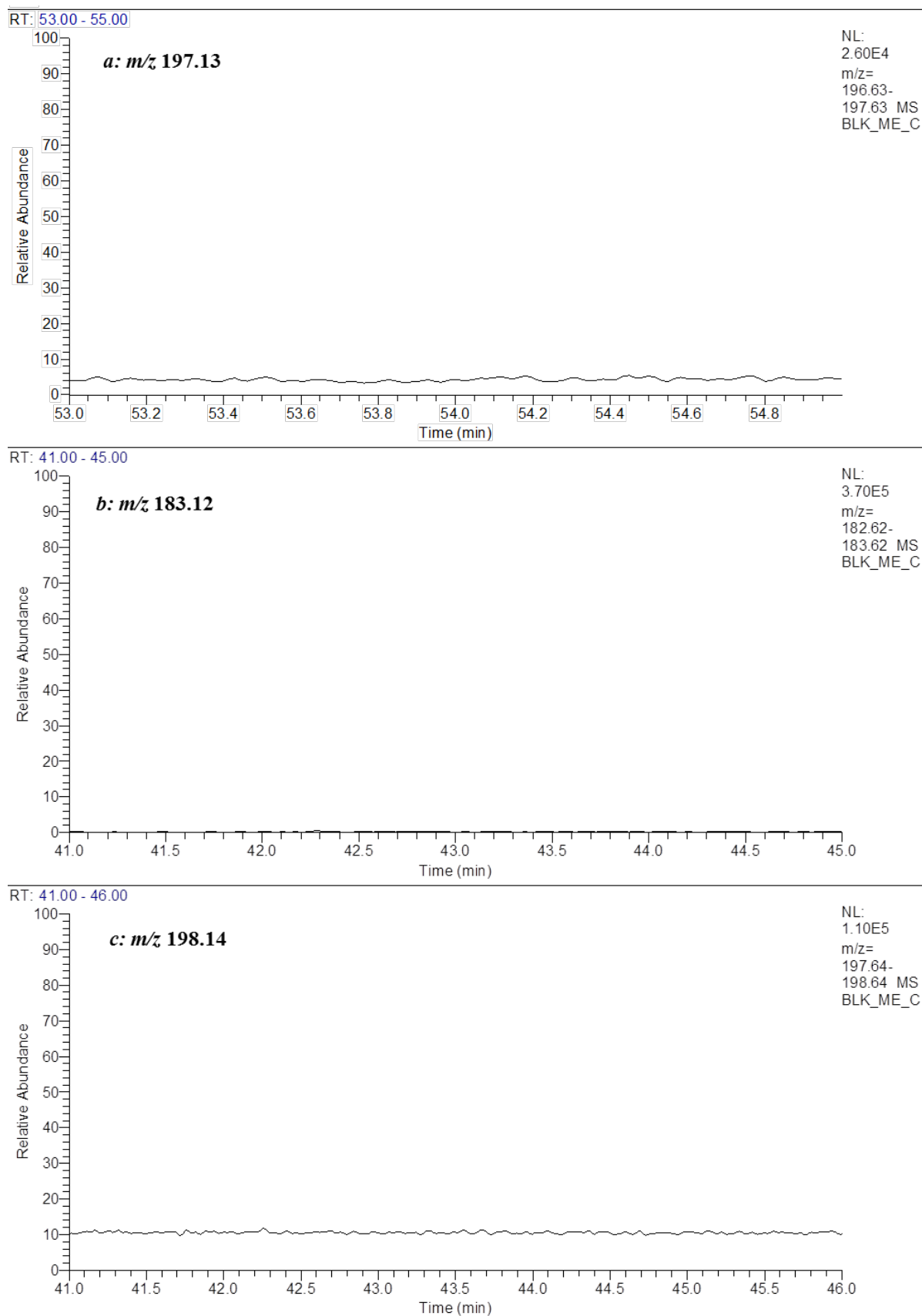


Figure A8-185: Partial m/z 197, 183 and 198 mass chromatograms for the Greenly-1 (4806-4818 m) FI system blank. Showing the distribution of (a) iso-hexylmethyl-naphthalene, and (b) and (c) cadalene. Peak abbreviations are listed in Table A5-41.

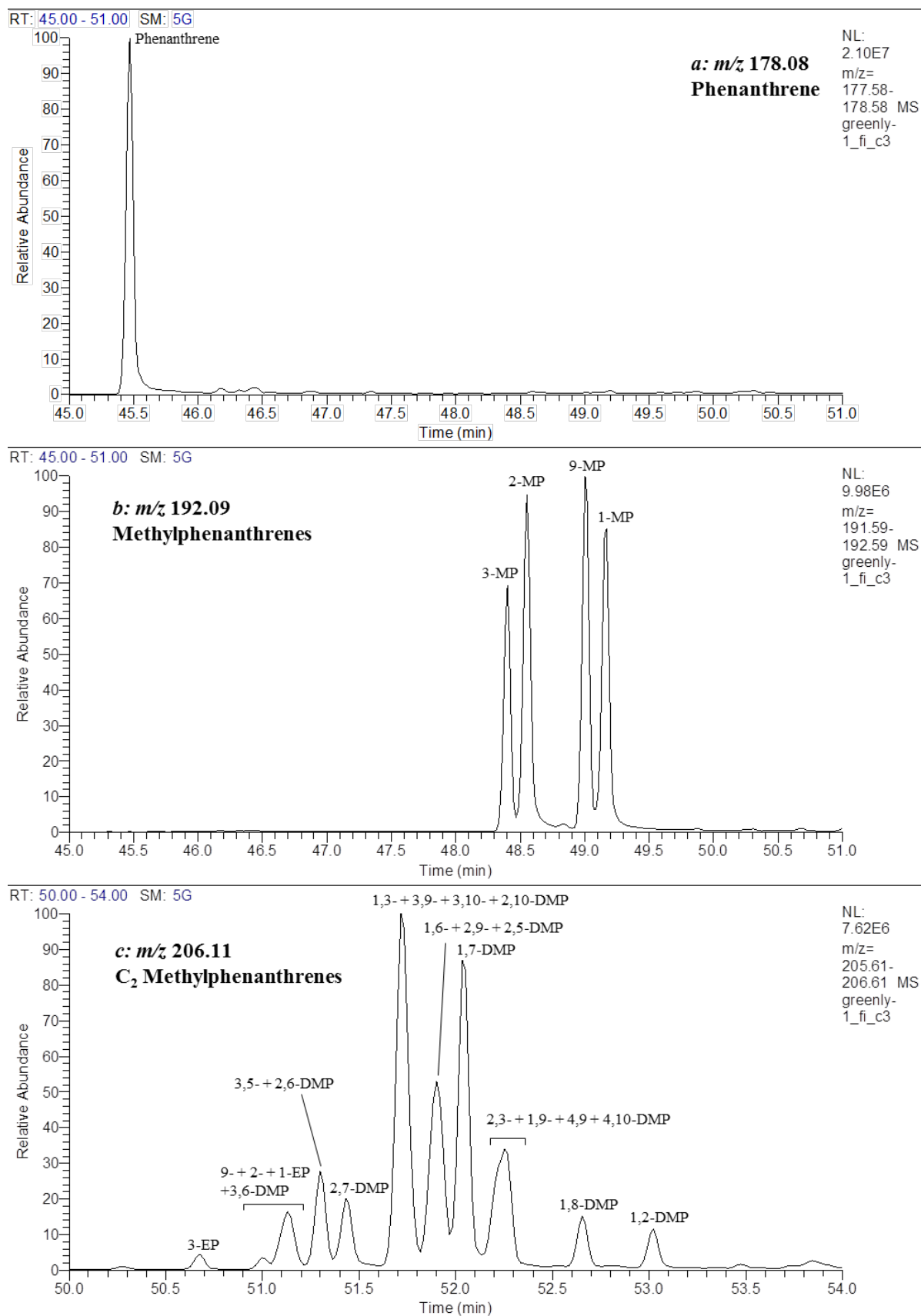


Figure A8-186: Partial m/z 178, 192 and 206 mass chromatograms for the Greenly-1 (4806-4818 m) FI oil. Showing the distribution of (a) phenanthrene, (b) methylphenanthrenes and (c) ethylphenanthrenes and dimethylphenanthrenes respectively. Peak abbreviations are listed in Table A5-41.

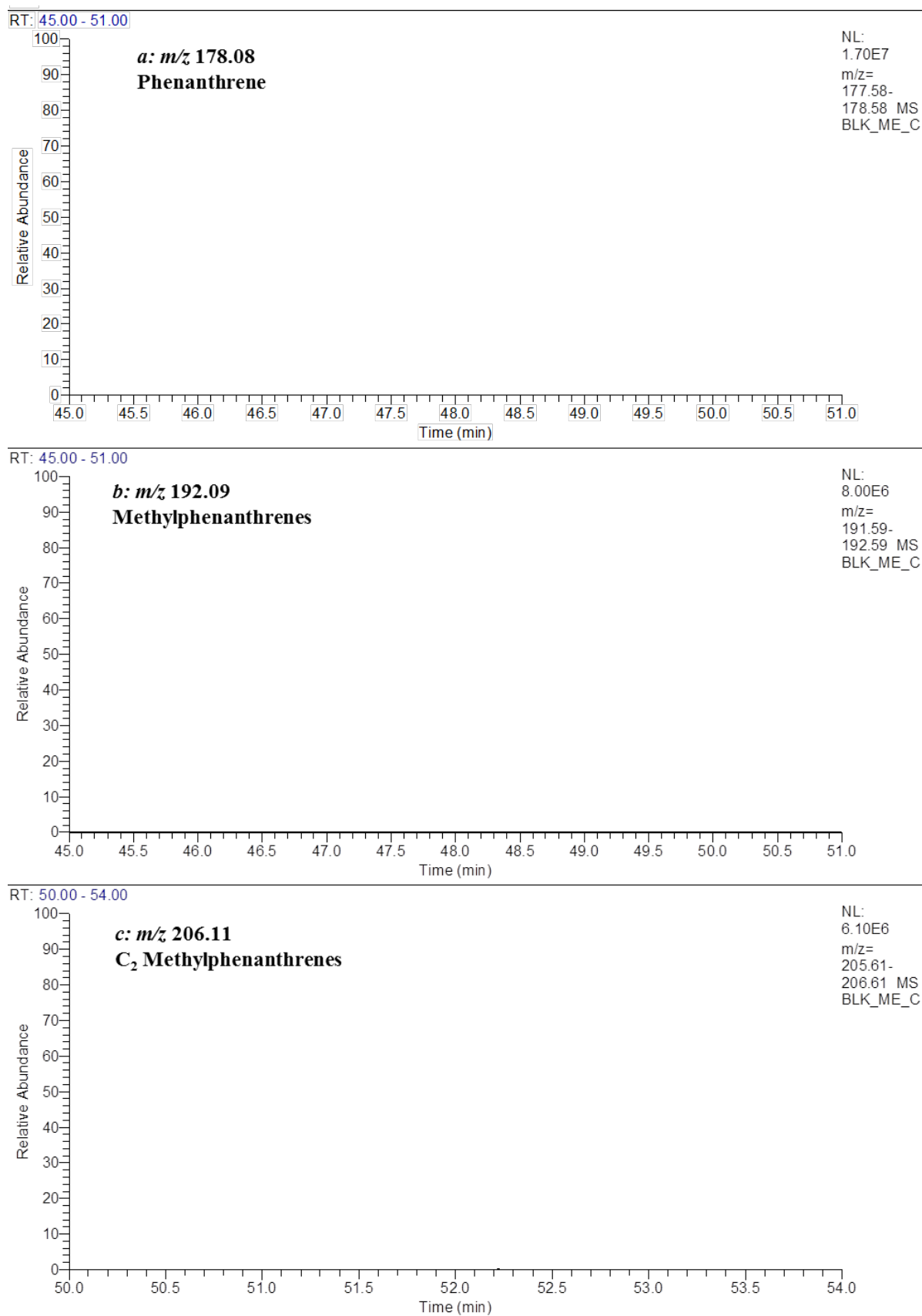


Figure A8-187: Partial m/z 178, 192 and 206 mass chromatograms for the Greenly-1 (4806-4818 m) FI system blank. Showing the distribution of (a) phenanthrene, (b) methylphenanthrenes and (c) ethylphenanthrenes and dimethylphenanthrenes respectively. Peak abbreviations are listed in Table A5-41.

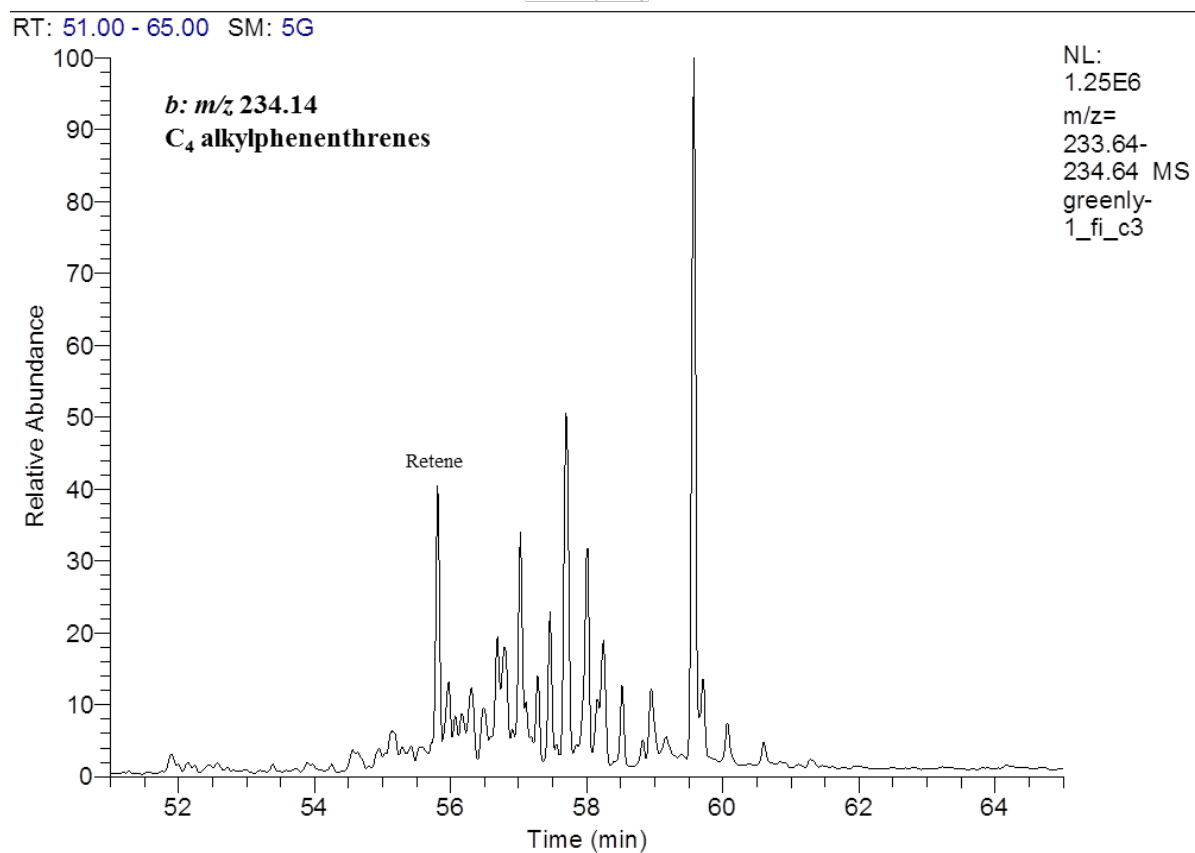
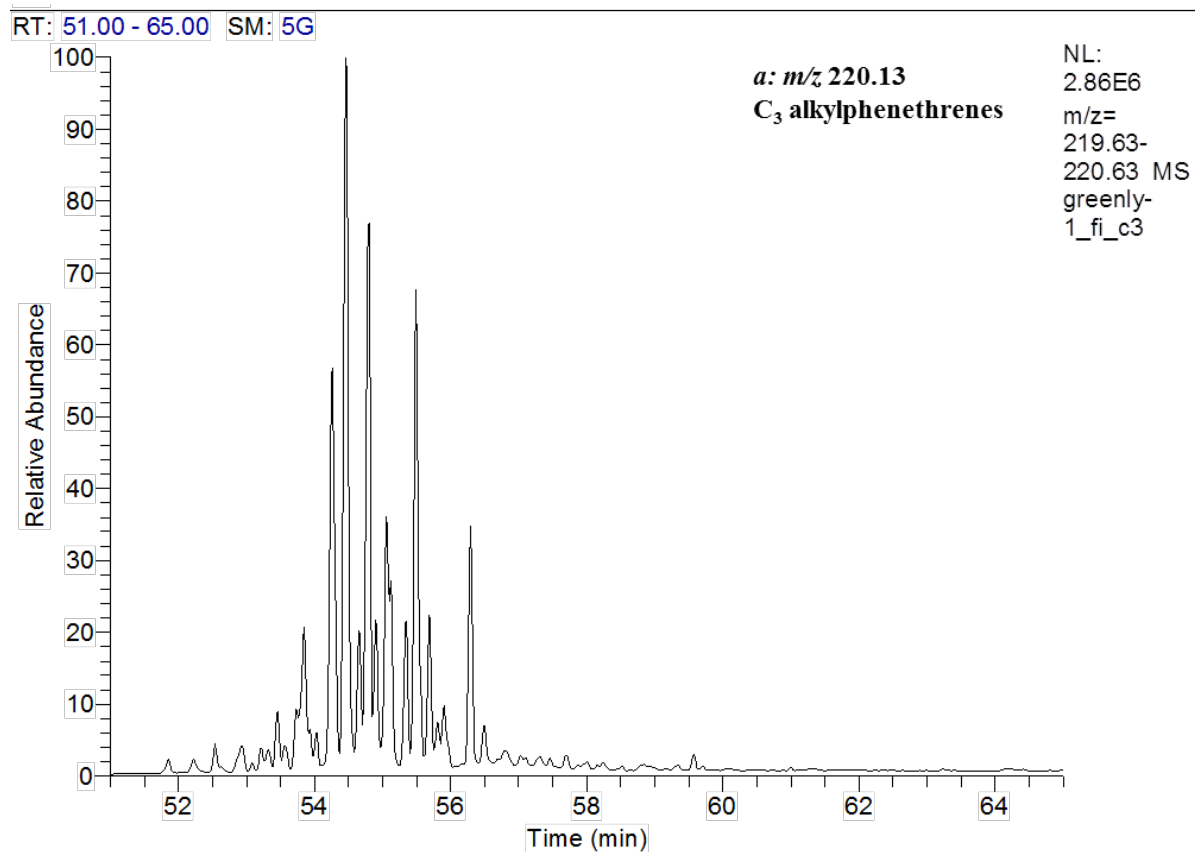


Figure A8-188: Partial m/z 220 and 234 mass chromatograms for the Greenly-1 (4806-4818 m) FI oil. Showing the distribution of (a) trimethylphenanthrenes and (b) retene and tetramethylphenanthrenes. Peak abbreviations are listed in Table A5-41.

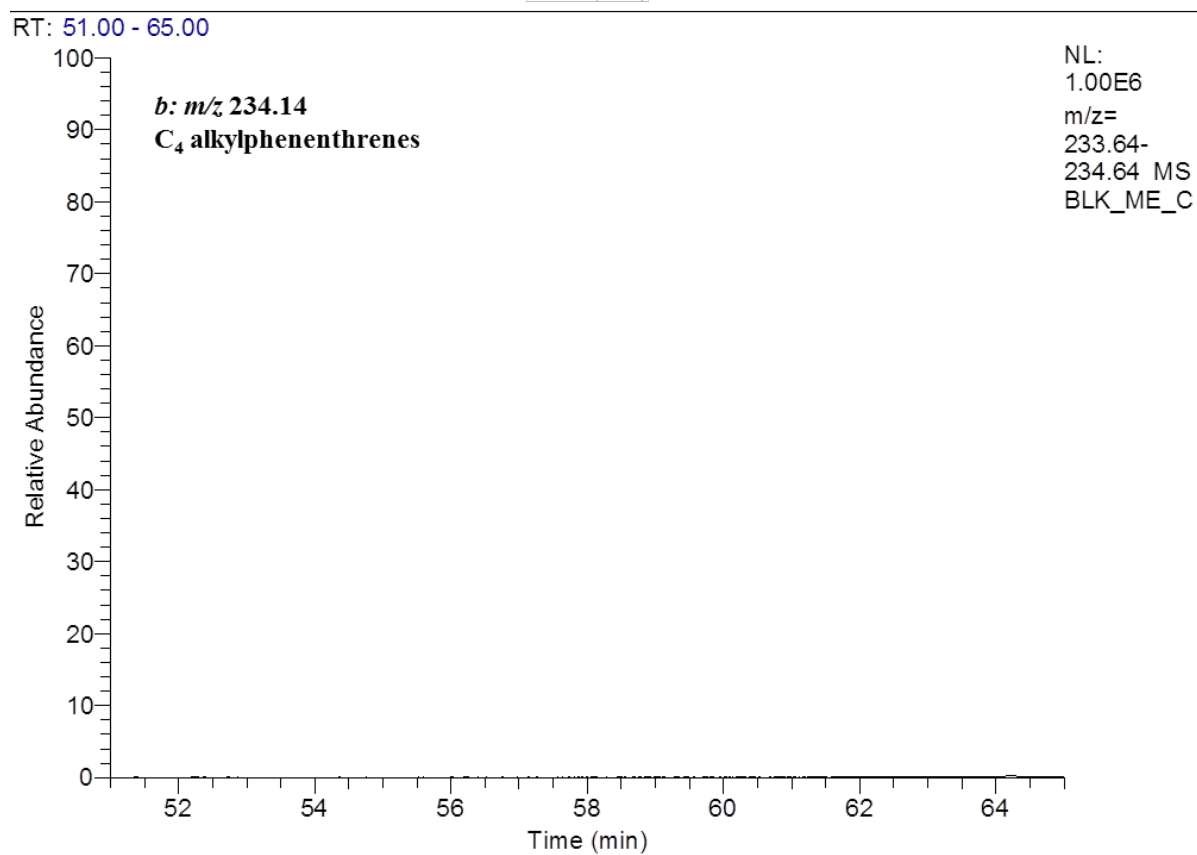
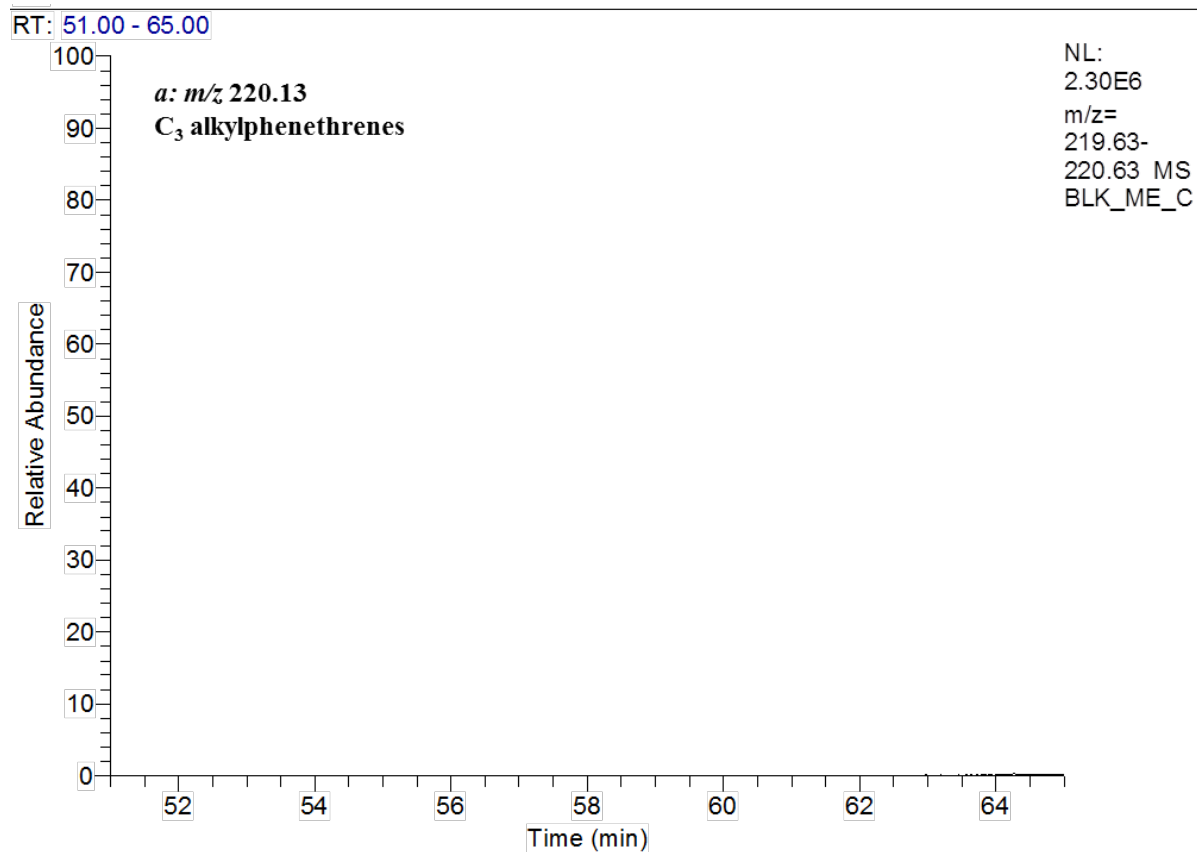


Figure A8-189: Partial m/z 220 and 234 mass chromatograms for the Greenly-1 (4806-4818 m) FI system blank. Showing the distribution of (a) trimethylphenanthrenes and (b) retene and tetramethylphenanthrenes. Peak abbreviations are listed in Table A5-41.

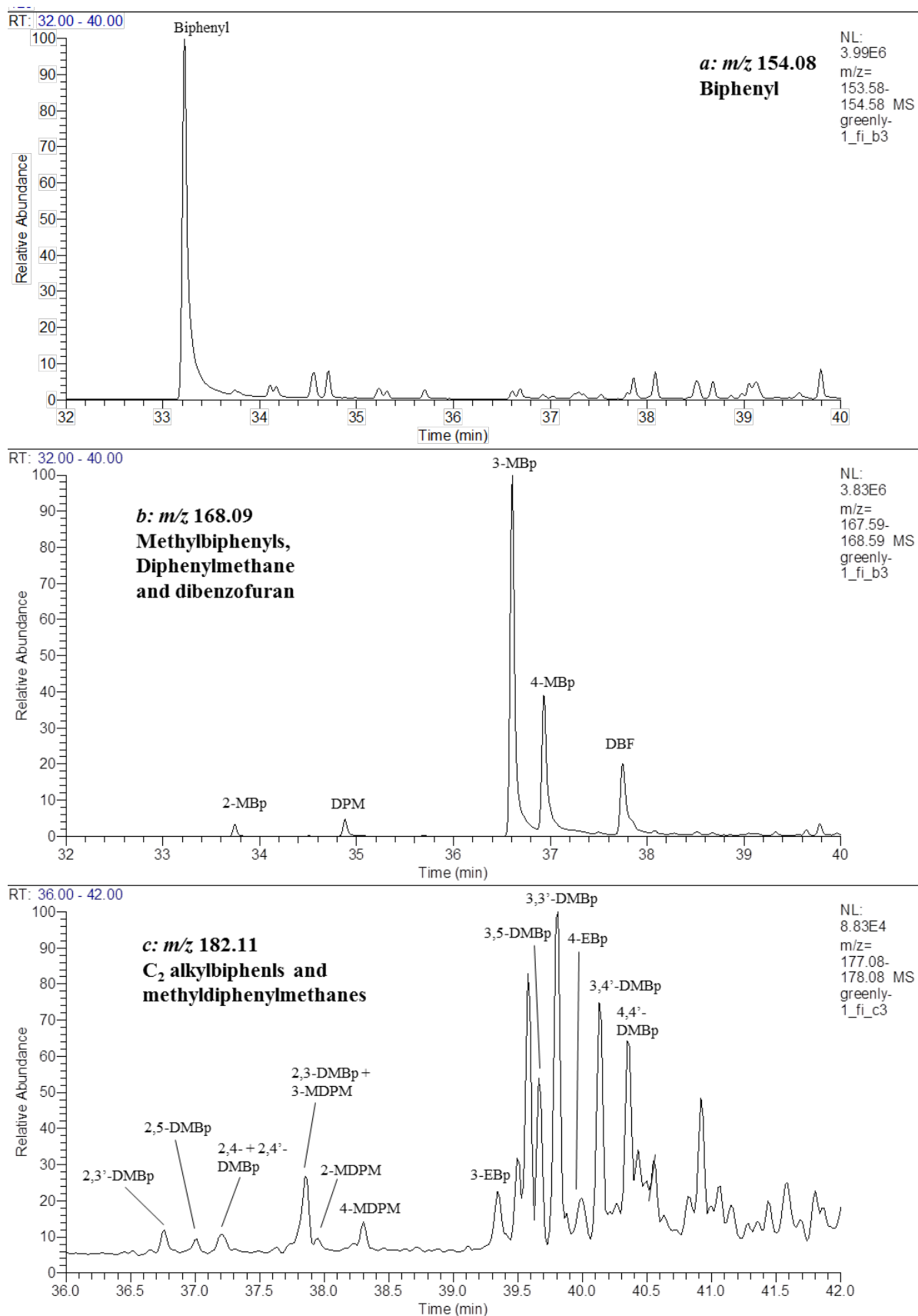


Figure A8-190: Partial m/z 154, 168 and 182 mass chromatograms for the Greenly-1 (4806-4818 m) FI oil. Showing the distribution of (a) biphenyl, (b) methylbiphenyls, diphenylmethane and dibenzofuran, and (c) dimethylbiphenyls, ethylbiphenyls and methyldiphenylmethanes, respectively. Peak abbreviations are listed in Table A5-41.

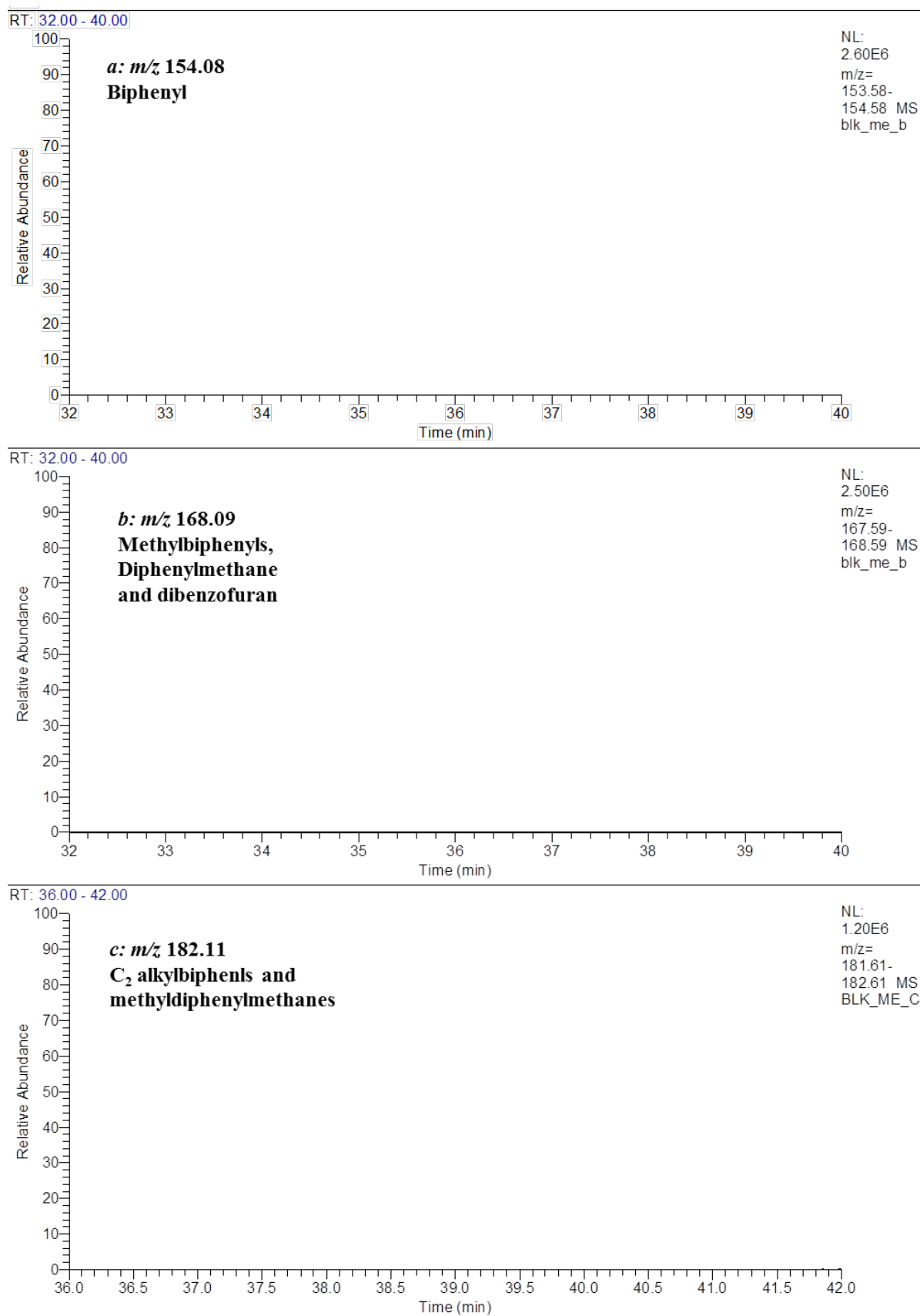


Figure A8-191: Partial m/z 154, 168 and 182 mass chromatograms for the Greenly-1 (4806-4818 m) FI system blank. Showing the distribution of (a) biphenyl, (b) methylbiphenyls, diphenylmethane and dibenzofuran, and (c) dimethylbiphenyls, ethylbiphenyls and methyldiphenylmethanes, respectively. Peak abbreviations are listed in Table A5-41.

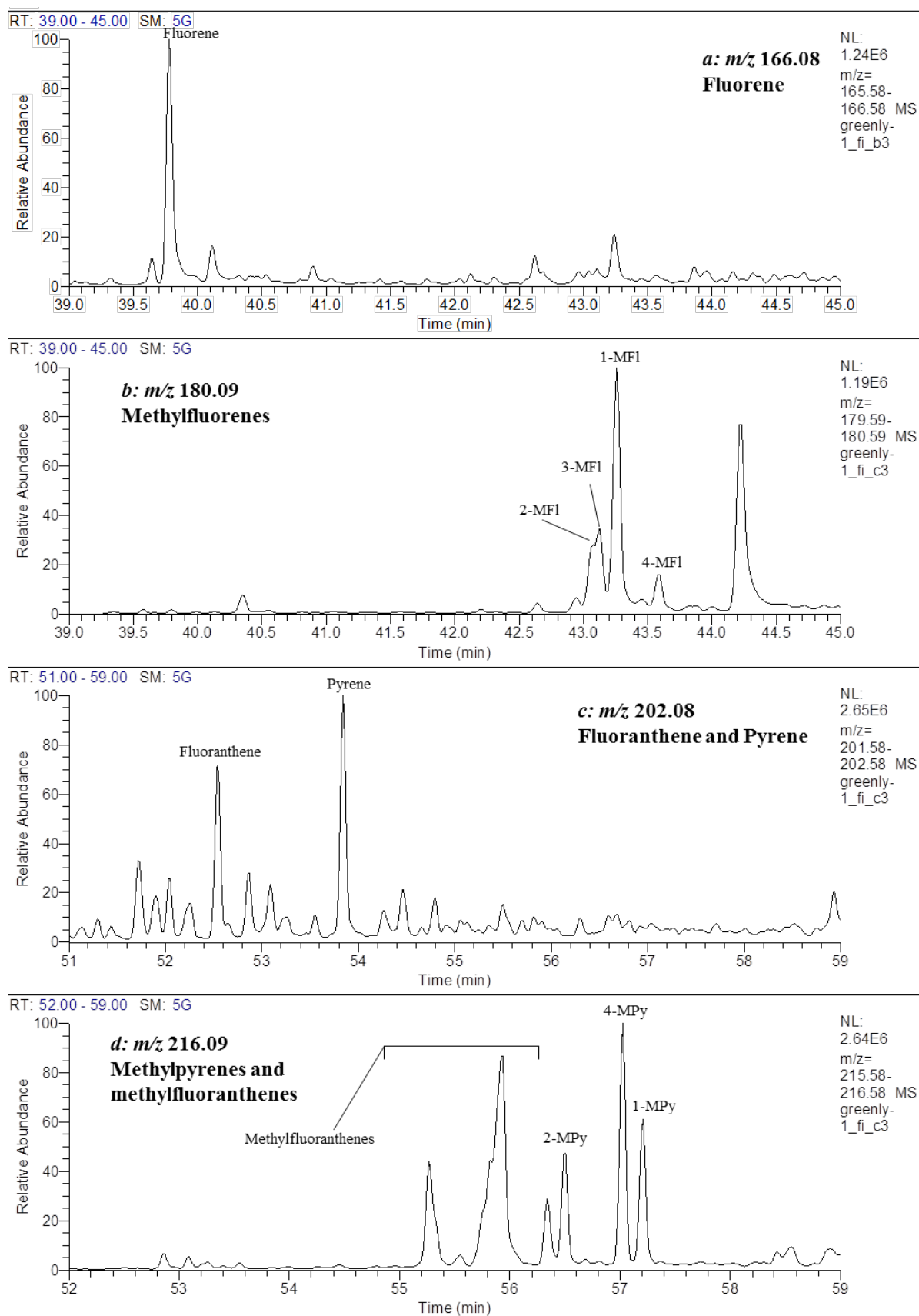


Figure A8-192: Partial m/z 166, 180, 202 and 216 mass chromatograms for the Greenly-1 (4806-4818 m) FI oil. Showing the distribution of (a) fluorene, (b) methylfluorenes, (c) fluoranthene and pyrene, and (d) methylfluoranthenes and methylpyrenes respectively. Peak abbreviations are listed in Table A5-41.

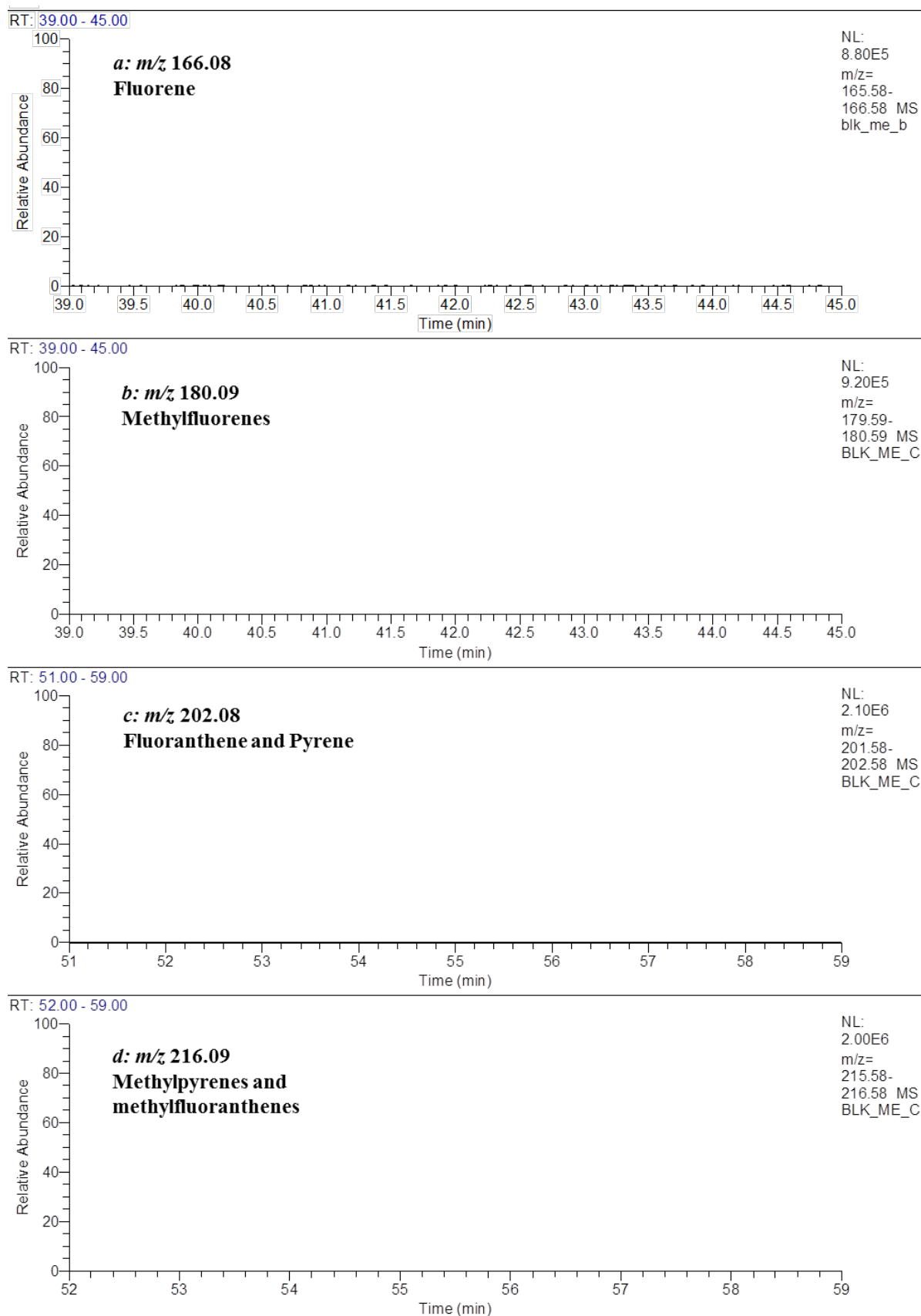


Figure A8-193: Partial m/z 166, 180, 202 and 216 mass chromatograms for the Greenly-1 (4806-4818 m) FI system blank. Showing the distribution of (a) fluorene, (b) methylfluorenes, (c) fluoranthene and pyrene, and (d) methylfluoranthenes and methylpyrenes respectively. Peak abbreviations are listed in Table A5-41.

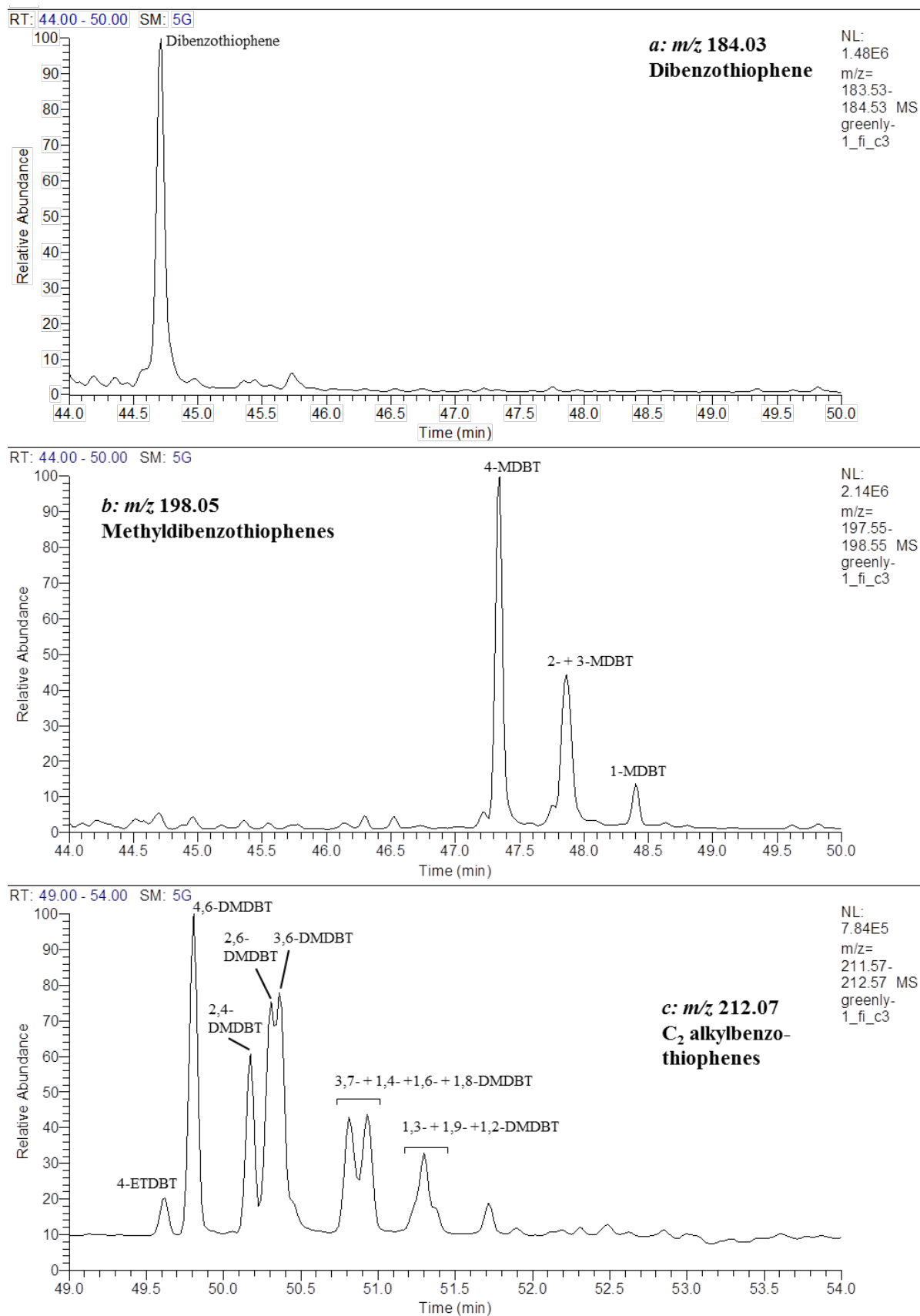


Figure A8-194: Partial m/z 184, 198 and 212 mass chromatograms for the Greenly-1 (4806-4818 m) FI oil. Showing the distribution of (a) dibenzothiophene, (b) methyldibenzothiophenes and (c) dimethyldibenzothiophenes and ethyldibenzothiophenes respectively. Peak abbreviations are listed in Table A5-41.

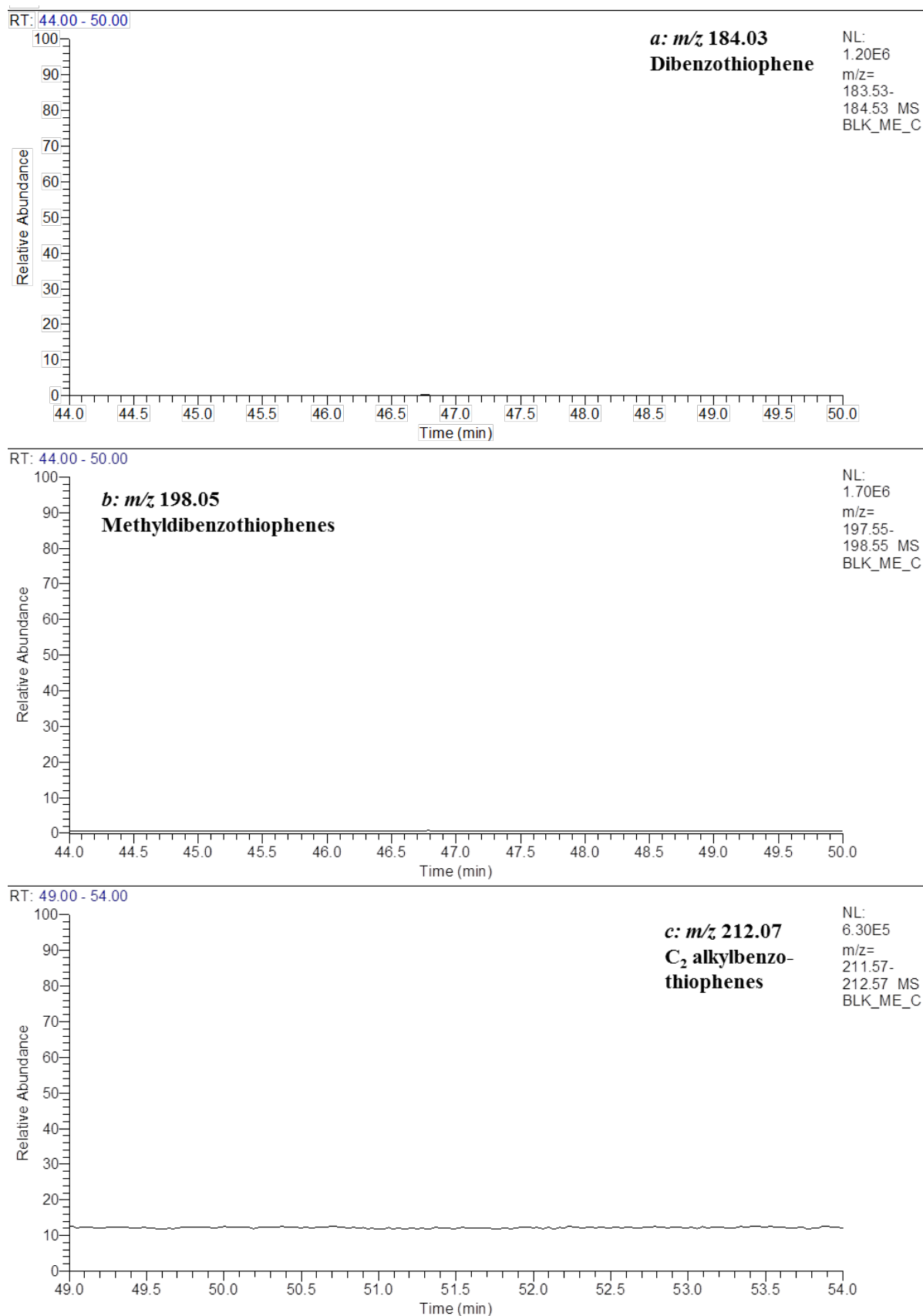


Figure A8-195: Partial m/z 184, 198 and 212 mass chromatograms for the Greenly-1 (4806-4818 m) FI system blank. Showing the distribution of (a) dibenzothiophene, (b) methyldibenzothiophenes and (c) dimethyldibenzothiophenes and ethyldibenzothiophenes respectively. Peak abbreviations are listed in Table A5-41.

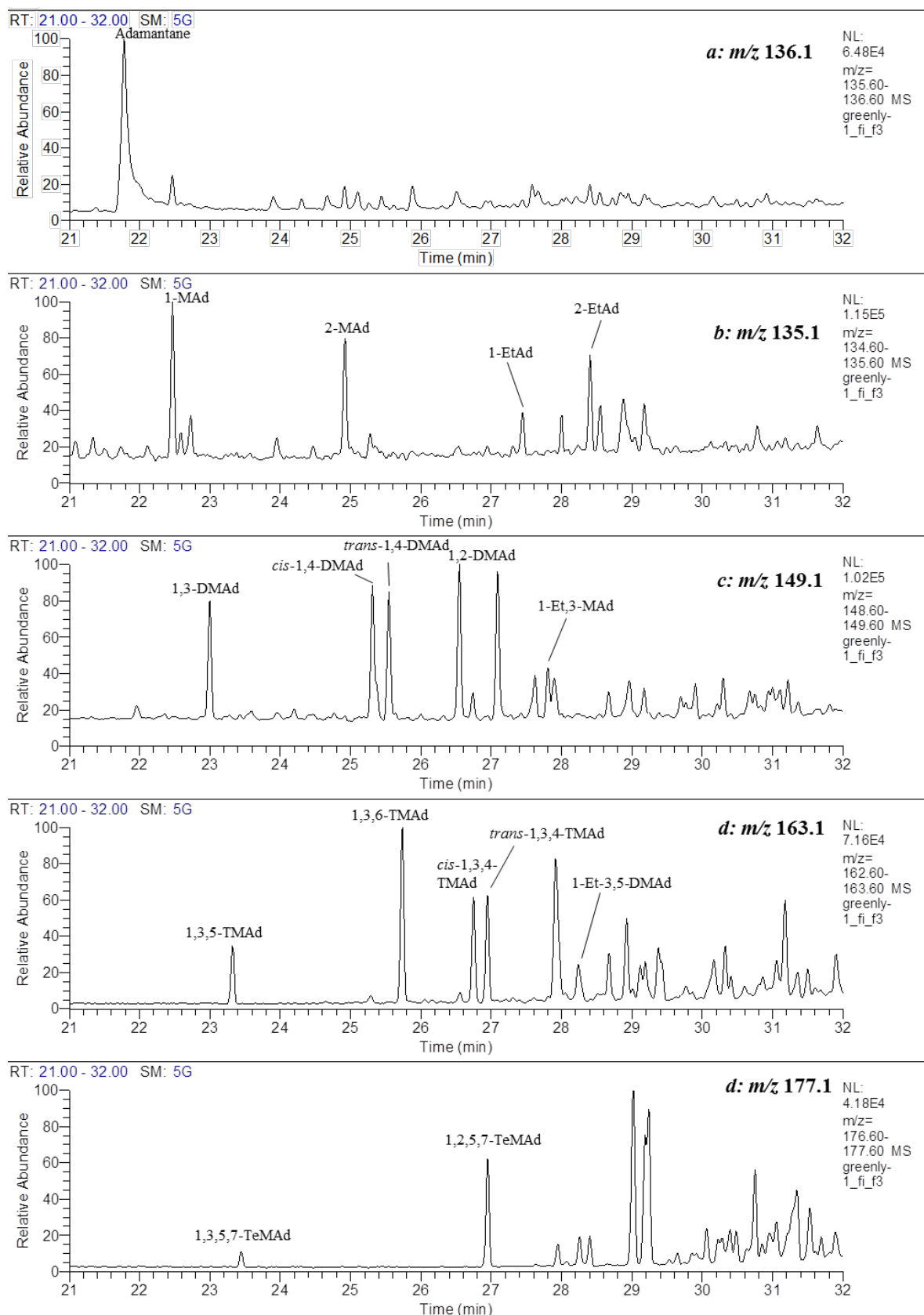


Figure A8-196: Partial m/z 136.1, 135.1, 149.1, 163.1 and 177.1 mass chromatograms for the Greenly-1 (4806-4818 m) FI oil. Showing the distribution of (a) adamantane, (b) methyladamantanes and ethyladamantanes, (c) dimethyladamantanes and ethylmethyladamantanes, (d) trimethyladamantanes and (e) tetramethyladamantanes. Peak abbreviations are listed in Table A5-B6.

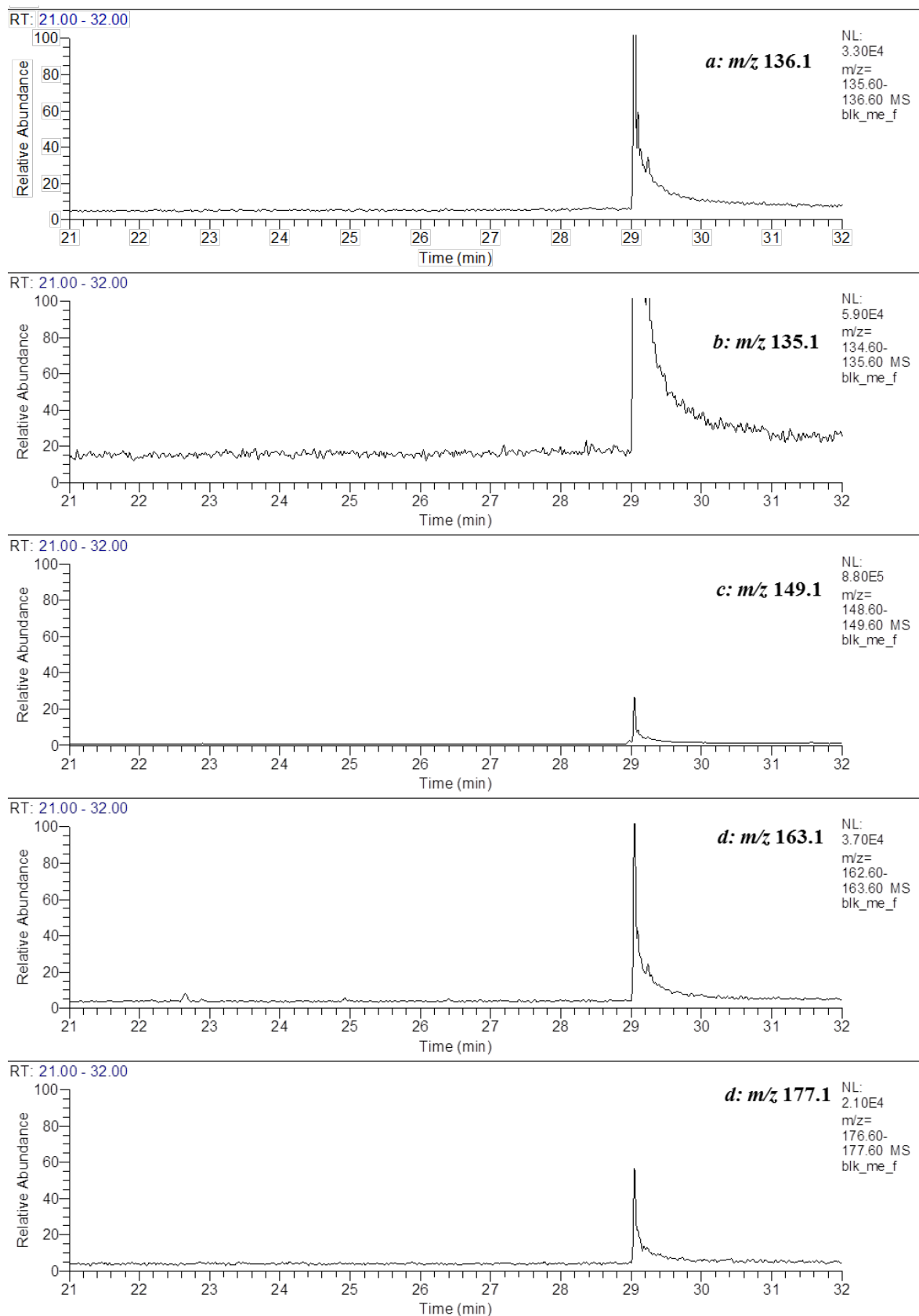


Figure A8-197: Partial m/z 136.1, 135.1, 149.1, 163.1 and 177.1 mass chromatograms for the Greenly-1 (4806-4818 m) FI system blank. Showing the distribution of (a) adamantane, (b) methyladamantanes and ethyladamantanes, (c) dimethyladamantanes and ethylmethyladamantanes, (d) trimethyladamantanes and (e) tetramethyladamantanes. Peak abbreviations are listed in Table A5-B6.

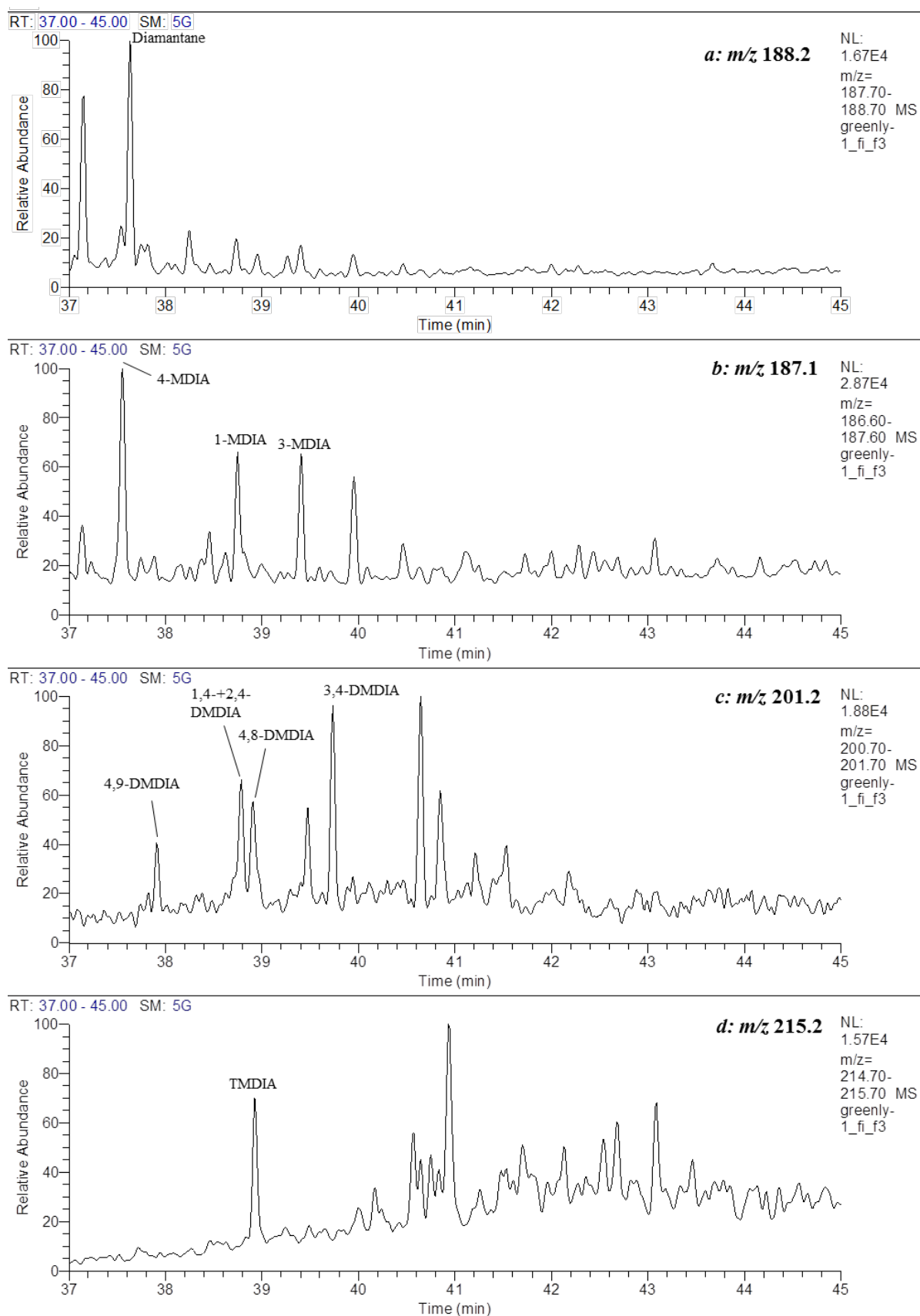


Figure A8-198: Partial m/z 188.2, 187.1, 201.2 and 215.2 mass chromatograms for the Greenly-1 (4806-4818 m) FI oil. Showing the distribution of (a) diamantane, (b) methyl-diamantanes, (c) dimethyl-diamantanes and (d) trimethyl-diamantanes respectively. Peak abbreviations are listed in Table A5-B6.

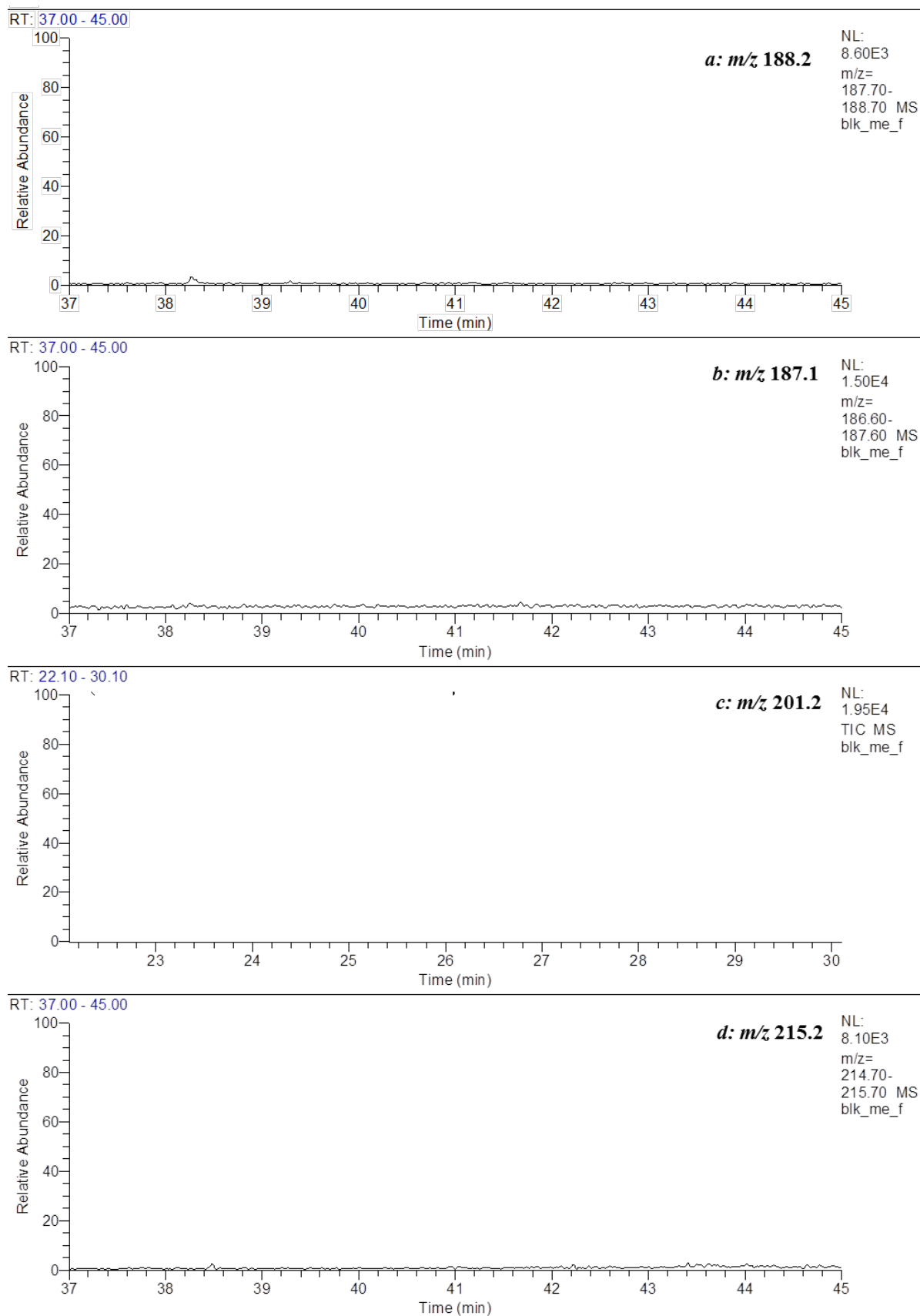
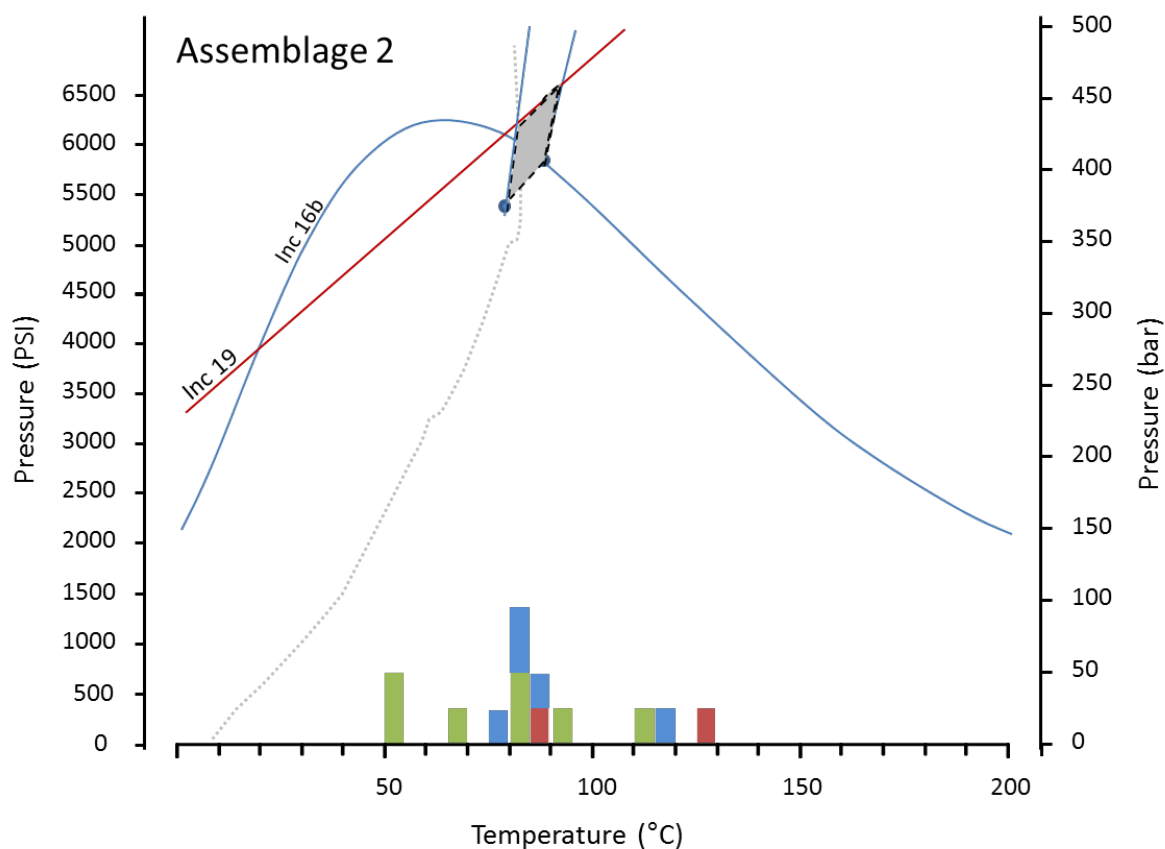
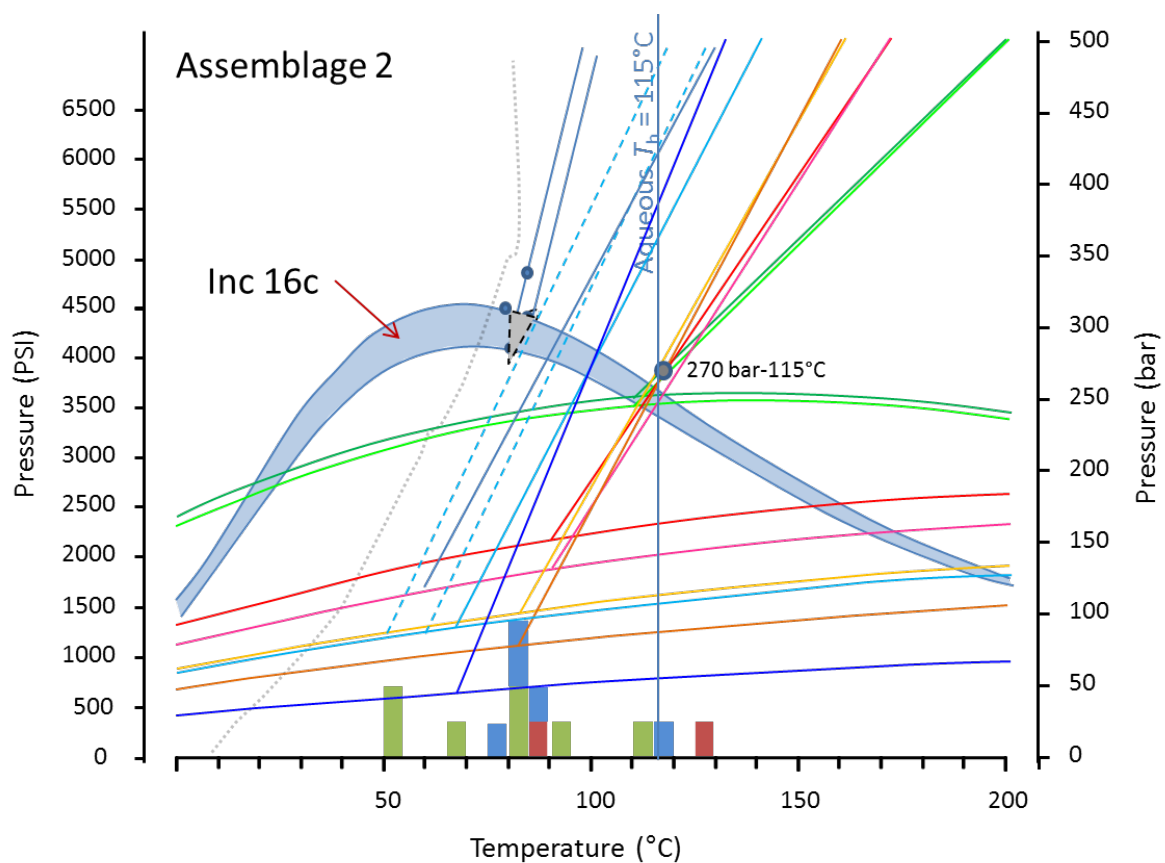


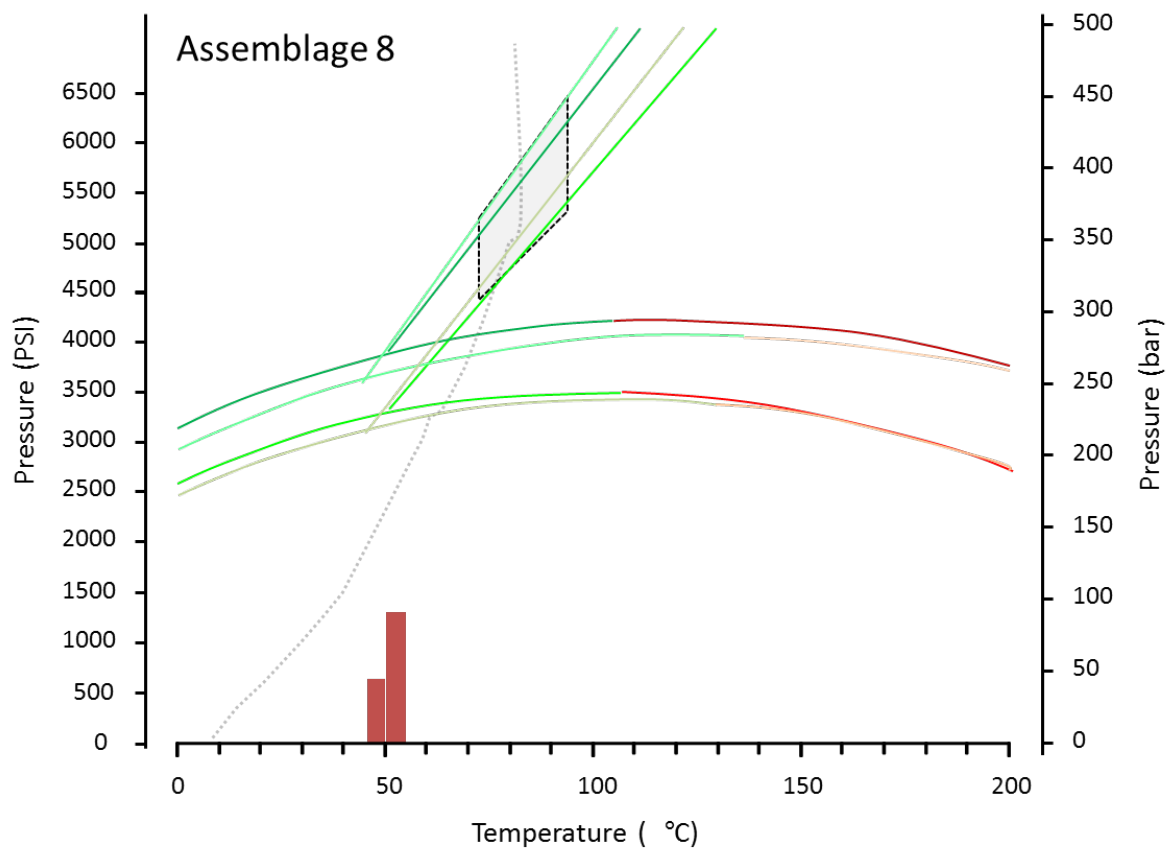
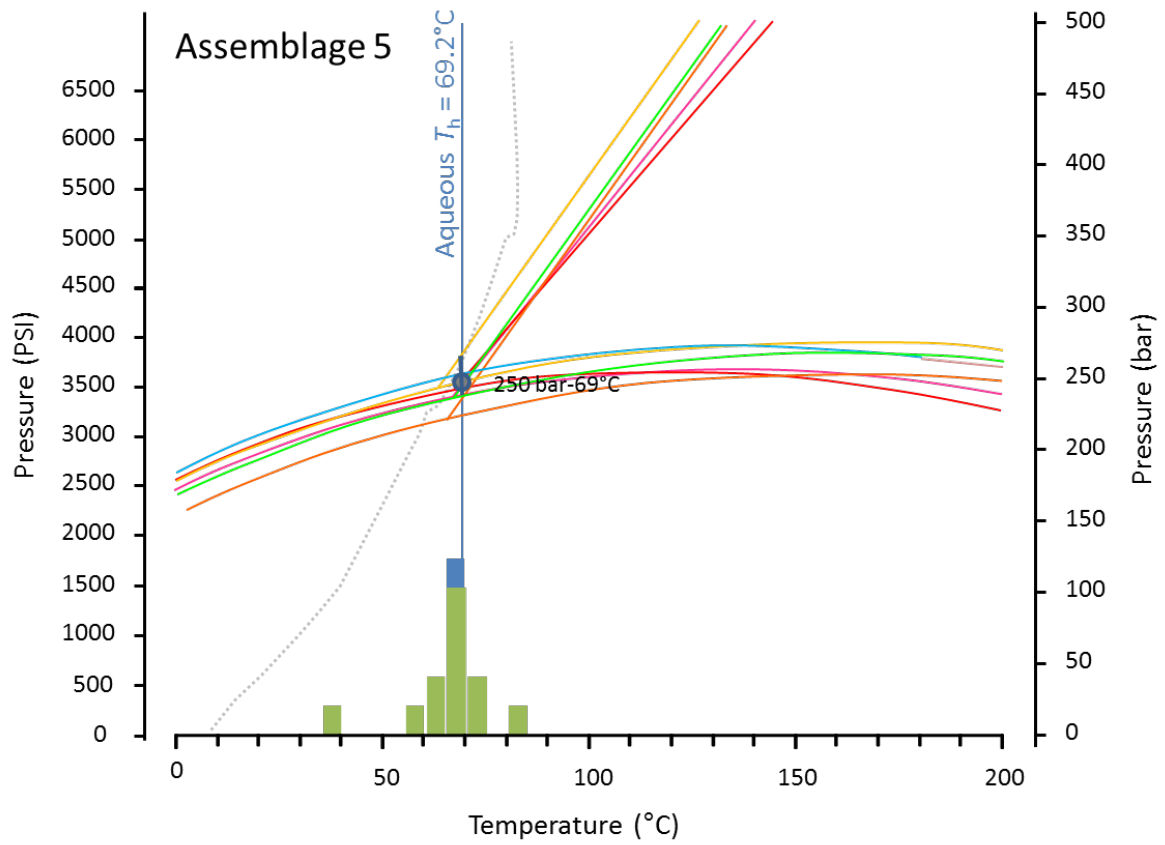
Figure A8-199: Partial m/z 188.2, 187.1, 201.2 and 215.2 mass chromatograms for the Greenly-1 (4806-4818 m) FI system blank.

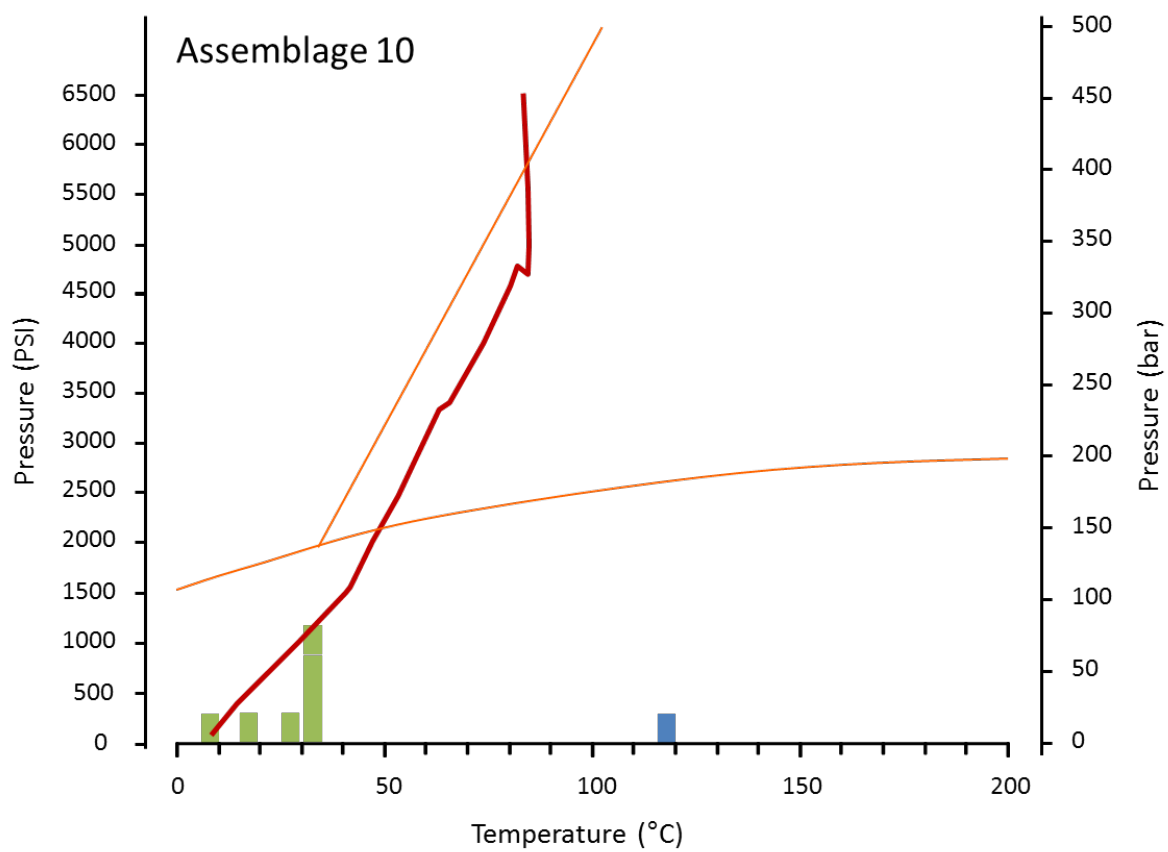
Showing the distribution of (a) diamantane, (b) methyldiamantanes, (c) dimethyldiamantanes and (d) trimethyldiamantanes respectively. Peak abbreviations are listed in Table A5-B6.

APPENDIX 9: PT diagrams Gnarlyknots-1A

Fluid Inclusion Oil Assemblages (4410-15 mMD)

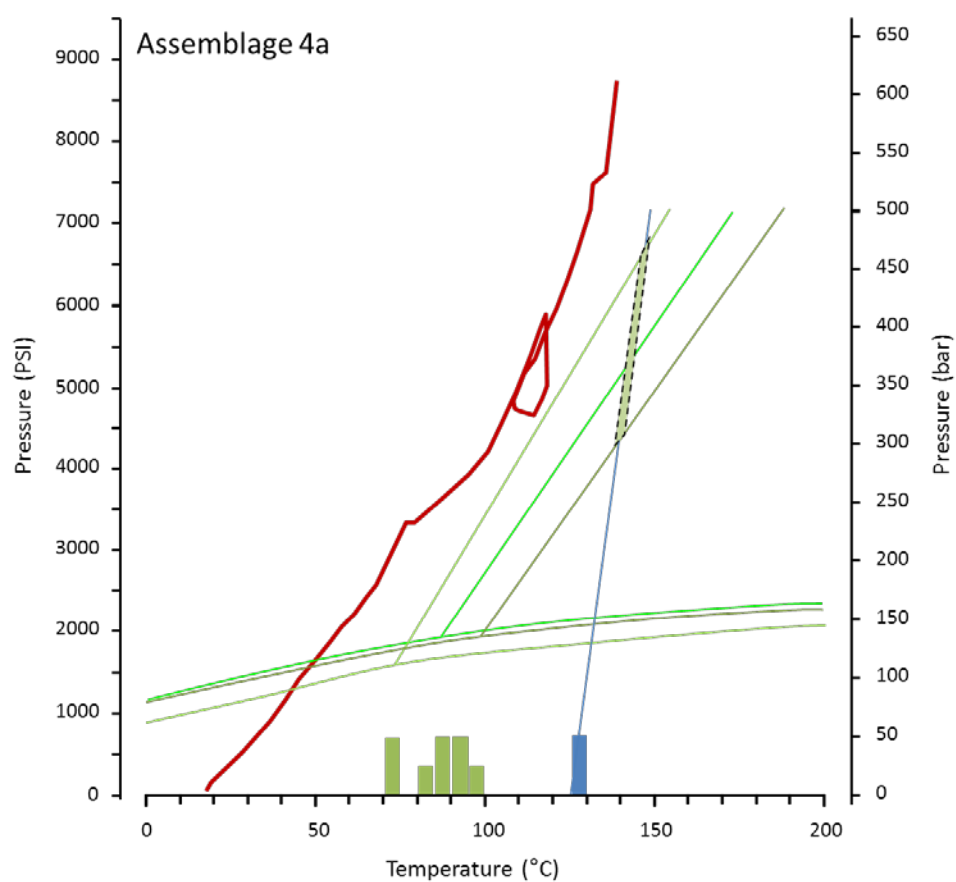
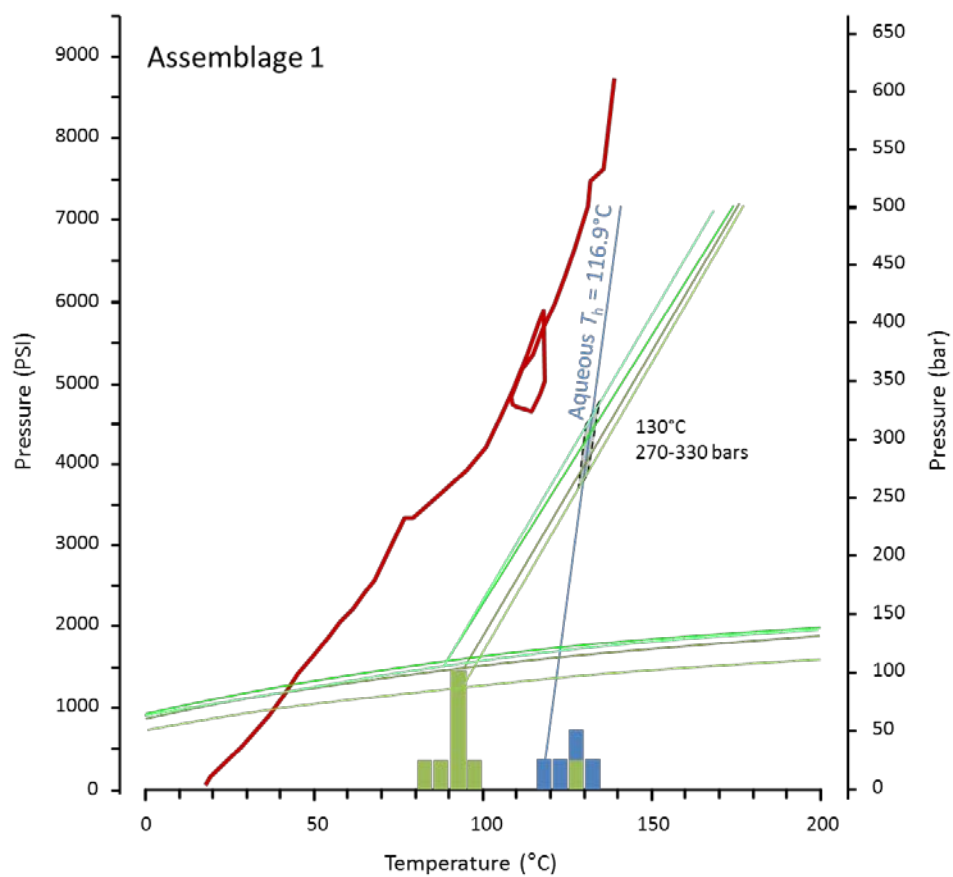


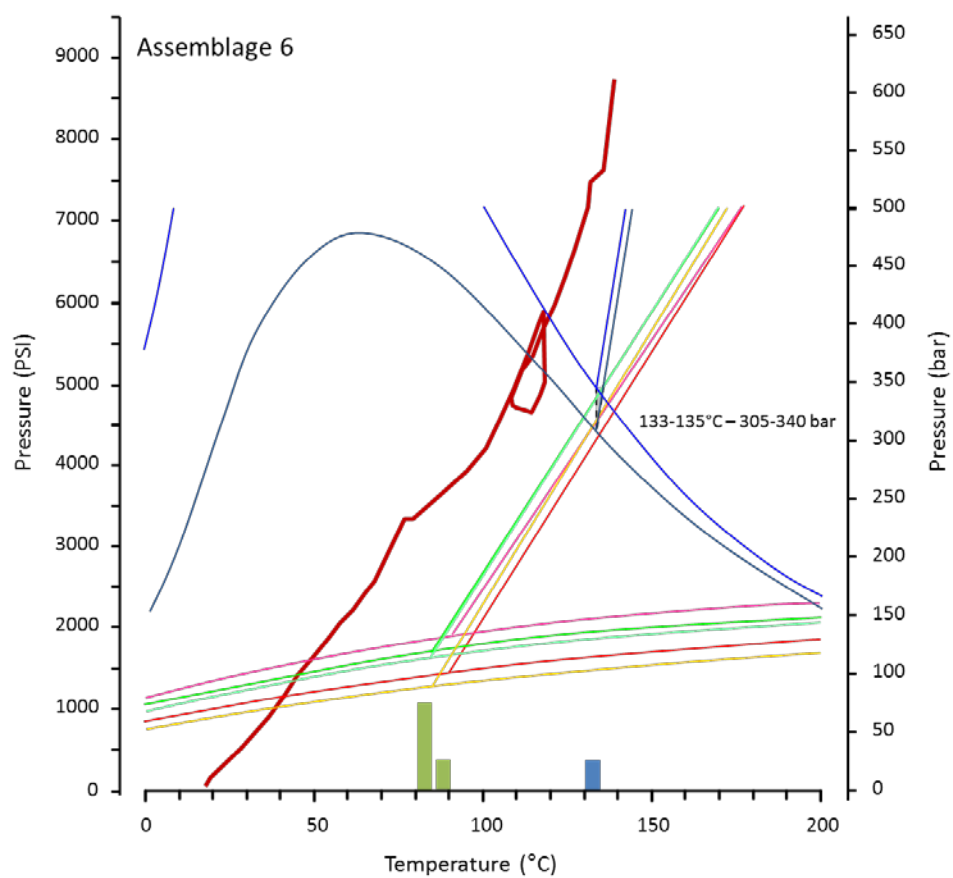
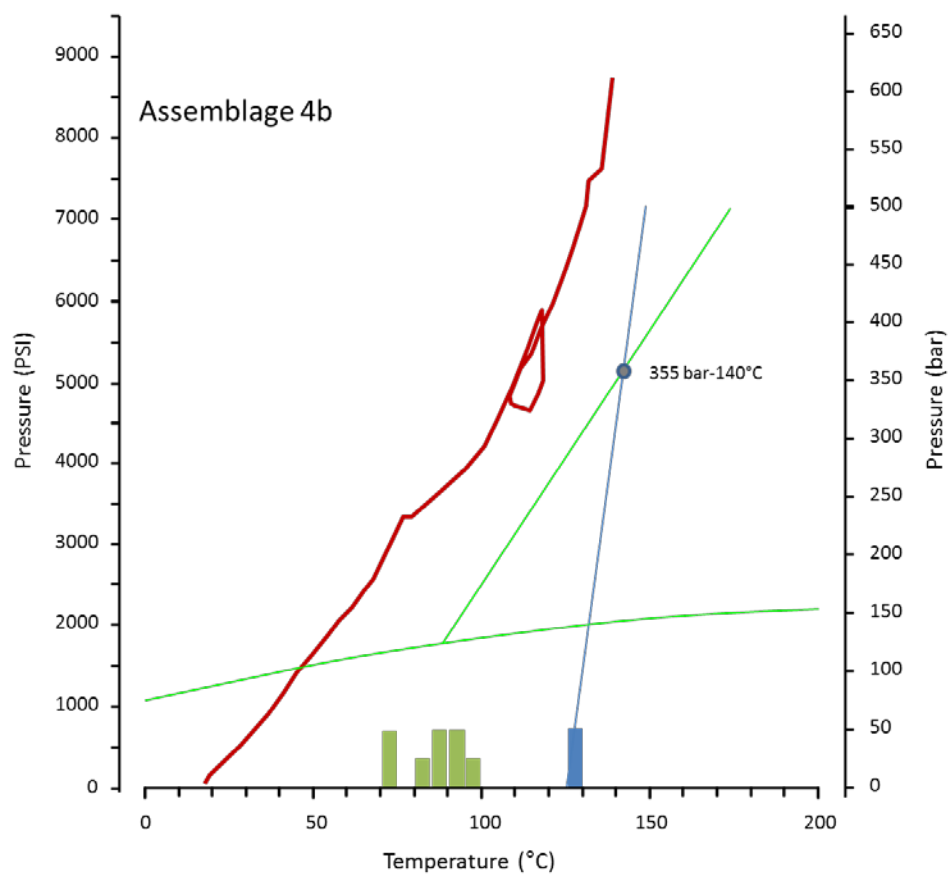


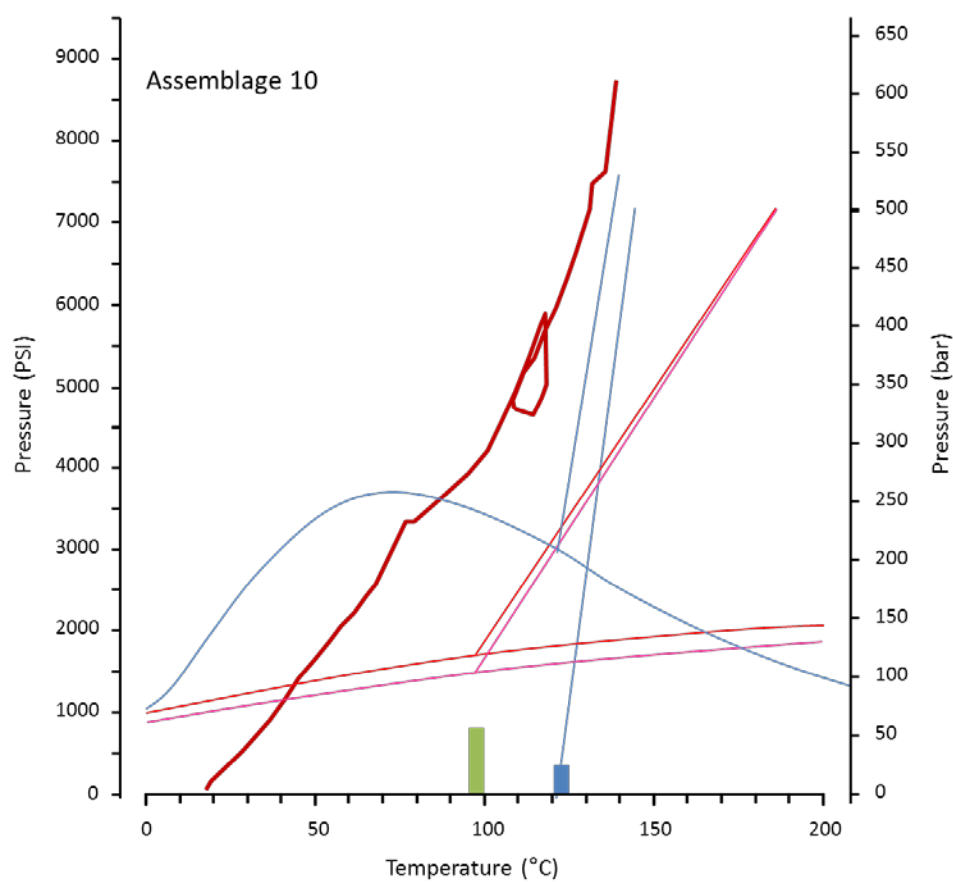
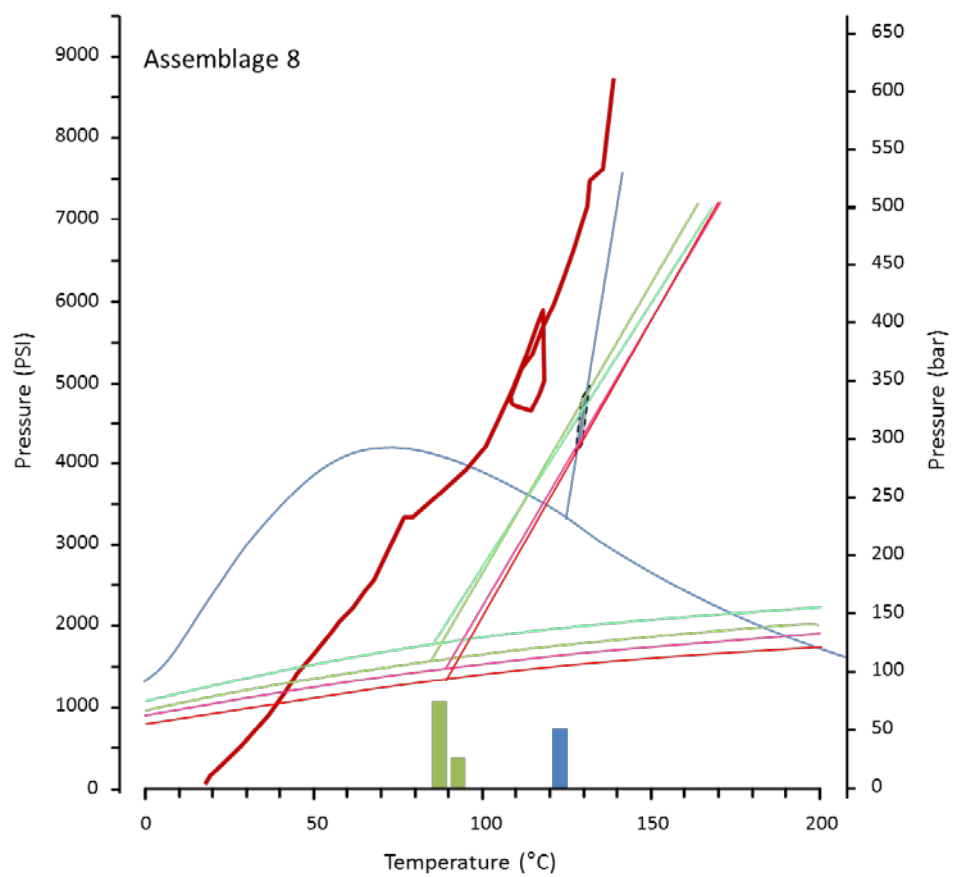


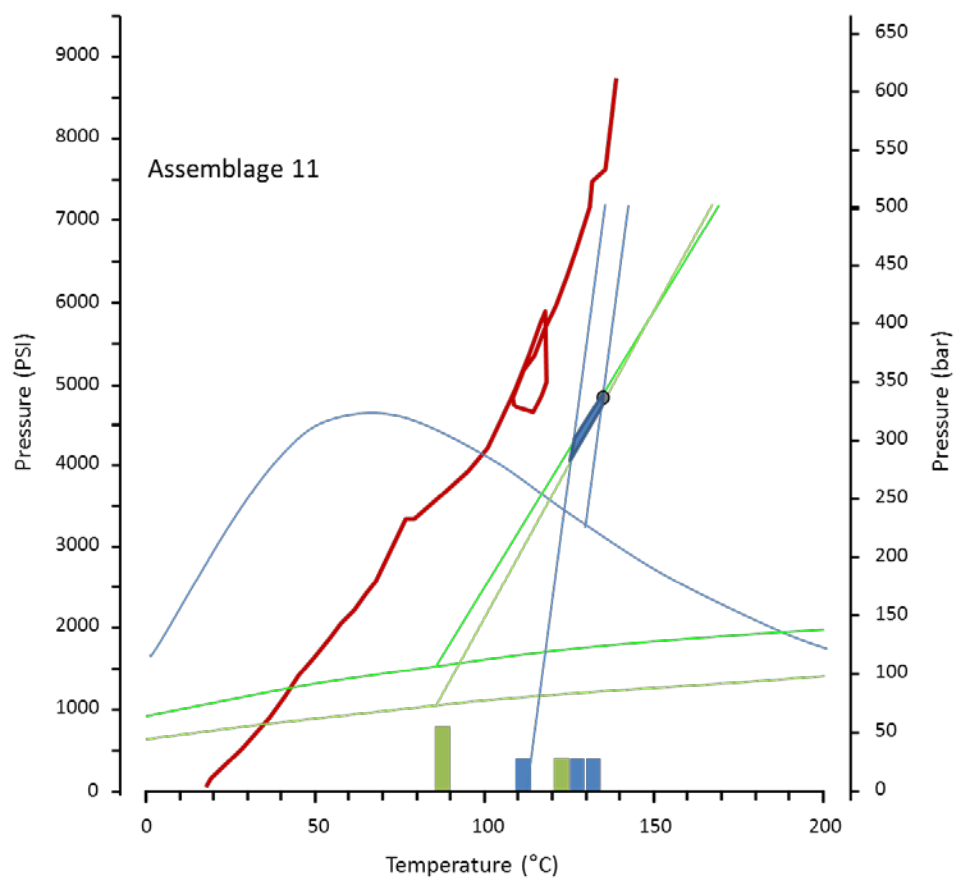
APPENDIX 10: PT diagrams Greenly-1

Fluid Inclusion Oil Assemblages (4809-12 mMD)



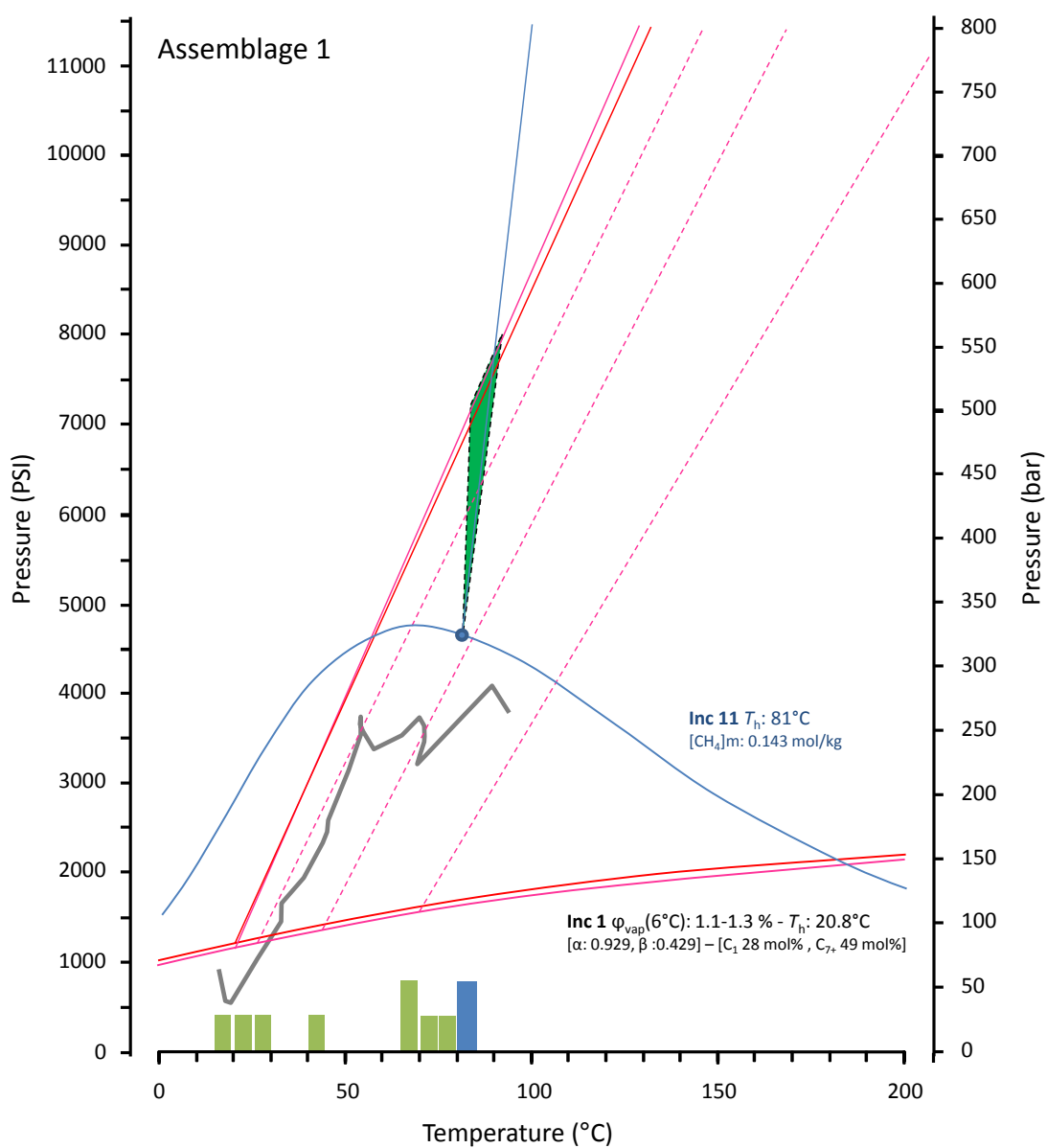


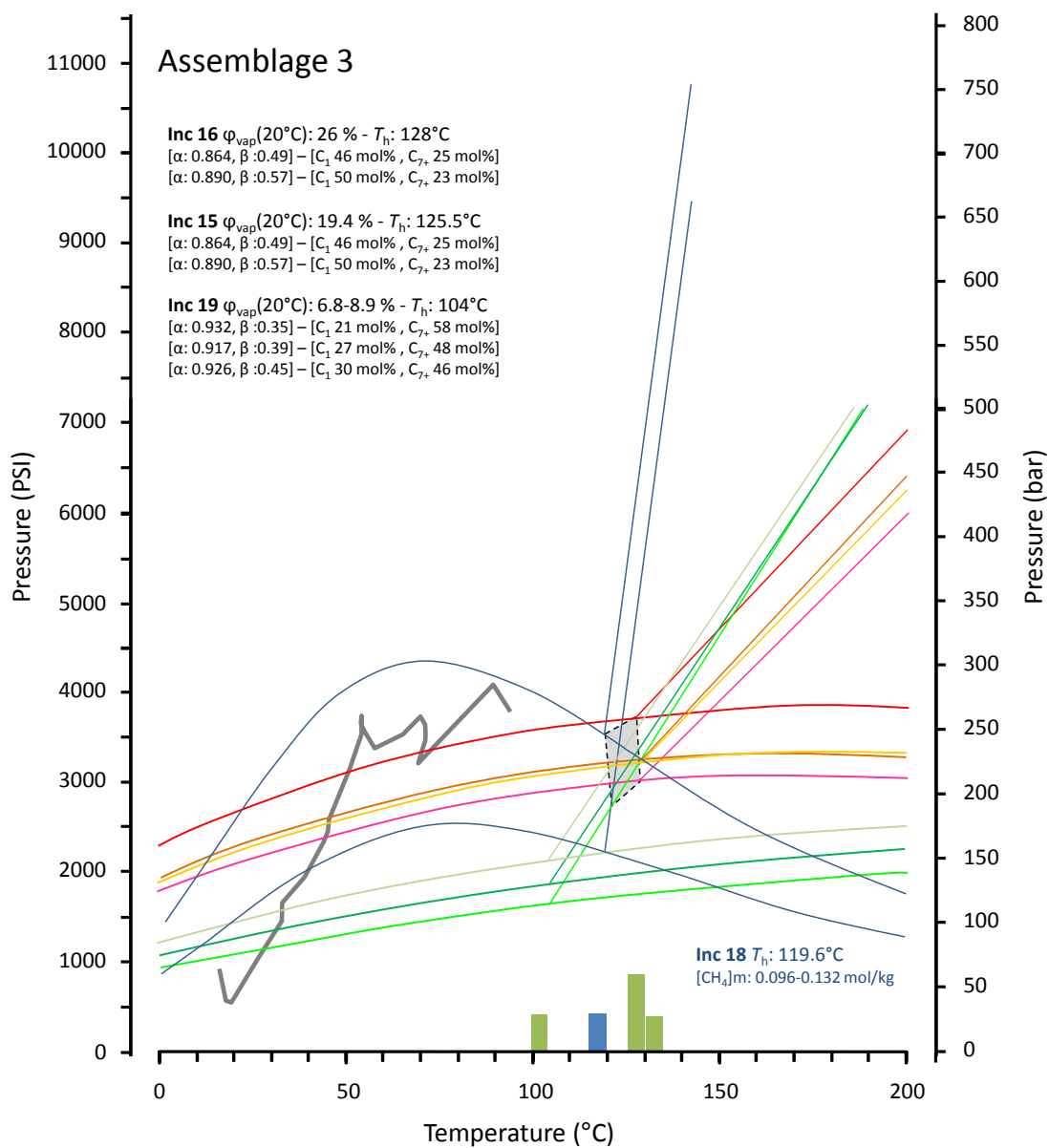


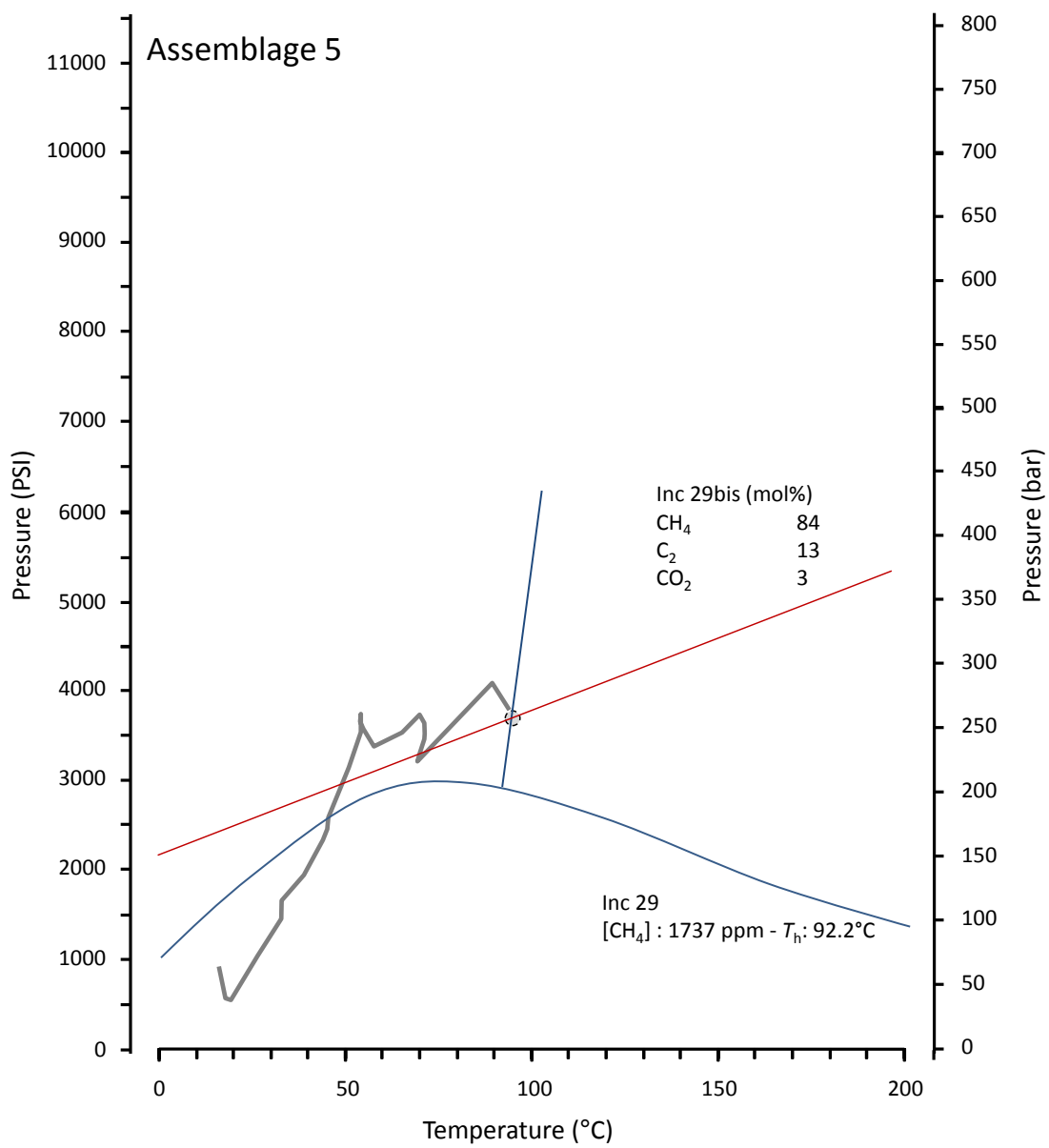


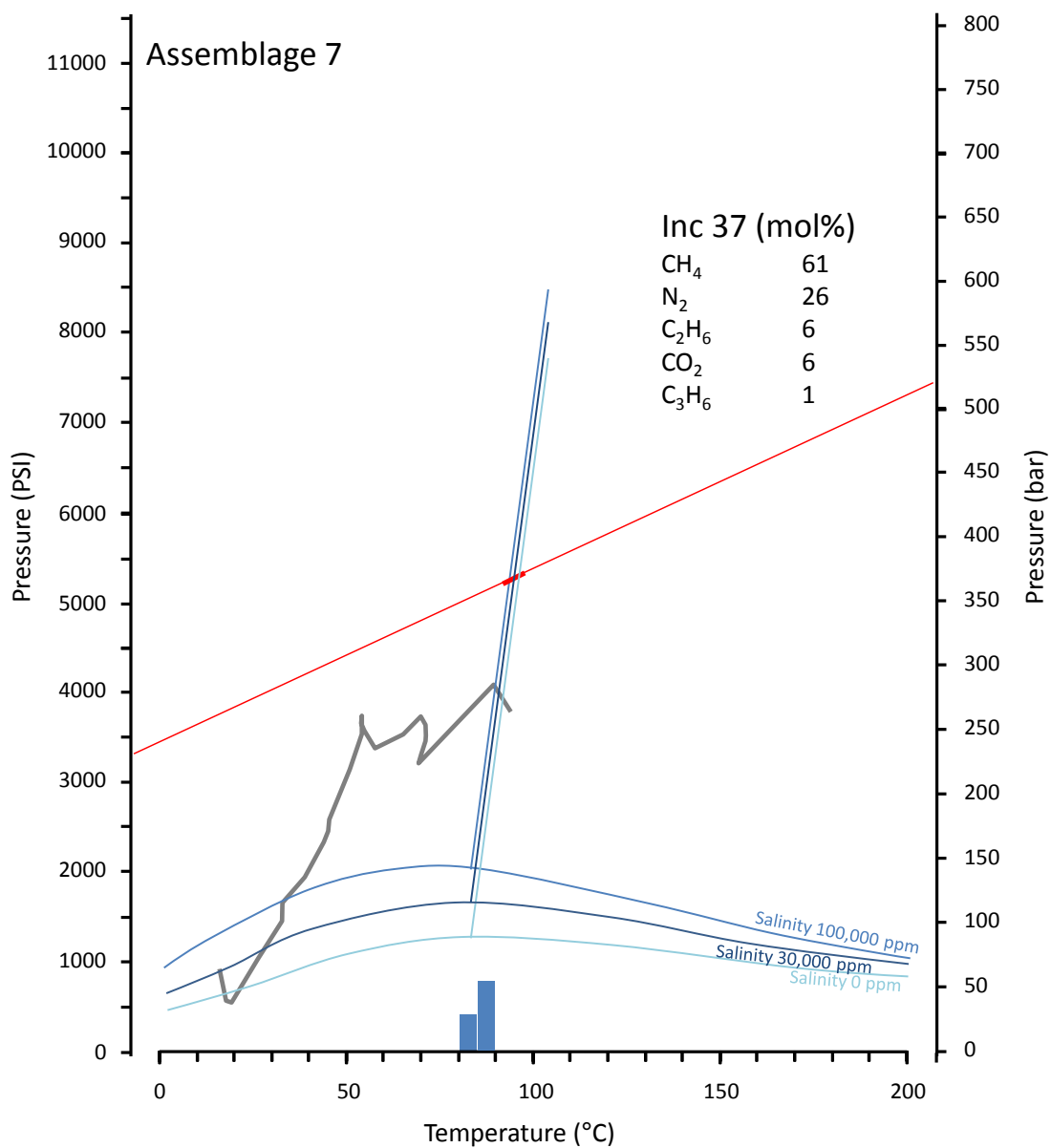
APPENDIX 11: PT diagrams Duntroon-1

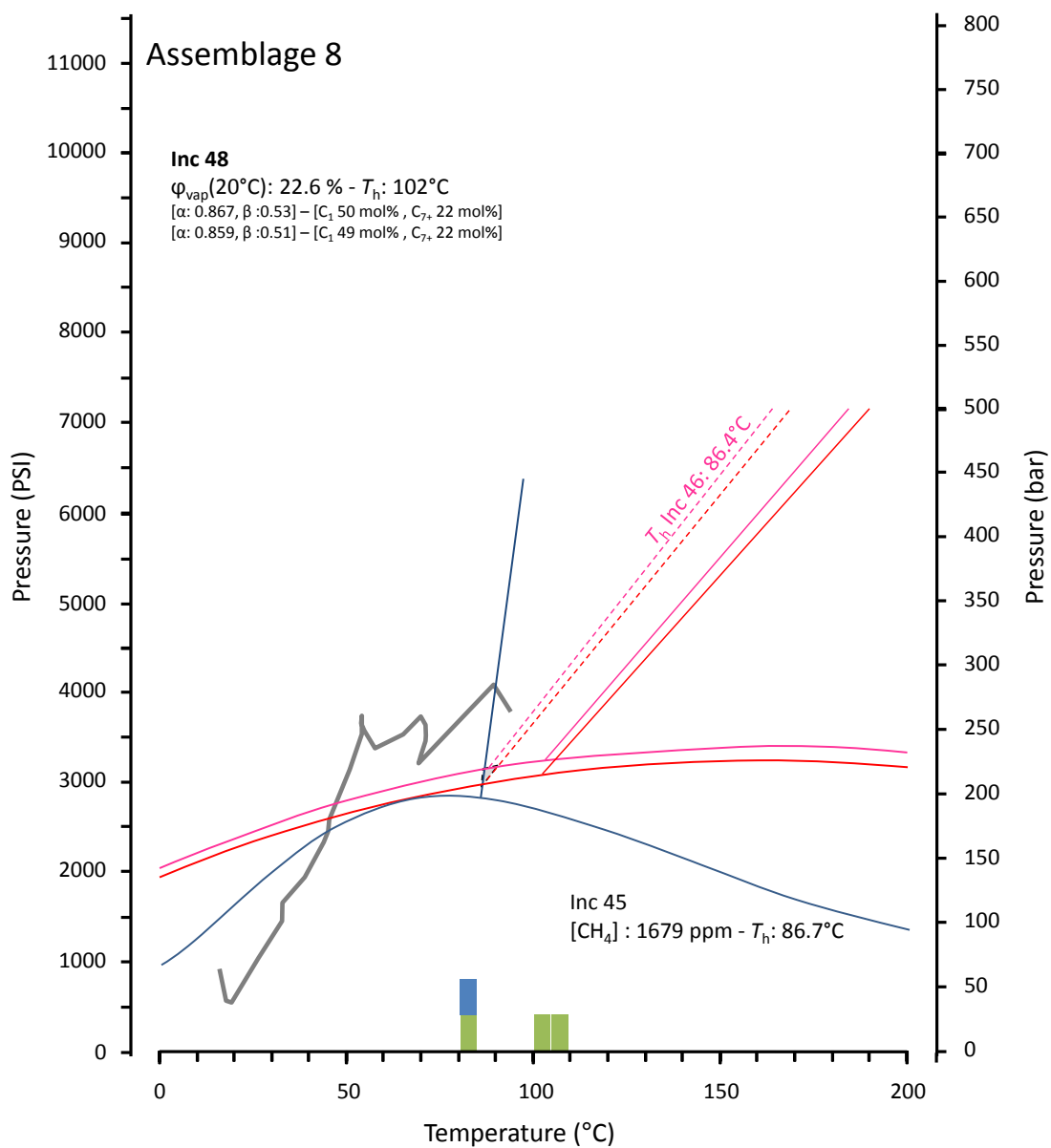
Fluid Inclusion Oil Assemblages (2505-10 mMD)

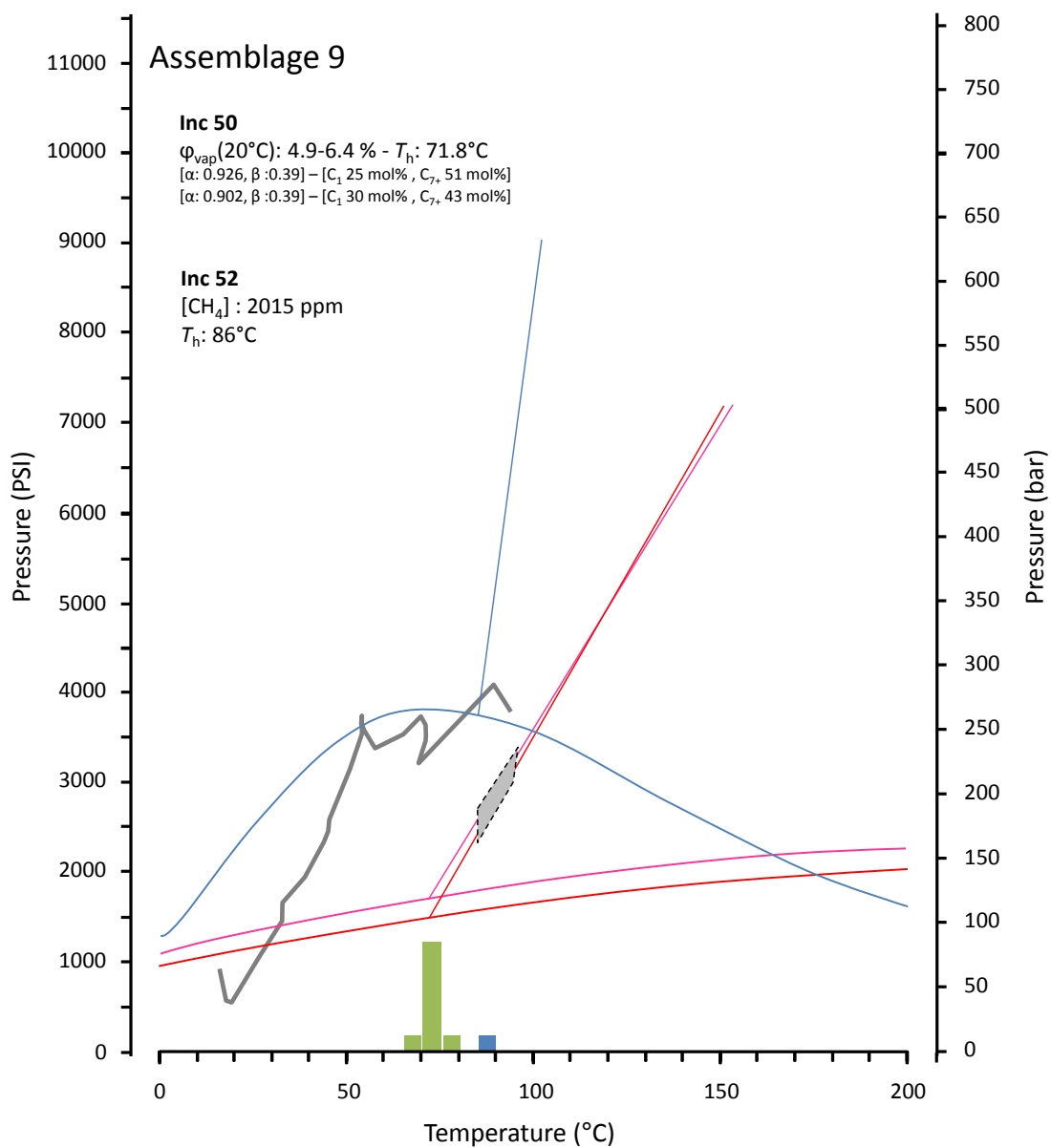


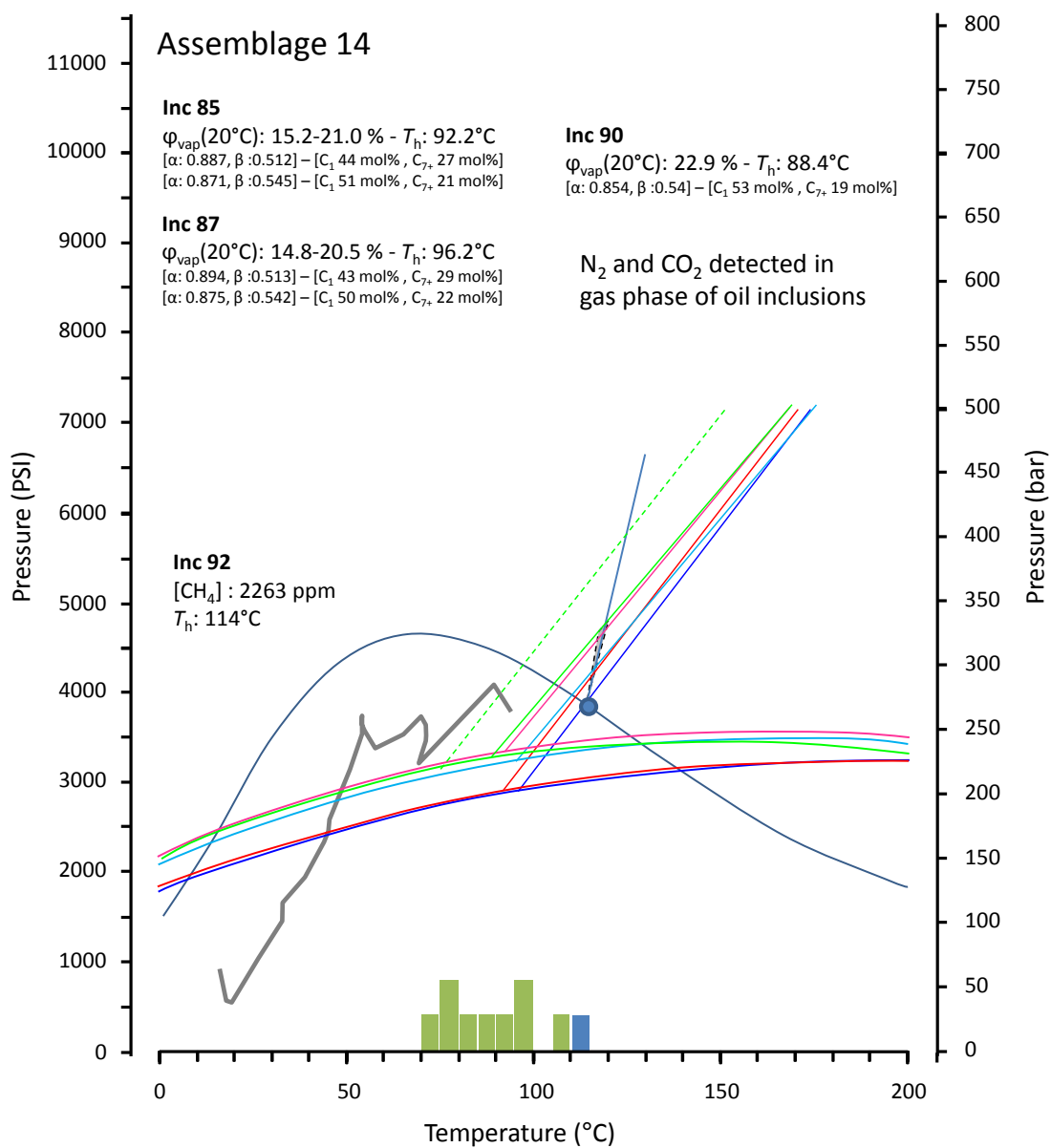






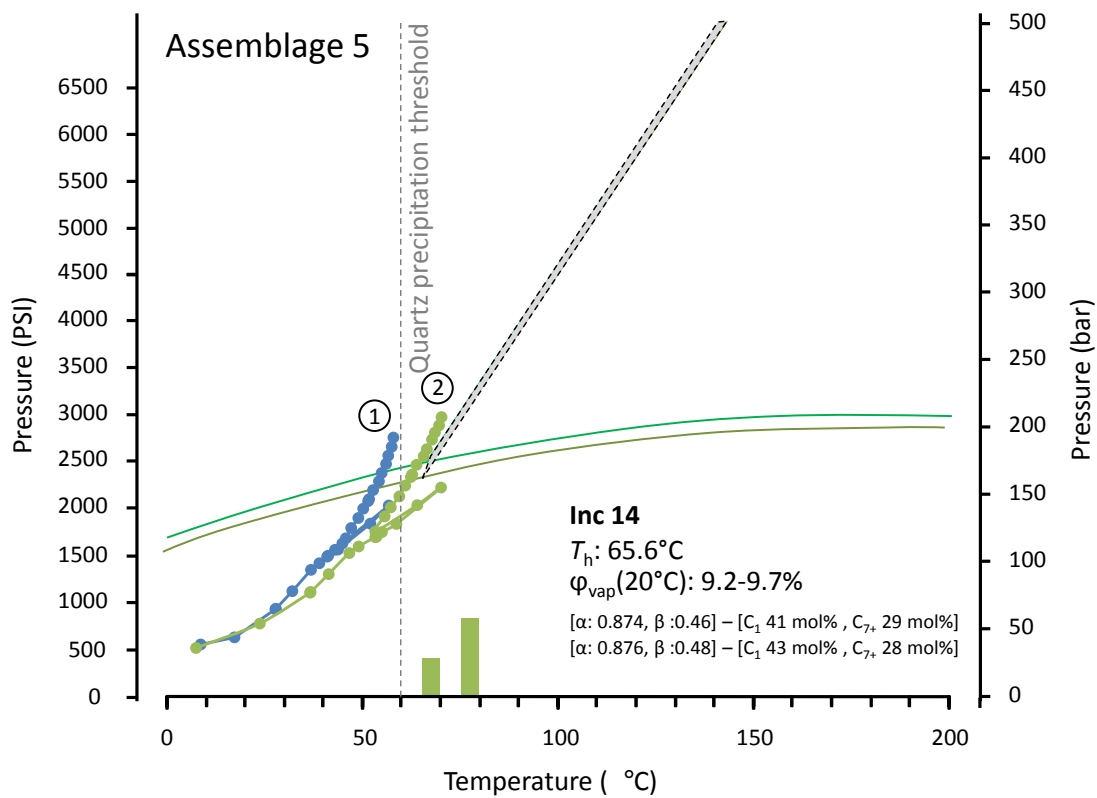
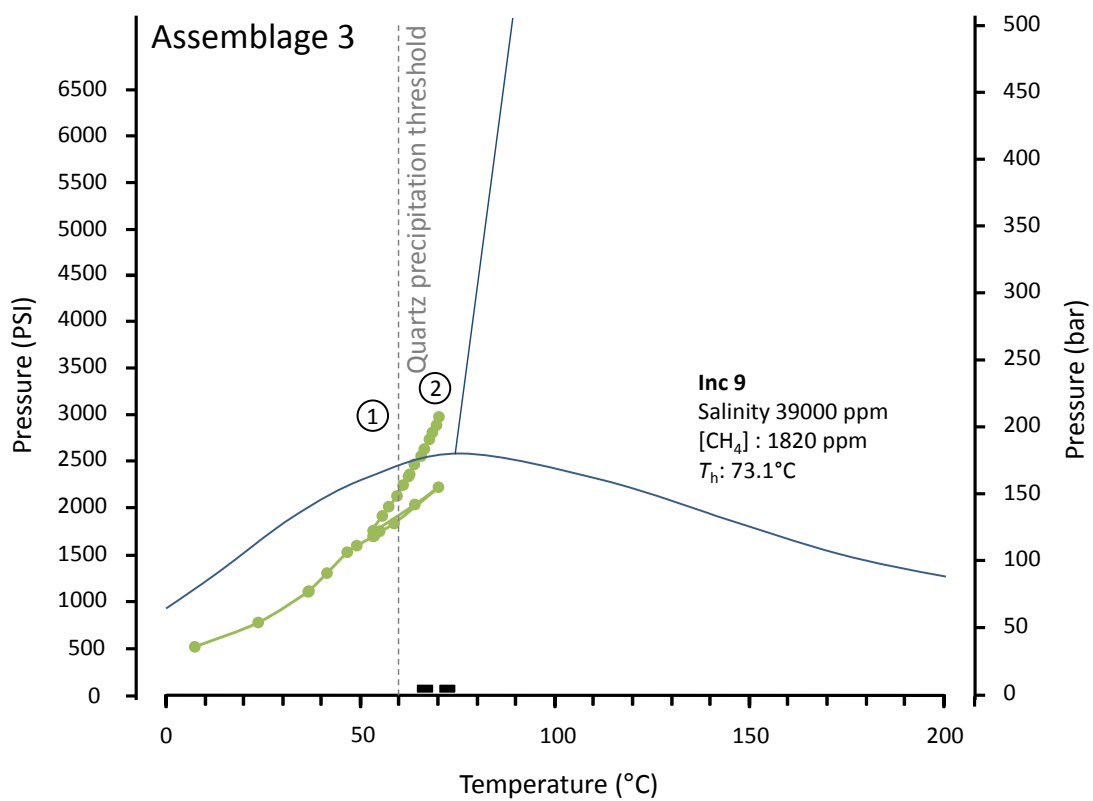


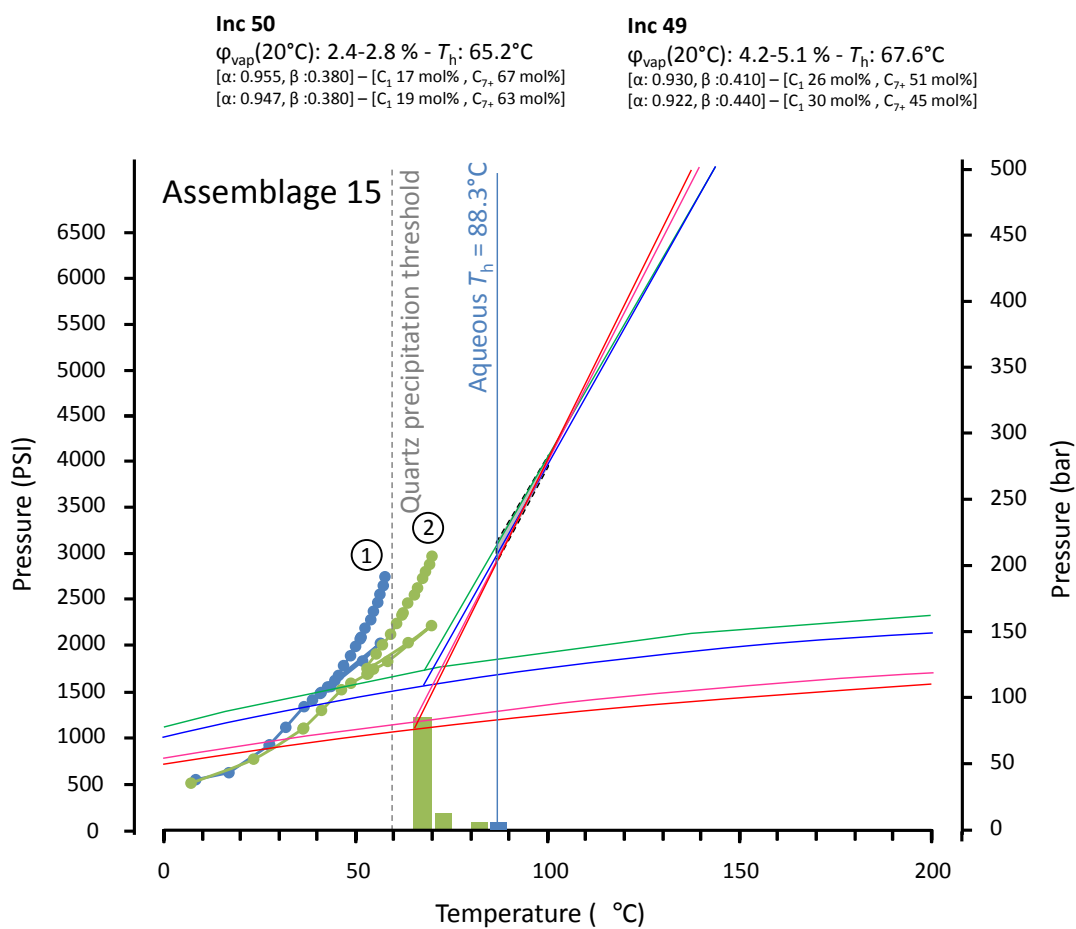
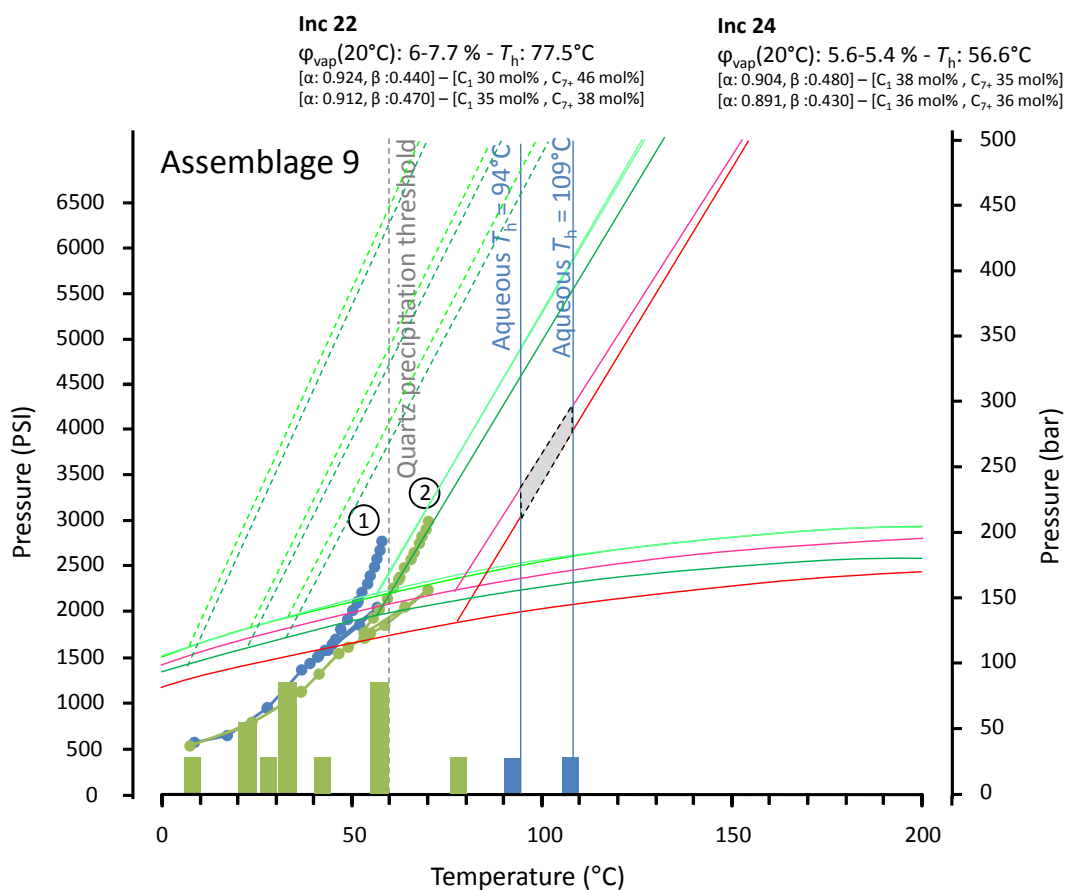




APPENDIX 12: PT diagrams Potoroo-1

Fluid Inclusion Oil Assemblages (1778-86 mMD)





APPENDIX 13: Phase envelopes of hydrocarbon fluid showing reversible precipitation at low temperatures

For oil of a fixed composition, asphaltene precipitation is most likely to take place near the bubble point. At the bubble point, the oil has the highest content of dissolved gas. The paraffinic gas components (C_1 , C_2 , etc.) increase in the oil is counterbalanced by the desorption of aromatics and resins around the asphaltenes which results in asphaltenes precipitation. The solubility of asphaltenes in paraffins also increases with pressure. Increasing the pressure from the bubble point will also make the asphaltene phase dissolve. At a sufficiently pressure, the upper asphaltene onset pressure (upper AOP), the asphaltene phase will disappear. The pressure at which the last asphaltenes go into solution is called the lower asphaltene onset pressure (lower AOP).

